MODELLING AND EXPERIMENTAL STUDIES ON A MIXED-MODE NATURAL CONVECTION SOLAR CROP DRYER WITH BACK UP HEATER

By

CHARLES KOFI KAFUI SEKYERE
(MSc. Mechanical Engineering)

KNUST

A thesis submitted to the School of Graduate Studies in partial fulfillment of the requirement for the award of the degree of Doctor of phylosophy in Mechanical Engineering

Department of Mechanical Engineering

College of Engineering

Kwame Nkrumah University of Science and Technology (KNUST), Kumasi

SEPTEMBER 2013

DECLARATION

I hereby declare that this thesis is my original research work towards a PhD undertaken at the Department of Mechanical Engineering, Kwame Nkrumah University of Science and Technology, Kumasi, Ghana, under the supervision of the undersigned, and that, to the best of my knowledge, it contains no material previously published by another person nor material which has been accepted for the award of any other degree of the University, except where due acknowledgement has been made in the write up.

.....
C.K.K. SEKYERE (PG 2676308)

1/10/2013
.....
Prof. F.K. Forson
(1ST SUPERVISOR)

01/10/13
.....
Dr. Y.A.K. Fiagbe
(2ND SUPERVISOR)

01/10/2013
.....
Dr. Richard Opoku
(3RD SUPERVISOR)

CERTIFICATION

I certify that this thesis has been assessed and all corrections have been made in accordance with the comments made by the examiners.

.....
Dr. S.M. Sackey
Head
Department of Mechanical Engineering

HEAD
DEPT. OF MECH. ENGINEERING
K.N.U.S.T., KUMASI
GHANA

KNUST

ABSTRACT OF THE RESEARCH

This thesis presents the design, experimental, and theoretical analysis of a Mixed-mode Natural Convection Solar Crop Dryer with back up heater (MNCSCDBH). The ultimate aim of the research is to study the thermal buoyancy characteristics and possible drying conditions of a mixed-mode natural convection solar crop dryer with integrated collector-storage and back-backup heater through modelling and experimental studies.

Experiments were carried out on a laboratory model of the system having similar geometrical construction as the designed prototype except for the burner used. The laboratory model was adopted in order to cut down on the cost of experimentation. The laboratory model, with a loading capacity of 2,262 g of wet agricultural produce, was designed and constructed at the Mechanical Engineering Laboratory, KNUST.

In all, thirty-one carefully planned tests, twenty-seven under no load conditions and 4 under load conditions, were conducted on the experimental dryer. The tests under no load conditions were performed in three modes of heating namely, solar, burner, and hybrid heating modes, for three different configurations of the plenum inlet gap and vent outlet gap whereas the tests under load conditions were performed in four modes of heating to reflect the possible drying conditions to be realised in practice.

The experimental dehydration results showed that in the solar mode of operation, the dryer reduced the moisture content of pineapple slices from about 1049.43% to 143.91% (db) in 23 hours; from 924.42% to 105.80% in solar drying with back up heating mode in 19 hours; from 1049.43% to 183.55% in burner drying mode in 10 hours; and from 912.23% to 154.58% in hybrid drying mode in 7 hours. The average values of the moisture pickup efficiency were 15.24%, 15.30%, 17.22%, and 13% in the solar, solar with back up heating, burner, and hybrid modes of drying, respectively.

An exergy analysis conducted on the drying air under no load conditions give the minimum and maximum rate of change of flow exergy values as 93.09 and 4,597.27 kW; 4,012.88 and 13,656.24 kW; and 5,549.866 and 17,319.27 kW for solar, heater, and hybrid heating modes respectively. These results show that the rate of change of flow exergy increases with increased heating effect.

Mathematical models, capable of predicting the performance of the MNCSCDBH for three heating modes were developed. The models were based on a one-dimensional steady-state operation of the dryer. A MATLAB code was developed and used to predict the performance of the dryer under no load conditions. The simulation results were validated with experimental data from the laboratory experiments and the simulation model was subsequently fine tuned.

Parametric studies were conducted by observing the effects of varying plenum inlet to vent outlet ratios of 1, 1.33, and 1.5 on the performance of the dryer. Results obtained indicate that for the proposed system a significant improvement can be made by maintaining the ratio of the vent outlet gap to plenum inlet gap of: 1:1.5.

LIST OF CONTENTS

	PAGE
DECLARATIONS	ii
ABSTRACT	iii
LIST OF CONTENTS	iv
LIST OF TABLES	viii
LIST OF FIGURES	xi
NOMENCLATURE AND ACRONYMS	xvii
ACKNOWLEDGEMENTS	xxii

CHAPTER ONE: INTRODUCTION

1.1 Background.....1

1.2 Objectives of the study.....4

1.3 Methodology and technical approach.....5

1.2 Organisation of the report.....8

CHAPTER TWO: THEORETICAL FRAMEWORK

2.0 Introduction.....9

2.1 Fundamentals of drying.....9

2.2 Drying Kinetics.....10

2.2.1 Constant-rate period.....12

2.2.2 Falling-rate period.....14

2.3 Drying: modeling requirements and dryer design calculations.....16

2.4 Thermo-physical properties of agricultural products.....17

2.4.1 Moisture content of agricultural products.....17

2.4.2 Specific heat capacity.....19

2.4.3 Heat of vaporization or latent heat of moisture from a crop.....20

2.5 The dynamics of drying wet products.....21

2.5.1 The equilibrium moisture content (EMC).....21

2.5.2 Drying constant.....25

KNUST

2.5.3 Moisture diffusivity.....26
2.6 Psychrometry in relation to drying.....28
2.7 Drying simulation.....32
2.7.1 Thin layer drying.....33
2.7.2 Analysis of deep-bed drying.....41
2.7.2.1 Non-equilibrium models.....42
2.7.2.2 Equilibrium models.....45
2.7.2.3 Logarithmic models.....46
2.8 Solar drying: an overview.....47
2.8.1 Dryer construction and functionality.....47
2.8.1.1 Main types of solar dryers.....48
2.8.1.2 Solar natural dryers.....48
2.8.1.3 Cabinet dryers fitted with a chimney.....51
2.8.1.4 Cabinet dryers fitted with a chimney and heat storage.....52
2.8.1.5 Structural design of solar dryers.....53
2.9 Crop dryer modeling equations and reviews.....56
2.9.1 Formulation of drying model.....57
2.9.1.1 Heat and mass transfer in layer drying.....58
2.9.1.2 The drying rate equation.....58
2.9.1.3 Mass balance equation on the drying air.....59
2.9.1.4 Heat balance on the drying air.....60
2.9.1.5 Heat balance on the wet material.....61
2.9.2 Energy balance on the walls of the drying chamber.....64
2.9.3 Finite difference formulation of the drying simulation model.....64
2.9.4 Solution procedure.....65
2.9.5 Programme termination.....67
2.9.6 Technical performance criteria model.....68
2.9.6.1 The system drying efficiency.....68
2.9.6.2 The pick-up efficiency.....69
2.9.7 Drying of pineapples.....70
2.9.8 Use of back up heating in solar crop drying.....70

KNUST

CHAPTER THREE: FORMULATION OF MATHEMATICAL MODELS

3.0 Introduction.....74

3.1 Formulation of the backup heating and air-heating models.....74

3.1.1. Energy balance equations on air heating model.....75

3.1.2 Radiation analysis of the plenum.....81

3.1.3 Modeling of air flow rate.....87

3.1.4 Estimation of heat transfer coefficients.....89

3.1.5 Thermo-physical properties of air.....93

3.1.6 Solution procedure.....94

3.2 Formulation of drying model.....99

CHAPTER FOUR: EXPERIMENTAL SET-UPS: DESCRIPTION, INSTRUMENTS, MEASUREMENT TECHNIQUES, AND TESTS

4.0 Introduction.....101

4.1 Description of experimental set-up.....101

4.1.1 Laboratory model.....101

4.1.2 Operation.....107

4.2 Instrumentation and measurement.....108

4.2.1 Laboratory model instrumentation.....109

4.3 An overview of the test series.....117

4.3.1 Laboratory test.....118

4.3.2 Determination of initial moisture content of pineapple.....120

KNUST

CHAPTER FIVE: EXPERIMENTAL RESULTS AND DISCUSSIONS

5.0 Introduction.....122

5.1 Laboratory experiments under no load conditions.....122

5.1.1 Solar heating mode.....125

5.1.2 Burner heating mode.....137

5.1.3 Hybrid heating mode.....149

5.2 Laboratory experiments under load conditions: Results and Discussions.....164

5.2.1 Experiments under load conditions.....164

CHAPTER SIX:COMPUTER SIMULATION: PROGRAMS, RESULTS AND DISCUSSIONS

6.0 Computer simulation code.....186

6.1 Air-heater performance simulations.....188

6.1.1 Air heater simulation results.....188

6.1.2 Comparison of simulation and experimental results on air heater.....198

6.2 Parametric studies and optimization of air ventilation process.....203

CHAPTER SEVEN:CONCLUSIONS AND SUGGESTIONS FOR FURTHER WORK

7.0 CONCLUSIONS.....206

7.1 SUGGESTIONS FOR FURTHER WORK.....209

LIST OF REFERENCE.....210

APPENDIX A.....222

APPENDIX B.....223

APPENDIX C.....231

APPENDIX D.....258

KNUST

LIBRARY
KWAME NKRUMAH
UNIVERSITY OF SCIENCE & TECHNOLOGY
KUMASI

LIST OF TABLES

Page

Table 1: Effective moisture diffusivity in some materials.....27
Table 2: Thermocouple calibration results.....115
Table 3: Summary of the test conditions for dryer characteristic studies.....119
Table 4: General input parameters for simulation process, either determined by design analysis or adopted from generally accepted literature.....123
Table 5: Solar drying only.....165
Table 6: Solar drying (system component temperatures).....167
Table 7: Solar drying with back up heating.....172
Table 8: Solar drying with back up heating-system component temperatures.....173
Table 9: Drying in burner mode.....177
Table 10: Drying in burner mode – system component temperatures.....178
Table 11: Hybrid drying.....181
Table 12: Drying in hybrid mode-system component temperatures.....182
Table 13: SIMULATION RESULTS: Solar heating mode 1.....189
Table 14: SIMULATION RESULTS: Solar heating mode 2.....190
Table 15: SIMULATION RESULTS: Solar heating mode 3.....191
Table 16: SIMULATION RESULTS: Burner heating mode 1.....192
Table 17: SIMULATION RESULTS: Burner heating mode 2.....193
Table 18: SIMULATION RESULTS: Burner heating mode 3.....194
Table 19: SIMULATION RESULTS: Hybrid heating mode 1.....195
Table 20: SIMULATION RESULTS: Hybrid heating mode 2.....196
Table 21: SIMULATION RESULTS: Hybrid heating mode 3.....197
Table 22: Comparison of simulation results (headed Sim) and experimental results (headed expt)-Solar heating mode 1.....199
Table 23: Comparison of simulation results (headed Sim) and experimental results (headed expt) - solar heating mode 2.....200
Table 24: Comparison of simulation results (headed Sim) and experimental results (headed expt) -Burner heating mode 1.....201
Table 25: Comparison of simulation results (headed Sim) and experimental results (headed expt) -Hybrid heating mode 2.....202

KNUST

LIST OF FIGURES

Page

Figure 1: Schematic representation of MNCSCDBH.....3

Figure 2: Classification of solar dryer and drying modes. 10

Figure 3(a): Moisture content versus time.....11

Figure 3(b): Drying rate versus moisture content.....11

Figure 3(c): Drying rate versus time.....12

Figure 4: Drying model information flow diagram.....16

Figure 5: Typical sorption isotherms showing hysteresis.....22

Figure 6: Control volume of a stationary bed of crop.....42

Figure 7: Cabinet type dryer for fruits and herbs.....49

Figure 8: Tent type solar dryer.....50

Figure 9: Shelf type cabinet dryer.....51

Figure 10: Cabinet dryer with chimney.....52

Figure 11: Cabinet dryer with chimney and latent heat storage.....53

Figure 12: Solar collectors.....55

Figure 13: Elemental volume of crop beds.....57

Figure 14: Hybrid solar/sawdust crop dryer (Bassey et al).....72

Figure 15(a):Energy balance on the components of the air-heater and its Surroundings.....75

Figure 15(b): Energy balance on glass cover.....75

Figure 16: Heat transfer scenario during solar heat charging.....79

Figure 17: Heat transfer scenario during backup heating.....80

Figure 18: The plenum as a seven surface enclosure.....81

Figure 19: Radiation network associated with plenum as a seven surface Enclosure.....82

Figure 20 View factor from absorber surface to upper wall.....83

Figure 21 View factor from thermal mass to lower wall.....85

Figure 22 MNCSCDBH showing flow passages.....87

Figure 23 Energy balance on components of drying chamber.....99

Figure 24(a): Pictorial view of the laboratory model of MNCSCDBH.....102

Figure 24(b): Pictorial view of the laboratory model of MNCSCDBH.....102

KNUST

Figure 24(c) Solar dryer and solar simulator arrangement.....103
Figure 24 (d) Solar simulator and supporting structures.....104
Figure 24 (e): Concrete absorber and rock pebble bed arrangement.....104
Figure 24 (f): Vent outlet configuration.....105
Figure 24 (g): 1800 Watts electric heater.....105
Figure 24 (h): Solar simulator platform.....106
Figure 25: Integrated absorber-thermal mass system showing slabs for controlling air flow.....106
Figure 26: MNCSCDBH showing drying trays.....107
Figure 27:Schematic illustration of the laboratory dryer showing the locations of the temperature measuring sensors.....109
Figure 28: PCE-FWS 20 Receiver and weather centre.....110
Figure 29:Vaisala H M34 and Macronta LCD humidity and temperature meters.....110
Figure 30: Barnant 115 thermocouple (model number: 600-2810).....111
Figure 31: Solar meter (model 776).....111
Figure 32: 21X Micrologger, Campbell Scientific Incorporation, U.S.A.....112
Figure 33: Set up for calibration of mercury-in-glass thermometer.....113
Figure 34: Set up for calibration of Barnant 115 thermocouple.....114
Figure 35: Set up for calibration of k-type thermocouple.....114
Figure 36: Calibration for k-type thermocouple wires.....116
Figure 37: Thermal buoyancy properties versus time in solar heating mode (pi=2cm, vo=2 cm).....125
Figure 38: Technical performance parameters versus time in solar heating mode (pi=2cm, vo=2 cm).....125
Figure 39: Pertinent hardware temperatures versus time in solar heating mode (pi=2cm, vo=2 cm).....126
Figure 40:Thermal buoyancy properties versus time in solar heating mode (pi=2 cm, vo=3 cm).....127
Figure 41: Technical performance parameters versus time in solar heating mode (pi=2 cm, vo=3 cm).....127
Figure 42: Pertinent hardware temperatures versus time in solar heating

KNUST

mode (pi=2 cm, vo=3cm).....127
Figure 43: Thermal buoyancy properties versus time in solar heating
mode (pi=2 cm, vo=4 cm).....128
Figure 44: Technical performance parameters versus time in solar heating
mode (pi=2 cm, vo=4 cm).....129
Figure 45: Pertinent hardware temperatures in solar heating mode
(pi= 2 cm, vo=4 cm).....129
Figure 46: Thermal buoyancy properties versus time in solar heating mode
(pi=2 cm, vo=4 cm).....130
Figure 47:Technical performance parameters versus time in solar heating
mode (pi=2 cm, vo=4).....130
Figure 48: Pertinent hardware temperatures versus time in solar heating
mode (pi=4cm, vo=2 cm).....130
Figure 49:Thermal buoyancy properties versus time in solar heating
mode (pi=4 cm, vo=3 cm).....131
Figure 50:Technical performance parameters versus time in solar heating
mode (pi=4 cm, vo=3 cm).....131
Figure 51:Pertinent hardware temperatures versus time in solar
heating mode (pi=4 cm, vo= 3 cm).....132
Figure 52:Thermal buoyancy properties versus time in solar heating
mode (pi=4 cm, vo=4 cm).....132
Figure 53:Technical performance parameters versus time in solar heating
mode (pi=4 cm, vo=4 cm).....133
Figure 54:Pertinent hardware temperatures versus time in solar heating
mode (pi=4 cm, vo=4 cm).....133
Figure 55:Thermal buoyancy properties versus time in solar heating
mode (pi=6 cm, vo=2 cm).....134
Figure 56: Technical performance parameters versus time in solar heating
mode (pi= 6cm, vo=2 cm).....134
Figure 57: Pertinent hardware temperatures versus tin in solar heating
mode (pi=6 cm, vo=2 cm).....134
Figure 58: Thermal buoyancy properties versus time in solar heating
mode (pi=6 cm, vo=3 cm).....135
Figure 59: Technical performance parameters versus time in solar heating
mode (pi=6 cm, vo=3 cm).....135

KNUST

Figure 60: Pertinent hardware temperatures versus time in solar heating mode (pi=6 cm, vo=3 cm).....135
Figure 61: Thermal buoyancy properties versus time in solar heating mode (pi=6 cm, vo=4 cm).....136
Figure 62: Technical performance parameters versus time in solar heating mode (pi=6 cm, vo=4 cm).....136
Figure 63: Pertinent hardware temperatures versus time in solar heating mode (pi=6 cm, vo=4 cm).....137
Figure 64: Thermal buoyancy properties versus time in burner heating mode (pi=2cm, vo=2 cm).....138
Figure 65: Technical performance parameters versus time in burner heating mode (pi=2cm, vo=2 cm).....138
Figure 66: Pertinent hardware temperatures versus time in burner heating mode (pi=2cm, vo=2 cm).....138
Figure 67:Thermal buoyancy properties versus time in burner heating mode (pi=2 cm, vo=3 cm).....139
Figure 68: Technical performance parameters versus time in burner heating mode (pi=2 cm, vo=3 cm).....139
Figure 69: Pertinent hardware temperatures versus time in burner heating mode (pi=2 cm, vo=3cm).....140
Figure 70: Thermal buoyancy properties versus time in burner heating mode (pi=2 cm, vo=4 cm).....140
Figure 71: Technical performance parameters versus time in burner heating mode (pi=2 cm, vo=4 cm).....141
Figure 72: Pertinent hardware temperatures in burner heating mode (pi= 2 cm, vo=4 cm).....141
Figure 73: Thermal buoyancy properties versus time in burner heating mode (pi=2 cm, vo=4 cm).....142
Figure 74:Technical performance parameters versus time in burner heating mode (pi=2 cm, vo=4) 142
Figure 75: Pertinent hardware temperatures versus time in burner heating mode (pi=4cm, vo=2 cm) 142
Figure 76:Thermal buoyancy properties versus time in burner heating mode (pi=4 cm, vo=3 cm) 143
Figure 77:Technical performance parameters versus time in burner heating

mode (pi=4 cm, vo=3 cm) 143
Figure 78:Pertinent hardware temperatures versus time in burner
heating mode (pi=4 cm,vo= 3 cm).....143
Figure 79:Thermal buoyancy properties versus time in burner heating
mode (pi=4 cm, vo=4 cm) 144
Figure 80:Technical performance parameters versus time in burner heating
mode (pi=4 cm, vo=4 cm) 144
Figure 81:Pertinent hardware temperatures versus time in burner heating
mode (pi=4 cm, vo=4 cm).....145
Figure 82:Thermal buoyancy properties versus time in burner heating
mode (pi=6 cm, vo=2 cm) 145
Figure 83: Technical performance parameters versus time in burner heating
mode (pi= 6cm, vo=2 cm).....146
Figure 84: Pertinent hardware temperatures versus tin in burner heating
mode (pi=6 cm, vo=2 cm).....146
Figure 85: Thermal buoyancy properties versus time in burner heating
mode (pi=6 cm, vo=3 cm).....147
Figure 86: Technical performance parameters versus time in burner heating
mode (pi=6 cm, vo=3 cm).....147
Figure 87: Pertinent hardware temperatures versus time in burner heating
mode (pi=6 cm, vo=3 cm).....147
Figure 88: Thermal buoyancy properties versus time in burner heating
mode (pi=6 cm, vo=4 cm).....148
Figure 89: Technical performance parameters versus time in burner heating
mode (pi=6 cm, vo=4 cm).....148
Figure 90: Pertinent hardware temperatures versus time in burner heating
mode (pi=6 cm, vo=4 cm).....149
Figure 91: Thermal buoyancy properties versus time in hybrid heating mode
(pi=2cm, vo=2 cm).....149
Figure 92: Technical performance parameters versus time in hybrid heating
mode (pi=2cm, vo=2 cm).....150
Figure 93: Pertinent hardware temperatures versus time in hybrid heating
mode (pi=2cm, vo=2 cm).....150
Figure 94:Thermal buoyancy properties versus time in hybrid heating mode
(pi=2 cm, vo=3 cm).....151
Figure 95: Technical performance parameters versus time in hybrid heating

KNUST

mode (pi=2 cm, vo=3 cm).....151
Figure 96: Pertinent hardware temperatures versus time in hybrid heating
mode (pi=2 cm, vo=3cm).....151
Figure 97: Thermal buoyancy properties versus time in hybrid heating
mode (pi=2 cm, vo=4 cm).....152
Figure 98: Technical performance parameters versus time in hybrid heating
mode (pi=2 cm, vo=4 cm).....152
Figure 99: Pertinent hardware temperatures in hybrid heating mode
(pi= 2 cm, vo=4 cm).....153
Figure 100: Thermal buoyancy properties versus time in hybrid heating mode
(pi=2 cm, vo=4 cm).....153
Figure 101:Technical performance parameters versus time in hybrid heating
mode (pi=2 cm, vo=4).....154
Figure 102: Pertinent hardware temperatures versus time in hybrid heating
mode (pi=4cm, vo=2 cm).....154
Figure 103:Thermal buoyancy properties versus time in hybrid heating
mode (pi=4 cm, vo=3 cm).....155
Figure 104:Technical performance parameters versus time in hybrid heating
mode (pi=4 cm, vo=3 cm).....155
Figure 105:Pertinent hardware temperatures versus time in hybrid
heating mode (pi=4 cm, vo= 3 cm).....155
Figure 106:Thermal buoyancy properties versus time in hybrid heating
mode (pi=4 cm, vo=4 cm).....156
Figure 107:Technical performance parameters versus time in hybrid heating
mode (pi=4 cm, vo=4 cm).....156
Figure 108:Pertinent hardware temperatures versus time in hybrid heating
mode (pi=4 cm, vo=4 cm).....157
Figure 109:Thermal buoyancy properties versus time in hybrid heating
mode (pi=6 cm, vo=2 cm).....157
Figure 110: Technical performance parameters versus time in hybrid heating
mode (pi= 6cm, vo=2 cm).....158
Figure 111: Pertinent hardware temperatures versus tin in hybrid heating
mode (pi=6 cm, vo=2 cm).....158
Figure 112: Thermal buoyancy properties versus time in hybrid heating

KNUST

mode (pi=6 cm, vo=3 cm).....151
Figure 113: Technical performance parameters versus time in hybrid heating
mode (pi=6 cm, vo=3 cm).....159
Figure114: Pertinent hardware temperatures versus time in hybrid heating
mode (pi=6 cm, vo=3 cm).....159
Figure 115: Thermal buoyancy properties versus time in hybrid heating
mode (pi=6 cm, vo=4 cm).....160
Figure 116: Technical performance parameters versus time in hybrid heating
mode (pi=6 cm, vo=4 cm).....160
Figure 117: Pertinent hardware temperatures versus time in hybrid heating
mode (pi=6 cm, vo=4 cm).....161
Figure 118 Percentage moisture content on dry basis versus time in
solar drying mode.....169
Figure 119 Product surface temperatures in trays 1, 2, and 3 versus
time in solar drying mode.....170
Figure 120 Air inlet and exit relative humidity values versus time in
solar drying mode.....171
Figure 121 Percentage moisture content on dry basis versus time
in back-up heating mode.....171
Figure 122 falling rate regime 1(top tray).....174
Figure 123 Falling rate regime 2(top tray).....174
Figure 124 Product surface temperatures at trays 1, 2, and 3
versus time in back-up heating mode.....175
Figure 125 Dryer air inlet and outlet relative humidity values versus
time in back-up heating mode.....175
Figure 126 Percentage moisture content on dry basis versus time in
burner drying mode.....176
Figure 127 Product surface temperatures at trays 1, 2, and 3,
versus time in burner drying mode.....179
Figure128 Dryer inlet and outlet relative humidity values versus
time in burner drying mode.....179
Figure 129 Percentage moisture content on dry basis versus time in hybrid
drying mode.....180
Figure 130 Product surface temperatures at trays 1, 2, and 3
versus time in hybrid drying mode.....183

KNUST

Figure 131 Dryer inlet and outlet relative humidity values versus time
in hybrid drying mode.....183
Figure 132 Flow chart for air heater simulation model.....187
Figure 133 Parametric studies-solar heating mode 1.....203
Figure 134 Parametric studies-solar heating mode 2.....203
Figure 135 Parametric studies-solar heating mode 3.....204

KNUST

NOMENCLATURE

Below is a partial listing of the symbols used throughout the thesis.Those symbols that are used infrequently are defined appropriately where they are used in the write up. In some cases reference is made to the equations in which these symbols are used.

a'', b''	empirical constants in the Angstrom relation
a_v	heat transfer area per unit volume of drying bed (equ. 2.4) (1/m)
A	characteristic area $\left(m^2\right)$
A_u	ratio of outside unwetted surface area to the evaporating surface of a wet product (equ. 2.2)
A_P	total product surface area (m^2)
A_W	total inner drying chamber wall surface area (m^2)
c_p	specific heat capacity of air $\left(kJ/kg.K\right)$
$C''m''$	equivalent heat capacity of the drying chamber (J/kg K)
C_{pl}	specific heat capacity of water (J/kg K)
$C_{p,s}$	specific heat capacity of the sample (J/kg K)
C_{pw}	specific heat capacity of water vapour (J/kg K)
C_{pc}	specific heat of calorimeter (J/kg K)
d_e	equivalent diameter of product particle (m)
d_t	thickness of a material, drying bed thickness (m) (equ. 2.2)
$d_{h,i}$	hydraulic mean depth of an air-heater duct (m)
D	diffusion coefficient (m^2/s)
E_b	activation or binding energy for diffusion (kJ/kmol)
f	friction factor
f_v	mass transfer coefficient (equation 2.1) (kg/s m^2).Pa
F	view factor
Gr	Grashof number
G_a	air-mass flux (kg/s.m^2)
g	acceleration due to gravity $\left(m/s^2\right)$
h_t	total heat transfer coefficient (W/m^2 K)
h_{fg}	latentheat of vaporisation of free water (J/kg K)
h_L	depth of a drying bed (m)
H	absolutehumidity (Equation 2.113) (kg_w/kg_{air})
H_s^*	saturated absolute humidity (kg_w/kg_{air})
L	length of primary collector m
L_t'	heat of evaporation of moisture from a product (J/kg K)
L_t'	heat of vaporisation of adsorbed product moisture (J/kg K)
$\dot{m}$	air mass flow rate $\left(kg/s\right)$

KNUST
LIBRARY
KWAME NKRUMAH
UNIVERSITY OF SCIENCE & TECHNOLOGY
KUMASI

M	moisture content	decimal
M_e	equilibrium moisture content	decimal
M_c	critical moisture content	decimal
$M_{c,wb}$	moisture content (wet basis)	decimal
$M_{c,\,d.b}$	moisture content (dry basis)	decimal
$M_{f,d.b}$	final moisture content, dry basis	decimal
$M_{f,w.b}$	final moisture content, wet basis	decimal
$M_{i,d.b}$	initial moisture content, dry basis	decimal
m_w	mass of water removed from a wet product	kg
MR	moisture content ratio of a product or material	decimal
Pr	Prandtl number	
$P_{v,\,\mathrm{db}}$	partial pressure of water vapour in moist air evaluated at T_{dp}	N/m^2
P_{cL}	critical pressure of water (212 bar)	bar
P_s	vapour pressure of water at surface of wet material	N/m^2
P_v	partial pressure of water vapour in moist air	N/m^2
$\dot{q}_u$	useful energy per unit time per unit area	W/m^2
$\dot{Q}$	energy transferred per unit time	W
$\dot{Q}_c$	energytransferred by convection	W
Ra	Rayleigh number	
R_v	gas constant of water vapour (J/kg K)	
R	gas constant of dry air (J/kg K)	
Re	Reynolds number	
R_o	universal gas constant	J/kmol K
RH	relative humidity of air	
T_{sk}	sky temperature (K)	
T_{ab}	average temperature of concrete absorber surface (K)	
T_c	average temperature of cover glass (K)	
T_f	mean temperature of heated air (K)	
T_{pt}	temperature of drying material or product (K)	
T_a	ambienttemperature (K)	
T_{dw}	drying chamber wall temperature (K)	
T_{cL}	critical temperature of water (K)	
T_{bL}	boiling point of water (K)	
v	velocity of system drying air (m/s)	
λ	thermal conductivity (W/mK)	
V	Local wind speed (m/s)	
β	Air thermal expansion coefficient $= 1/T\ (1/K)$	
V	volume (m^3)	

KNUST

V_T	total volume of a wet product (m^3)	
W	width (m) of collector	
W_T	mass of a wet material or product (kg)	
W_d	mass of dry matter content of a wet product or material (kg)	
W_m	mass of water content of a wet product or material (kg)	

Greek symbols

α_c	absorptance of collector cover	
α_p	absorptance of the air-heater absorber plate	
ΔT	difference in temperature	K
ε	bulk porosity	
ε_p	emittance of absorber plate	
ε_c	emittance of collector cover	
η_c	air-heater efficiency	%
η_d	drying efficiency	%
η_p	pick-up efficiency	%
θ	temperature of air (or angle between normal to collector surface and the incident radiation)	^{o}C (deg)
θ_{pt}	temperature of product	^{o}C
μ	dynamic viscosity	kg/s m
ν	kinematic viscosity	m^2/s
ρ_b	bulk density	kg/m^3
ε	emissivity of surface	
ρ	air mass density $\left(kg/m^3\right)$	
σ	Stefan-Boltzman constant $\left(W/m^2K^4\right)$	
τ	transmittance of glazing	
θ	angle of tilt	
h_c	convection heat transfer coefficient $\left(W/m^2K\right)$	
ρ_{pr}	density of the product	kg/m^3
ρ_w	density of water	kg/m^3
σ	Stefan-Boltzman constant	
τ_c	transmittance of collector cover	
θ_a'	temperature of air (^{o}F)	

KNUST

Subscripts

a	ambient
ab	absorber
ab-f	absorber fluid interface
ab-rp	absorber rock pile interface
bg	burner housing floor
br	burner rock-pile interface
bu	burner unit
c	cover plate/glazing/glass cover
cu	collector unit
dd	drying bed
db	dry bulb
d.b	dry basis
dp	dew point
f	fluid/air
gr	ground
in	inlet
lw	burner housing wall
out	outlet
pst	product surface temperature
rp	rock pile
rp-bu	rock pile burner interface
uw	wall of plenum
wa	wall
w.b	wet basis
wb	wet bulb

KNUST

ACRONYM

MNCSCDBH: Mixed-Mode Natural Convection Solar Crop Dryer with Back up Heater

SHM: Solar Heating Model
BHM: Burner Heating Model
HHM: Hybrid Heating Model
AIRFM: Air Flow Model
DCHM: Drying Chamber Heating Model

KNUST

ACKNOWLEDGEMENTS

The author wishes to express his appreciation to Prof. F. K. FORSON, Dr. Y.A.K. Fiagbe, and Dr. R. Opoku his supervisors, for continued support and guidance during the research, and to Mr. Robert Kyere, technician at the department of Mechanical Engineering, Kwame Nkrumah University of Science and Technology, Kumasi, for helping in the setting up of the power supply system for the data logger.

Thanks are due to the following personnel for their assistance during the testing programme and in the execution of the computer simulation model: Mr. Edwin Adjei, and Mr. Faisal Wahib Adams, both of the Department of Mechanical Engineering, Kwame Nkrumah University of Science and Technology, Kumasi.

KNUST

I also wish to express my appreciation to Dr. C.K. Idun of the Department of Mechanical Engineering for taking two days off his busy schedule to get me a laptop that was compatible with the storage module of the data logger.

My deepest gratitude goes to: my beloved sister Rebecca Ama Sekyere and her husband Mr. Peter Otta of 13 Balderstone Close, Leicester (U.K.) and to the staff of the Mechanical Engineering Department at De Montfort University in the United Kingdom for accommodating me and allowing me access to their research and laboratory facilities. I also want to say a big thank you to my most treasured brother Divine Comla Sekyere (Estate Manager, Kumasi Polytechnic) for the moral support and words of encouragement offered throughout the stressful period of research.

Last but not the least, I thank God, for the wisdom, direction and protection offered me.

September 2013

CHARLES KOFI KAFUI **SEKYERE**

CHAPTER ONE

INTRODUCTION

1.1 Background

Sun drying is currently the commonest mode of drying in Ghana. In Ghana, this inefficient traditional drying technique is used by the rural and commercial farmers to dry about 90 % of the total agricultural produce (Dapaah, 1991). Most farmers cannot afford to import expensive mechanical drying equipment, which is either electricity or diesel engine-powered, with the additional financial burden of maintenance and other running expenses. Though the traditional method of drying crops is cheap and environmentally friendly yet it is labour intensive, and requires a large area of land to dry a relatively small quantity of crop. In addition, the method provides no control over the drying process and no crop protection against unexpected rain and/or strong wind. Furthermore, the crop being dried is subject to contamination by dirt and infestation by insects, rodents, moulds, and pests. All these problems result in a poor quality dried product and in post-harvest losses (for example, in Ghana the figure can be as high as 20 to 30 %). The economic consequences to the farmer and to the country arising from these losses can be substantial (Dapaah, 1991).

Some of the problems associated with open sun drying can be solved through the use of solar dryers. Solar dryers are less labour intensive, have high temperatures, can produce low relative humidity heated air which improves the rate of drying and final moisture content of the produce which is the most important factor that can affect the growth of micro-organisms in stored grains and agricultural products. Nevertheless, one disadvantage of solar drying is that the dehydration process is interrupted and is slowed down at night and there can be re-absorption of water by the partially dried products resulting in the dried product being of poor quality.

When using the sun's radiation as the energy source for drying, two principal difficulties must be overcome in order to exploit the full potential of solar dryers: the periodic character and the time dependence of the solar radiation. The influence of weather changes must be considered.

The periodic character of the solar radiation can partly be balanced by employing an intermittent drying operation. However, because the number of hours of available sunshine is very much dependent on the prevalent weather conditions, the use of a heat storage unit may be needed. Water can be used as the heat storage medium in indirect systems, and phase-change materials or a rock bed in direct drying systems.The dependence of the dryer performance on the weather, especially in large systems, should be minimised by providing an auxiliary energy source, which would normally be based on natural gas, oil or biomass. It is connected to the dryer by means of a heat exchanger and operates in emergency situation only.

To overcome the defect of poor quality drying in solar dryers at night and in bad weather a mixed mode solar crop dryer with integrated back up heater was adopted. The addition of a transparent top part was to increase the thermal buoyancy during drying to enhance uniform drying during sun hours.An air vent was used instead of a chimney (see figure 1). This was to prevent the effect of reversed thermosiphoning observed during night drying by Madhlopa et al (2006).

The goal of the present study is, therefore, to develop a solar dryer with a storage component for both solar and thermal energy for drying of agricultural produce.

Figure 1 illustrates the schematic diagram of a conceptual design of such a solar drying system.

KNUST
NYANSAPƆ WƆSANE NO BADWENMA

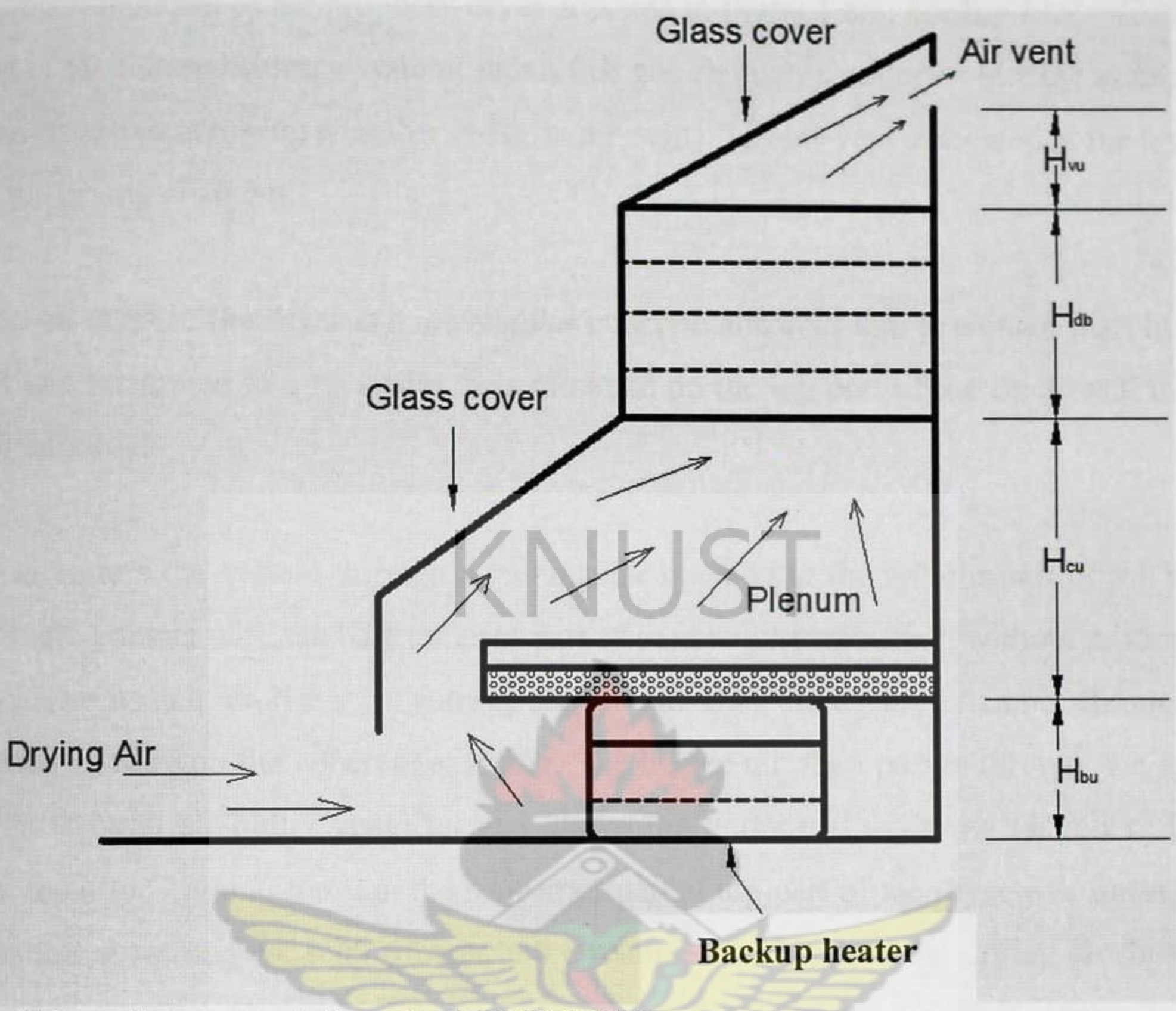

Figure1: Schematic representation of a MNCSCDBH

Ghana lies within latitude 4°46' south and 11°11' north and longitude 3°11' west and 1°11' east. Ghana, therefore, receives abundant solar energy all year round. The mean annual solar radiation received in different parts of the country ranges from 15.84 - 20.16 MJ/m^2-day (i.e. 4.4 to 5.6 kWh/m^2-day). Mean annual sunshine duration is in the range of 1800 to 2820 hours, with very little seasonal variation. These conditions make the use of solar energy for drying crops particularly attractive. This work seeks to achieve in the ultimate a natural convection solar crop drying system that maximizes the suns radiant energy when available during the day for drying during the day and provides a means of drying during periods of adverse or unfavourable conditions.

Description of proposed dryer

The main components of the proposed dryer depicted in figure 1 are: *backup heater* located at the base of the thermal storage system(with a flue gas chimney), collector-storage thermal mass, and semi-transparent drying chamber (with an air-vent). The air vent is located at the top back side of the drying chamber.

The thermal mass of the dryer is a rectangular concrete absorber that is painted matt black on its top part and integrated to a rock pile. It is mounted on the top part of the brick wall that houses the backupheater.

Drying air enters the system through a rectangular opening at the bottom part of the brick wall and gets into contact with the bare exterior part of the cylindrical burner, without mixing with the flue gas. The heated air rises, by natural convection, into the drying chamber through another rectangular openingon the concrete absorber. The heated air, then passes through the drying bed and exits through air outlet vents located above the doors to the drying chamber. The direct incident radiation coming through the semi-transparent top part of the dryer will further increase the moisture absorbing capacity (decrease the relative humidity) of the drying air thus ensuring uniform drying across all trays.

As the drying air leaves the burner enclosure, it passes through a narrow horizontal rectangular slot, resulting in contraction and pressure loss. In the collector, the drying air flows from a narrower cross-sectional area to a wider section at the exit from the collector resulting in air expansion and pressure loss.

1.2 Objectives of the study

The main objective of the research is to study the thermal buoyancy characteristics and possible drying conditions of a mixed-mode natural convection solar crop dryer with integrated collector-storage and back-backup heater through modeling and experimental studies.

The specific objectives are to:

(a) develop a mathematical model for the proposed system which incorporates the air heater model, drying chamber heater model, and the air flow model under no load conditions,

(b) evaluate the overall performance of the proposed system by carrying out appropriate numerical predictions including:

(i)determining airflow rate through the dryer in the various modes of operation

(ii) determining the air vent outlet and plenum inlet thicknesses that optimizes the dryer performance,

(c) design, construct and evaluate a small-scale laboratory model of the dryer to be tested in three modes of operation under no load conditions namely, solar, backup heater, and hybrid modes using fresh pineapples,

(d) evaluate the principal dryer characteristics: capacity, drying time, and uniformity of drying

(e) investigate the comparative performance of the backup heater.

1.3 Methodology and technical approach

To develop a mathematical model capable of effectively simulating the performance of the proposed dryer under no load conditions, the following tasks were undertaken:

- an extensive literature search to develop the theoretical framework and the essential empirical relations required to formulate the models,
- a small-scale laboratory model of the prototype dryer was designed and constructed,
- a series of experiments were conducted on the small-scale laboratory model of the proposed dryer,
- the computer code was run to simulate the performance of the dryer operating under varied conditions,
- the predicted results were compared with the experimental data in order to fine tune and validate the model.

KNUST
LIBRARY
KWAME NKRUMAH
UNIVERSITY OF SCIENCE & TECHNOLOGY
KUMASI

Full investigation of the effect of design variables on system performance would involve studying the implications of a number of different configurations under varied operating conditions. In order to achieve an optimal design, data from long-term extensive experimentation on several designs operating under different climatic conditions is required. This exercise will be time consuming and costly for the prototype development of the dryer. The alternative is to perform experiments on a small-scale model under varied preset conditions. The resulting information, however, must be extrapolated to full scale. The specific rules for doing this are in most cases unavailable. Furthermore, the small-scale model cannot simulate all the features of the full-scale system. Alternatively, a mathematical model of the physical system can be developed and used for investigating the effect of changes in the design and operating conditions on performance at a relatively low cost. Simulation models, as noted by Diamante and Munro (1991a), are needed in the development of dryer designs and in the operation of drying systems.

The performance evaluation criteria for solar crop dryers developed by Leon et al (2002) were extensively used in this research. Parameters measured during experimentation included:

(i) average temperature at vent exit,

(ii) mean temperature of the drying air at the exit of the collector unit

(iii) temperature variation and mean temperature rise of air inside the drying chamber,

(iv) mean operating temperatures of the components of the thermal mass,

(v) the flow rate of air through the drying chamber,

(vi) the drying rates of the material to be dried, and

(vii) ambient temperature

(viii) product surface temperatures

Quantities determined during evaluation included:

Product

Initial Moisture Content: (% w.b)

Average ambient temperature, (°C)

Average ambient relative humidity, (%)

Parameters

Quantity loaded (full load), kg

Loading density, kg per m^2 of solar aperture

Collector area, m^2

Tray surface area, m^2

Drying time, up tobetween 20% and 35% moisture content on dry basis, (including nights), hr

Heat collection efficiency, %

Pick-up efficiency, (%)

Average temperature and Relative Humidity of exit air: °C, %

Maximum drying air temperature under no-load conditions, (°C)

Maximum drying air temperatureunder loading, (°C)

Equipment used for instrumentation included:

1. Thermocouples: for temperature measurement
2. Humidity probe/sensor: for measurement of humidity
3. Weather station: for measuring wind speed
4. Electronic balance for measurement of mass.

Facilities available for the research

- Library and internet facilities, KNUST
- The Mechanical Engineering laboratory, College of Engineering, KNUST
- Weather station
- Humidity probes/sensors
- 21X Micrologger
- Electronic balance (PM 15-N; Mettler)

KNUST

1.4 Organisation of the report

This thesis is organised in seven main chapters. Chapter 1, the introductory chapter, provides the socio-economic- and technical background information. It outlines the objectives of the study and the methodology adopted in solving the problem at stake. A summary of the organisation of the report is also provided in chapter 1. Chapter 2 provides the theoretical framework related to the fundamentals of crop drying, the review of theoretical and experimental studies on solar crop drying, and crop drying simulation techniques.The mathematical model developed for the design and predictions of the performance of the proposed dryer configuration is provided in Chapter 3.The description of the laboratory dryer, and the experimental set-ups and procedures are presented in Chapter 4. In Chapter 5 the results and discussion of all the tests conducted on the laboratory model are presented, while the simulation results are presented and discussed in Chapter 6. The comparison of the predicted and experimental results is also included in chapter 6. Chapter 7 presents the conclusions from the study and suggestions for further work.

KNUST

CHAPTER TWO

THEORETICAL FRAMEWORK

2.0 Introduction

In this chapter, a review of the fundamentals of drying theory is undertaken to gather necessary information required to successfully design and model a solar drying system. The chapter provides an overview of the physical, transport and thermodynamic properties of the wet product along with the psychrometric properties of the drying medium required as input parameters for developing a drying process model.The review also includes the theoretical and numerical models currently available for analysing crop drying processes.

KNUST

2.1 Fundamentals of drying

Drying is traditionally defined as an operation during which a liquid, solid or semi-solid feed material is converted into a solid product of significantly lower moisture content. In most cases, drying involves the application of thermal energy, which causes water to evaporate into the vapour phase.

Classification of solar crop dryers

Solar crop dryers are generally classified, depending on the mode of heating or operation. According to mode of heating, solar crop dryers can be categorisedinto: (a) direct, (b) indirect and, (c) mixed mode systems with natural or forced circulation of the heated drying air. In the direct dryer, solar radiation passes through a transparent cover fitted on the top part of the dryer and is directly absorbed by the crop placed on the drying bed under the transparent cover. In an indirect dryer, air is heated in a separate solar collector and circulated through the drying bed where it picks moisture fromthe crop. The mixed mode possesses both features of the direct and indirect categories of solar dryers. In particular, dryers of the natural-convection variety are popular because they are relatively cheap and simple to operate and maintain (Soponronnarit, 1995).

Most solar dryers developed are designed for specific products or class of products. Products such as pepper, onion, cocoa bean, ginger, corn, mushroom, cassava and coconut, are commonly dried in Ghana. A systematic classification of available solar food dryers, based on the design of system components and the mode of utilization of solar energy, is presented in figure 2.

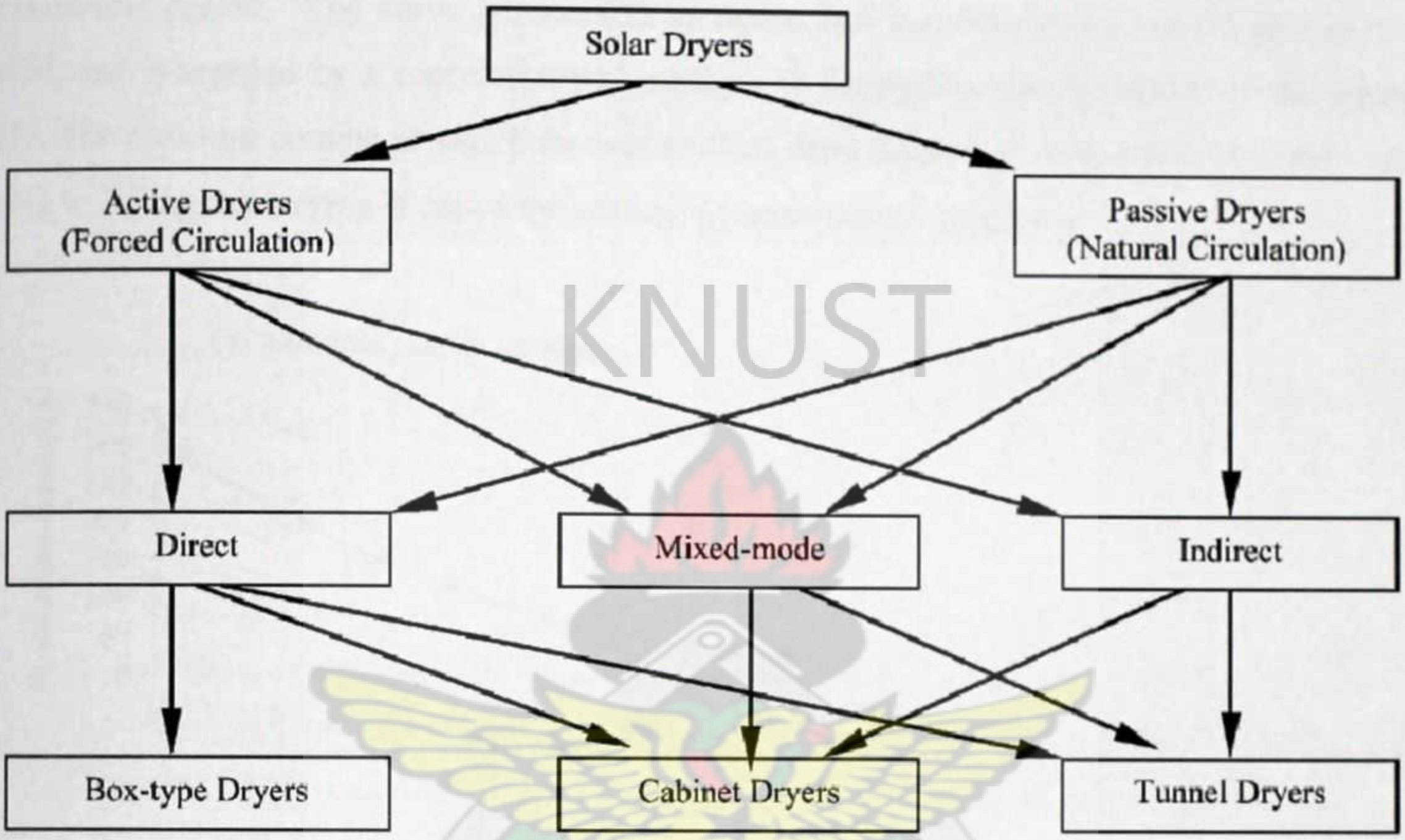

Figure 2Classification of solar dryers and drying modes (Source: Leon et al, 2002)

2.2 Drying Kinetics

In drying experiments, data are usually obtained relating to moisture content and time. These data are plotted as moisture content *M*, either on dry or wet basis, versus time, *t*. A typical experimental drying curve is shown in figure 3(a). This curve represents the general case when a wet product loses moisture first by evaporation from a surface saturated with water, followed in turn by a period of evaporation from a partially saturated surface of gradually decreasing area, and finally when water evaporates from the interior of the product.

Although figure 3(a) indicates that the drying rate is subject to variation with time or moisture content, this variation can be better illustrated by graphically differentiating the curve and plotting dM/dt versus M, as shown in figure 3(b), or as dM/dt versus t, as shown in figure 3(c).

The portion AB represents a warming-up period. Section BC on each curve represents the constant-rate period. The curve portion CD of figure 3(a) and 3(b) is termed the falling-rate period, and is typified by a continuously changing rate throughout the remainder of the drying cycle. The moisture content at which the wet product demonstrates a change from constant rate drying to falling rate drying is called the critical moisture conten (point C).

KNUST

(a) Moisture content vs. time

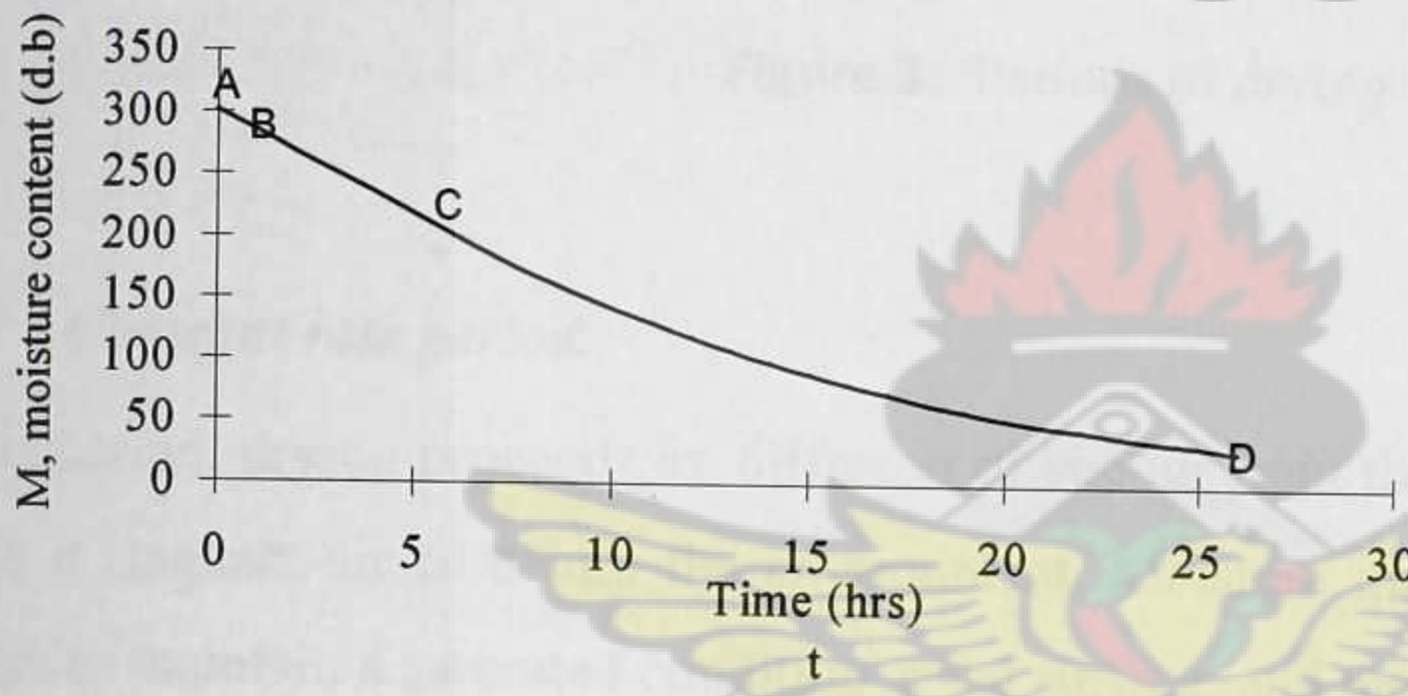

(b) Drying rate vs. moisture content

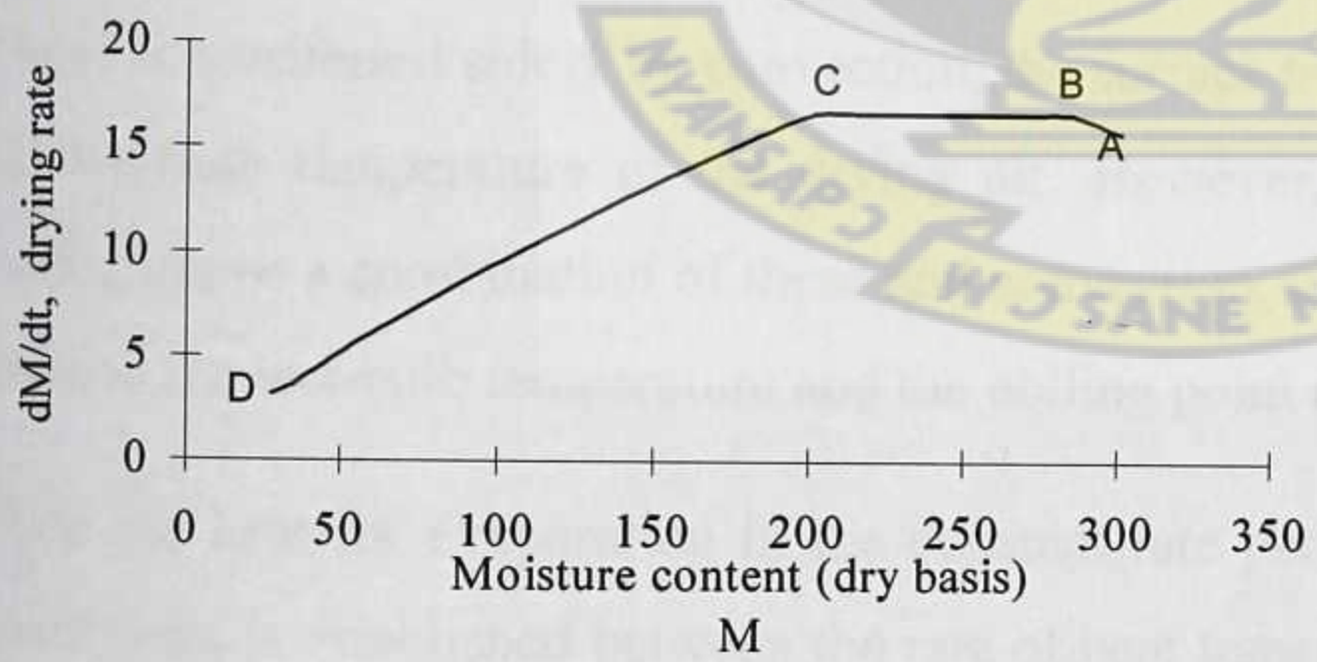

(c) Drying rate vs. time

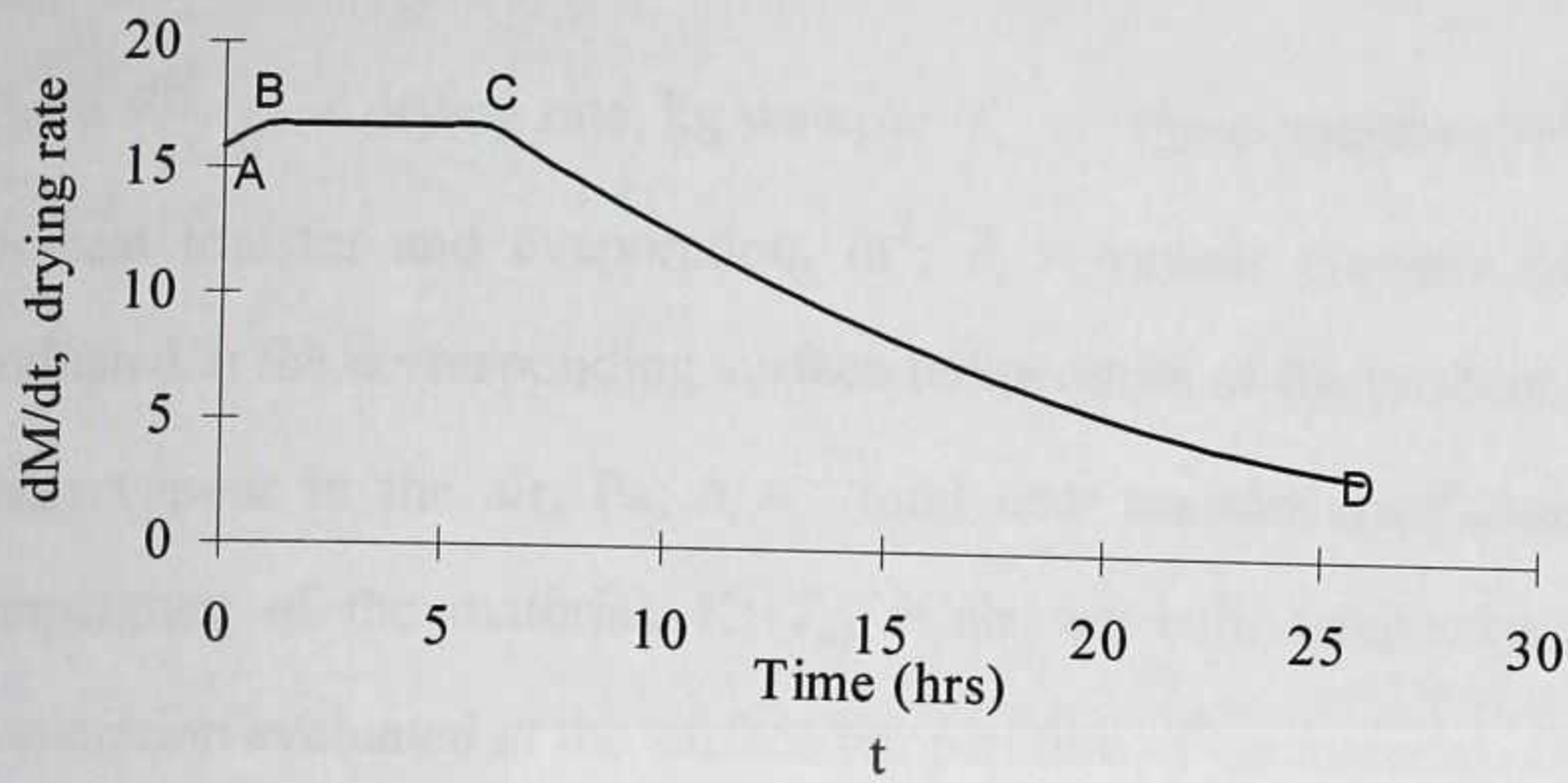

KNUST

Figure 3: Periods of drying

2.2.1 Constant rate period.

In this period, drying proceeds by diffusion of vapour from the saturated surface of the material across a stagnant-air film into the environment. Moisture movement within the solid is rapid enough to maintain a saturated condition at the surface, and the rate of drying is controlled by the rate of heat transfer to the surface. The mechanism of moisture removal in this period is independent of the nature of the product (Porter *et al*, 1973).

If heat is transferred solely by convection, the surface temperature of the wet product approaches the wet-bulb temperature of the drying air. However, when heat is transferred by radiation, conduction or a combination of these and convection, the temperature of the saturated surface is between the wet-bulb temperature and the boiling point of water.

When the heat for evaporation in the constant-rate period is supplied by heated air or gas, an equilibrium is established between the rate of heat transfer to the material and the rate of vapour removal from the surface. The driving force of moisture movement and the internal factors of crop resistance to flow, during the constant rate period, are represented by equation (2.1) (Porter *et al*, 1973; Henderson and Perry, 1976; Hall, 1980):

$$\frac{dW}{dt} = -f_v A\left(P_s - P_{v,wb}\right) = -\frac{h_t A(T_{s'} - T_{wb})}{h_{fg}} \tag{2.1}$$

where dW/dt = drying rate, kg water/s; f_v = mass-transfer coefficient, kg/s m^2 Pa; A = area for heat transfer and evaporation, m^2; P_s = vapour pressure of water in the product and is evaluated at the corresponding surface temperature of the product, $T_{s'}$; $P_{v,wb}$ = partial pressure of water vapour in the air, Pa; h_t = total heat transfer coefficient, W/m^2 K, $T_{s'}$ = the surface temperature of the material, K; T_{wb} = air wet-bulb temperature, K and h_{fg} = latent heat of evaporation evaluated at the surface temperature of the material, J/kg.

When h_t is the coefficient of heat transfer by convection only, then $T_{s'}$ under equilibrium conditions is taken as the wet-bulb temperature of the inlet air, and P_s as the vapour pressure at this temperature. If heat is also supplied by radiation, then h_t is the total of the heat transfer coefficients by the two different modes and $T_{s'}$ becomes higher than the wet-bulb temperature. In batch drying in trays, heat arrives at the evaporation surface from the tray walls by conduction through the wet materials. The total heat transfer under the combined modes of heat transfer is given by Porter *et al*, (1973) as:

$$h_t = (h_c + h_r)\left[1 + \frac{A_u}{1 + d_t(h_c + h_r)/k_{ws}}\right] \tag{2.2}$$

where h_t is the total heat-transfer coefficient; A_u is defined as the ratio of the outside unwetted surface to the evaporating-surface area; d_t is the depth of the material in the tray; k_{ws} is the thermal conductivity of the wet material.

The magnitude of drying achieved in the constant rate-period depends upon three external variables (Porter *et al*, 1973).: (1) the heat- or mass-transfer coefficient, (2) the area of wet product exposed to the drying medium, and (3) the difference in temperature or humidity between the air stream and the wet surface of the product.

For drying calculations, it has been suggested (Porter *et al*, 1973) that it is convenient to express equation (2.1) in terms of the decrease in the moisture content rather than the amount of water

evaporated. For evaporation from a tray of wet product, assuming no change in volume during drying, equation (2.1) becomes:

$$\frac{dM}{dt} = -\frac{h_t}{\rho_p d_t h_{fg}}(T_{wb} - T_s) \tag{2.3}$$

where dM/dt = drying rate, kg water/(s) (kg dry product); ρ_p = bulk density of the dry product (kg/m^3); d_t = thickness of the bed, (m). For through-circulation drying, a similar equation is written of the form

$$\frac{dM}{dt} = -\frac{h_t a}{\rho_p h_{fg}}(T_{wb} - T_s) \tag{2.4}$$

where a = heat transfer area per unit volume of the bed (1/m); other symbols are the same as defined for equation (2.3). In practice, the volume of the wet product decreases as the drying progresses and therefore equation (2.3) or its modified form, equation (2.4) is not totally correct. To take care of the shortfall in equ. (2.4) a function has to be introduced into the equation to account for the change in volume. This can be done by carrying out dehydration experiments and measuring changes in product dimensions and coming out with an empirical relation that describes the shrinkage of the product in relation to volume, depth, and surface area of the product being dried.

2.2.2 Falling-rate period.

The falling-rate period follows the constant rate period. The moisture content at which the drying rate of a product changes from a constant rate to a falling rate (shown as point C in figs. 3(a) - (c)), is called the critical moisture content of the product. If the desired final moisture content is above the critical moisture content (for specified drying conditions), the whole drying process will occur under constant-rate conditions. It has been observed and proposed by several investigators that, if the initial moisture content is below the critical moisture content, the entire drying process will occur in the falling-rate period. This period is, generally, divided into two

KNUST
LIBRARY
KWAME NKRUMAH
UNIVERSITY OF SCIENCE & TECHNOLOGY
KUMASI

zones: (1) the zone of unsaturated surface drying, and (2) the zone where internal moisture movement controls the drying process (Porter *et al*, 1973).

In the first period, the entire evaporating surface can no longer be maintained at saturated level by the moisture within the solid. The drying rate decreases for the unsaturated portion, and hence the rate for the total surface decreases. The drying rate depends on the factors affecting the diffusion of water vapour away from the evaporating surface and those affecting the rate of internal moisture movement. As drying proceeds, the plane of evaporation moves into the product, and the drying process enters into the second falling-rate period. In drying to low moisture contents, the falling-rate period predominates in determining the total drying time. This latter statement is supported by experimental evidence of Ayensu and Bondzie (1986).

KNUST

Studies of internal moisture movement indicate the possibility of several controlling mechanisms, the more significant ones being postulated as liquid or vapour diffusion, capillarity, and pressure gradients caused by shrinkage. According to Brenndorfer *et al*, (1987), the principal controlling mechanism that explains the migration of moisture from the interior of an agricultural product to the surface, and its subsequent evaporation from the surface, is diffusion. The general equation for diffusion of liquid through a porous solid according to Sherwood (1936) is given by Fick's law:

$$\frac{\partial M}{\partial t} = \nabla.(D\nabla M) \tag{2.5}$$

Equation 2.5 has been applied by several researchers (Becker and Sallans, 1956; Steffe and Singh, 1982; Suarez *et al*, 1980) to model the rate of moisture removal from wet products during the falling-rate period under the assumption that the functional dependencies of D are known or can be estimated.

The following relationship can also be used to describe the rate of drying in the falling-rate period (Sokhansanj and Jayas, 1995):

$$\frac{dM}{dt} = -KA\frac{dP}{dx} \tag{2.6}$$

where K is a moisture transfer (diffusion) coefficient, and dP/dx is the driving force for the moisture movement in terms of water vapour pressure gradient within the product. It must be emphasised that the choice between equations (2.5) and (2.6) to describe the rate of drying in the falling-rate period depends on whether concentration or vapour pressure gradient is considered as the potential for the moisture movement.

2.3 Drying: modelling requirements and dryer design calculations

An information flow diagram for a drying model is shown in figure 4. The part of the model that contains equations for heat and mass transfer phenomena is termed the *process model*, while the equations describing the dependence of drying conditions on transport properties form the *properties model*.

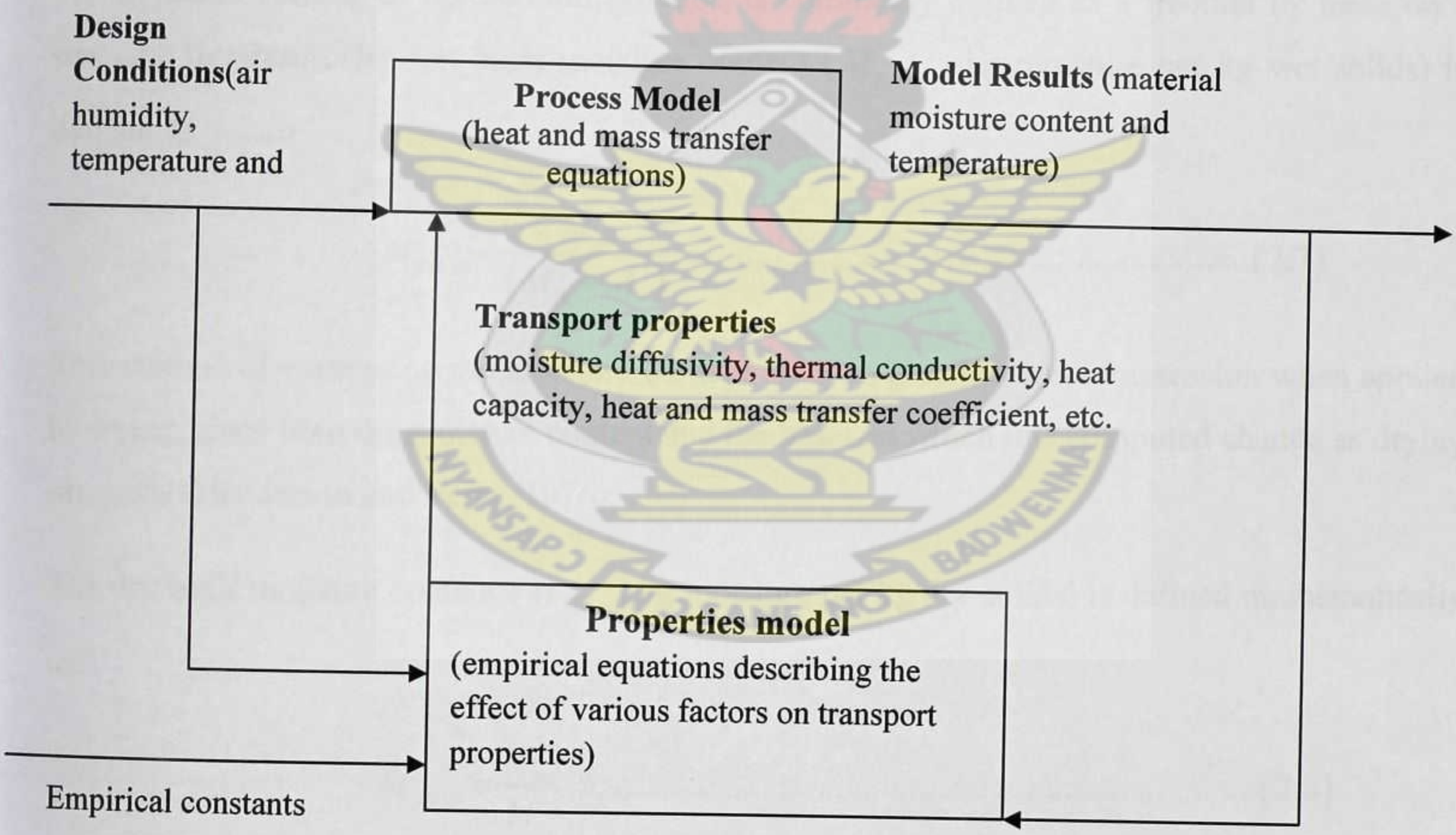

Figure 4 Drying ~~model~~ information flow diagram

2.4 Thermo-physical properties of agricultural products

In the food processing industry, most processes involve heat transfer operations. Knowledge of thermal properties of food materials is a must, so that energy-efficient processes and equipments can be attained. The major thermal properties of foods are specific heat, thermal conductivity and thermal diffusivity.

This section presents some of the thermal and physical properties of food substances required for the heat transfer analysis of food substances.

2.4.1 Moisture content of agricultural products

Although not a property itself, water content significantly influences all thermal properties. Values of specific heat and latent heat of vaporisation are calculated directly from water content.

The moisture content of agricultural products is commonly defined as a fraction by mass on a wet or a dry basis.The wet basis moisture content ($M_{c,w,p}$, kg moisture per kg wet solids) is defined as

$$M_{c,w,p} = \frac{M_w}{(M_w + M_s)} \quad \ldots\ldots\ldots\

$$M_{c,d,p} = \frac{M_{c,w,p}}{\left(1 - M_{c,w,p}\right)} \quad \text{.....(2.9)}$$

$$M_{c,w,p} = \frac{M_{c,d,p}}{\left(1 + M_{c,d,p}\right)} \quad \text{.....(2.10)}$$

At low moisture levels, $M_{c,w,p}$ and $M_{c,d,p}$ are numerically very similar. For example, a wet basis moisture content of 5% ($M_{c,w,p} = 0.0500$ kg moisture per kg wet solids) is equivalent to a dry basis value of 0.0526 kg moisture per kg dry solids. In contrast, there are large differences at higher moisture contents; $M_{c,w,p} = 0.50$, for instant, is equivalent to $M_{c,d,p} = 1.00$.

The quantity of moisture (m_w, in kg) to be evaporated from a crop to bring it to a safe level for storage is defined in terms of the initial and final moisture contents of the crop as

$$m_w = \frac{W_i\left(M_{i,c,w.p} - M_{f,c,w,p}\right)}{\left(1 - M_{f,w,c,p}\right)} \quad \text{.....(2.11)}$$

The procedures for determining the moisture content of products are classified as primary and secondary methods by Henderson and Perry, (1976) or direct and indirect methods by Brooker *et al*, (1974) and Hall, (1980). The primary (or direct) procedures are such that the moisture in a sample is removed and the quantity is determined by weighing or measuring. The secondary (or indirect) procedures namely, electrical resistance methods, dielectric methods, chemical methods, hygrometric methods, neutron scattering method and the nuclear resonance-absorption method all involve the measurement of a property of the material including mechanical, electrical, or thermal property, which is related to moisture content and must be calibrated against a standard primary method. The two most common and useful primary procedures for determining moisture content are the vacuum oven and the air oven method (Brenndorfer *et al*, 1987). In the vacuum oven method, a given sample of a wet material is placed on a metal dish in a vacuum oven at 70° C and dried to constant weight. The ratio of the difference in the initial and final weights of the material to the original weight of the wet material, gives the moisture content fraction on wet basis. In the air oven method, a sample of the wet material of known weight is placed on a metal dish in an air oven at 105° C and dried to a constant weight. The moisture content fraction on wet basis is then evaluated as in the vacuum oven method.

KNUST

2.4.2 Specific heat capacity

The specific heat at constant pressure is normally used for heat transfer problems during the drying of agricultural crops, since the pressure change is very small. The pressure dependence of specific heat is very little for solids and liquids until extremely high pressure is encountered. Specific heat is also a function of temperature; however, it has been established that at ordinary temperatures and over temperature intervals which are not too great, specific heat may be considered as a constant physical property.

Many articles have been reported on the determination of specific heat of agricultural crops. Most of this research involved determination of specific heat by the method of mixtures or by the method of differential scanning calorimetry (DSC). The DSC instrument is very expensive and is hardly used. The method of mixtures consists of adding a given quantity of a given crop to a known mass of water in a calorimeter. The equilibrium temperature, T_e attained by the calorimeter and its contents is then noted. At equilibrium, the heat lost by the crop is equated to the heat gained by the water and the calorimeter, from which relation the specific heat is calculated as:

$$C_{p,s}m_s(T_i - T_e) = m_w C_{p,w}(T_e - T_w) + m_c C_{p,c}(T_e - T_w) \tag{2.12}$$

where the subscripts c, s and w refer to calorimeter, dry sample and water respectively, and T_i the initial temperature of the sample, T_w initial temperature of the calorimeter and water. The specific heat capacity of the wet sample is then expressed as:

$$C_p = C_{ps} + C_{pw} M_{d.b} \tag{2.13}$$

where C_{ps} is the specific heat of the dry matter, C_{pw} is the specific heat of water and M_d is the moisture content of the material on dry basis.

Siebel (1892) proposed that the specific heat of food materials might be estimated from the weighted sum of the specific heat of water and that of the solid matter. These equations have long been used and reported in the literature (ASHRAE, 1989 and Wallapapan *et al*, 1986) and they are given as:

$$C_p = 0.84 + 0.0335 M_{Wb}\text{ , (for values above freezing)} \quad (2.14)$$

$$C_p = 0.84 + 0.0126 M_{Wb}\text{ , (for values below freezing)} \quad (2.15)$$

where: C_p is the specific heat, kJ/kg K, and M_{Wb} is the moisture content, % wet basis.

Equations 2.14 and 2.15 are recommended by Wallapapan *et al*, (1986) for estimating specific heat only when data are lacking and there are no better alternative methods of determining the specific heat. It is reported by Choi and Okos (1986), that the equations proposed by Siebel are limited to food products with relatively high moisture content.

KNUST

2.4.3 Heat of vaporisation or latent heat of moisture from a crop

The heat of vaporisation or latent heat of moisture from a crop is defined as the energy required to vaporise moisture from the crop. Its value is determined at the wet-bulb temperature of the air in contact with the surface of the crop (Daly, 1992). The energy required to vaporise water from a crop is dependent upon its moisture content, and its temperature. The lower the moisture content and the temperature, the higher the heat of vaporisation.

Othmer (1940), starting with the Clapeyron equation, developed the following relationship for calculating the heat of vaporisation of absorbed moisture from a product:

$$\frac{\log P_s'}{\log P_v} = \frac{L_t'}{h_{fg}} + q \quad (2.16)$$

where P_v and P_s' are vapour pressures and h_{fg} and L_t' are the heats of vaporisation of free water and of the adsorbed crop moisture, respectively. The constant q is product- and temperature-dependent.

The heat of vaporisation has been observed to decrease steadily with temperature (Liley and Gambill, 1973). A known or calculated value of the heat of vaporisation of moisture from a wet product at a known temperature may be accurately extrapolated to other temperatures with the Watson's correlation (Reid *et al*, 1987):

$$L_{t,2} = L_{t,1}\left(\frac{1 - T_2/T_{cL}}{1 - T_1/T_{cL}}\right)^n \tag{2.17}$$

where n = 0.375 or 0.38 and T_c (= 647.3 K) is the critical temperature of water. A dimensionless equation which allows one to estimate the heat of evaporation at any temperature without the vapour-pressure data is given by Liley and Gambill (1973) as:

$$L_t = R_v T_{cL} T_{bL} \ln(P_{cL}) \frac{(T_{cL} - T)^{0.38}}{(T_{cL} - T_{bL})^{1.38}} \tag{2.18}$$

where,

T_{bL} is the boiling point of water, P_{cL} (221 bar) is the critical pressure of water, and R_v is the gas constant for water vapour. Equation 2.18 gives an average error of about 5%.

KNUST

2.5 The dynamics of drying wet products

This section talks about the availability of water molecules for dehydration in relation to water binding mechanism. The sorption isotherm is used to explain hysteris exhibited by many wet products under adsorption and desorption conditions.

2.5.1 Equilibrium moisture content (EMC)

The moisture content of a wet solid in equilibrium with air of given humidity and temperature is termed the equilibrium moisture content (EMC). A plot of EMC at a given temperature versus the dry-basis moisture content of the solid is called the sorption isotherm (Baker 1997). An isotherm obtained by exposing the wet solid to air of increasing humidity is termed the adsorption isotherm. That obtained by exposing the solid to air of decreasing humidity is known as the desorption isotherm. The latter is of interest in drying as the moisture content of the solids progressively decreases. Most food materials display 'hysteresis' in that the two isotherms are not identical.

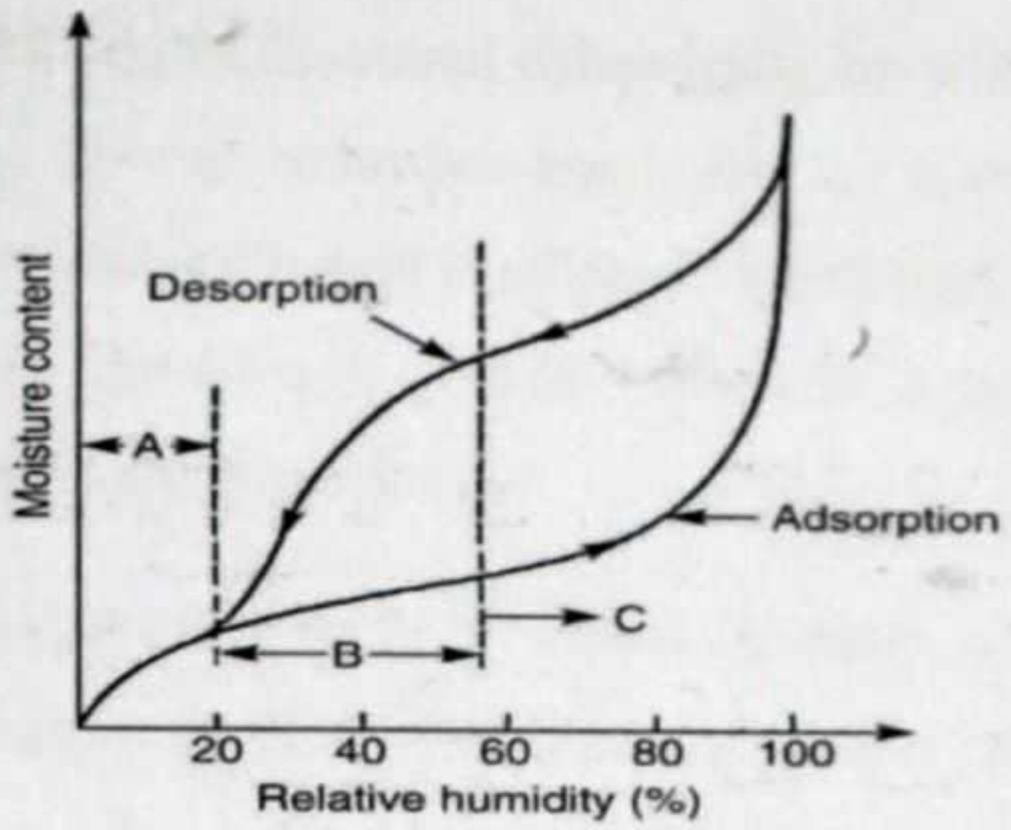

Figure 5 Typical sorption isotherms showing hysteresis

KNUST

Figure 5 shows the general shape of the sorption isotherm for food material. They are characterized by three distinct zones, A, B and C, which are indicative of different water binding mechanism at individual sites on the solid matrix. In region A, the water is tightly bound to the sites and is unavailable for reaction. In this region, there is essentially monolayer adsorption of water vapour and no distinction exists between the adsorption and desorption isotherms. In region B, the water is more loosely bound. The vapour pressure depression below the equilibrium vapour pressure of water at the same temperature is due to its confinement in small capillaries. Water in region C is even more loosely held in larger capillaries. It is available for participation in reactions and as a solvent (Baker, 1997).

Determination of EMC values may be made under static and dynamic conditions, although the latter case is preferred. A simple static procedure is to place samples in ordinary laboratory desiccator containing sulphuric acid solutions of known concentrations which produce atmospheres of known relative humidity. The sample in each desiccator is weighed periodically until a constant weight is obtained. Moisture content at this final weight represents the equilibrium moisture content for the particular conditions.

The value of equilibrium moisture content, for many materials, depends on the direction in which the equilibrium is approached because it is relatively easier to add moisture to a dried product than to remove moisture from a wet product. For drying calculations the de-sorption values are preferred as opposed to adsorption values, since they give higher values.

Equilibrium moisture content can be measured dynamically by placing the sample in a U-tube through which a continuous flow of controlled-humidified air is drawn. Again the sample is weighed periodically until a constant weight is reached. Humidified air for this experiment can be obtained by bubbling dry air through a large volume of a saturated salt solution which produces a definite degree of saturation of the air.

In the absence of facilities for determining EMC values, a number of theoretical, semi-theoretical and empirical models have been proposed. Notwithstanding the extensive research efforts in this area, no theoretical EMC is yet capable of predicting accurately the moisture equilibrium contents of even cereal grains, the well researched field of study, over the full temperature and relative humidity ranges. A review of the frequently used EMC models is presented in this sub-section.

KNUST

Smith (1947) suggested that static equilibrium moisture content expressed on wet basis provides an accurate correction to the isotherm equations for shrinking materials. He developed the following EMC equation:

$$M_{s,w} = M_b - g\ln(1 - RH) \tag{2.19}$$

where M_b is the bound moisture content and g is a constant which depends on temperature. The Smith equation has been found to fit the experimental EMC de-sorption curves of cereal grains rather well in the region $0.5 \leq RH \leq 0.95$ (Becker and Sallans, 1956).

Henderson (1952) proposed the following semi-empirical model for predicting the static moisture equilibrium curves of biological products, including grains:

$$1 - RH = e^{-c\,T_{abs}\,M_e{}^n} \tag{2.20}$$

in which RH, the relative humidity is represented as a fraction; T, the absolute temperature, M_e, the static equilibrium moisture content, %, d.b.; and c and n are material-dependent constants. Henderson's equation, in the form described above, has been found to be inadequate for cereal grains (Brooker *et al*, 1974). A number of empirically established modifications of the Henderson equation have been proposed. Day and Nelson (1965) modified Henderson's equation for calculating the EMC values for wheat as

$$1 - RH = \exp\left(-fM_e^{\,k}\right) \tag{2.21}$$

Where,

$$f = \left(5.7336\times10^{-10}\right)\theta_F^{\,3.3718}$$

$$k = 14.863\theta_F^{\,-0.41733}$$

and θ_F is the temperature, °F.

Thompson (1967) modified the Henderson's equation for corn as:

$$1 - RH = \exp\left[-3.8195\times10^{-5.0}(T+50)M_e^{\,2.0}\right] \tag{2.22}$$

Data from drying of hygroscopic materials have also been fitted to an empirical relation of the form:

$$\ln\left(\frac{M_e}{p_o+p_1RH+p_2RH^2+p_3RH^3}\right)=q_o+\left(q_1+q_2RH+q_3RH^2+q_4RH^3+q_5RH^4\right)T_{abs} \tag{2.23}$$

Testing of expression (2.23) was performed for hygroscopic data of rice (Anon, 1962), coffee and corn (Teter and Citelly, 1970) and cassava (Roa, 1974). The results were found to be adequate for practical applications. The values of the constants p_i and q_i are listed in the literature (Roa, 1974).

An EMC equation based on the potential theory and a simplified equation of state was developed by Chung and Pfost (1967). The equation is of the form:

$$\ln(RH)=\frac{-A}{R_o\,T_{abs}}\exp(-BM_e) \tag{2.24}$$

where constants A and B are temperature-dependent and M_e is the static equilibrium moisture content, dry basis. The constants A and B can be calculated for shelled corn from the following relationships (Brooker *et al*, 1974)

KNUST
WJ SANE NO BADWEMA
LIBRARY
KWAME NKRUMAH
UNIVERSITY OF SCIENCE & TECHNOLOGY
KUMASI

$$\ln A = R_o T'_{abs}\left(1.544\times10^{-2} - 1.383\times10^{-5} T'_{abs}\right) \quad (2.25)$$

$$B = R_o T'_{abs}\left(3.211\times10^{-3} + 2.069\times10^{-5} T'_{abs}\right) \quad (2.26)$$

where T'_{abs} denotes the absolute temperature in ^{o}R. Equation 2.24 is valid if $0.20 < RH < 0.90$.

beans, dried peas, cereal derivatives other than flour, oilseeds and almonds, the Hasley relation was found to be the best.

2.5.2Drying constant.

The drying constant depends on both material and air properties since it is phenomenological property representative of several transport phenomena. It is a function of the material moisture content, temperature, and thickness, as well as air humidity, temperature and velocity (Marinos-Kouris and Maroulis, 1995). Lewis (1921) suggested that during the drying of porous hygroscopic materials in the falling-rate period, the rate of change in material moisture content is proportional to the instantaneous difference between material moisture content and the expected material moisture content when it comes into equilibrium with the drying air. If it is assumed that the material layer is thin enough or the air velocity is sufficiently high so that the conditions of the drying air (humidity, temperature) are kept constant throughout the drying of the material, the thin-layer equation has the following form:

$$\frac{dM}{dt} = -K(M - M_e) \quad (2.27)$$

where$M$ (kg/kg) is the material moisture content (dry basis), M_e (kg/kg) the material moisture content in equilibrium with the drying air (dry basis), and t (s) is the time. The drying constant is estimated by fitting the thin-layer equation to experimental data. If the controlling mechanism of moisture removal during a drying process is diffusion then the drying constant can be determined as a function of moisture diffusivity. For slabs, for example, the following equation is valid:

$$K = \pi^2 D/L^2 \quad (2.28)$$

where D (m^2/s) is the effective diffusivity and L (m) is the thickness of the slab. In the drying of grains, Henderson and Pabis (1961) showed that the drying rate coefficient K can be related to the effective diffusion, D, and an equivalent grain radius, R, by:

$$K = D\frac{\pi^2}{R^2} \tag{2.29}$$

O'Callaghan (1954) observed that for wheat, in the temperature range 10-66° C, the drying constant is independent of the relative humidity of the drying air but is dependent on its temperature. He proposed the following equation:

$$K = A\exp(BT) \tag{2.30}$$

KNUST

Henderson and Pabis (1961) proposed an Arrhenius-type equation to relate the thin-layer drying constant to drying air temperature.

$$K = p\exp(-q/T) \tag{2.31}$$

where p, q are material-dependant constants.

Syarief *et al* (1984) observed that the drying constant of sunflower seeds is a function of the drying air temperature and its relative humidity according to the equation:

$$K = 5.16\times10^{-4}T^{1.8387} + 3.45\times10^{-5}RH^2 \tag{2.32}$$

Nellist (1974) observed during the drying of ryegrass seeds that the inclusion of moisture content and humidity in the form:

$$K = a\exp(bT+cH+dM_o) \tag{2.33}$$

improved the fit of the curve to the experimental data.

2.5.3 Moisture diffusivity

Diffusion in solids during drying is a complex process involving several mechanisms including liquid and vapour diffusion, surface diffusion, hydrodynamic or bulk flow, and capillary flow

(Marinos-Kouris and Maroulis, 1995). Combining all these phenomena into one, the effective diffusivity can be defined from Fick's law (see Equation 2.5).Table 1 gives some literature values of the effective diffusivity of moisture in various materials.

Table 1: Effective moisture diffusivity in some materials

Material	Moisture content fraction (kg/kg d.b)	Temperature (°C)	Diffusivity (m^2/s)
Alfafa stems	< 3.70	26	$2.6x10^{-12}$ - $2.6x10^{-9}$
Apple	0.12	60	$6.5x\ 10^{-12}$ - $1.2x10^{-10}$
	0.15 - 7.0	30 – 76	$1.2\ x10^{-10}$ - $2.6x10^{-10}$
Avocado		31 – 56	$1.1x\ 10^{-10}$ - $3.3x10^{-10}$
Beet	0.10 - 0.65	65	$1.54x10^{-9}$
Biscuit	0.10-0.65	20-100	$9.4x10^{-9}$ - $9.7x10^{-8}$
Bread	0.10 - 0.70	20 – 100	$2.5x10^{-9}$ - $5.5x10^{-7}$
Carrot	0.03 - 11.6	42 – 80	$9.0x10^{-10}$ - $3.3x10^{-9}$
Corn	0.05 - 0.23	40	$1.0x10^{-12}$ - $1.0x10^{-10}$
Corn	0.19 - 0.27	36 – 62	$7.2x10^{-11}$ - $3.3x10^{-10}$
Muffin	0.10 - 0.65	20 – 100	$8.4x10^{-10}$ - $1.5x10^{-7}$
Onion	0.05 - 18.7	47 – 81	$7.0x10^{-10}$. $4.9x10^{-9}$
Fish muscle	0.05 - 0.30	30	$8.1x10^{-11}$ - $3.4x10^{-10}$
Pepper, green	0.04 - 16.2	47 – 81	$5.0x10^{-10}$ - $9.2x10^{-9}$
Pepperoni	0.19	12	$4.7x10^{-11}$ - $5.7x10^{-11}$

Source: Marinos-Kouris and Maroulis, 1995

Moisture diffusivity for food materials have been found to depend on several factors including temperature, moisture content, shape of the material, and relative humidity of the surrounding

KNUST

medium. However, because of the problem with the measurement of the product temperature some authors have measured the air temperature instead of the product temperature (Igbeka *et al*, 1976). Husain *et al* (1972) suggested that for high moisture foods, the use of variable diffusivity in a model describing a drying process is appropriate, if shrinkage effect is neglected.

Pabis and Henderson (1961) expressed the dependence of diffusion coefficient at high moisture levels with temperature in terms of an Arrhenius-type expression:

$$D = D_o \exp(-E/RT_g) \tag{2.34}$$

where,

D_o (m^2 / s) is the Arrhenius factor, E (kJ / kmol) is the activation energy for diffusion at high moisture levels, R (kJ / kmol K) the gas constant, T_g (K) the temperature of the material.

Xiong *et al* (1992) postulated that the decrease in the effective diffusivity at lower moisture contents is a result of a decrease in the availability of water molecules for diffusion. Their resulting expression relating the effective diffusivity and the proportional amount of free water is of the form:

$$D = D_o \exp(-E_b/RT_g)\frac{K\exp(-E_b/RT_g)}{1 + K\exp(-E_b/RT_g)} \tag{2.35}$$

where E_b is the binding energy and is inversely related to the moisture content (Iglesias and Chirife, 1982), and K is an equilibrium constant. At higher moisture levels (> 70% wet basis) the binding energy is zero signifying that at these levels the effective moisture diffusivity is independent of moisture content.

2.6 Psychrometry in relation to drying

Two processes occur simultaneously during the thermal process of drying a wet product: heat transfer, to change the temperature of the wet product and to evaporate its surface moisture, and mass transfer of moisture to, and its subsequent evaporation from, the surface of the product to the surrounding medium. The drying medium is moist air, which is a binary mixture of dry air

and water vapour. Relationships that can be used to model the inter-relationships between air and water vapour are provided in the literature (ASHRAE, 2009).

The water vapour saturation pressure for the temperature range of 0 to 200° C is given by (ASHRAE, 2009):

$$\ln(p_{vs}) = C_1/T_{db} + C_2 + C_3 T_{db} + C_4 T_{db}^{\ 2} + C_5 T_{db}^{\ 3} + C_6 \ln(T_{db}) \qquad (2.36)$$

where C_1 =-5.800 220 6 × 10^3, C_2 = 1.3914993, C_3= -4.864 023 9×10^{-2},

C_4 = 4.176 476 8 ×10^{-5}, C_5 = -1.445 209 3×10^{-8}, C_6 = 6.545 967 3 and T_{db} is the dry-bulb temperature.

KNUST

or by (Brooker *et al*, 1974):

$$P_{vs} = R \exp\left(\frac{A + BT_{db} + CT_{db}^{\ 2} + DT_{db}^{\ 3} + ET_{db}^{\ 4}}{FT_{db} - GT_{db}^{\ 2}}\right) \qquad (2.37)$$

where,

P_{vs} = saturated water vapour pressure of the drying air, N/m^2

R = 0.2210564925×10^8, A = -0.274055258361×10^5, B = 0.54189×10^2,
C = -0.451370×10^{-1}, D = 0.2153214×10^{-4}, E = -0.462027×10^{-8}
F = 0.241613×10, G = 0.121547×10^{-2}

T_{db} = dry bulb temperature, K.

The absolute humidity of moist air (kg water vapour/kg dry air) in the temperature range of 255 K to 533 K is given by:

$$H = \frac{0.6219 P_v}{P_{atm} - P_v} \qquad (2.38)$$

where, P_v is the partial pressure of water vapour in the moist air sample which is evaluated from equation (2.37) or (2.38) by putting T_{db} equal to the wet bulb temperature of the surrounding air.

The saturated humidity, H_s , is the absolute humidity of moist air saturated with respect to water at the same temperature, T, and pressure, P. Its value is obtained from the equation (2.38) by putting $P_v = P_{vs,wb}$.

The wet-bulb temperature can be estimated from the relationship below (ASHRAE, 2009)

$$\theta_{wb} = \frac{\left(2501(H_s - H_s^*) + \theta_{db}(1.805H_s + 1)\right)}{\left(1 - 2.381H_s^* + 4.186H_s\right)} \tag{2.39}$$

where H_s^* is the humidity of moist air at saturation thermodynamic wet-bulb temperature,

or from the following relationship given by Brooker *et al*, (1974)

$$T_{wb} = T_{db} - \frac{P_{vs,db} - P_{vs,wb}}{B} \tag{2.40}$$

where,

$$B = \frac{1006.9254\left(P_{vs,wb} - P_{atm}\right)\left(1 + 0.15577P_{vs,db}/P_{atm}\right)}{0.62194h_{fg,wb}} \tag{2.41}$$

and the latent heat of vaporisation of water vapour from moist air, h_{fg} , (J/kg) is calculated using one of the following relationships (Bakker-Arkema *et al*, 1978):

$$h_{fg} = 2502535.259 - 2385.764244(T - 338.72), \text{ for } 273 \leq T \leq 339\ K \tag{2.42}$$

$$h_{fg} = \left(7329155978000 - 15995964.08T^2\right)^{1/2}, \quad \text{for } 339 < T \leq 533\ K \tag{2.43}$$

To evaluate the wet-bulb temperature by using either equation (2.39) or (2.40) requires a trial and error or a numerical solution method. The latent heat or heat of evaporation is evaluated at the wet-bulb temperature of the air in contact with the surface of the product (Daly, 1992). This statement assumes that at steady-state, the temperature of the wet surface of the material being dried is equal to the wet-bulb temperature of the air in contact with the surface of the product. However, in a mixed mode dryer since the surface temperature of the wet product is greater than

KNUST

the wet bulb temperature of the surrounding air, it is reasonable to assume a value of about 5 to 15K more than the wet bulb temperature as an initial guess.

The dew-point temperature, θ_d, of moist air with humidity H and pressure P is defined by (ASHRAE, 1993)

$$P_{ws}(t_d) = P_v = (pH)/(0.62198 + H) \tag{2.44}$$

where, P_v is the water vapour partial pressure for the moist air sample and $P_{ws}(t_d)$ is the saturation vapour pressure at temperature θ_d. Alternatively, the dew-point temperature can be calculated from the following equation (ASHRAE, 1993)

$$\theta_d = a + b\alpha + c\alpha^2 + d\alpha^3 + e(P_w)^{0.1984} \tag{2.45}$$

where, θ_d = dew point temperature, °C

α = $\ln(P_w)$

P_w = water vapour partial pressure, kPa

a = 6.54, b = 14.526, c = 0.7389, d = 0.09486 and e = 0.4569

The specific volume of moist air (m^3/kg. dry air) can be determined, by assuming ideal gas behaviour, by the following equation (ASHRAE, 1989):

$$\upsilon = \frac{R_a T}{P_{atm}}(1 + 1.608H) \tag{2.46}$$

The density of moist air is evaluated as the reciprocal of the humid air specific volume from equation (2.46).

The relative humidity fraction is calculated from the following relation given by (Daly, 1992):

$$RH = \frac{1}{P_{vs,db}}\left\{P_{vs,wb} - 66.6\left(\frac{P_{atm}}{10{,}000}\right)(\theta_{db} - \theta_{wb})\right\} \tag{2.47}$$

or from the definition

$$RH = \frac{P_v}{P_{vs,\,db}} \tag{2.48}$$

where, θ_{db} and θ_{wb} are the dry-bulb and wet-bulb temperatures in $^{\circ}C$, $P_{vs,db}$ and $P_{vs,wb}$ are the saturation vapour pressure in Pa at θ_{db} and θ_{wb} respectively, and P_{atm} is the barometric pressure in Pa.

The specific enthalpy (or total heat) of moist air, per kilogram of dry air, is given by:

$$h = C_{p,a}\theta_{db} + C_{pw}H\theta_{db} + Hh_{fg} \tag{2.49}$$

where C_{pa} is the specific heat capacity of dry air and the other dependent variables are as previously defined.

KNUST

2.7 Drying simulation

This section references the two methods of analysing the rate of drying of wet agricultural products. The first part considers the drying of the product as individual particles or in thin-layers and the next section considers the practical situation in which the products are dried in deep-beds. A review of mathematical expressions describing the drying rate of agricultural crops in thin-layers is presented. The use of these expressions in predicting the moisture loss from crops in conventional dryers is reviewed. The practical importance of thin-layer expressions, according to Bakker-Arkema *et al* (1978), is limited since agricultural crops, as they stated, are dried not as individual particles or in thin-layers; instead, crops are dried in either a stationary or a moving deep-bed. Nevertheless, the set of equations describing the drying of agricultural crops always include an expression that describes the rate of moisture removal from a thin-layer. Hence, in the second part of this section, the method of analysis of drying of a deep-bed of agricultural crops is reviewed.

2.7.1 Thin layer drying

A thin layer may be defined, contrary to a deep bed layer, as one in which there is no moisture gradient through the layer during drying. The thin-layer drying concept assumes that the ratio of the material volume to air is such that there is only a small change in temperature and relative humidity of the drying air when it exits the crop bed compared to its inlet conditions (ASHRAE, 1989). In crop drying, material depths of up to 200 mm are considered as thin-layers (Hall, 1975); but as pointed out by Henderson and Perry (1976), even material depths as small as 25 mm provide evidence of moisture gradient and, thus may be considered as 'deep beds'.

The search for an accurate method of describing the drying rate of a thin-layer of material in a stream of air at constant temperature, velocity and absolute humidity (constant external drying conditions) has often been reported in the literature (Karel *etal,* 1975; Suarez *etal*, 1980; Igbeka, 1982; Hutchinson and Otten, 1983; and Chiang and Peterson, 1985).

Thin layer drying equations relate the rate of moisture loss to the drying conditions (drying air temperature, velocity and relative humidity) and the initial moisture content of the crop; they are based on empirical studies, or derived from theoretical or semi-theoretical considerations. In the theoretical approach, the equation is derived from either the diffusion equation or from simultaneous heat and mass transfer equations. In the semi-theoretical approach, approximated theoretical equations are used. In the empirical approach, experiments are conducted and empirical equations are developed to fit the experimental data. The main justification of the empirical equation is a satisfactory fit to experimental data (Zaman and Bala, 1989) and the subsequent benefit in describing thin-layer and deep bed drying of crops.

The following mechanisms have been proposed to account for moisture movement in capillary-porous solids such as agricultural crops (van Brakel, 1980; Brooker *et al*, 1974; Bakker-Arkema *et al*, 1978):

1) *liquid diffusion* due to moisture concentration gradient;

2) *vapour diffusion* due to partial vapour pressure gradient;

3) *capillary flow*, liquid movement due to surface forces;

4) *surface diffusion,* liquid movement due to diffusion of moisture on the crop surfaces;

5) *thermal diffusion,* vapour movement due to temperature differences; and

6) *hydrodynamic flow or filtration,* liquid or vapour flow due to differences in total pressure.

Liquid and/or vapour diffusion have been assumed to be the primary mass transfer mechanism(s) in drying studies on cereal grains and similar products (Hutchinson and Otten, 1983). The most widely investigated theoretical model in the thin-layer drying literature is the diffusion model, given by Fick's law (see equation 2.5).

The assumptions inherent in the diffusion model are as follows:

1) the primary mechanism for moisture transport is diffusion;

2) the principal driving force for mass transport is the internal moisture content gradient;

3) temperature within the kernel is assumed constant;

4) the resistance to moisture flow is uniformly distributed throughout the interior of the material; and

5) either vapour or liquid diffusion predominates. If both processes occur simultaneously, the diffusion coefficient must represent the combined effects of liquid and vapour diffusion.

Van Arsdel (1947) suggested that the diffusion equation could be used to describe the rate of moisture movement from a solid, if the potential for the moisture diffusion is represented by concentration gradient. Wang and Hall (1961) hypothesised that if the temperature distribution within a product being dried is assumed uniform, then the diffusion equation with concentration as the driving force is adequate in describing moisture movement from the product. The selection of either moisture content gradient or vapour pressure gradient as the driving force for diffusion has been a subject of controversy. Babbitt (1949) and Bramhall (1979) maintain that vapour pressure gradient more consistently accounts for experimentally observed phenomena than does the concentration gradient. Babbitt explains that since vapour pressure is a function of moisture content and temperature, moisture transfer in response to a temperature gradient follows easily using the vapour pressure gradient as the driving force. Referring to this explanation, then under

KNUST
LIBRARY
KWAME NKRUMAH
UNIVERSITY OF SCIENCE & TECHNOLOGY
KUMASI

non-isothermal drying conditions as experienced in conventional dryers, it might be prudent to recognise vapour pressure gradient as the driving force for moisture diffusion rather than concentration gradient.

The exact solutions of the diffusion equation characterising moisture transfer in plane sheets, finite cylinders and spheres are listed by Young and Whitaker (1971a,b) and Crank (1975). The solution for a sphere, cylinder and the plane sheet commonly used for simulating moisture transfer in crops are respectively:

$$\frac{\overline{M} - M_e}{M_o - M_e} = \frac{6}{\Pi^2} \sum_{n=1}^{\infty} \frac{1}{n^2} \exp\left[-n^2 D\pi^2 t / r^2\right] \tag{2.50}$$

$$\frac{\overline{M} - M_e}{M_o - M_e} = \sum_{n=1}^{\infty} \frac{4}{a^2 \alpha_n{}^2} \exp(-D \alpha_n{}^2 t) \tag{2.51}$$

$$\frac{\overline{M} - M_e}{M_o - M_e} = \frac{8}{\pi^2} \sum_{n=0}^{\infty} \frac{1}{(2n+1)^2} \exp\left[-(2n+1)^2 D\pi^2 t / z^2\right] \tag{2.52}$$

wherethe $\alpha_n{}'s$ are the Bessel function roots of the first kind and order zero, D is the diffusion coefficient, M_e is the equilibrium moisture content, M_o is the initial moisture content, and $\overline{M}$ is the average moisture content at time t in seconds.

Solutions to the diffusion equations are restricted to conditions where the temperature, humidity, pressure, and velocity of the drying air are constant (Hougen *et al*, 1940). Referring to this statement, the assumption of a quasi-steady state analysis of the dynamic phenomena of drying could be justified.

In addition to the exact solutions of equation (2.5), other relations or simplified solutions have frequently been employed in crop drying analyses. Lewis (1921) suggested that the rate of drying during the falling rate period is directly proportional to the difference between the actual moisture content of the material and the equilibrium moisture content, i.e:

$$\frac{dM}{dt} = -k(M - M_e) \tag{2.53}$$

After separating variables, equation (2.53) can be integrated to equation (2.54) or (2.55):

$$\ln\left(\frac{M-M_e}{M_o-M_e}\right)=-kt \tag{2.54}$$

$$\frac{M-M_e}{M_o-M_e}=\exp(-kt) \tag{2.55}$$

Equation 2.54 or 2.55 is commonly known as the exponential model. It was derived based on the approximated differential equation for diffusion on the following assumptions:

a) the resistance to moisture movement is concentrated in a layer at the surface of the material,

b) the initial moisture content of the material is not very high (less than 100 to 200 per cent on dry basis, depending on the material), since the drying rate no longer increases with moisture content but remains constant,

c) the material does not shrink greatly during drying , and

d) the drying coefficient , k , is a constant, though for a given material it varies with rate of diffusion and of surface evaporation and with its thickness.

It has been noted (ASHRAE, 2009) that equation (2.54) or (2.55) alone does not describe the usual drying process where grain is dried in a deep-bed because the drying air changes condition but does not necessarily reach moisture equilibrium with the crop. This notwithstanding, it has been widely used by a number of researchers.

Sherwood (1936) contends that equation (2.53) should not be applied to the constant-rate drying period. If no constant rate period occurs, according to Sherwood, equation (2.53) will hold reasonably well, particularly when the drying curve is in the falling rate period. Sherwood (1936) noted that in certain slow-drying solids no constant rate period appeared, and internal liquid diffusion controlled the process from the start. The models of Lewis (1921) and Henderson and Pabis (1962) assumed that all the resistance to moisture flow was concentrated in a layer at the surface of the material. On the other hand, if it is assumed that the resistance to moisture flow is uniformly distributed throughout the interior of the material, then the fundamental diffusion

equation would be an appropriate model describing the rate of moisture loss from an agricultural crop (Sherwood, 1936).

A modified form of the basic exponential drying equation, sometimes referred to as the Hustrulid & Flikke equation (Hustrulid and Flikke, 1959), has also been used by a number of researchers (Ross and White, 1972; Sharaf-Eldeen *et al*, 1980; White *et al*, 1981; Chiang and Petersen, 1985; Patil and Ward, 1989; Diamante and Munro, 1991b, 1994); it is of the form:

$$\frac{M - M_e}{M_o - M_e} = a\exp(-kt) \tag{2.56}$$

Equation (2.56) has been one of the most widely used equations in modelling drying rates of crops of high moisture content (Chirife and Cachero, 1970; Vaccarezza *et al*, 1974; Igbeka, 1982; Diamante and Munro, 1993).

$$\frac{M - M_e}{M_o - M_e} = a\exp(-\frac{\pi^2}{4}\frac{D}{L^2}t) \tag{2.57}$$

An alternative approach to the analysis of thin-layer drying data has been to use purely empirical relationships. Very good fits of experimental data have been reported by researchers using purely empirical relationships (Hutchinson and Otten, 1983; Morey *et al*, 1978; Brooker *et al*, 1974). One equation that has been widely used in thin-layer studies of a variety of materials (Hutchinson and Otten, 1983) is Page equation.

Page (1949) (cited by Hall and Rodgriguez-Arias, 1958 and Van Rest and Isaacs, 1968), on the basis of his investigation on the basic drying rates of shelled corn at Purdue University, proposed an empirical equation for describing thin-layer drying of the form:

$$\frac{M - M_e}{M_o - M_e} = \exp(-kt^n) \tag{2.58}$$

where n is an experimental constant, and the value of the constant k was determined on the basis of time, t, expressed in half-response units. Page found that the constant n was a function of the relative humidity and obtained values of 0.60, 0.65 and 0.83 for relative humidity values of 35, 50 and 70% respectively, and 0.68 for k.

Li and Morey (1984) obtained satisfactory fits for their drying data using equation (2.57) and found that within the limits of drying airflow rates and air relative humidity values used, k and n can be expressed as functions of air temperature and initial grain moisture only. Their equations for k and n apply to air temperatures ranging from 27 to 116° C, initial grain moistures in the range of 23 to 36% dry basis, airflow rates from 0.27 to 1.34 m/s, and air relative humidity ranging from 5 to 40%.

Equation (2.53) may be modified to include the dependence on sample thickness as a simplification of the Fick's diffusion equation to give the modified Page equation (Diamante and Munro, 1991b):

$$\frac{M - M_e}{M_o - M_e} = \exp(-k[t / L^2]^n) \tag{2.59}$$

KNUST

The effect of air dry bulb temperature on drying is well documented in the literature (Igbeka, 1982; Hutchinson and Otten, 1983; Chiang and Petersen, 1985). Contrary to the observation of Diamante and Munro (1991b), several investigators have shown that air relative humidity below 20% has an insignificant effect on drying rates (White *et al*, 1973; Chiang and Petersen, 1985). It is revealing from the above studies that the effect of the air relative humidity on the rate of drying cannot be ignored. A number of researchers have chosen to neglect the effect of air flow rates in the analysis of thin-layer drying data, citing the conclusion of Henderson and Pabis (1962) that resistance to moisture movement at the surface is negligible compared to internal resistance for turbulent flows, which occur in most conventional dryers. However, Islam and Flink (1982) pointed out that at air velocities of 2.5 m/s or less, the external mass transport resistance is significant and needs to be considered in the analysis of the drying data. The study of Diamante and Munro (1991b) showed this to be the case for air velocity within the range of 0.5-3.0 m/s. In natural convection solar dryers, air flow rates are relatively low enough for external mass transport resistance to be considered.

Thompson, Peart and Foster (1968) performed a series of thin-layer drying test at Purdue University in 1963. The main variable of their investigation in the tests conducted was the drying air temperature; however, other explanatory tests were performed to evaluate the effect of airflow rate and the product (corn) variety on drying rate. The tests were performed with corn at

initial moisture contents of 19, 23, or 33% expressed on wet basis, for drying air flow rates of 20 and 60 cfm/ft^2 and at temperatures ranging from 49 to 171°C. They reported the results of each drying test were analysed by fitting the experimental data to two thin-layer equations. The first was the simple exponential drying relation and second was a second-order exponential curve of the form:

$$t = A \ln MR + B (\ln MR)^2 \tag{2.60}$$

They reported from the plots of the experimental data and those predicted using the simple exponential relation that the simple exponential relation did not adequately represent the experimental results.

KNUST

They assumed the Henderson (1955) equilibrium moisture content relation and hence developed by trial and error the following equation for shelled corn from the data by Rodriguez-Arias (1956) for a given air state point:

$$1 - RH = \exp \{-c (T + 50) M_e^{\,n}\} \tag{2.61}$$

They reported that the constants that represent the experimental results the best are:

$c = 3.8195 \times 10^{-5}$, and $n = 2.0$. They found that the second order equation which involves time and natural logarithm of moisture ratio adequately represented drying characteristics of shelled corn.

Bunn *et al*, (1972) also proposed another empirical equation, simple in form, to describe the dynamic process of drying a variety of materials with high initial moisture content (100% d.b and above). The equation is of the form:

$$W = A\left[\frac{t + BC}{t + AB}\right] \tag{2.62}$$

By applying the initial and boundary conditions (when $t = 0$, $W = W_o$ and when $t = \infty$, $W = W_e$) and defining the time, t, when the weight ratio is equal to one-half as, $t_{1/2}$, the weight ratio in terms of half-life, equation (2.62) then becomes:

initial moisture contents of 19, 23, or 33% expressed on wet basis, for drying air flow rates of 20 and 60 cfm/ft^2 and at temperatures ranging from 49 to 171°C. They reported the results of each drying test were analysed by fitting the experimental data to two thin-layer equations. The first was the simple exponential drying relation and second was a second-order exponential curve of the form:

$$t = A \ln MR + B (\ln MR)^2 \tag{2.60}$$

They reported from the plots of the experimental data and those predicted using the simple exponential relation that the simple exponential relation did not adequately represent the experimental results.

KNUST

They assumed the Henderson (1955) equilibrium moisture content relation and hence developed by trial and error the following equation for shelled corn from the data by Rodriguez-Arias (1956) for a given air state point:

$$1 - RH = \exp \{-c (T + 50) M_e^{\,n}\} \tag{2.61}$$

They reported that the constants that represent the experimental results the best are:

$c = 3.8195 \times 10^{-5}$, and $n = 2.0$. They found that the second order equation which involves time and natural logarithm of moisture ratio adequately represented drying characteristics of shelled corn.

Bunn *et al*, (1972) also proposed another empirical equation, simple in form, to describe the dynamic process of drying a variety of materials with high initial moisture content (100% d.b and above). The equation is of the form:

$$W = A\left[\frac{t + BC}{t + AB}\right] \tag{2.62}$$

By applying the initial and boundary conditions (when $t = 0$, $W = W_o$ and when $t = \infty$, $W = W_e$) and defining the time, t, when the weight ratio is equal to one-half as, $t_{1/2}$, the weight ratio in terms of half-life, equation (2.62) then becomes:

$$\frac{W - W_e}{W_o - W_e} = \frac{t_{1/2}}{t + t_{1/2}} \tag{2.63}$$

Equation (2.63), according to Bunn *et al*, was developed through many theoretical and empirical trials with weight-loss data from stalk-cut burley tobacco curing studies. They reported that the following form of the equation, in fact a re-arrangement, describes the weight-time relationship down to about 5 % moisture content (dry basis).

$$W = W_e + (W_o - W_e)\left[\frac{t_{1/2}}{t + t_{1/2}}\right] \tag{2.64}$$

They also indicated that their different sets of data were fitted to the Page's equation, as a way of comparison, and found that Bunn's equation fitted better than the Page's equation.

Sharaf-Eldeen *et al*, (1979a) applied the general solution to the diffusion equation and developed a two term exponential thin layer drying equation of the form:

$$\frac{M - M_e}{M_o - M_e} = A\exp(-kt) + (1 - A)\exp(-Bkt) \tag{2.65}$$

They assumed a constant diffusivity and observed that the two-term exponential model adequately describes the behaviour of fully exposed shelled corn, rough rice and soybeans. They also observed that Page equation gives a better description compared to the basic logarithmic model proposed by Lewis.

Verma *et al* (1985) carried out an extensive experimental study in a vertical airflow dryer to evaluate the effects of the temperature, velocity and relative humidity of the drying air on the drying constants of steamed and unsteamed rough rice. Thirty-seven tests were conducted with unsteamed rice and thirty-five with steamed treated rice. Relative humidity varied from 3 to 60%, velocity from 0.025 to 0.50 $m^3/s.m^2$ and temperature from 35 to 95° C for unsteamed rice. In the case of steamed rice, the relative humidity varied from 10 to 58%, velocity from 0.05 to 0.50 $m^3/s.m^2$ and temperature from 30 to 75° C. They developed a two term exponential drying equation (an approximated form of the infinite series solution of the diffusion equation for a plane sheet) that describes the single layer drying of steamed and unsteamed rice of the form:

$$\frac{M - M_e}{M_o - M_e} = A\exp(-kt) + F\exp(-gt) \qquad (2.66)$$

in which the drying the drying constant was expressed by an Arrhehius-type relation.

A number of researchers (Hustrulid and Flikke, 1959; Newman, 1931; Sharaf-Eldeen *et al* 1979b) have also pointed out that the second and subsequent terms of the series solution of the diffusion equation are negligible after extended drying.

Chhinnan (1984) designed and fabricated an experimental dryer for thin layer drying studies of pecans. Thin layer drying data was obtained for in-shell pecans for varying drying conditions. Four mathematical models were evaluated to fit the drying data, namely: the simple exponential model, the diffusion model, one term approximation of the infinite series solution of the diffusion model and the Page equation. The Page equation was found to be most suitable in describing drying characteristics of single layer of in-shell pecans and was recommended for bulk modelling studies. The exponent of the time, *n* was found to be a constant and equal to 0.6996. The basic exponential model was found to give the worst fit and diffusion model was found to give a better fit than the approximated diffusion model.

KNUST

2.7.2 Analysis of deep-bed drying.

The conditions of agricultural crops and of air change with position and time during deep bed drying processes (Boyce, 1965 and Thompson *et al*, 1968). Mathematical models have been used for studying low and high temperature deep-bed drying processes in the past. In these models, the drying phenomenon is analysed by calculating the drying of a thin layer of crop and then combining many thin layers to form the deep bed. The continuous drying process can be simulated by consecutively calculating the air and moisture changes that occur during short increments of time as the drying air passes from one layer to the next. Thus each layer is dried for a short time interval using exhaust air from the preceding layer. The process is repeated with consecutive short increments of time until a desired final moisture content of the crop bed is achieved.

2.7.2.1 Non-equilibrium models.

The non-equilibrium drying models assume that there is no heat nor mass equilibrium between the drying air and the crop throughout the deep-bed. Based on this assumption a system of partial differential equations (PDE) is derived from the laws of heat and mass transfer, the mathematical theory of drying of single solid bodies, and the general crop drying theory to represent the crop drying model.

Four of the many non-equilibrium models applicable to situations in which the wet product is dried in a stationary bed are referenced in this section.

The non-equilibrium model derived by Bakker-Arkema *et al*, (1967) and also presented by Brooker *et al*, (1974) is based on a control volume isolated from a stationary crop bed (see fig. 6).

KNUST

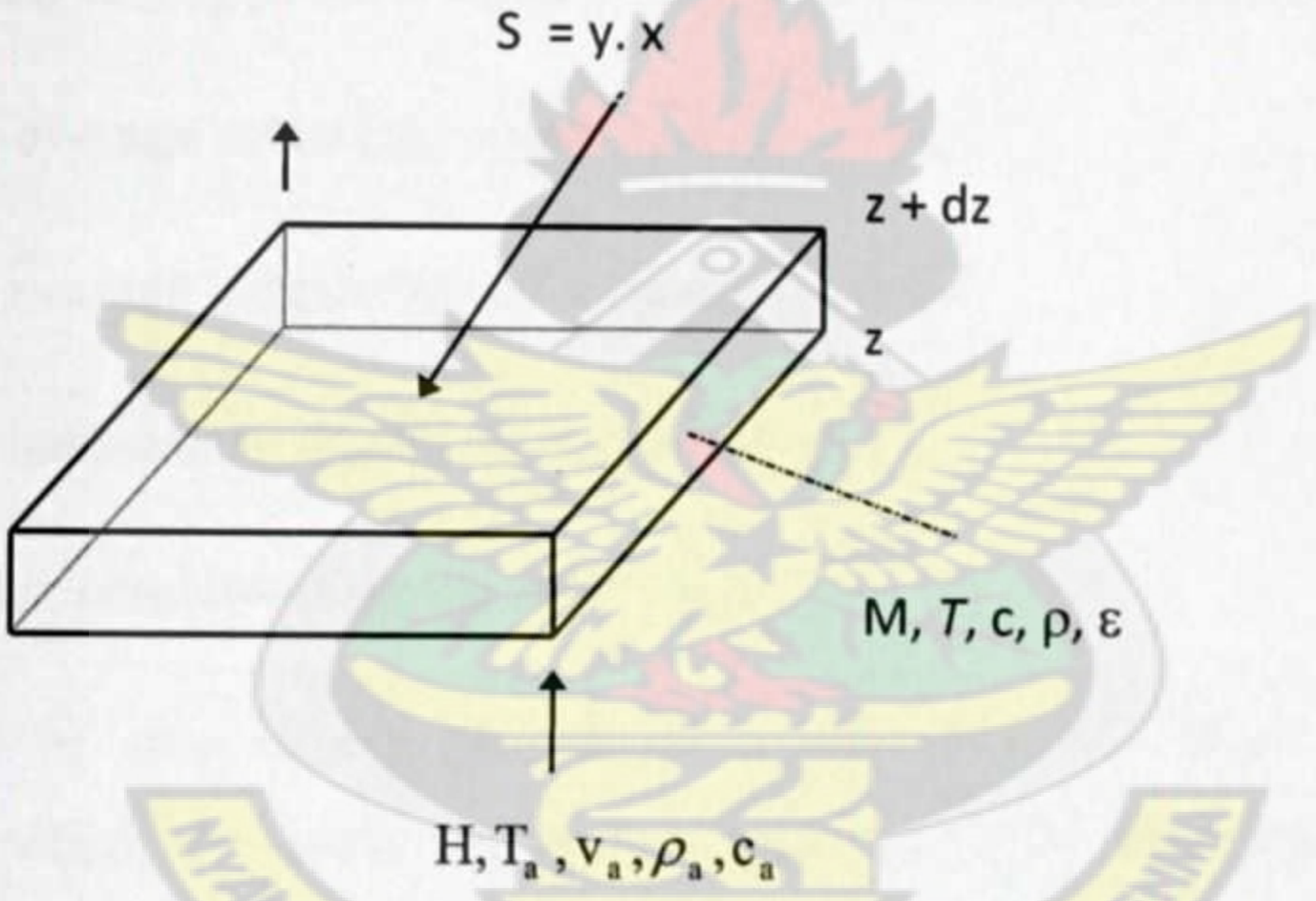

Figure 6: Control volume of a stationary bed of crop (Bakker-Arkema *et al*, 1967).

Their model is developed based on the following assumptions:

(i) volume shrinkage of a crop bed is negligible during drying,

(ii) temperature gradients within the individual kernels of grain are negligible,

(iii) conduction heat and mass transfer between crop particles is negligible,

(iv) airflow and grain flow are plug-type,

(v) changes in temperature and humidity of the drying air over time are negligible when compared to air temperature and humidity changes over a thickness *dz* of the deep-bed in the direction of airflow,

(vi) bin walls are adiabatic with negligible heat capacity,

(vii) heat capacities of moist air and grain are constant over short periods, and

(viii) accurate thin-layer equation and moisture content equilibrium isotherms are known.

In practice a drying process is a non-stationary process, therefore, moisture content and temperature depend on position, z, and drying time, t, i.e. $M = M(z,t)$ and $\theta = \theta(z,t)$. For a quasi-steady solution, moisture content can be calculated or expressed as the average distribution of moisture within the crop bed.

KNUST

When modelling the crop drying process in deep bed, the following unknowns are identified:

1. $M = M(z,t)$, the average moisture content of the crop bed,

2. $\vartheta = \vartheta(z,t)$, the average temperature of a product particle,

3. $H = H(z,t)$, the humidity of drying air in the bed, and

4. $T = T(z,t)$, the temperature of drying air in the bed.

Therefore, the model of crop drying process in a stationary bed must comprise of four differential equations which are: mass and energy balances of the crop and drying air and a drying rate equation of a thin-layer of the product. Bakker-Arkema *et al* (1967) and Brooker *et al*, (1974) presented the following set of differential equations for describing drying of grain in a stationary bed:

$$\frac{\partial H}{\partial z} = -\frac{\rho}{G_a}\frac{\partial M}{\partial t} \tag{2.67}$$

$$\frac{\partial T}{\partial z} = \frac{-ha}{G_a c_a + G_a c_v H}(T_a - T) \tag{2.68}$$

(v) changes in temperature and humidity of the drying air over time are negligible when compared to air temperature and humidity changes over a thickness *dz* of the deep-bed in the direction of airflow,

(vi) bin walls are adiabatic with negligible heat capacity,

(vii) heat capacities of moist air and grain are constant over short periods, and

(viii) accurate thin-layer equation and moisture content equilibrium isotherms are known.

In practice a drying process is a non-stationary process, therefore, moisture content and temperature depend on position, *z*, and drying time, *t*, i.e. $M = M(z,t)$ and $\theta = \theta(z,t)$. For a quasi-steady solution, moisture content can be calculated or expressed as the average distribution of moisture within the crop bed.

KNUST

When modelling the crop drying process in deep bed, the following unknowns are identified:

1. $M = M(z,t)$, the average moisture content of the crop bed,

2. $\vartheta = \vartheta(z,t)$, the average temperature of a product particle,

3. $H = H(z,t)$, the humidity of drying air in the bed, and

4. $T = T(z,t)$, the temperature of drying air in the bed.

Therefore, the model of crop drying process in a stationary bed must comprise of four differential equations which are: mass and energy balances of the crop and drying air and a drying rate equation of a thin-layer of the product. Bakker-Arkema *et al* (1967) and Brooker *et al*, (1974) presented the following set of differential equations for describing drying of grain in a stationary bed:

$$\frac{\partial H}{\partial z} = -\frac{\rho}{G_a}\frac{\partial M}{\partial t} \tag{2.67}$$

$$\frac{\partial T}{\partial z} = \frac{-ha}{G_a c_a + G_a c_v H}(T_a - T) \tag{2.68}$$

$$\frac{\partial \theta}{\partial t} = \frac{ha(T_a - T)}{\rho c + \rho c_w M} + \frac{h_v + c_v(T_a - T)}{\rho c + \rho c_w M} G_a \frac{\partial H}{\partial z} \tag{2.69}$$

$$\frac{\partial M}{\partial t} = \text{an appropriate thin layer equation.} \tag{2.70}$$

where: $G_a = v_a \rho_a$ is the air mass flow rate per unit area (air mass-flux).

Spencer (1969) presented a PDE grain drying model for a stationary deep-bed, but derived it based on premises different from the above model. He used the following assumptions in deriving his model:

(i) thermal properties of dry grain, moisture, and air are constant,

(ii) conduction heat transfer within the deep-bed is negligible,

(iii) the effect of condensation within the deep-bed is negligible, and

(iv) the problem is one dimensional.

The model also consists of four partial differential equations, and is based on an elemental volume of unit area and depth, *dz*.

$$v_a \frac{\partial \rho_v}{\partial z} + \varepsilon \frac{\partial \rho_v}{\partial t} = \rho(1 - \varepsilon) \frac{\partial M}{\partial t} \tag{2.71}$$

$$c_a \left(G_a \frac{\partial T_a}{\partial z} + \varepsilon \rho_a \frac{\partial T_a}{\partial t} \right) = h(T - T_a) \tag{2.72}$$

$$\frac{\partial \theta}{\partial t} = \frac{h(T_a - T) + h_v(1 - \varepsilon)\rho \dfrac{\partial M}{\partial t}}{(c + c_w M)(1 - \varepsilon)\rho} \tag{2.73}$$

$$\frac{\partial M}{\partial t} = f(M, M_e, T, t, ..) \tag{2.74}$$

Sharp (1982) reviewed low temperature grain drying models for stationary beds. He presented a model based on an elemental bed of unit cross-sectional area with respect to airflow. By

conducting the energy and mass balances, similar to Bakker-Arkema *et al*, (1967), he presented the following set of partial differential equations for describing drying of grain in a stationary bed:

$$G_a \frac{\partial H}{\partial z} = -\rho \frac{\partial M}{\partial t} - \varepsilon \rho_a \frac{\partial H}{\partial t} \tag{2.75}$$

$$G_a (c_a + c_v H) \frac{\partial T_a}{\partial z} = \rho c_v (T_a - T) \frac{\partial M}{\partial t} - h(T_a - T) - \rho_a \varepsilon (c_a + c_v H) \frac{\partial T_a}{\partial t} \tag{2.76}$$

$$\rho (c + c_w M) \frac{\partial T}{\partial t} = h(T_a - T) + h_v \rho \frac{\partial M}{\partial t} \tag{2.77}$$

$$\frac{\partial M}{\partial t} = -K(M - M_e) \tag{2.78}$$

Sharp suggested that the terms containing $\frac{\partial T_a}{\partial t}$ and $\frac{\partial H}{\partial t}$ in the above set of equations can be neglected, in which case the resulting set of equations will be very similar to the model of Bakker-Arkema *et al*, (1967).

2.7.2.2 Equilibrium models

Under equilibrium conditions, the simplifying assumptions reduce the four equations in the partial differential equation model to two equations based on balances of moisture content in the grain and air humidity. For heat and mass equilibrium between the moist air and the grain throughout the stationary deep-bed, it is assumed that there is no resistance to heat and mass transfer within this bed. It is also assumed under equilibrium analysis that the air temperature is equal to the grain temperature. In equilibrium model analysis it is further assumed that under mass equilibrium M is equal to M_e (Cenkowski *et al*, 1993).

Thompson *et al*, (1968) developed an equilibrium grain model based on the empirical formula of the type

$$t = A\ln MR + B(\ln MR)^2 \tag{2.79}$$

where MR is the moisture content ratio.

2.7.2.3 Logarithmic models.

The logarithmic drying models are based on direct relationship between the rate of drying of a layer of grain in a deep bed, $\partial M/\partial t$, and the temperature gradient $\partial T_a/\partial z$ across this layer. This relationship can be derived from partial differential equations describing grain drying in a deep-bed presented by Sharp (1982). According to Cenkowski *et al*, (1993), these models have a low prediction accuracy yet most researchers still use them because of their simplicity.

Assuming a unique relationship between the rate of moisture content change with time in deep bed drying, and the temperature change of air with respect to position, Hukill (1954) developed an equation and a series of a dimensionless curves to predict the moisture content at any depth in a grain mass after a specified drying time as:

$$MR = \frac{M - M_e}{M_o - M_e} = \frac{2^D}{2^D + 2^Y - 1} \tag{2.80}$$

D = dimensionless depth factor

Y = dimensionless time.

One depth factor is defined as the depth of crop that contains, DM' of dry matter content given by

$$DM' = \frac{G'C_a(T_a - T_g)t_{1/2}}{vh_{fg}(M_{in} - M_e)} \tag{2.81}$$

where G' is the volumetric flow rate (m^3/s), and $t_{1/2}$ is the time for crop with a depth factor of zero to dry from a moisture ratio of 1.0 to a moisture ratio of 0.50. The depth factor of zero represents the drying of crop in a very thin layer. Also T_a and T_g represent the air temperature at inlet and outlet respectively. The dimensionless time, Y, is defined as

$$Y = t / t_{1/2} \tag{2.82}$$

where t is the drying time.

Equation (2.82) is referred to as the logarithmic model. Barre *et al* (1971) applied the modified form of Hukill's logarithmic model to cross-flow, low-temperature deep bed grain (ear corn) drying, and subsequently Barre and Hamdy (1974) employed the model to determine the optimal filling rates for in-storage drying of grain. Barre *et al* (1971) obtained quite good agreement between observed and predicted mean moisture contents for ear corn. Sabbah *et al* (1979) used a logarithmic model to simulate, forced-convection solar grain drying performance.

It may be concluded from the above that the equilibrium and logarithmic models are nothing but simplified variants of the partial differential equation models. It will therefore not be contentious if drying models are based non-equilibrium models.

KNUST

2.8 Solar Drying:an overview

2.8.1 Dryer construction and functionality

The main functional part of a solar dryer is the drying space, where the drying process takes place. In directly irradiated solar dryers, the energy is absorbed directly by the drying material. In this case the drying space has a transparent (glass or foil) cover.

In solar convective dryers, the drying medium is air preheated by solar energy in a collector, which converts solar radiation into heat. In direct heat transfer systems, the working fluid of the solar collector is the drying air itself. In the case of indirect systems, the working fluid is a liquid (e.g. water) and a liquid-air heat exchanger is used to preheat the drying air. This can be kept in motion by means of a fan driven by an electric motor. The latter is normally connected to the power grid or, in more remote rural areas, to an autonomous photovoltaic system or a wind turbine driven electric generator (Esper and Muhlbauer, 1993; Bansal and George, 1993). A chimney can also be connected to the drying space to induce air flow through a thermosyphon effect (Ekechukwu and Norton, 1993).

2.8.1.1 Main types of solar dryers

Solar dryers can be classified into three main groups, according to the type of energy used for drying and the equipment employed (1mre, 1988a, 1989, 1993, 1995):

- Solar natural dryers
- Semi-artificial solar dryers
- Solar-assisted dryers

(a) Solar natural dryers. These devices use only ambient energy and have no active elements. The air flow, if there is any, is maintained by natural convection or, in some cases, by themosyphon effects induced by a chimney.

KNUST

Solar natural dryers are mainly used as substitutes for traditional open-air drying methods in areas where no other source of energy is available. In contrast to these traditional methods, however, losses and damage to the product caused by rain, dust, insects, birds and other animals, as well as the pollution from the atmosphere are avoided by the purpose built construction. Their use results in a better quality product, which should be considered as a positive cash contribution in any economic evaluation.

(b) Solar-assisted dryers. Solar assisted dryers are conventional dryers having a solar collector. They are generally fitted with a heat storage system and are always fitted with an auxiliary energy source, such as a thermo-generator fuelled by natural gas or oil, for use in situations where the solar energy collected is insufficient for drying purposes. They are normally fitted with modern control systems.

2.8.1.2 Solar natural dryers

(a) Cabinet dryers. These are the simplest and cheapest type of solar dryer. They are generally used for drying agricultural products, such as fruits, herbs, vegetables, and spices, in small quantities (Wibulswas and Niyomkarn, 1980; Reuss, 1993).

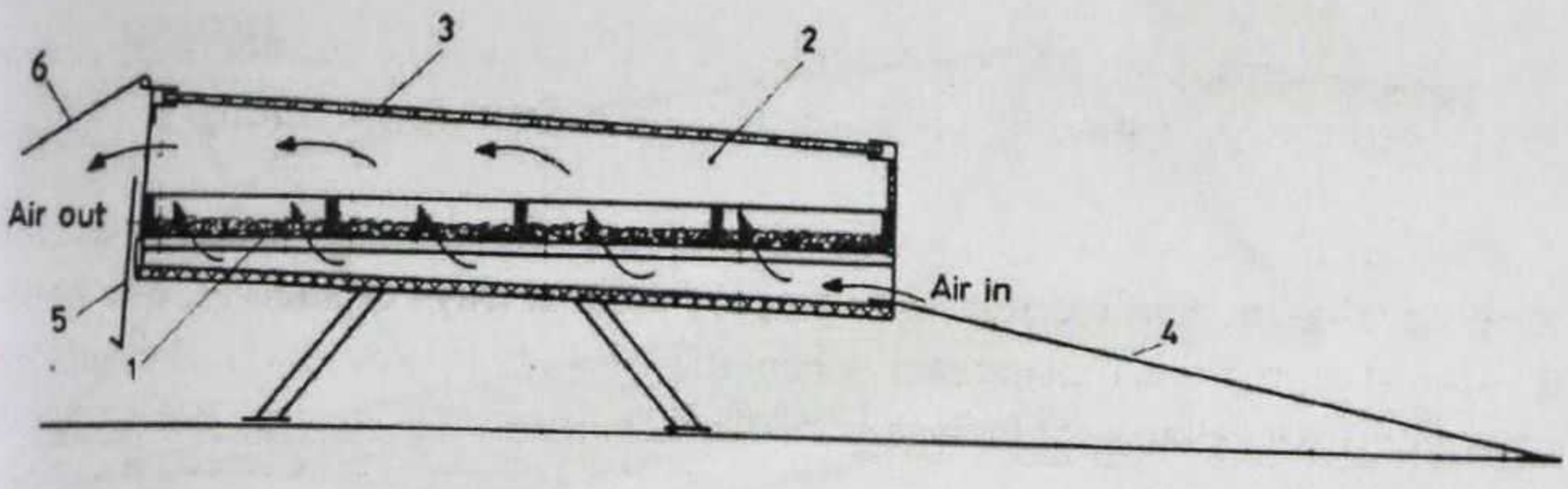

Figure 7 Cabinet type dryer for fruit and herbs

Simple cabinet dryers consist of a south-facing drying space covered by a transparent material, which also serves as a roof to protect against rain and pollution. The material to be dried is spread in a thin layer on a tray having a perforated bottom and is directly exposed to the solar radiation. Holes are provided in the lower part of the front wall and in the upper part of the back wall of the cabinet to induce an air flow by natural convection. This carries away the water evaporated from the material and prevents its overheating.

An improved version of the simple cabinet dryer designed for household use is illustrated in Figure 7.The trays with perforated bottoms 1 are arranged under the transparent cover3, making it possible to dry simultaneously various kinds of foodstuffs, such as fruits, herbs and vegetables. Each product, in its individual tray, may have its own specific drying time. Air, preheated by a black-painted aluminum sheet 4, is introduced into the dryer and regulated by the throttling device 5 and 6. The open cross-sectional area of the air outlet can gradually be decreased as drying proceeds. At night time, the slide 6 should be closed and the sheet 4 should be fitted to the transparent cover of the cabinet 2 (Baker, 1997).

(b) Tent type dryers. The drying capacity of cabinet type dryers can be increased by enlarging the basic surface area of the dryer. Tent type dryers represent the simplest and cheapest way to achieve this goal. A schematic representation of a tent type solar dryer is shown in Figure 8. The drying space 2 is located within a tent, which may have a triangular or semi-circular cross-section. The south-facing surface of the over 1 should be transparent; the other sides are opaque. The material to be dried (e.g. coffee beans) is spread on a perforated tray 3 or directly on a concrete floor (Sunworld, 1980).

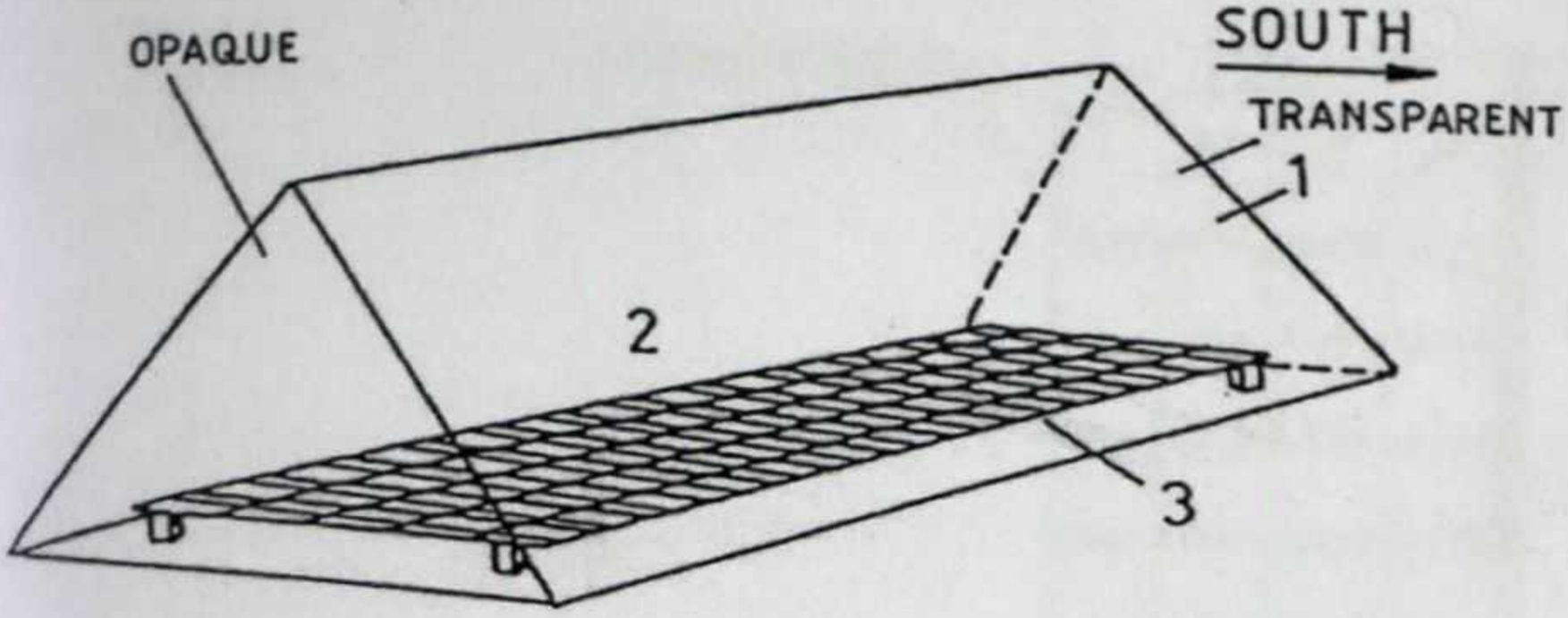

Figure8 Tent type solar dryer

(c) Shelf type dryers. Another way to increase the drying capacity, without enlarging the basic surface area, is to employ several trays or shelves, one above the other. Figure 9 illustrates a schematic of a shelf type dryer (Wibulswas and Niyomkarn, 1980). Thin layers of fruit, vegetables, etc. to be dried are loaded on the perforated shelves 1. The south-facing surfaces 2 of the dryer are transparent; the back wall 3 and the floor are painted black and insulated. Since the lower trays or shelves partly shade each other, a separate solar collector 4 should be connected to the drying space to produce the energy required. Air flow is generated by natural convection through the collector and the material layers on the shelves; moist air leaves the dryer through the upper opening 5.

In the shelf type arrangement, the flow resistances of the separate material layers are coupled in series and the total resistances is their sum. To ensure satisfactory air flow rate, the height of the dryer should be sufficient to produce an adequate chimney effect.

KNUST
WJSANE NO BADWENHWA

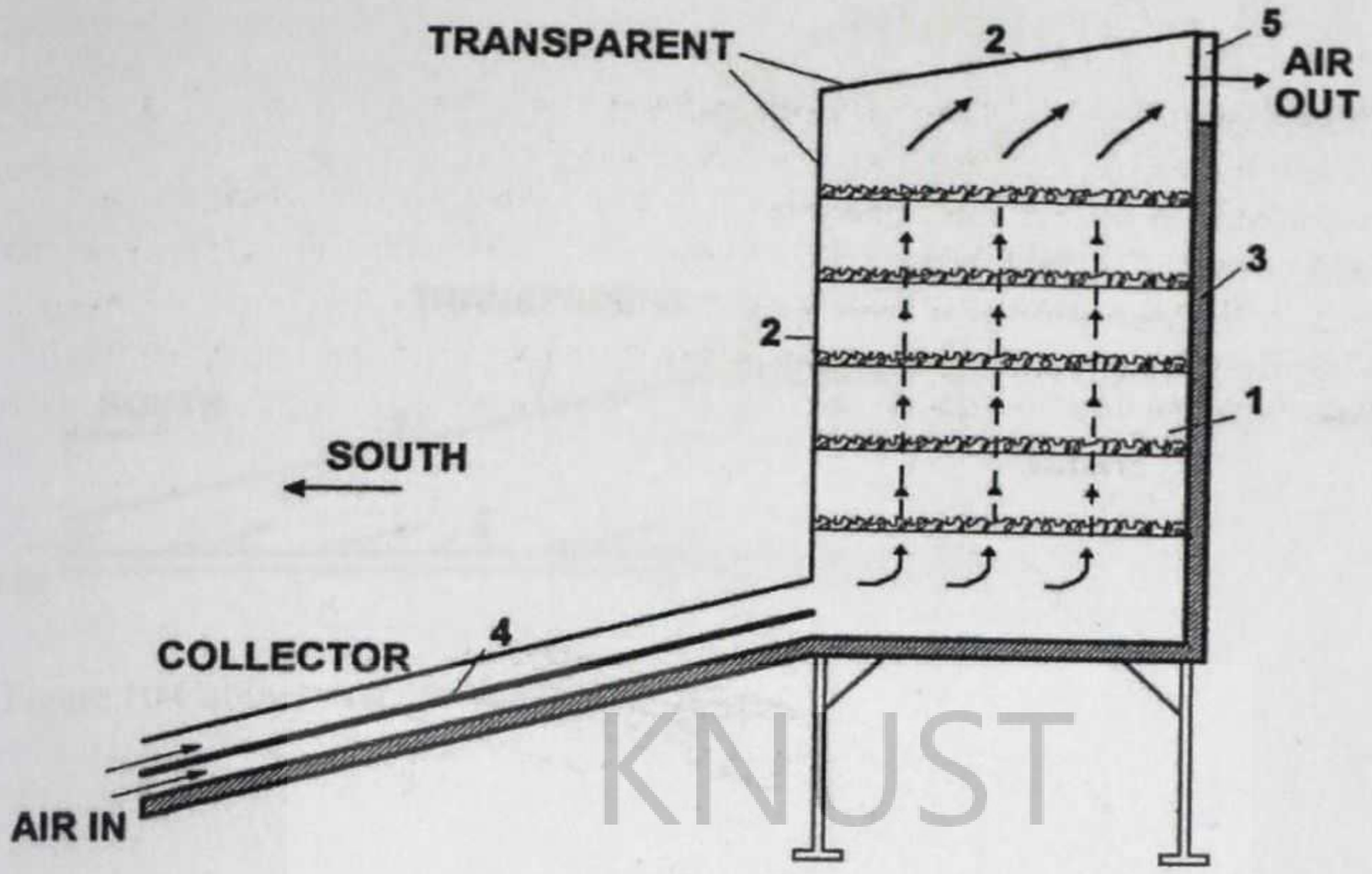

Figure 9 Shelf type cabinet dryer

2.8.1.3 Cabinet dryers fitted with a chimney

The themosyphon effect required to induce an adequate flow through a solar dryer can be increased by means of a chimney. A simple version of a chimney type solar dryer is presented in Figure 10 (Sunworld, 1980). The lower part of the dryer acts as an integrated solar collector with a transparent cover 2; the bottom surface 4 functions as an absorber. Material to be dried is arranged in a static bed 1. Cover 3 over the bed is also transparent. Chimney 5 is connected to the upper part of the drying space. Drying time (at 15 $MJm^{-2}day^{-1-}$ mean global irradiation), 3-4days

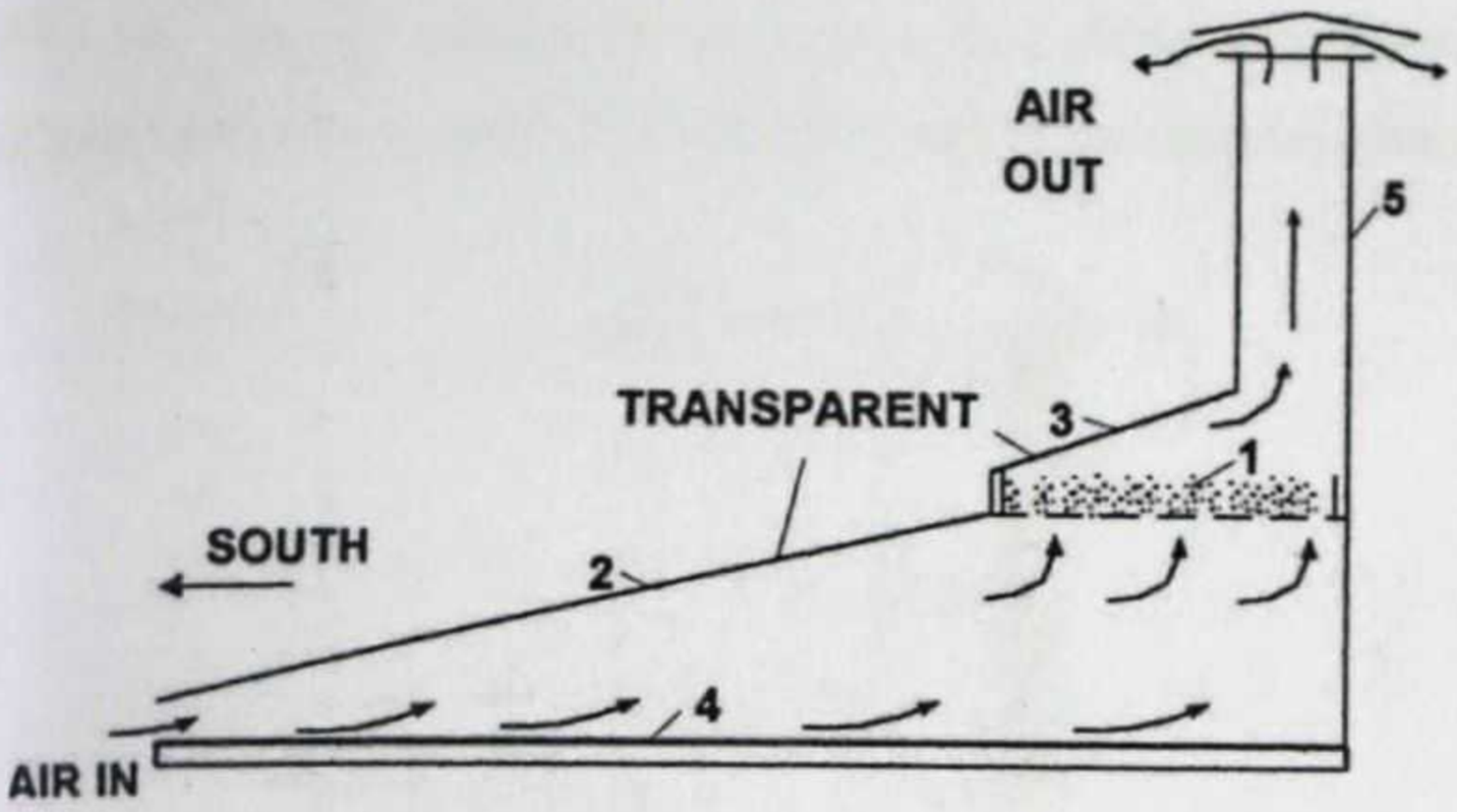

Figure 10 Cabinet dryer with chimney

KNUST

2.8.1.4 Cabinet dryers fitted with a chimney and heat storage

To extend the drying process into the non-sunny hours of the day, heat storage should be employed. Water vessels have been used as a relatively low cost means of heat storage (Puigalli and Lara, 1982).

Sensible-heat storage capacity can be increased by using phase change materials. Figure 11 shows a simplified schematic of a chimney type cabinet dryer in which calcium chloride hexahydrate ($CaCl_2.6H_2O$) is employed for this purpose (1mre, 1986b, 1989). The phase change material is enclosed in plate shaped containers. The fixed latent heat storage plates 4 are arranged as the absorber of the separate collector 2, and of the northern wall of the chimney as well. The outer-wall surfaces 6 of the chimney 3 are thermally insulated. Additional heat storage plates 5 are movable and arranged below the cover of the collector. In sunny hours, these plates 5 are pulled out of the collector on both sides and are directly irradiated and charged. During night-time operation, they are pushed back below the collector covering (see figure), forming an air duct with hot upper and lower surfaces. Since the phase change process occurs at constant temperature, a constant thermosyphon effect and a continuous air flow through the dryer will be maintained until the heat storage unit has been fully discharged. The material to be dried is spread in thin layers on trays 7 having perforated bottoms located in the drying space 1. Upper and lower trays can be exchanged during drying to equalize differences in drying rates. The air

flow rate through cabinet dryers fitted with a chimney can also be enhanced by using a wind-driven ventilator connected to the upper end of the chimney (Bansal and George, 1993).

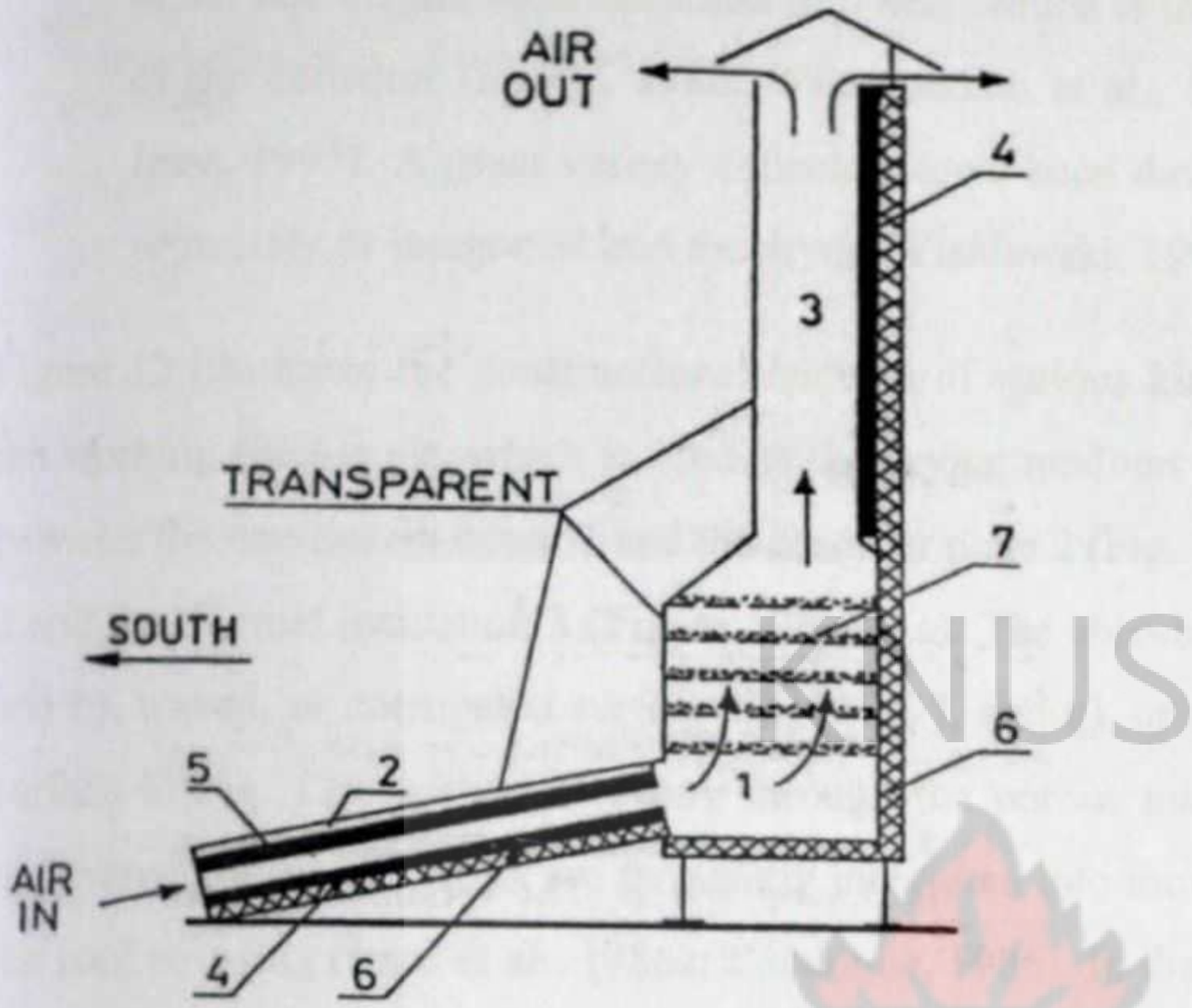

Figure 11 Cabinet dryer with chimney and latent heat storage

KNUST

2.8.1.5 Structural design of solar dryers

In order to undertake the structural design of a solar dryer, it is essential to be aware of the technological capability of the dryer manufacturer. Therefore, the designer should keep close contact with the technical and production staff at the factory. The structural design will greatly influence the investment and maintenance costs as well as the service life of the dryer. These factors have a major influence on the return on investment.

(a) Selection of the materials of construction. The materials of construction of the structural elements is of great importance. The designer should consider:

- the UV effects of the solar radiation;
- possible counter-effects between the structural elements and the material to be dried
- The corrosive effects of the atmosphere

(b) Structural design of the solar collector. The solar collector serves to provide the primary supply of energy to the dryer. Essentially, the absorber within the collector converts the direct and diffuse solar radiation into heat, which is then transferred to the working fluid of the collector (Lunde, 1980; Wijeysundera et al., 1982; Duffie and Beckman, 1993; Imre, 1995). A great variety collectors have been developed. These can either be used separately or integrated into the dryer (Wisniewski, 1993).

Figure 12 illustrates the constructional features of various kinds of solar collector. Frequently, the working fluid is air, which is used as the drying medium (Direct type solar dryers). It flows between the transparent cover 1 and the absorber plate 2 (Fig. 12a), or between the absorber plate 2 and the thermal insulation 3 (Figure 12b and c). The absorber 2 may have a plane (Figure 12a and b), waved, or corrugated surface (Fig. 12c, f, and g), or a stepwise divided and overlapped surface in Fig. 12e, with air flowing through the porous matrix. Figures 12f and g illustrate uncovered collectors, which are frequently integrated into the rood of a drying room and used as the roof covering (Imre et al., 1986a; Catalogue, 1986). In the case of solar dryers incorporating an indirect heat transfer system and heat storage, the collector working fluid is usually water or antifreeze solution, flowing in the tubes of the tube sheet type or finned tube type (Figure 12h) absorber.

KNUST

LIBRARY
KWAME NKRUMAH
UNIVERSITY OF SCIENCE & TECHNOLOGY
KUMASI

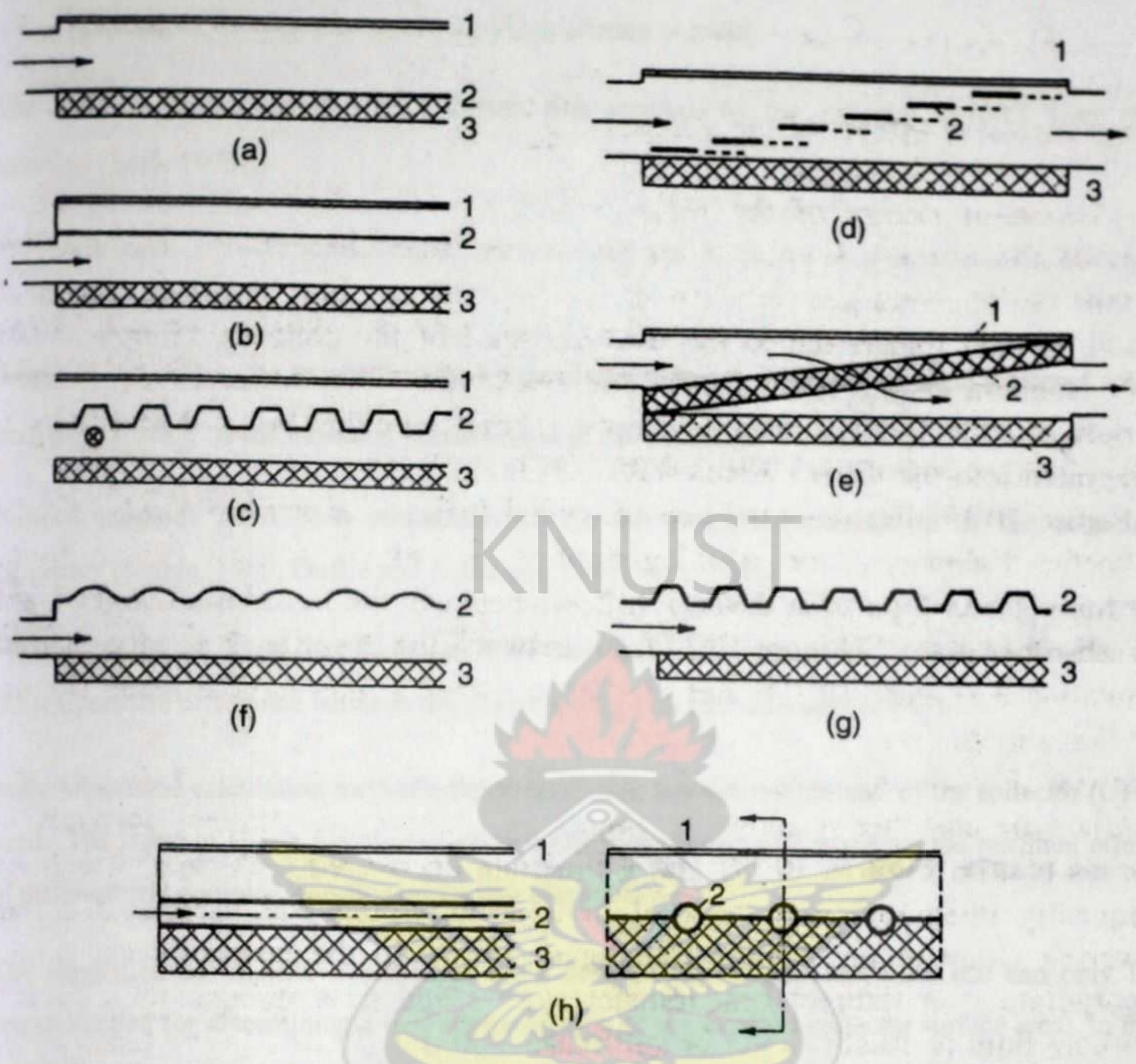

Figure 12 Solar collectors: (1) transparent cover; (2) absorber; and (3) thermal insulation (Source: Baker, 1997).

In hybrid (air-liquid) collectors, air is directed between the transparent covering and the liquid absorber. In combined collectors, latent heat storage elements serve as absorber (Imre and Kiss, 1983; 1mre, 1995). The materials of construction commonly used in solar collectors are as follows.

- Transparent covering; glass, UV stabilized plastic or foil
- Absorber, with air as working fluid: aluminum, copper, steel, UV stabilized plastic; with water as working fluid: copper, UV stabilized plastic.

- Coating of the absorber: selective black coating or paint.

The designer should determine the energy flux required by the collector, ϕ_u (W), from the equation (Imre, 1995):

$$j_u = \xi A_c I \quad \text{.....(2.90)}$$

Where A_c (in m^2) is the required surface area of the collector, I (in Wm^{-2}) is the expected solar energy flux, and ξ is the expected effectiveness of the collector.

Various methods have been recommended for the simplified calculation of the collector efficiency (Lunde, 1980; Duffie and Beckman, 1993; Imre, 1995).

These methods are based on calculation of the heat loss from the collector, which is a function of the temperature difference between the absorber (T_{abs}) and the atmosphere (T_a).

In the simplified calculation methods, the 'overall heat transfer coefficient' of the collector (U) is used. The value of U is a function of several other parameters and describes the resultant effect of different and complex non-linear heat transfer processes.

The simplified calculation methods do have several weak points and their use can only be recommended for determining a first approximation of the required collector surface area. In the detailed design phase, the performance of the collector should be checked using computer simulation methods (Imre, 1974, 1995; Imre and Kiss, 1983; Mahapatra and Imre, 1995). These methods can also be used to undertake a sensitivity analysis and to optimise the design.

2.9 Crop dryer modeling equations and reviews

This section examines other pertinent theories used in the modelling and analysis of solar crop drying systems. Additionally, the section also reviews relevant studies conducted in the area of solar crop drying involving the use of back up heating.

2.9.1 Formulation of the drying model

The deep-bed drying process is approached by writing energy and mass balance equations on an arbitrary elemental layer of the fixed crop bed. The drying of this element can be simulated by considering changes that occur in the crop and the drying air as represented in figure 13. The drying air is passed through this elemental layer of crop for a time interval (Δt). During this period, moisture is evaporated from the crop bed into the drying air causing the moisture content of the crop to decrease and the absolute humidity of the air to increase. For a specified air flow rate, the values of the following variables are determined after each incremental drying period (Δt): T, the drying air temperature; T_{pt}, the crop temperature; H, the absolute humidity of the drying air; and M, the average moisture content.

KNUST

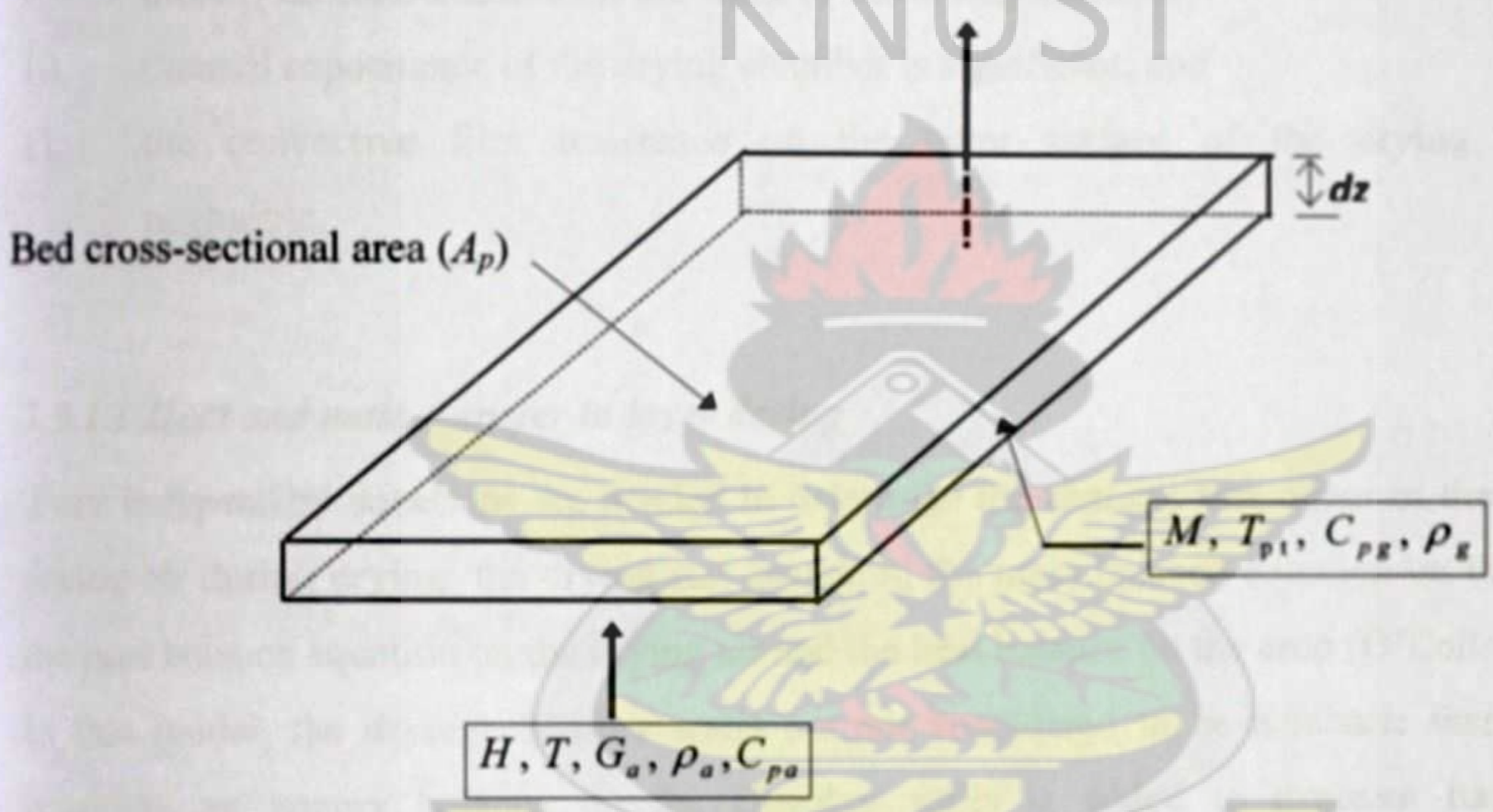

Figure 13: Elemental volume of crop bed

In deriving the mathematical model for analysing the drying process, the following assumptions are made:

1. no temperature gradients exist within individual pieces of crop material;
2. conduction between adjacent crop slices is negligible;
3. changes in heat capacities of the air and of the wet crop during the short time interval of the passage of drying air are negligible;

4. the changes in temperature and humidity of air over an elemental layer of the crop bed are more significant than the changes that occur in a short time interval;
5. at the commencement of the drying process, the drying air displaces all air within the dryer without heat or mass transfer taking place. This assumption although not exact, it allows for the initial boundary conditions of the process to be specified;
6. moisture evaporated from the crop is at a temperature equal to that of the drying material;
7. the crop-bed is a rectangular slab with void spaces;
8. the change in enthalpy of the air trapped in the crop-bed void spaces is negligible compared to the change in the enthalpy of the flowing air.
9. there is no condensation on the walls of the drying chamber;
10. thermal capacitance of the drying chamber is significant; and
11. the convective film resistance on the outer surface of the drying chamber is negligible.

KNUST

2.9.1.1 Heat and mass transfer in layer drying

Four independent equations are needed to determine the changes that occur in the product and drying air during drying: the drying rate equation, the mass balance equation on the drying air, the heat balance equation on the drying air and the heat balance on the crop (O'Callaghan, 1971). In this model, the drying chamber walls are not considered to be adiabatic therefore a fifth equation, an energy balance on the chamber walls is added to evaluate its steady-state temperature. These five equations are derived as explained in the subsequent sections.

2.9.1.2 The drying rate equation

The rate of moisture removal from pineapple can be expressed by the diffusion equation, (equation 2.5) which describes the removal of water vapour from the wet product. The solution of this equation for a slab-shaped crop bed is given as (Crank, 1975):

$$\frac{\overline{M} - M_e}{M_o - M_e} = \frac{8}{\pi^2} \sum_{n=0}^{\infty} \frac{1}{(2n+1)^2} \exp\left[-(2n+1)^2 D\pi^2 t / z^2\right] \qquad (2.84)$$

LIBRARY
KWAME NKRUMAH
UNIVERSITY OF SCIENCE & TECHNOLOGY
KUMASI

where, D is the diffusion coefficient of the wet material, z is the thickness of the crop bed and t is the drying time. A simplified solution is sought by using the first few terms of the series solution of equation (2.84). The diffusion coefficient chosen for pineapple is an Arrhenius-type expression which expresses the dependence of diffusion coefficient at high moisture levels with temperature of the material being dried.

$$D = D_o \exp(-E / RT_g) \qquad (2.85)$$

This relation is chosen because of the high initial moisture content of fresh pineapple and its use is supported by literature (Shahab et al, 2007). Shahab et al (2007) determined the effective diffusivity (D_o) and activation energy (E) for pineapple to be in the order of 10^{-10} m^2/s and 35.5 kJ/mol respectively. A power law equation was used to correlate the shrinkage in thickness with the moisture content of the sample.

KNUST

A generalised empirical relation is used to describe the equilibrium moisture content isotherm for pineapple. This relation is of the form (Teter and Citelly, 1970; Roa, 1974):

$$\ln\left(\frac{M_e}{p_o + p_1 RH + p_2 RH^2 + p_3 RH^3}\right) = q_o + \left(q_1 + q_2 RH + q_3 RH^2 + q_4 RH^3 + q_5 RH^4\right)T \quad (2.86)$$

In equation (2.86), $p_i$and q_i are product-dependent constants.

2.9.1.3 Mass balance equation on the drying air

The mass balance equation relates the exchange of moisture between material being dried and the drying air. Consider an element of material in a deep-bed dryer and the associated quantities (see figure 13). Under steady-state, the difference between the amount of moisture flowing into and out of the control volume during the time interval *dt* is equal to the moisture leaving the material in the control volume. The change in humidity of the air in the void spaces can be neglected (Brooker *et al*, 1974).

Under steady-state, assuming no condensation on the walls of the drying chamber, the mass balance on the control volume is

$$G_a A_p H dt - G_a A_p (H + \frac{\partial H}{\partial z} dz) dt = \rho_p A_p dz \frac{\partial M}{\partial t} dt \quad (2.87)$$

which simplifies to:

$$G_a \frac{\partial H}{\partial z} = -\rho_p \frac{\partial M}{\partial t} \quad (2.88)$$

where, G_a (kg/s-m^2) is the mass-flux of air through the drying chamber and is related to the mass-flow rate and the effective cross-sectional area of the drying chamber by the relation:

$$G_a = \frac{\dot{m}}{A_{dc}} \quad (2.89)$$

KNUST

2.9.1.4 Heat balance on the drying air

Energy balance on air:

the change in enthalpy of the air = heat lost to the product and the drying chamber + heat carried by vapour to the air.

The enthalpy of the air flowing into the control volume in time dt at location z is

$$G_a A_p \left[\left(C_{pa} + C_{pw} H(z) \right) T(z) + L_a H(z) \right] dt$$

Similarly, the enthalpy of the air flowing out of the control volume in the same time dt from location $(z + dz)$ is

$$G_a A_p \left[\left(C_{pa} + C_{pw} H(z + dz) \right) T(z + dz) + L_a H(z + dz) \right] dt$$

But the heat lost from the drying air to the product and the walls of the drying chamber is

$$= \left[h_v A_p \left(T - T_{pt} \right) + h_v A_w (T - T_w) \right] dz\, dt$$

Assuming that moisture is evaporated from the wet material at the same temperature of the crop, the gain in enthalpy of vapour during the passage of air through a crop bed in time (dt) is given by

$$\left(C_{pw}T_{pt} + L_a\right)\rho_p A_p \frac{\partial M}{\partial t} dz\, dt$$

The change in enthalpy of the drying air is given by the difference between the enthalpies of the air flowing into and out of the control volume as:

$$G_a A_p\left[\left(C_{pa} + C_{pw}H(z)\right)T(z) + L_a H(z)\right] dt$$

$$G_a A_p\left[\left(C_{pa} + C_{pw}H(z+dz)\right)T(z+dz) + L_a H(z+dz)\right] dt$$

KNUST

Simplifying and re-arranging the terms of the mathematical statement of the energy balance for the drying air results in the relation:

$$G_a A_p\left[\left(C_{pa} + C_{pw}H\right)\frac{\partial T}{\partial z} + C_{pw}T\frac{\partial H}{\partial z} + L_a\frac{\partial H}{\partial z}\right]dtdz$$

$$= -h_v A_p(T - T_{pt})\,dtdz - \left(\rho_p C_{pw}T_{pt} + \rho_p L_a\right)A_p\frac{\partial M}{\partial t}dtdz - h_v A_w\left(T - T_w\right)dtdz \quad (2.90)$$

Substituting equation (2.86) into equation (2.90), the following expression relating the average temperature, T, at which air transfers heat in the control volume, to the drying conditions is obtained as:

$$\frac{\partial T}{\partial z} = \frac{1}{G_a(C_{pa} + C_{pw}H)}\left[h_v\left(T_{pt} - T\right) + \rho_p C_{pw}\left(T - T_{pt}\right)\frac{\partial M}{\partial t} - \frac{h_v A_w}{A_p}(T - T_w)\right] \quad (2.91)$$

2.9.1.5 Heat balance on the wet material

In writing the energy balance on the wet material, it is assumed that the external energy supplied to the drying chamber is used by the wet material and the drying chamber walls during the drying period in the following ways:

- heat to evaporate moisture from the wet material and heat to raise the evaporated moisture temperature to that of the drying air
- heat to raise the temperature of the dry solid and its residual moisture
- heat lost from the crop through the chamber walls to the surrounding
- heat to raise the temperature of the drying trays and the chamber walls.

It is further assumed that the moisture evaporated from the wet material in time (dt) is carried away by the drying air.

Thus,

the change in enthalpy of the crop = convective and radiant energy transferred to the crop − Heat supplied to evaporate the moisture from the wet material to the drying air − Heat lost from the crop to the chamber walls by radiation −radiation heat exchange from a layer of the crop bed to the adjacent layer(s).

In addition to convective heat from the solar/burner heated air passing through the elemental layer, solar energy is transferred directly to the top layer by radiation from the top and through the sides of the drying chamber to all other layers. As a result, the effective surface temperature of the wet material will rise above the wet-bulb temperature of the air and this will subsequently reduce the rate at which heat is drawn from the heated air, but will increase the rate of evaporation. The incident solar energy absorbed by an elemental layer at the top layer is progressively reduced by the absorptance-transmittance factor of the subsequent layers. Following from this assumption, the intensity of solar radiation on each layer, $\overline{H}_s$ is approximately modeled as an exponential decaying function with its maximum value, $\overline{H}_T$ at the top layer and one-half its maximum halfway through the entire bed and is represented by

$$\overline{H}_s = \overline{H}_T \exp(2\ln 2\{JM(dz)/z_o - 1\}) \tag{2.92}$$

At the beginning of the time step t, the enthalpy of the material is

$$A_p \rho_p dz\{C_{pg} + C_{pl} M(t)\} T_{pt}(t)$$

and at time $t+dt$, is

$$A_p \rho_p dz\left(C_{pg} + C_{pl} M(t)\right)\ T_{pt}(t+dt)$$

The difference in the enthalpy of the material is given by

$$\rho_p\left(C_{pg} + C_{pl} M\right) A_p dz \frac{\partial T_{pt}}{\partial t} dt$$

The amount of moisture evaporated in the time dt is equal to the change in the humidity ratio of the air as it passes through the elemental volume, $A_p dz$, of the crop bed and is given as

$$G_a\ A_p dz \frac{\partial H}{\partial z} dt$$

The energy required for the evaporation of moisture from the wet material in the time dt is

$$L_a\, G_a\ A_p \frac{\partial H}{\partial z} dz\, dt$$

The energy required for heating the moisture evaporated from the wet material at temperature T_{pt} to air temperature in time dt is

$$C_{pl}(T - T_{pt})\, G_a\ A_p dz \frac{\partial H}{\partial z} dt$$

The energy required to raise the temperature of the mass of the drying chamber is given by

$$C''m'' \frac{\partial T_{pt}}{\partial t} dz\, dt$$

The enthalpy balance on the wet material is

$$(\rho_p A_p(C_{pg} + C_{pl} M) + C''m'') \frac{\partial T_{pt}}{\partial t} dt\, dz = \alpha_p \tau_p \overline{H}_s\ A_{sc} dt\, dz + h_v A_{dc}(T - T_{pt}) dt\, dz$$
$$-\rho_p A_p \frac{\partial M}{\partial t}\left[C_{pl}(T - T_{pt}) + L_g\ \right] dt dz - h_{rpw} A_w (T_{pt} - T_w) dt\, dz \qquad (2.93)$$

$$\frac{\partial T_{pt}}{\partial t} = \frac{1}{\rho_p(C_{pg} + C_{pl} M) + C''m''}\left[\alpha_p{}^{i} \tau_p \frac{\overline{H}_s}{\cos\beta} + \frac{h_v A_w}{A_p}(T - T_{pt})\right.$$
$$\left. G_a \frac{\partial H}{\partial z}\left[C_{pl}(T - T_{pt}) + L_g\ \right] - \frac{h_{rpw} A_w}{A_p}(T_{pt} - T_w)\ \right] \qquad (2.94)$$

KNUST

2.9.2 *Energy balance on the walls of the drying chamber*

Performing an energy balance on the drying chamber walls under load conditions yields

$$\alpha \bar{S}_c A_{w_T} + h_v A_{w_p}(T - T_{dw}) + h_{r_{pw}} A_{w_p}(T_{pt} - T_{dw}) = h_{r_{ws}} A_{w_p}(T_{dw} - T_{sk}) + h_w A_{w_p}(T_{dw} - T_a) \quad (2.95)$$

It is assumed that there is no condensation on the inner surface of the cover of the drying chamber. The above equation is used to establish the temperature of the walls of the drying chamber as:

$$T_{dw} = \frac{\alpha_c \bar{S}_c + h_{r_{pw}} T_{pt} + h_{r_{ws}} T_s + h_w T_a + h_v T}{h_w + h_{r_{ws}} + h_v + h_{r_{pw}}} \quad (2.96)$$

KNUST

2.9.3 *Finite difference formulation of the drying simulation model.*

The finite difference numerical technique is used to discretise the governing equations of the deep-bed drying mathematical model. A first-order implicit finite difference scheme (in both time and space), is employed to solve the governing equations described. The dependent variables (H and T) are to be evaluated at the time ($t + dt$). The independent variables (M and T_{pt}) are evaluated as the mean value of each layer representative of a given time interval. The following definitions are also applied in arriving at the finite difference model:

$$T_{z+\frac{1}{2}\Delta z, t+\Delta t} = \frac{T_{z+\Delta z, t+\Delta t} + T_{z, t+\Delta t}}{2} \quad (2.97)$$

$$H_{z+\frac{1}{2}\Delta z, t+\Delta t} = \frac{H_{z+\Delta z, t+\Delta t} + H_{z, t+\Delta t}}{2} \quad (2.98)$$

$$\frac{\partial M}{\partial t} = \frac{M_{z+1/2\Delta z, t+\Delta t} - M_{z+1/2\Delta z, t}}{\Delta t} \quad (2.99)$$

$$\frac{\partial H}{\partial z} = \frac{H_{z+\Delta z, t+\Delta t} - H_{z, t+\Delta t}}{\Delta z} \quad (2.100)$$

$$\bar{M} = M_{z+1/2\Delta z, t+\Delta t} \quad (2.101)$$

$$\overline{T} = T_{z,\,t+\Delta t} + T_{z+\Delta z,\,t+\Delta t} \tag{2.102}$$

Equations (2.91), (2.95), (2.98), and (2.102) can be written as

$$M_{z+1/2\,\Delta z,\,t+\Delta t} = M_e + (M_o - M_e)\frac{8}{\pi^2}\sum_{n=0}^{\infty}\frac{1}{(2n+1)^2}\exp\left[-(2n+1)^2\, D\pi^2 t / z^2\right] \tag{2.103}$$

$$H_{z+\Delta z,\,t+\Delta t} = H_{z,\,t+\Delta t} - \frac{\rho_p}{G_a}\frac{dz}{dt}\left(M_{z+\frac{1}{2}\Delta z,\,t+\Delta t} - M_{z+\frac{1}{2}\Delta z,\,t}\right) \tag{2.104}$$

$$\frac{T_{z+\Delta z,\,t+\Delta t} - T_{z,\,t+\Delta t}}{dz} = \frac{1}{G_a\left(C_{pa} + C_{pw}\,H_{z+\frac{1}{2}\Delta z,\,t+\Delta t}\right)}\left[\begin{array}{l} h_v\left(T_{pt\,z+\frac{1}{2}\Delta z,\,t+\Delta t} - T_{z+\frac{1}{2}\Delta z,\,t+\Delta t}\right) + \\ \rho_p C_{pw}\left(T_{z+\frac{1}{2}\Delta z,\,t+\Delta t} - T_{pt\,z+\frac{1}{2}\Delta z,\,t+\Delta t}\right)\left(\dfrac{\partial M}{\partial t}\right) \\ -\dfrac{h_v A_w}{A_p}\left(T_{z+\frac{1}{2}\Delta z,\,t+\Delta t} - T_w\right) \end{array}\right] \tag{2.105}$$

$$\begin{aligned} T_{pt\,z+\frac{1}{2}\Delta z,\,t+\Delta t} &= T_{pt\,z+\frac{1}{2}\Delta z,\,t} + [\{\alpha_p{}^{i}\,\tau_g\,\overline{H}/\cos\beta\}dt \\ &+ G_a\Delta t/dz(H_{z+\Delta z,\,t} - H_{z,\,t})(L_g + C_{pl}(T_{pt\,z+\frac{1}{2}\Delta z,\,t} - \frac{T_{z+\Delta z,\,t} + T_{z,\,t}}{2})) - \frac{h_{rws}A_w dt}{A_p}(T_w{}^4 - T_s{}^4) \\ &- \frac{h_{rpw}A_w}{A_p}(T_{pt\,z+\frac{1}{2}\Delta z,\,t} - T_w) + h_v dt(\frac{T_{z+\Delta z,\,t} + T_{z,\,t}}{2} - T_{pt\,z+\frac{1}{2}\Delta z,\,t}) - \frac{h_v A_w dt}{A_p}(\frac{T_{z+\Delta z,\,t} + T_{z,\,t}}{2} - T_w)] \\ &/(\rho_p C_{pg} + \rho_p C_{pl} M_{z+\frac{1}{2}\Delta z,\,t} + C''m'') \end{aligned} \tag{2.106}$$

Additionally, the relative humidity of the drying air is evaluated from the following expressions:

$$P_w = \frac{p(H_{z+\Delta z,\,t+\Delta t} + H_{z,\,t+\Delta t})/2}{(0.62198 + \{H_{z+\Delta z,\,t+\Delta t} + H_{z,\,t+\Delta t}\}/2)} \tag{2.107}$$

$$P_{ws} = C_8 / DTMT + C_9 + C_{10}(DTMT) + C_{11}(DTMT)^2 + C_{12}(DTMT)^3 + C_{13}\ln(DTMT) \tag{2.108}$$

where, $DTMT = (T_{z+\Delta z,\,t+\Delta t} + T_{z,\,t+\Delta t})/2$

and, $RH = \frac{P_w}{P_{ws}}$

2.9.4 Solution procedure

To solve equations (2.103), (2.104), (2.105) and (2.106), the finite difference model, the values of M, H, T and T_{pt} must be initialised at each position within the bed. First the following initial conditions are applied:

$M_{z,0} = M_o$; $H_{z,0} = H_{\text{inlet}}$; $T_{z,0} = T_{\text{inlet}}$; $T_{\text{pt, (z,0)}} = T_{\text{pt, initial}}$; and $T_{pt,(0,0)} = T_{\text{a}}$.

KNUST

Second, equations (2.103), (2.104), (2.105) and (2.106) are solved from the bottom elemental layer to the top layer of the crop bed. This then completes the initialisation process. The temperature of the material at the first time step is estimated as the average of the initial air and product temperature.

The discretised equations are solved as an uncoupled set. After the calculation of the first time step is completed, the following calculations are pursued until the required solution is achieved:

i) Guess the air mass flow rate, $\dot{m}_o$ through the system and the drying chamber wall temperature, T_{dw}

ii) Using equations (3.26) and (3.30), the air mass flow rate, $\dot{m}_o$, through the system is estimated.

iii) Progress the drying time from t to $t + dt$. . The value of increment in time, dt , is calculated using equation (2.109).

iv) Solve equation (2.106) for temperature of the material at the current time.

v) Solve equation (2.103) for moisture content of the material.

vi) Solve equation (2.104) for relative humidity of the drying air.

vii) Solve equation (2.104) for the temperature of the air.

viii) Increase z by dz and repeat steps (iii) through to (vii) until the top layer is reached. Calculate the average moisture content, $\overline{M}$, of the entire crop bed after the time $(t + dt)$. Compare the average moisture content after time $(t + dt)$ with the desired moisture content, $\overline{M}_f$. The program is then terminated subject to the conditions for the termination of the program. Otherwise you go back to step (ii) and then follow the subsequent steps through to step (vii).

The size of the increments dz and dt are critical since their choice will affect the stability of the solution procedure. Bakker-Arkema *et al* (1974) pointed out that if their values are too large, the equations will diverge from the true solution and if too small, the solution will require excessive computation time. To determine the expression for evaluating the time step the mass transfer terms in equations (2.92) and (2.93) are neglected. Furthermore, it is assumed that the change in temperature of the drying air is approximately equal to the change in the temperature of the product; then dividing equation (2.92) by (2.93) an approximate expression for evaluating the time step is obtained as:

$$dt \cong dx \frac{(\rho_p C_{pg} + \rho_p C_{pl} M + C'' m'')\cos\beta}{(G_a C_{pa} + G_a C_{pw} H)\alpha_g \tau_g \bar{H}_s} \qquad (2.109)$$

Equation 2.109 is used to evaluate the time step during the simulation run.

2.9.5 Program termination

The drying model terminates in one of the following ways:

(i) when a desired or specified drying time has been attained (in this programme the time should be less than 30 hours); and /or

(ii) when the average moisture content in the drying bed falls below a specified value.

2.9.6 Technical performance criteria model

In this model, the equations that allow for the assessment of the performance of the dryer are considered. For solar drying, three criteria have been defined (Brenndorfa et al, 1987): the system drying efficiency, and the pick up efficiency.

2.9.6.1 The system drying efficiency, η_d

This parameter is defined as the ratio of the energy required to evaporate the moisture to the energy supplied to the dryer. The energy supplied to the dryer is the quantified as the solar energy incident on energy collection surfaces of the dryer over a given time interval. The system drying efficiency is a measure of the overall effectiveness of the system and is calculated from the following mathematical formula:

$$\eta_d = \frac{W_m L_t}{\overline{H}_T A_c t} \tag{2.110}$$

where, W_m (kg) is the mass of moisture evaporated in time t, L_t (J/kg) is the latent heat of evaporation of water from the product, $\overline{H}_T$ (W/m^2) is the insolation on the energy collection surfaces in a given time interval, A_c (m^2) is the effective energy collection area, and t (s) total drying time. Equation (2.110) is redefined in terms of the moisture content of the product as:

$$\eta_d = \frac{W_d (M_{\mathrm{i,db}} - M_{\mathrm{f,db}}) L_t}{\overline{H}_T A_c t} \tag{2.111}$$

It evident from equation (2.111) that for a given dryer, the load will have a significant effect on the drying efficiency. To isolate the effect of the initial crop mass on the drying efficiency, its value is normalised to obtain the normalised drying efficiency defined as:

$$\eta_{dN} = \frac{\eta_d}{W_d} \tag{2.112}$$

where W_d is the mass of dry matter (i.e. bone dry matter) in the initial crop mass. Equation (2.112) gives an indication of the efficiency of the drying system reckoned per mass of the crop.

LIBRARY
KWAME NKRUMAH
UNIVERSITY OF SCIENCE & TECHNOLOGY
KUMASI

2.9.6.2 The pick-up efficiency, η_p

This parameter is used for evaluating the actual evaporation of moisture from the commodity inside the dryer. It is a direct measure of how efficiently the capacity of the (solar) heated air is utilised to dry a commodity. The pick-up efficiency is defined as the ratio of the moisture picked up by the air in the drying chamber to the theoretical capacity of the air to absorb moisture. Pick-up efficiency of 30 %, as an average over the whole drying period, is considered to be relatively good (Brenndorfer *et al*, 1987). The pick-up efficiency can be calculated from the formula:

$$\eta_p = \frac{W_o - W_t}{\dot{m}t(H_s^* - H_i)} \tag{2.113}$$

where, W_o (kg) is the initial mass of the commodity, W_t (kg) is the mass of the commodity at the time t, H_s^* (kg dry water/kg dry air) adiabatic saturation humidity of the air entering the drying chamber, H_i (kg dry water/kg dry air) is the absolute humidity of the ambient air (which is theoretically the same as the absolute humidity at the exit of the air-heater). The calculation of the pick-up efficiency necessitates the use of the psychrometric chart and or empirical relations to determine the adiabatic saturation humidity and the absolute humidity of the heated air at the inlet of drying chamber. The adiabatic saturation humidity is evaluated from the following expression:

$$H_s^* = \frac{H_i(2501 + 1.805\theta_i - 4.186\theta^*) + (\theta_i - \theta^*)}{2501 - 2.381\theta^*} \tag{2.114}$$

where, θ_i ($^\circ$C) is the dry-bulb temperature of air entering the drying chamber, and

θ^* ($^\circ$C) is the wet-bulb temperature of the air entering the drying chamber. Combining equations (2.113) and (2.11), equation (2.112) is redefined as:

$$\eta_p = \frac{W_d(M_{i,d.b} - M_{t,d.b})(2501 - 2.381\theta_i^*)}{\dot{m}t(\theta_i - \theta_i^*)(1.805H_i + 1)} \tag{2.115}$$

The determination of the wet bulb-temperature of the heated air involves a try and error method. While equation (2.114) is to be used in mathematical models, equation (2.112) is easy to use in situations in which a physical experiment has been conducted.

2.9.7 Drying of pineapple

Pineapple is a seasonal tropical fruit rich in proteins, vitamins and minerals (Barnell, 1974; Ihekoronye and Ngoddy, 1985). Being highly perishable, it requires preservation in some form. Drying is one of the methods commonly used for preserving pineapple (Ramallo and Mascheroni, 2012; Gujral *et al*., 2013); other methods may be freezing, canning, irradiation and controlled atmosphere storage.

KNUST

The establishment of curves of hygroscopic equilibrium is important to define limits of dehydration of the product, estimate the changes of humidity under specific condition of temperature and relative humidity of the environment and to define the moisture contents conducive to the activity beginning of agents that will cause the deterioration of the product
In the case of the pineapple, it is important to highlight that the appropriate drying and storage conditions are essential to maintain the quality of the product due to its high water activity.

Bala (2009) used a multilayer neural network approach to predict the performance of the solar tunnel drier using fresh pineapples. It was reported that the solar tunnel drying required 3 days to dry pineapple samples from 87.32% to 14.13% as compared to 87.32% to 21.52% in 3 days.

2.9.8 Use of back-up heater in solar crop drying

Several attempts have been made to overcome the problem of intermittent drying in natural convection solar drying. One approach has been the use of thermal storage. The use of a supplementary source of heat cannot be economical in many cases, e.g., for very small-scale applications, because of the initial capital cost investment needed, but for larger drying systems the volume of the crop may justify such a system. *Khanna (1967)* studied design data for solar heating of air using a heat exchanger (heat transfer by both natural and forced modes). It was

heating of air using a heat exchanger (heat transfer by both natural and forced modes). It was found that the data would assist in obtaining the final design of a shell-and-tube heat exchanger for use in drying a specific material.*Ayensu and Asiedu-Bondzie (1986)*constructed a dryer with thermal storage, from locally available materials. The system was capable of transferring 118 W m^{-2} to the drying air. *Ayensu (1997)* designed and constructed a solar dryer with a rock storage system. It was found that the rock pile stored enough energy to enhance nocturnal drying. The duration of crop drying in the solar dryer was shorter than that in the open air. *Aboul-Enein et al. (2000)*developed a solar air heater and tested it with and without thermal storage for drying agricultural products. They found that the drying process continued at night when a thermal mass was used. *El-Sebaii et al. (2002)*developed a solar dryer with a thermal storage system. The dryer was tested with and without thermal storage. They found that the storage material reduced the drying period. *Enibe (2002)* used a phase change material to store thermal energy in a solar air heating system. It was found that the system could be operated for crop drying and poultry egg incubation. In all these studies, solar energy was used exclusively. However, the intensity of solar radiation is sometimes so low that the temperature of the thermal mass may rise by an insignificant margin above the ambient level, and thereby limiting the continuity of dehydration. All these interventions notwithstanding, there is still the need to address the intermittent drying process in natural convection solar dryers by employing a supplementary energy source and it is suggested in this study to employ a back-up heater that utilizes biomass feedstock as the fuel source.

Akyurt and Selcuk (1973) developed an indirect solar dryer with a backup gas burner. They found that the drying time could be shortened due to the inclusion of the backup heater. *Bassey et al. (1987)* used a sawdust burner to provide heat to a direct type solar dryer during bad weather and at night. In their study, the burner was not integrated to the dryer but used steam as a heat transfer medium.The burner consisted of 28 burner holes (2.5 cm initial diameter), spaced at 10 cm between centres, and arranged in four rows. Four galvanized iron pipes (110 cm long, 2.5 cm diameter) were mounted directly over the burner holes. Water in these pipes was evaporated and the steam passed through the heat-exchanger pipes in the drying cabinet and then vented to the atmosphere. It was assumed in the design that the energy input by the burner to the drying cabinet was 400 W/m^2, burner efficiency to convert water to steam was 10%, and condenser

LIBRARY
KWAME NKRUMAH
UNIVERSITY OF SCIENCE & TECHNOLOGY
KUMASI

Figure 14 shows the hybrid solar/sawdust crop dryer designed and tested by Bassey et al.

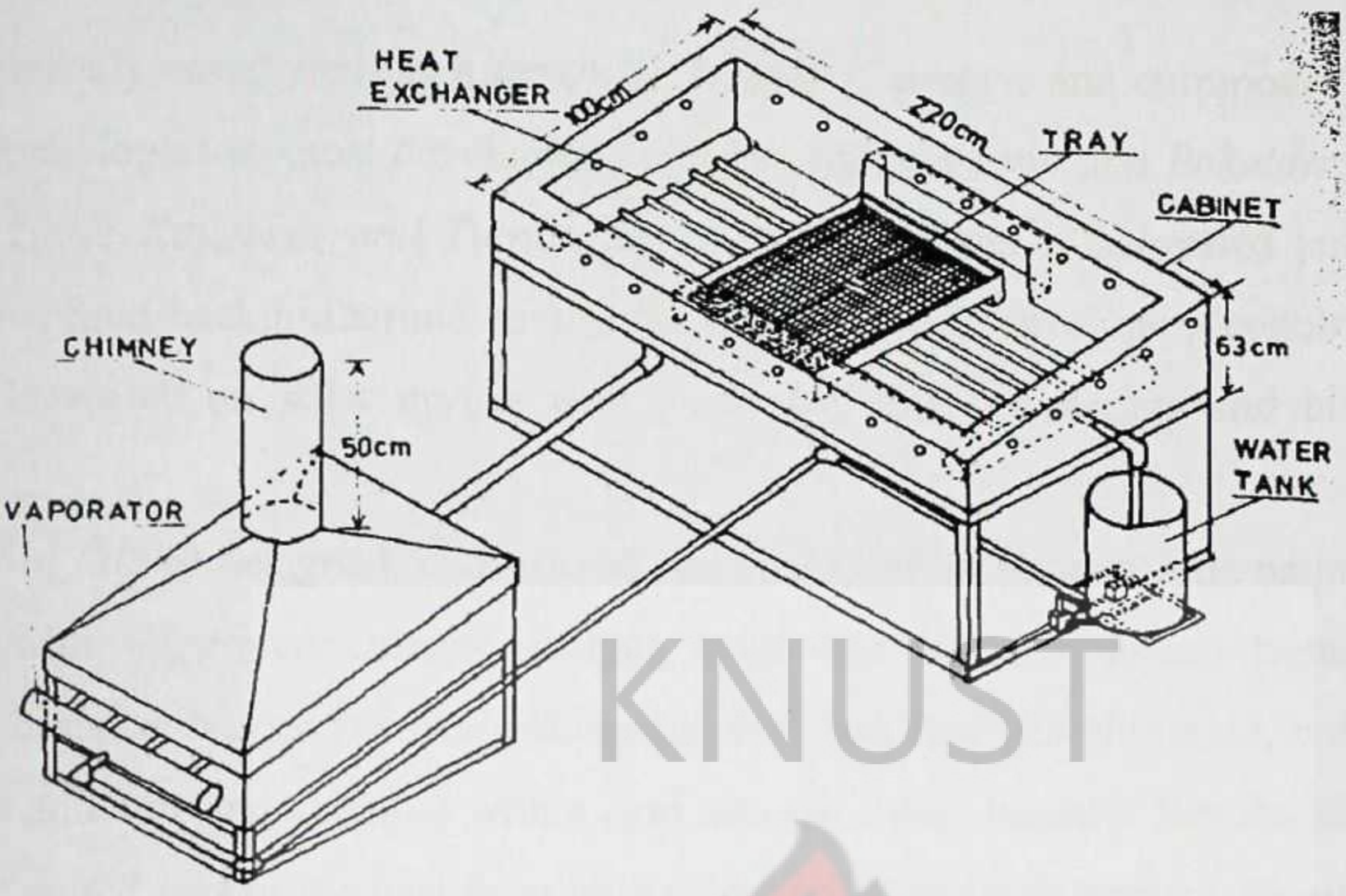

KNUST

Figure 14 Hybrid solar/sawdust crop dryer (Bassey et al)

Bena and Fuller (2002) designed a direct solar dryer with an integrated biomass-backup heater. The thermal performance of their system was reported to be satisfactory. *Prasad and Vijay (2005)* also developed a direct solar–biomass dryer. The biomass burner had a rock slab on the top part which helped in moderating the temperature of the drying air. These dryer designs had a backup heater without thermal storage to capture solar energy. Consequently, the air temperature in the drying chamber dropped down to ambient level immediately after sunset, requiring backup heating even when the preceding day was sunny. This leads to wastage of both solar and fuel resources.

Biomass (especially wood fuel) is a dominant source of energy, and commonly burned using inefficient technologies in most developing countries *(Kristoferson and Bokalders, 1991; Bena and Fuller, 2002; Kaygusuz and Tu¨rker*, 2002). This resource, if harvested sustainably, can provide the required backup thermal energy for solar drying in developing countries. However, information is scarce on solar drying with integrated collector-storage and biomass-backup heaters.

requiring backup heating evenwhen the preceding day was sunny. This leads to wastageof both solar and fuel resources.

Biomass (especially wood fuel) is a dominant source of energy, and commonly burned using inefficient technologies in most developing countries *(Kristoferson and Bokalders, 1991; Bena and Fuller, 2002; Kaygusuz and Tu¨rker*,2002). This resource, if harvested sustainably, can provide the required backup thermal energy for solar drying in developing countries. However, information is scarce on solar drying with integrated collector-storage and biomass-backup heaters.

Madhlopa et al (2006) designed, constructed and evaluated an indirect type natural convection solar dryer with integrated collector-storage solar and biomass-backup heater. The dryer consisted of biomass burner (with a rectangular duct and flue gas chimney), collector-storage thermal mass and a drying chamber with a conventional solar chimney. Results showed that the thermal mass stored part of the heat from both solar and biomass air heaters, thereby moderating temperature fluctuations in the drying chamber and reducing wastage of energy. However, there were two defects with their system:

(1) the drying was not uniform across the trays. Consequently, there was need for interchanging the trays periodically during drying to achieve uniform dried products

(2) reverse thermosiphoning was observed in the solar chimney during the night.

KNUST

CHAPTER THREE

FORMULATION OF MATHEMATICAL MODELS

3.0 Introduction

In this chapter, the mathematical models developed for predicting and evaluating the performance of the mixed-mode solar crop dryer with integrated backup heater under no load conditionsare presented. Four models are presented namely; the air-heater model (solar, burner, and hybrid), the drying chamber heating model, the air flow model, and the technical performance model. The air-heatermodel, as presented in section 3.1, incorporates a model for predicting the pertinent temperatures of the air heater components of the system. The air flow model predicts the average velocity and mass flow rate of air through the dryer. The technical performance model predicts the collector efficiency, supply of energy from the burner to the collector-storage thermal mass, exergy transfer rate of air, and the total entropy change of the thermal mass. The drying chamber heater model, as presented in section 3.2, predicts the temperatures of the drying chamber components.

3.1 Formulation of the backup heating and solar air-heating models

The equations governing the performance of the system are formulated by coupling energy balance equations on the components of the air-heater (solar, biomass, and hybrid heating) with energy balance for the air. The equations are formulated based on the following assumptions:

1. The backup heater operates under steady-state conditions.
2. The concrete absorber is subjected to constant insolation and hence, variations in its operating temperatures in a horizontal plane are negligible.
3. The temperature of the air varies only in the direction of the flow.
4. The sky is considered a black-body for long wavelength radiation.
5. The heat flow through the glazing and the collector-storage thermal mass is one-dimensional.

6. The physical properties of air are assumed to vary linearly with temperature in the range $293K < T < 333K$.
7. The ambient temperature and wind speed are constant and equal to the long-term, monthly-average day-time values.
8. The plenum inlet is small compared to other dimensions of the plenum, so that the plenum walls together with the concrete and absorber and drying chamber inlet form a complete enclosure over the burner housing
9. The air media within the dryer does not participate in the radiant energy transmission

KNUST

3.1.1 *Energy balance equations on air heating model*

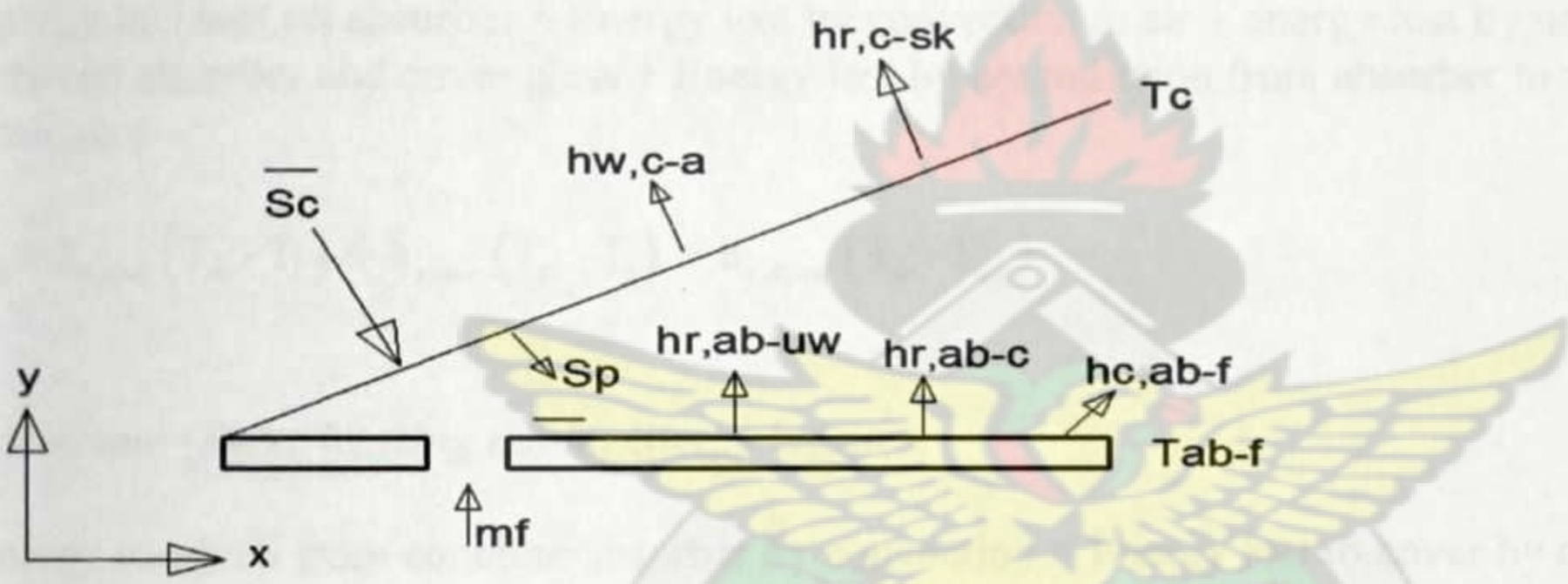

Figure 15(a)Energy balance on the components of the air-heater and its surrounding

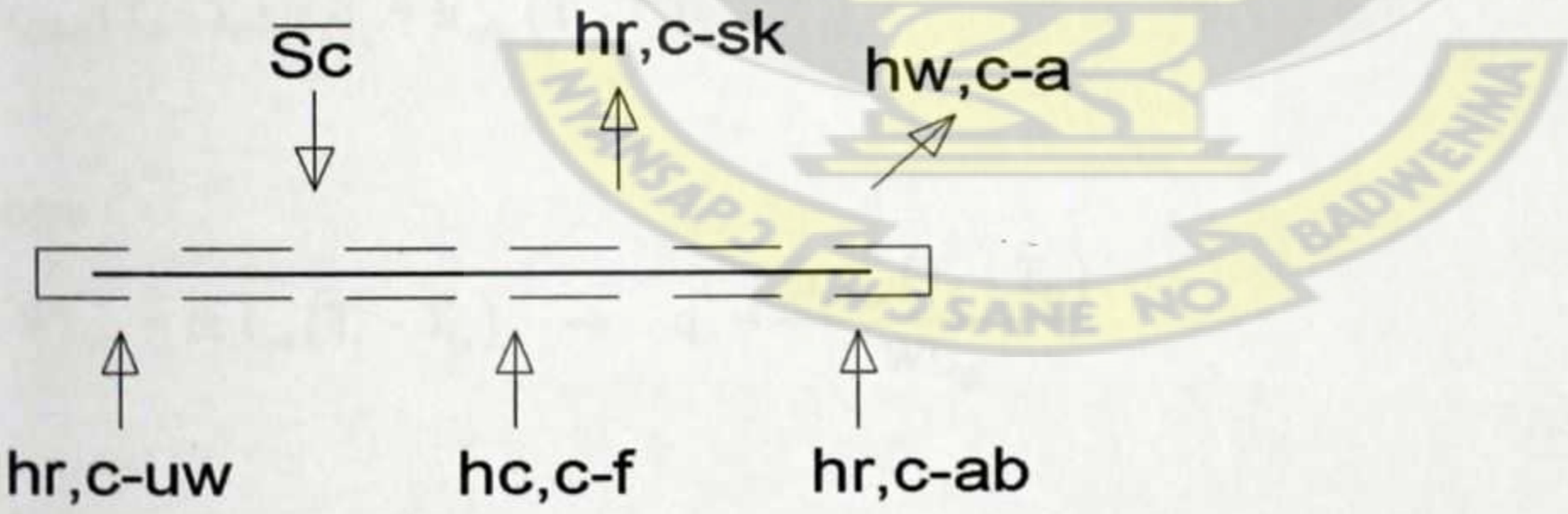

Figure 15(b) Energy balance on glass cover

The energy-balance equations on the two components of the air heater as illustrated in figures15(a) and15(b), and expressions relating the useful energy absorbed by the heated air in

the heater passages to the incident energy (solar radiation) on the system are presented as follows:

Absorber cover plate (refer to figure 15(a)):

Radiant energy incident on cover glass + net radiation gained by cover from absorber + net radiation heat gained by cover from plenum enclosure walls + heat gained by cover as a result of convection between cover and drying air = heat lost through convection by cover to ambient air + heat lost by net radiation from cover to sky

$$\alpha_c \bar{S}_c + h_{r,c\text{-}ab}(T_{ab} - T_c) + h_{c,f\text{-}c}(T_f - T_c) + h_{r,uw\text{-}c}(T_{uw} - T_c) = h_{w,c\text{-}a}(T_c - T_a) + h_{r,c\text{-}sk}(T_c - T_{sk}) \quad (3.1)$$

where

KNUST

Concrete absorber energy balance (solar heating mode):

Energy incident on absorber = Energy lost by convection to air + energy lost by net radiation between absorber and cover glass + Energy lost by net radiation from absorber to wall of plenum enclosure

$$\bar{S}_p = h_{c,ab\text{-}f}(T_{ab} - T_f) + h_{r,ab\text{-}c}(T_{ab} - T_c) + h_{r,ab\text{-}uw}(T_{ab} - T_{uw}) \quad (3.2)$$

Air stream (***Solar heating mode***) energy balance:

Energy received from concrete absorber by convection = Energy lost to cover by convection + Energy stored by the air

$$h_{c,ab\text{-}f}(T_{ab} - T_f) = q'' + h_{c,f\text{-}c}(T_f - T_c) \quad (3.3a)$$

where

$$q'' W L_{ab} = \dot{m}_a c_{pa}(T_f - T_{f,i}) \quad \rightarrow \quad q'' = \frac{\dot{m}_a c_{pa}(T_f - T_{f,i})}{W L_{ab}} \quad (3.3b)$$

Air stream (***backup heating and hybrid heating modes***) energy balance:

(Energy received from bare exterior surface of burner) = (Energy lost to cover by convection) +(Energy received by convection from absorber) + (Energy stored by the air)

$$\pi r_{bu} h_{c,fi\text{-}bu}(T_{bu} - T_{f,i}) + h_{c,ab\text{-}f} W (T_{ab} - T_f) = q'' + h_{c,f\text{-}c} W (T_f - T_c) \quad (3.3c)$$

where $q^{"}(\pi r + W)L_{ab} = \dot{m}_a c_{pa}(T_f - T_{f,i}) \rightarrow q^{"} = \dfrac{\dot{m}_a c_{pa}(T_f - T_{f,i})}{(\pi r + W)L_{ab}}$ (3.3d)

For the purpose of modeling the experimental dryer, equation (3.3c) has been modified since a resistance heater is used instead of a burner drum. The resultant equation is:

$$h_{c,fi\text{-}bu}(T_{rp\text{-}bu} - T_{f,i}) + h_{c,ab\text{-}f}(T_{ab} - T_f) = q^{"} + h_{c,f\text{-}c}(T_c - T_f) \quad (3.3e)$$

Performance of the air-heater under a given set of conditions

The overall effectiveness of the solar air-heater is indicated by its energy collection efficiency, η_c, which is a measure of how effectively the energy available in the solar energy incident upon the solar collector is transferred to the air flowing through it. In solar heating mode, it is defined as the ratio of the heat absorbed by the drying air to the solar energy incident upon the absorber surface, and is calculated from the equation:

$$\eta_c = \frac{\dot{m}\, C_{p,a}(T_f - T_{f,i})}{A_{ab}\bar{S}_c} \quad (3.4a)$$

Burner heating mode:

$$\eta_c = \frac{\dot{m}\, C_{p,a}(T_f - T_{f,i})}{\dot{Q}_{tm}} \quad (3.4b)$$

Hybrid heating mode:

$$\eta_c = \frac{\dot{m}\, C_{p,a}(T_f - T_{f,i})}{A_{ab}\bar{S}_c + \dot{Q}_{tm}} \quad (3.4c)$$

Average heat absorbed by thermal mass:

$$Q_{tm} = m_{ab}c_{ab}(T_{ab,av} - T_{fi}) + m_{rp}c_{rp}(T_{rp,av} - T_{fi}) \quad (3.4d)$$

Where

$$T_{ab,av} = \frac{1}{2}(T_{ab} + T_{ab\text{-}rp}) \text{ and } T_{rp,av} = \frac{1}{2}(T_{rp\text{-}bu} + T_{ab\text{-}rp})$$

Rate of change of flow exergy of air from dryer inlet to plenum exit:

KNUST
NYANSAPO WO SANE NO BADWENMA

$$\Delta\dot{\psi} = \dot{\psi}_2 - \dot{\psi}_1 = \dot{m}\left\{(h_2 - h_1) + T_o(s_2 - s_1) + \frac{1}{2}(v_2^2 - v_1^2) + g(z_2 - z_1)\right\} \quad (3.4e)$$

where

$$s_2 - s_1 = c_v \ln\left(\frac{T_2}{T_1}\right) + R\ln\left(\frac{p_2}{p_1}\right)$$

Total entropy change equation for thermal mass:

$$(\Delta S)_{tm} = m_{ab} c_{v,ab} \ln\left(\frac{T_{ab\text{-}rp}}{T_{ab}}\right) + m_{rp} c_{v,rp} \ln\left(\frac{T_{rp}}{T_{ab\text{-}rp}}\right) \quad (3.4f)$$

KNUST

Solar heat charging

During solar heating, the top part of the thermal mass heats up faster than the bottom part. The thermal energy is conducted through the rock pile until an equilibrium state is established. Heat is conducted from the top surface of the concrete absorber (Tab-f) to the interface (Tab-rp)between the absorber and the rock pile matrix, and from the interface to the bottom of the rock pile (Trp-bu). In steady state, the rate of heat transfer from the interface to the bottom of the rock pile is equal to the rate of heat loss from the bottom of the rock bed (Figure 16). The energy balance can be represented by the following equations, assuming heat transfer is one-dimensional:

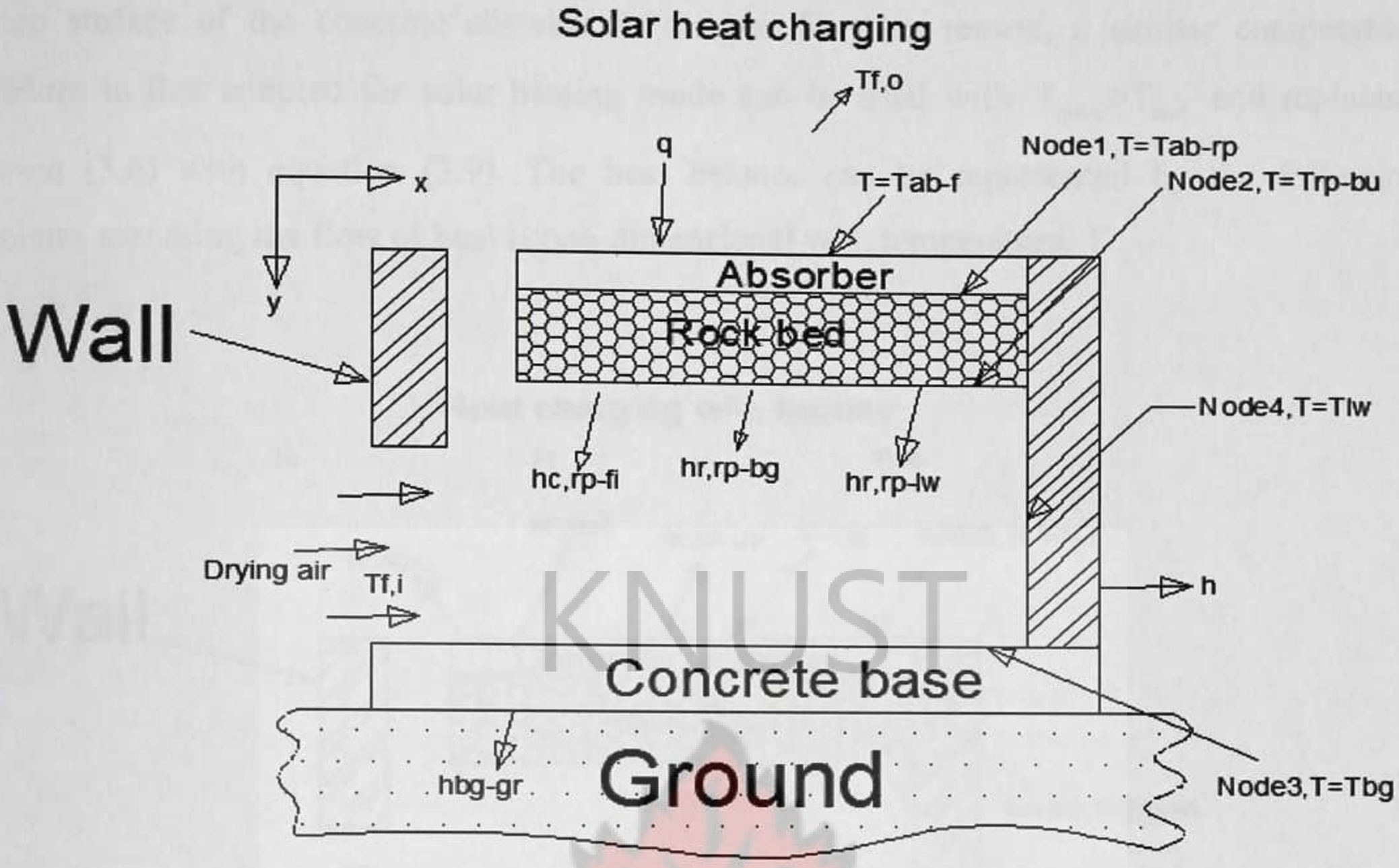

Figure 16 Heat transfer scenario during solar heat charging

$$\text{Node 1: } \lambda_{ab}\frac{\left(T_{ab\text{-}f}-T_{ab\text{-}rp}\right)}{x_{ab}}=\lambda_{rp}\frac{\left(T_{ab\text{-}rp}-T_{rp\text{-}bu}\right)}{x_{rp}} \tag{3.5}$$

$$\text{Node 2: } \lambda_{rp}\frac{\left(T_{ab\text{-}rp}-T_{rp\text{-}bu}\right)}{x_{rp}}=h_{r,rp\text{-}bg}\left(T_{rp\text{-}bu}-T_{bg}\right)+h_{r,rp\text{-}lw}\left(T_{rp\text{-}bu}-T_{lw}\right)+h_{c,rp\text{-}a}\left(T_{rp\text{-}bu}-T_{a}\right) \tag{3.6}$$

$$\text{Node 3: } h_{r,rp\text{-}bg}\left(T_{rp\text{-}bu}-T_{bg}\right)=\lambda_{bg}\frac{\left(T_{bg}-T_{gr}\right)}{x_{bg}} \tag{3.7}$$

$$\text{Node 4: } h_{r,rp\text{-}lw}\left(T_{rp\text{-}bu}-T_{lw}\right)=\left[R_1+\left(R_2R_3\right)/\left(R_3+R_2\right)\right]^{-1}\left(T_{lw}-T_{a}\right) \tag{3.8}$$

where $R_1=x_{lw}/\lambda_{lw}$; $R_2=1/h_{c,lw\text{-}a}$; $R_3=1/h_{r,lw\text{-}a}$

Backup heating mode

Heat is conducted from the backup heater through the bottom face of the rock pile $\left(T=T_{rp\text{-}bu}\right)$ to the interface $\left(T=T_{rp\text{-}ab}\right)$ between the rock matrix and concrete absorber and from the interface to the top surface of the concrete absorber $\left(T=T_{ab\text{-}f}\right)$. In steady state, the rate of heat transfer from the interface to the top part of the concrete absorber is equal to the rate of heat dissipation from

the top surface of the concrete absorber to the air. For this reason, a similar computation procedure to that adopted for solar heating mode can be used with $T_{rp\text{-}bu} > T_{ab\text{-}f}$ and replacing equation (3.6) with equation (3.9). The heat balance can be represented by the following equations, assuming the flow of heat is one-dimensional with temperature, T:

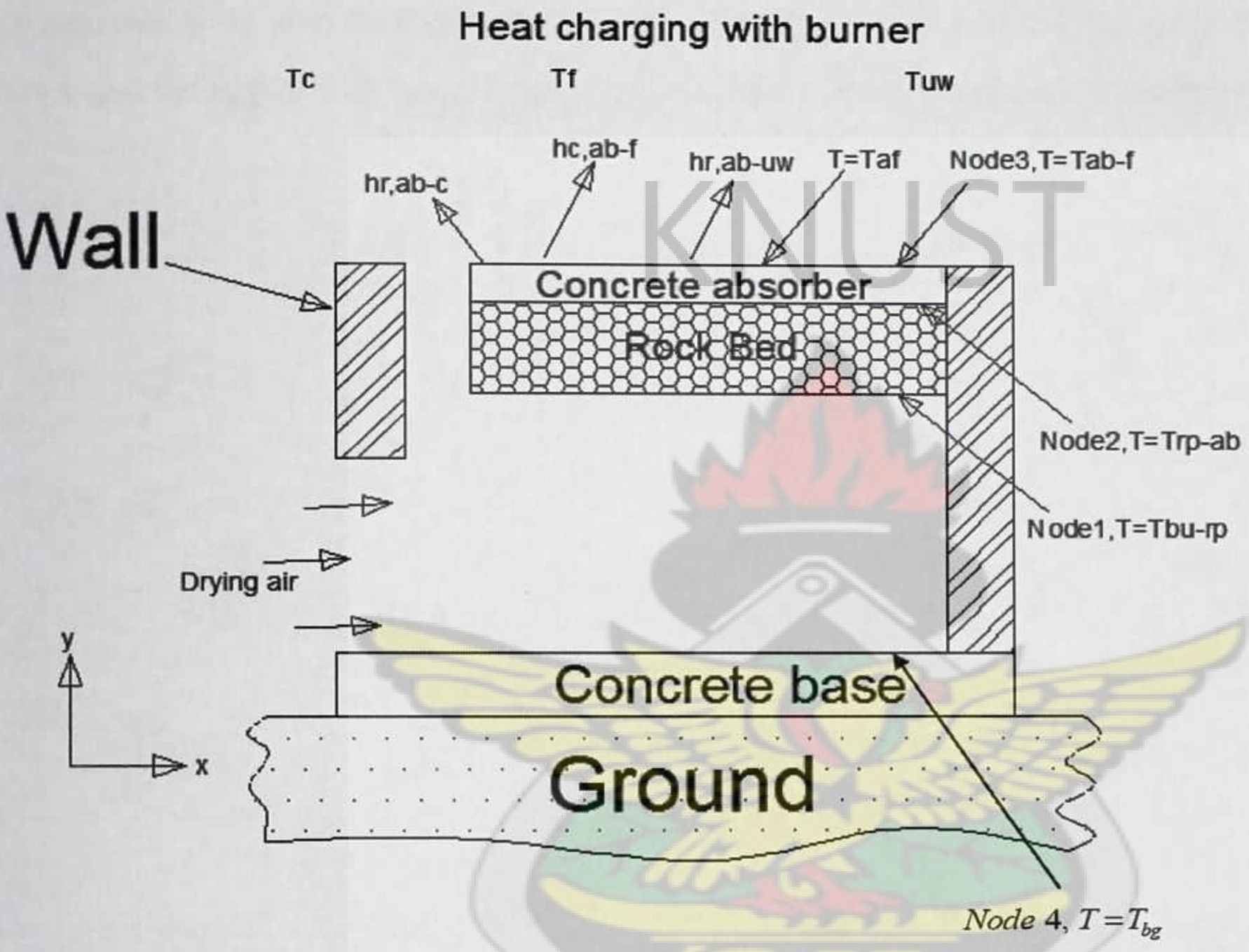

Figure 17 Heat transfer scenario during backup heating

$$\text{Node 1:}\lambda_{rp}\frac{\left(T_{rp\text{-}bu}-T_{rp\text{-}ab}\right)}{x_{rp}}+h_{r,rp\text{-}bg}\left(T_{rp\text{-}bu}-T_{bg}\right)+h_{r,rp\text{-}lw}\left(T_{rp\text{-}bu}-T_{lw}\right)+h_{c,rp\text{-}f}\left(T_{rp\text{-}bu}-T_{f,i}\right)=0 \qquad (3.9)$$

$$\text{Node 2: }\lambda_{rp}\frac{\left(T_{rp\text{-}bu}-T_{rp\text{-}ab}\right)}{x_{rp}}=\lambda_{ab}\frac{\left(T_{rp\text{-}ab}-T_{ab\text{-}f}\right)}{x_{ab}} \qquad (3.10)$$

$$\text{Node 3:}\lambda_{ab}\frac{\left(T_{ab\text{-}rp}-T_{ab\text{-}f}\right)}{x_{ab}}=h_{r,ab\text{-}c}\left(T_{ab\text{-}f}-T_{c}\right)+h_{r,ab\text{-}uw}\left(T_{ab\text{-}f}-T_{uw}\right)+h_{c,ab\text{-}f}\left(T_{ab\text{-}f}-T_{f}\right) \qquad (3.11)$$

$$\text{Node 4:}h_{r,rp\text{-}bg}\left(T_{rp\text{-}bu}-T_{bg}\right)=\lambda_{bg}\frac{\left(T_{bg}-T_{gr}\right)}{x_{bg}} \qquad (3.12)$$

purpose of simplicity surfaces 2, 5, 6, and 7 are collectively called the upper wall (designated with subscript uw). The inner surfaces of the enclosure are relabeled as follows:

top surface of integrated collector-thermal mass system: surface 1

upper vertical wall (2, 5, 6, and 7): surface 2

inner inclined surface of glass cover: surface 3

drying chamber entrance: surface 4

In this analysis it is assumed that the surfaces are isothermal and diffuse-gray surfaces with surfaces 1 and the upper wall being opaque and surface 3, a semitransparent surface.

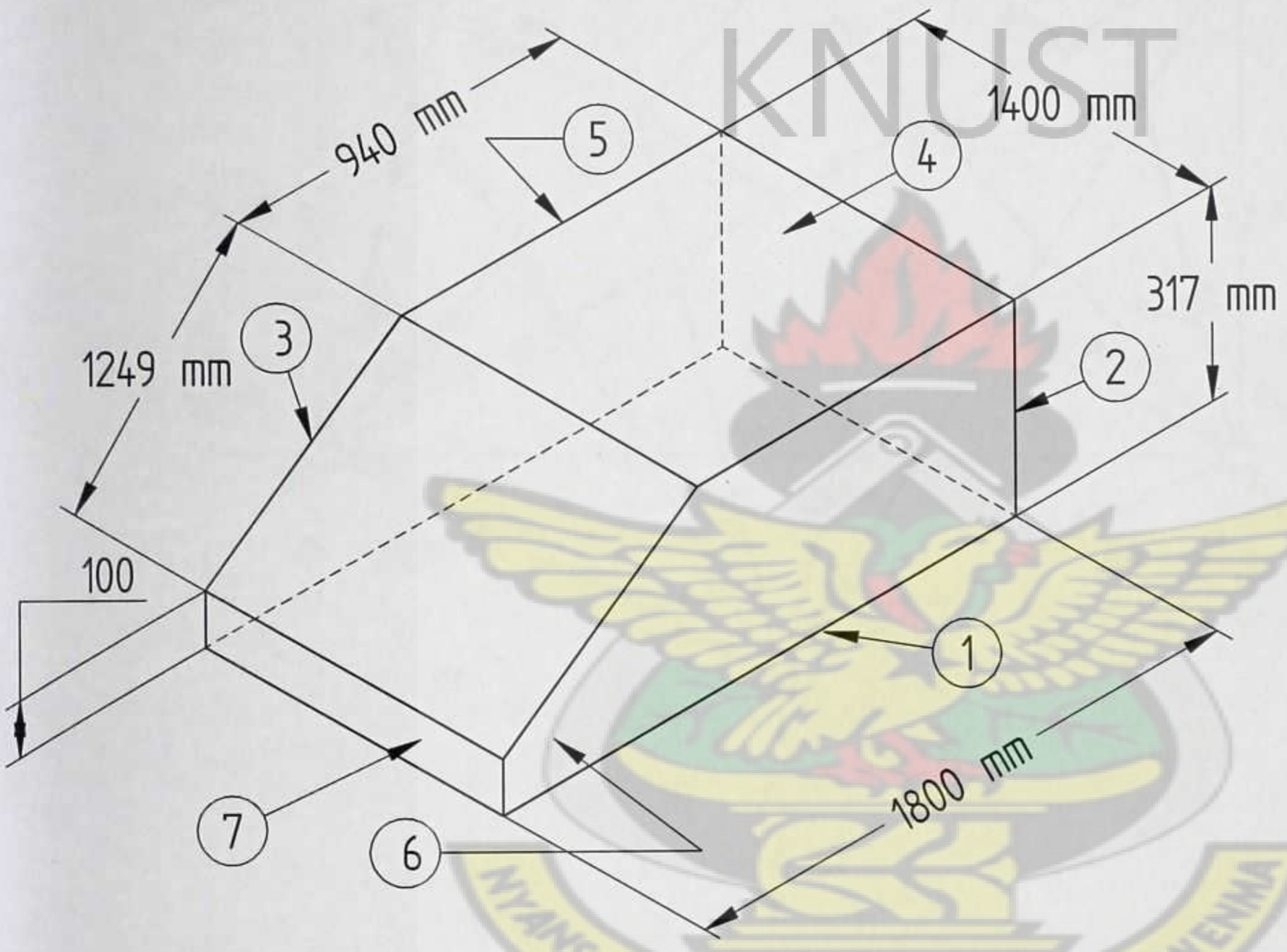

Figure 18 The plenum as a seven surface enclosure

The radiation network of this geometry is shown in figure 19.

KNUST

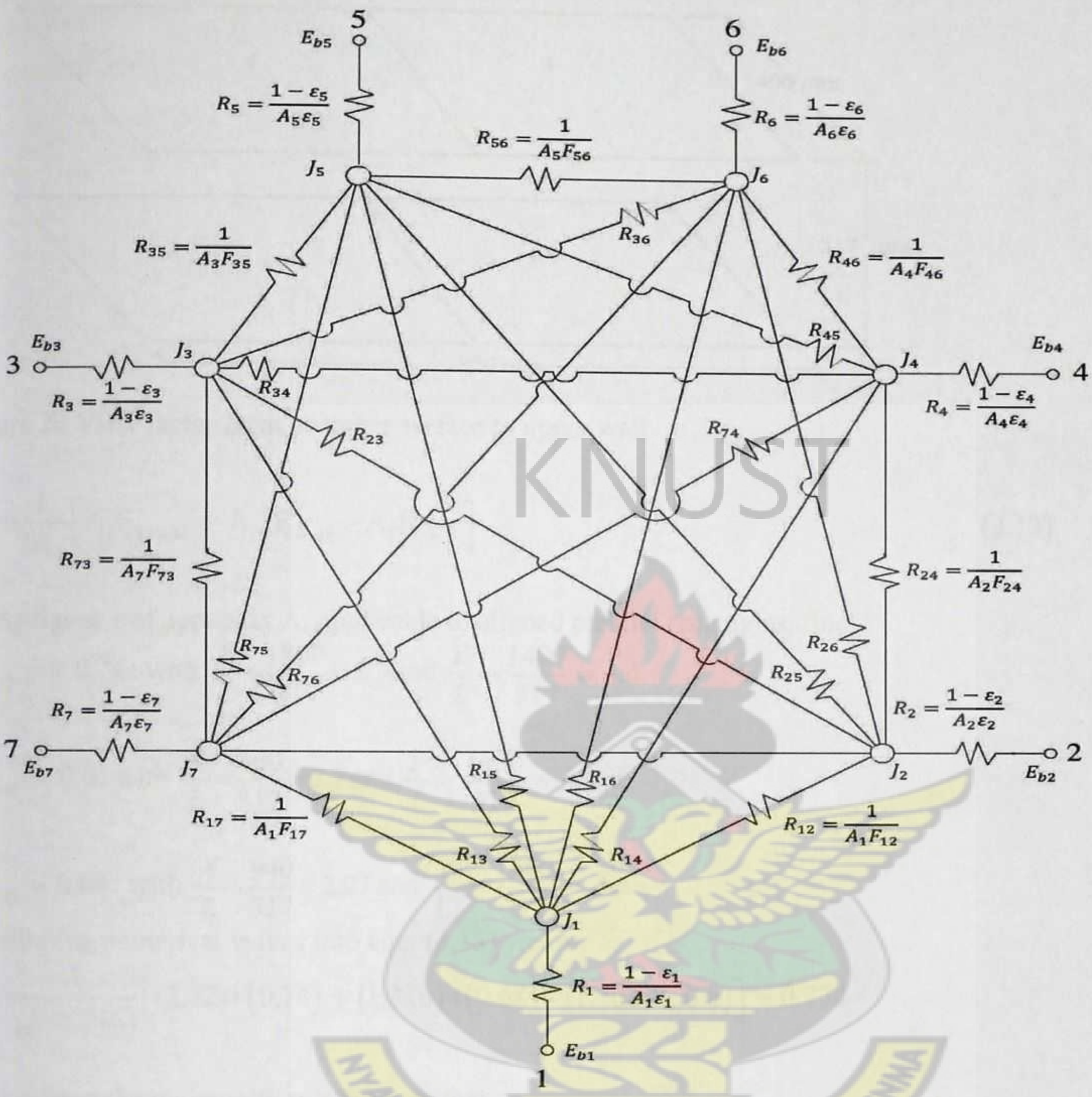

Figure 19 Radiation network associated with plenum as a seven surface enclosure

Determination of view factors

The view factors $F_{11} = F_{33} = F_{44} \cong 0$ since these surfaces are plane surfaces.

The view factor F_{41} can be determined with reference to figure 20 as follows:

Surface 4 is extended to include a fictitious surface labeled f whereas surface 1 is subdivided into two equal halves labeled as 1A and 1B as shown in figure 20. The view factor can then be determined using the superposition (Cengel, 2006) rule as

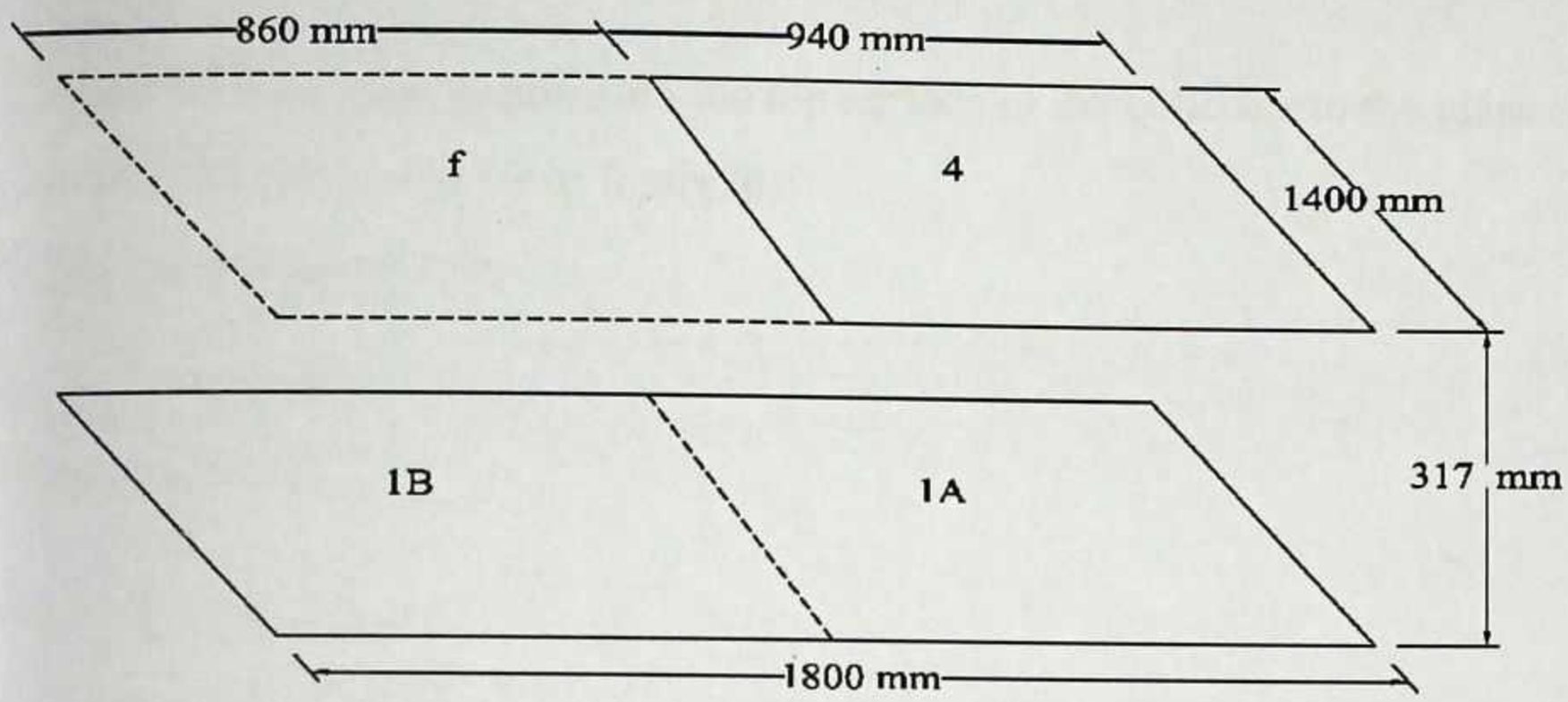

Figure 20 View factor from absorber surface to upper wall

KNUST

$$F_{41} = \frac{1}{2A_4}\left[A_1 F_{(4,f)\to 1} + A_{1A} F_{1A\to 4} - A_f F_{f\to 1B}\right] \qquad (3.13)$$

Using figure 1 of appendix A, applicable to aligned parallel rectangles, find

$F_{(4,f)\to 1} = 0.74$: with $\frac{X}{L} = \frac{1800}{317} = 5.7$ and $\frac{Y}{L} = \frac{1400}{317} = 4.4$

$F_{f\to 1B} = 0.6$: with $\frac{X}{L} = \frac{860}{317} = 2.7$ and $\frac{Y}{L} = \frac{1400}{317} = 4.4$

$F_{1A\to 4} = 0.68$: with $\frac{X}{L} = \frac{940}{317} = 2.97$ and $\frac{Y}{L} = \frac{1400}{317} = 4.4$

Substituting numerical values into equ. (3.13) yields

$$F_{41} = \frac{1}{(2\times 1.316)}\left[(2.52)\times(0.74) + (1.316)\times(0.68) - (1.204)\times(0.6)\right] = 0.774$$

Hence, from the reciprocity rule we note that

$$A_1 F_{14} = A_4 F_{41} \qquad (3.14)$$

Substituting numerical values into equ. (3.14), the view factor from the top surface of the collector to the drying chamber opening,

$$F_{14} = \frac{A_4}{A_1} F_{41} = \frac{1.316}{2.52}\times 0.774$$
$$= 0.404$$

LIBRARY
KWAME NKRUMAH
UNIVERSITY OF SCIENCE & TECHNOLOGY
KUMASI

The approximate view factor from the top surface of the collector to the glass cover can be calculated as follows (refer to figure20):

By the superposition rule,

$$F_{1\to(4,3))} = F_{14} + F_{13} \tag{3.15}$$

From equ. (3.15)

$$F_{1\to3} = F_{1\to(4,3)} - F_{1\to4} \tag{3.16}$$

Substituting numerical values into equation (3.16) yields

$$F_{1\to3} = 0.74 - 0.404$$
$$= 0.336$$

KNUST

Applying the summation rule to surface 1 (top surface of integrated collector-thermal mass):

$$F_{11} + F_{12} + F_{13} + F_{14} = 1 \tag{3.17}$$

Equation (4.17) implies that

$$F_{12} = 1 - (F_{13} + F_{14}) \tag{3.18}$$

Substituting numerical values into equation (3.18),

$$F_{12} = 1 - (0.336 + 0.404)$$
$$= 0.260$$

Calculation of F_{23}

F_{23} can be calculated from the application of the summation rule to surface 3 as follows:

$$F_{31} + F_{32} + F_{33} + F_{34} = 1 \tag{3.19}$$

But $F_{33} = 0$

$$F_{31} = \frac{A_1}{A_3} \times F_{13} = \frac{2.52}{2.048} \times 0.336 = 0.413$$

F_{34} can be calculated from the application of the triangle rule (Cengel, 2006) to surfaces 3 and 4 as labeled on figure 18 by connecting the edges of surfaces 3 and 4 with a fictitious surface to form a triangle.

Let D denote the fictitious surface.

Then,

$$F_{34} = \frac{L_3 + L_4 - L_D}{2L_3} = \frac{1249 + 1800 - 2362}{2 \times 1249} = 0.275$$

Substituting the values of F_{34} and F_{31} into equation (3.19),

$$0.413 + F_{32} + 0 + 0.275 = 1 \rightarrow F_{32} = 0.312$$

$$\therefore F_{23} = \frac{A_3}{A_2} F_{32} = \frac{2.048}{1.776} \times 0.312 = 0.360$$

KNUST

The view factors between the bottom surface of the thermal mass and the inner surfaces of the four vertical walls of the burner enclosure (collectively called lower wall) and between the bottom surface of the thermal mass and the burner floor can be determined as follows:

The entire burner housing including the bottom surface of the thermal mass and the burner housing floor is regarded as a three surface enclosure. The surfaces are labeled as follows:
Bottom plane surface of thermal mass is labeled as surface 5; the burner housing floor as surface 6; and the inner plane surfaces of the four vertical walls of the burner enclosure (also called the lower wall, lw) are collectively designated as surface 7. Surfaces 5 and 6 are shown in figure 21. Surface 5 is extended to include a fictitious designated as f. surface 6 is subdivided into two surfaces called 6A and 6B. The view factor from surface 5 to 6 can be determined as follows:

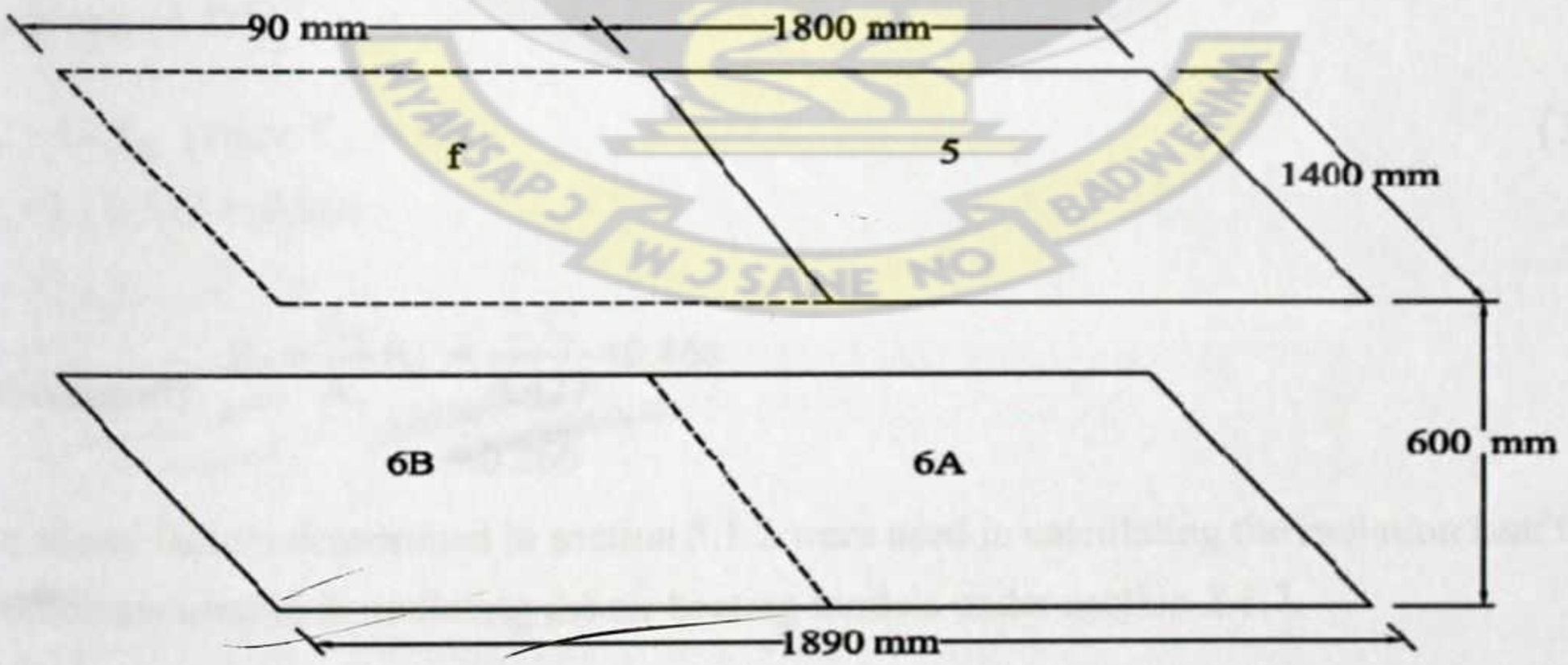

Figure 21 View factor from thermal mass to lower wall

$$F_{56} = \frac{1}{2A_5}\left[A_6 F_{(5,f)\to 6} + A_{6A} F_{6A\to 5} - A_f F_{f\to 6B}\right] \qquad (3.20)$$

Using figure 1 of appendix A, applicable to aligned parallel rectangles, we find

$$F_{(5,f)\to 6} = 0.52 : \text{with} \frac{X}{L} = \frac{1890}{600} = 3.2 \text{ and } \frac{Y}{L} = \frac{1400}{600} = 2.3$$

$$F_{f\to 6B} = 0.04 : \text{with} \frac{X}{L} = \frac{90}{600} = 0.15 \text{ and } \frac{Y}{L} = \frac{1400}{600} = 2.3$$

$$F_{6A\to 5} = 0.52 : \text{with} \frac{X}{L} = \frac{1800}{600} = 3 \text{ and } \frac{Y}{L} = \frac{1400}{600} = 2.3$$

Substituting numerical values into equ. (3.19) yields

$$F_{56} = \frac{1}{(2\times 2.52)}\left[(2.646)\times(0.52) + (2.52)\times(0.52) - (0.126)\times(0.04)\right] = 0.532$$

$$F_{65} = \frac{A_5}{A_6} F_{56} = \frac{2.52}{2.646}\times 0.532$$
$$= 0.507$$

Applying the summation rule to surface 5:

$$F_{55} + F_{56} + F_{57} = 1 \qquad (3.21)$$

From equ. (4.21),

$$F_{57} = 1 - F_{56} \quad (\text{since } F_{55} = 0) \qquad (3.22)$$

$$F_{57} = 1 - 0.532 = 0.468$$

Subsequently, $$F_{75} = \frac{A_5}{A_7} F_{57} = \frac{2.52}{4.427}\times 0.468$$
$$= 0.266$$

The views factors determined in section 3.1.2 were used in calculating the radiation heat transfer coefficients used in formulating the air heating models under section 3.1.7.

KNUST

3.1.3 Modelling of air flow rate

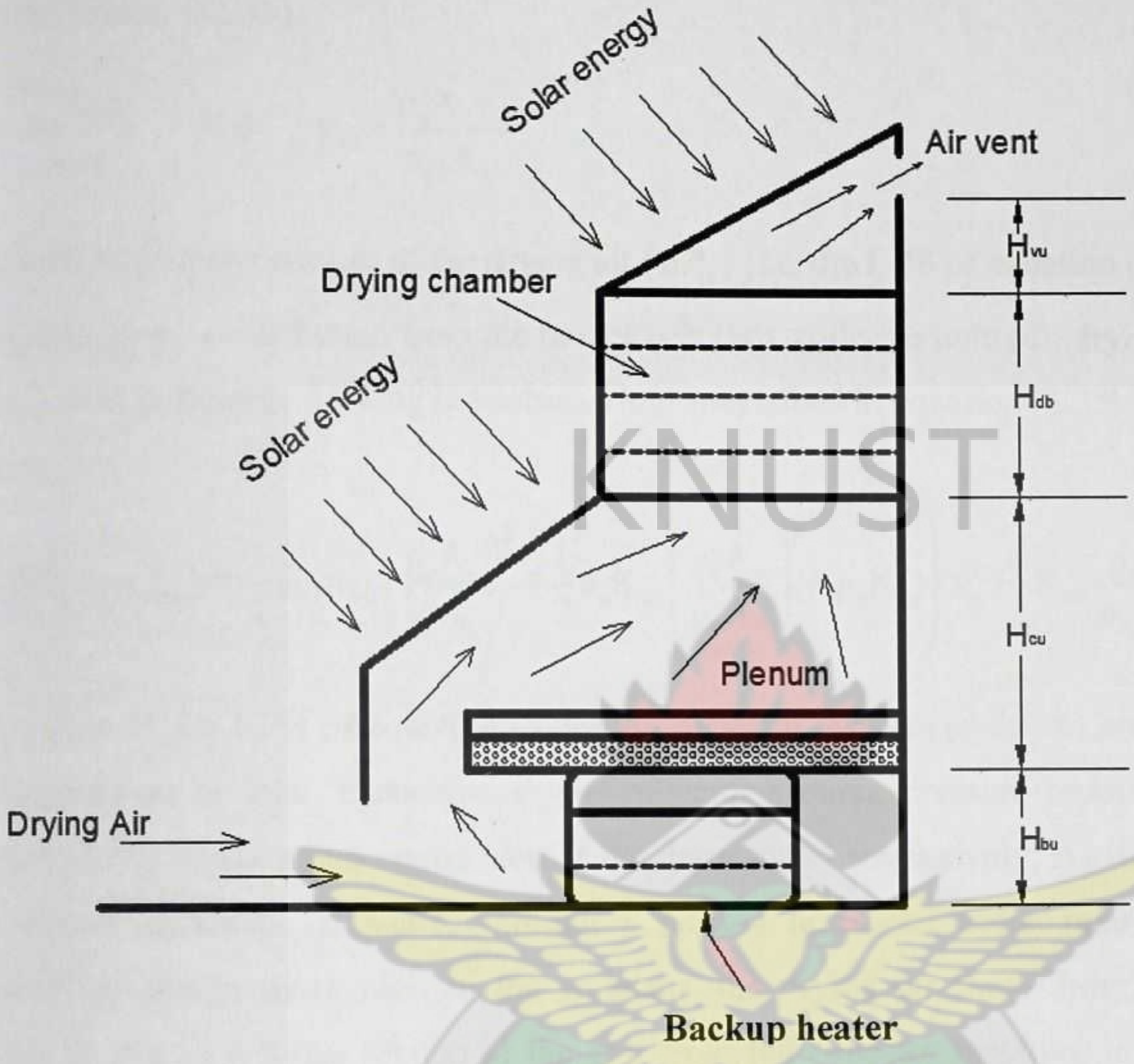

Figure 22 MNCSCDBH showing flow passages

Air flow is induced by the difference between temperatures of air in the system components and ambient air (figure 22). The thermal buoyancy (ΔP) in the system components is given by (Bala and Woods, 1994)

$$\beta \rho_a g H(\Delta T) = \Delta P_{bu} + \Delta P_{cu} + \Delta P_{dd} + \Delta P_{vu} \qquad (3.23)$$

Resistive pressure within air passage components is given by:

$$\Delta P = \frac{1}{2}\left(\rho_i K_{bu,i} v_i^2 + \rho_p K_{cu} v_p^2 + \rho_o K_{vu} v_o^2 \right) + K_{dd} v_{db} \qquad (3.24)$$

where v_i is the average dryer inlet velocity, v_p is the average plenum velocity, v_{db} is the average drying cabinet velocity, and v_o is the average vent outlet velocity.

The continuity of mass for the flow passage requires that

$$\dot{m}=\rho_i A_i v_i=\rho_p A_p v_p=\rho_{db} A_{db} v_{db}=\rho_o A_o v_o \quad (3.25a)$$

From equation (3.25b)

$$v_p=\frac{\rho_o A_o v_o}{\rho_p A_P} \quad \text{and} \quad v_{dd}=\frac{\rho_o A_o v_o}{\rho_{dd} A_{dd}} \quad (3.25b)$$

The total buoyancy pressure of the drying air (ΔP_{tb}) (i.e. the LHS of equation (3.23) is found by summing up the contribution from the burner unit (bu), collector unit(cu), drying bed (dd) and vent (vu) as indicated. Making the substitutions prescribed in equation (3.25b), equation (3.23) becomes

$$\beta\rho_a gH\left(T_{f,o}-T_{f,i}\right)=\frac{1}{2}\left\{\rho_i K_{bu}\left(\frac{\rho_o A_o}{\rho_i A_i}\right)^2+\frac{1}{2}\rho_p K_{cu}\left(\frac{\rho_o A_o}{\rho_p A_P}\right)^2+\rho_o K_{vu}\right\}v_o^2+\left(K_{dd}\frac{\rho_o A_o}{\rho_{dd} A_{dd}}\right)v_o \quad ....(3.26)$$

The terms on the RHS of equation (3.26) are pressure resistances due to contraction, bending, and expansion at inlet, expansion at the collector section, pressure resistance in the drying chamber, and bending and contraction at the dryer outlet respectively. As the drying air leaves the burner enclosure, it passes through a narrow horizontal rectangular slot, resulting in contraction and pressure loss. In the collector, the drying air flows from a narrower cross-sectional area to a wider section at the exit from the collector resulting in air expansion and pressure loss. These losses are included in thecomputation of pressure loss coefficients.

The coefficients K_{bu} , K_{cu} and K_{vu} are calculated according to ASHRAE (2009) based on the following assumptions: (a) the burner enclosure/unit is rectangular in section, (b) the collector is an asymmetric diffuser, and (c) the flow of air is viscous and fully developed.

$$K_{bu}=f_{bu}H_{bu}/D_{bu}+K_c \quad (3.27)$$

where K_c accounts for pressure loss during contraction and is computed according to Miller (1978).

$$K_{cu}=f_{cu}H_{cu}/D_{cu}+K_c \quad (3.28)$$

The loss coefficient associated with expansion of air from a narrow section into a room (K_e) was computed according to ASHRAE (2009).

For laminar flow, the friction factor f can be calculated from (Bala and Woods, 1994; ASHRAE, 2001)

$$f = 64/Re \tag{3.29a}$$

$$Re = \frac{\rho v_i D}{\mu} \tag{3.29b}$$

where v_i is the fluid inlet velocity.

The resistive pressure coefficient in the drying bed (K_{dd}) was calculated from the correlation reported byAyensu (1997).

Equation (3.26) is solved for v_o and the mass rate of flow of drying air,

$$\dot{m} = \rho_o A_o v_o \tag{3.30}$$

The input variables to the air flow model are $T_{f,i}$ (dryer air inlet temperature), T_f the plenum air temperature, and $T_{f,o}$ the dryer outlet temperature. The dryer inlet temperature is periodic in nature.

3.1.4 Estimation of heat transfer coefficients

The radiation heat transfer coefficient between the glass cover and the sky (i.e. from a collector to the surroundings) is given by

$$h_{r,c\text{-}sk} = \sigma \varepsilon_c (T_c^2 + T_{sk}^2)(T_c + T_{sk}) \tag{3.31}$$

where T_{sk}, the sky-temperature, is evaluated from an equation given by Ong (2003) as

$$T_{sk} = 0.0552(T_a)^{1.5} \tag{3.32}$$

For a rough assessment of sky temperature, Whillier (1967) provides even a simpler expression

$$T_{sk} = T_a - 6 \tag{3.33}$$

The effective sky temperature is related to the dew point temperature, dry bulb temperature, and the hour from midnight, t_h, by the following equation (Duffie and Beckman, 2006):

$$T_{sk} = T_a(0.711 + 0.0056\theta_{dp} + 0.000073\theta_{dp}^2 + 0.013\cos(15t_h) \tag{3.34}$$

KNUST

where T_{sk} and T_a are in Kelvin and θ_{dp} is the dew point temperature in degree Celsius. The experimental data on which equation (3.34) is based is valid for dew points ranging from - 20° C to 30° C. It is reported that in general, the difference between the sky temperature and the ambient air temperatures range from 5° C in hot, moist climate to 30° C in a cold, dry climate. In this study equation (3.32) was used since it is relatively simple and also gives fairly accurate results. It has been noted that a cloud cover will tend to increase the sky temperature over that for a clear sky.

A number of models have been proposed for the wind induced heat transfer coefficient between a solid boundary and the ambient as noted by Duffie and Beckman (2006). But, there is no well established model that is applicable to all situations. However, in situations similar to the current study, one equation that has been used on a number of occasions with acceptable results is (Ong, 2003; Ong chow, 2003)

$$h_{w,c-a} = 5.7 + 3.8V \qquad (3.35)$$

The radiative heat transfer coefficient from the concrete absorber to the cover plate (glazing), $h_{r,ab-c}$ is given as:

$$h_{r,ab-c} = \frac{\sigma\left(T_{ab} + T_c\right)\left(T_{ab}^2 + T_c^2\right)}{\frac{1-\varepsilon_{ab}}{A_{ab}\varepsilon_{ab}} + \frac{1}{A_{ab}F_{ab\to c}} + \frac{\rho_c}{A_c\varepsilon_c}} \qquad (3.36)$$

The radiative heat transfer coefficients from the concrete absorber to the three vertical walls adjoining the upper part of the thermal mass, $h_{r,ab-uw}$ are given by the general expression (Cengel, 2006):

$$h_{r,ab-uw} = \frac{\sigma\left(T_{ab} + T_{uw}\right)\left(T_{ab}^2 + T_{uw}^2\right)}{\frac{1-\varepsilon_{ab}}{A_{ab}\varepsilon_{ab}} + \frac{1}{A_{ab}F_{ab\to uw}} + \frac{1-\varepsilon_{uw}}{A_{uw}\varepsilon_{uw}}} \qquad (3.37)$$

Assuming (a) rock bed and the ~~conerete~~ base are parallel plates, and (b) rock bed is perpendicular to the wall enclosing the burner:The radiative heat transfer coefficients between the ~~bottom~~ surface of the rock pile and thegroundand between the bottom surface of the rock pile and the walls of the burner enclosure are given by the following expressions:

KNUST
LIBRARY
KWAME NKRUMAH
UNIVERSITY OF SCIENCE & TECHNOLOGY
KUMASI

$$h_{r,rp\text{-}bg} = \sigma \frac{\left(T_{rp} + T_{bg}\right)\left(T_{rp}^2 + T_{bg}^2\right)}{\frac{1}{\varepsilon_{rp}} + \frac{1}{\varepsilon_{bg}} - 1} \tag{3.38}$$

and

$$h_{r,rp\text{-}lw} = \frac{\sigma\left(T_{rp} + T_{lw}\right)\left(T_{rp}^2 + T_{lw}^2\right)}{\frac{1-\varepsilon_{rp}}{A_{rp}\varepsilon_{rp}} + \frac{1}{A_{rp}F_{rp\to lw}} + \frac{1-\varepsilon_{lw}}{A_{lw}\varepsilon_{lw}}} \tag{3.39}$$

The average Nusselt number for flow upwards (free convection) at the bottom surface of a heated plate (Incopera, F.P., De Witt, D.P., 2007) with angle $0 \le \theta \le 60$ and characteristic dimension $L_{c-f} = A_s / P$ is given as:

$$\overline{Nu_L} = 0.68 + \frac{0.670 Ra_L^{1/4}}{\left[1 + \left(0.492/Pr\right)^{9/16}\right]^{4/9}}, \text{ for laminar flow } \left(0 < Ra_L < 10^9\right) \tag{3.40}$$

$$\overline{Nu_L} = \left\{0.825 + \frac{0.387 Ra_L^{1/6}}{\left[1 + \left(0.492/Pr\right)^{9/16}\right]^{8/27}}\right\}^2, \text{ for turbulent flow } \left(Ra_L > 10^9\right) \tag{3.41}$$

where

$$Ra_L = Gr_L Pr = \frac{(g\cos\theta)\beta\left(T_c - T_f\right)L^3}{\nu\alpha} \tag{3.42}$$

where e.g. $Pr_{ab\text{-}f} = \frac{c_{p,ab\text{-}f}\mu_{ab\text{-}f}}{\lambda_{ab\text{-}f}}$, $\beta = \frac{1}{T_{c\text{-}f}}$

All fluid properties are evaluated at the surface film temperature, $T = \frac{T_c + T_f}{2}$. The g term in equation (3.42) is replaced with $g\cos\theta$ to account for the effect of inclination of the solid boundary. For θ above 60°, the Ra_L is interpolated between 60° and 90° as information for that range is lacking.

According to Incopera et al (2007) the recommended correlation for average Nusselt number for the upper surface of a heated horizontal plate based on a characteristic length $L = A_s/P$ is given as:

$$\overline{Nu_L} = 0.54 Ra_L^{1/4} \qquad \left(10^4 \le Ra_L \le 10^7\right) \qquad (3.43)$$

Equation (3.43) will be used for calculating the natural convection heat transfer coefficient between the top surface of the concrete absorber and the drying air.

Assuming the rock bed is a horizontal plate cooled from the bottom, the recommended correlation for calculating the average Nusselt number for flow over the bottom surface of a hot plate (Incopera, F.P., De Witt, D.P., 2007) is given by:

$$\overline{Nu_L} = 0.27 Ra_L^{1/4} \qquad \left(10^5 \le Ra_L \le 10^{10}\right) \qquad (3.44)$$

KNUST

For improved accuracy a characteristic dimension $L_{rp\text{-}f} = A_{rp}/P_{rp}$ is used for calculating the Rayleigh number which is given by:

$$Ra_L = \frac{g\beta\left(T_{rp} - T_f\right)L_{rp}Pr}{\nu^2} \qquad (3.45)$$

Equation (3.44) is used to calculate the convection heat transfer coefficient for convection between the bottom surface of the rock pile and ambient air.

The recommended correlation for the average Nusselt number for natural convection over the bare exterior surface of the cylindrical burner based on the diameter of the burner cylinder is given by

$$\overline{Nu_D} = \left\{0.6 + \frac{0.387 Ra^{1/6}}{\left[1 + \left(0.559/Pr\right)^{9/16}\right]^{8/27}}\right\}^2 \qquad (3.46)$$

where $Ra_D \le 10^{12}$ (Cengel, 2006).

The recommended correlation for the average Nusselt number for natural convection between a fluid stream and a plane vertical surface is:

$$\overline{Nu_L} = \left\{0.825 + \frac{0.387 Ra^{1/6}}{\left[1 + \left(0.492/Pr\right)^{9/16}\right]^{8/27}}\right\}^2 \qquad (3.47)$$

The convection heat transfer coefficients for natural convection is generally given as

$$h_c = \frac{\lambda \overline{Nu}}{L} \tag{3.48}$$

The total radiation $\overline{S_C}$ incident on the glazing surface may come in various proportions of direct, diffuse and reflected (either from the ground or neighbouring surfaces). It may be given as monthly, daily or hourly average total radiation. The irradiation absorbed by the concrete absorber is given as

$$\overline{S}_P = (\tau_c \alpha_{ab}) \overline{S}_C \tag{3.49}$$

KNUST

3.1.5 Thermo-physical properties of air

The air inside the plenum undergoes heating after going over the bare exterior surface of the burner before rising through the rectangular aperture located in the thermal mass into the plenum.

The thermo-physical properties of air (density, thermal conductivity, specific heat and kinematic viscosity) are assumed to vary linearly with temperature T (K). The following relations valid for 293 K < T < 333 Kare assumed for various thermo-physical properties of air(Ong, 2003; Ong and Chow, 2003):

$$\rho = -0.0038T + 2.3180 \tag{3.50a}$$

$$k = [0.0732\,T + 4.1672] \times 10^{-3} \tag{3.50b}$$

$$C_p = 0.0000098\,T + 1.0038 \tag{3.50c}$$

$$\nu = [0.0942\,T + 2.3180] \times 10^{-6} \tag{3.50d}$$

$$\mu = \left[1.846 + 0.00472\left(T - 300\right)\right] \times 10^{-5} \tag{3.50e}$$

The recommended (Kern and Harris, 1975; Duffie and Beckman, 1991) value of the collector tiltβ, for maximum annual collection of solar radiation is the latitude of the site. However, from experiments the minimum slope for rain-water to drop off a sloped surface is 6°. Hence, the minimum value of the collector tilt is 6°.

3.1.6 Solution procedure

The subscripts ab-f and rp-f are used to denote the interactions between concrete absorber and plenum air, and between rock pile and inlet air.

Solar heating mode (thermal mass equations)

By manipulating equations (3.5) to (3.8), we obtain

$$T_{ab\text{-}rp} = A_1 T_{ab} + B_1 T_{rp\text{-}bu} \quad (3.51a)$$

$$T_{rp\text{-}bu} = B_2 A_2 T_{ab\text{-}rp} + C_2 A_2 T_{bg} + D_2 A_2 T_{lw} + E_2 A_2 \quad (3.51b)$$

$$T_{bg} = P_1 T_{rp\text{-}bu} + C_3 \quad (3.51c)$$

$$T_{lw} = A_4 T_{rp\text{-}bu} + B_4 \quad (3.51d)$$

KNUST

where

$$A_1 = \frac{\lambda_{ab}}{x_{ab}}\left(\frac{\lambda_{rp}}{x_{rp}} + \frac{\lambda_{ab}}{x_{ab}}\right)^{-1}, B_1 = \frac{\lambda_{rp}}{x_{rp}}\left(\frac{\lambda_{rp}}{x_{rp}} + \frac{\lambda_{ab}}{x_{ab}}\right)^{-1}, A_2 = \left(h_{r,rp\text{-}bg} + h_{r,rp\text{-}lw} + h_{c,rp\text{-}fi} + \frac{\lambda_{rp}}{x_{rp}}\right)^{-1}$$

$$B_2 = \frac{\lambda_{rp}}{x_{rp}}, \quad C_2 = h_{r,rp\text{-}bg}, \quad D_2 = h_{r,rp\text{-}lw}, \text{ and } \quad E_2 = h_{c,rp\text{-}f,i} T_{f,i}$$

$$A_3 = h_{r,rp\text{-}bg} + \frac{\lambda_{bg}}{x_{bg}}, \quad B_3 = \left(\frac{\lambda_{bg}}{x_{bg}} + h_{r,rp\text{-}bg}\right)^{-1}, P_1 = h_{r,rp\text{-}bg} B_3, \quad C_3 = \left(\lambda_{bg} / x_{bg}\right) T_{gr} B_3$$

$$A_4 = h_{r,rp\text{-}lw} P_2, \; P_2 = \left\{\left(R_1 + 1/h_{c,lw\text{-}f,i}\right)^{-1} + h_{r,rp\text{-}lw}\right\}^{-1} \text{ and } B_4 = P_2\left(R_1 + \left(R_2 R_3 / R_3 + R_2\right)\right) T_a$$

Equations for cover glass and absorber(solar heating mode)

Equations (3.1) and (3.2) can be simplified into the following expressions:

$$T_c = F_2 F_1 T_{ab} + F_1 G_2 T_f + F_1 M_1 T_{uw} + F_1 G_1 \quad (3.52a)$$

$$T_{ab} = G_3 T_f + F_4 T_c + G_4 T_{uw} + C_8 \quad (3.52b)$$

where $F_1 = \left(h_{w,c\text{-}a} + h_{r,c\text{-}sk} + F_2 + G_2 + M_1\right)^{-1}$, $F_2 = h_{r,c\text{-}ab}$, $G_1 = \alpha_c \bar{S}_c + h_{w,c\text{-}a} T_a + h_{r,c\text{-}sk} T_{sk}$, $G_2 = h_{c,f\text{-}c}$

$M_1 = h_{r,uw\text{-}c}$

$F_3 = \left(h_{c,ab\text{-}f} + h_{r,ab\text{-}c} + h_{r,ab\text{-}uw}\right)^{-1}$, $C_8 = \bar{S}_p F_3$, $G_3 = h_{c,ab\text{-}f} F_3$, $F_4 = h_{r,ab\text{-}c} F_3$, $G_4 = h_{r,ab\text{-}uw} F_3$

In solar heating mode, the air stream model (from equations 3.3aand 3.3b) becomes:

$$T_f = \lambda_3 \lambda_2 T_{ab} + \mu_2 \lambda_2 T_c + C_{10} \qquad (3.53)$$

where $\lambda_2 = \left(\frac{\dot{m}_a c_{pa}}{WL_{ab}} + h_{c,f\text{-}c} + h_{c,ab\text{-}f}\right)^{-1}$; $\mu_2 = h_{c,f\text{-}c}$; $\gamma_3 = \frac{\dot{m}_a c_{pa}}{WL_{ab}} T_{f,i}$; $C_{10} = \gamma_3 \lambda_2$

$\lambda_3 = h_{c,ab\text{-}f}$

KNUST

Equations (3.51a), (3.51b), (3.51c), (3.51d), (3.52a), (3.52b), and (3.53) constitute a set of linear equations. This system of equations was solved to simulate heating in solar mode. The variables investigated are $T_{ab\text{-}f}$, $T_{ab\text{-}rp}$, $T_{rp\text{-}bu}$, $T_{bg} = T_a$, T_{lw}, T_c, T_f, and T_{uw}. The ground temperature T_{gr} is assumed to be at ambient (meaning $T_{gr} = T_a$). Equation 3.32 (i.e. $T_{sk} = 0.0552(T_a)^{1.5}$) was used to calculate sky temperature.

Burner heating mode (thermal mass equations)

Manipulation of equations (3.9), (3.10), (3.11), and (3.12) give:

$$T_{rp\text{-}bu} = A_5 T_{rp\text{-}ab} + B_5 T_{bg} + C_5 T_{lw} + D_5 \qquad (3.54a)$$

$$T_{rp\text{-}ab} = A_6 T_{rp\text{-}bu} + B_6 T_{ab\text{-}f} \qquad (3.54b)$$

$$T_{ab\text{-}f} = A_7 T_{ab\text{-}rp} + B_7 T_c + C_7 T_{uw} + D_7 T_f \qquad (3.54c)$$

$$T_{bg} = A_8 T_{rp\text{-}bu} + B_8 \qquad (3.54d)$$

where $A_5 = \frac{\lambda_{rp}}{x_{rp}}\left(\frac{\lambda_{rp}}{x_{rp}} + h_{r,rp\text{-}bg} + h_{r,rp\text{-}lw} + h_{c,rp\text{-}f}\right)^{-1}$; $B_5 = h_{r,rp\text{-}bg}\left(\frac{\lambda_{rp}}{x_{rp}} + h_{r,rp\text{-}bg} + h_{r,rp\text{-}lw} + h_{c,rp\text{-}f}\right)^{-1}$,

$C_5 = h_{r,rp\text{-}lw}\left(\frac{\lambda_{rp}}{x_{rp}} + h_{r,rp\text{-}bg} + h_{r,rp\text{-}lw} + h_{c,rp\text{-}f}\right)^{-1}$, $D_5 = h_{c,rp\text{-}f} T_{f,i}\left(\frac{\lambda_{rp}}{x_{rp}} + h_{r,rp\text{-}bg} + h_{r,rp\text{-}lw} + h_{c,rp\text{-}f}\right)^{-1}$

$$A_6 = \frac{\lambda_{rp}}{x_{rp}}\left(\frac{\lambda_{rp}}{x_{rp}} + \frac{\lambda_{ab}}{x_{ab}}\right)^{-1}; \quad B_6 = \frac{\lambda_{ab}}{x_{ab}}\left(\frac{\lambda_{rp}}{x_{rp}} + \frac{\lambda_{ab}}{x_{ab}}\right)^{-1}$$

$$A_7 = \left(\frac{\lambda_{ab}}{x_{ab}}\right)\left(h_{r,ab\text{-}c} + h_{r,ab\text{-}uw} + h_{c,ab\text{-}f} + \frac{\lambda_{ab}}{x_{ab}}\right)^{-1}, \quad B_7 = h_{r,ab\text{-}c}\left(h_{r,ab\text{-}c} + h_{r,ab\text{-}uw} + h_{c,ab\text{-}f} + \frac{\lambda_{ab}}{x_{ab}}\right)^{-1}$$

$$C_7 = h_{r,ab\text{-}uw}\left(h_{r,ab\text{-}c} + h_{r,ab\text{-}uw} + h_{c,ab\text{-}f} + \frac{\lambda_{ab}}{x_{ab}}\right)^{-1}, \quad D_7 = h_{c,ab\text{-}f}$$

$$A_8 = h_{r,rp\text{-}bg}\left(\frac{\lambda_{bg}}{x_{bg}} + h_{r,rp\text{-}bg}\right)^{-1}; \qquad B_8 = \lambda_{bg}/x_{bg}T_{gr}\left(\frac{\lambda_{bg}}{x_{bg}} + h_{r,rp\text{-}bg}\right)^{-1}$$

KNUST

Equation for heated air (burner heating mode)

Combination of (3.3b) and (3.3e) can be simplified into the following expressions:

$$T_f = \lambda_1\mu_1 T_{rp\text{-}bu} + \lambda_1\lambda_5 T_{ab} - \gamma_1\lambda_1 T_c + C_9 \qquad (3.55)$$

Collector efficiency:

$$\eta_c = \frac{\dot{m}\, C_{p,a}\,(T_f - T_{f,i})}{\dot{Q}tm} \qquad (3.56)$$

$$\lambda_1 = \left(h_{c,ab\text{-}f} - h_{c,f\text{-}c} + \frac{\dot{m}_a c_{pa}}{WL_{ab}}\right)^{-1}; \ \mu_1 = h_{c,bu\text{-}fi}; \ \lambda_5 = h_{c,ab\text{-}f}; \ \gamma_1 = h_{c,f\text{-}c}; \ C_9 = \lambda_1\lambda_7$$

$$\lambda_7 = \left(\frac{\dot{m}_a c_{pa}}{WL_{ab}} - h_{c,bu\text{-}fi}\right)T_{fi}$$

Equations (3.54a), (3.54b), (3.54c), (3.54d), and (3.55) constitute the air heater model in the burner heating mode. This system of linear equations was used to predict temperatures in burner heating mode.The variables investigated are cover glass temperature T_c, plenum fluid temperature ($T_f \leq 80\ ^{o}C$), concrete absorber surface temperature ($T_{ab\text{-}f}$), burner external surface temperature or burner rock pile interface temperature ($T_{rp\text{-}bu}$), rock pile absorber interface temperature ($T_{rp\text{-}ab}$), lower wall temperature ($T_{lw} = T_a + 39.7$), plenum wall or upper wall temperature (T_{uw}), and burner floor temperature ($T_{bg} = T_a + 20$).

Combined (hybrid) heating mode

Equations for cover glass and heated air:

From equations (3.1) and (3.2) the following expressions can be formulated for the cover glass and heated air respectively:

$$T_c = F_2F_1T_{ab} + F_1G_2T_f + F_1M_1T_{uw} + F_1G_1 \qquad (3.57a)$$

$$T_{ab} = G_3T_f + F_4T_c + G_4T_{uw} + C_8 \qquad (3.57b)$$

where $F_1 = \left(h_{w,c\text{-}a} + h_{r,c\text{-}sk} + h_{r,c\text{-}ab} + h_{c,f\text{-}c} + h_{r,uw\text{-}c}\right)^{-1}$, $F_2 = h_{r,c\text{-}ab}$, $G_1 = \alpha_c\bar{S}_c + h_{w,c\text{-}a}T_a + h_{r,c\text{-}sk}T_{sk}$, $G_2 = h_{c,f\text{-}c}$ $M_1 = h_{r,uw\text{-}c}$ and

$F_3 = \left(h_{c,ab\text{-}f} + h_{r,ab\text{-}c} + h_{r,ab\text{-}uw}\right)^{-1}$, $C_8 = \bar{S}_pF_3$, $G_3 = h_{c,ab\text{-}f}F_3$, $F_4 = h_{ab\text{-}c}F_3$, $G_4 = h_{r,ab\text{-}uw}F_3$

The air stream model for burning heat charging is applicable to hybrid heat charging.

$$T_f = \lambda_1\mu_1T_{bu} + \lambda_1\lambda_5T_{ab} - \gamma_1\lambda_1T_c + C_9 \qquad (3.58)$$

$$\lambda_1 = \left(\frac{\dot{m}_a c_{pa}}{(\pi r_{bu} + W)L_{ab}} + h_{c,f\text{-}c} + h_{c,ab\text{-}f}\right)^{-1};\ \mu_1 = h_{c,f\text{-}bu};\ \lambda_5 = h_{c,ab\text{-}f};\ \gamma_1 = h_{c,f\text{-}c};\ C_9 = \lambda_1\lambda_7$$

or

$$\lambda_1 = \left(h_{c,ab\text{-}f} - h_{c,f\text{-}c} + \frac{\dot{m}_a c_{pa}}{(\pi r_{bu} + W)L_{ab}}\right)^{-1};\ \mu_1 = h_{c,bu\text{-}fi};\ \lambda_5 = h_{c,ab\text{-}f};\ \gamma_1 = h_{c,f\text{-}c};\ C_9 = \lambda_1\lambda_7$$

$$\lambda_7 = \left(\frac{\dot{m}_a c_{pa}}{WL_{ab}} - h_{c,bu\text{-}fi}\right)T_{fi}$$ for the laboratory model

Equation (3.10) can be applied to hybrid heating mode under steady state assumptions. The resulting equation is:

$$T_{rp\text{-}ab} = Y_1Y_2T_{rp\text{-}bu} + Y_1Y_3T_{ab\text{-}f} \qquad (3.59)$$

$$Y_1 = \left(\frac{\lambda_{ab}}{x_{ab}} + \frac{\lambda_{rp}}{x_{rp}}\right)^{-1};\quad Y_2 = \frac{\lambda_{ab}}{x_{ab}};\quad Y_3 = \frac{\lambda_{rp}}{x_{rp}}$$

Equation (3.9) can be adopted for hybrid heating mode on the premise that total thermal energy gained by rock pile in the combined heating mode is lost from below the burner by convection to

inlet air, net radiation exchange between rock pile and burner floor as well as lower burner walls. For this application, equation (3.9) becomes:

$$T_{rp\text{-}bu} = A_5 T_{rp\text{-}ab} + B_5 T_{bg} + C_5 T_{lw} + D_5 \qquad (3.60)$$

where $A_5 = \frac{\lambda_{rp}}{x_{rp}}\left(\frac{\lambda_{rp}}{x_{rp}} + h_{r,rp\text{-}bg} + h_{r,rp\text{-}lw} + h_{c,rp\text{-}f}\right)^{-1}$; $B_5 = h_{r,rp\text{-}bg}\left(\frac{\lambda_{rp}}{x_{rp}} + h_{r,rp\text{-}bg} + h_{r,rp\text{-}lw} + h_{c,rp\text{-}fi}\right)^{-1}$,

$C_5 = h_{r,rp\text{-}lw}\left(\frac{\lambda_{rp}}{x_{rp}} + h_{r,rp\text{-}bg} + h_{r,rp\text{-}lw} + h_{c,rp\text{-}fi}\right)^{-1}$, $D_5 = h_{c,rp\text{-}fi} T_{f,i}\left(\frac{\lambda_{rp}}{x_{rp}} + h_{r,rp\text{-}bg} + h_{r,rp\text{-}lw} + h_{c,rp\text{-}fi}\right)^{-1}$

Equation (3.11) can be used in hybrid heating mode because of the similarities to burner heating mode. The resulting equation is:

$$T_{ab\text{-}f} = A_7 T_{ab\text{-}rp} + B_7 T_c + C_7 T_{uw} + D_7 T_f \qquad (3.61)$$

where

$A_7 = \left(\frac{\lambda_{ab}}{x_{ab}}\right)\left(h_{r,ab\text{-}c} + h_{r,ab\text{-}uw} + h_{c,ab\text{-}f} + \frac{\lambda_{ab}}{x_{ab}}\right)^{-1}$, $B_7 = h_{r,ab\text{-}c}\left(h_{r,ab\text{-}c} + h_{r,ab\text{-}uw} + h_{c,ab\text{-}f} + \frac{\lambda_{ab}}{x_{ab}}\right)^{-1}$

$C_7 = h_{r,ab\text{-}uw}\left(h_{r,ab\text{-}c} + h_{r,ab\text{-}uw} + h_{c,ab\text{-}f} + \frac{\lambda_{ab}}{x_{ab}}\right)^{-1}$, $D_7 = h_{c,ab\text{-}f}$

Equation (3.12) can be adopted for hybrid heating to take care of net radiation exchange between thermal mass and burner enclosure from which is subsequently conducted to the ground. The resulting modeling equation is

$$T_{bg} = A_8 T_{rp\text{-}bu} + B_8 \qquad (3.62)$$

where $A_8 = h_{r,rp\text{-}bg}\left(\frac{\lambda_{bg}}{x_{bg}} + h_{r,rp\text{-}bg}\right)^{-1}$; $B_8 = \lambda_{bg}/x_{bg} T_{gr}\left(\frac{\lambda_{bg}}{x_{bg}} + h_{r,rp\text{-}bg}\right)^{-1}$

In hybrid heating mode, the empirical correlation $T_{bg} = 8.66T_a - 2237.3$ was used for calculating the burner floor temperature (T_{bg})

Collector efficiency:

KNUST

$$\eta_c = \frac{\dot{m}\, C_{p,a}\,(T_f - T_{f,i})}{(\bar{S}_c \times A_{ab}) + \dot{Q}_{tm}} \qquad (3.63)$$

3.2 Drying chamber heater model

The subscripts dc, fo, and dw refer to drying chamber cover glass, temperature of air exiting drying section, and drying chamber wall, respectively.

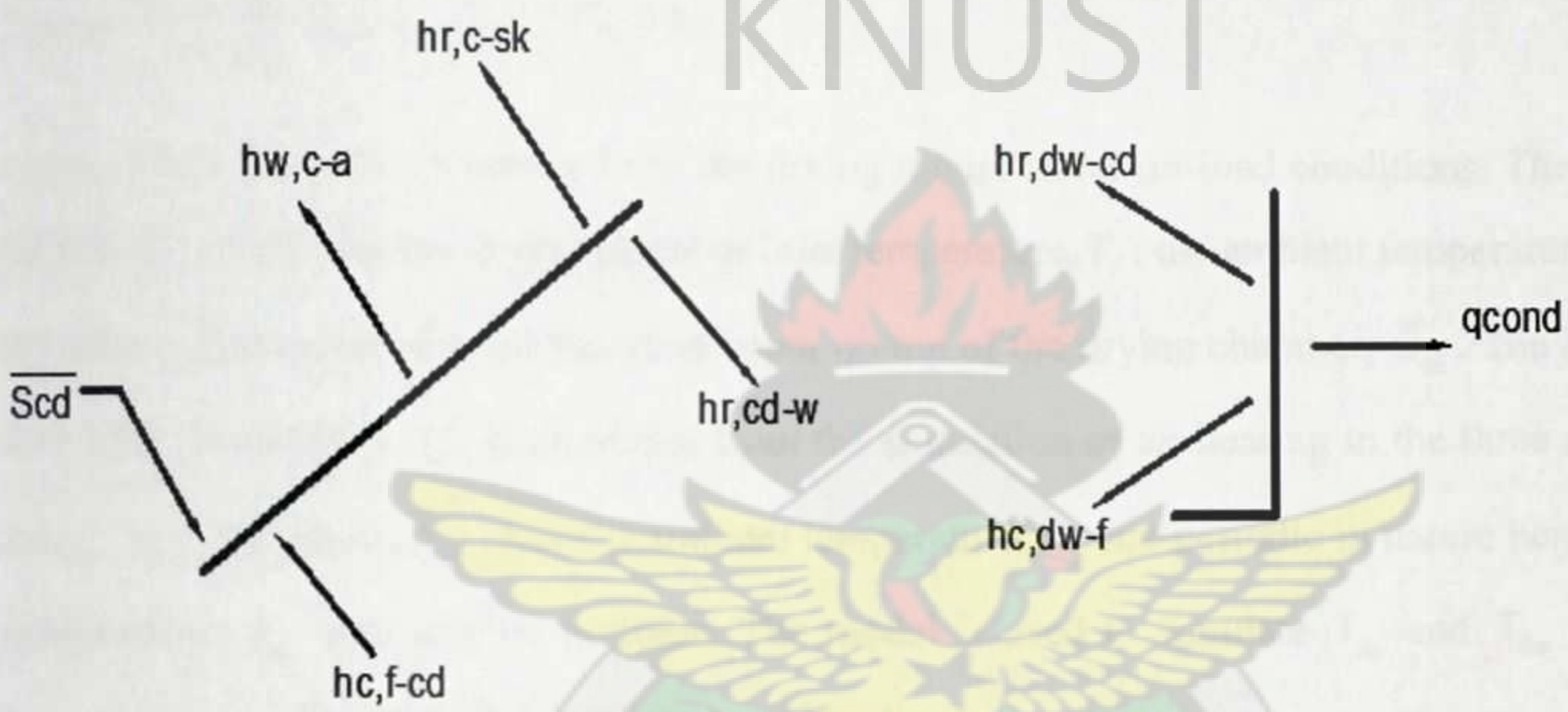

Figure 23 Energy balance on components of drying chamber

Under no-load, steady state conditions the energy balance equations on the drying chamber (see figure 23) are as follows:

Energy balance on drying chamber glazing (T_{dc}):

$$A_{dc}\left(\alpha_c \bar{S}_{cd}\right) + A_{dc} h_{c,dc\text{-}fo}\left(T_{f,o} - T_{dc}\right) = A_{dw} h_{r,dc\text{-}dw}\left(T_{dc} - T_{dw}\right) + A_{dc} h_{w,dc\text{-}a}\left(T_{dc} - T_a\right) + A_{dc} h_{r,dc\text{-}sk}\left(T_{dc} - T_{sk}\right) \qquad (3.64)$$

Energy balance on drying chamber wall under no load conditions:

$$A_{dw} h_{c,dw\text{-}f}\left(T_{dw} - T_f\right) + A_{dw} h_{r,dw\text{-}dc}\left(T_{dw} - T_{dc}\right) = A_{dw} \lambda_{dw} \frac{\left(T_{dw} - T_{dwo}\right)}{x_{dw}} \qquad (3.65)$$

Equations (3.64) and (3.65) can be transformed and simplified as follows:

$$T_{dc} = \frac{K_2 + K_3 T_{f,o}}{K_1} \tag{3.66}$$

$$T_{dw} = Z_2 Z_1 T_{dc} + Z_3 Z_1 T_f - Z_4 Z_1 \tag{3.67}$$

where

$$K_1 = A_{dc} h_{w,dc\text{-}a} + A_{dc} h_{r,dc\text{-}sk} + A_{dc} h_{c,dc\text{-}fo};\ K_2 = A_{dc} \alpha_c \bar{S}_{cd} + A_{dc} h_{w,dc\text{-}a} T_a + A_{dc} h_{r,dc\text{-}sk} T_{sk};\ K_3 = A_{dc} h_{c,dc\text{-}fo}$$

$$Z_1 = \left(h_{c,dw\text{-}f} + h_{r,dw\text{-}dc} - \frac{\lambda_{dw}}{x_{dw}} \right)^{-1},\ Z_2 = h_{r,dw\text{-}dc}$$

$$Z_3 = h_{c,dw\text{-}f},\ Z_4 = \frac{\lambda_{dw}}{x_{dw}} T_{dw,o},\qquad T_{dw,o} = T_a + 5$$

KNUST

Equations (3.66) and (3.67) together form the drying model under no-load conditions. The input variables to the model are the drying chamber inlet temperature, T_f, the ambient temperature, T_a, and the solar radiation incident on the glass cover on top of the drying chamber, $\bar{S}_{cd}$. The drying chamber inlet temperature, T_f, is an output from the simulation of air heating in the three modes of heating. The irradiation, $\bar{S}_{cd}$, and the ambient temperature, T_a are periodic in nature hence the sky temperature, T_{sk} will also be periodic. The model is used to simulate T_{dc} and T_{dw} under varying ambient conditions in the three modes of heating.

CHAPTER FOUR

EXPERIMENTAL SET-UPS: DESCRIPTION, INSTRUMENTS, MEASUREMENT TECHNIQUES, AND TESTS

4.0 Introduction

Experimental data needed for the development and validation of the mathematical model was obtained using a laboratory model of the dryer. The laboratory model adopted for experimentation is of geometrically similar construction to the designed prototype dryer. This model of the dryer which is able to simulate all the features of the designed dryer was adopted as a measure to cut down the cost of experimentation. The dryer is a mixed-mode natural convection solar crop-dryer. The laboratory model can accommodate two thousand two hundred and sixty-two grammes (2,262 g) of wet agricultural produce at any time. The general description of the small scale dryer used is provided in section 4.1. The description of the instruments and the measurement techniques adopted during the experiments is presented in section 4.2. A summary of the test series is provided in section 4.3. A more detailed description of the design principles including sample calculations for the determination of the various dimensions of the laboratory model is outlined in Appendix B.

4.1 Description of experimental set-ups

4.1.1 Laboratory model

Figures 24(a) and 24(b) show pictorial views of the laboratory model of the mixed-mode solar crop dryer with backup heater and the solar and burner simulators in operation. Figure 24(a) shows the laboratory dryer with manual instrumentation whereas figure 24(b) shows the dryer with a data logger. Manual instrumentation was used in the characteristic studies of the dryer under no load conditions whilst the data logger was used for experiments involving dehydration of products.

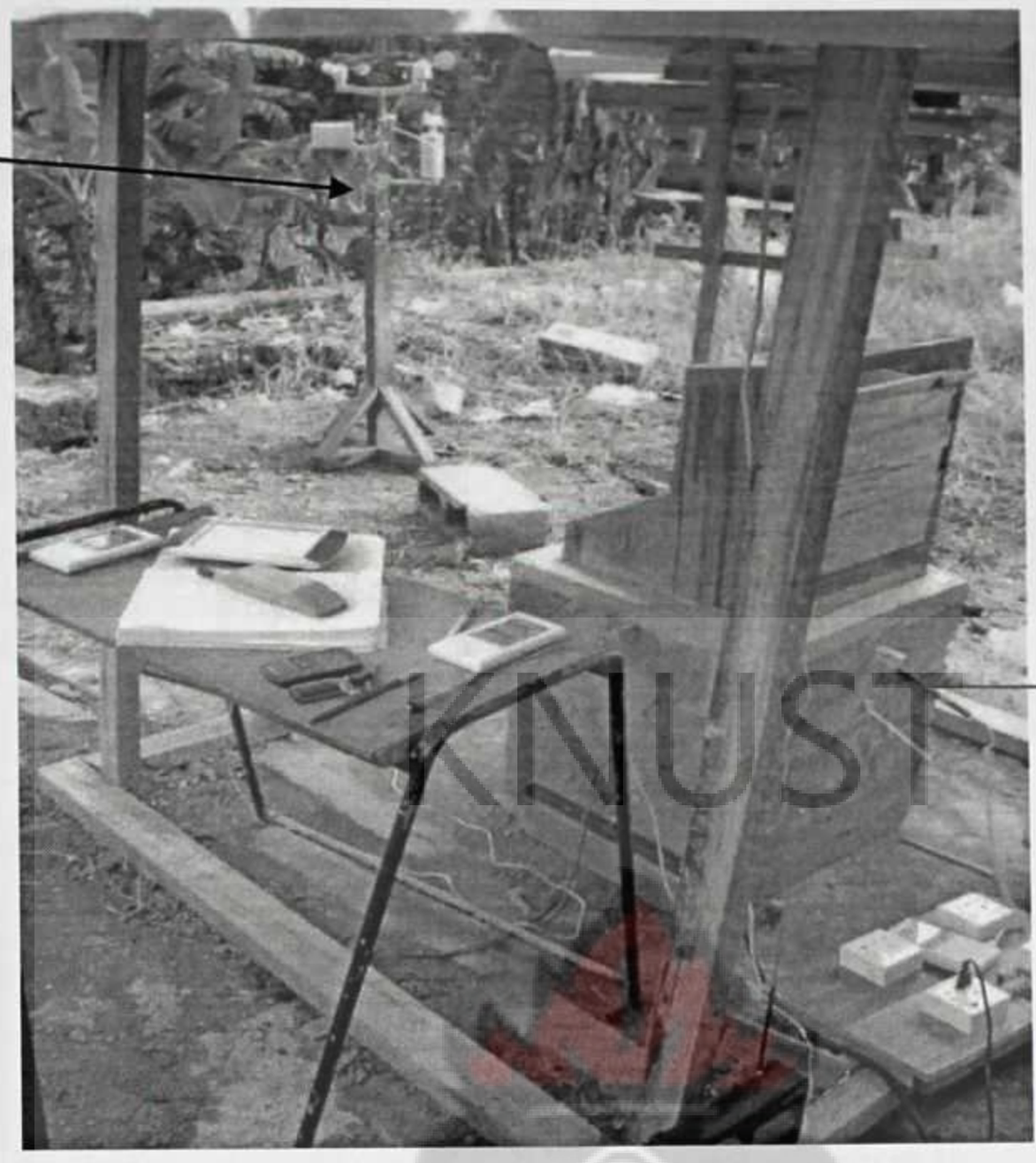

Figure 24(a): Pictorial view of the laboratory model of MNCSCDBH.

Figure 24(b): Pictorial view of the laboratory model of MNCSCDBH.

Figures 24 (c), 24(d), 24(e), and 24 (f) show sketches of the dryer and solar simulator unit with some important dimensions, the solar simulator platform and supporting member, the concrete absorber and rock pebble bed unit, and the vent outlet openings integrated into the dryer hardware to control the outflow of air.

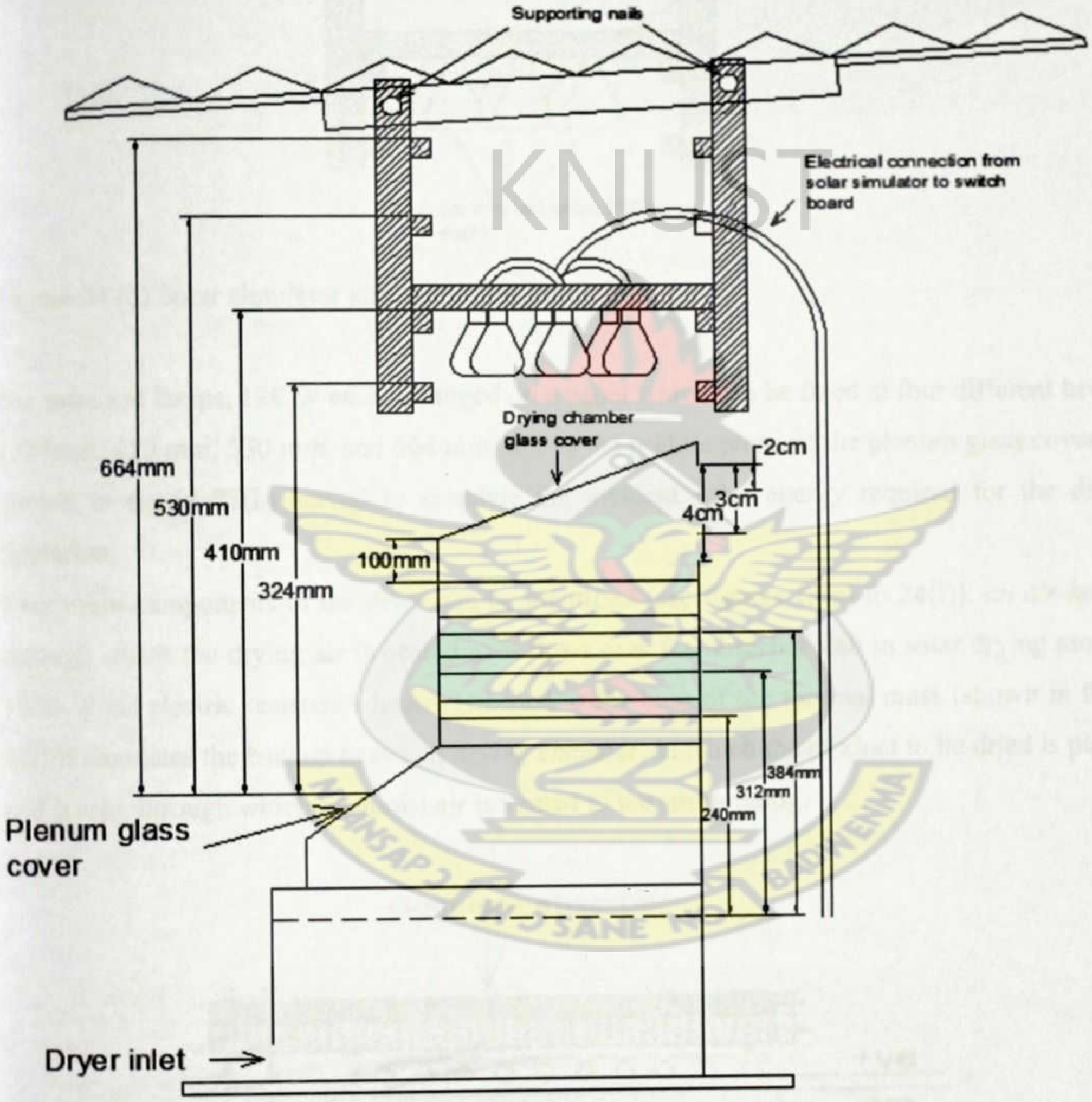

Figure 24 (c) Solar dryer and solar simulator arrangement

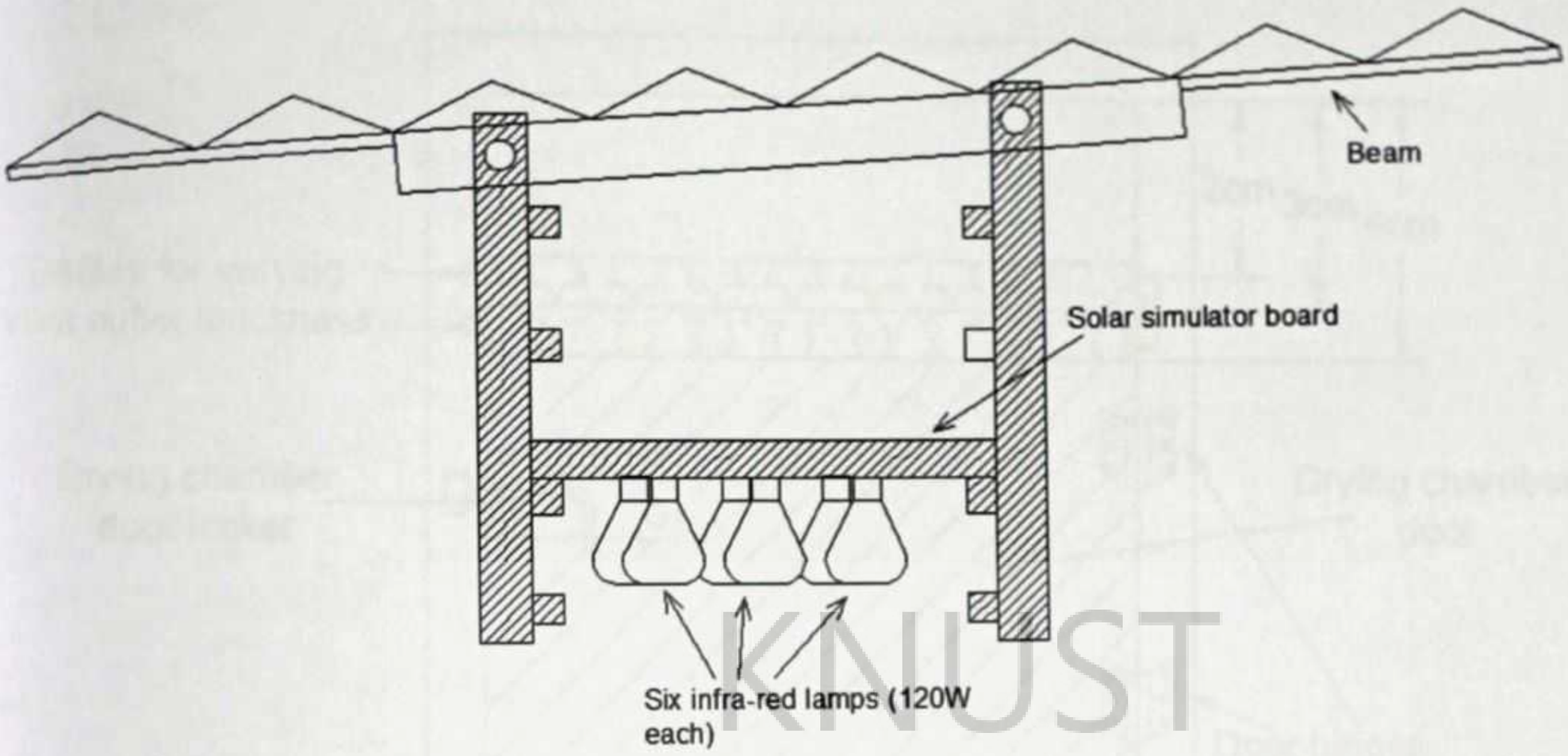

Figure 24 (d) Solar simulator and supporting structures

Six infra-red lamps, 120 W each, arranged on a panel which can be fixed at four different heights (324mm, 410 mm, 530 mm, and 664 mm) above the middle plane of the plenum glass cover, (as shown in figure 23(h) served to simulate the incident solar energy required for the drying operation.

Four main components of the dryer can be identified (see figures 24(a) to 24(f)): *an air-heater*, through which the drying air is heated as it flows over the absorber slab in solar drying mode; a 1800 Watts electric resistance heater attached to the base of the thermal mass (shown in figure 24(g)) simulates the backup heater*; a drying chamber*, in which the product to be dried is placed; and *a vent*, through which the moist air is vented to the surrounding.

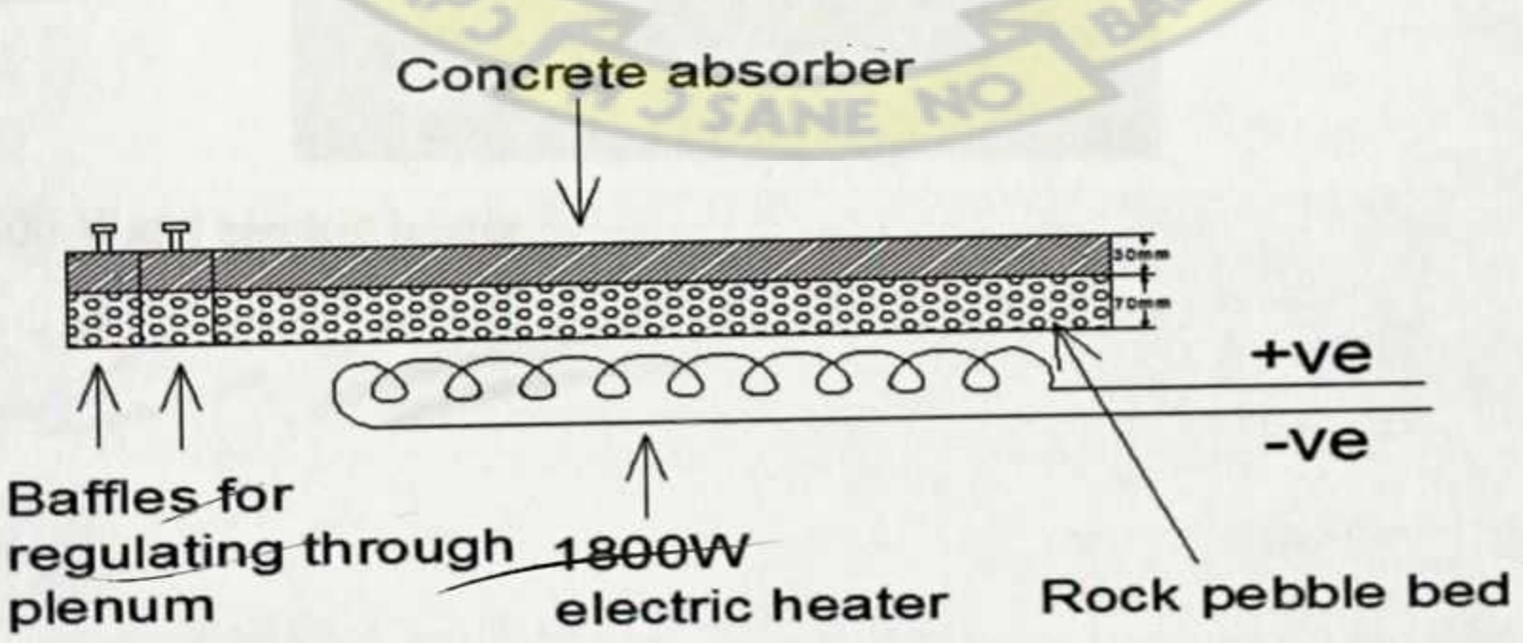

Figure 24 (e) Concrete absorber and rock pebble bed arrangement

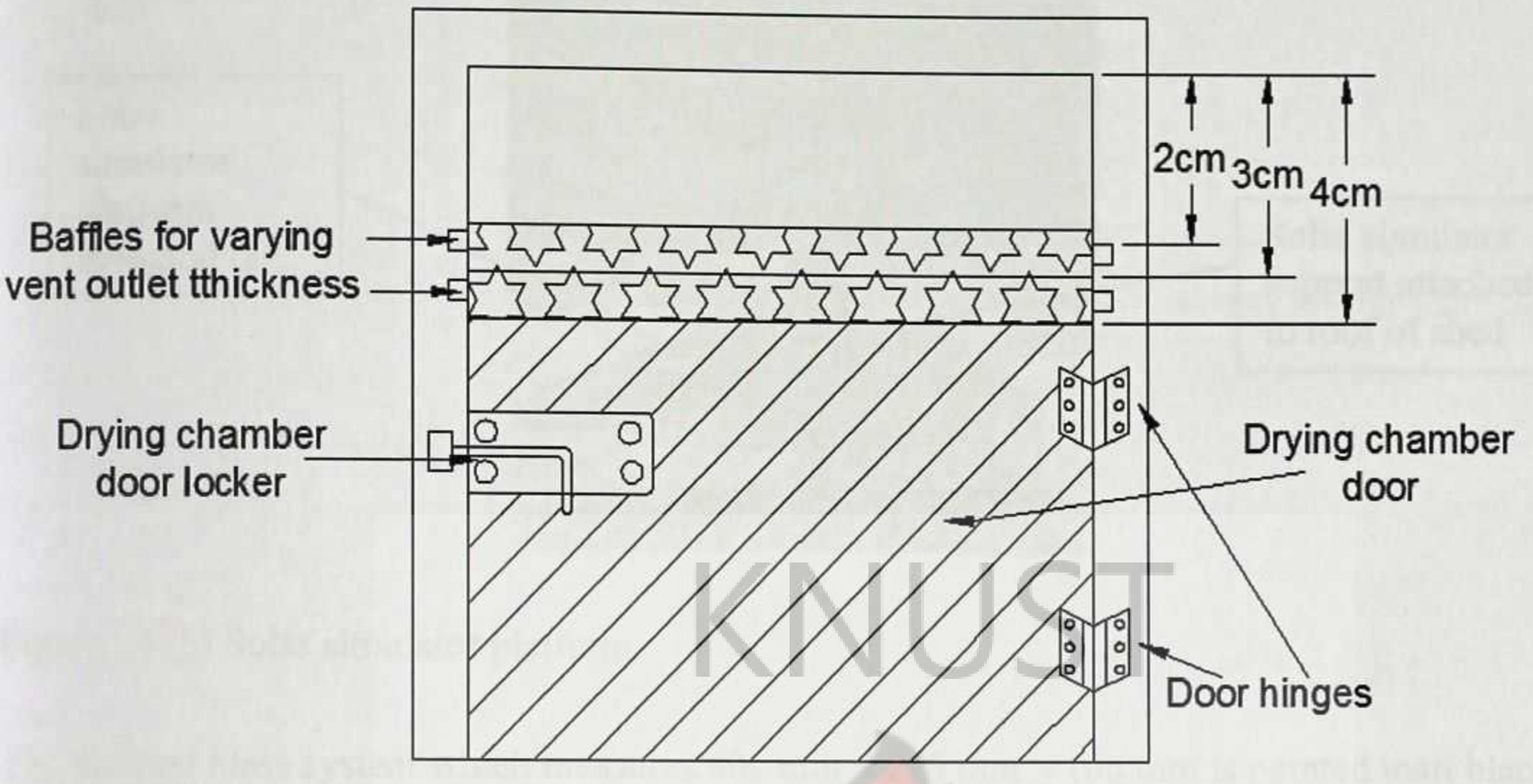

Figure 24(f) Vent outlet configuration

The *air-heater* consists of a concrete slab absorber integrated with a rock pile bed which constituted a thermal mass system. The thermal mass system serves as a temporary heat storage medium when the biomass burner is used.

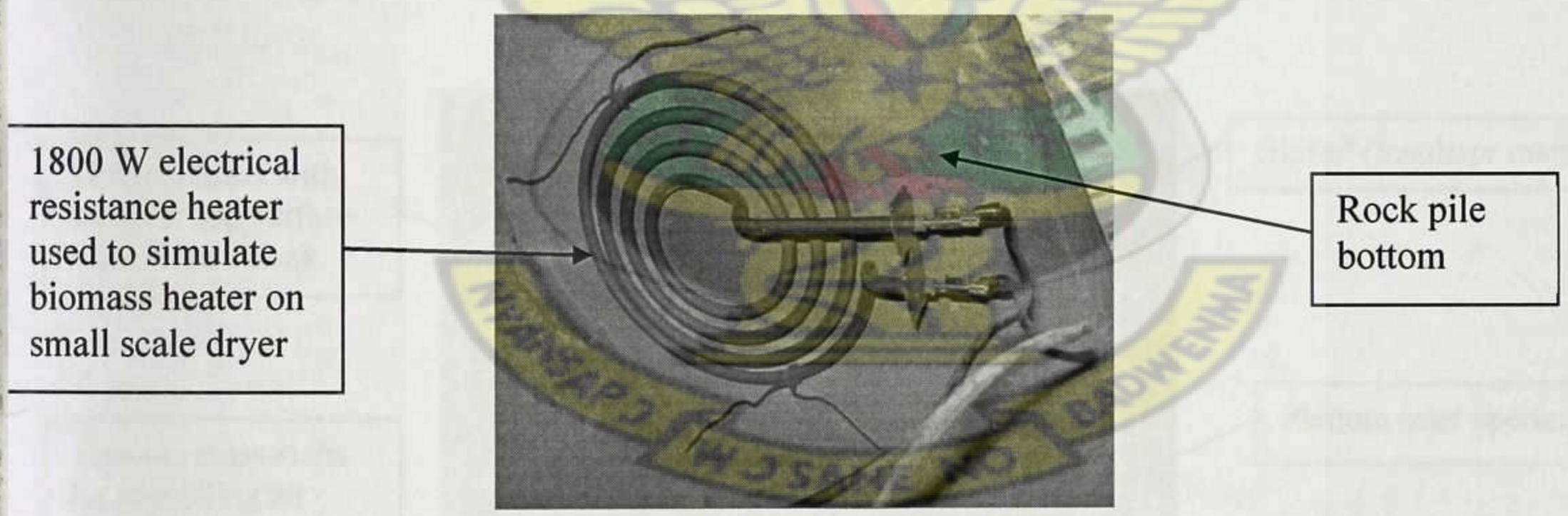

Figure 24(g) 1800 Watts electric heater

LIBRARY
KWAME NKRUMAH
UNIVERSITY OF SCIENCE & TECHNOLOGY
KUMASI

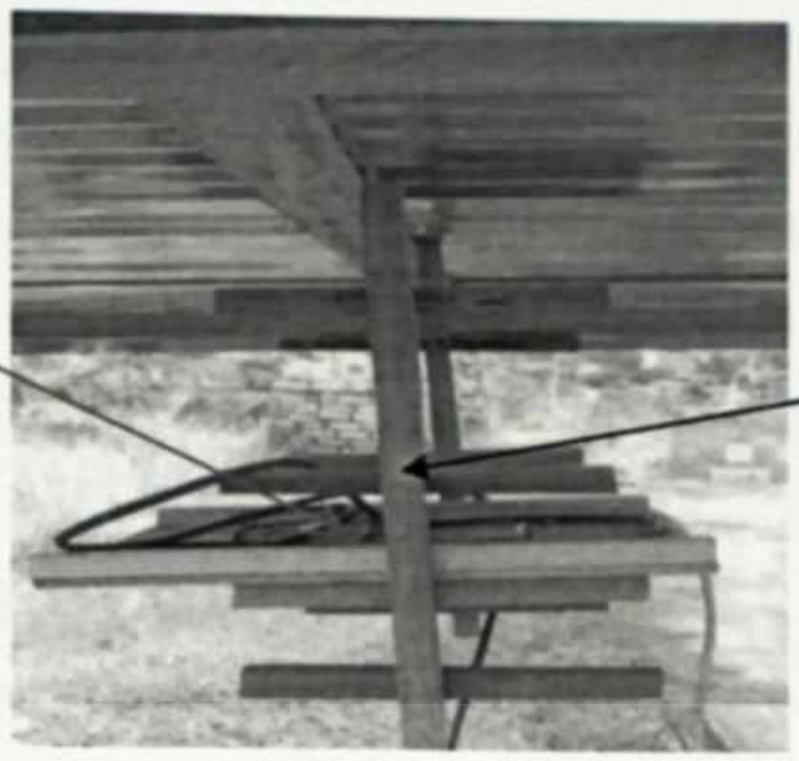

Figure 24 (h) Solar simulator platform

KNUST

The thermal mass system which measures 400 mm ×275 mm ×100 mm is painted matt black on its top surface to improve its thermal absorptivity. The plenum air inlet opening (31 cm by length internal) has two 2 cm thick baffles (shown in figure 25) for regulating air flow through the dryer. The rectangular air gap can be adjusted to 20, 40, and 60 mm widths. The rock bed (which makes up 70 mm thickness of the integrated concrete absorber thermal mass and has a rock pebble volume of 0.00355 m^3 whereas the concrete absorber is 30 mm thick.

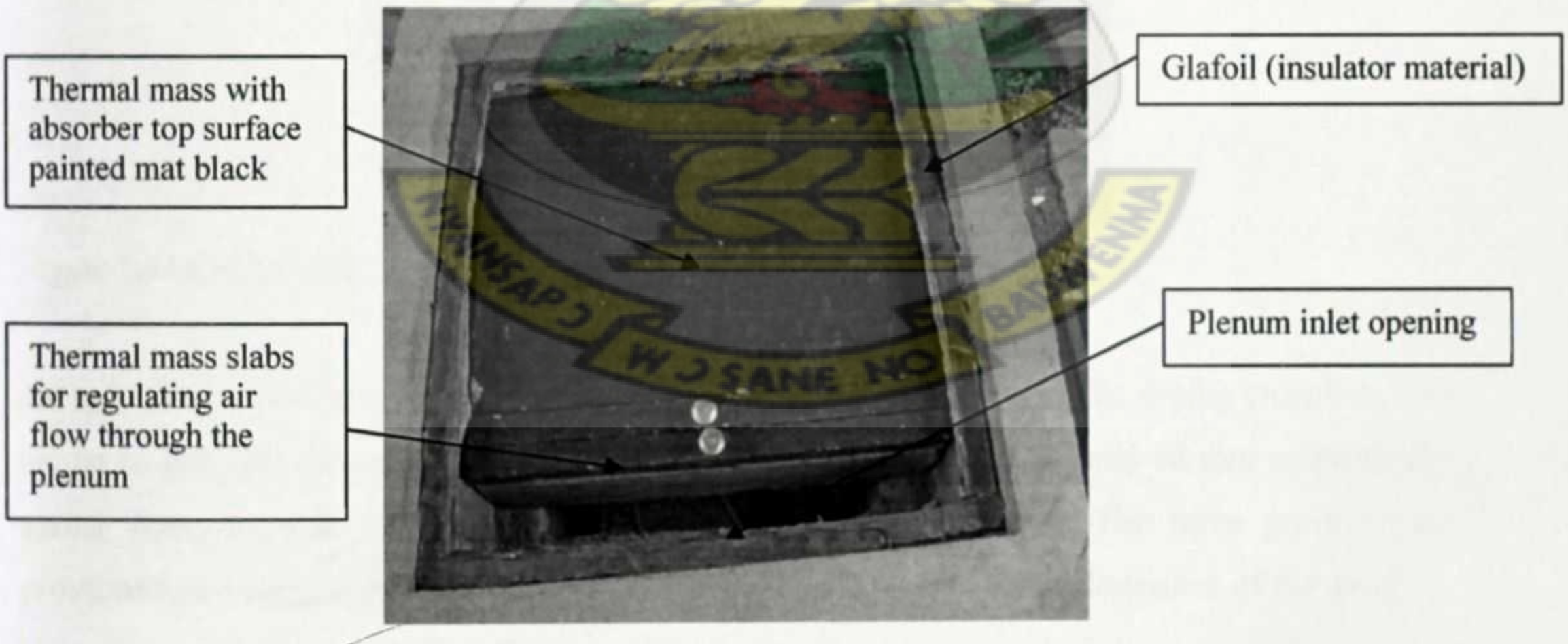

Figure 25 Integrated absorber-thermal mass system showing slabs for controlling air flow

The *drying chamber* has a trapezoidal section but with a rectangular drying surface measuring 141 mm x 367 mm. It houses three removable extended metal-mesh trays, arranged vertically in

line on guides that are spaced 72 mm apart with the lower tray at a height of 240 mm from the base of the plenum. The second and third trays as shown in figure 25 are 312 mm and 376 mm from the plenum base, respectively. The distance from the top of the third tray to the lower edge of the drying chamber roof is 100 mm. The side walls are made up of block board and the roof is made of glazing. There is a door that provides access to the chamber for loading, and unloading the crop and it measures 200 mm × 402 mm. The entire wooden structure that makes up the plenum and drying chamber fits into a rectangular slot (measuring 440 mm ×425 mm internally) with a glass foil insulation material between the wooden components of the system and the burner compartment (see figure 25).

KNUST

Figure 26 MNCSCDBH showing drying trays

An exit air vent 400 mm wide runs across the width of the top back of the drying chamber. The height of the vent can be adjusted to three positions (20 mm, 30 mm, and 40 mm respectively) giving three variable air exit areas for dryer characteristic studies. The three positions are provided to investigate the effect of varying the exit vent size on the performance of the dryer.

4.1.2 Operation

The dryer is designed to operate with solar radiation as the main energy source. The back-up heater is used when radiation is inadequate and at night so that continuous drying is not

interrupted. When the dryer is run on solar energy as the main energy source, atmospheric air picks up heat energy absorbed by the concrete absorber and rises through the drying cabinet to effect drying. In addition, direct solar radiation entering through the transparent top cover, is absorbed by the interior surfaces of the cabinet and by the crop, thus, providing additional energy for drying. The heated surfaces further warm the surrounding air, which rises by natural convection, passing through the drying trays and picking up moisture from the product being dried. The moist air finally exits the dryer through the vents on the upper back side of the cabinet. This action reduces the pressure inside the cabinet and ambient air is drawn into the dryer through the inlet holes in the brick wall. A continuous flow of air is thus established.

KNUST

During periods of low radiation, the back-up heater is used to supply heat energy. The resistance heater heats up the rock pile bottom surface, which in turn warms the air naturally aspirated through the system as it moves over the rock pile surface. The warm air rises up into the drying chamber, evaporating and picking up crop moisture as it passes through the trays, and then escapes through the top vents as before. By regulating the amount of air entering the burner the heat delivery rate can be controlled.

4.2 Instrumentation and measurement

The laboratory dryer was fully instrumented for the various measurements. The following parameters were measured during experimentation: mass of pineapple, temperature, relative humidity, moisture content levels, wind speed and air flow through dryer. A combination of hand-held instruments and sensors and a data logger (21X Micrologger) were used to make and record the measurements under load conditions. Under no load conditions the instrumentation was done manually. Figure 27 shows the experimental dryer with the locations of the temperature measuring sensors and humidity probes.

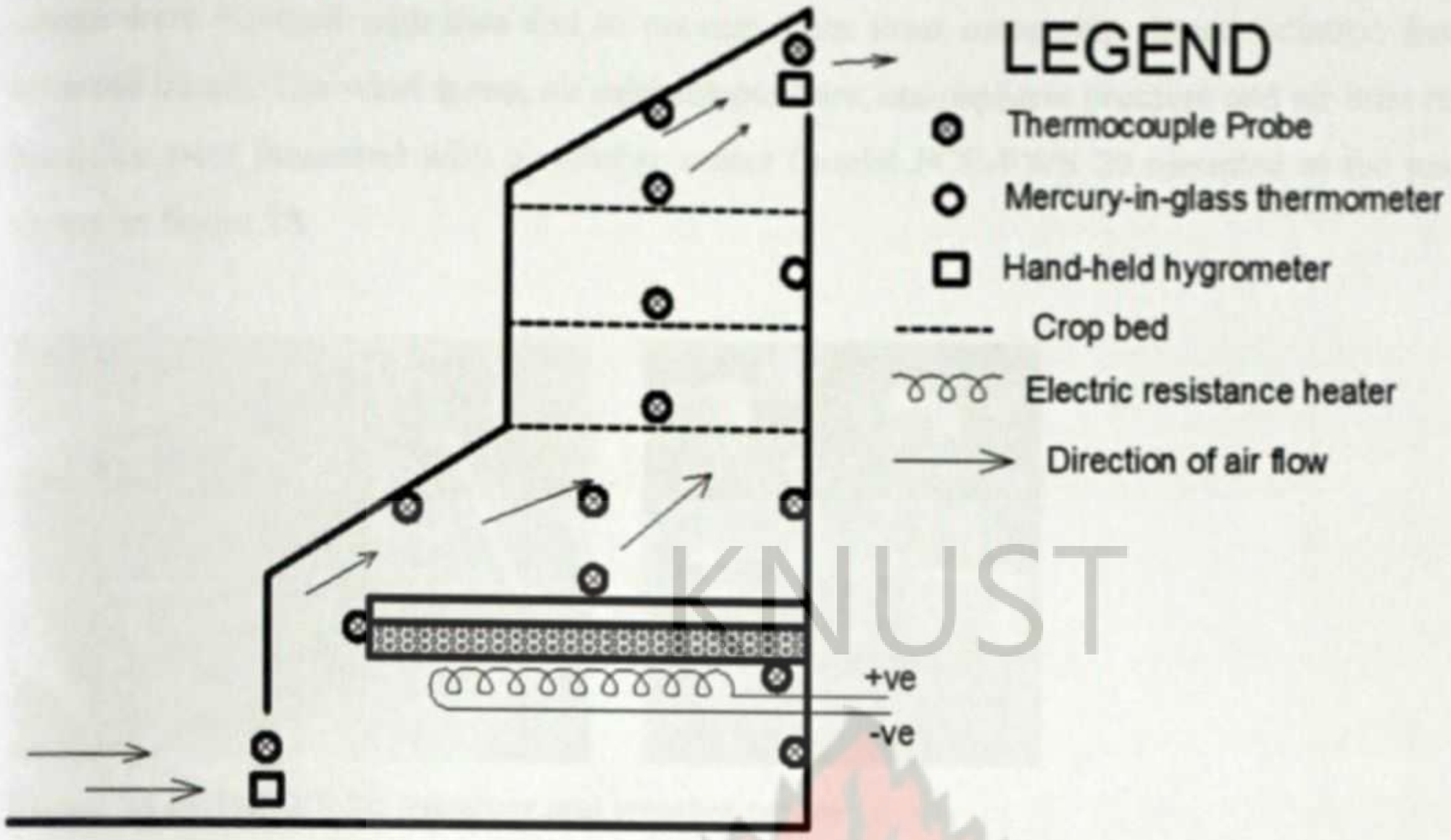

Figure 27 Schematic illustration of the laboratory dryer showing the locations of the temperature and relative humidity measuring sensors.

The instruments and the techniques used to measure the various parameters during the experiments carried out on the laboratory model described in section 4.1 are provided below.

4.2.1 Laboratory model instrumentation

Air speed, relative humidity, and temperature measurement

The concrete absorber top surface and rock pebble bed underside surface temperatures; the glazing temperatures of the plenum and the drying chamber; the inner wall temperatures of the burner housing and the plenum; the burner floor temperature; the drying chamber wall temperature; the absorber-rockpile interface temperature; and the average plenum air temperature were measured at intervals of twenty minutes between consecutive readings in solar heating mode and intervals of fifteen minutes in burner heating and hybrid heat charging modes respectively, with Mercury-in-glass thermometers (the mercury-in-glass thermometers used could measure up to 250 °C) with accuracy of ± 0.1°C during the dryer characteristic studies. The thermometers were attached to the various parts using sellotape. The bulbs of the mercury-in-glass thermometers connected to the inner surfaces of the plenum and drying chamber glass

covers were covered with thin foil to prevent them from measuring direct radiation from the infra-red lamps. The wind speed, air inlet temperature, atmospheric pressure and air inlet relative humidity were measured with a weather center (model PCE-FWS 20 mounted at the test site) shown in figure 28.

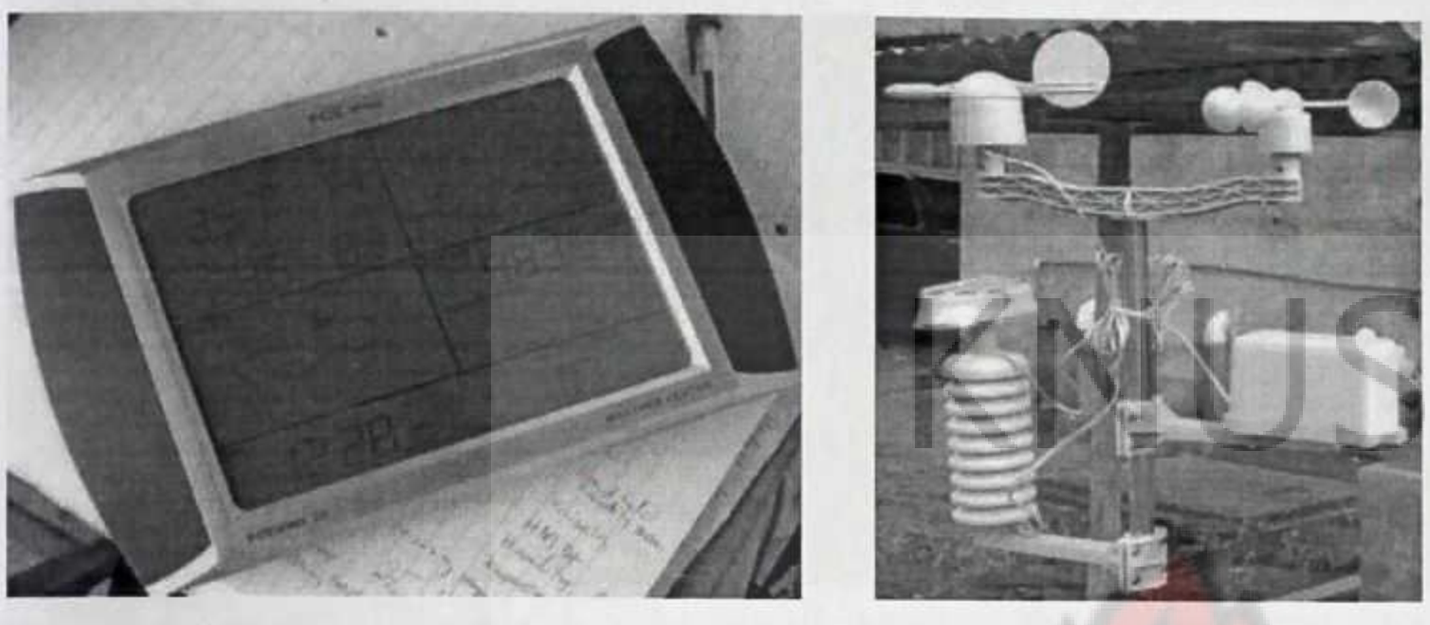

Figure 28 PCE-FWS 20 Receiver and weather centre

The air outlet temperature and relative humidity were measured with a portable Macronta LCD Indoor/Outdoor thermometer/hygrometer (CAT 63-867) in conjunction with a Vaisala H M34 humidity and temperature meter (measuring range: 0 – 100% RH and -4 to +140 °F) as shown in Figure28.

Figure 29 Vaisala H M34 and Macronta LCD humidity and temperature meters

A Barnant 115 thermocouple (model number: 600-2810) was used to measure the rock bed-absorber interface temperature.

The mercury-in-glass thermometers used to measure the absorber top surface, thermal mass lower surface, and burner housing floor surface temperatures could measure temperatures up to 482 °F (250 °C). The intensity of infra red radiation (from infra red lamps) on the inclined plane of the plenum glass cover was measured with a solar meter (model 776).

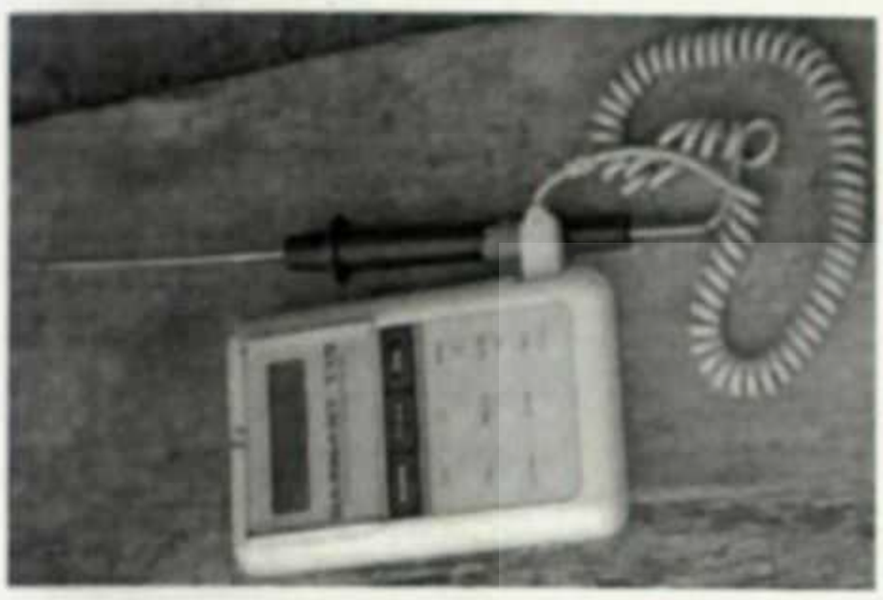

Figure 30 Barnant 115 thermocouple (model number: 600-2810)

Figure 31 Solar meter (model 776)

Under load conditions copper-constantan thermocouples (type K) suitable for temperatures ranging from 0 to 200° C were used to measure the following temperatures:

air inlet temperature, T_{fi}

average burner housing floor temperature, T_{bg}

average inner burner housing wall temperature, T_{lw}

average rock bed bottom surface temperature, T_{rp-f}

average rock pile-absorber interface temperature, T_{rp-ab}

average absorber top surface temperature, T_{ab-f}

average inner plenum wall temperature, T_{uw}

average plenum fluid temperature, T_f

average product surface temperatures in trays 1, 2, and 3 respectively T_1, T_2, and T_3

average air outlet temperature, Tfo

The output terminals from twelve thermocouples, measuring the temperatures listed above, were connected to a thermocouple temperature logger (21X micrologger, Campbell Scientific; S/N 11552). The logger, which measures temperatures up to an accuracy of ± 0.01°C was programmed using the 21X prompt sheet. The programme and, hence, data collected were stored

on storage module SM 192 (S/N 11487). The temperatures were continuously monitored and logged out using the 21X Micrologger from Campbell Scientific Incorporation, U.S.A (see figure 32). The logger was programmed in the single channel mode to select an input to a channel every 5 minutes and the recorded data integrated to give the hour-by-hour values.

Figure 32 21X Micrologger, Campbell Scientific Incorporation, U.S.A

Measurement of product moisture loss

The weight loss of the samples were measured hourly by the use of an electronic scale with accuracy of ± 0.1 g (Metler PM 34) by removing the trays from the drying chamber one after the other.

Calibration of instruments

Calibration of mercury-in glass thermometers

Ice Point Method

A measuring cylinder was filled with a uniform mixture of potable crushed ice and water to within 1 inch of top of container to provide an environment of 32°F (see figure 33).

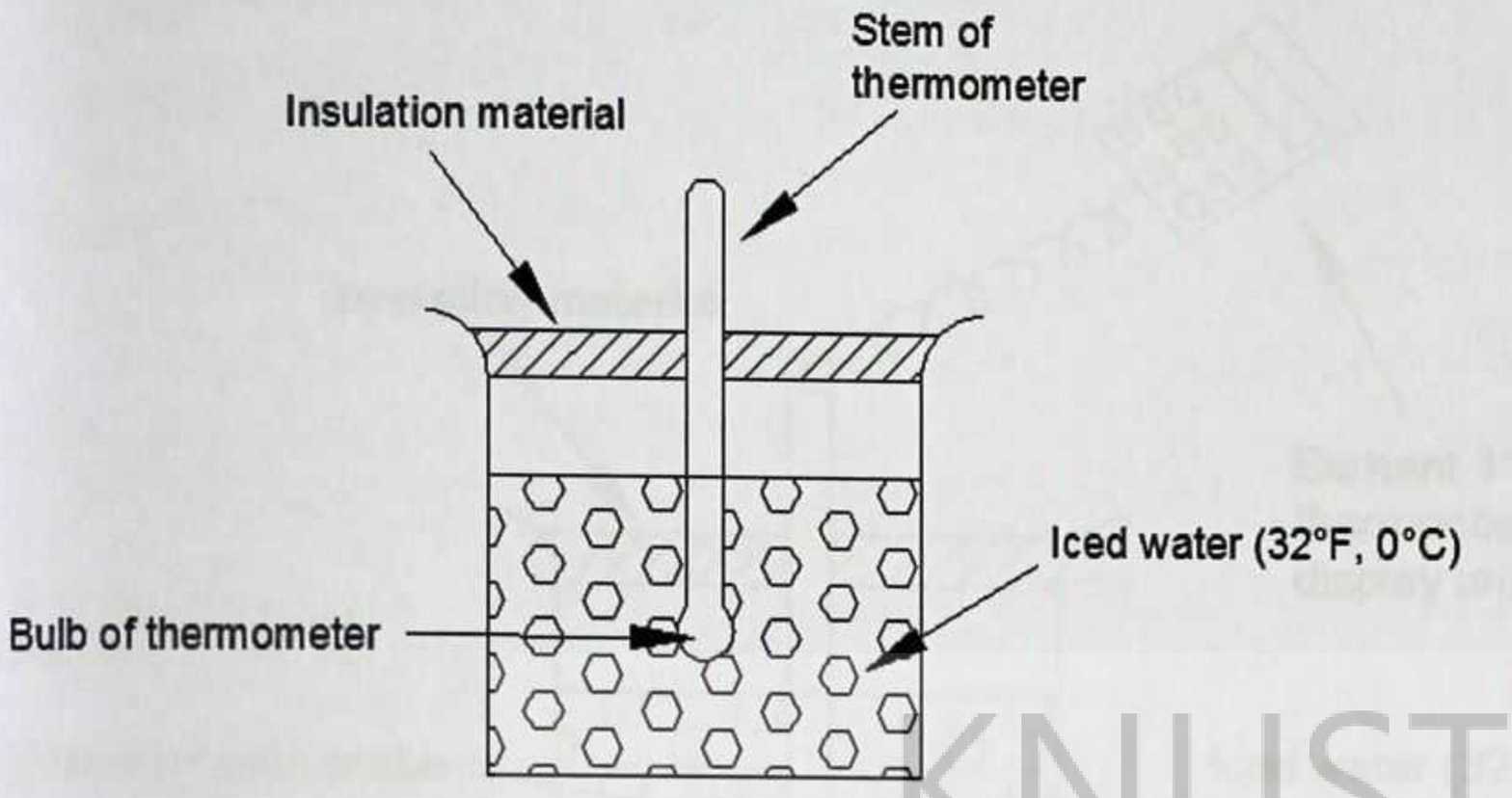

Figure 33 Setup for calibration of mercury-in-glass thermometers

When the mixture of the water and ice had stabilised after about five minutes, the mercury-in-glass thermometer to be calibrated was inserted such that the sensing portion (from tip of thermometer to the dimple on stem) which is about five (5) centimeters depth from the bulb was immersed in the mixture.

Measures were put in place to ensure that the stem of the instrument did not touch the bottom and sides of the container. Sufficient time was allowed for the thermometer reading to stabilise. Thermometers that were not accurate within +/- 2°F of 32°F were replaced.

Calibration of the Barnant 115 thermocouple

The steps taken to calibrate the Barnant 115 thermocouple were similar to those described for the mercury-in-glass thermometer. The exception was that the Barnant 115 thermocouple had a reset button that had to be pushed to recalibrate the setting (see figure 34). The resetting was done by holding the on/off button located behind the digital display unit for about 8 seconds to enter the calibration mode.

Procedure:

The stem of the Barnant 115 thermocouple was immersed into the ice water bath ensuring that the tip was in the mixture deep enough and not touching the bowl. When the display had become stable, the "CAL" button was pressed until the display read 32°F (0°C)

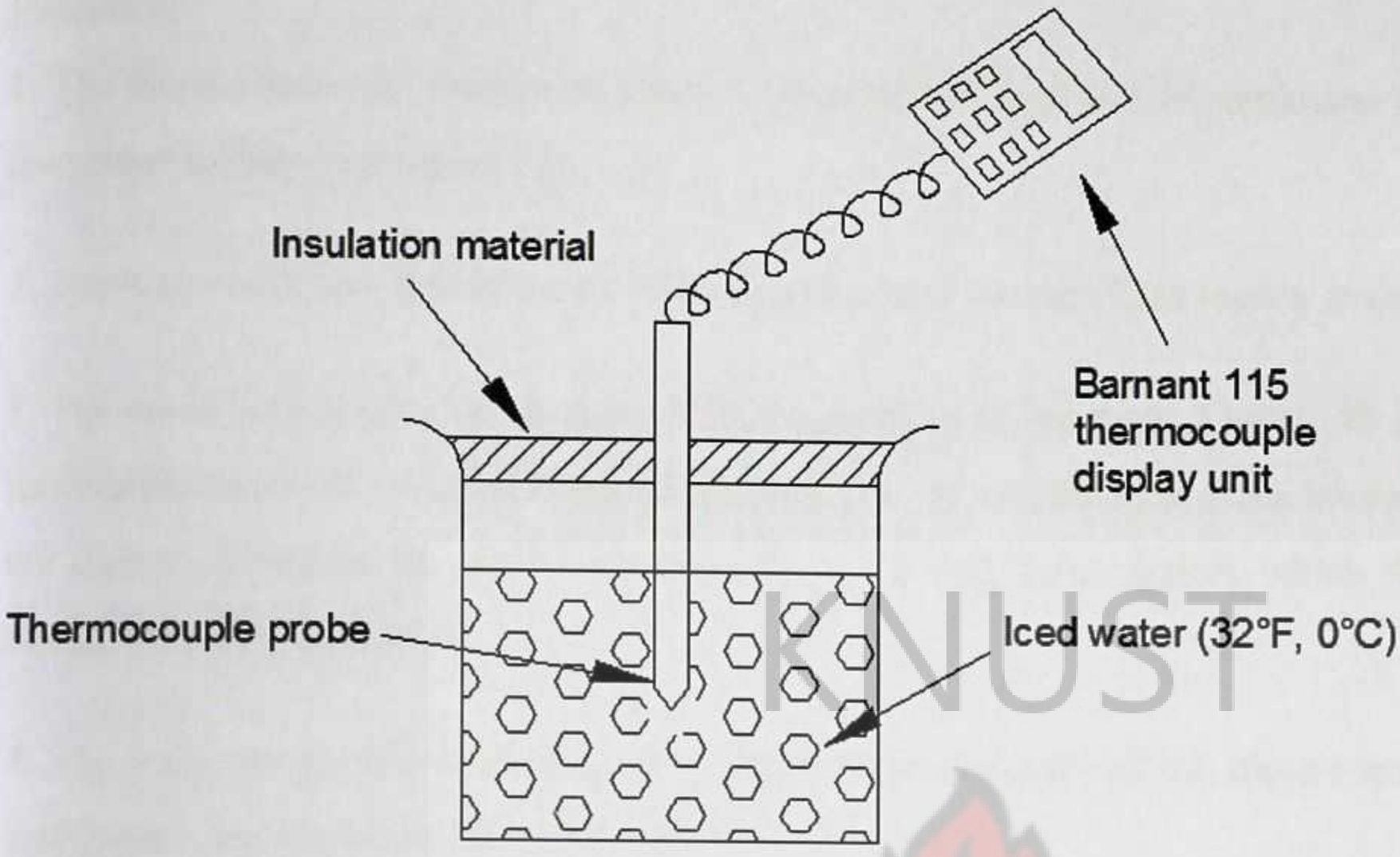

Figure 34 set up for calibration of Barnant 115 thermocouple

Calibration of type k thermocouple (Chromel / Alumel) wires

Thermocouple composition: a positive leg, which is approximately 90% nickel, 10% chromium and a negative leg, which is approximately 95% nickel, 2% aluminum, 2% manganese and 1% silicon.

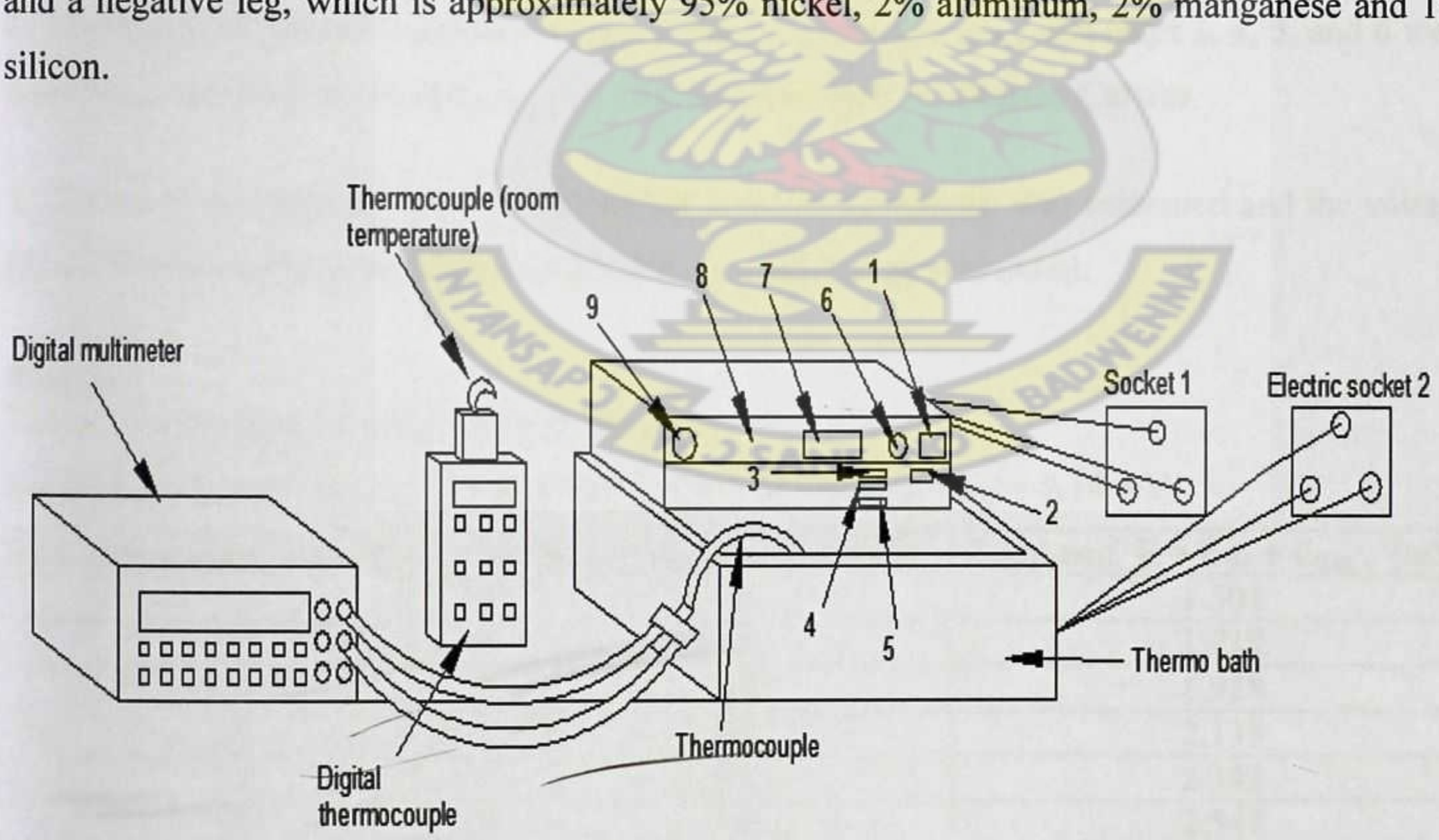

Figure 35 set up for calibration of k- type thermocouple wires

Procedure:

1. The thermo bath was filled with water to the required level and the apparatus was connected to the power supply (see figure 35).

2. The water bath was turned on by switching the main switch (1) as shown in the figure.

3. The set-in switch (8) was used to set the temperature to the desired level (30 deg C to start) by turning the knob (6) and observing the display (7). In normal mode, the temperature shown on the digital display is the actual temperature of the bath (T_B) against which the thermocouple sensor would be calibrated.

KNUST

4. The ends of the thermocouple were connected to the ends of the digital multimeter and the multimeter was set to read in millivolts DC.

5. One end of the thermocouple junction was immersed in the thermo-bath liquid and the device was left for few minutes to stabilise (i.e. the reading on the multimeter became steady except the last digit).

6. The digital multimeter readings were recorded in millivolts (E_M) and steps 3, 4, 5, and 6 were repeated in temperature increments of 5 degrees from 30 to 60 degrees Celsius.

7. The room temperature at which the experiment was conducted was measured and the voltage for the thermocouple type at the measured room temperature was noted.

Results:

Table 2 Thermocouple calibration results

Room temperature: 28.5 °C; corresponding millivolt reading, E_{RM} = 1.14 mV

Bath temperature, T_B, (°C)	Millivolt reading, Em (mV)	Total emf, E = Em + E_{RM} , (mV)
30	0.361	1.501
35	0.579	1.719
40	0.788	1.928
45	0.995	2.135
50	1.202	2.342
55	1.407	2.547
60	1.613	2.753

Figure 36 shows the "standard response curve" for the type-K thermocouple used in collecting data during the dehydration tests. Equation (4.1) matches the standard curves for a type-K thermocouple with error less than 0.1 degrees Celsius through the range 30 degrees C to 60 degrees Celsius.

$$3\times10^{-14}V^3 - 9\times10^{-13}V^2 + 25 \qquad (4.1)$$

where V is voltage in units of millivolts and T is temperature in degrees Celcius.

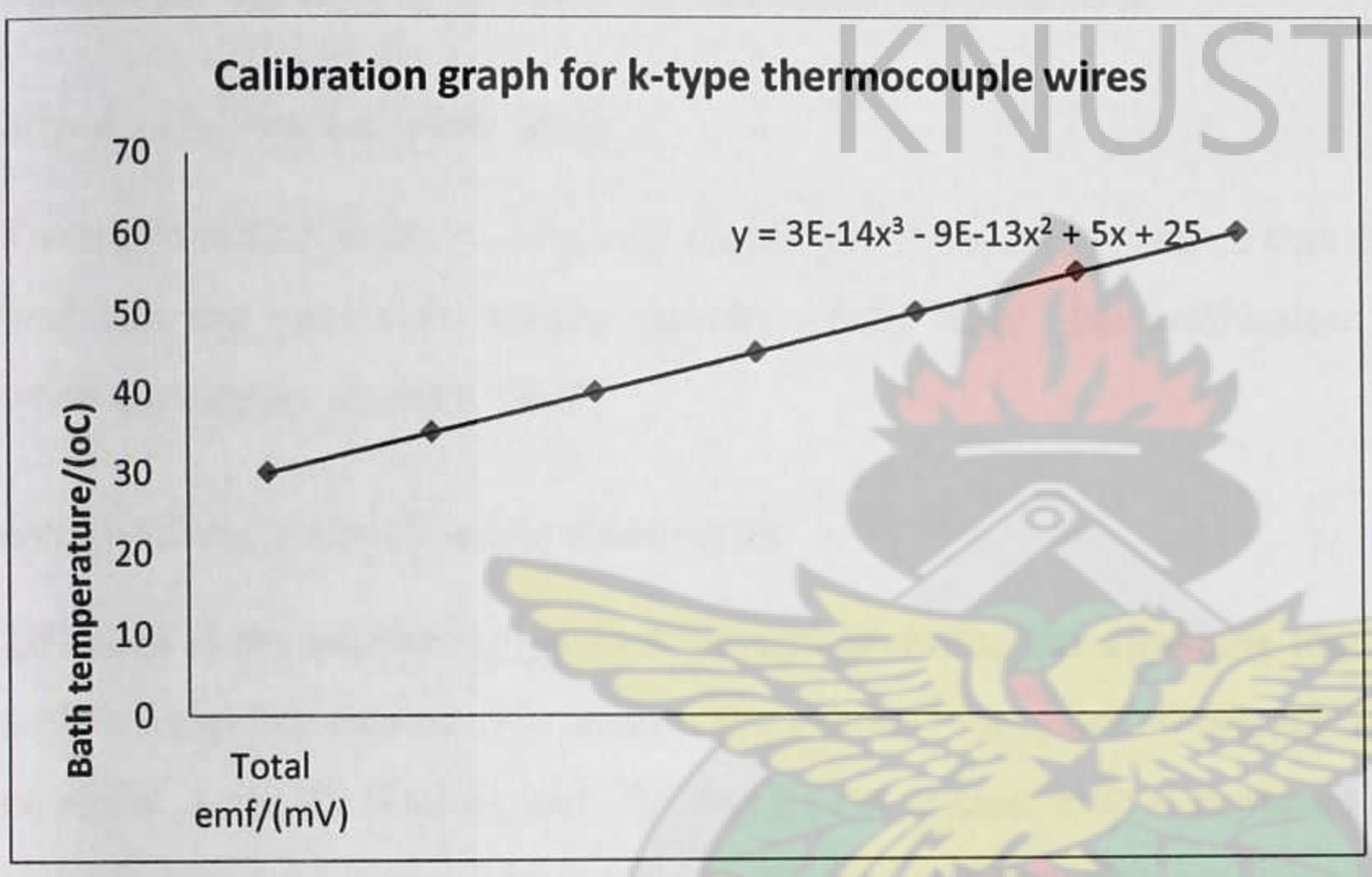

Figure 36 Calibration curve for k-type thermocouple wires

Calibration of electronic scale for measuring mass

Apparatus: electronic scale, level surface, a tin of ideal milk (170 grammes), 6 mini bags of gino rice (5 kilogrammes each).

Step 1 – Determination of the mass Capacity of the scale

The standardised mass capacity of the electronic scale was read and recorded from a tag on the scale as 30 kilogrammes. The 6 mini bags of gino rice making a total of 30 kilogrammes was chosen as a substitute weight since there were no standard weights readily available at the time

Step 2 – Activation of the Scale

The scale was set on a flat, level surface and was switched on and left for a few seconds for the readings to stabilise. After the scale reading had stabilised, the mode setting button on the scale was selected.

Step 3 – Loading the scale with the substitute mass

The substitute weight was placed on the scale's measuring surface in the center and left for a few seconds for the scale to calculate the total mass imposed on it.

KNUST

Step 4 – Calibration of the Scale

The mode setting button was pressed again and the scale registered that the mass of the substitute load was the maximum weight capacity of the scale. The calibration process was completed when the display showed "End".

Step 6 – Double Checking the Calibration

To check if the calibration process worked properly, the substitute load was removed from the scale's weighing surface. The scale was turned off for about 60 seconds after which it was turned on again. After the reading had stabilised, a tin of ideal milk was placed on the weighing surface and left for about 5 seconds for the reading to stabilise. The scale read the correct mass of the load as 170 grammes confirming that the calibration process was successful.

4.3 An overview of the test series

Tests performed using the laboratory model of the mixed mode natural convection solar crop dryer with back-up heater described in section 4.1 can be classified broadly into two categories as: a) tests under no load conditions and, b) tests under load conditions. In each test under load conditions, pineapple was used as the drying material. Under the load conditions, the test was performed in four different modes namely, (i) solar drying during the day with the use of back up heater during the night; (ii) continuous burner drying during the day and at night; (iii) hybrid drying to simulate drying in extremely poor weather; and (iv) total solar drying on a good sunny

day. Under no load conditions, the thermal buoyancy characteristics of the experimental dryer was investigated in three different heating modes namely, (1) solar heating, (2) burner heating, and (3) hybrid heating modes under varied plenum inlet area and vent outlet area scenarios. The fresh fruits were washed, peeled, sliced (rectangular-shaped slices, thickness of about 0.01 m) and cored. The slices were weighed on a digital electronic balance and loaded into the dryer for dehydration in single layers on each tray of the three drying trays and the weight loss of the product was monitored continuously every hour.

4.3.1 Laboratory tests

In all, thirty-one carefully planned tests were conducted using the same dryer model. Twenty seven of the tests were performed under no load conditions with the same dryer model but with three different variations of the plenum inlet opening and the air outlet vent opening in three heating modes. Four of the tests were performed under load conditions in four heating modes. The results for solar drying mode were used as the baseline values for comparative analysis.

The tests under no load conditions were performed by adjusting the rectangular air inlet gap to three different positions. For each rectangular air inlet gap size chosen, the air outlet vent size was also adjusted to three different sizes while measuring temperatures, air flowrate and other performance characteristics for each of the three drying modes.

The test under load conditions investigated (i) the drying rates of the product, (i) the product surface temperatures, and (ii) the overall performance of the dryer.

(a) Test under no load conditions

Purpose: to examine relative performance of the dryer under no load conditions

The plenum inlet gaps and vent outlet gaps shown in table 3 were chosen because they affect the rate of air flow through the dryer. The values were systematically chosen for the purposes of comparative performance studies.

Table 3: Summary of the test conditions for dryer characteristic studies

Test condition	*Test mode*	*Vent width 1 (20 mm)*	*Vent width 2 (30 mm)*	*Vent width 3 (40)*
Plenum inlet opening 1 (20 mm)	Solar heating	1	2	3
	Burner heating	1'	2'	3'
	Hybrid heating	1''	2''	3''
Plenum inlet opening 2 (40 mm)	Solar heating	4	5	6
	Burner heating	4'	5'	6'
	Hybrid heating	4''	5''	6''
Plenum inlet opening 3 (60 mm)	Solar heating	7	8	9
	Burner heating	7'	8'	9'
	Hybrid heating	7''	8''	9''

KNUST

Apparatus: small scale mixed mode natural convection solar crop dryer with back up heater, mercury-in-glass thermometers, micronta LCD humidity and temperature probe, vaisala H M 34 humidity and temperature probe, Barnant 115 thermocouple, PCE-FWS 20 weather station, and solar simulator

Description of tests:

The tests 1 to 27 (see table 3) were conducted with the primary aim of examining the relative performance of the dryer operated with the three different rectangular plenum air inlet openings and three different vent outlet openings for the three heating modes investigated. For instance, when plenum inlet opening 1 (20 mm width) was chosen under solar heating mode, the experiment was run for vent outlet opening 1 (20 mm width), vent outlet opening 2 (30 mm width), and vent outlet opening 3 (40 mm width). After that, plenum inlet opening 2 (40 mm width) was chosen and the experiment was conducted for the vent outlet openings 1, 2, and 3 respectively. After running the experiment for the last plenum inlet opening, a new heating mode was chosen and the experiments repeated.

Under no load conditions, the tests in burner and hybrid heating modes were done with recordings being made over a period of three hours with twelve readings taken every fifteen minutes. In solar heating mode, recordings were made over a period of four hours with twelve readings taken every twenty minutes.

(b) Tests under load conditions

Purpose: to examine the overall performance of the dryer under load conditions for the four options of air heating modes

Apparatus: small scale mixed mode natural convection solar crop dryer with biomass back up heater, 21X Microloger and 12 k-type thermocouple wires, SN 192 storage module, solar module, miconta LCD humidity and temperature probe, vaisala H M 34 humidity and temperature probe, Barnant 115 thermocouple, PCE-FWS 20 weather station, electronic scale (Metler PM 34) and solar simulator

KNUST

Description of tests:

Four tests were conducted under load conditions to examine the performance of the dryer at a plenum inlet opening of 60 mm and an air outlet vent opening of 40 mm under four different heating scenarios. The experiments were devised for the material moisture content to be monitored continuously at full loading capacity in each heating mode considered and drying proceeded till the desired moisture content of between 20% and 35% (giving a terminal values of between 203 grammes and 307 grammes wet products) was achieved or the experiment was terminated. In each test, 2,262 grammes of pineapple (occupying a bed 35 mm depth) was dried from an initial moisture content of 91.3 % (wet basis). In each of the above tests, the specified quantity of pineapple was spread on three metal mesh trays on a total area of about 0.156 m^2.

4.3.2 Determination of initial moisture content of pineapple

The aim of the experiment was to determine the average initial moisture content of the fresh pineapple used for the drying experiment by the evaporation method. Fresh pineapple was procured from a retailer at Kotei, a township at the peripheral of KNUST at 11.30 am on July 26, 2012. The pineapple was washed, peeled, and two different test samples were prepared from it and placed into test containers labeled D17 and D1 respectively. The samples were quickly placed on an electronic balance (Metler PM 34) in turns and the initial masses of the freshly prepared pineapple test samples with the test containers were measured. The test samples were subsequently placed in an air oven and kept at a constant temperature of 105 ^{o}C at the Civil

Engineering laboratory at the College of Engineering, KNUST, at 12:10 pm on July 26, 2012. The masses of the test samples were measured regularly until constant masses were obtained for each test sample. The dehydration experiment was terminated at 8:20 am on July 31, 2012. The analysis of the results is as follows:

Test Sample I

Mass of empty container (container D17), $m_{D17} = 9.58$ g

Initial mass of sample plus container, $m_{D17+s1,i} = 79.15$ g

Final mass of sample plus container, $m_{D17+s1,f} = 15.46$ g

Total mass of moisture removed, $m_{D17,T} = (79.15\text{-}9.58)\text{-}(15.46\text{-}9.58) = 63.69$ g

Therefore, the moisture content (wet basis), $M_w = \frac{63.69}{(79.15\text{-}9.58)} \times 100\% = 91.55\%$

Test Sample II

Mass of empty container (container D17), $m_{D1} = 9.54$ g

Initial mass of sample plus container, $m_{D1+s2,i} = 67.32$ g

Final mass of sample plus container, $m_{D1+s2,f} = 14.72$ g

Total mass of moisture removed, $m_{D1,T} = (67.32-9.54)-(14.72-9.54) = 52.6\,g$

Therefore, the moisture content (wet basis), $M_w = \frac{52.66}{(67.32\text{-}9.54)} \times 100\% = 91.03\%$

Therefore, an average of $\frac{91.55 + 91.03}{2} = 91.3\%$ is used

KNUST

CHAPTER FIVE

EXPERIMENTAL RESULTS AND DISCUSSIONS

5.0 Introduction

In this chapter, the results from the experiments conducted on the laboratory model are presented and discussed under two sections. In section 5.1, the results of the experimental investigation of the laboratory dryer under no load conditions are presented and discussed while the results obtained under load conditions are presented and discussed in section 5.2.

KNUST

5.1 Laboratory experiments under no load conditions

The objective of these set of experiments was to establish the effects of the inlet and outlet areas as well as the various heating modes on thermal buoyancy (ventilation) through the dryer Experimental results and discussion are, therefore, presented under three subsections: subsection 5.1.1 is devoted to tests in solar heating mode; subsection 5.1.2 to test under burner heating mode, and subsection 5.1.3 to tests in hybrid heating mode respectively. Tables 5.1 shows design parameters, dimensions and properties obtained for the laboratory model dryer used for experimentation.

Table 4: The general input parameters for the simulation, either determined by design analysis or adopted from generally accepted figures in the literature

Parameter	Symbol	Numerical value	Units
1. Granite pebble properties:			
Mass of 7 cm thick granite pebble	m_{gr}	9,346	G
Thermal conductivity of granite pebble bed	λ_{gr}	2.79	W/m.K
Gross density of granite pebble bed	ρ_{gr}	2630	kg/m3
Specific heat capacity of granite pebble bed	c_{gr}	775	J/kg.K
Emissivity of granite pebble bed	ε_{gr}	0.92	
2. Mortar properties:			
Mass of 3 cm thick mortar used as concrete absorber	m_{3cmM}	8,907	G
Mass of mortar used to bind 7 cm thick rock pebble bed	m_{bngM}	4,925	G
Total mass of mortar used in 10 cm thermal mass	m_{MT}	13,832	G
Emissivity of absorber surface	ε_{ab}	0.88	
Bulk density of mortar	ρ_{mo}	2,162	kg/m3
Specific heat capacity of mortar	c_{mo}	780	J/kg.K
3. Brick fire clay:			
Bulk density	ρ_{br}	2,403	kg/m3
Emissivity	ε_{br}	0.95	
Specific heat capacity	c_{br}	835	J/kg.K
Thermal conductivity	λ_{br}	0.72	W/m.K
Thickness of brick (flat)	t_{br}	115	Mm
4. Plenum glass cover (single layer):			
Emissivity of glass	ε_c	0.93	
Bulk density	ρ_c	2,400	kg/m3
Specific heat capacity	c_c	840	J/kg.K
Plenum glass cover dimensions:			
Length		41	Cm
Breadth		22.5	Cm
Transmissivity	τ_c	0.7	
Thermal conductivity	λ_c	0.036	W/m.K
5. Burner housing:			
Total external dimensions:			
Length	l_{bhe}	55	Cm
Breadth	b_{bhe}	54	Cm
Height	h_{bhe}	50	Cm
Total internal dimensions:			
Length	l_{bhi}	31	Cm
Breadth	b_{bhi}	31	Cm
Height	h_{bhi}	37.5	Cm

Dryer air inlet opening dimensions:			
Length	l_{dio}	32	Cm
Height	h_{dio}	10	Cm
6. Thermal mass:			
Granite pebble bed dimensions:			
Length	l_{gr}	40	cm
Breadth	b_{gr}	27.5	cm
Height	h_{gr}	7	cm
Granite pebble bed volume	V_{gr}	0.00355	m3
Concrete absorber dimensions:			
Length	l_{ca}	40	cm
Breadth	b_{ca}	27.5	cm
Height	h_{ca}	3	cm
7. Shed:			
Height of shed (higher side)	h_s	163	cm
Distance across supports (longer side side)	d_{ls}	146	cm
Distance across supports (shorter side)	d_{ss}	133	cm
8. Drying chamber:			
Tray dimensions (internal):			
Length	l_t	36.7	cm
Breadth	b_t	14.1	cm
Height	h_t	3.5	cm
Drying chamber cover glass dimensions:			
length	l_{dc}	40.2	Cm
breadth	b_{dc}	18.8	Cm
Internal dimensions of plenum base:			
Length		40.3	Cm
Breadth		38.8	Cm
Drying chamber door dimensions:			
Height			Cm
width			Cm
Thermal conductivity of drying chamber wall material	λ_{dw}	0.15	W/m.K
Vent outlet length	l_v	40	Cm
Plenum length	l_p	31	Cm

KNUST

5.1.1 **Solar Heating Mode**

The experimental results obtained for the MNCSCDBBH under no load conditions are presented as follows:

Figures 37 to 45 show the characteristics of the dryer under no load conditions in solar heat charging mode. Tables C1 to C9 in Appendix C cover the experimental data on dryer characteristic studies in solar heating mode.

The following definitions apply to the captions in section 5.1:

Pi: plenum inlet opening

vo: vent outlet opening

KNUST

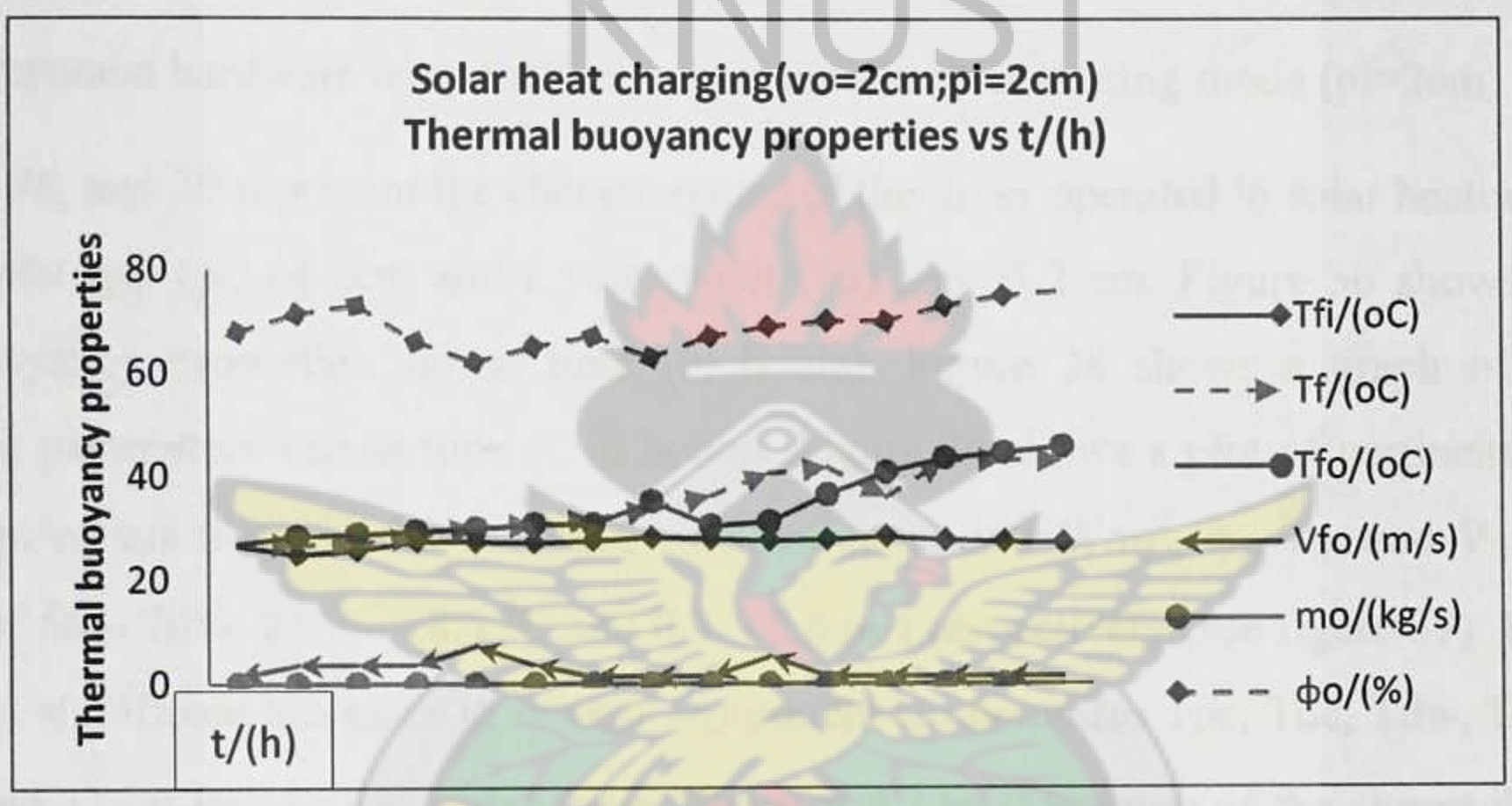

Figure 37 Thermal buoyancy properties versus time in solar heating mode (pi=2cm, vo=2 cm)

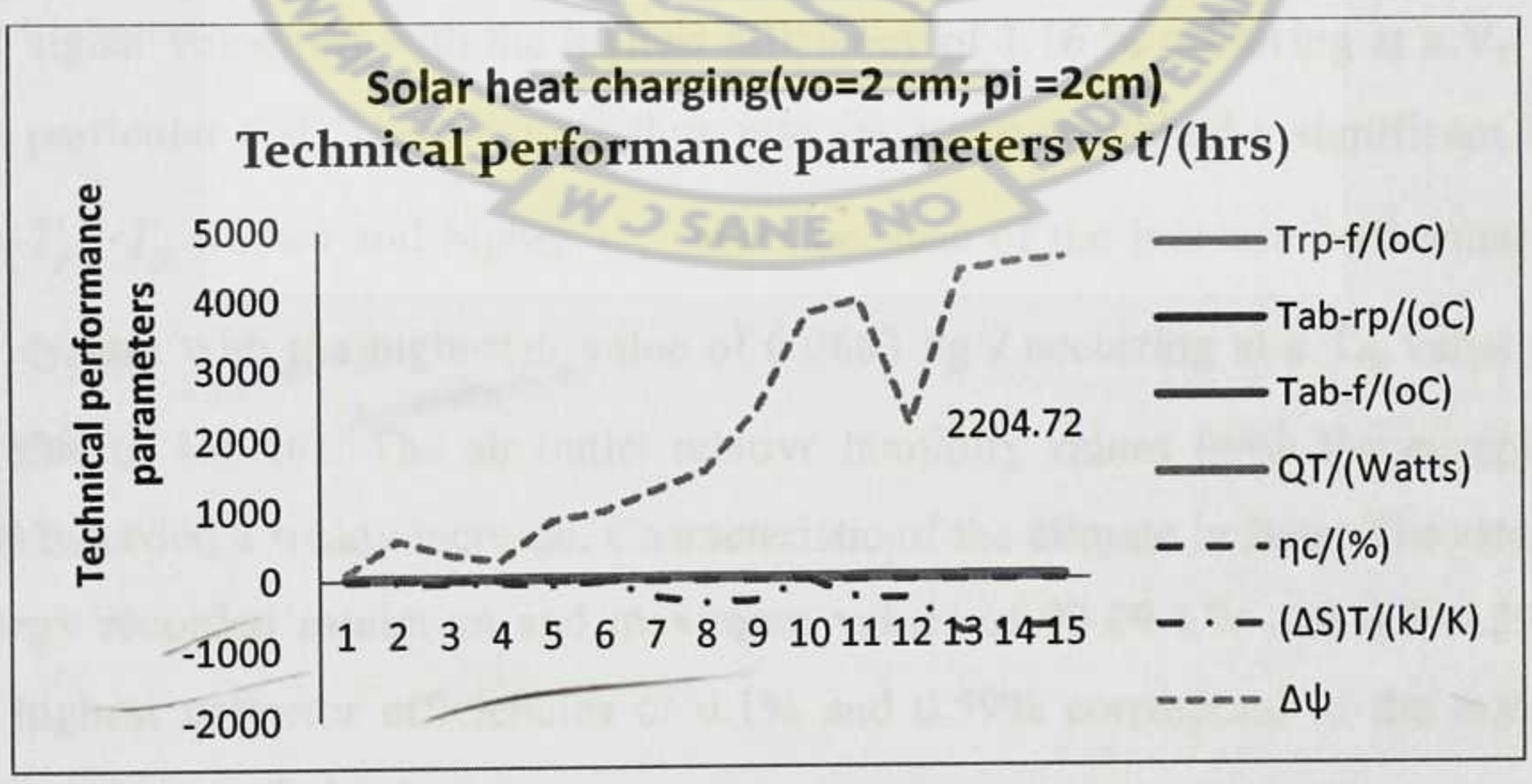

Figure 38 Technical performance parameters versus time in solar heating mode (pi=2cm, vo=2 cm)

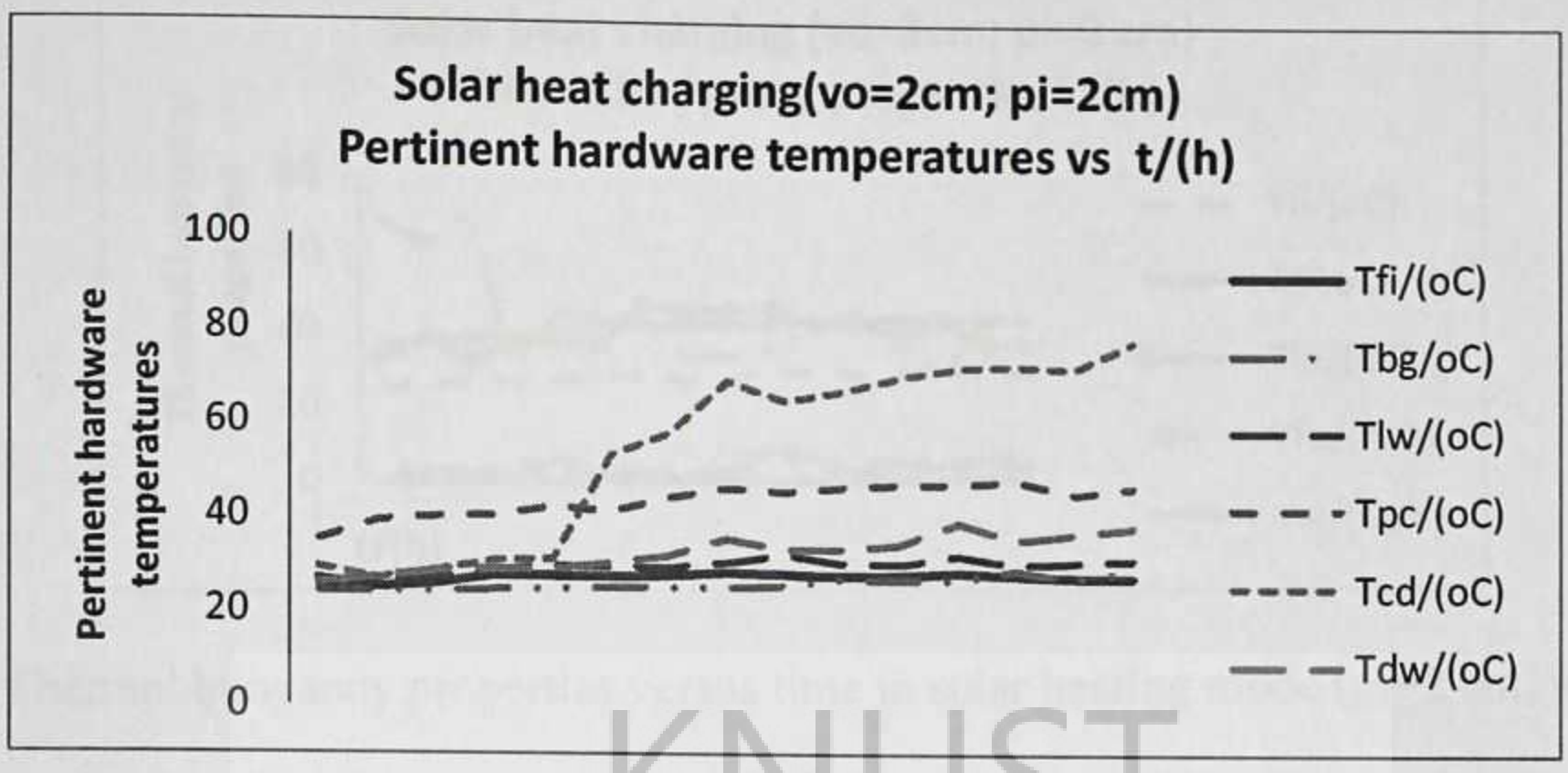

KNUST

Figure 39 Pertinent hardware temperatures versus time in solar heating mode (pi=2cm, vo=2 cm)

Figures 37, 38, and 39 represent the characteristics of the dryer operated in solar heating mode at a plenum inlet gap (pi) of 2cm and a vent outlet (vo) gap of 2 cm. Figure 36 shows a plot of thermal buoyancy properties versus time (in hours). Figure 38 shows a graph of technical performance parameters versus time (t, in hours). Figure 39 shows a plot of pertinent hardware temperatures versus time. Under a constant insolation of 350 W/m^2, ϕ_i, T_{fi}, and V_{fi} exhibited variations of 56 – 70%, 24.9 – 28.4 °C and 0.3 – 5.0 m/s respectively (see figure 37). Figures 38 and 39 show significant increases in system component temperatures Tpc, Tdc, Tdw, Tab-f, Tab-rp, Trp-f, and $\dot{Q}_T$ at low air velocities (particularly at 0.3 m/s) because of the abrupt decrease in heat absorption from the thermal mass. The collector efficiency (η_c) also showed remarkable increases at higher velocities with the highest efficiency of 1.16 % occurring at a V_{fi} value of 1 m/s for this particular test. The air mass flow rate ($\dot{m}_o$) also exhibited a significant increase at higher $\Delta T = T_{fo} - T_{fi}$ values and higher V_{fi} values because of the increase in thermal buoyancy through the system with the highest $\dot{m}_o$ value of 0.0663 kg/s occurring at a T_{fo} value of 29.9 °C and a V_{fi} value of 1.4 m/s. The air outlet relative humidity values (with the exception of the initial value) recorded a steady increase. Characteristic of the climate in June. The rate of change of flow exergy recorded minimum and maximum values of 93.09 kW and 4,597.29 kW. The lowest and highest collector effieiencies of 0.1% and 0.59% correspond to the minimum and maximum exergy rates of change.

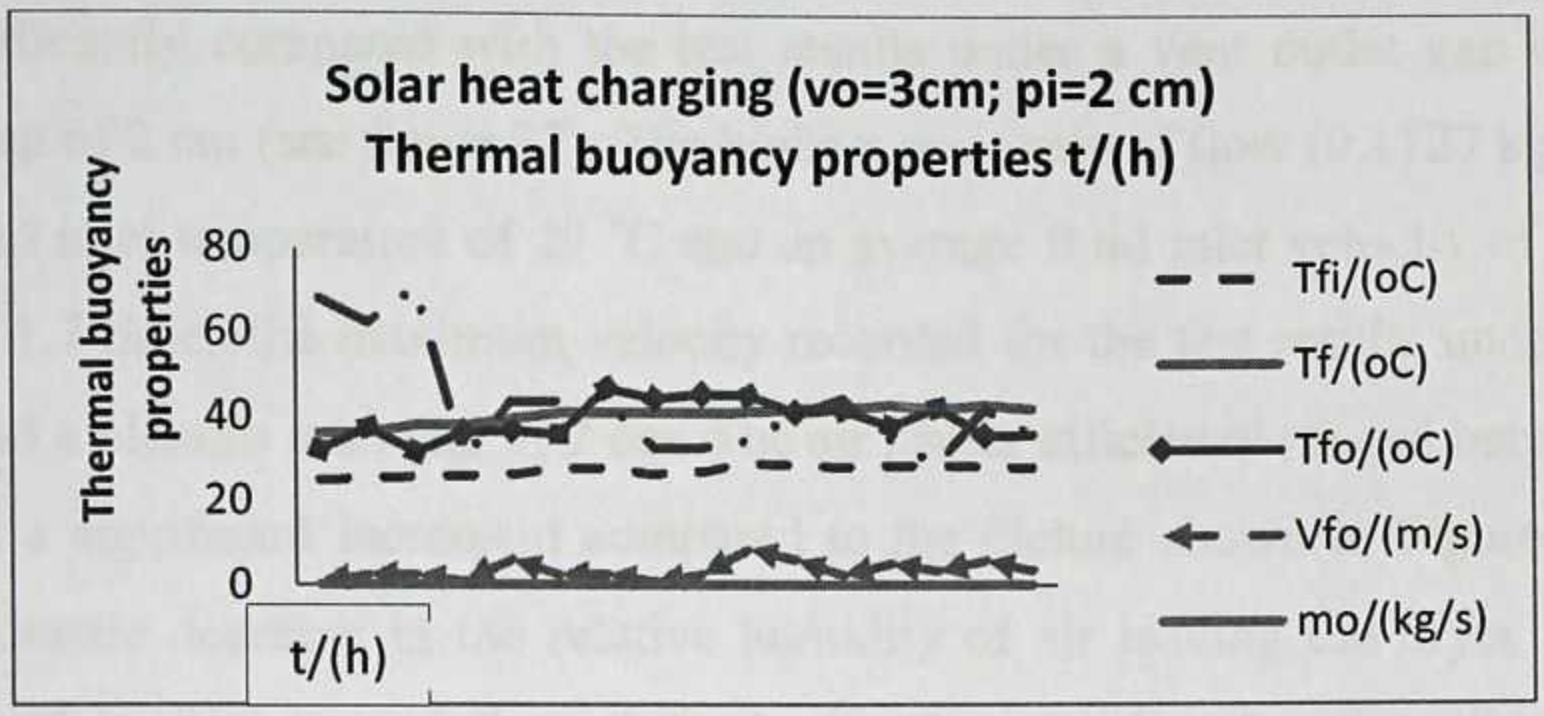

Figure 40 Thermal buoyancy properties versus time in solar heating mode (pi=2 cm, vo=3 cm)

KNUST

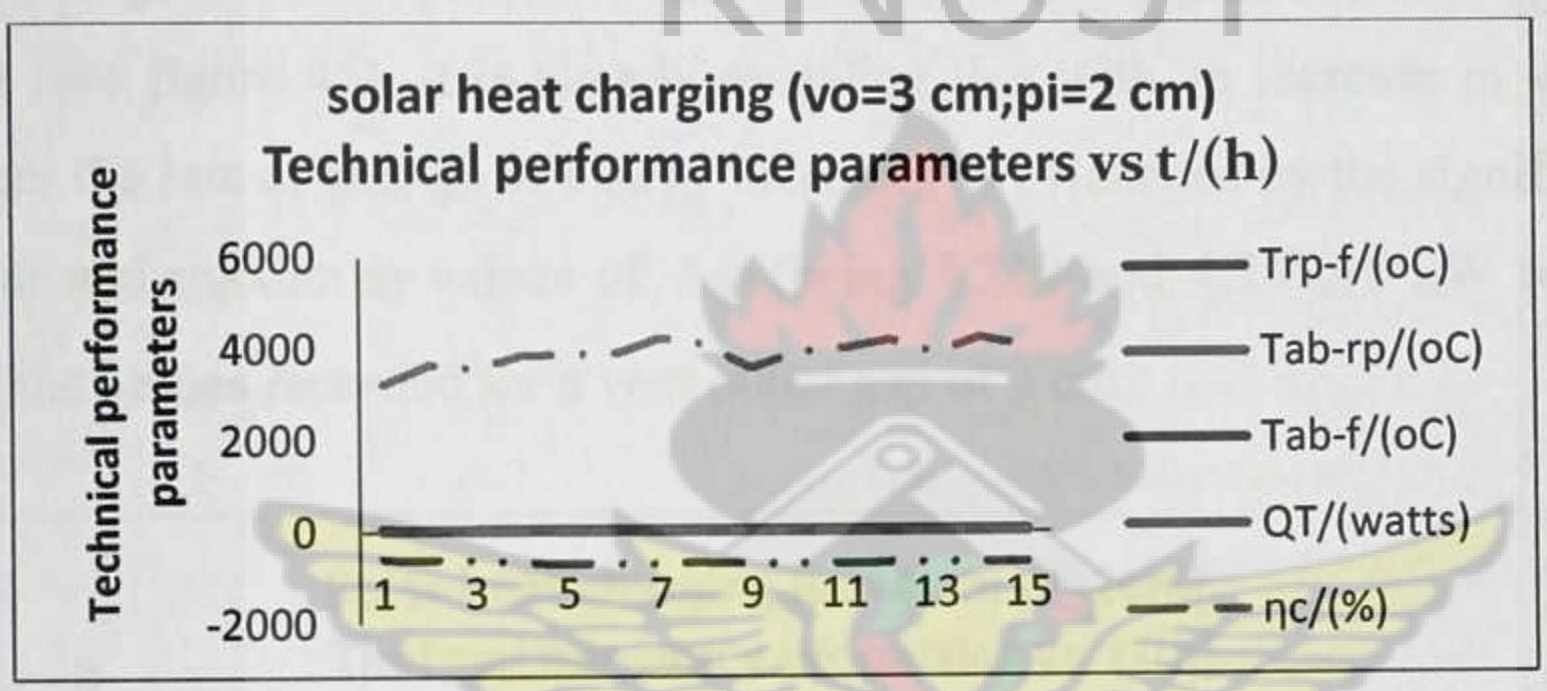

Figure 41 Thermal buoyancy properties versus time in solar heating mode (pi=2 cm, vo=3 cm)

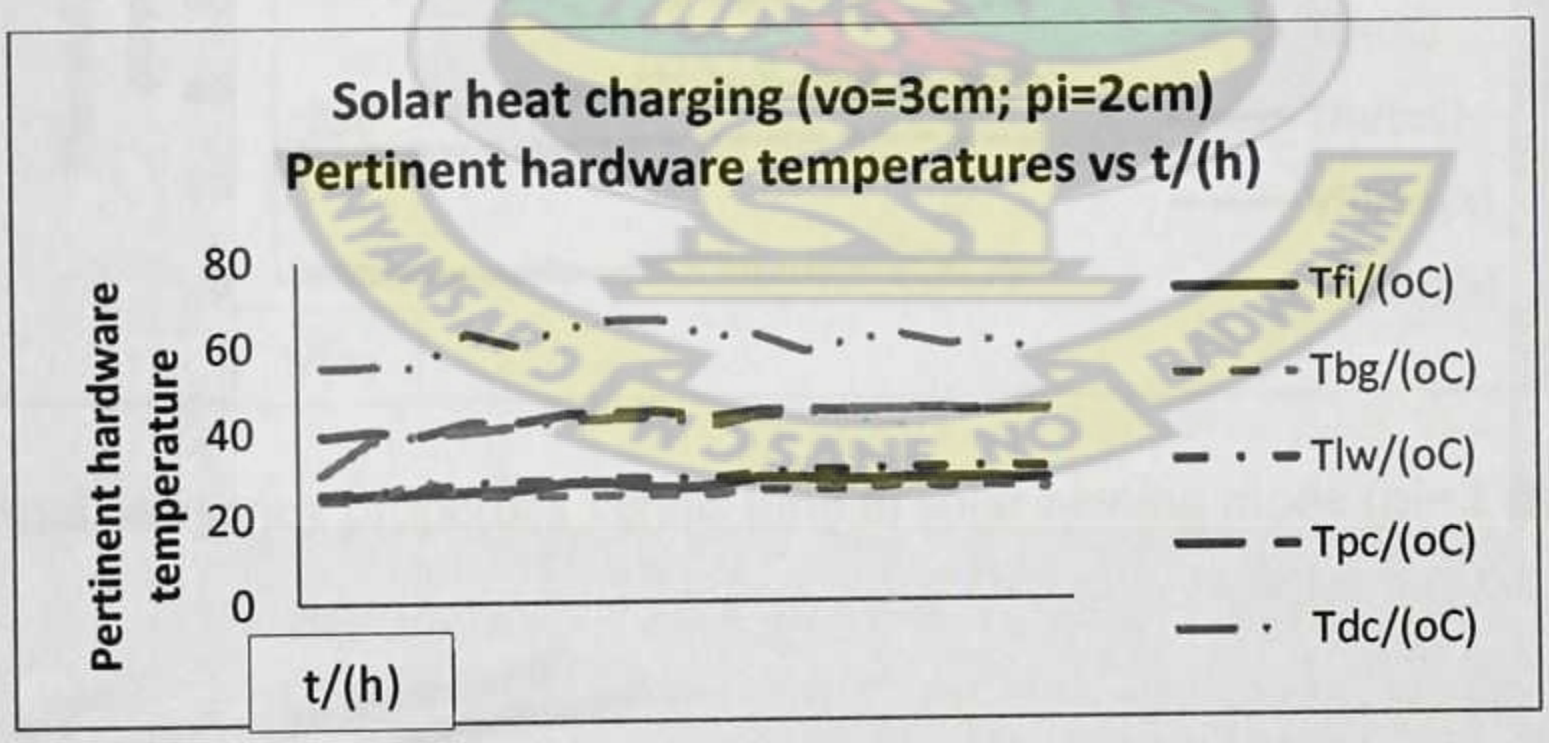

Figure 42 Pertinent hardware temperatures versus time in solar heating mode (pi=2 cm, vo=3cm)

Figures 40, 41, and 42 show graphical variations in performance indicators at a plenum inlet gap of 2 cm and a vent outlet gap of 3 cm under no load conditions in solar heating mode. Results show the average air inlet temperature and average fluid inlet velocities varying between 24.9 – 28.6 °C, and 0.3 – 2.4 m/s respectively. Noticeably, the outlet air mass rates of flow have

increased significantly compared with the test results under a vent outlet gap of 2 cm and a plenum inlet gap of 2 cm (see figure 37). The highest mass rate of flow (0.1127 kg/s) occurred at an average fluid inlet temperature of 29 °C and an average fluid inlet velocity of 2.4 m/s and is approximately 1.7 times the maximum velocity recorded for the test results under a vent outlet gap of 2 cm and a plenum inlet gap of 2 cm. The air heater efficiency ranged between 0.457 and 3.6% which is a significant increment compared to the picture shown in Figure 37. Figure 40 also shows a drastic decrease in the relative humidity of air leaving the dryer because of the comparatively high air rates of flow through the dryer under the prevailing experimental conditions. The heat transmission rate across the thermal mass as represented by Q_T has increased from a range of 7.20 – 25.87 W from the first test (see figure 38) to 13.99 – 80.74 W in the second test (see figure 41). It is already revealing that with an increase in vent outlet gap from 2cm to 3cm the rate of change of exergy increases as evidenced by the significant increases in the minimum and maximum values of $\Delta\dot{\psi}$ (being 3,219 and 4,255.48 kW respectively) as compared with the values recorded for a vent outlet gap of 2 cm.

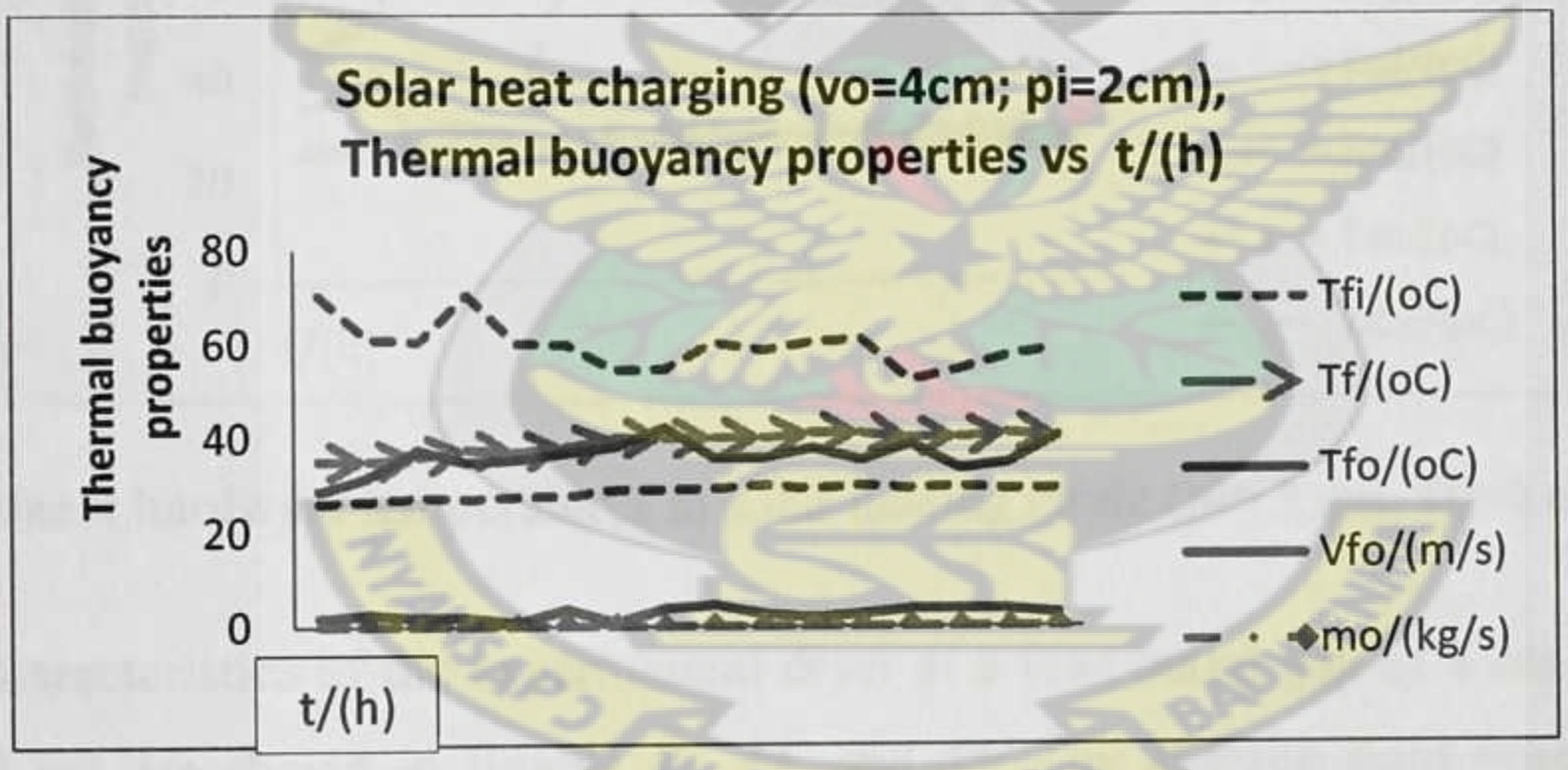

Figure 43 Thermal buoyancy properties versus time in solar heating mode (pi=2 cm, vo=4 cm)

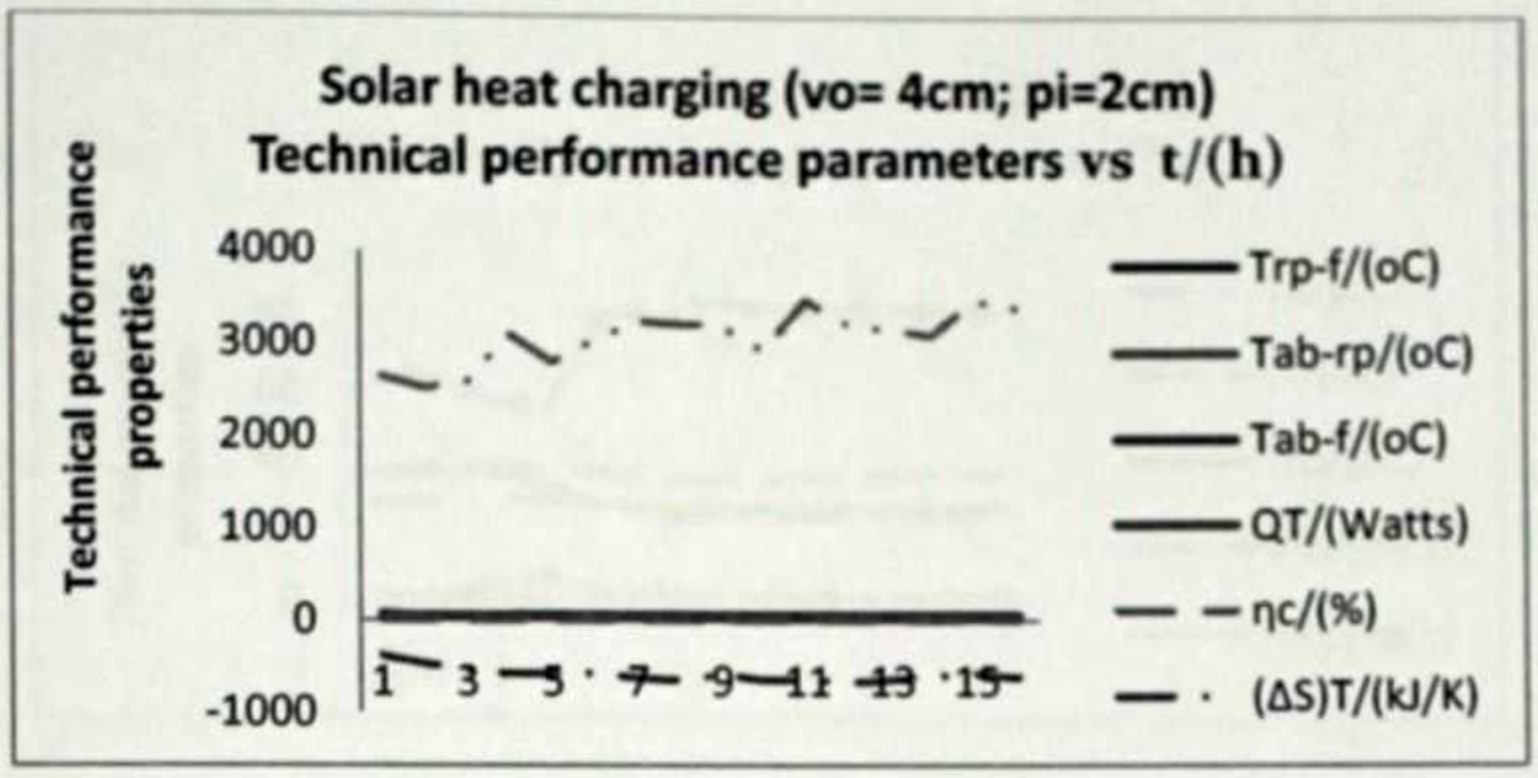

Figure 44 Technical performance parameters versus time in solar heating mode (pi=2 cm, vo=4 cm)

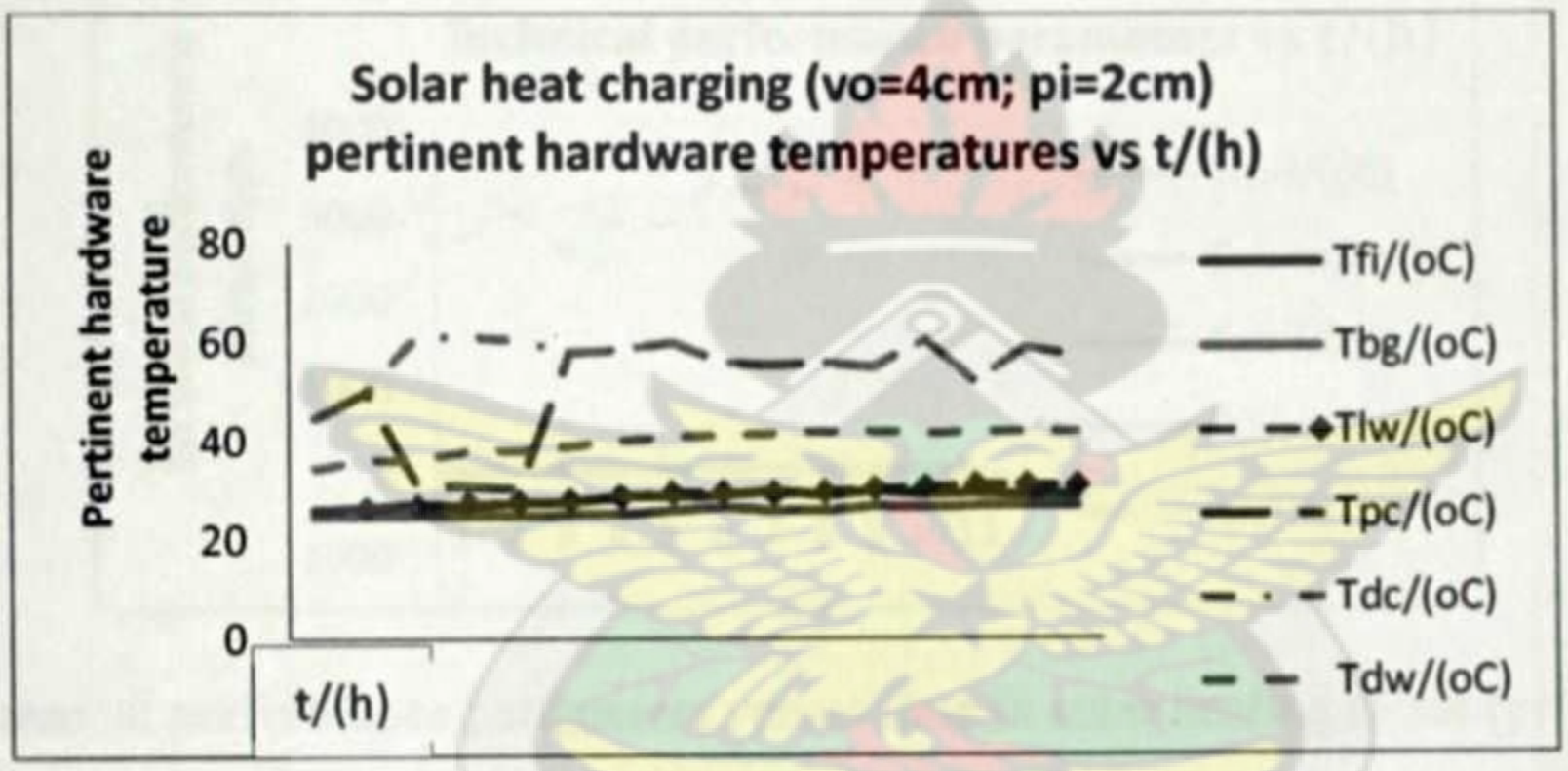

Figure 45 Pertinent hardware temperatures in solar heating mode (pi= 2 cm, vo=4 cm)

The heating characteristics of the experimental dryer at a vent outlet gap of 4 cm and a plenum inlet gap of 2 cm are shown in figures 43, 44, and 45. The average fluid inlet temperatures ranged between 26.1 – 29.6 °C. The air going through the dryer experienced a reasonable degree of heating as evidenced by the range of fluid outlet relative humidity values (ϕ_o: 52.2 – 70.2%). The air heater efficiency values are slightly lower than the values recorded for the previous test with the minimum and maximum air heater efficiency values being 0.77% and 2.28% respectively. A significant increase in the mass rate of flow can be observed for this particular vent outlet opening although the plenum inlet opening remains the same as cases shown on Figures 36, 37, 38, 39, 40, and 41. The minimum and maximum values of rate of exergy change are 2,511.43 and 3,468.20 kW respectively.

LIBRARY
KWAME NKRUMAH
UNIVERSITY OF SCIENCE & TECHNOLOGY
KUMASI

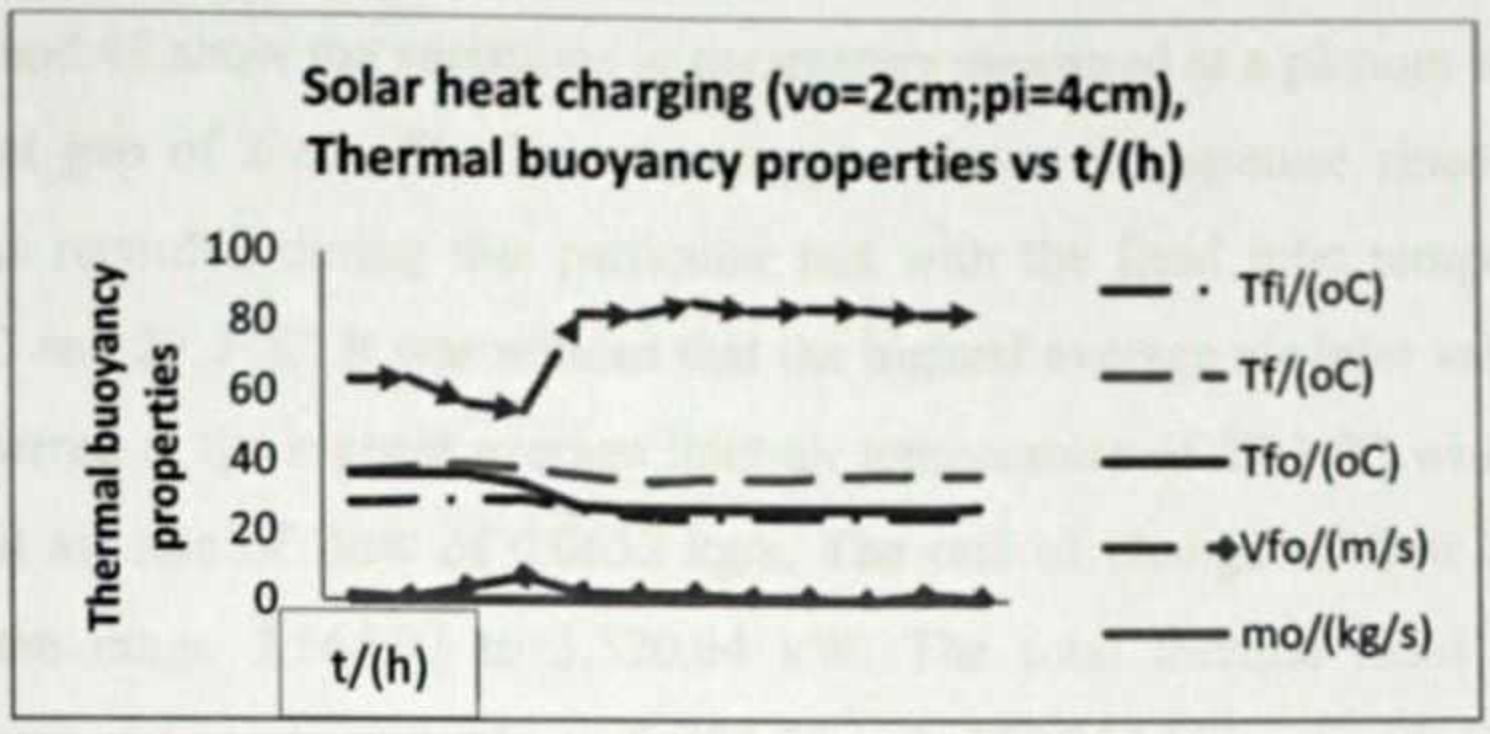

Figure 46 Thermal buoyancy properties versus time in solar heating mode (pi=2 cm, vo=4 cm)

KNUST

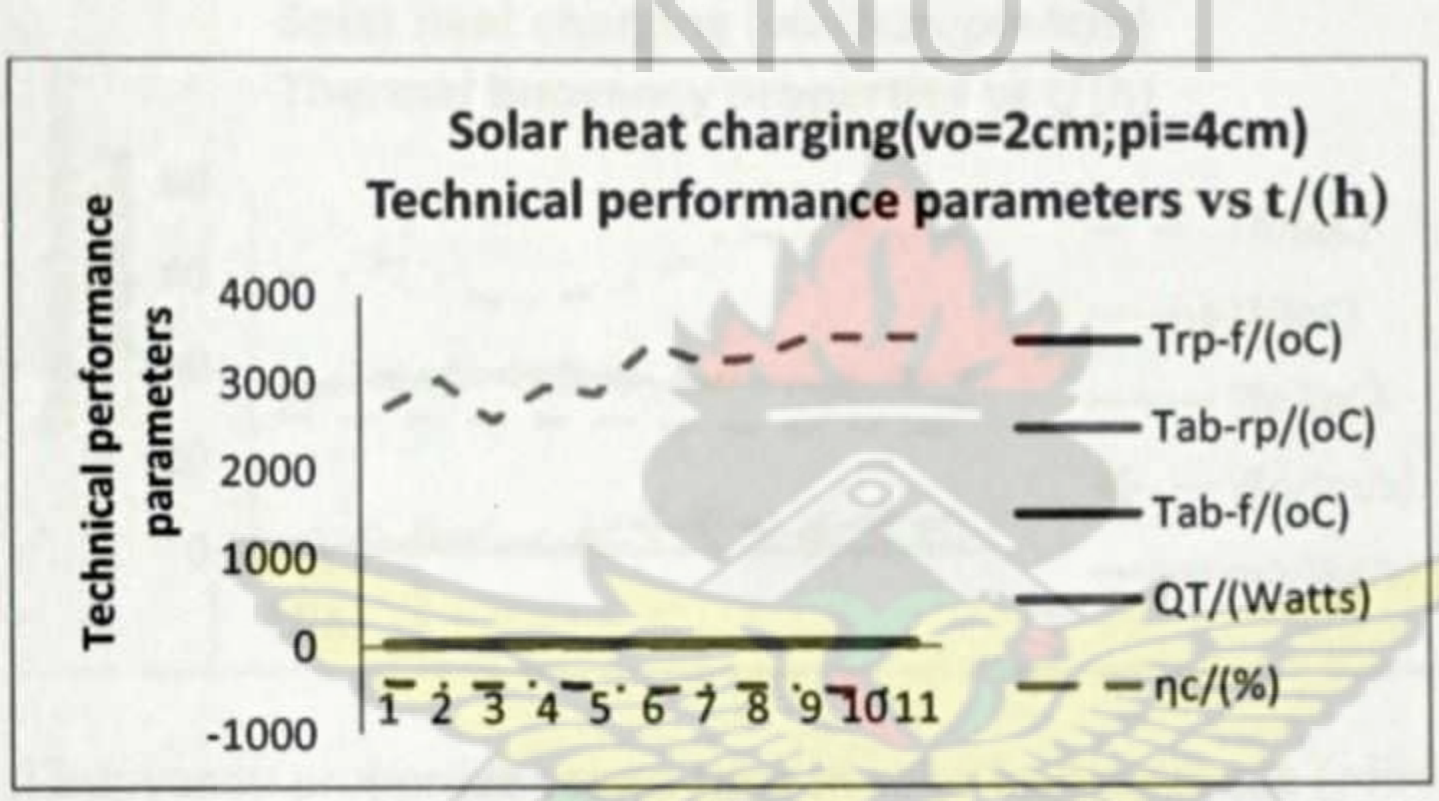

Figure 47 Technical performance parameters versus time in solar heating mode (pi=2 cm, vo=4 cm)

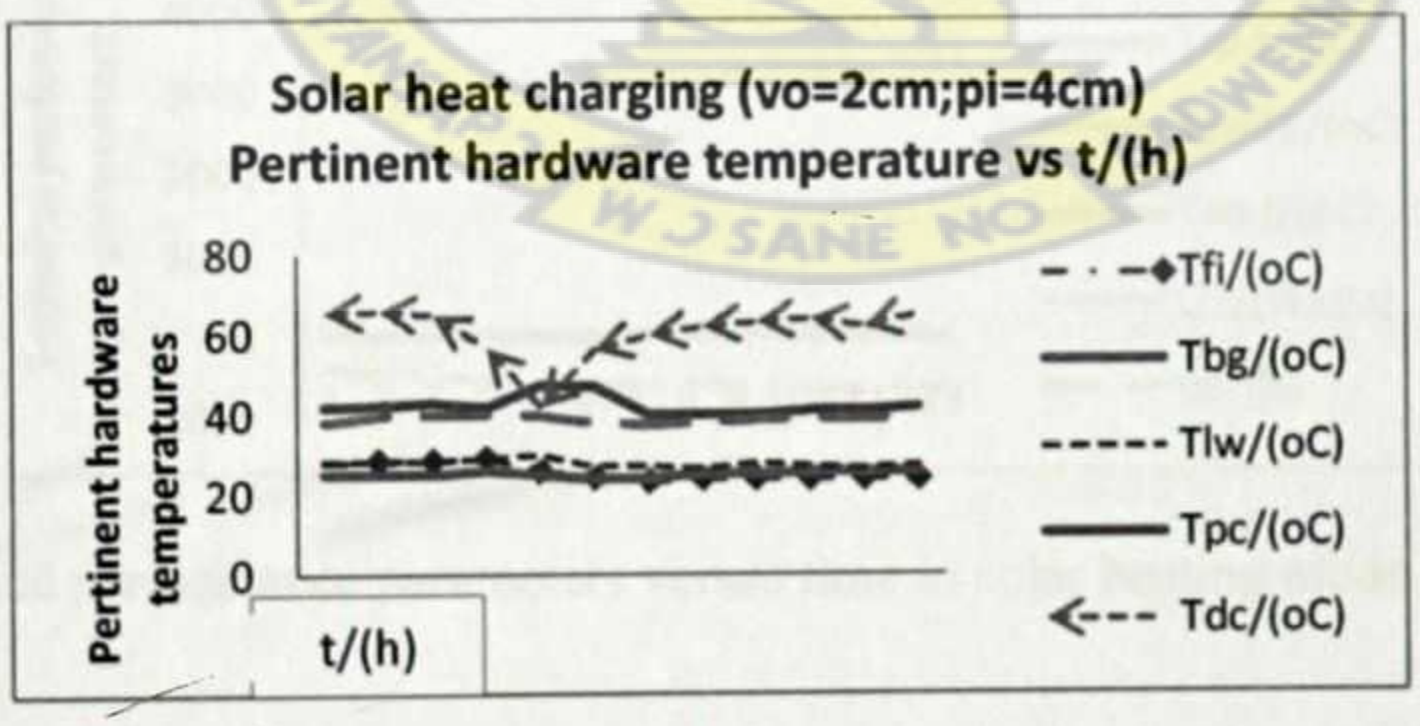

Figure 48 Pertinent hardware temperatures versus time in solar heating mode (pi=4cm, vo=2 cm)

Figures 46, 47, and 48 show the variations in parameters measured at a plenum inlet gap of 4 cm and a vent outlet gap of 2 cm. The lowest average ambient temperature since the start of the experiments was recorded during this particular test with the fluid inlet temperatures ranging between 23.4 °C and 29.3 °C. It was noticed that the highest average air inlet velocity of 2.7 m/s for this test occurred at the highest average inlet air temperature of 29.3 °C which subsequently gave the highest air rate of flow of 0.0632 kg/s. The rate of change of flow exergy recorded values within the range 2,564.92 to 3,520.64 kW. The total thermal mass entropy change recorded minimum and maximum values of -404.25 and -520.06 kJ/K respectively.

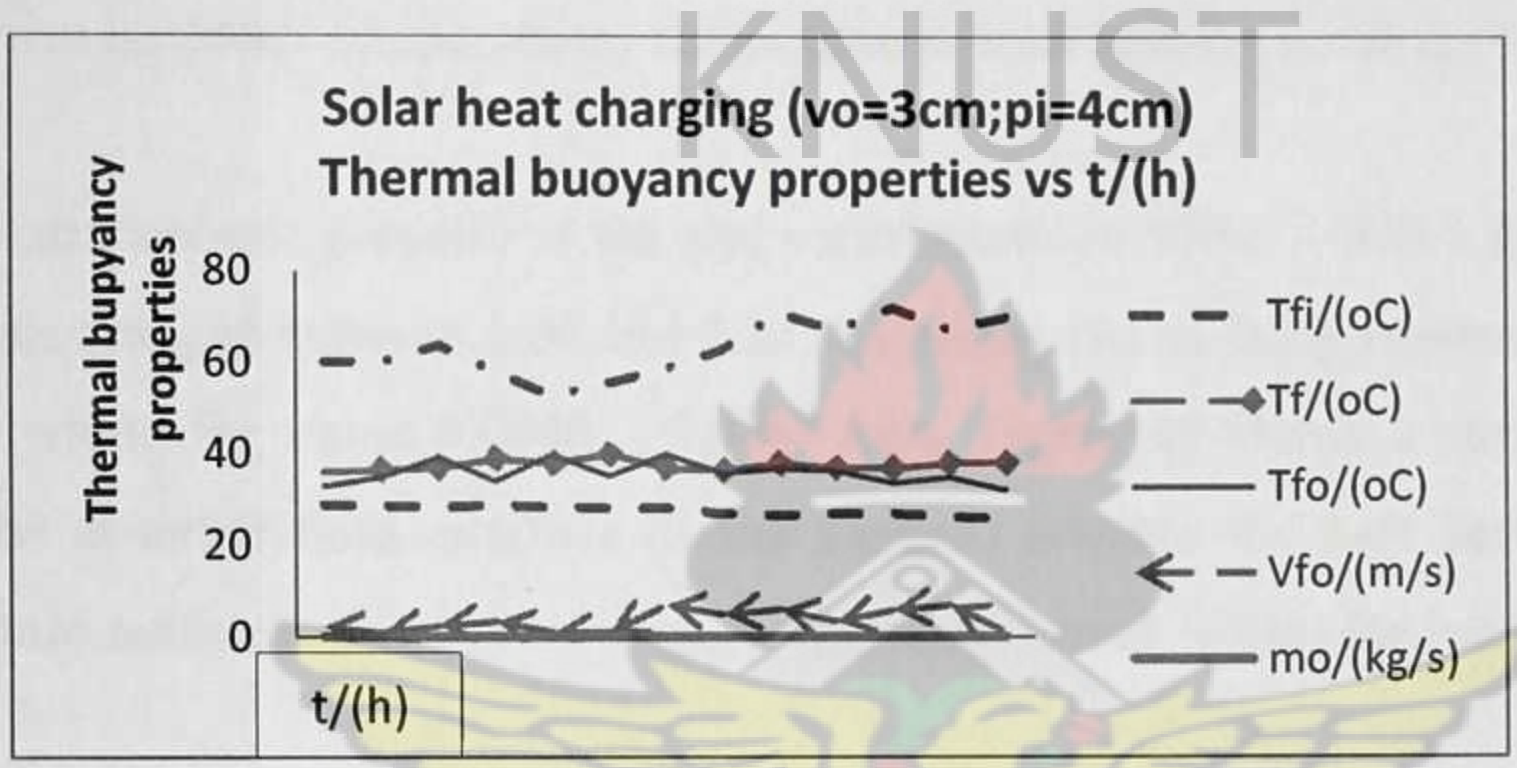

Figure 49 Thermal buoyancy properties versus time in solar heating mode (pi=4 cm, vo=3 cm)

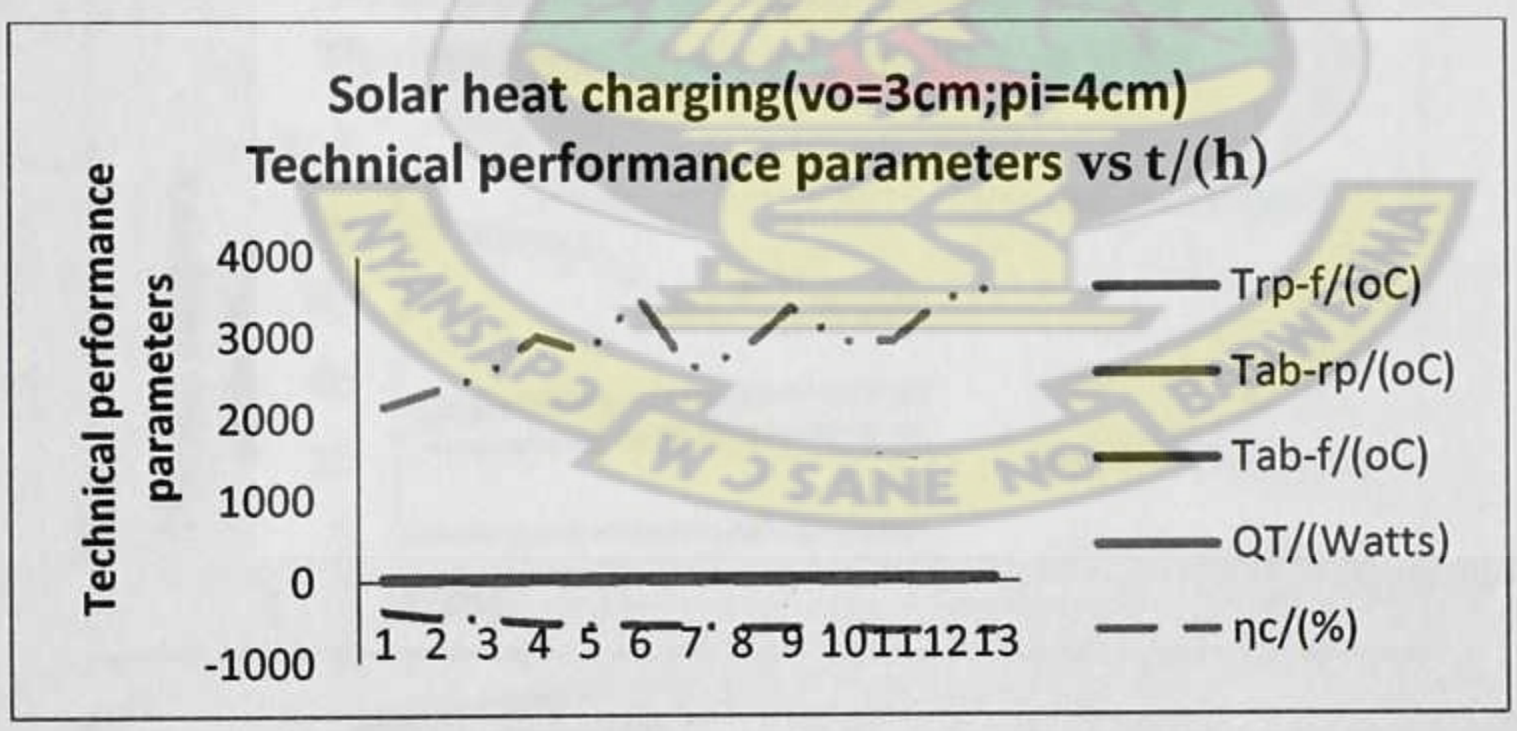

Figure 50 Technical performance parameters versus time in solar heating mode (pi=4 cm, vo=3 cm)

Figures 49, 50, and 51 show the dryer characteristics in solar heating mode at a plenum inlet gap of 4 cm and a vent outlet gap of 3 cm. Average air inlet temperatures ranged between 25.9 – 28.7 °C with average air inlet velocities varying within the range 0.3 – 1.7 m/s.

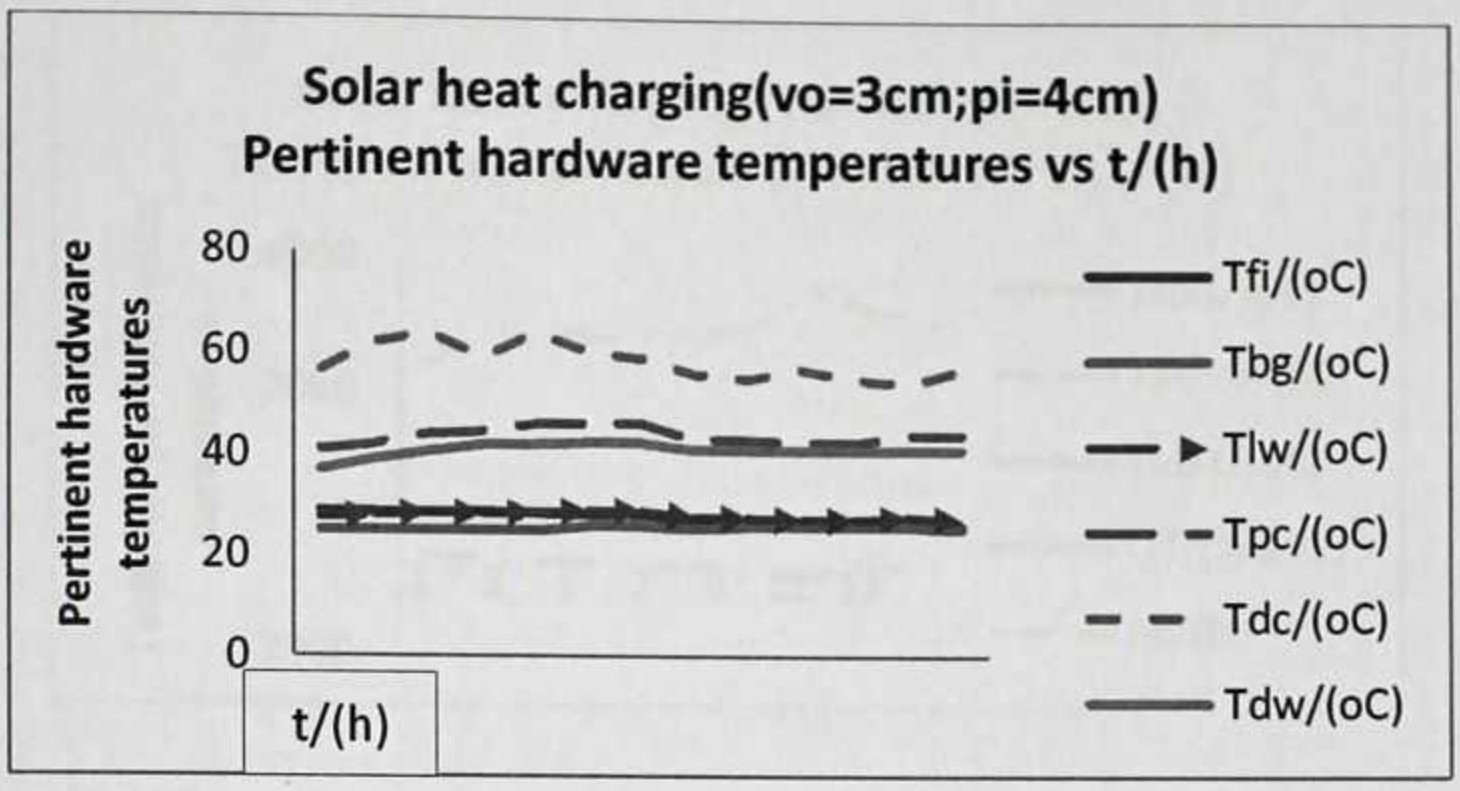

Figure 51 Pertinent hardware temperatures versus time in solar heating mode (pi=4 cm, vo= 3 cm)

KNUST

While the local atmospheric pressure at the site varied between 976.6 – 978.1 hPa, the average air outlet velocities ranged between 1.06 and 7.20 m/s giving rise to fairly reasonable average air mass flow rate within the range 0.0040 – 0.0265 kg/s. Figure 49 shows a steady decrease in entropy from the absorber-fluid interface (hotter surface) towards the rock bed-fluid interface (lower temperature surface). The rate of change of exergy varied within the range 2,146.13 and 3,614.22 kW.

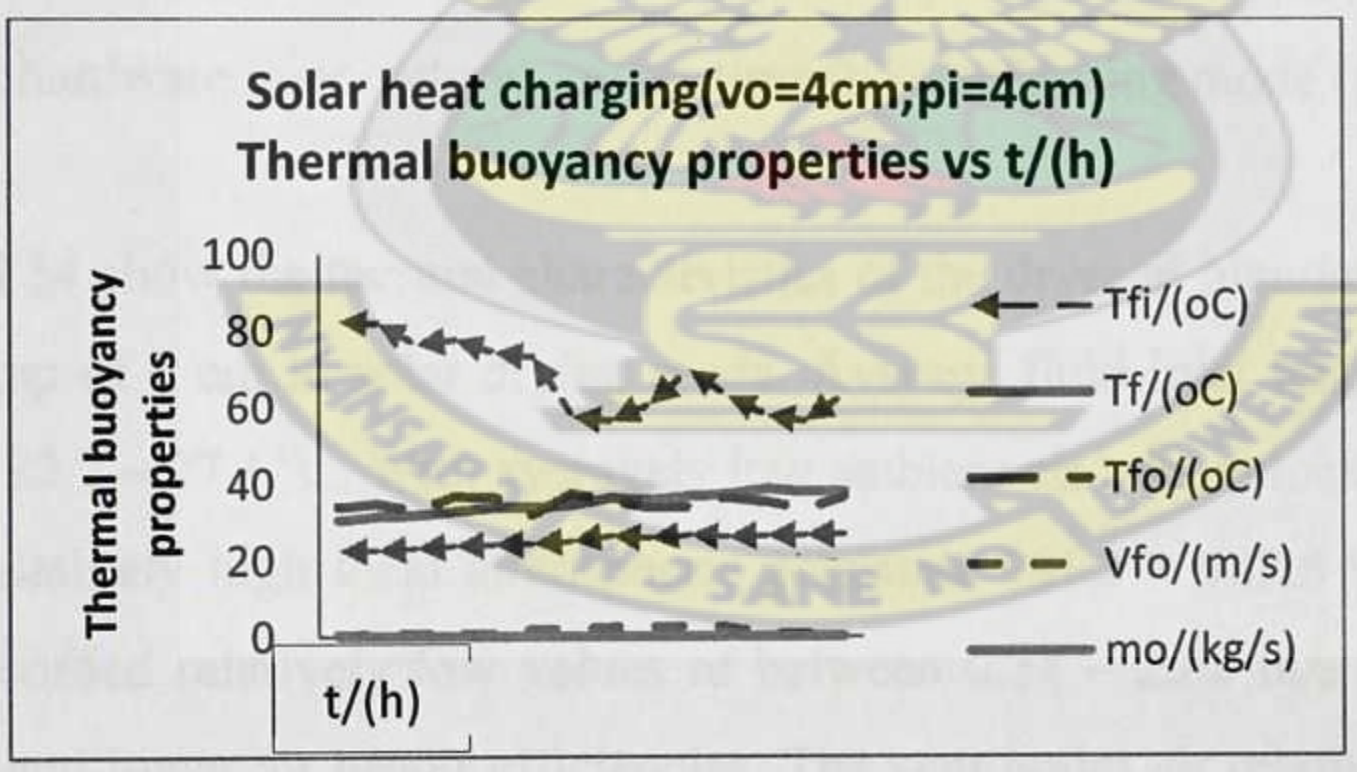

Figure 52 Thermal buoyancy properties versus time in solar heating mode (pi=4 cm, vo=4 cm)

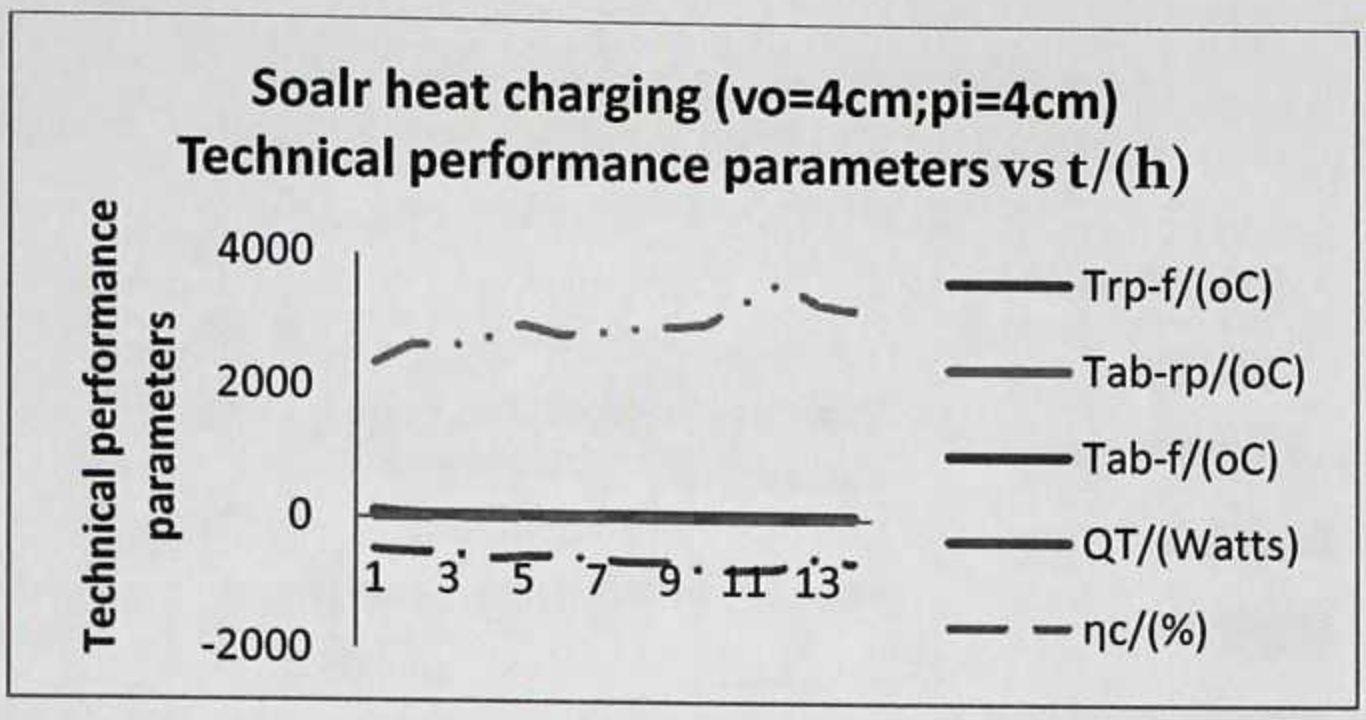

Figure 53 Technical performance parameters versus time in solar heating mode (pi=4 cm, vo=4 cm)

KNUST

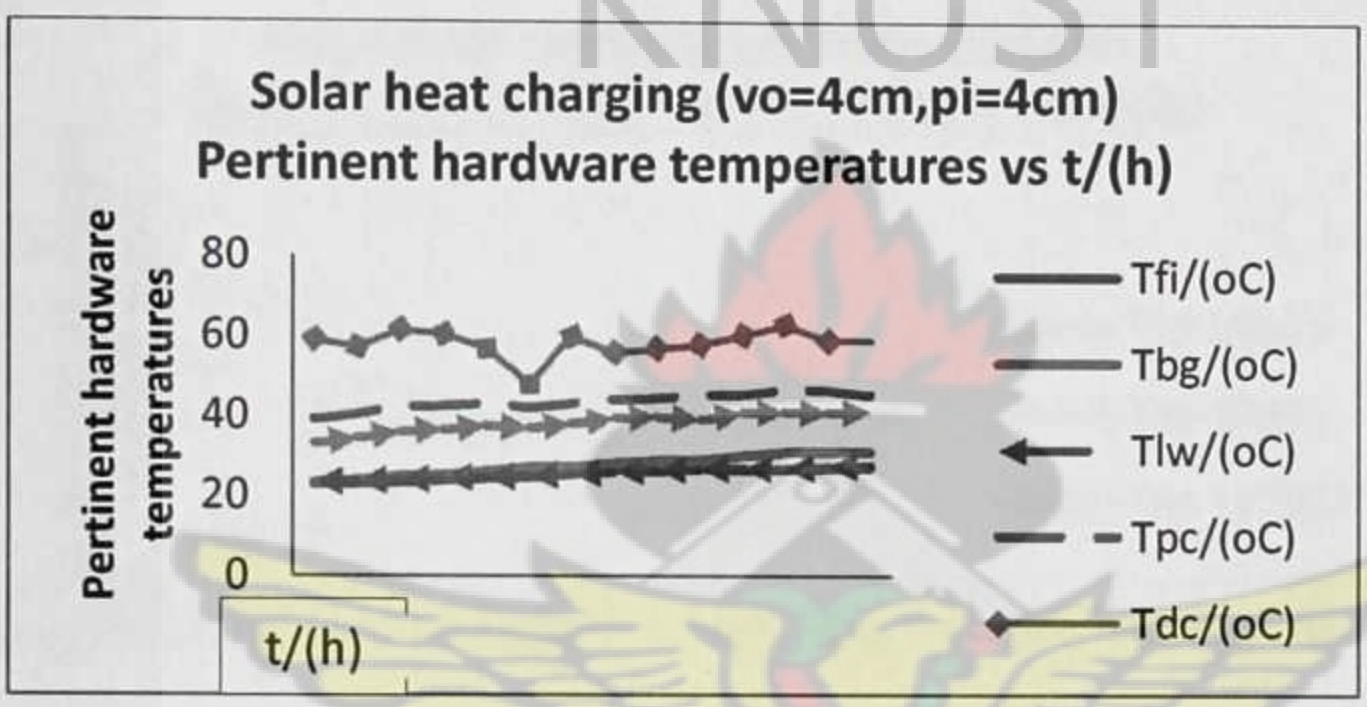

Figure 54 Pertinent hardware temperatures versus time in solar heating mode (pi=4 cm, vo=4 cm)

Figures 52, 53, and 54 show the thermal characteristics of the dryer at plenum inlet gap of 4 cm and a vent outlet gap of 4 cm in solar drying mode. Average fluid inlet temperatures recorded values in the range 22.7 – 27.1 °C. With averagely low ambient air inlet velocities of between 0.2 and 1.0 m/s and relatively high local atmospheric pressures 981.1 – 982.6 hPa. Average vent outlet velocities recorded relatively low values of between 0.54 – 2.68 m/s giving rise to low mass rates of flow and lower air heater efficiencies. The vent outlet air relative humidity values observed were within reasonable limits, making it desirable for drying. The average rate of change of exergy varied between 2,333.90 and 3,604.56 kW respectively.

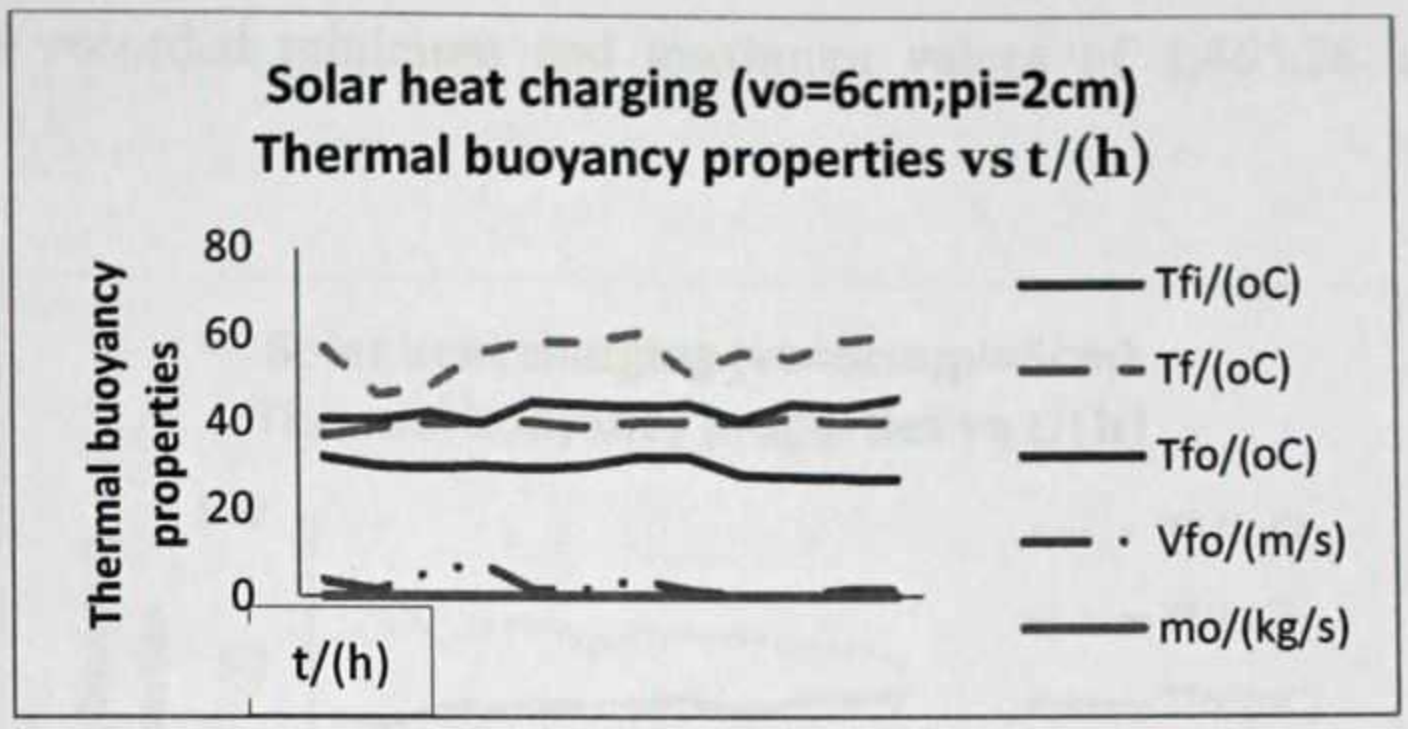

Figure 55 Thermal buoyancy properties versus time in solar heating mode (pi=6 cm, vo=2 cm)

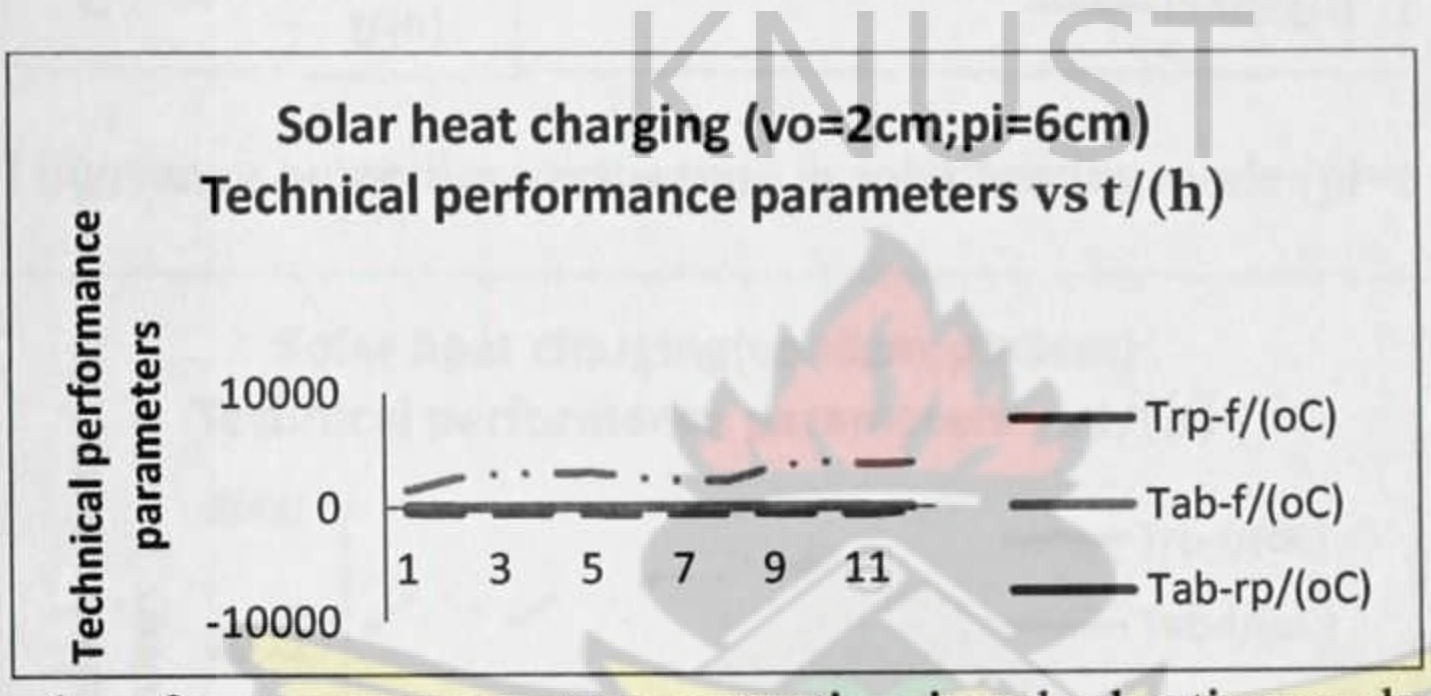

Figure 56 Technical performance parameters versus time in solar heating mode (pi= 6cm, vo=2 cm)

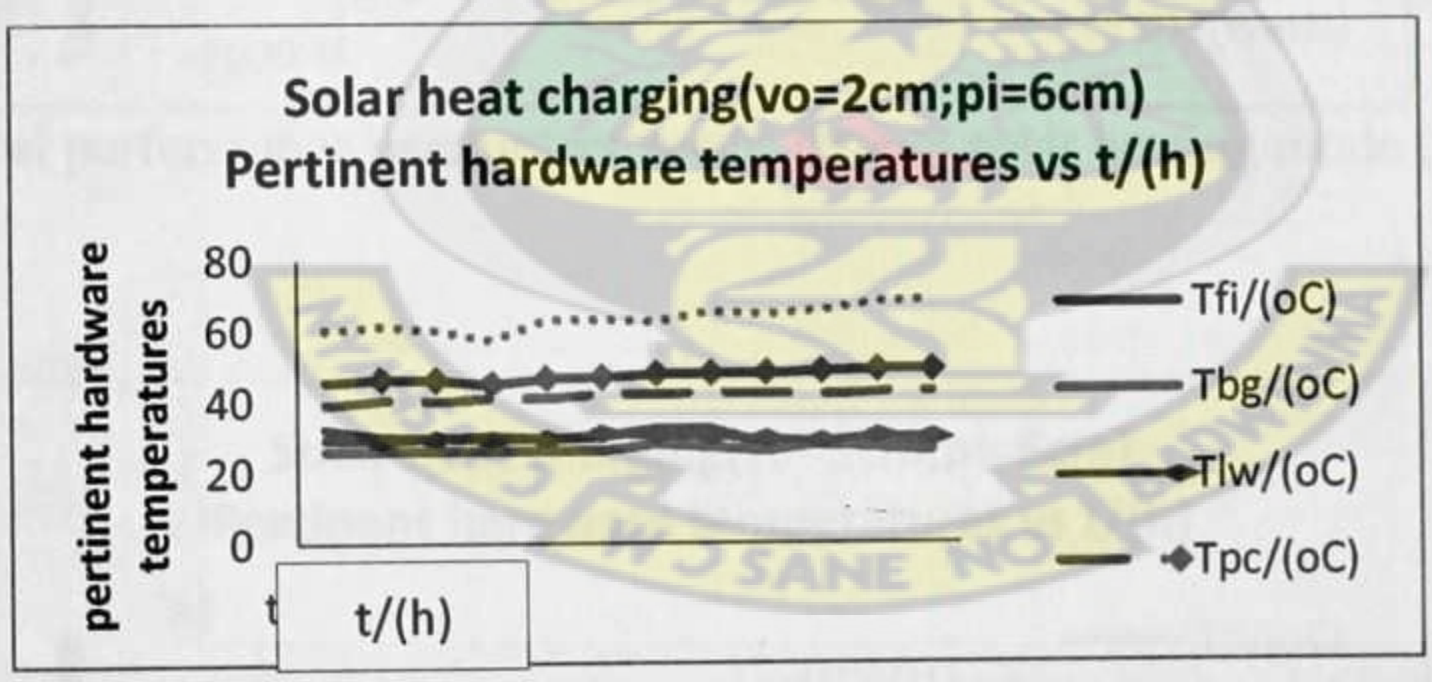

Figure 57 Pertinent hardware temperatures versus tin in solar heating mode (pi=6 cm, vo=2 cm)

Figures 55, 56, and 57 represent the experimental dryer characteristics conducted at plenum inlet gap of 6 cm and air vent outlet gap of 2 cm in solar heating mode. The average fluid inlet temperature varies between 26.9 and 32.2 °C whereas the average inlet velocities range between 0 and 1.4 m/s. The average drying chamber wall temperature also shows insignificant changes in value throughout the duration of the test with values within the range 39 – 42.6 °C. The rate of

change of exergy recorded minimum and maximum values of 1,465.26 and 3,889.68 kW respectively.

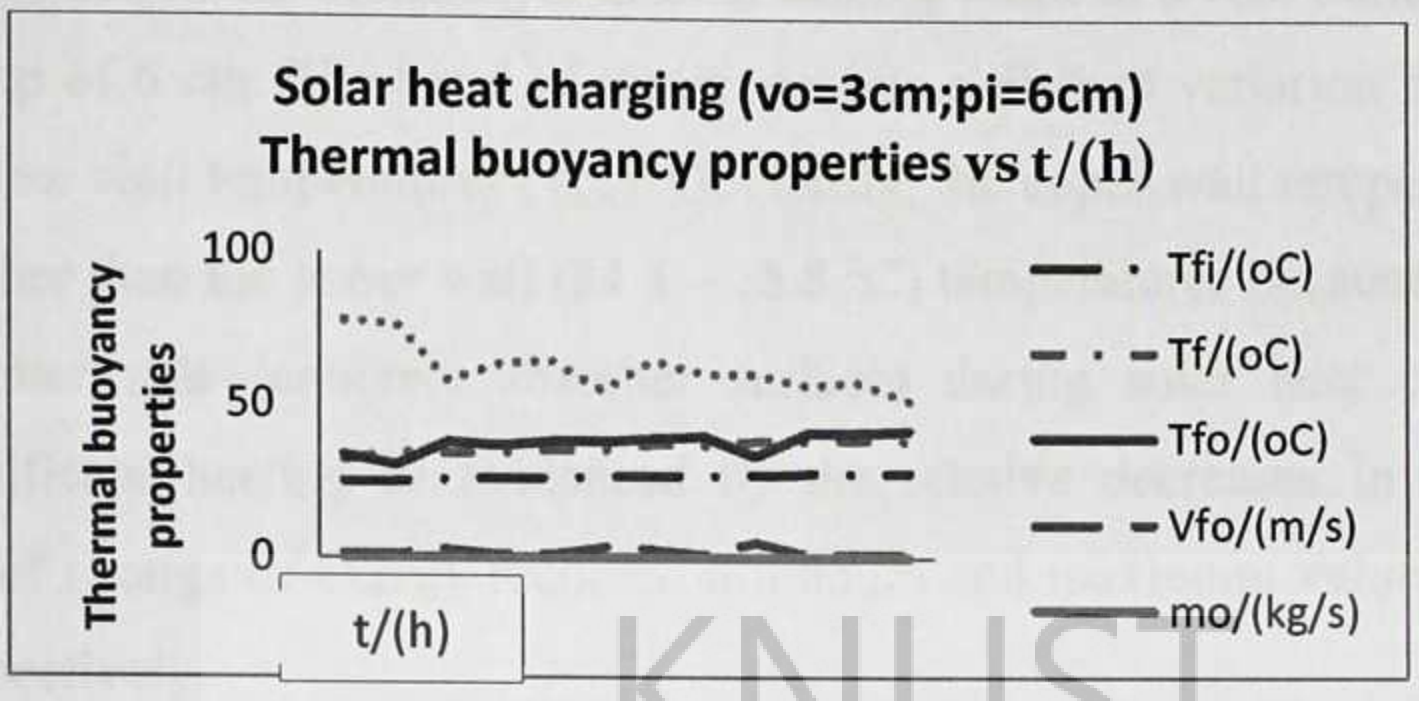

Figure 58 Thermal buoyancy properties versus time in solar heating mode (pi=6 cm, vo=3 cm)

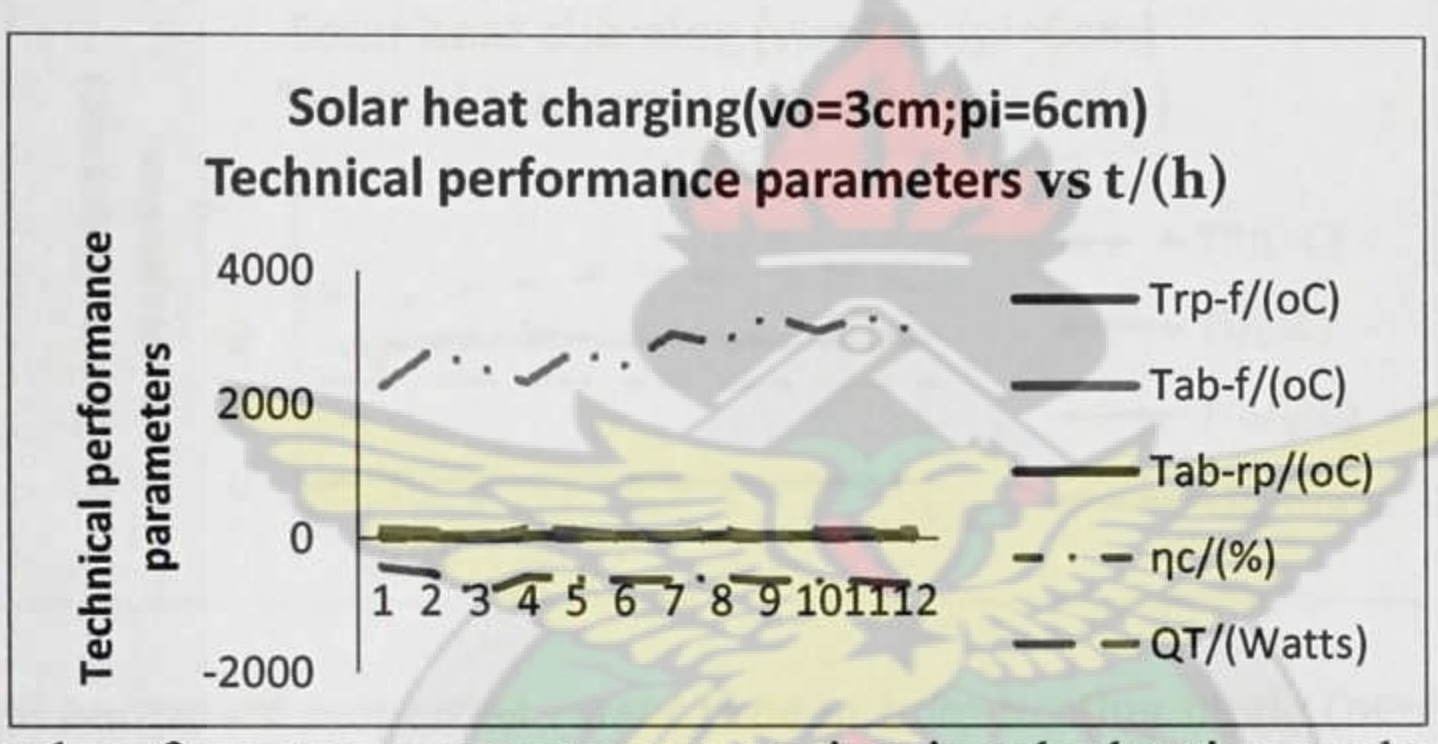

Figure 59 Technical performance parameters versus time in solar heating mode (pi=6 cm, vo=3 cm)

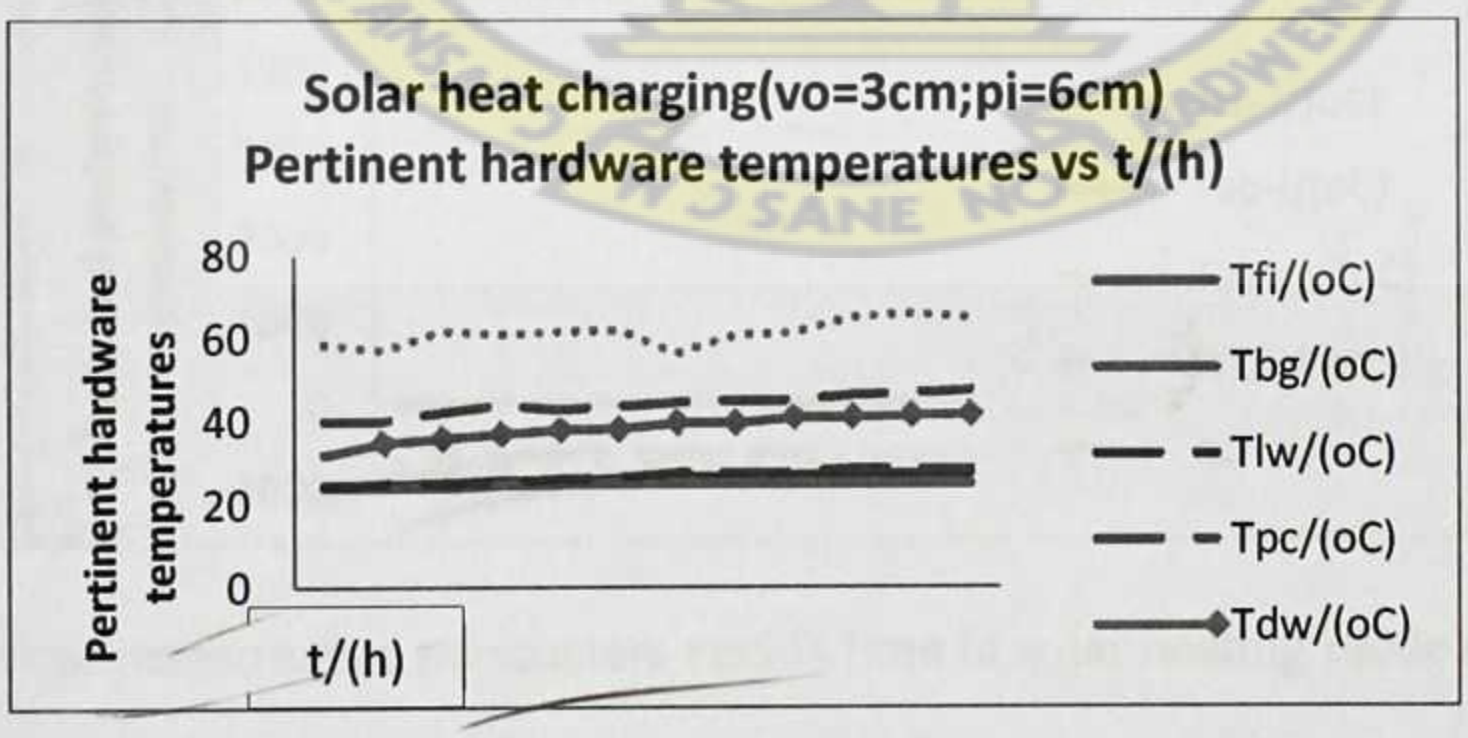

Figure 60 Pertinent hardware temperatures versus time in solar heating mode (pi=6 cm, vo=3 cm)

The trend of results as depicted in figure 60 shows that the burner housing floor temperature in solar heating mode remains fairly unchanged during heating. Figures 58, 59, and 60 show the general heating characteristics of the dryer in solar heating mode at a vent outlet gap of 4 cm and a plenum inlet gap of 6 cm. The trend of results depicts a distinct variation between the lower wall (T_{lw}) and upper wall temperatures (T_{uw}). Obviously, the upper wall temperatures (34 – 41.3 °C) are much higher than the lower wall (24.4 – 28.8 °C) temperatures because the upper wall is closer to the hotter side (concrete absorber surface) during solar heat charging. The air experienced significant heating as evidenced by the relative decreases in relative humidity values. The rate of change of exergy recorded minimum and maximum values of 2,262.48 and 3,325.91 kW respectively.

KNUST

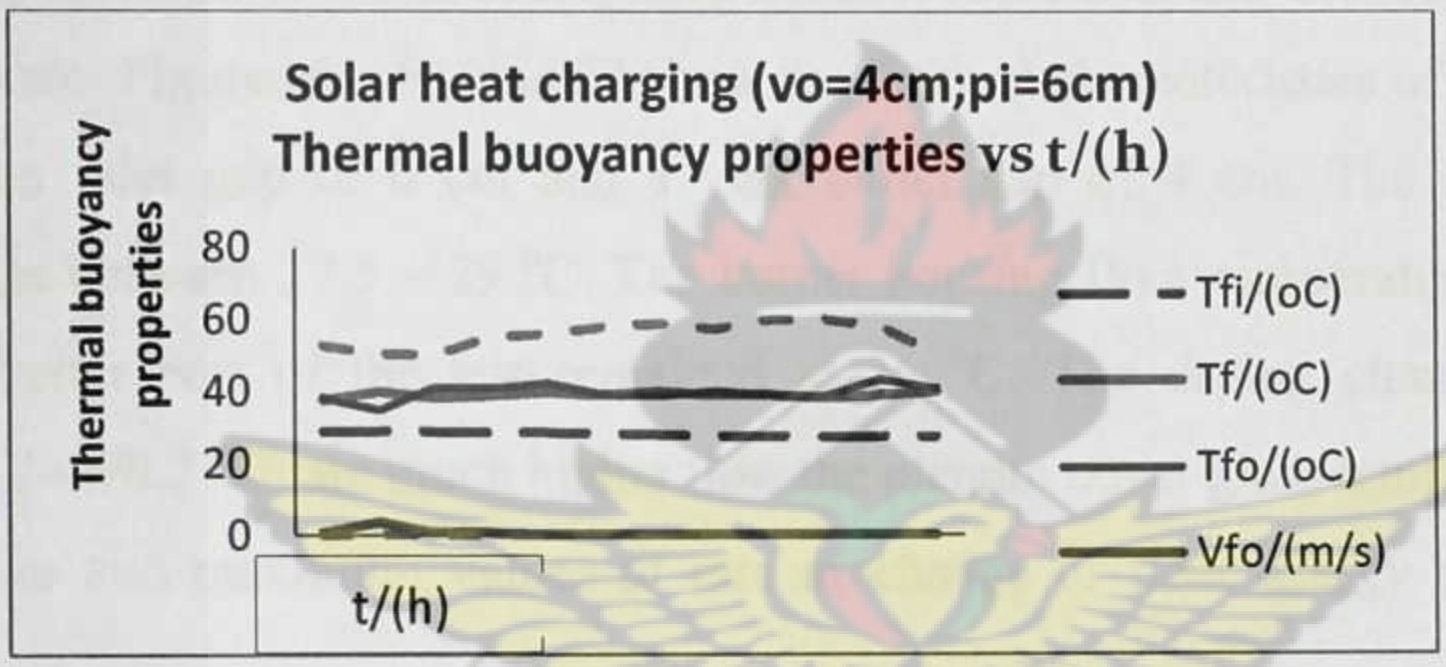

Figure 61 Thermal buoyancy properties versus time in solar heating mode (pi=6 cm, vo=4 cm)

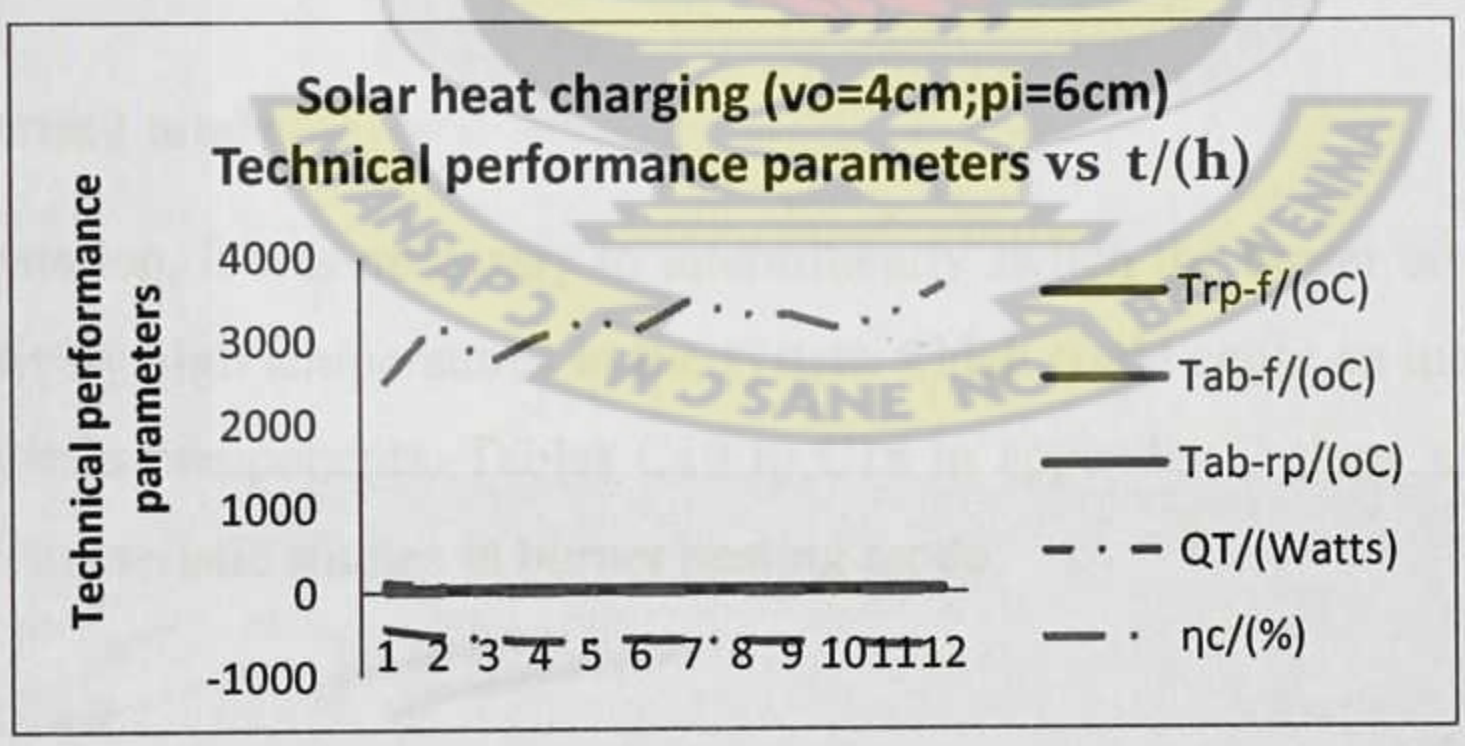

Figure 62 Technical performance parameters versus time in solar heating mode (pi=6 cm, vo=4 cm)

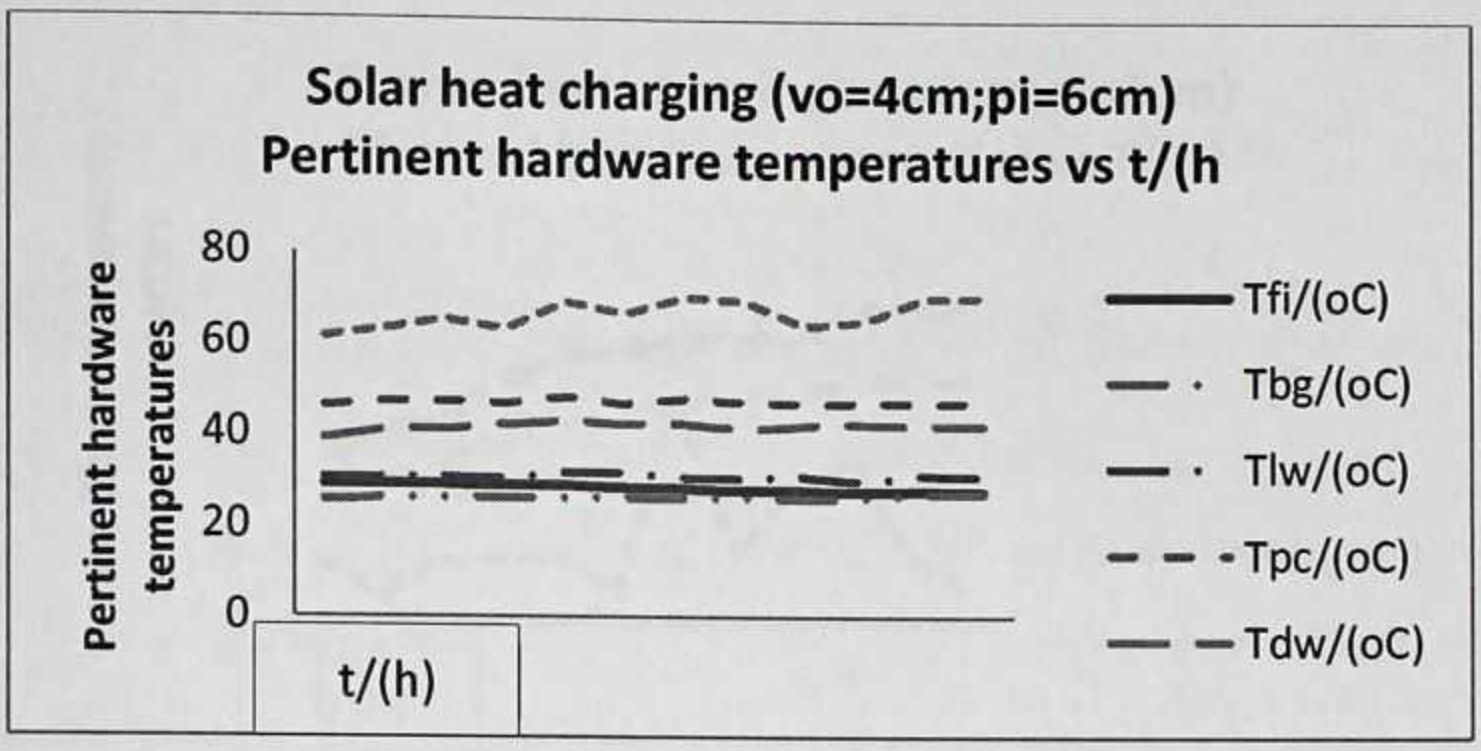

Figure 63 Pertinent hardware temperatures versus time in solar heating mode (pi=6 cm, vo=4 cm)

About 65% of this test was characterised by zero air inlet velocities as evidenced by the air mass flow rates being zero. Figures 61, 62, and 63 show the thermal characteristics of the experimental dryer at a plenum inlet gap of 6 cm and a vent outlet gap of 4 cm. The average air inlet temperature ranges between 27.5 – 29 °C. The burner housing floor temperature started at 25.5 °C and for the better part of the test remained at 26 °C. The drying chamber cover glass temperatures (61.2 – 70.2 °C) are much higher than the plenum cover glass temperatures (46 – 47 °C). The minimum and maximum values of rate of change of flow exergy are 2,517.98 and 3,652.16 kW

5.1.2 **Burner Heating mode**

During experimentation, it was necessary to intermittently switch the heater on and off in order to prevent excessively high temperatures in the system which could cause an increase in thermal stresses in the system components. Tables C10 to C18 in appendix C show experimental data covering dryer characteristic studies in burner heating mode.

KNUST

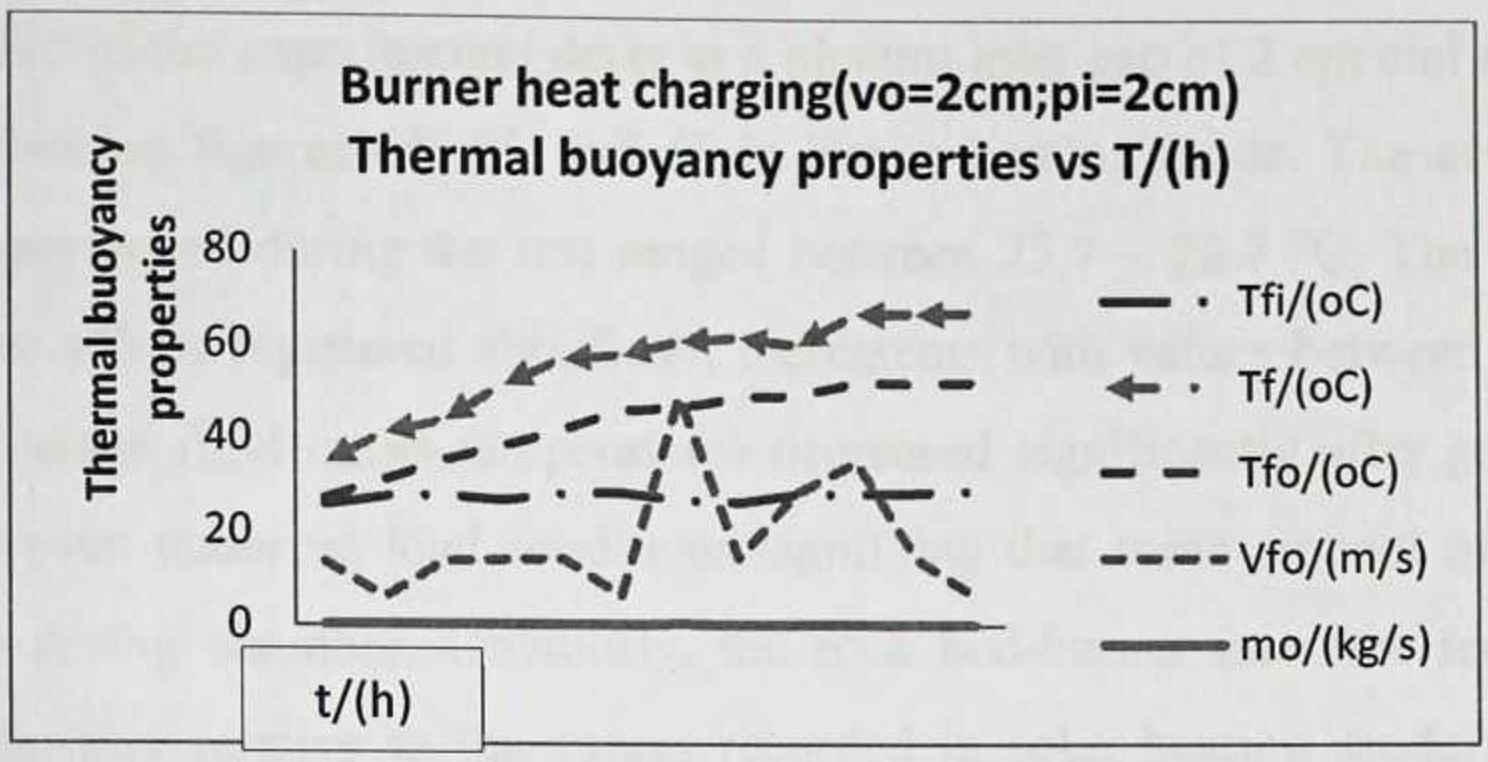

Figure 64 Thermal buoyancy properties versus time in burner heating mode (pi=2 cm, vo=2 cm)

KNUST

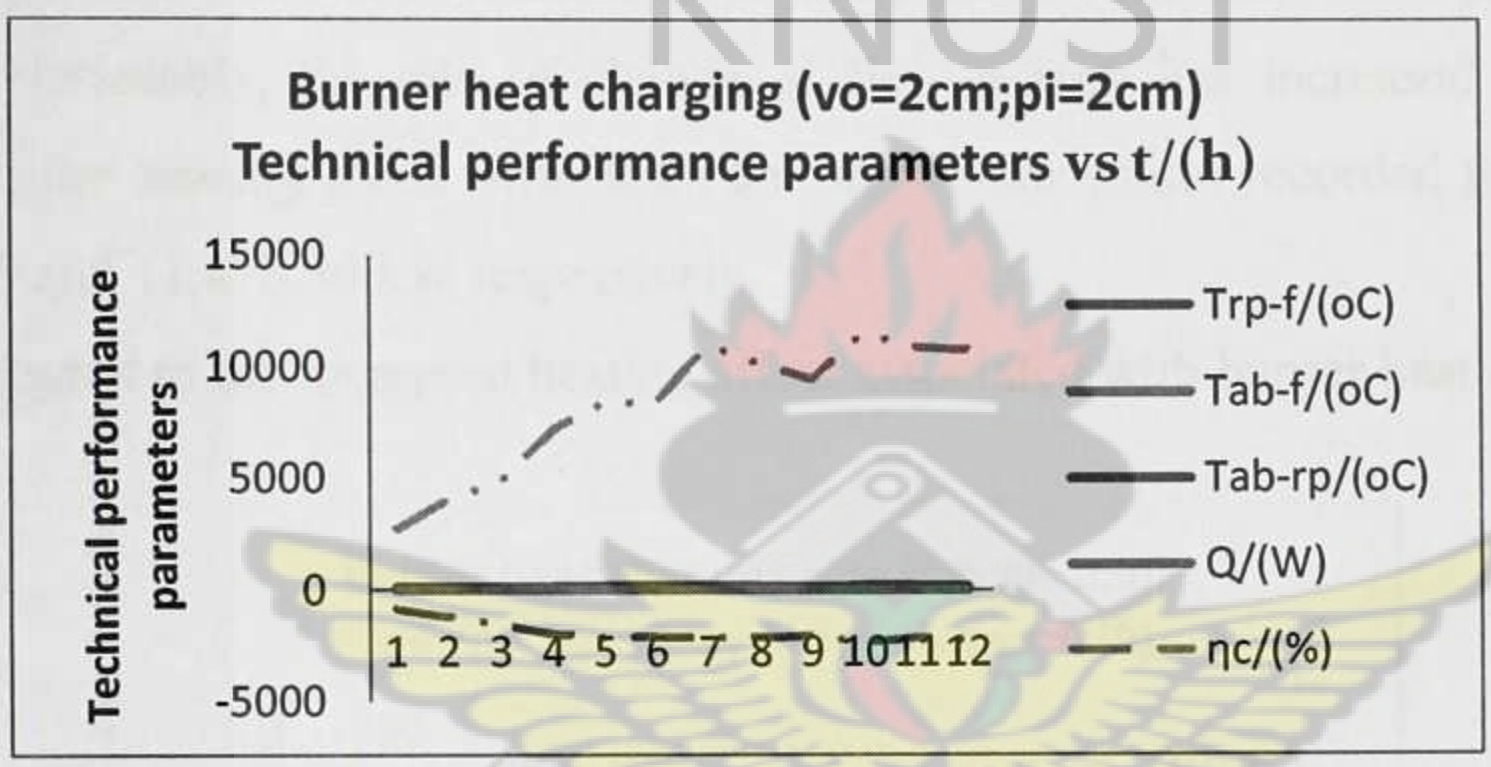

Figure 65 Technical performance parameters versus time in burner heating mode (pi=2 cm, vo=2 cm)

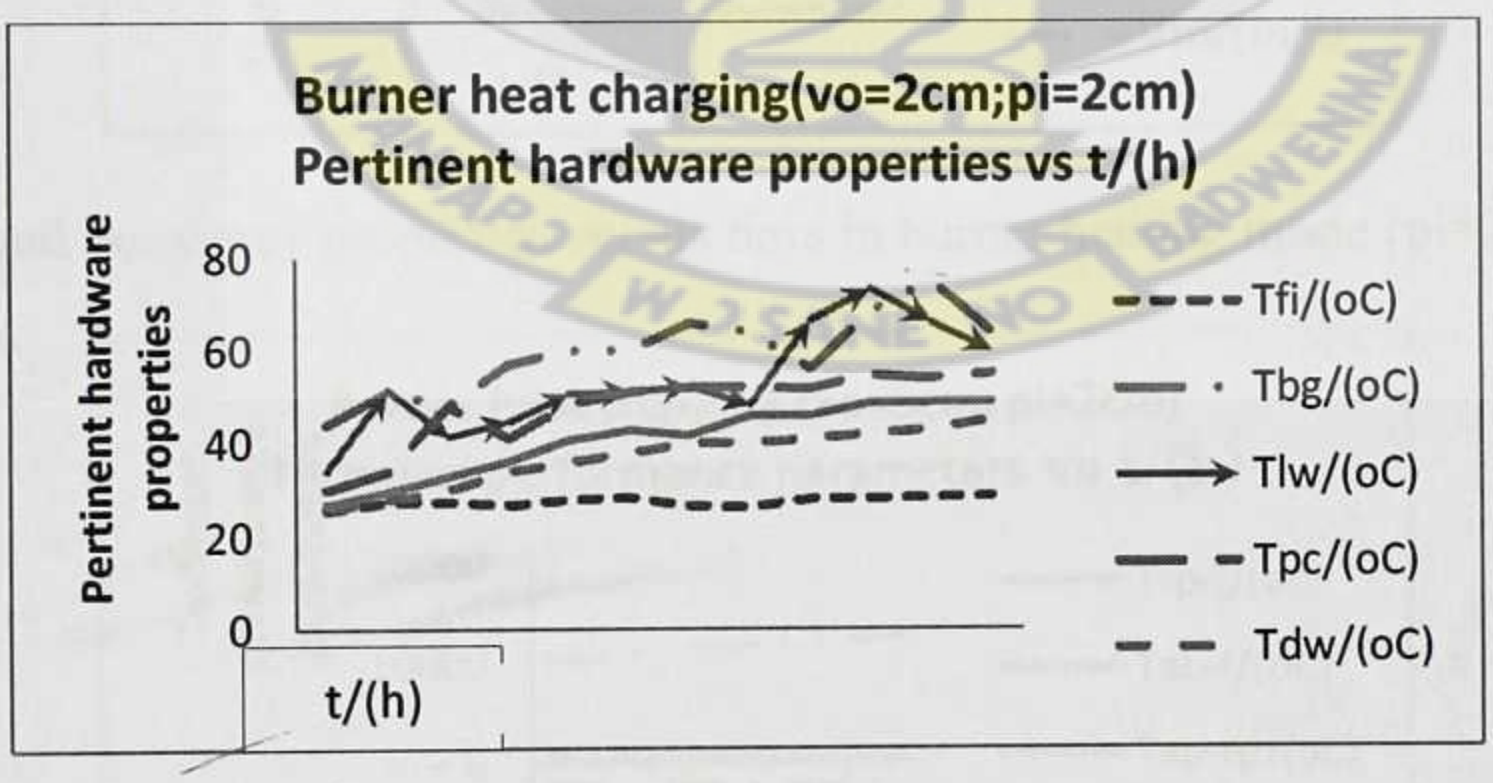

Figure 66 Pertinent hardware properties versus time in burner heating mode (pi=2 cm, vo=2 cm)

The characteristics of the experimental dryer at a plenum inlet gap of 2 cm and a vent outlet gap of 2 cm are shown on figures 64, 65, and 66 in burner heating mode. The average fluid inlet temperatures experienced during the test ranged between 25.7 – 28.7 °C. The average plenum fluid temperature values registered significant increments with values between 34.5 – 67.2 °C. However, the average fluid outlet temperatures decreased significantly after going through the drying chamber even under no load conditions signifying that some amount of heat absorption occurred in the drying chamber. Obviously, the rock bed-burner interface temperature (T_{rp-f}) increased significantly relative to the values recorded in solar heating mode with T_{rp-f} values ranging between 89 – 201 °C. Another significant observation is that the burner housing floor temperatures have also increased remarkably in comparison with the values recorded in solar heating mode. Noticeably, the rate of change of flow exergy has increased significantly as compared with solar heating mode. Minimum and maximum values recorded for this particular test are 2,687.25 and 11,478.30 kW respectively.

This can be attributed to the increased heating effect associated with burner heat charging.

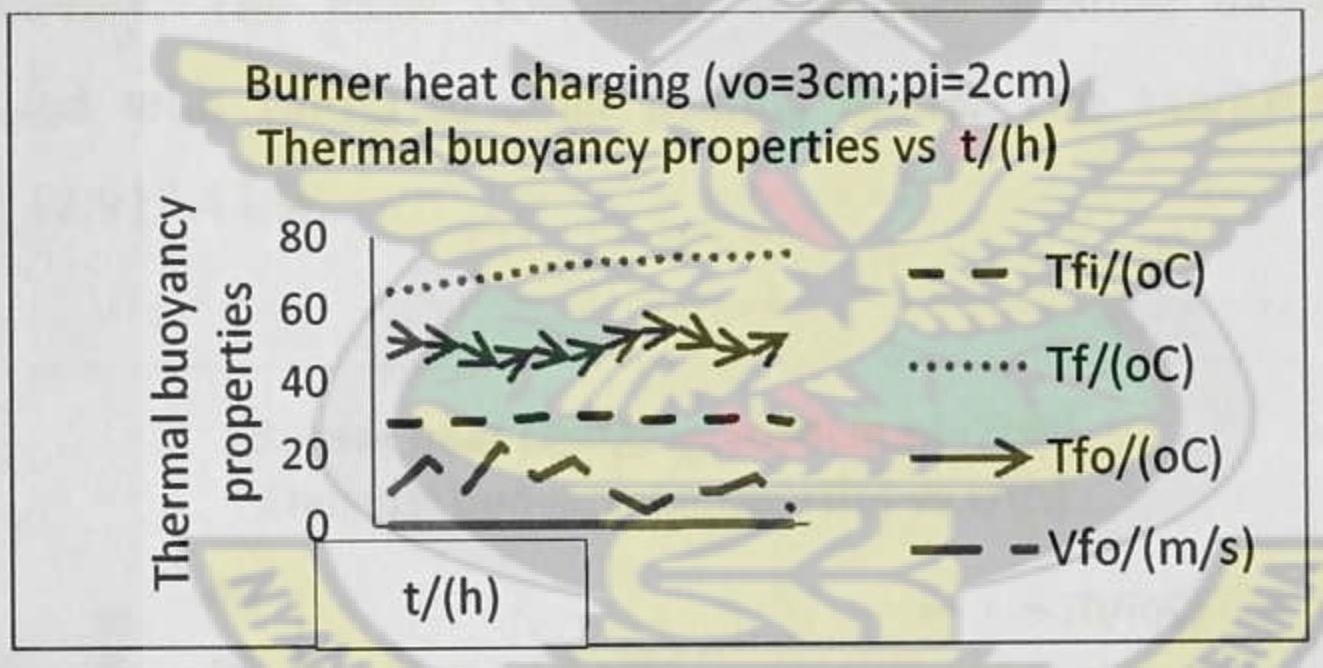

Figure 67 Thermal buoyancy properties versus time in burner heating mode (pi=2 cm, vo=3 cm)

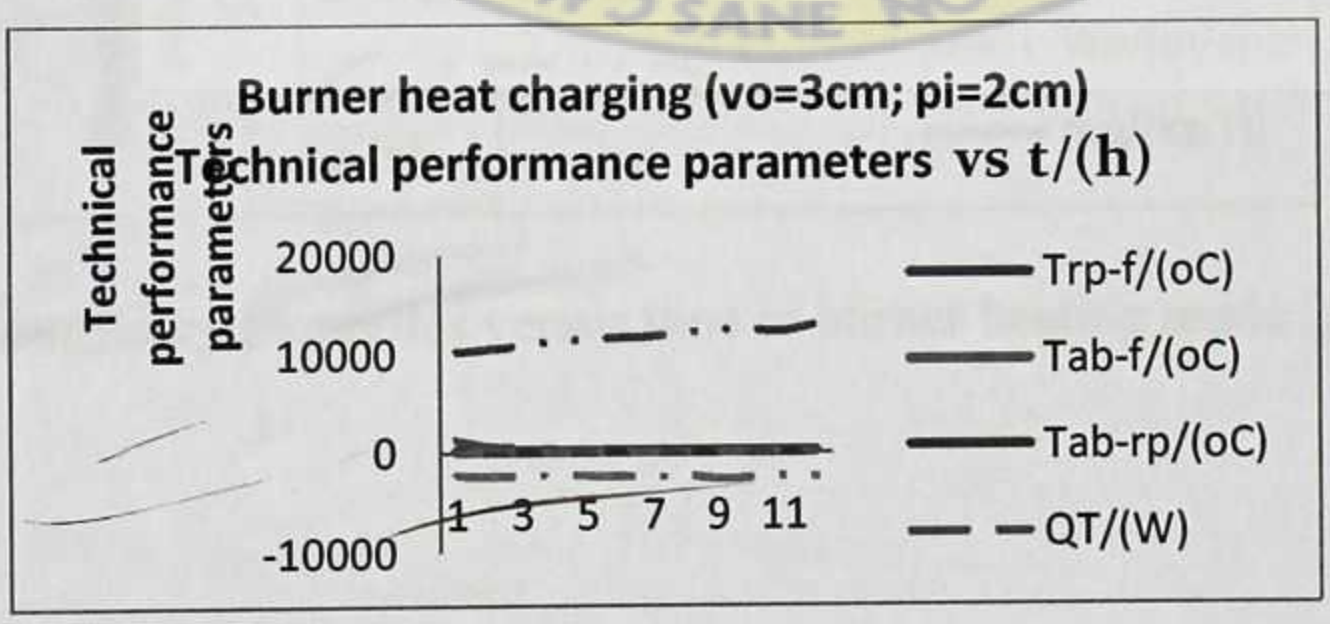

Figure 68 Technical performance parameters versus time in burner heating mode (pi=2 cm, vo=3 cm)

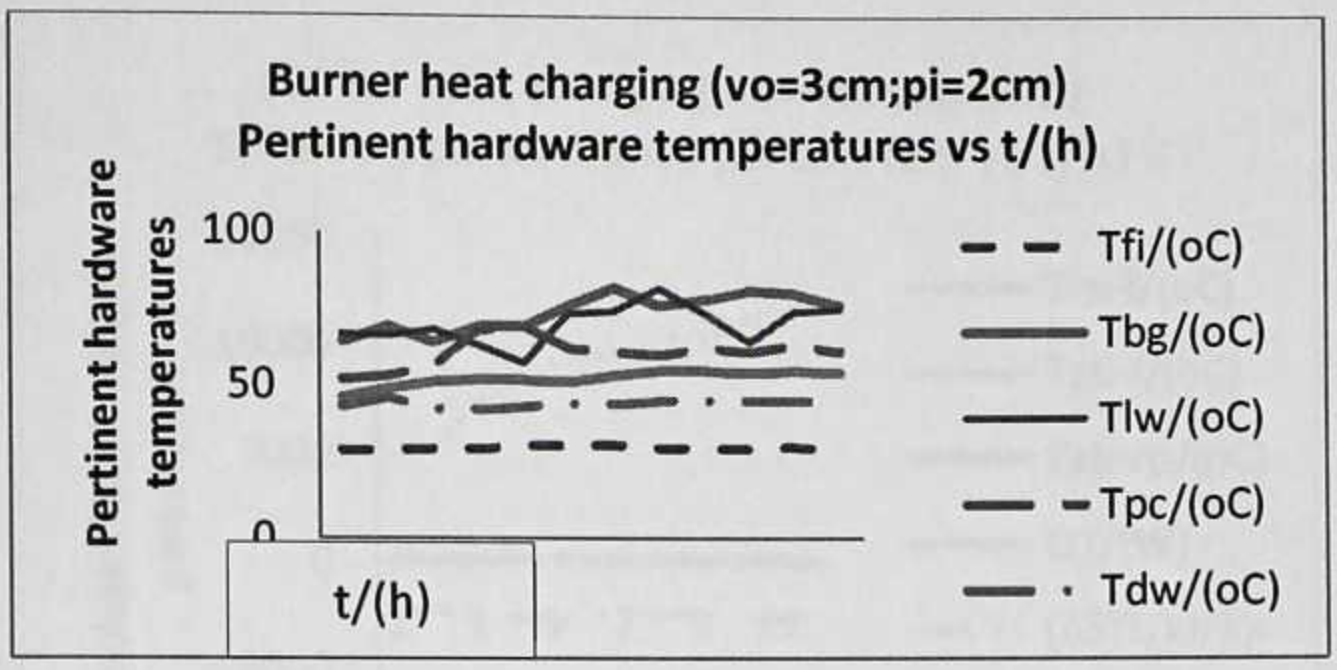

Figure 69 Pertinent hardware temperatures versus time in burner heating mode (pi=2 cm, vo=3 cm)

Figures 67, 68, and 69 show the characterisitcs of the experimental dryer in burner heating mode at a plenum inlet gap of 2 cm and a vent outlet gap of 3 cm. The average plenum fluid temperature showed a steady increase from 64.8 – 75.1 °C. The test recorded average fluid inlet temperatures in the range 28.4 – 30.4 °C with the average air inlet velocity range being 1.0 to 6.1 m/s. The minimum and maximum rock bed – burner interface temperatures recorded were 178 and 224 °C respectively. The mass flow rates in burner heating mode have appreciated significantly compared with values in solar heating mode. The exergy change rate ranged between 10,255 and 12,913.4 kW.

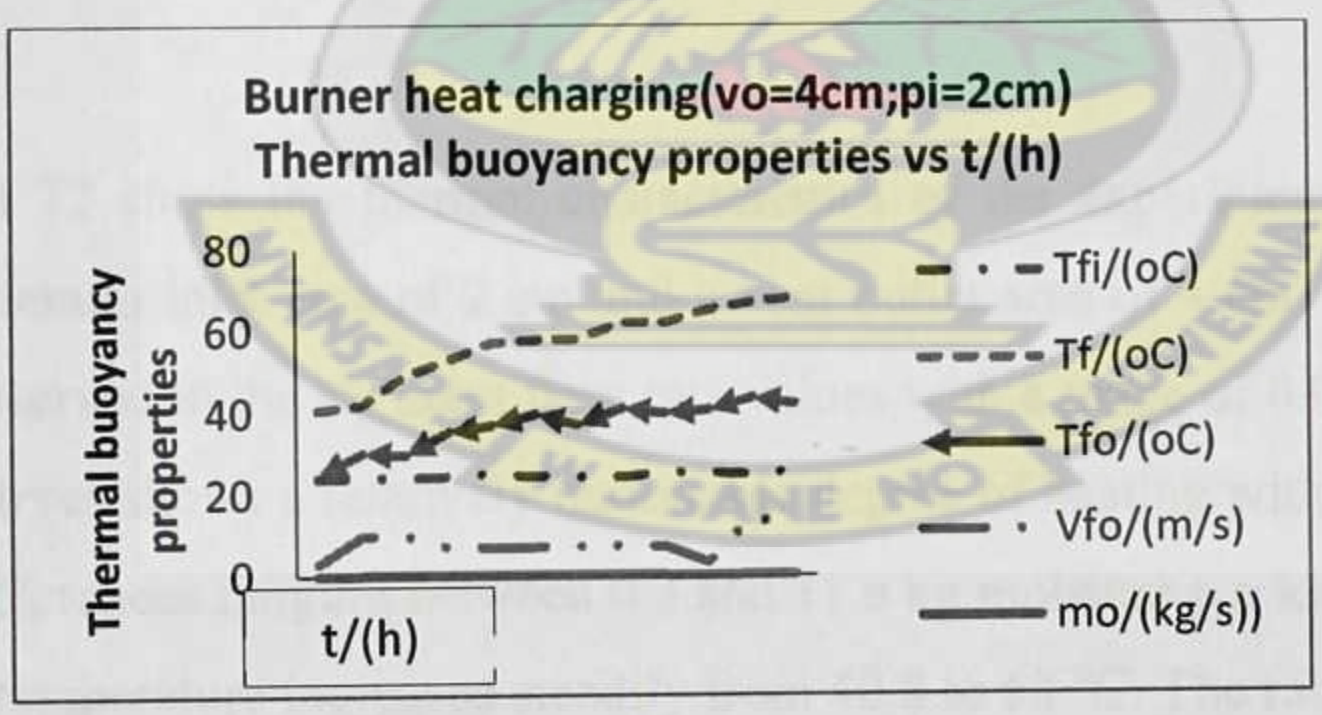

Figure 70 Thermal buoyancy properties versus time in burner heating mode (pi=2 cm, vo=4 cm)

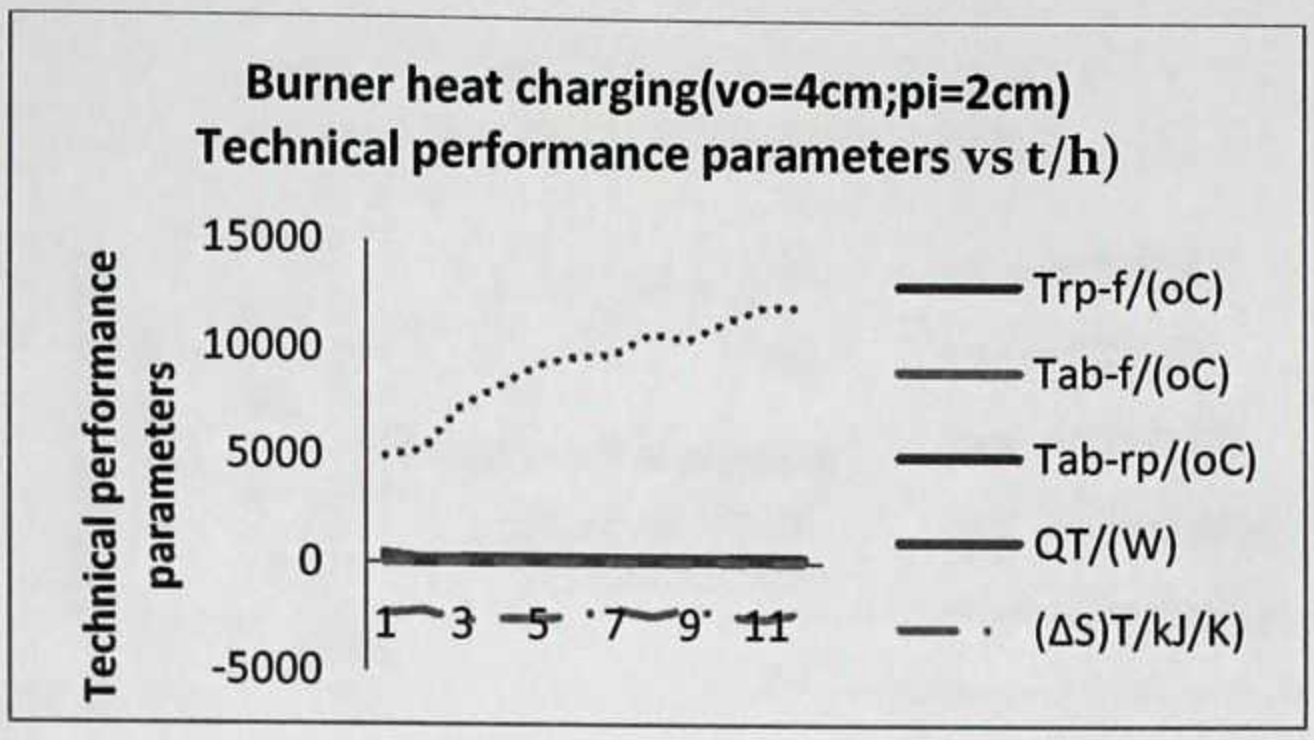

Figure 71 Technical performance parameters versus time in burner heating mode (pi=2 cm, vo=4 cm)

KNUST

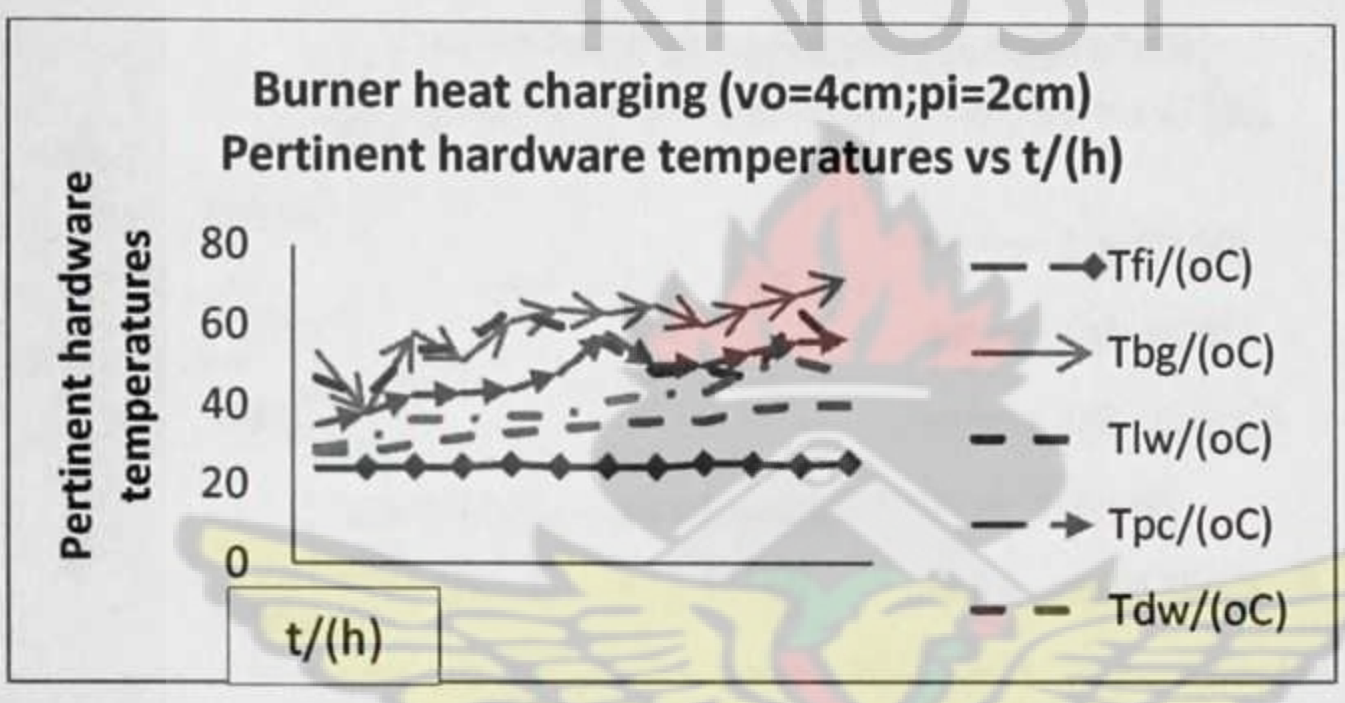

Figure 72 Pertinent hardware temperatures versus time in burner heating mode (pi=2 cm, vo=4 cm)

Figures 70, 71, and 72 show the thermal characteristics of the experimental dryer in burner heating mode at a plenum inlet area of 2 cm and a vent outlet area of 4 cm. A remarkably high increment can be observed in the air mass flow rate values with a range of 0.0524 – 0.2387 kg/s. The air exiting the dryer shows a relatively reasonable degree of heating with air inlet and outlet relative humidity differences ranging between 0.3 and 11.6 kg moisture per kilogram dry air. The average plenum air temperature increased steadily from 40.8 to 68 °C. The rate of change of flow exergy recorded 4,963.99 minimum and 11,974.02 kW maximum.

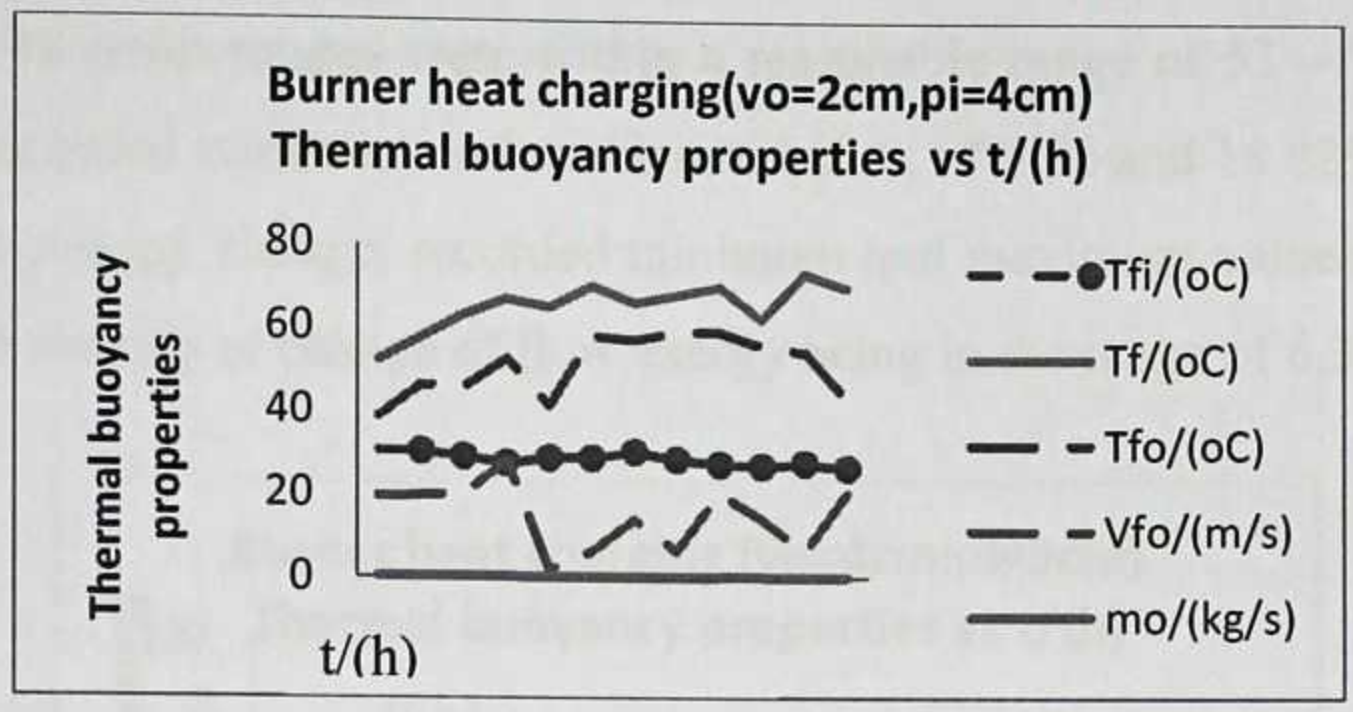

Figure 73 Thermal buoyancy properties versus time in burner heating mode (pi=4 cm, vo=2 cm)

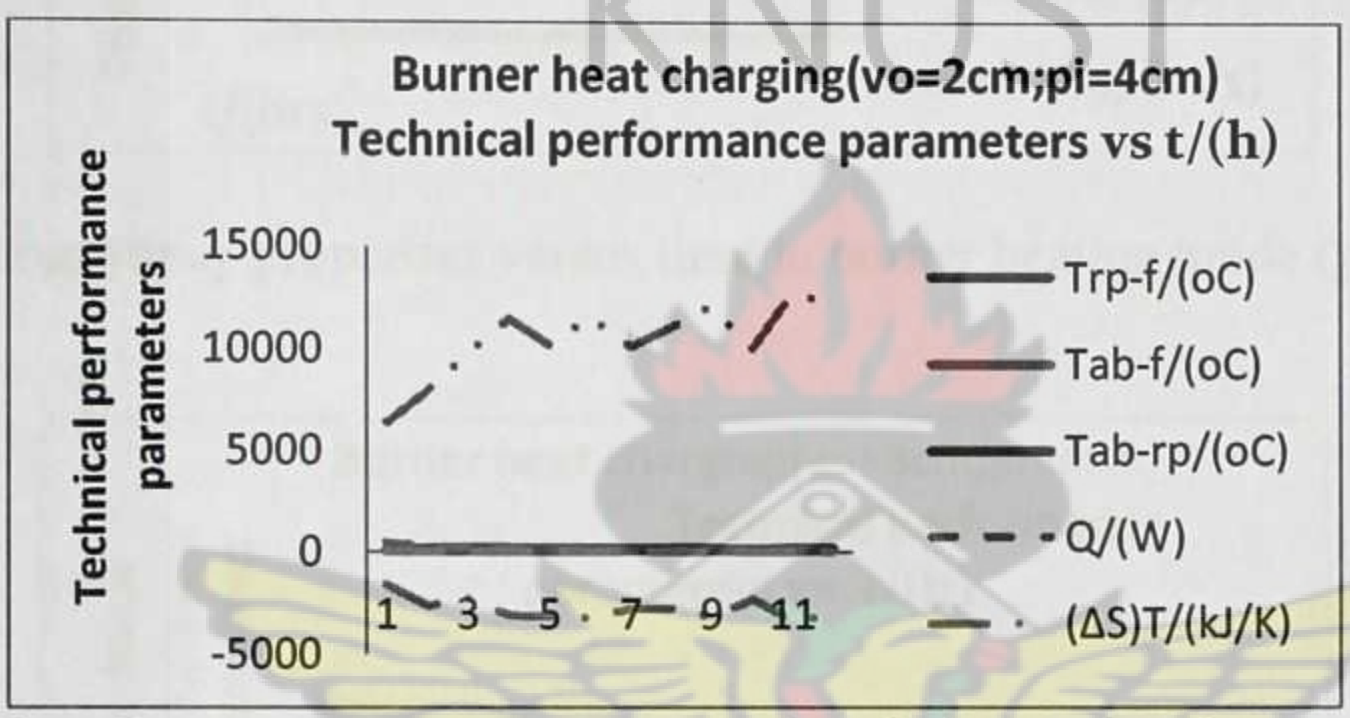

Figure 74 Technical performance parameters versus time in burner heating mode (pi=4 cm, vo=2 cm)

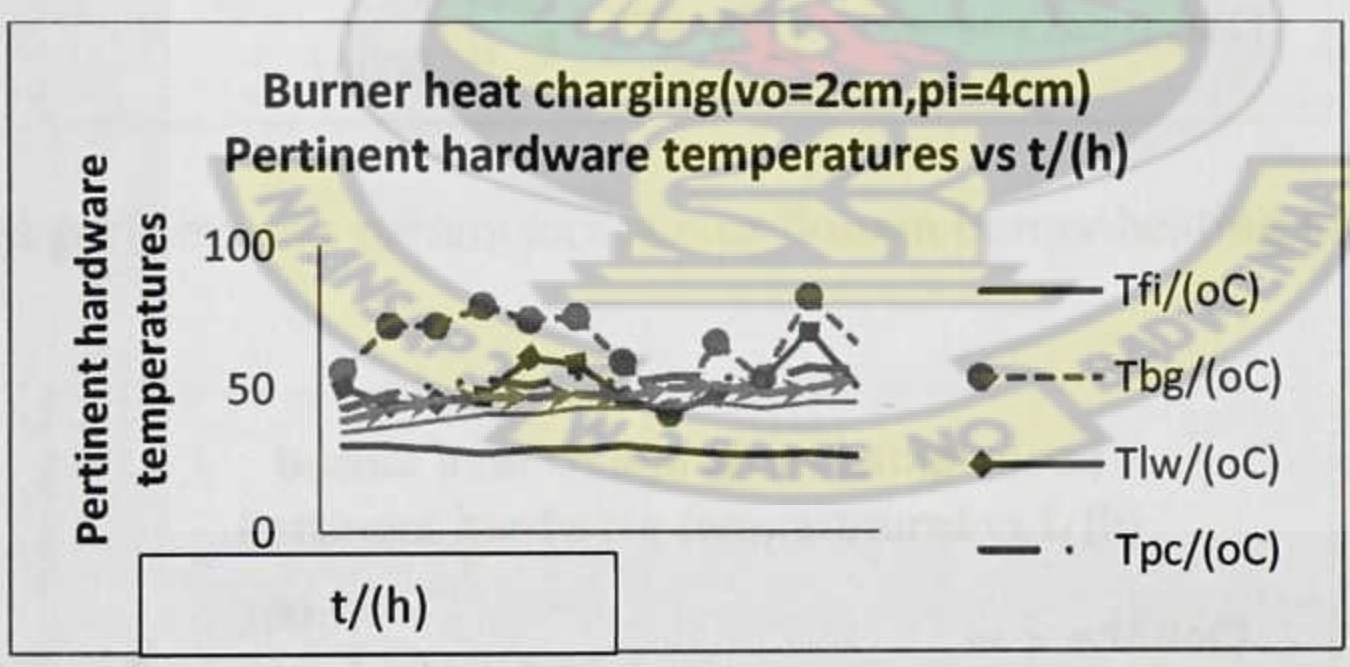

Figure 75 Pertinent hardware temperatures versus time in burner heating mode (pi=4 cm, vo=2 cm)

Figures 73, 74, and 75 show the characteristics of the dryer at a plenum inlet gap of 4 cm and a vent outlet gap of 2 cm in burner heating mode. The average air inlet temperatures ranged between 26.5 – 30.3 °C with the average air inlet velocities ranging from 0.3 – 5.0 m/s. The

average plenum inlet temperatures were within a reasonable range of 52 – 73.2 °C and the air heater efficiency recorded minimum and maximum values of 0.76 and 18.82% respectively. The thermal mass total entropy change, recorded minimum and maximum values of -1,595.76 and -3,143.62 kJ/K with the rate of change of flow exergy being in the range of 6,371 and 12,671 kW.

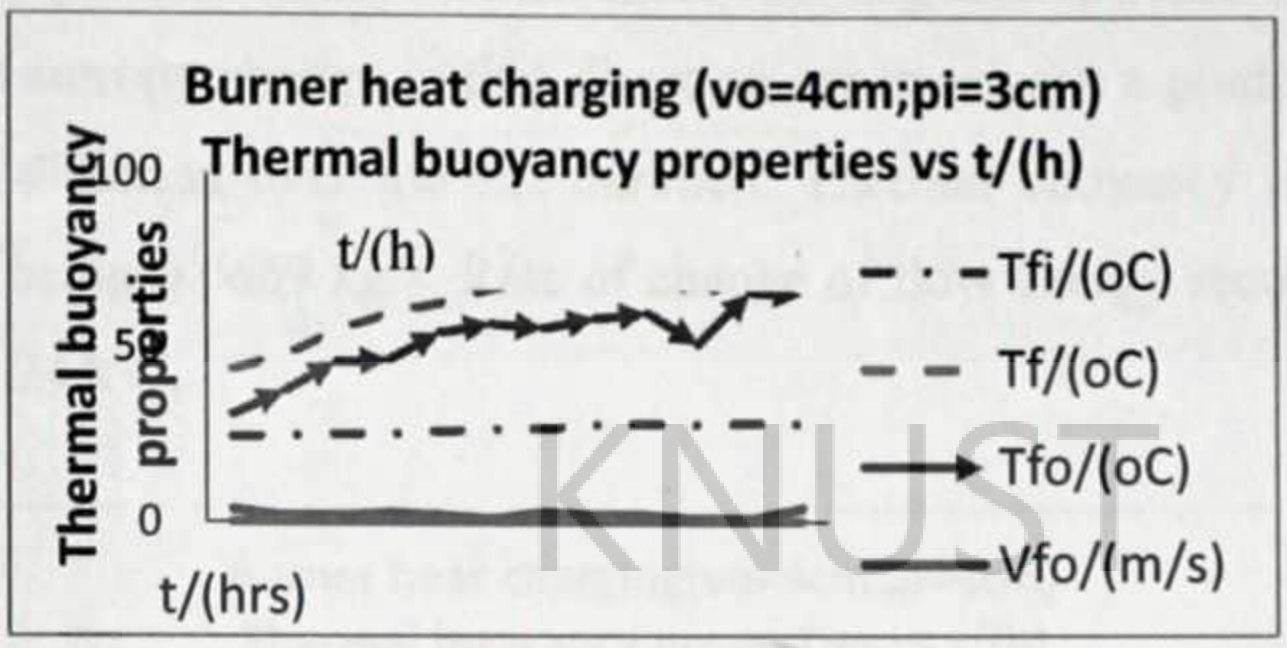

Figure 76 Thermal buoyancy properties versus time in burner heating mode (pi=3 cm, vo=4 cm)

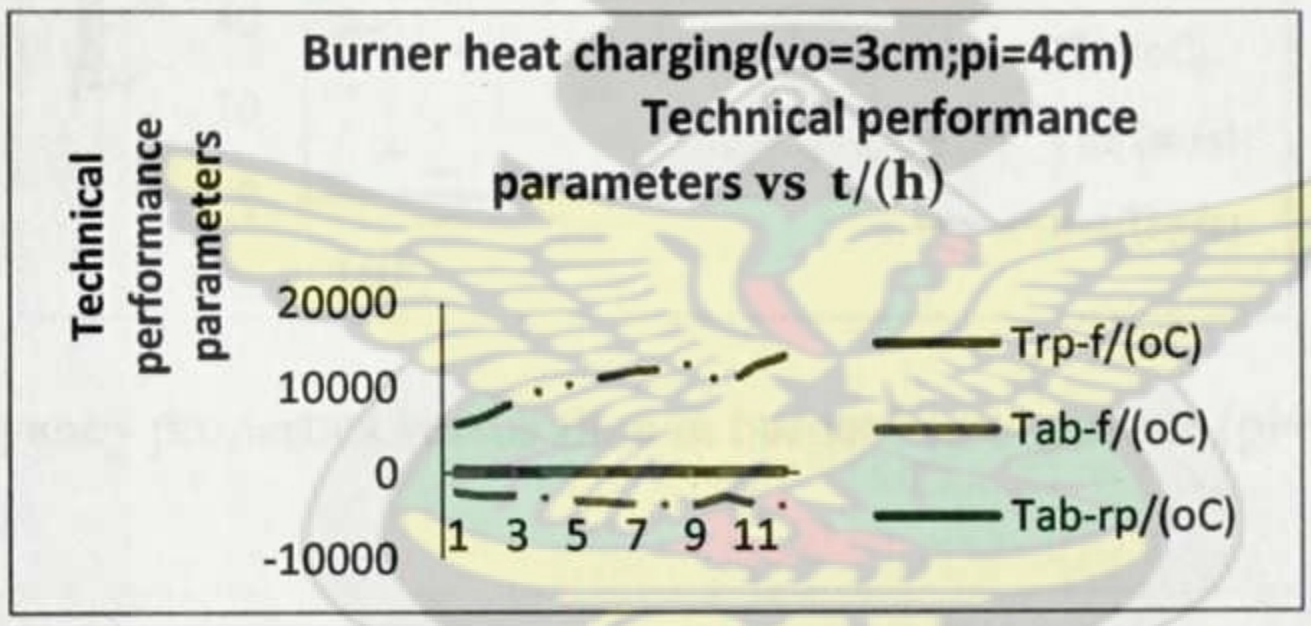

Figure 77 Technical performance parameters versus time in burner heating mode (pi=4 cm, vo=3 cm)

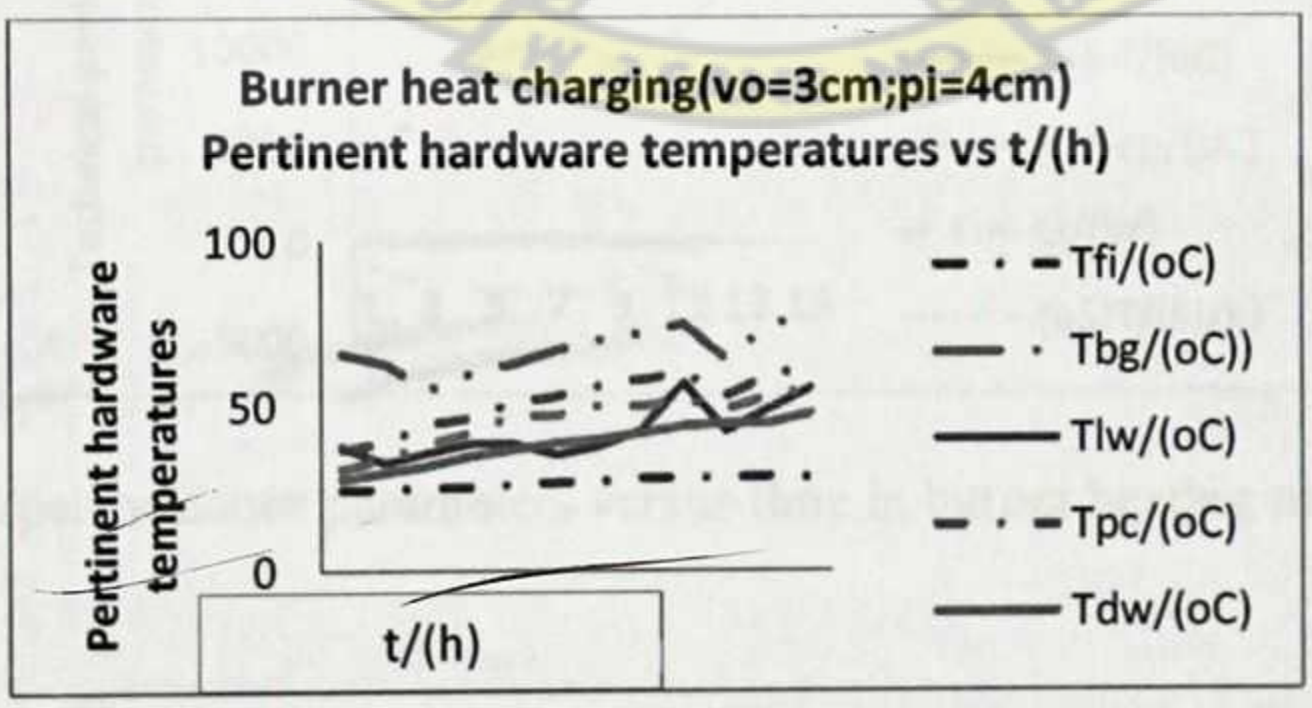

Figure 78 Pertinent hardware temperatures versus time in burner heating mode (pi=4 cm, vo=3 cm)

The thermal properties of the dryer at a plenum inlet gap of 4 cm and a vent outlet gap of 3 cm in burner heat charging mode is shown in figures 76, 77, and 78. On a characteristically cloudy day with relatively high local atmospheric pressures (981.3 – 981.6 hPa) the average fluid inlet temperatures ranged between 24.6 – 28.6 °C and average fluid inlet velocities not exceeding 1.4 m/s. The temperature gradient in the thermal mass was negative towards the concrete absorber surface making total entropy change in that direction negative with a gradually decreasing heat transfer rate in that direction over the test duration. Thermal buoyancy is moderate with the maximum flow rate being 0.0669 kg/s. Rate of change of flow exergy recorded values between 5,663.83 and 13,656.24 kW.

KNUST

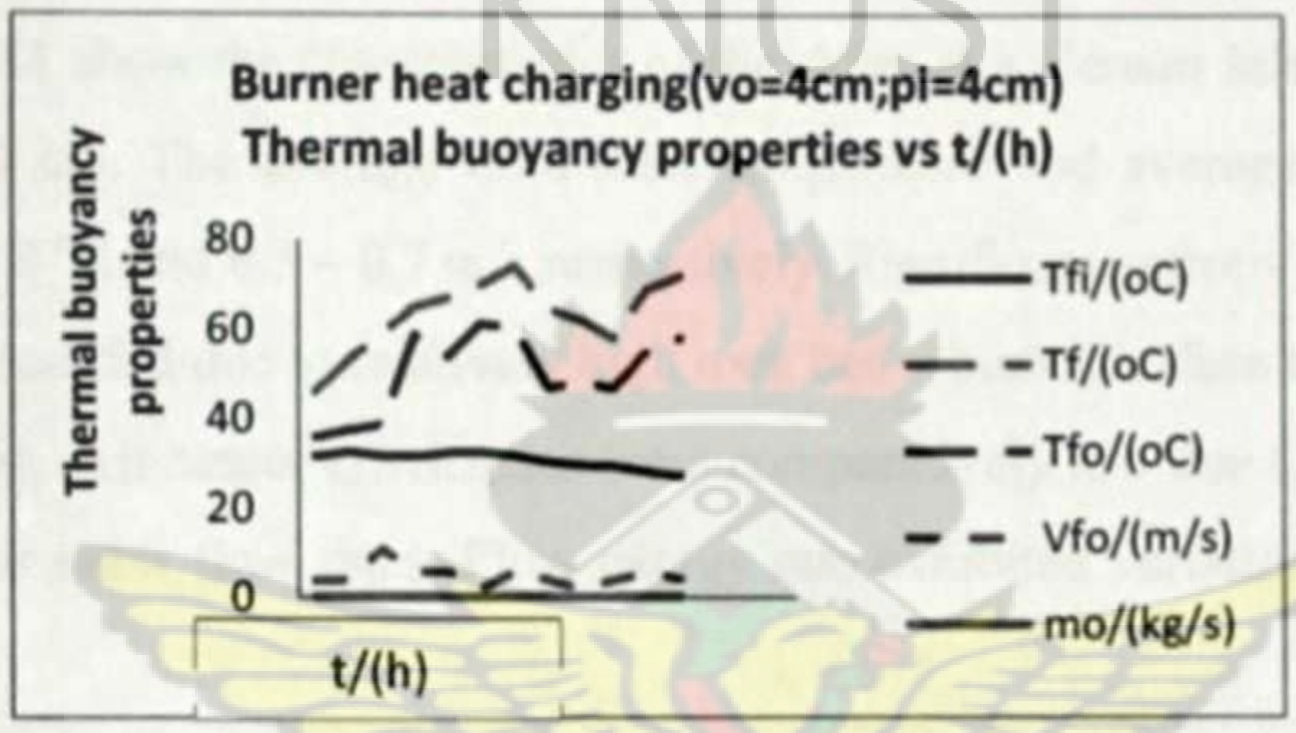

Fig 79 Thermal buoyancy properties versus time in burner heating mode (pi=4 cm, vo=4 cm)

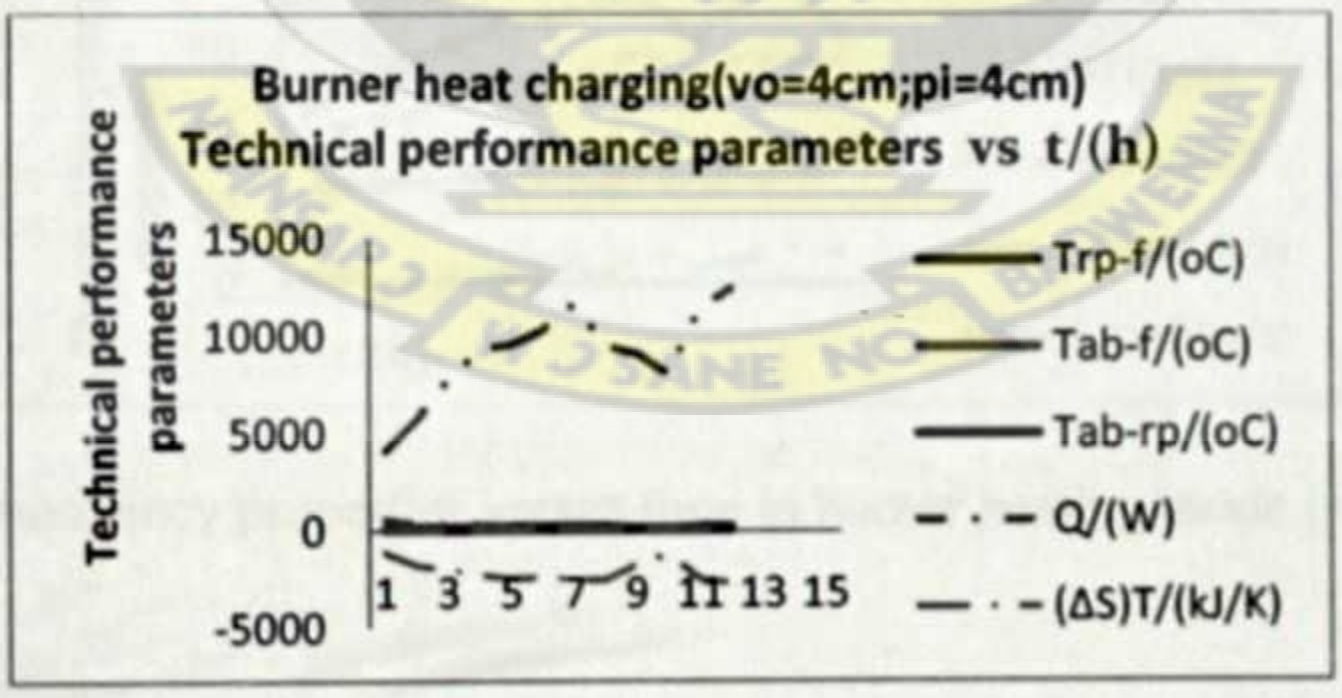

Figure 80 Technical performance parameters versus time in burner heating mode (pi=4 cm, vo=4 cm)

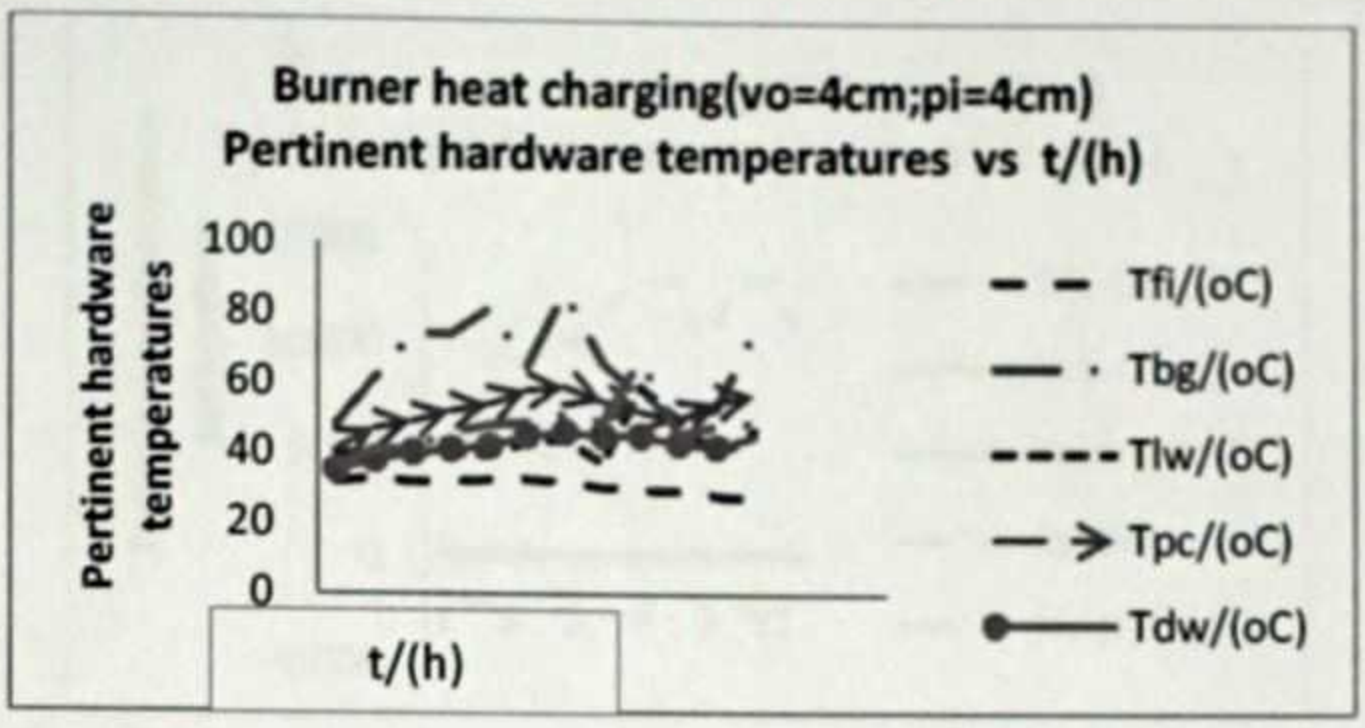

Figure 81 Pertinent hardware temperatures versus time in burner heating mode (pi=4 cm, vo=4 cm)

KNUST

Figures 79, 78, and 81 show the characteristics of the dryer at a plenum inlet gap of 4 cm and a vent outlet gap of 4 cm. The average fluid inlet temperature and average fluid inlet velocity ranges are 27.2 – 32.8 °C and 0.3 – 0.7 m/s respectively. Significant entropy decreases across the thermal mass were recorded due to relatively high rock bed – burn interface temperature and low ambient temperatures. Air heater efficiencies were comparatively low due to low inlet velocities and relatively low air mass flow rates. Flow exergy rate exhibited variations between 4,145.81 and 12,469.08 kW.

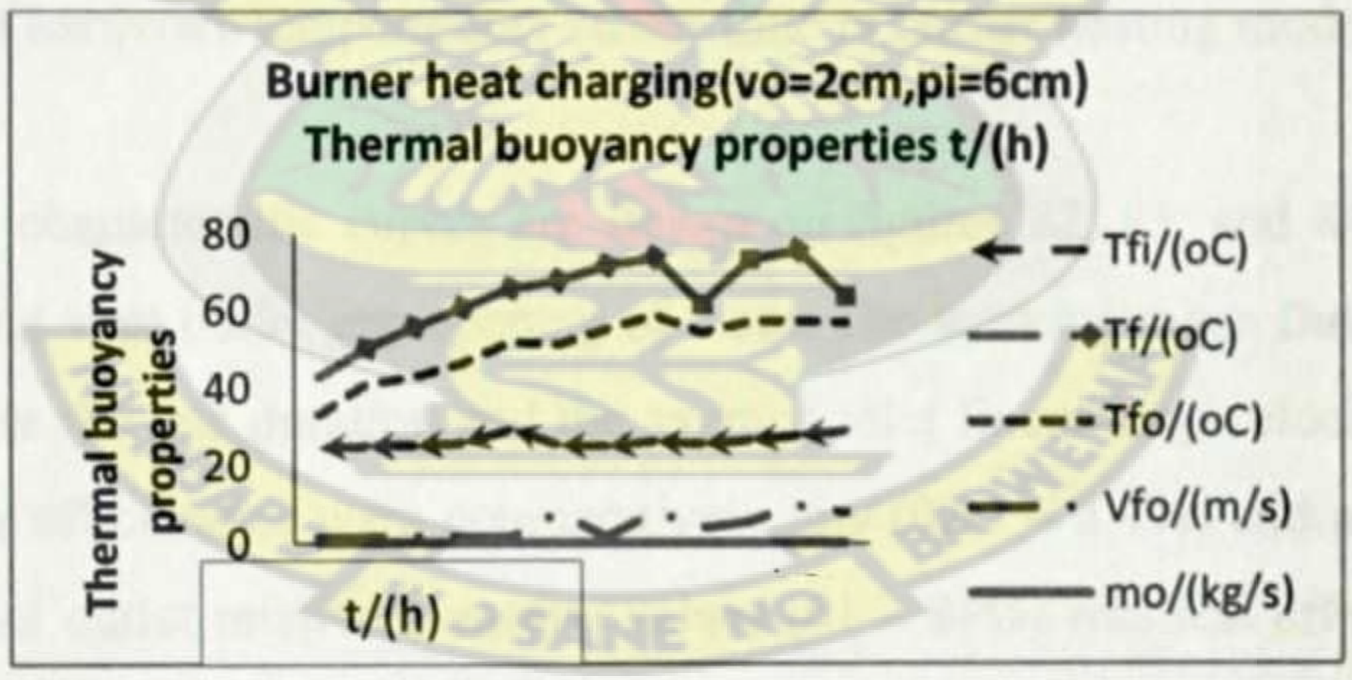

Figure 82 Thermal buoyancy properties versus time in burner heating mode (pi=6 cm, vo=2 cm)

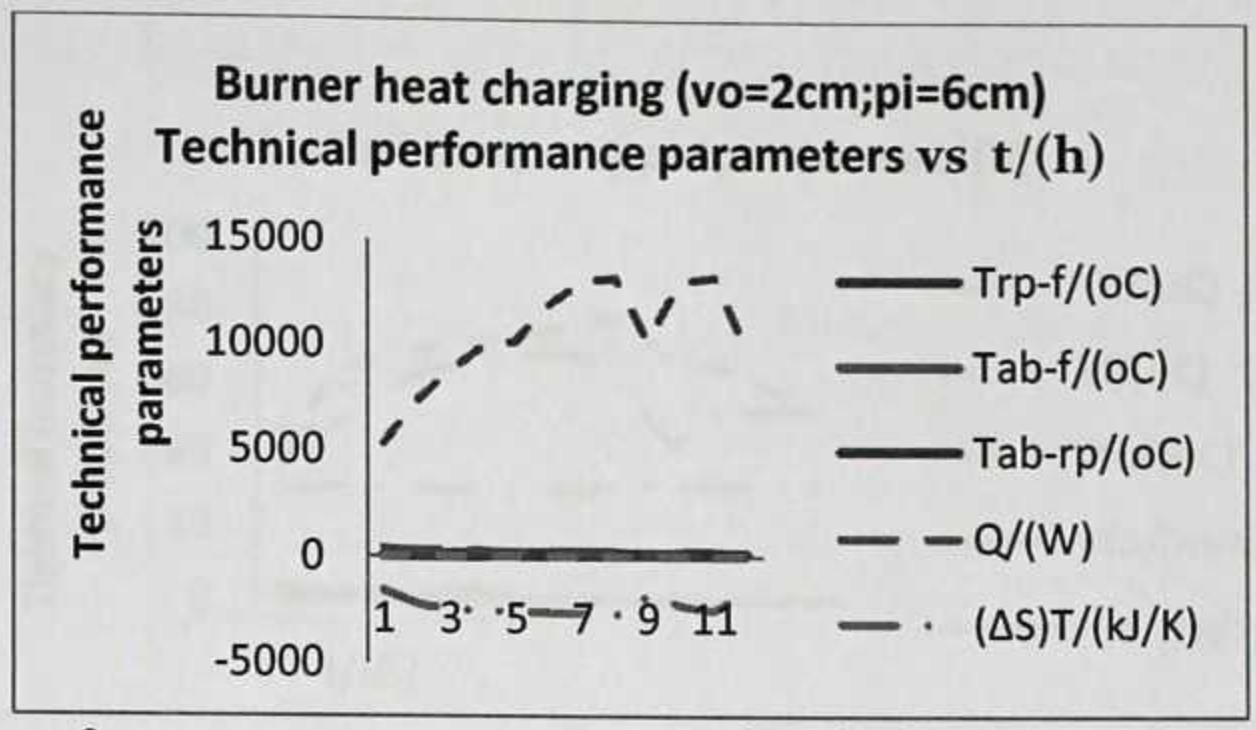

Figure 83 Technical performance parameters versus time in burner heating mode (pi=6 cm, vo=2 cm)

KNUST

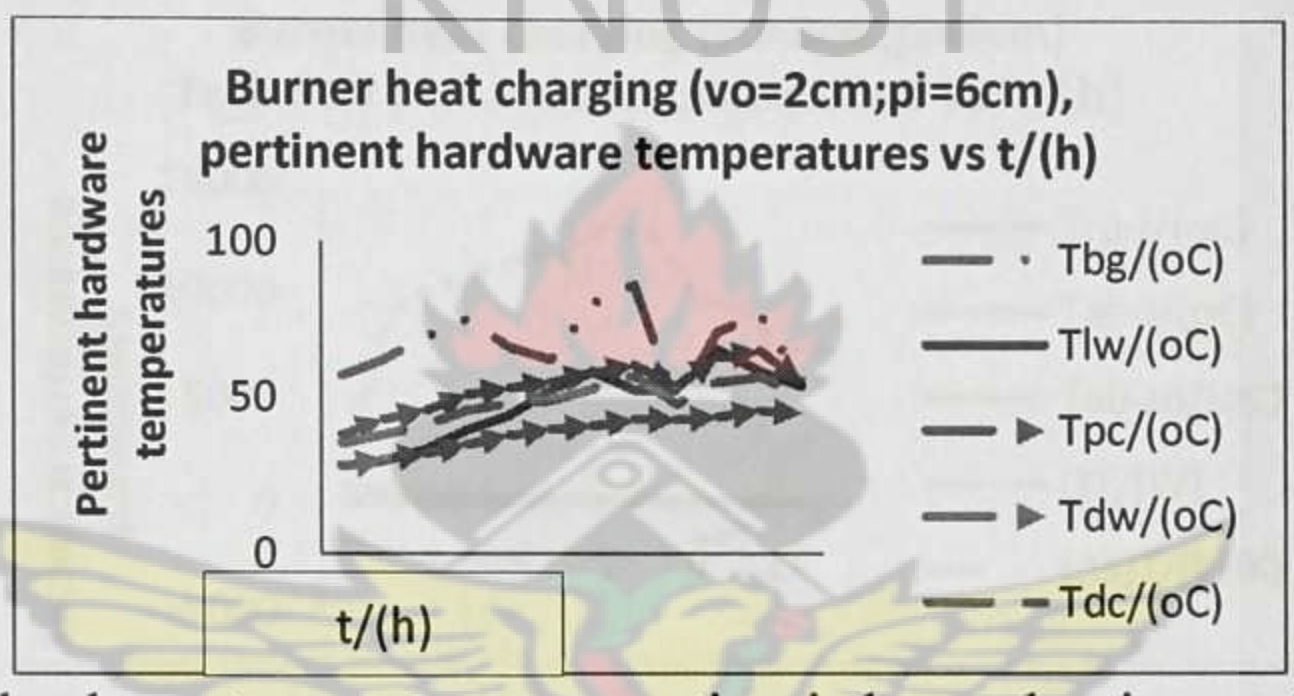

Figure 84 Pertinent hardware temperatures versus time in burner heating mode (pi=6 cm, vo=2 cm)

The dryer thermal characteristic curves are shown on figures 82, 83, and 84 at a plenum inlet opening of 6 cm and vent outlet gap opening of 2 cm. The working mean fluid inlet temperature range was 24.8 over the test duration and the average inlet fluctuating velocity range was 0.3 – 1.7 m/s. Air heater efficiencies were comparatively low (0.07 – 2.4%) and air heating effect as reflected by trend of outlet relative humidity values (61 – 84%) was less effective. Flow exergy varied between 5,315.99 and 13,271.61 kW.

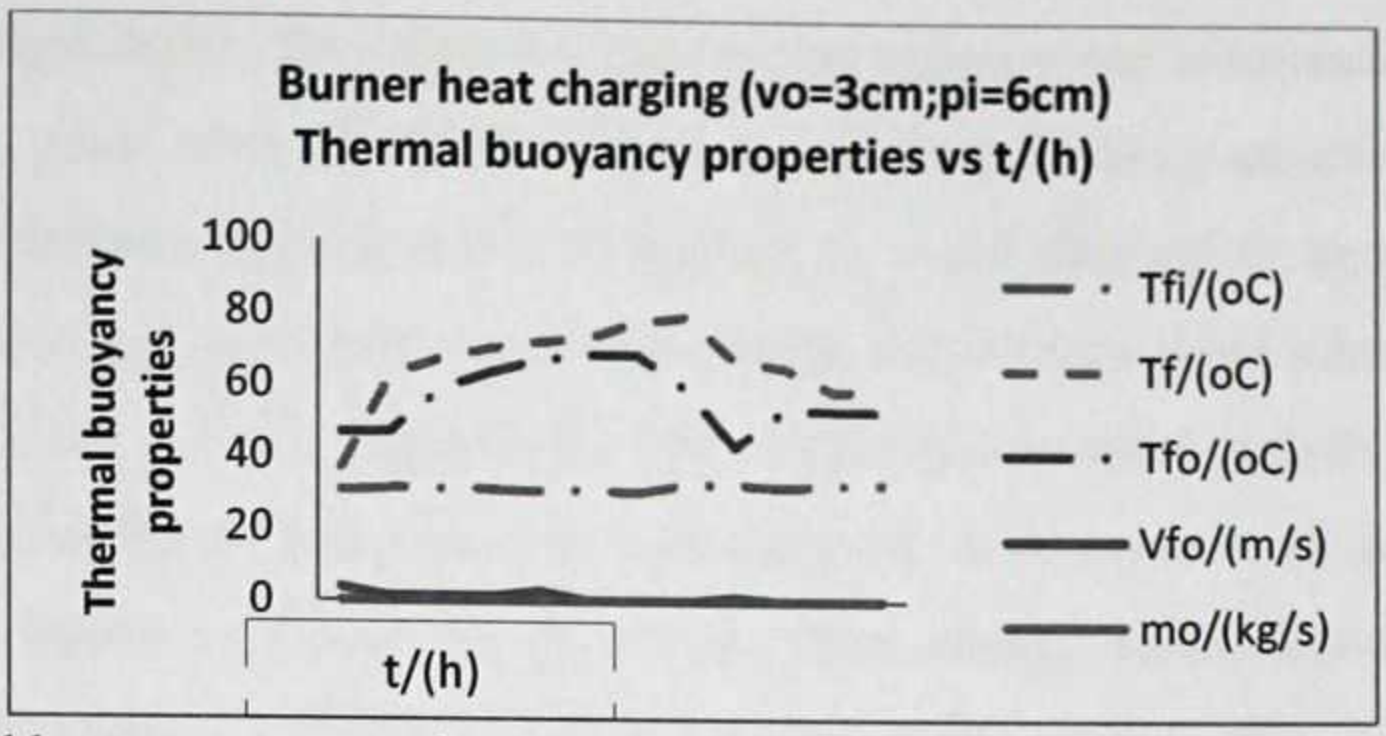

Figure 85 Thermal buoyancy properties versus time in burner heating mode (pi=6 cm, vo=3 cm)

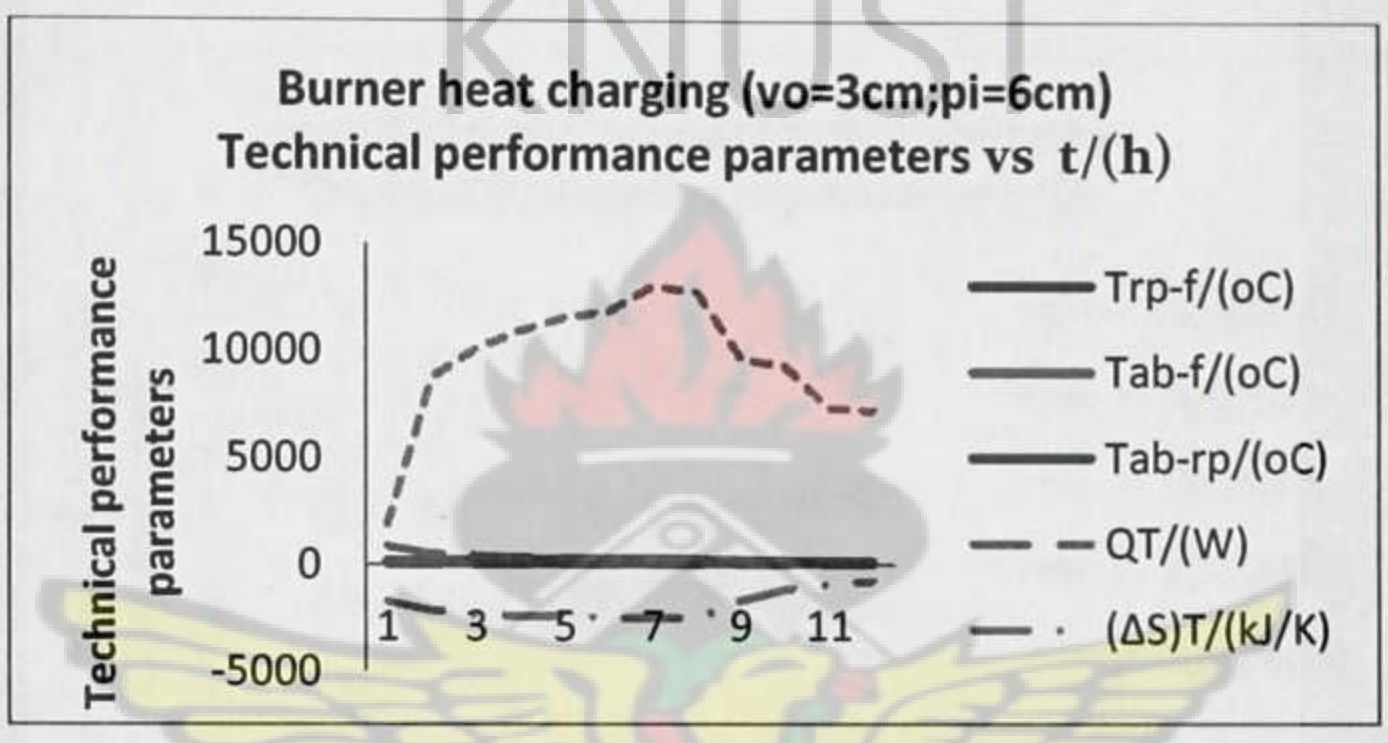

Figure 86 Technical performance parameters versus time in burner heating mode (pi=6 cm, vo=3 cm)

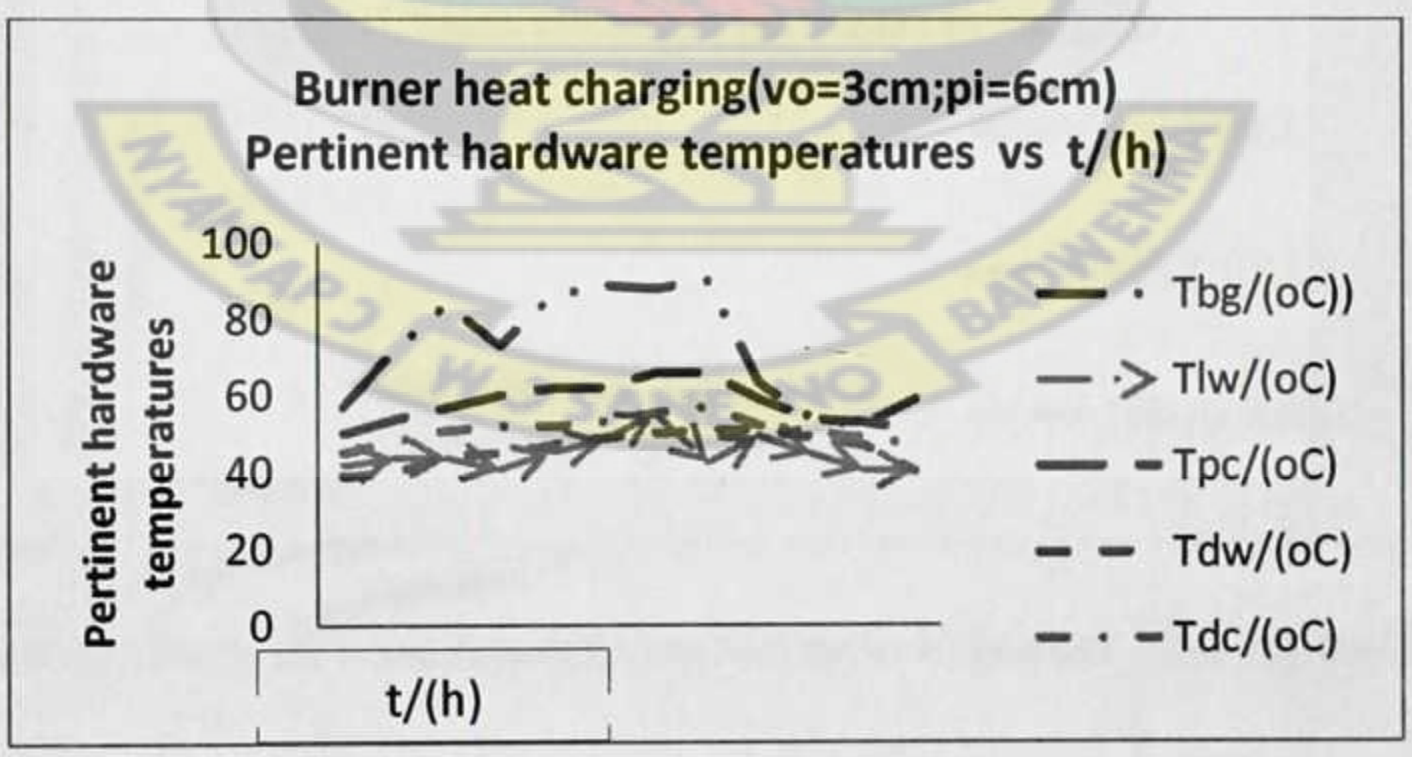

Figure 87 Pertinent hardware temperatures in burner heating mode (pi=6 cm, vo=3 cm)

Figures 85, 86, and 87 give graphical representations of the thermal characteristics of the experimental dryer at a plenum inlet gap of 6 cm and vent outlet gap of 3 cm. The average plenum glass cover temperature range and drying chamber glass cover range were 50 – 66 °C,

and 45 – 57 °C respectively. The relatively high plenum glass cover temperature range is due to the nearness of the glass cover to the thermal mass which has a burner attached to its underside. However, the temperature regime was safe enough to avoid damage to heat sensitive system components. The average fluid inlet temperature range and average wind inlet speed range were 30.3 – 32.5 °C and 0.3 – 1 m/s respectively. The relatively low wind activity accounted for the relative decrease in outlet air velocities and, subsequently, a decrease in air mass efflux and air heater efficiency values as shown on figure 84. Flow exergy varied between 7,182.77 and 13,013.46 kW. Air heater efficiency varied between 0.033 and 0.47% with 0% efficiency occurring at three test points characterised by 0 m/s fluid inlet velocity.

KNUST

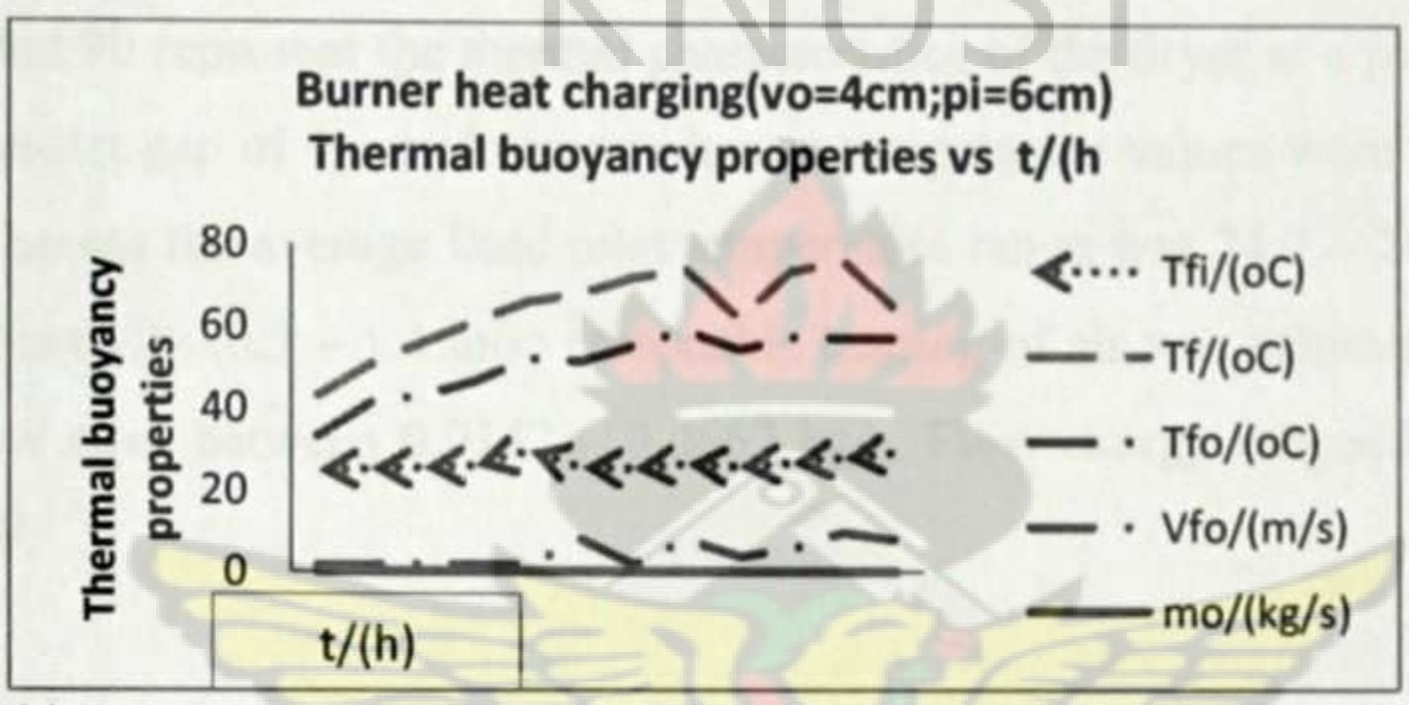

Figure 88 Thermal buoyancy properties versus time in burner heating mode (pi=6 cm, vo=4 cm)

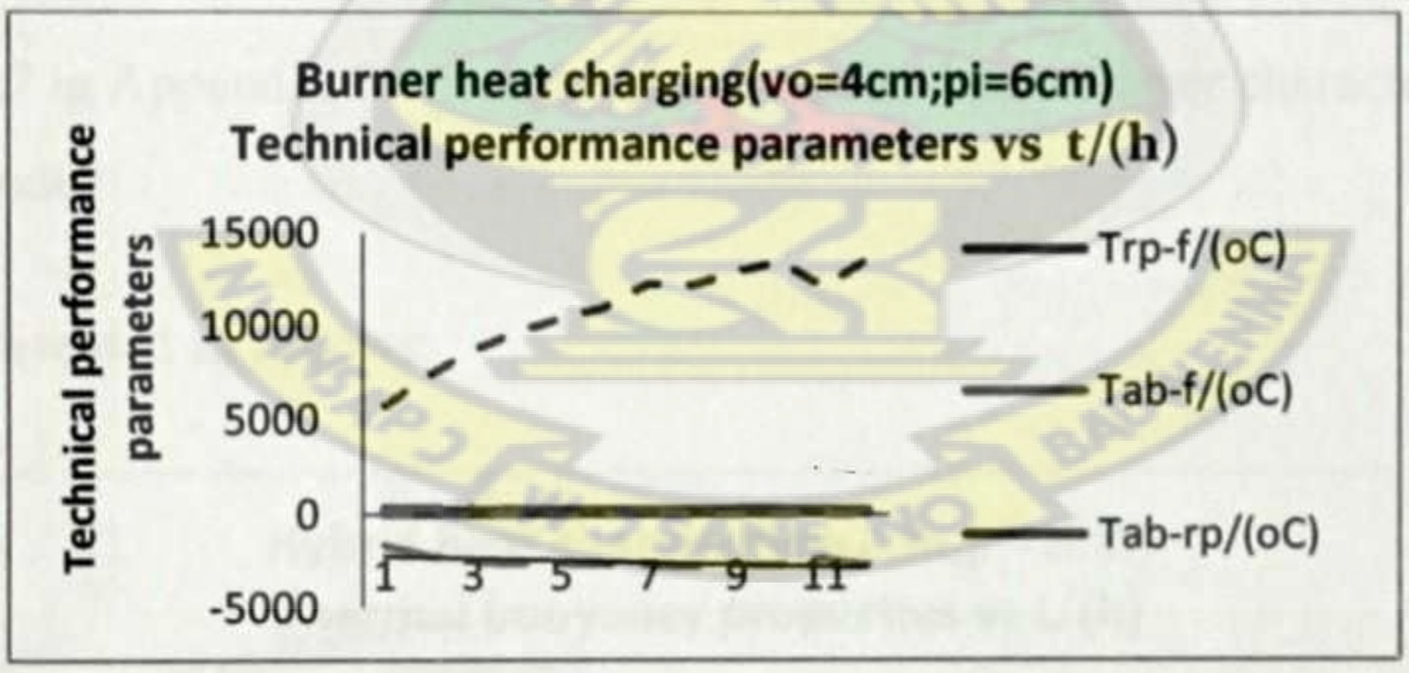

Figure 89 Technical performance parameters versus time in burner heating mode (pi=6 cm, vo=4 cm)

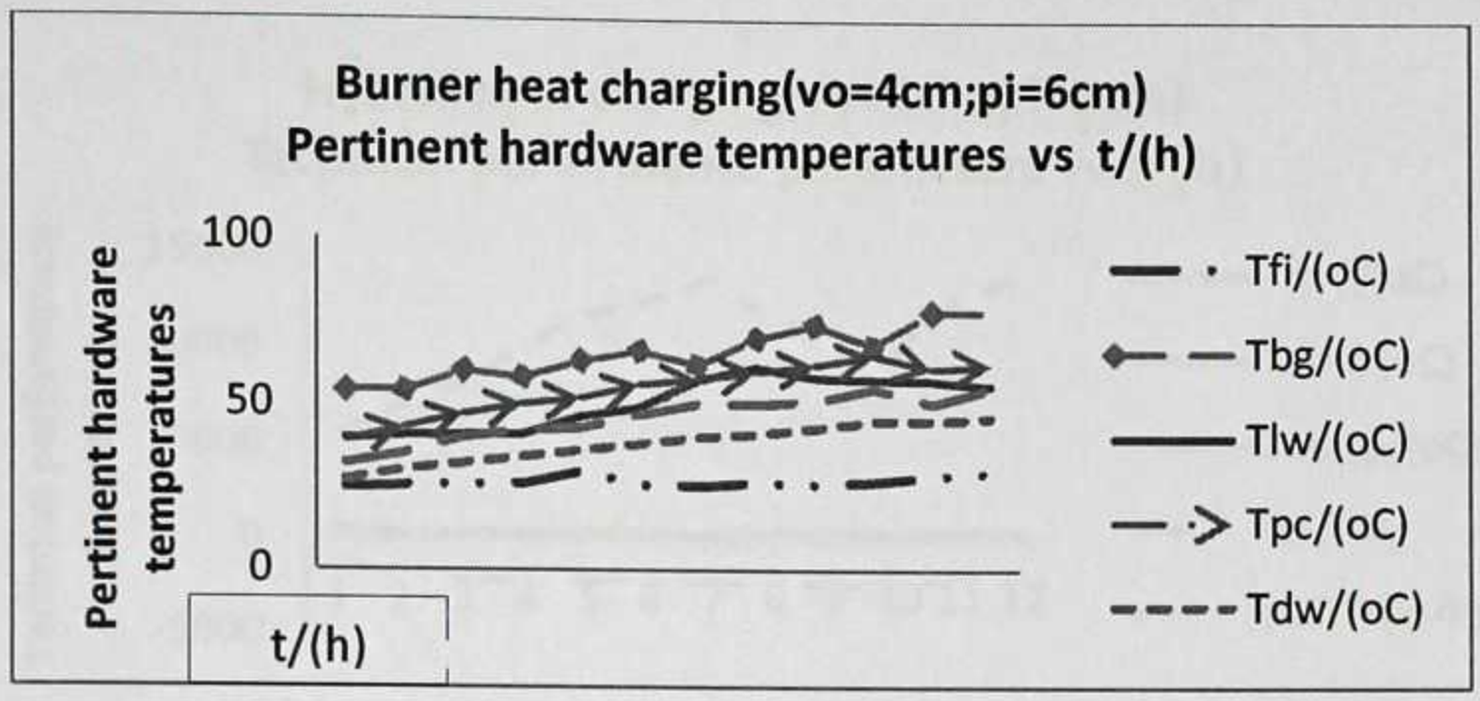

Figure 90 Pertinent hardware temperatures versus time in burner heating mode (pi=6 cm, vo=4 cm)

Figures 88, 89, and 90 represent the thermal characteristics of the dryer at a plenum inlet gap of 6 cm and a vent outlet gap of 4 cm. Average plenum temperature values were within safe limits (44 – 75.6 oC) whereas the average fluid inlet temperature range was 24.2 – 26.8 °C. Even with the average wind activity (0.3 – 1.4 m/s) reasonable heating of air was achieved (64.4 – 81.6%) with air mass flow rates between 0.0142 – 0.0667 kg/s. Flow exergy ranged between 5,749.71 and 13,574.04 kW.

5.1.3 **Hybrid Heat Charging**

Tables C19 to C27 in Appendix C cover the experimental data on dryer characteristic studies in hybrid heating mode.

The results are presented as follows:

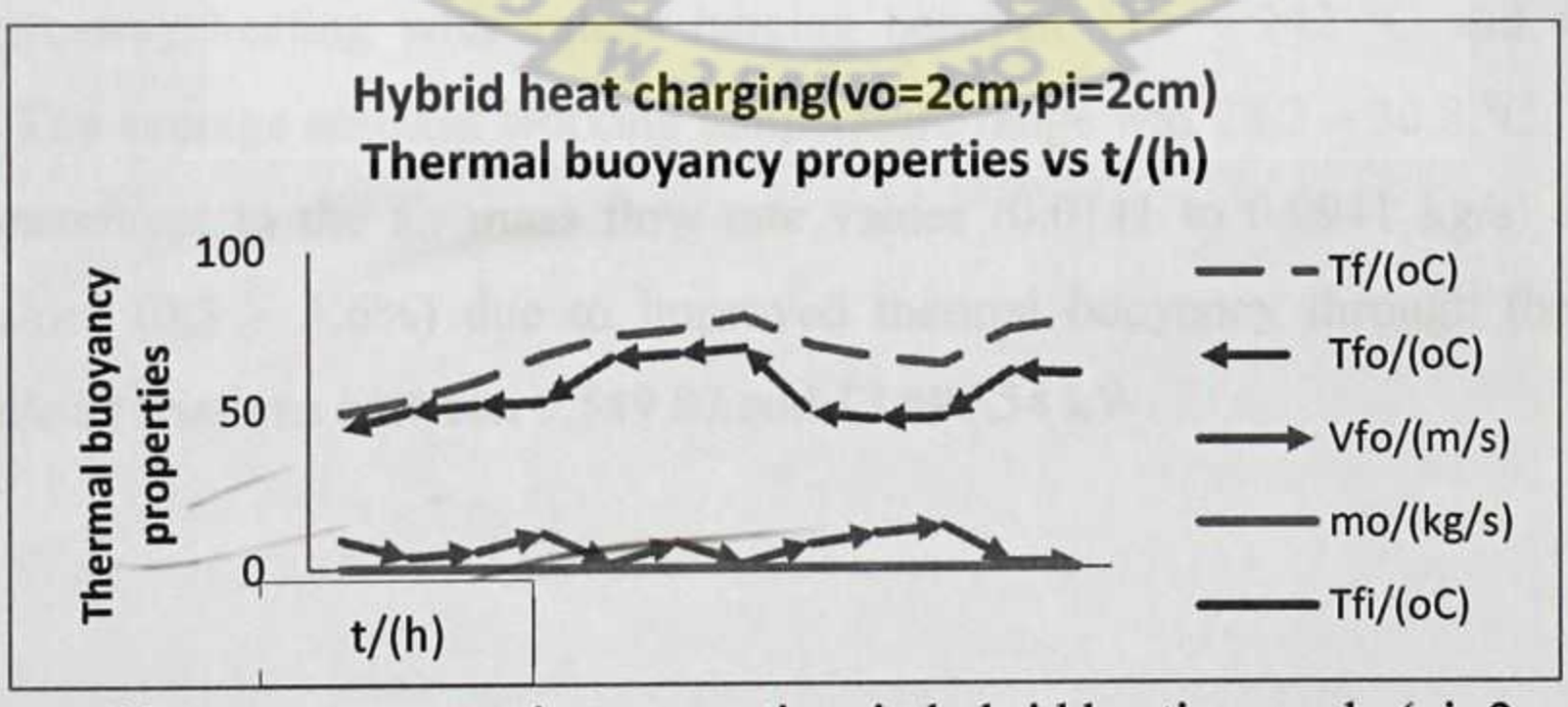

Figure 91 Thermal buoyancy properties versus time in hybrid heating mode (pi=2 cm, vo=2 cm)

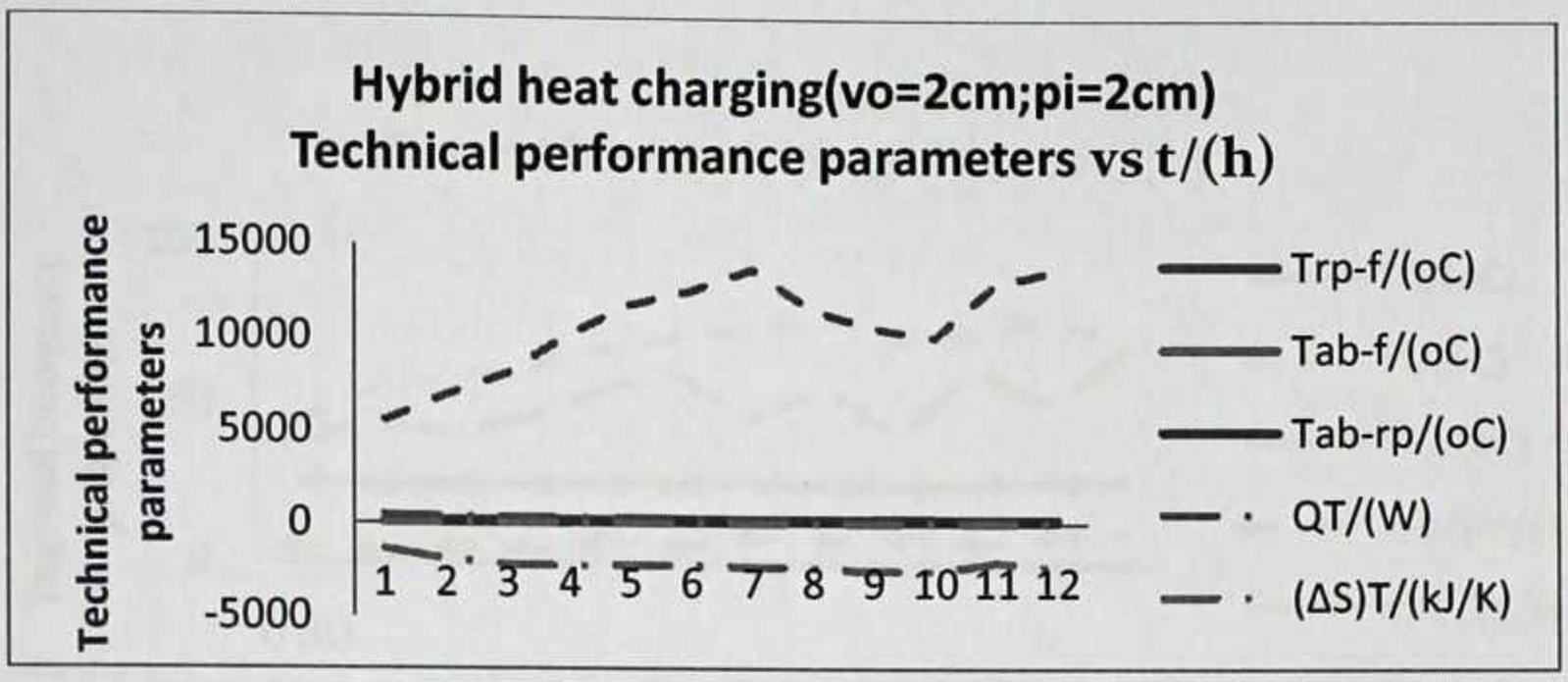

Figure 92 Technical performance parameters versus time in hybrid heating mode (pi=2 cm, vo=2 cm)

KNUST

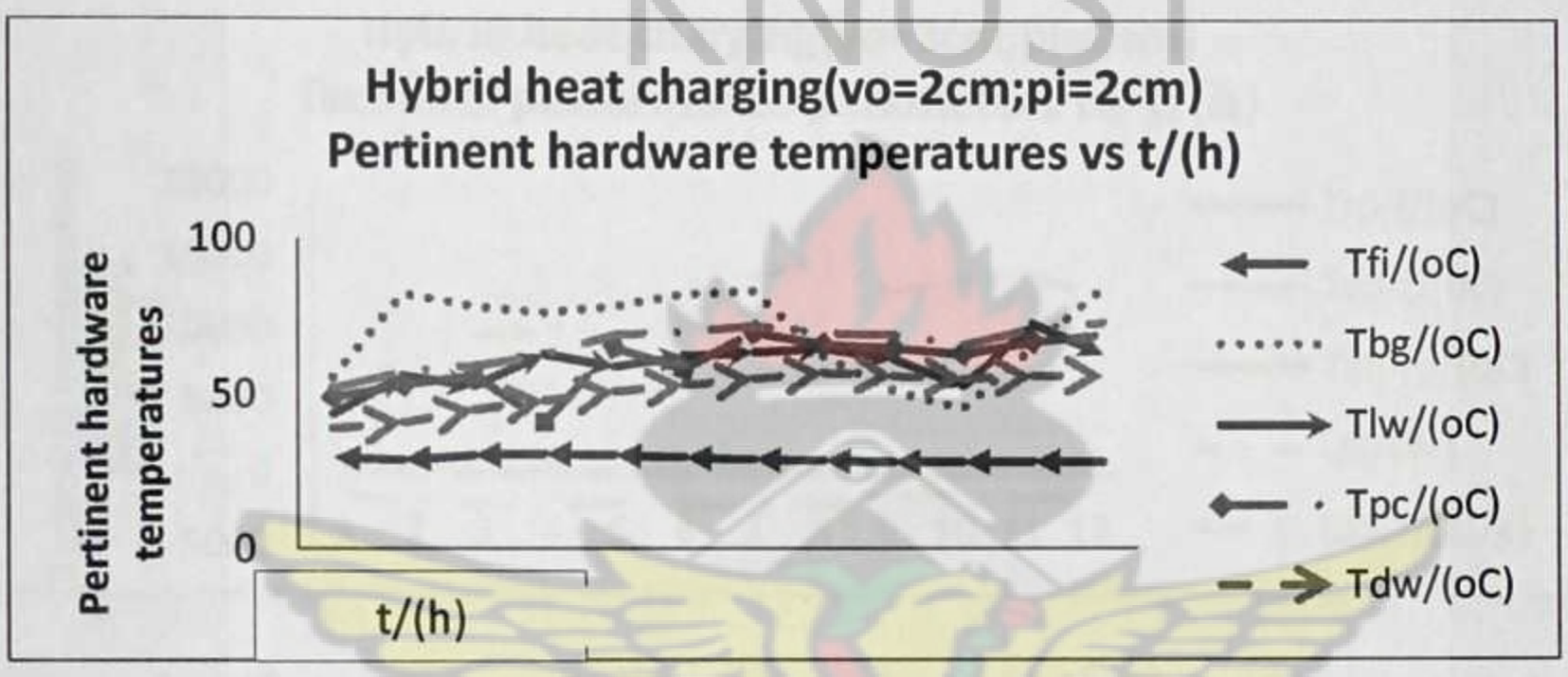

Figure 93 Pertinent hardware temperatures versus time in hybrid heating mode (pi=2 cm, vo=2 cm)

Figures 91, 92, and 93 show the hybrid heating mode characteristics of the dryer at a plenum inlet opening of 2 cm and a vent outlet opening of 2 cm. Noticeably, both the rock bed- burner interface and the absorber top surface temperature values have experienced increases in value due to the two-way heating with values ranging between 114 – 242 °C and 43 – 98.8 °C respectively. The average ambient working temperature range was 28.2 – 30.8 °C. There is also an obvious increment in the air mass flow rate values (0.0141 to 0.0941 kg/s) and air heater efficiency values (0.3 – 1.6%) due to improved thermal buoyancy through the dryer. Flow exergy exhibited variations between 5,549.87 and 13,697.54 kW.

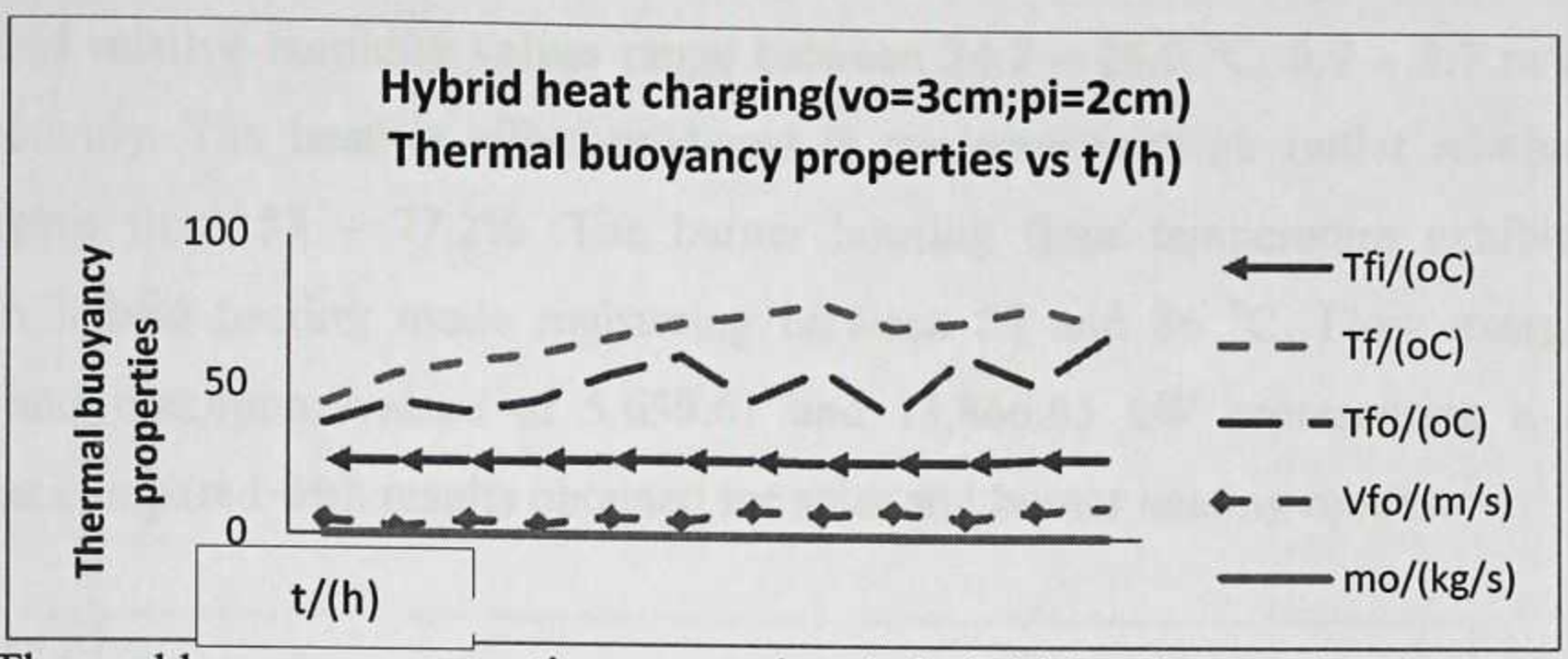

Figure 94 Thermal buoyancy properties versus time in hybrid heating mode (pi=2 cm, vo= 3 cm)

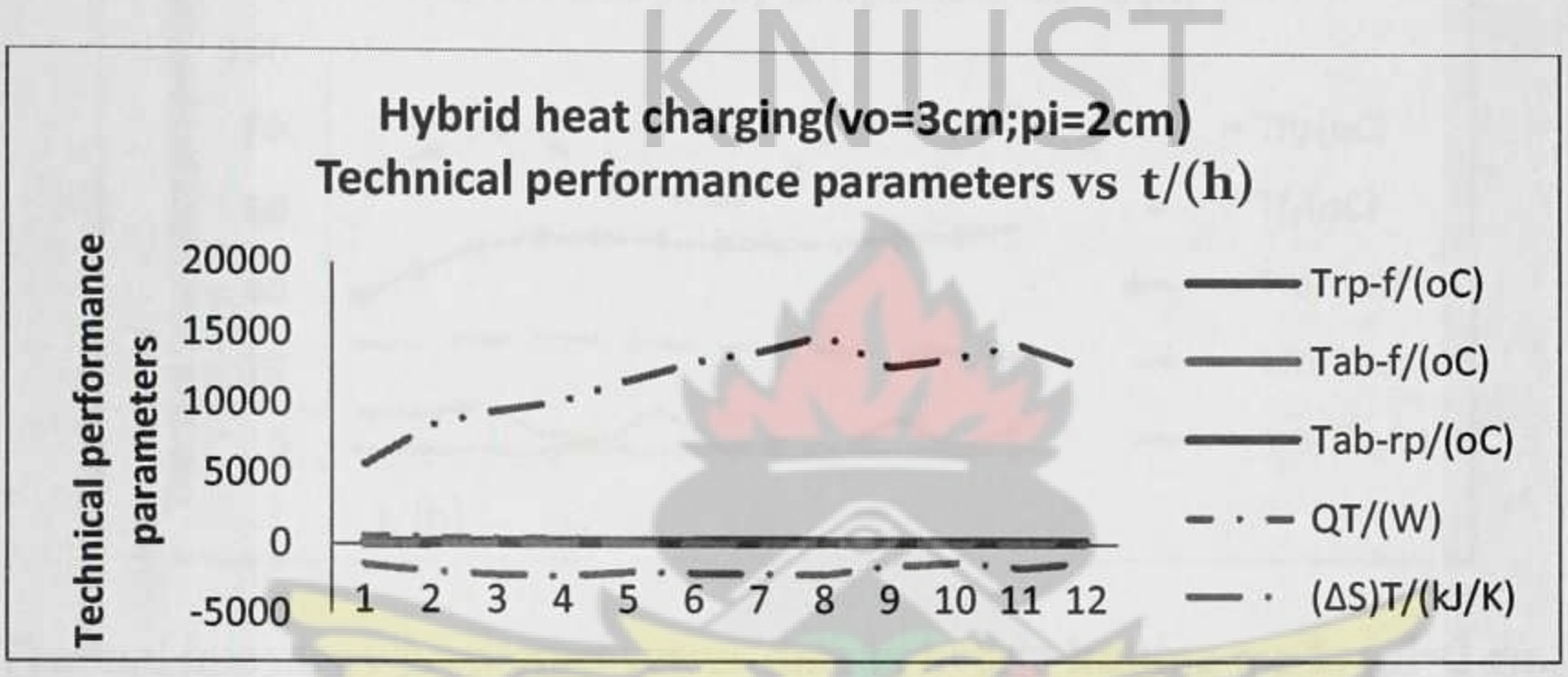

Figure 95 Technical performance parameters versus time in hybrid heating mode (pi=2 cm, vo=3 cm)

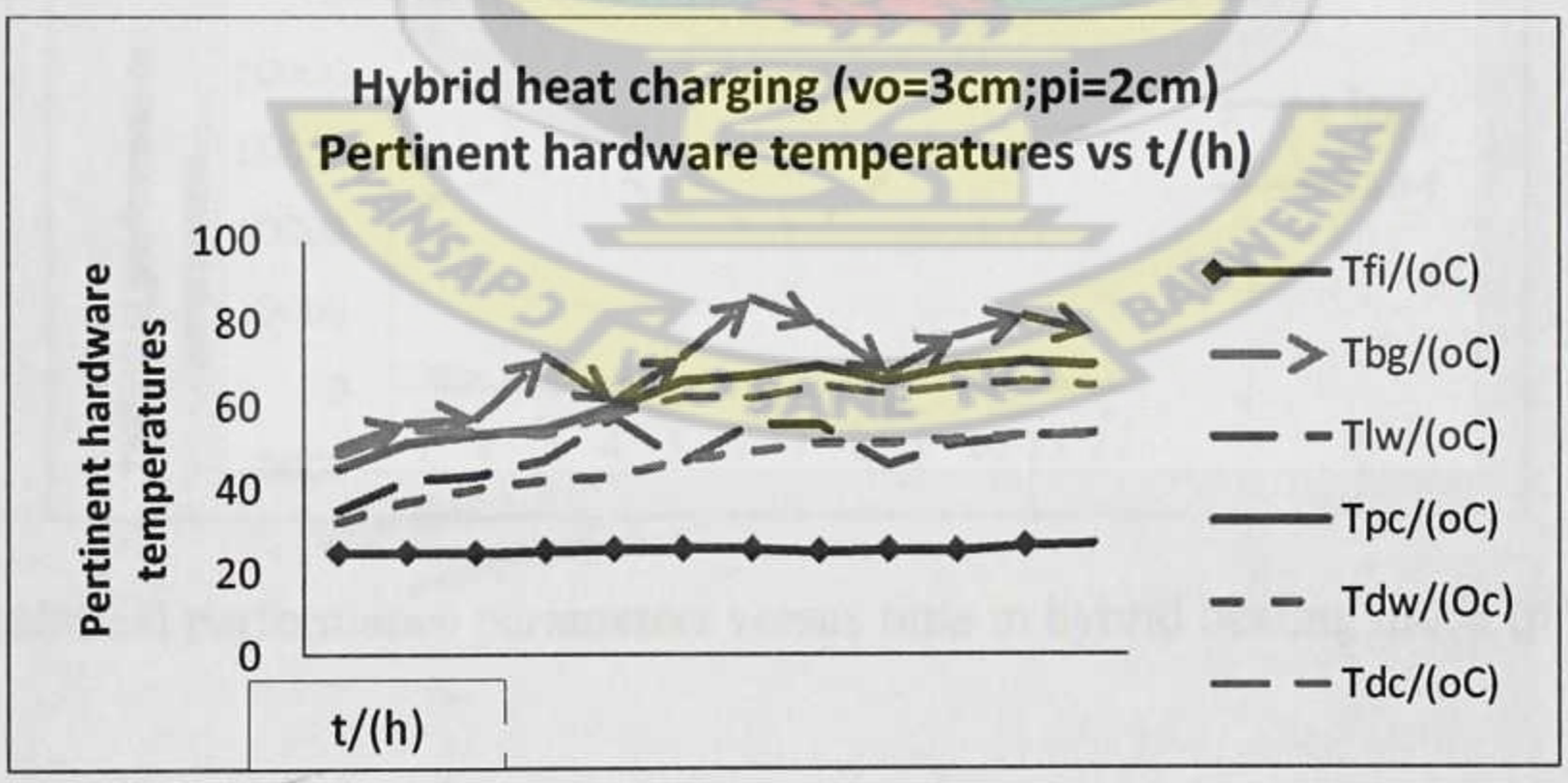

Figure 96 Pertinent hardware temperatures versus time in hybrid heating (pi=2 cm, vo=3 cm)

Figures 94, 95, and 96 show the characteristics of the dryer in hybrid heating mode at a plenum inlet opening of 2 cm and a vent outlet opening of 3 cm. The mean fluid inlet temperatures,

velocities and relative humidity values range between 24.7 – 26.9 °C, 0.7 – 2.7 m/s, and 76 – 88% respectively. The heating effect produced is moderate with air outlet relative humidity values ranging from 57 – 77.2%. The burner housing floor temperature exhibited a wide variation in hybrid heating mode registering between 50 and 86 °C. Flow exergy recorded minimum and maximum values of 5,639.61 and 14,866.05 kW representing a remarkable increment as compared with results obtained for solar and burner heating modes.

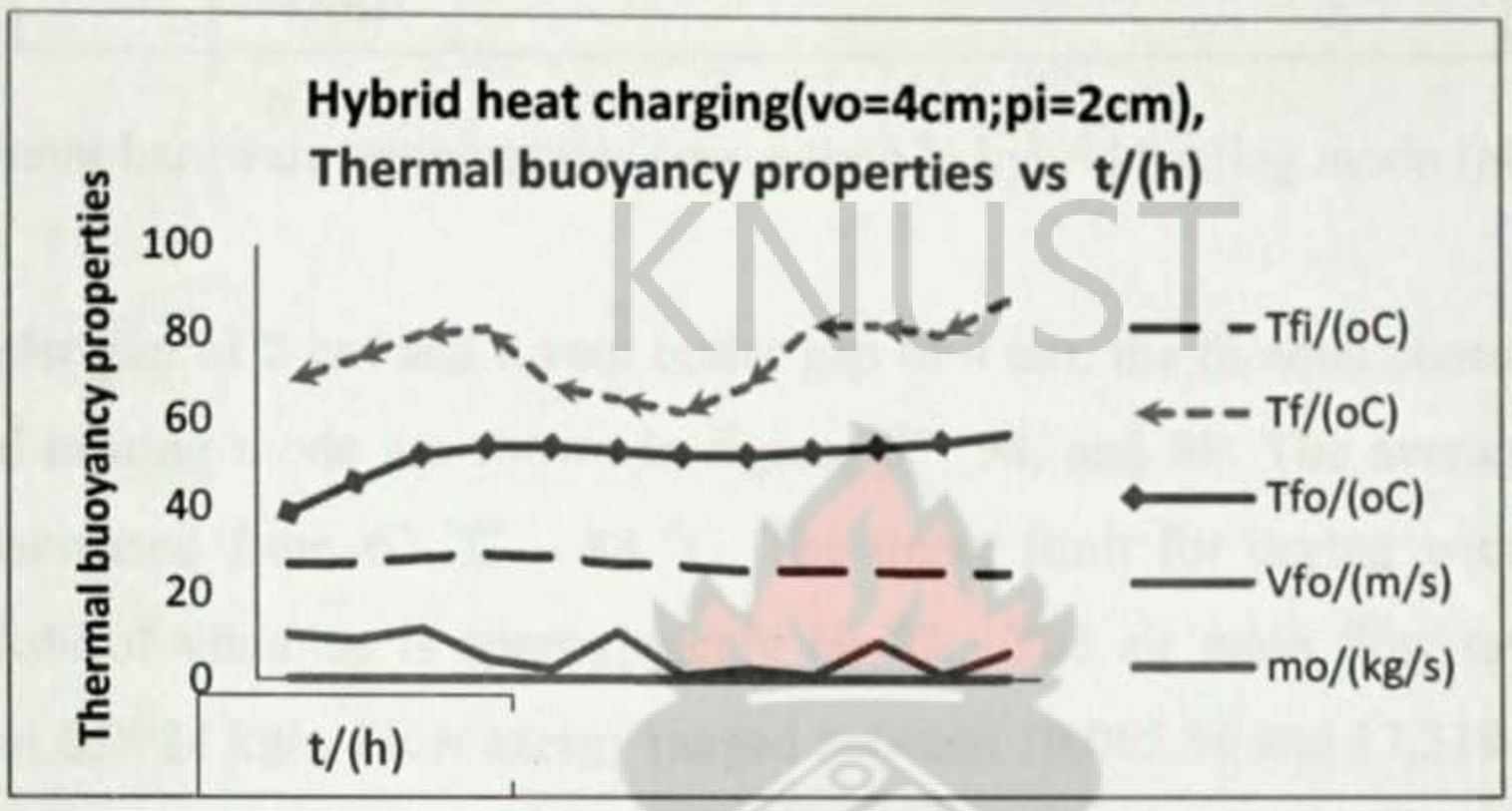

Figure 97 Thermal buoyancy properties versus time in hybrid heating mode (pi=2 cm, vo= 4 cm)

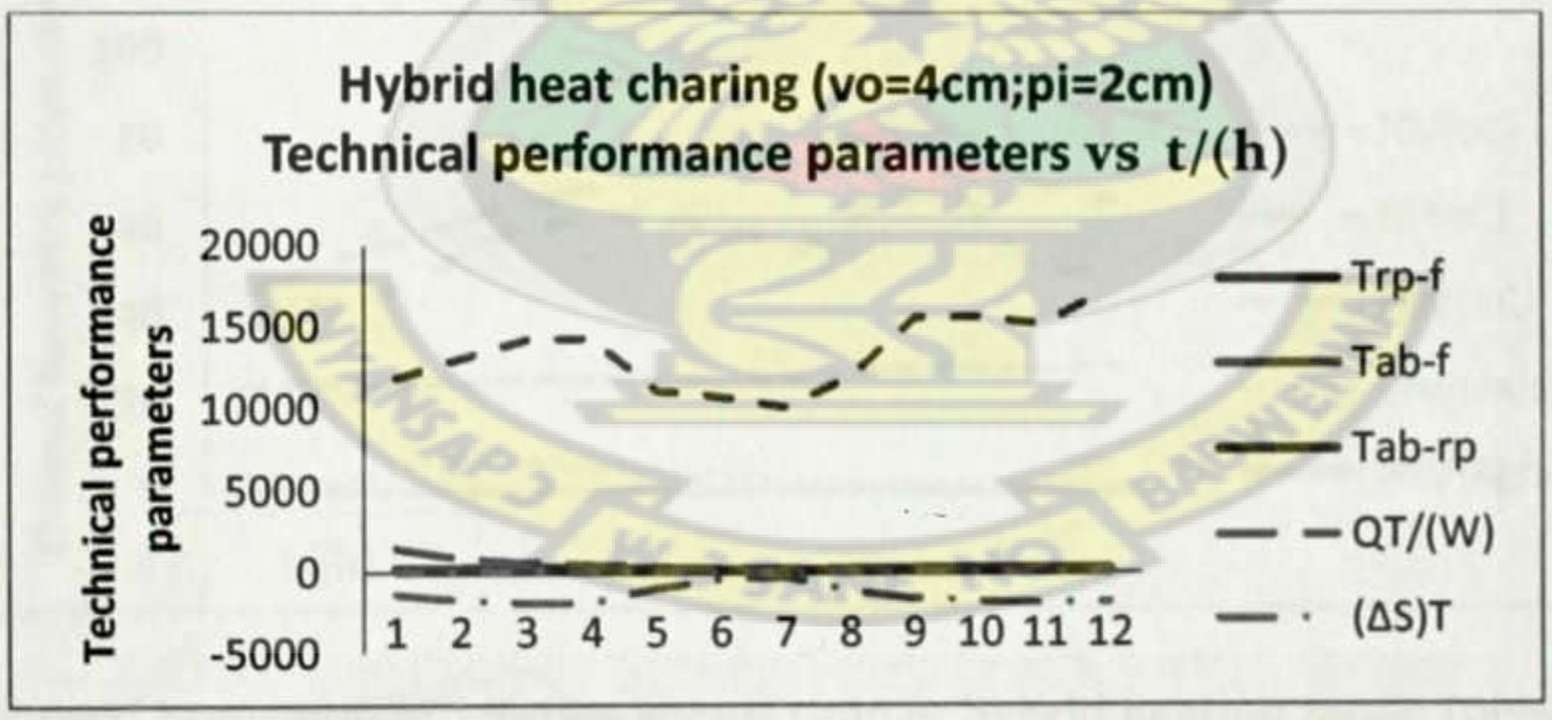

Figure 98 Technical performance parameters versus time in hybrid heating mode (pi=2 cm, vo=4 cm)

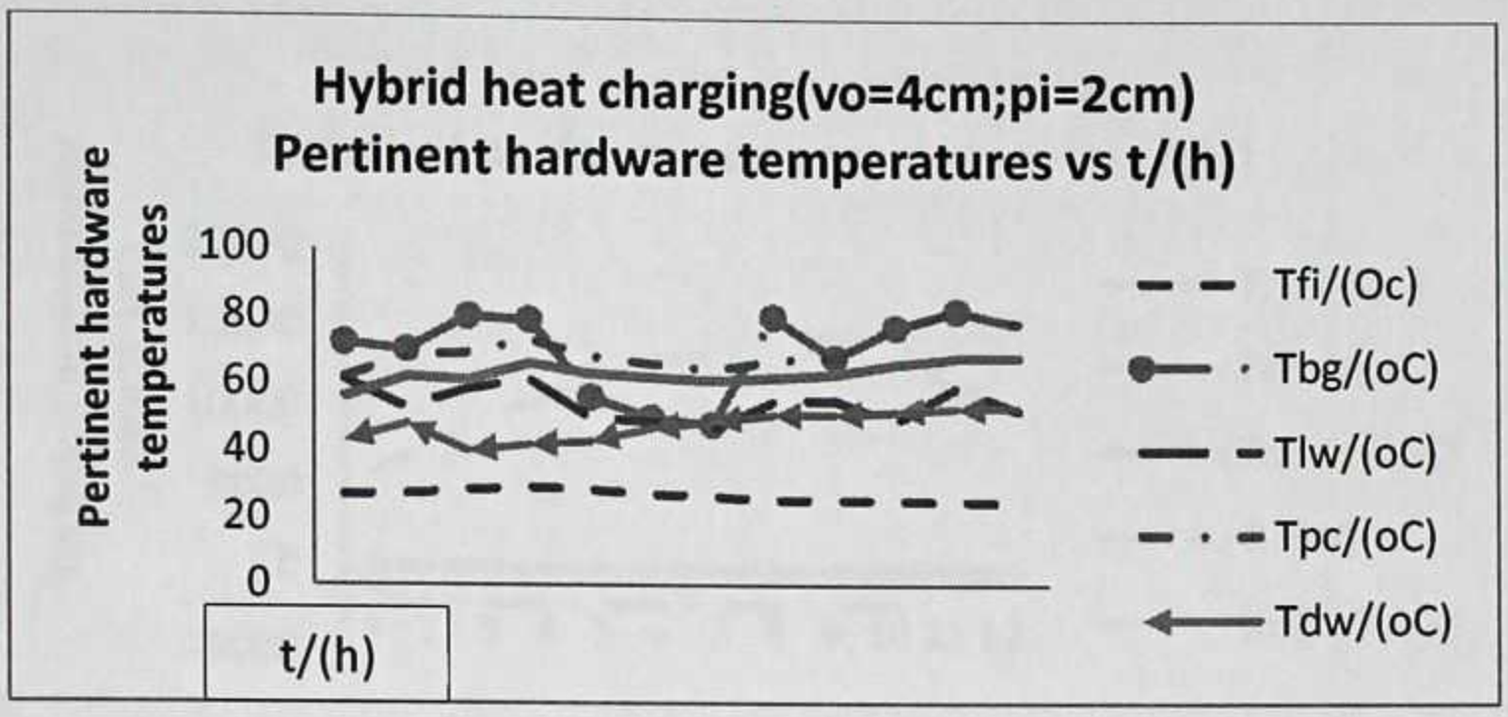

Figure 99 Pertinent hardware temperatures versus time in hybrid heating mode (pi=2 cm, vo=4 cm)

At a plenum inlet gap of 2 cm and a vent outlet gap of 4 cm, the thermal characteristics of the dryer in hybrid heating mode are shown in figures 97, 98, and 99. The average plenum fluid temperatures increased from 62 °C – 88 °C. The upper limit for drying without damage to products and loss of vitamins is approximately 80 °C. The air mass flow rates recorded an average value of 0.0984 kg/s. Flow exergy ranged between 10,065.56 and 17,319.27 kW.

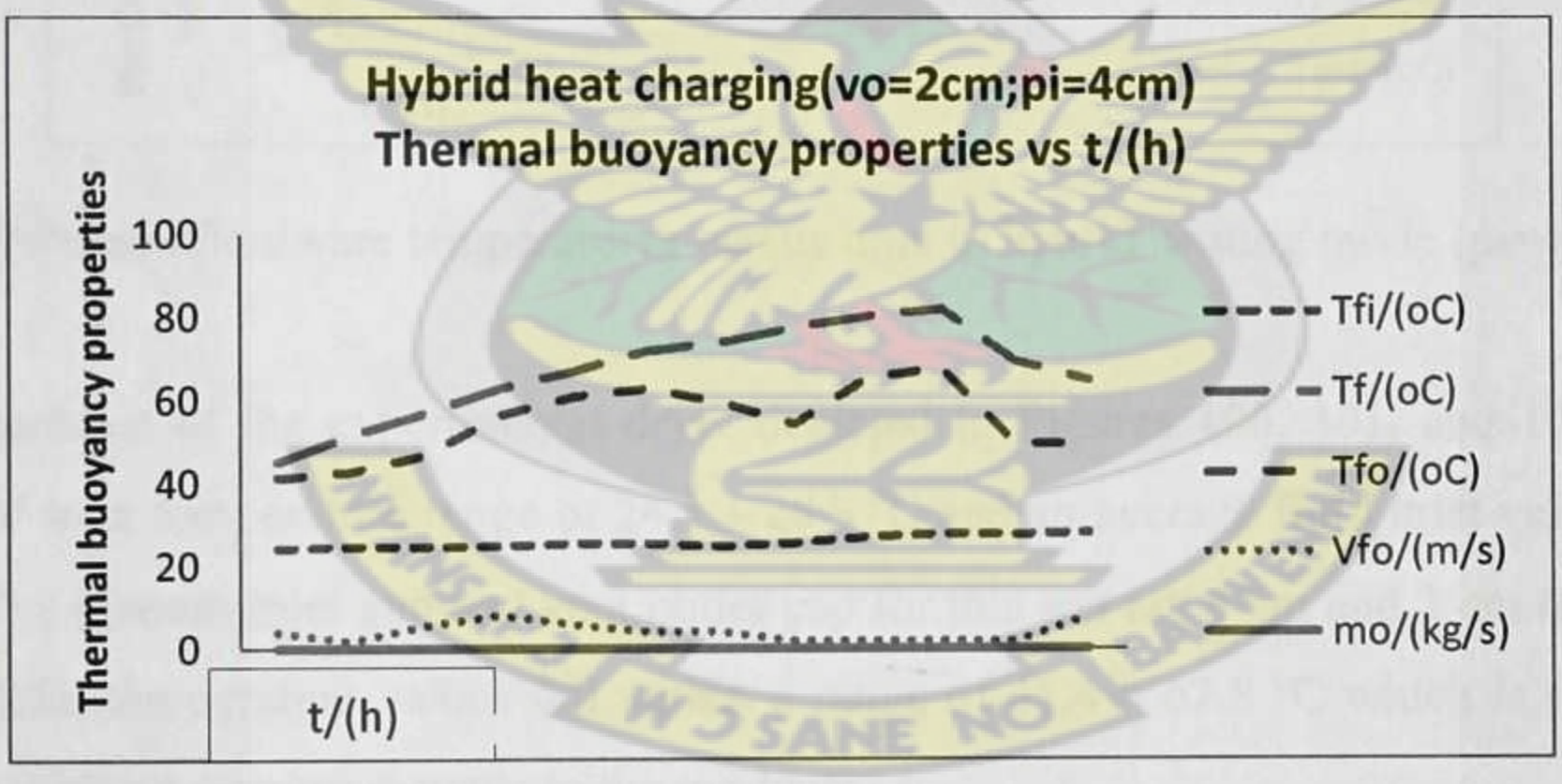

Figure 100 Thermal buoyancy properties versus time in hybrid heating mode (pi=4 cm, vo=2 cm)

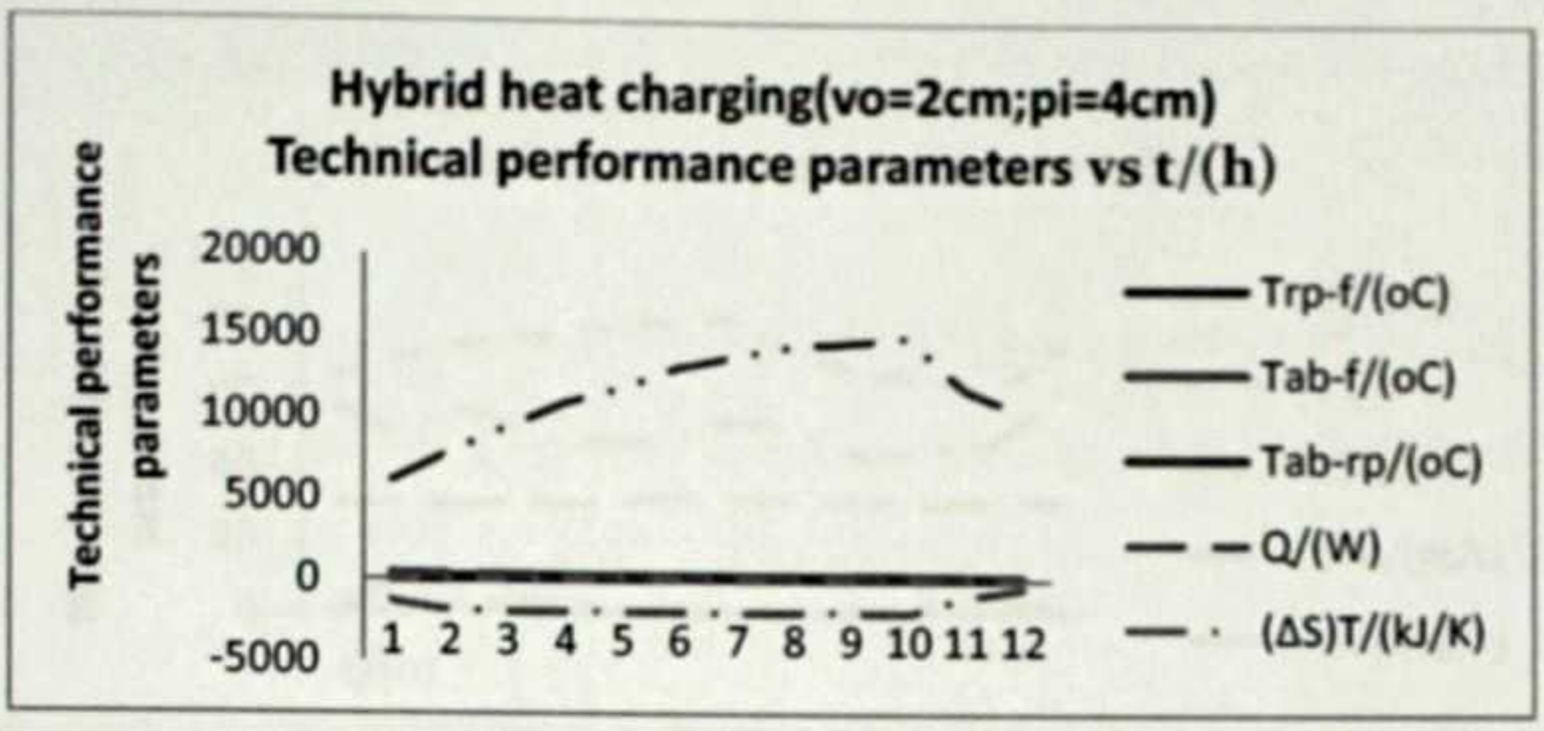

Figure 101 Technical performance parameters versus time in hybrid heating mode (pi=4 cm, vo=2 cm)

KNUST

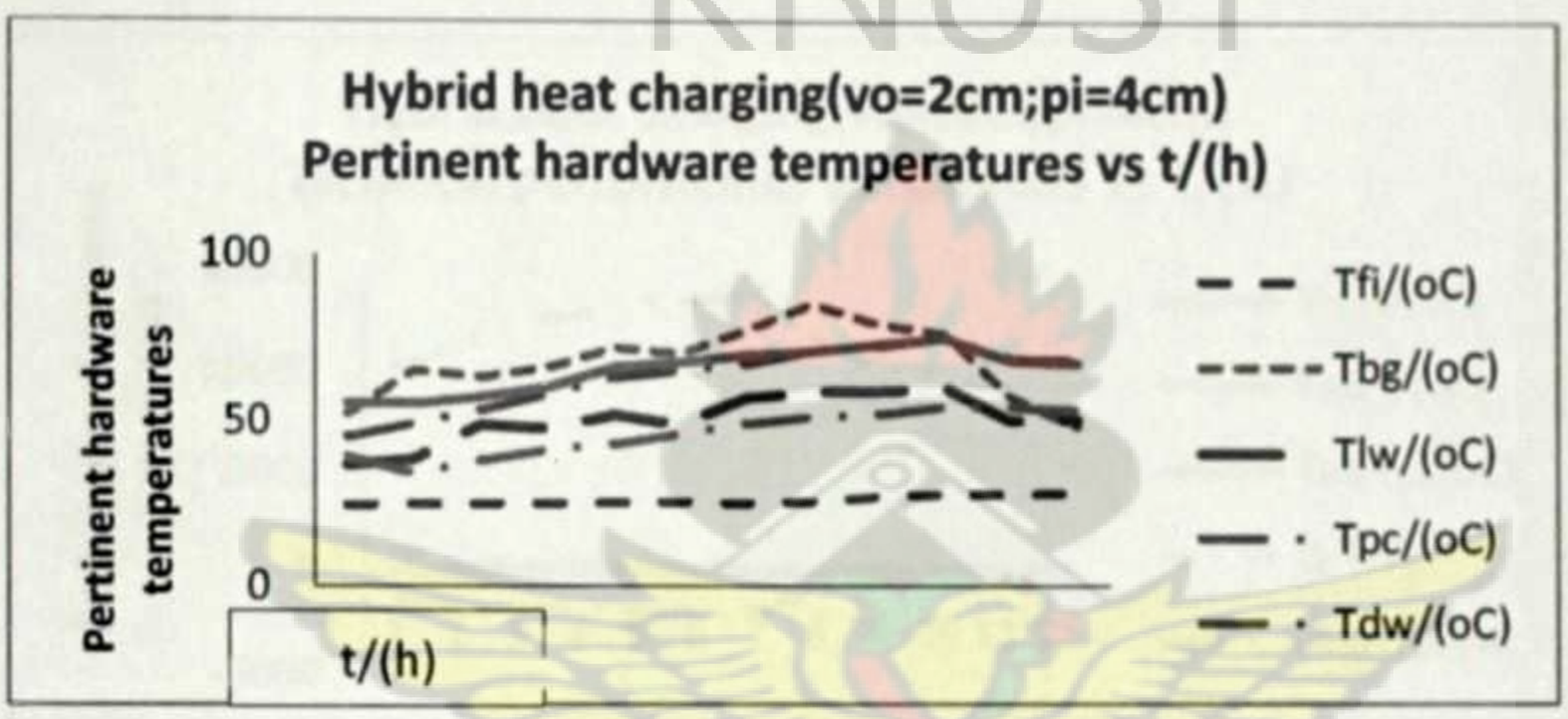

Figure 102 Pertinent hardware temperatures versus time in hybrid heating mode (pi=4 cm, vo=2 cm)

The characteristics of the experimental dryer depicted in Figures 100, 101, and 102 cover an average fluid inlet temperature range of 24.3 – 28.3 °C and an average fluid inlet velocity of 0.3 – 1.4 m/s. The plenum inlet gap and vent outlet gap for this test are 4 cm and 2 cm respectively. The fluid outlet temperature values fell within a range of 41.4 – 67.8 °C which is effective for dehydration without causing damage to the products.

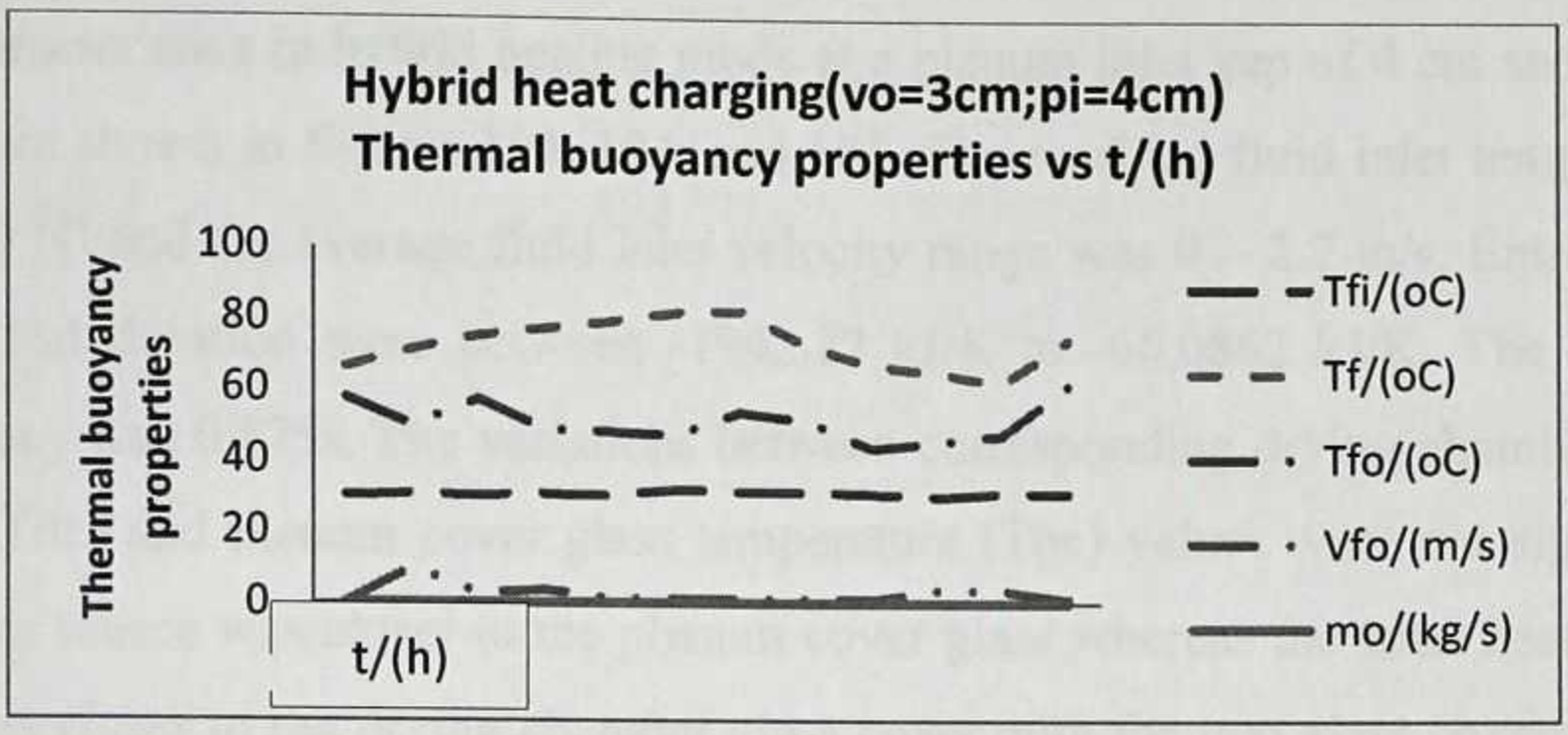

Figure 103 Thermal buoyancy properties versus time in hybrid heating mode (pi=4 cm, vo=3 cm)

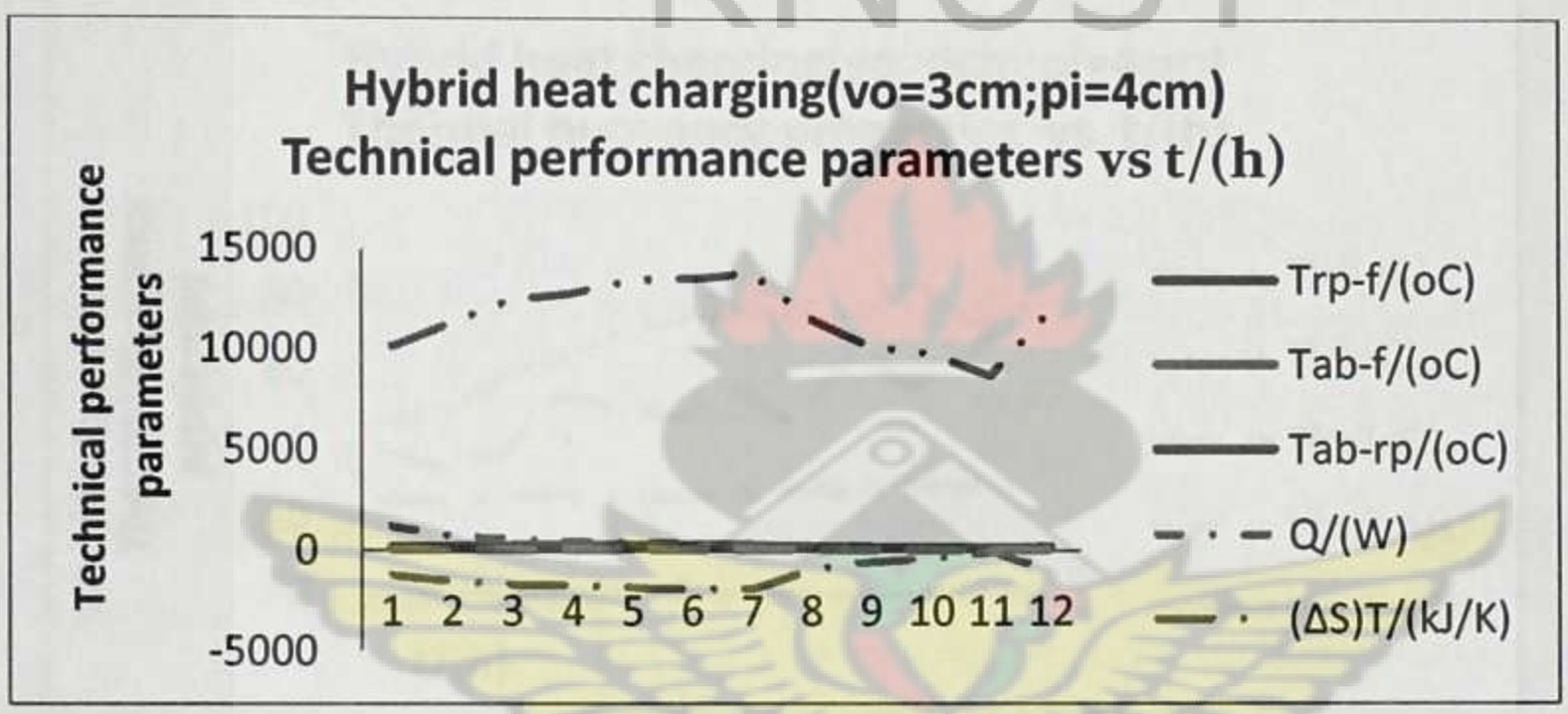

Figure 104 Technical performance parameters versus time in hybrid heating mode (pi= 4cm, vo=3 cm)

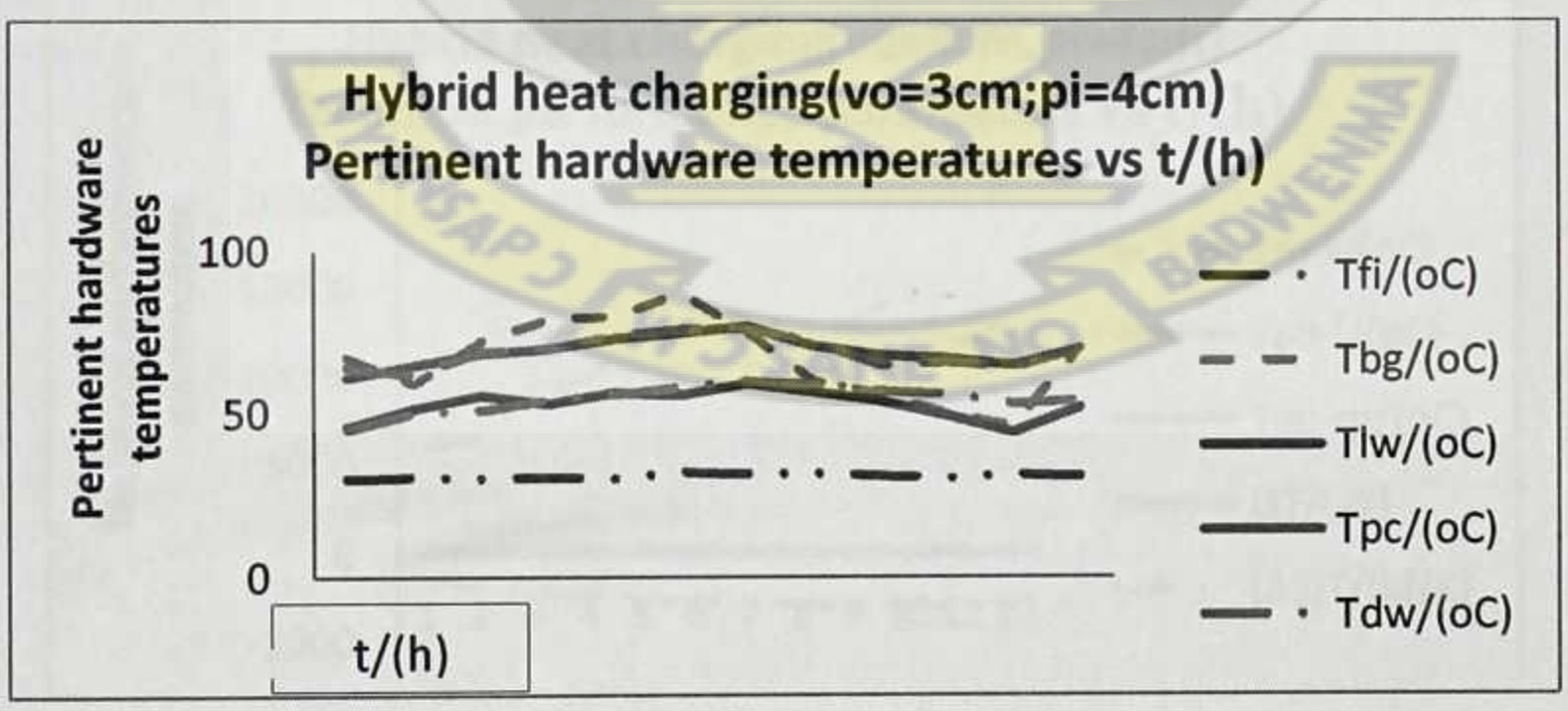

Figure 105 Pertinent hardware temperatures versus time in hybrid heating mode (pi=4 cm, vo=3 cm)

LIBRARY
KWAME NKRUMAH
UNIVERSITY OF SCIENCE & TECHNOLOGY
KUMASI

The dryer characteristics in hybrid heating mode at a plenum inlet gap of 4 cm and a vent outlet gap of 3 cm are shown in figures 103, 104, and 105. The working fluid inlet temperature range was 30 – 31.9 °C and the average fluid inlet velocity range was 0 – 2.7 m/s. Entropy decreases covering the test duration were between -1942.27 kJ/K to -66.0862 kJ/K. The maximum air heater efficiency was 0.87%. The variations between corresponding drying chamber glass cover temperature (Tdc) and plenum cover glass temperature (Tpc) values were not significant since the burner heat source was closer to the plenum cover glass whereas the solar heat source (infra red lamps) was closer to the drying chamber glass cover with the two glass covers experiencing nearly the same amount of heating.

KNUST

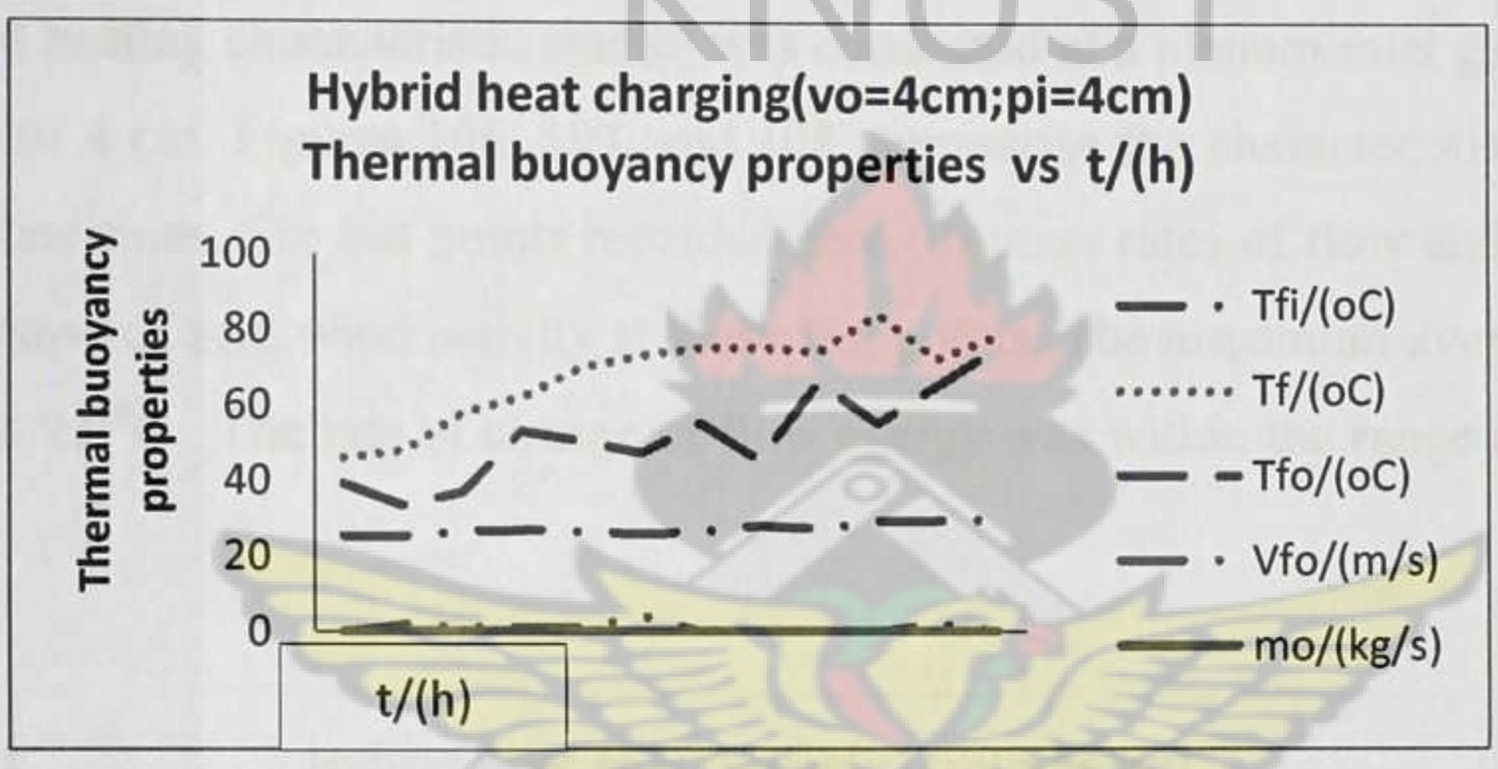

Figure 106 Thermal buoyancy properties versus time in hybrid heating mode

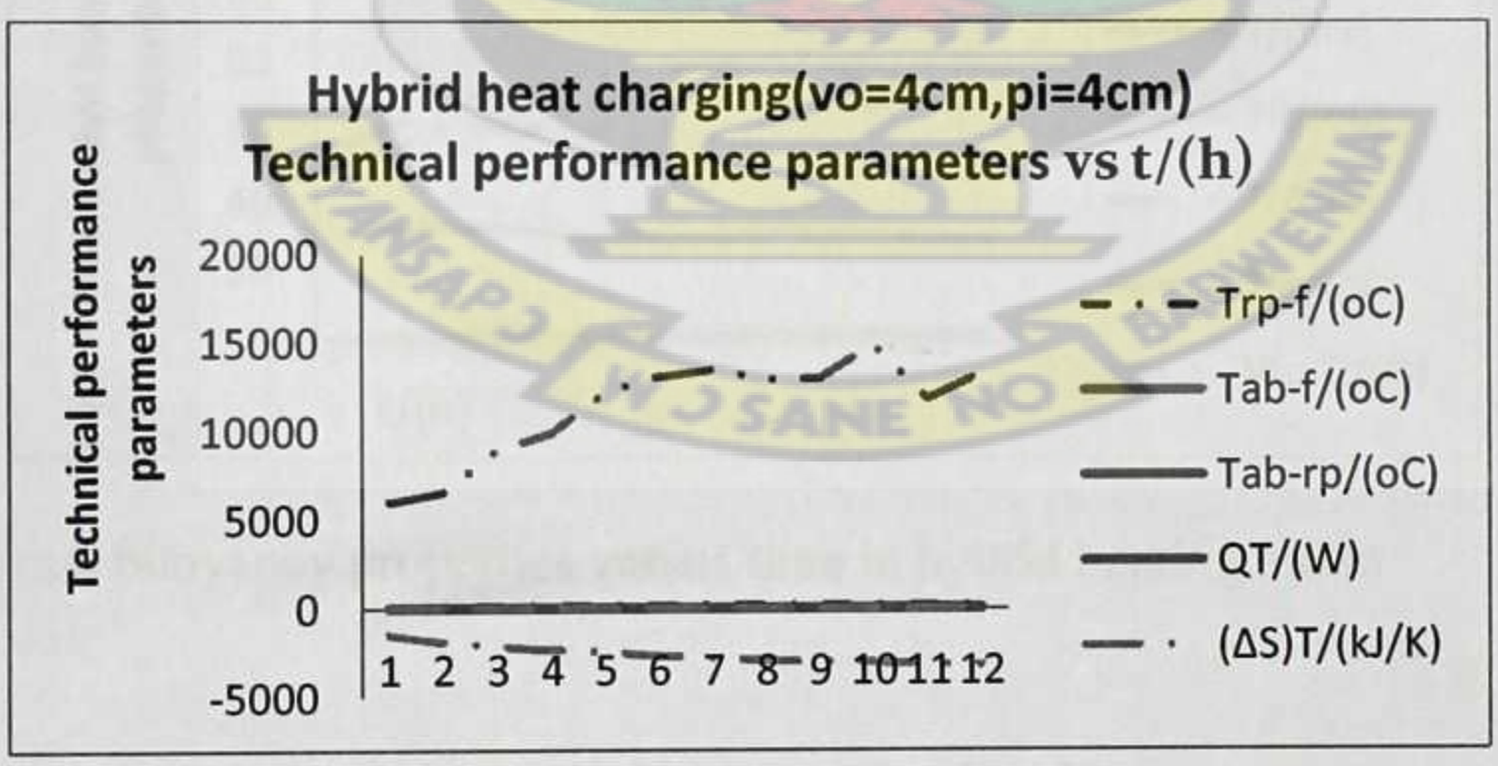

Figure 107 Technical performance parameters versus time in hybrid heating mode (pi=4 cm, vo=4 cm)

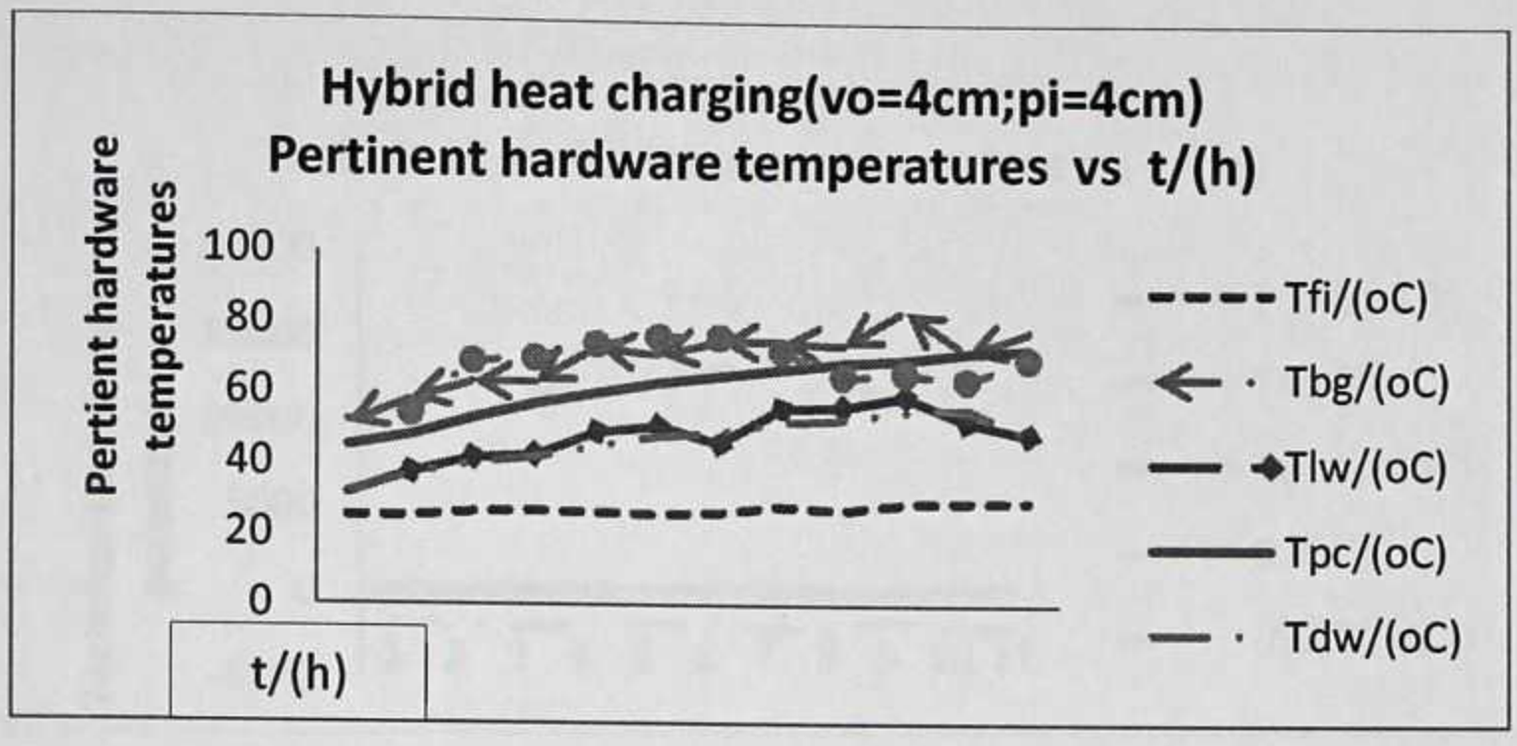

Figure 108 Pertinent hardware temperatures versus time in hybrid heating mode

The sixth hybrid heating characteristic studies was conducted at a plenum inlet gap of 4cm and a vent outlet gap of 4 cm. Figures 106, 107, and 108 summarise the characteristic studies results for this set of conditions. Six test points recorded zero (0) mass rates of flow and zero air heater efficiencies because of zero wind activity at those test points. The maximum average fluid outlet temperature was 75 °C. The rate of change of flow exergy was within the range of 6,040.86 and 13,475.97 kW.

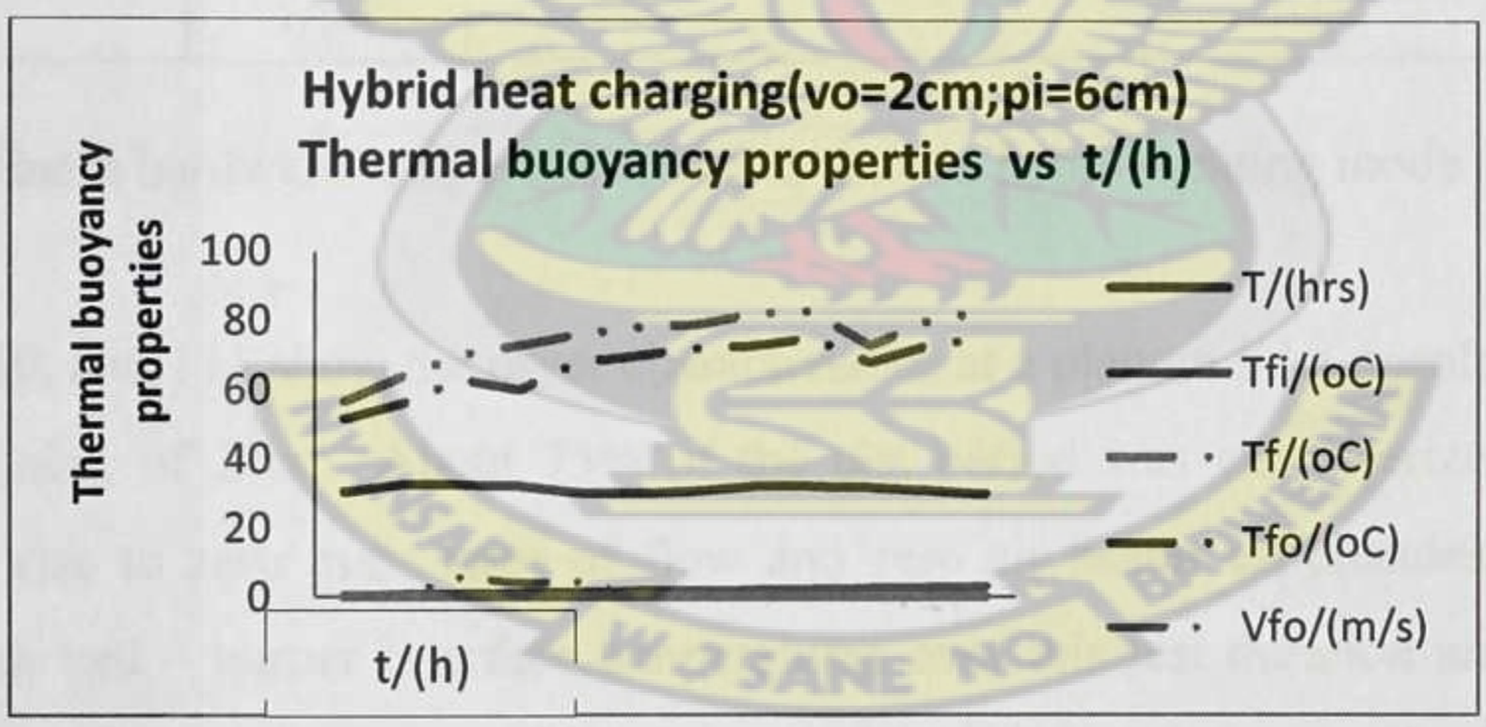

Figure 109 Thermal buoyancy properties versus time in hybrid heating mode

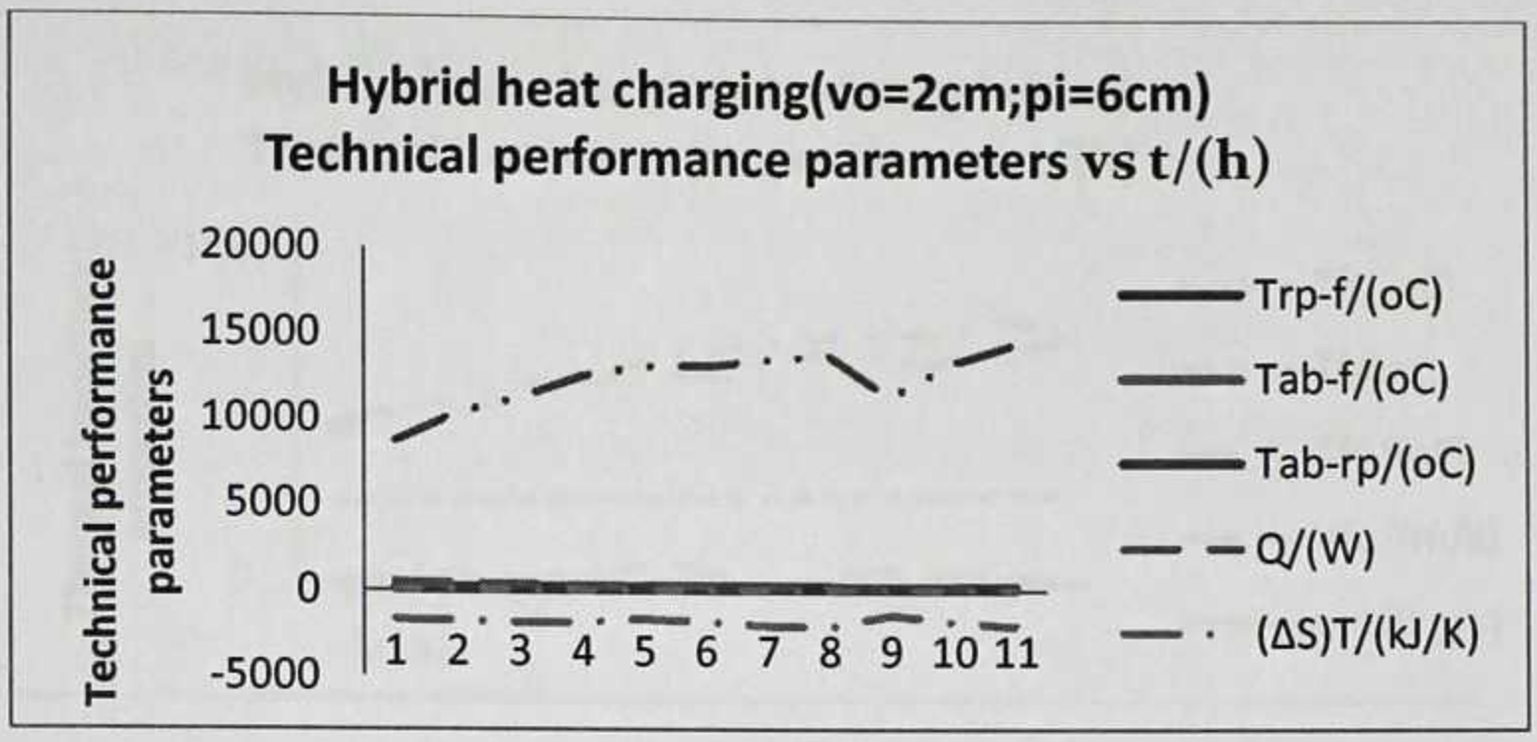

Figure 110 Technical performance parameters versus time in hybrid heating mode (pi=6 cm, vo=2 cm)

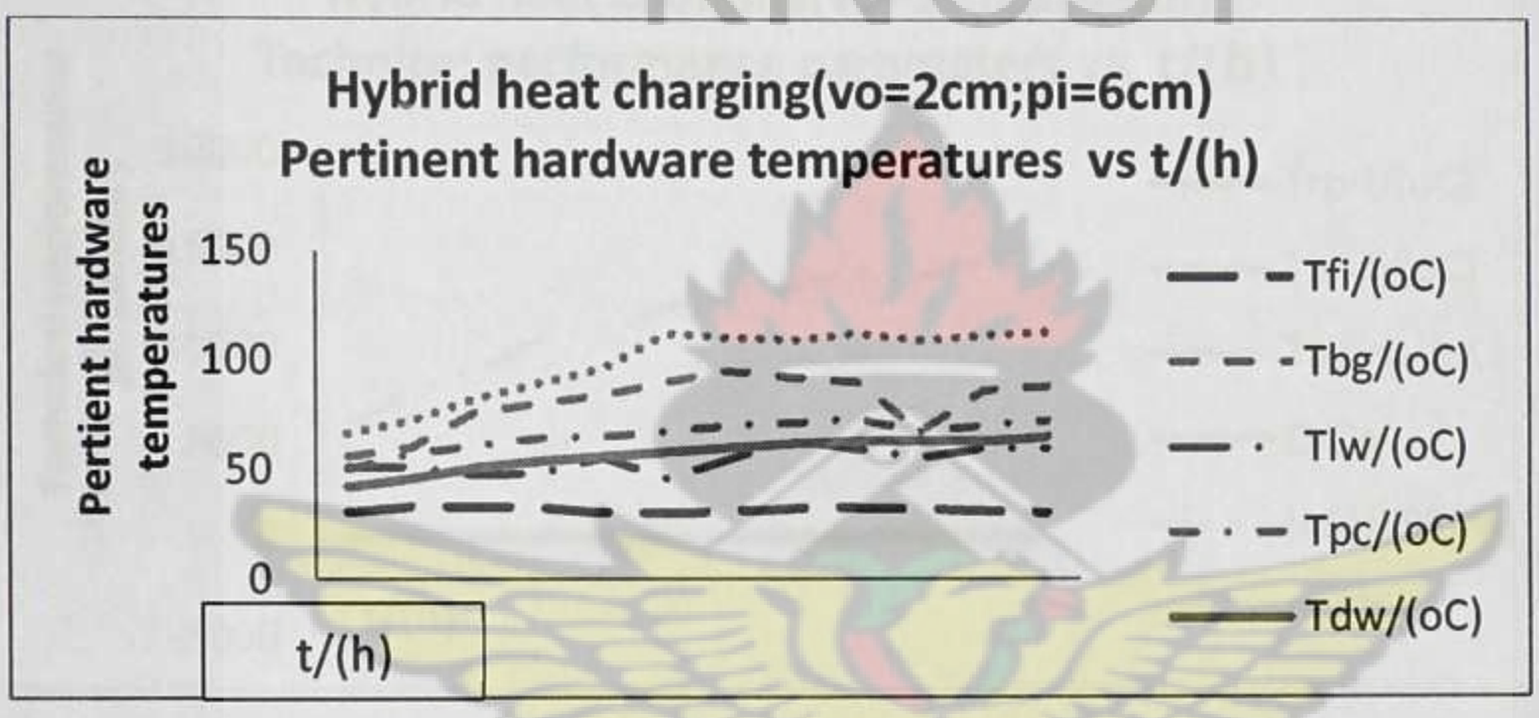

Figure 111 Pertinent hardware temperatures versus time in hybrid heating mode (pi=6 cm, vo=2 cm)

Figures 109, 110, and 111 show the dryer characteristics at a plenum inlet opening of 6 cm and a vent outlet opening of 2 cm. About 75% of the test period was characterized by zero wind activity giving rise to zero mass rates of flow and zero air heater efficiencies at ten (10) test points. The rock bed – burner interface temperatures over this test duration are relatively high compared with other tests because of the low wind activity, and, hence, the low rate of heat absorption from the concrete absorber surface. The outlet relative humidity values showed a reasonable extent of heating with the lowest relative humidity value being 32.6%.

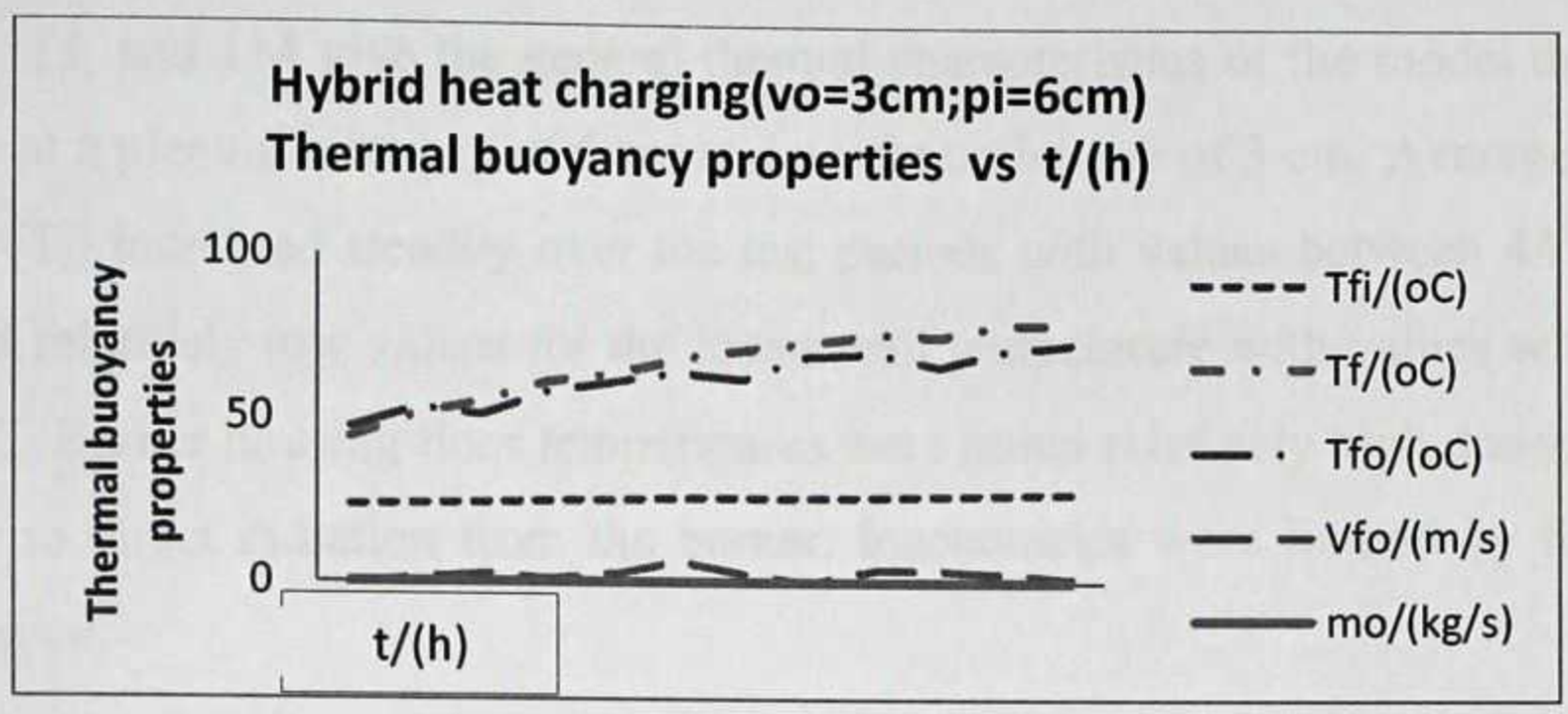

Figure112 Thermal buoyancy properties versus time in hybrid heating mode (pi=6 cm, vo=3 cm)

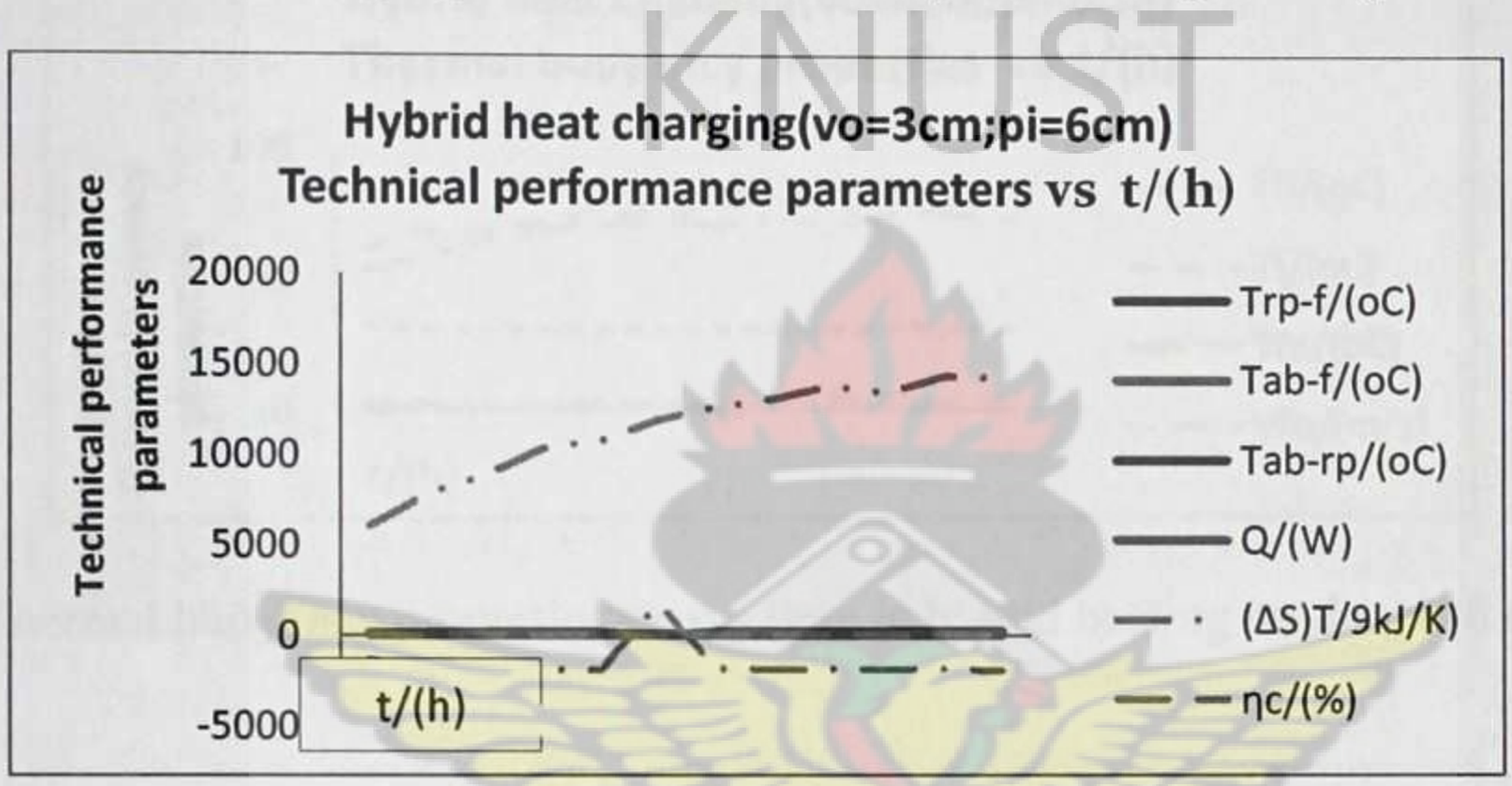

Figure 113 Technical performance parameters versus time in hybrid heating mode (pi=6 cm, vo=3 cm)

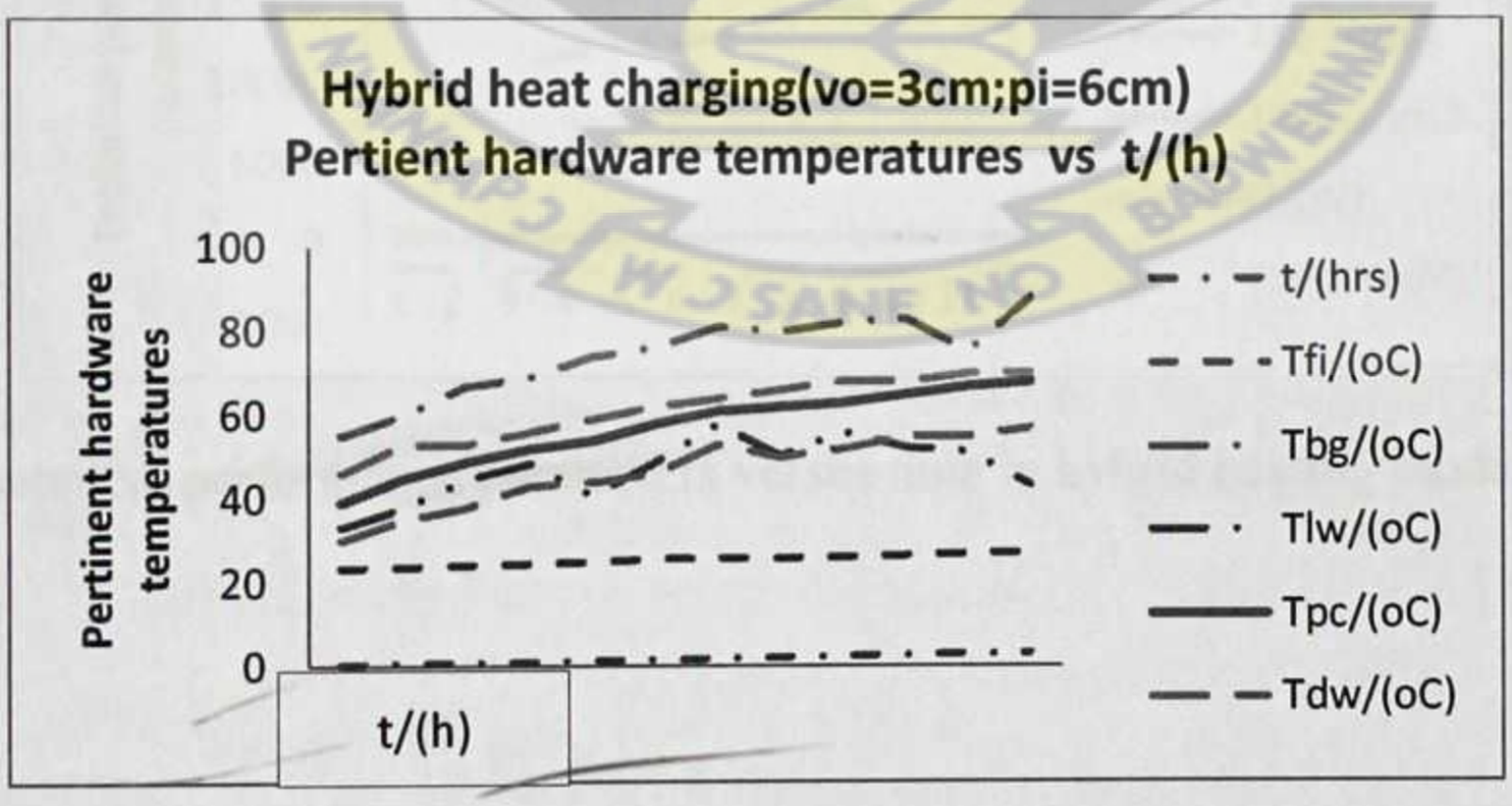

Figure 114 Pertinent hardware temperatures versus time in hybrid heating mode (pi=6 cm, vo=3

Figures 112, 113, and 114 give the general thermal characteristics of the model dryer in hybrid heating mode at a plenum inlet gap of 6 cm and a vent outlet gap of 3 cm. Average plenum fluid temperatures (T_f) increased steadily over the test periods with values between 44 – 79 °C. The test registered relatively low values for the lower wall temperature with values within the range 33.1 – 57.8 °C. Burner housing floor temperatures were rather relatively high due to the exposure of the sensor to direct radiation from the burner. Inaccuracies were limited by folding tin foil around the sensor.

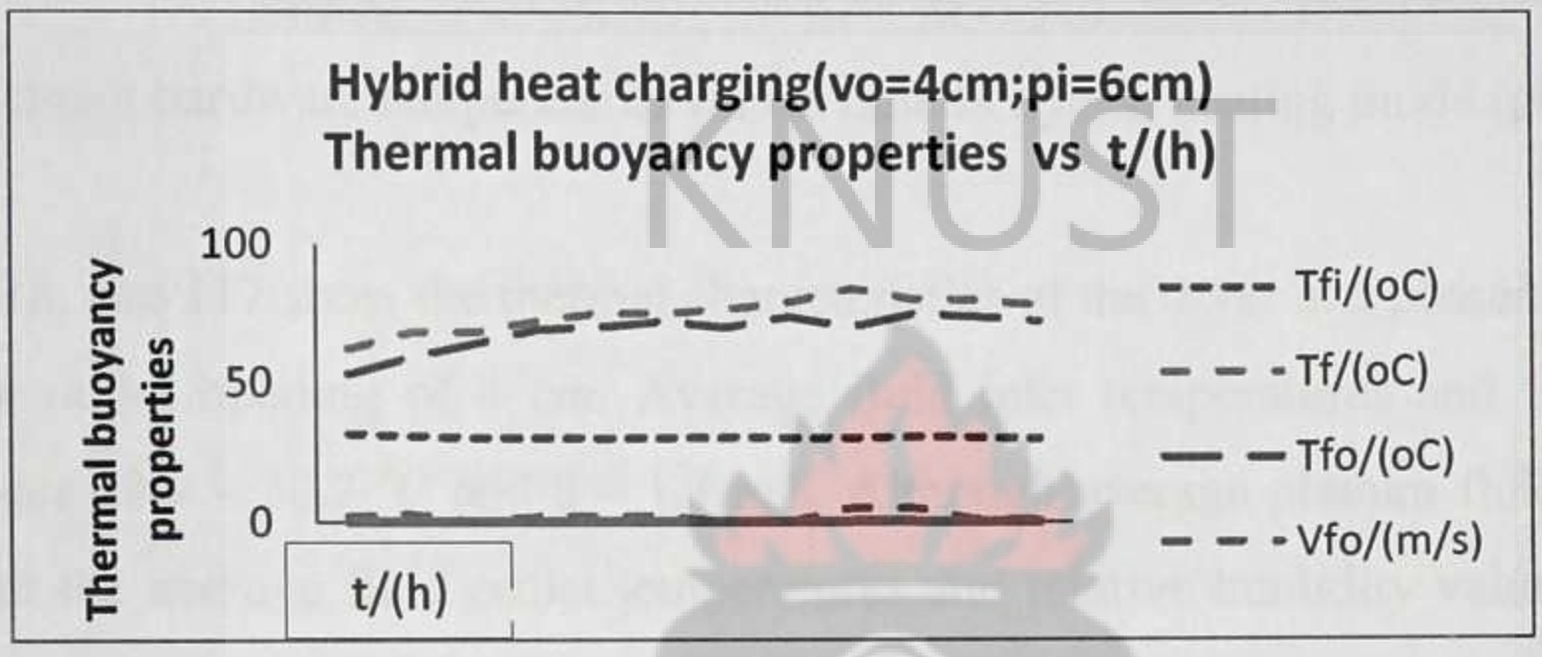

Figure 115 Thermal buoyancy properties versus time in hybrid heating mode (pi=6 cm, vo=4 cm)

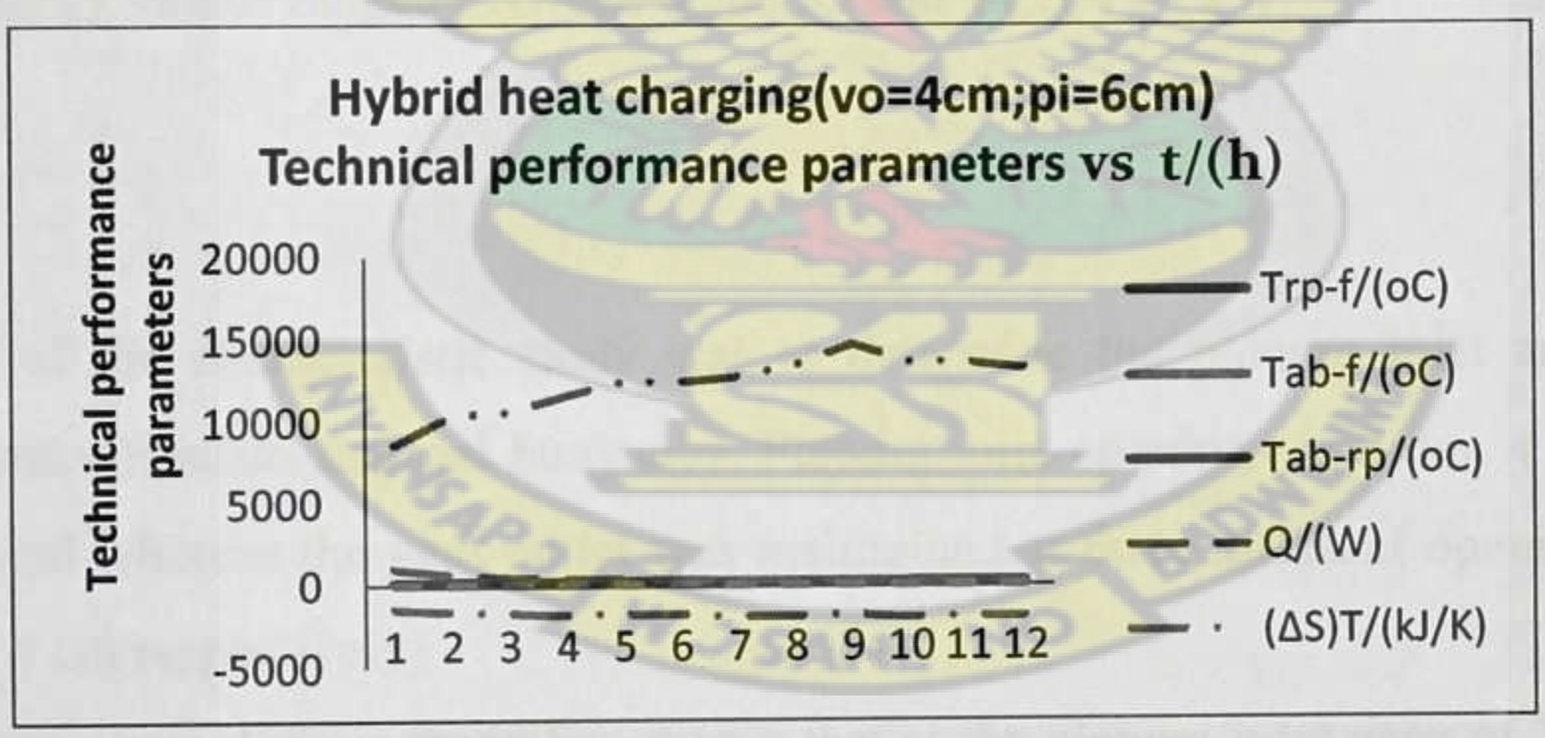

Figure 116 Technical performance parameters versus time in hybrid heating mode (pi=6 cm, vo=4 cm)

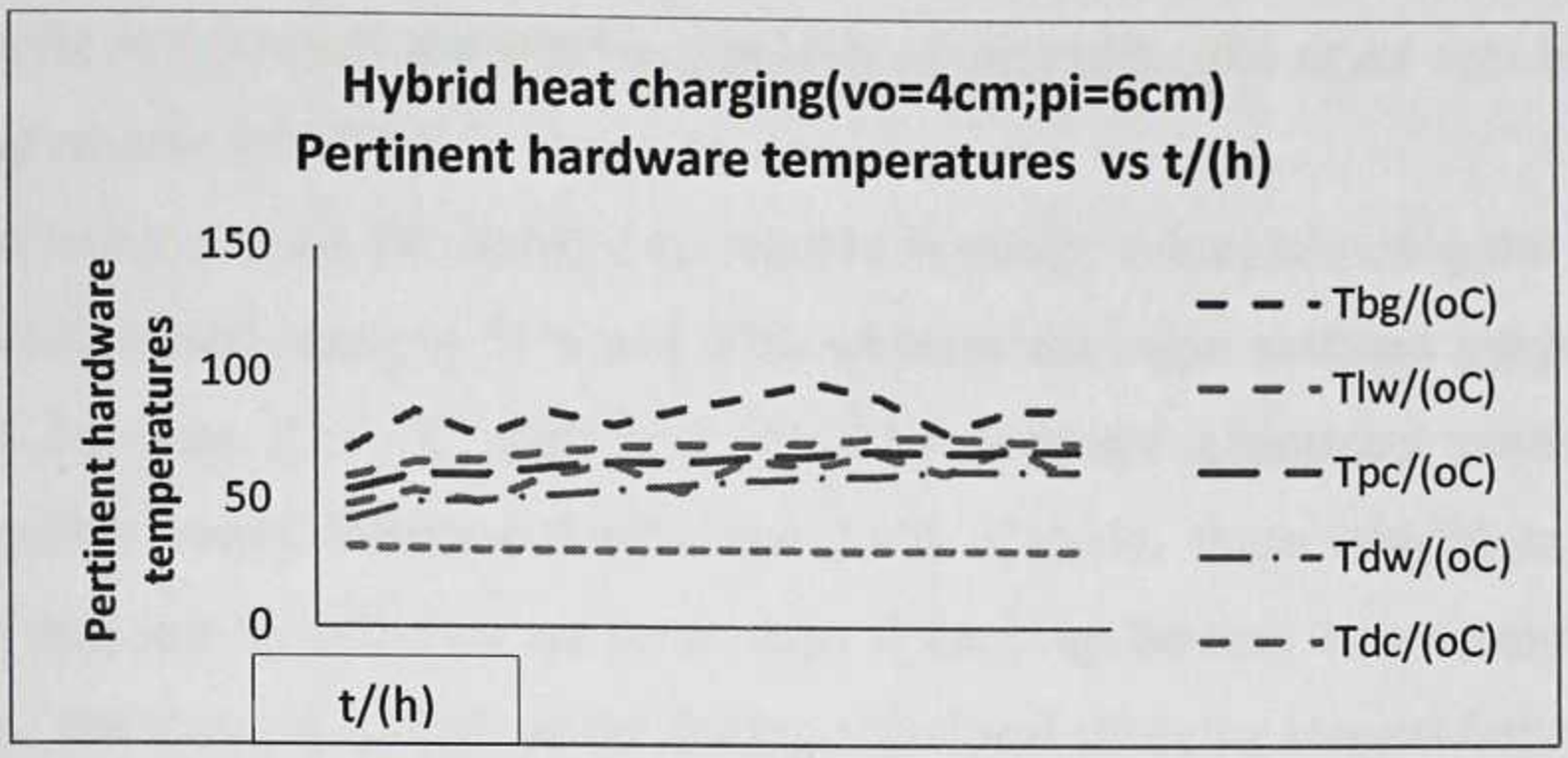

Figure 117 Pertinent hardware temperatures versus time in hybrid heating mode (pi=6 cm, vo=4 cm)

Figures 115, 116, and 117 show the thermal characteristics of the dryer at a plenum inlet gap of 6 cm and a vent outlet opening of 4 cm. Average fluid inlet temperatures and velocities were within the ranges 29.9 – 30.7 °C and 0 – 1.7 m/s. Although average plenum fluid temperatures were quite high the average fluid outlet temperatures and relative humidity values were within reasonable ranges (53 – 75 °C, and 45.9 – 52.5% respectively). Burner housing floor temperature values were comparatively high in hybrid heating mode due to the double heating effect. Flow exergy values ranged between 8,583.55 and 14,704.54 kW

Comments:

The objective of the characteristic study was to determine the plenum inlet and vent outlet combination that optimises thermal buoyancy. Plenum inlet openings of 2 cm, 4 cm, and 6 cm were investigated whereas the vent outlet was maintained at three different openings namely, 2 cm, 3 cm, and 4 cm respectively.

1. The dryer characteristic study has shown that at the plenum inlet gaps of 2 cm and 4 cm and vent openings of 2 cm, and 3 cm, in each of the three heating modes, air flow rate through the dryer was extremely low, temperatures in system components become high giving rise to relatively high plenum outlet temperatures (which can burn the product), low air heater efficiency (because of extremely low air flow rates). It was also noticed under these conditions that the relative humidity of the air exiting the vent did not follow any particular pattern due to observed irregularities in the outlet air relative humidity

values. At some points the relative humidity of air exiting the dryer was higher than the air inlet relative humidity

2. In solar heating mode the ambient air relative humidity values covering the 9 experiments conducted varied between 51% and 95% whereas the mean ambient temperature values ranged between 22.7 °C and 32.2 °C. The collector efficiency covering the nine experiments varied between 0.01% and 3.6%. Clearly, these conditions indicate that drying will not be effective on some days if back up heating is not employed. This is because the thermal energy stored during solar heat charging ranged between 0.029 MJ and 0.251 MJ and this range of values is inadequate to sustain night drying
3. During burner heat charging the average air outlet relative humidity values covering the 9 experiments conducted in solar heating mode varied between 41.1% and 84% whereas the mean ambient temperature values ranged between 23.9 °C and 32.8 °C. The thermal energy stored during burner heat charging ranged between 0.36 MJ and 1.8 MJ. The collector efficiency values ranged between 0.03% and 8.8%. This range of values show a significant improvement in the heating effect associated with burner heating as compared to solar heating.
4. With hybrid heat charging the average air relative humidity values covering the 9 experiments conducted varied between 31.2% and 78.1 % whereas the mean ambient temperature values ranged between 23.4 °C and 32.9 °C. The thermal energy stored during solar heat charging ranged between 0.3997 MJ and 1.9 MJ. The collector efficiency values ranged between 0.18% and 3.5 %. Apparently, the average air heater efficiency associated with hybrid heating is higher than solar heating. It can, therefore, be concluded that solar heating combined with burner heating is a more effective means of heating for solar drying than solar heating only.
5. At a plenum inlet gap of 6 cm and vent outlet gap of 4 cm comparatively high mass flow rates of between 0.0141 to 0.0798 kg/s were recorded with comparatively high air heater efficiency values of between 0.093% and 1.89%. Against this background it is concluded that a plenum inlet gap of 6 cm and a vent outlet gap of 4 cm optimizes the thermal performance of the dryer. For design purposes a plenum inlet gap to vent outlet gap ratio of 1.5:1 optimises heating and is therefore adopted for the drying experiments.

KNUST

6. An exergy analysis conducted on the air from dryer inlet to plenum exit give the minimum and maximum rate of change of exergy values as 93.09 and 4,597.27 kW; 4,012.88 and 13,656.24 kW; and 5,549.866 and 17,319.27 kW for solar, burner, and hybrid heating modes respectively. These results show that the availability (exergy) rate of the dryer increases with increased heating effect (solar being the lowest and hybrid the highest). In comparison with the range of collector efficiency values recorded for the three heating modes, it can be concluded that as the availability increases the collector efficiency increases. Therefore, the performance of the system can be improved by adopting a heating effect that optimises exergy. It can further be concluded that the performance of the system can be improved by adopting a design that minimizes heat losses since that will increase the ***availability*** of the system.

KNUST

5.2 Laboratory experiments under load conditions: results and discussions

Investigations on the laboratory model were conducted under load conditions at full capacity with fresh pineapple in four heating modes (solar drying with backup heating, use of only backup heater for drying, use of a combination of solar energy and backup heater for drying, and use of only solar energy for drying) to correspond to specified drying periods for four demarcated seasons in Ghana. The first heating mode was adopted for periods of inclement weather (July, August, and September in Ghana) which are the months of harvest in the forest regions, the second for night drying only or drying in extremely poor weather (almost zero insolation), the third for partly cloudy weather seasons, and the last drying mode for sun drying during peak sunshine seasons (March, April, and May in Ghana). A plenum inlet gap of 6 cm and a vent outlet gap of 4 cm were used for each drying test since that combination optimizes the dryer performance as established in section 5.1. The drying experiments are presented in section 5.2.1

5.2.1 Experiments under load conditions

The results covering tests under load conditions are presented in tables 4 to 11.

The water vapour saturation pressure (P_{vs}), the absolute humidity of moist air, system drying efficiency, and moisture pick up efficiency were calculated using equations (2.77), (2.79), (2.172), and (2.174) respectively.

SOLAR DRYING MODE (Scenario 1)

Tables 5 and 6 show experimental data as well as performance parameters obtained from the analysis of data for drying in solar mode at full dryer capacity (2,262 grammes)

KNUST

Table 5 Solar drying only; loading density = 14.54 kg/m2; radiation intensity used: 350 W/m^2 for the first 4 hours and 450 W/m2 between 12:00 GMT and 17:00 GMT; Average Volume flow rate = 160.68 m^3/h

Test date: Tuesday, July 24, 2012; Time started: 08:30 am

$T/(h)$	$T_{f,i}$ ± 0.1°C	$T_{f,o}$	V_i	$\dot{m}_o$	ϕ_i	ϕ_o	P_{atm}	η_p	η_d	TRAY 1 $m_1/(g)$	TRAY 2 $m_2/(g)$	TRAY 3 $m_3/(g)$
0	23.7	30	0.3	0.01445	88	83.7	982.7			754	754	754
1	25.1	31	1.4	0.06715	82	87.3	982.7	0.5944	0.2765	740	739	680
2	24.5	33	0.3	0.01432	83	91.4	982.8	0.6654	0.1466	724	724	601
3	24.0	34	0.3	0.01429	90	88.9	982.3	0.2439	0.0878	706	708	536
4	24.0	35	0.7	0.03332	90	91.5	982.3	0.3326	0.0652	686	691	475
5	24.1	35	0.3	0.01428	85	90.1	982.0	0.4280	0.0633	665	673	395
6	26.2	42	0.3	0.01423	67	86.4	980.5	0.3551	0.0415	643	643	353
7	25.4	36	1.4	0.00663	79	88.4	980.6	0.0755	0.0254	629	624	319
8	24.7	45	0.7	0.03312	81	80.3	980.7	0.0649	0.0275	609	599	281
9	24.1	50	0.3	0.01422	89	88.7	980.6	0.1249	0.0263	587	568	245
Day 2 of solar drying (Wednesday, July 25, 2012); Time started: 9:30 am												
0	24.3	52	1.4	0.00000	79	77.7	982.5	0	0.000	587	568	245
1	24.2	47	2.0	0.09558	82	78.3	982.4	0.0194	0.0464	530	505	174
2	25.5	53	1.4	0.06679	77	79.6	981.8	-		514	475	
There was power interruption between 12:00 pm and 02:00 pm. The test was re-started at 2:00 pm												
3	26.2	58	0.7	0.03312	77	78.2	980.4	0.1415	0.0124	455	381	
4	25.9	55	1.7	0.08036	77	79.5	980.5	0.0264	0.0099	433	333	
5	25.8	56	1.4	0.06619	77	79.0	980.4	0.0209	0.0227	407	289	
6	24.7	56	1.7	0.08048	83	83.4	980.7	0.0970	0.0075	379	257	

Day 3 of solar drying (Thursday, July 26, 2012); Time started: 08:48

0	25.1	1.0	0.0481	79	76	983.6	0.0013	0.0051	310	180
1	26.3	0.7	0.03349	75	72	983.4	0.0071	0.0041	283	156
2	27.7	1.7	0.0809	68	45.3	982.7	0.0012	0.0038	247	
3	29.1	1.0	0.04736	65	43.9	982.0	0.0002	0.0021	216	
4	29.6	0.3	0.01414	60	47.3	981.0	0.0003	0.0010	186	
5	30.0	1.0	0.04691	61	47.3	980.5	0.0006	0.00068	169	
7	29.8	1.7	0.07954	58	40.7	980.3	-	0.0000	154	

KNUST

Table 6 Solar drying (system component temperature)

Test date: July 24, 2012; Time started: 08:30 am; plenum inlet gap = 6cm, vent outlet gap = 4 cm

Day	Hour	T_{fi}	T_{bg}	T_{lw}	T_{rp}	T_{ab-rp}	T_{ab}	T_{uw}	T_f	T_{pst1}	T_{pst3}	T_{pst2}	T_{fo}
206	800	22.7	22.7	22.7	22.7	22.7	22.7	22.7	22.7	22.7	22.7	22.7	22.7
206	900	23.97	23.97	23.97	23.97	23.97	23.97	23.97	23.97	23.97	30.92	28.14	23.97
206	1000	25.36	25.36	25.36	25.36	25.36	25.36	28.14	25.36	25.36	42.02	33.69	25.36
206	1100	25.94	25.94	25.94	25.94	25.94	25.94	38.42	25.94	25.94	42.58	38.42	25.94
206	1200	26.11	26.11	26.11	26.11	26.11	26.11	39.97	26.11	26.11	42.74	37.2	26.11
206	1300	25.99	25.99	25.99	25.99	25.99	25.99	41.24	25.99	25.99	42.62	38.47	25.99
206	1400	26.6	26.6	26.6	26.6	26.6	26.6	41.83	26.6	26.6	45.89	43.21	26.6
206	1500	27.02	27.02	27.02	27.02	27.02	27.02	43.62	27.02	27.02	43.62	40.85	27.02
206	1600	27.44	27.44	27.44	27.44	27.44	27.44	44.02	27.44	27.44	44.02	42.64	27.44
206	1700	26.8	26.8	26.8	26.8	26.8	26.8	43.4	26.8	26.8	50.1	37.87	26.8
Day 2 of experiments (Wednesday, July 25, 2012); Time started: 9:30 am													
207	1000	24.95	24.95	24.95	24.95	24.95	24.95	24.95	24.95	24.95	31.89	24.95	24.95
207	1100	25.28	25.28	25.28	25.28	25.28	25.28	25.28	25.28	25.28	44.63	25.28	25.28
207	1200	ELECCTRICAL POWER WAS INTERUPTED BETWEEN 12:00 AND 14:00 GMT											
207	1300												
207	1400	POWER WAS RESTORED AT 14:00 GMT											
207	1500	27.36	27.36	27.36	27.36	27.36	27.36	30.12	27.36	41.18	43.94	28.74	27.36
207	1600	27.66	27.66	27.66	27.66	27.66	27.66	38.71	27.66	44.24	52.25	35.95	27.66
207	1700	27.59	27.59	27.59	27.59	27.59	27.59	44.16	27.59	44.16	50.84	34.49	27.59
207	1800	27.25	27.25	27.25	27.25	27.25	27.25	43.84	30.02	43.84	53.21	36.93	27.25

208	900	23.4	23.4	23.4	23.4	23.4	23.4	23.4	23.4	26.19	28.93	23.4	23.4
208	1000	24.92	24.92	24.92	24.92	24.92	24.92	24.92	26.31	41.6	52.35	33.26	24.92
208	1100	26.31	26.31	26.31	26.31	26.31	26.31	37.39	29.08	42.93	53.65	37.39	26.31
208	1200	27.52	27.52	27.52	27.52	27.52	27.52	42.72	41.33	42.72	56.13	42.72	27.52
208	1300	28.71	28.71	28.71	28.71	28.71	28.71	45.25	45.25	46.58	50.58	45.25	34.22
208	1400	29.95	29.95	29.95	29.95	29.95	29.95	46.44	45.06	50.43	50.43	43.69	46.44
208	1500	30.71	30.71	30.71	30.71	30.71	30.71	47.17	49.82	48.49	72	47.17	43.05

KNUST

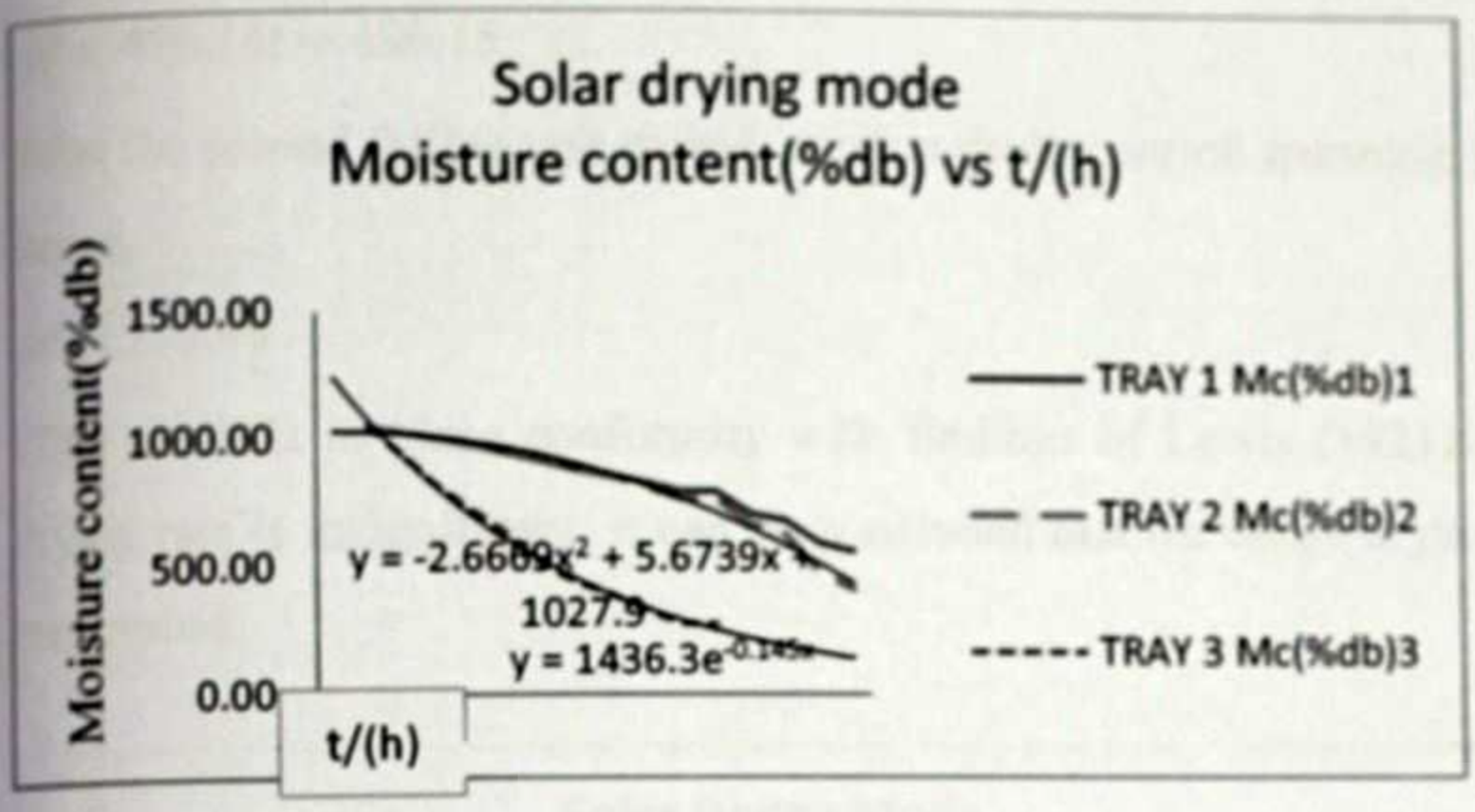

Figure 118 Percentage moisture content on dry basis versus time in solar drying mode

KNUST

Figure 118 shows the dehydration curves for pineapple at tray levels 1, 2, and 3. It is can be seen that the samples in the top tray (tray 3) dried fastest, with the bottom tray exhibiting the lowest drying rate. This drying pattern is attributed to the fact that the product in the top tray is exposed to direct, high intensity radiation from the infra red lamps. Hot air from the collector starts picking moisture from the bottom tray (thereby increasing its humidity ratio) before reaching the middle and top trays. Hence the middle tray exhibited an intermediate drying rate with the bottom tray exhibiting the least drying rate in solar mode of operation. At full loading capacity, drying in solar mode took a total of 23 hours with an average volumetric flow rate of 160.68 m^3/h. Moisture pick up efficiency recorded an average value of 15.24% with the initial overall drying efficiency being 27.65%. The falling-rate period characterised a significant proportion of the drying process from the start for tray 1. Two stages of the falling-rate period were identified. The first falling rate period which ends at a moisture content (Mc_1) of 624.11 (%db) is characterised by the exponential function

$$M = 1205.7\exp(-0.131t),$$

and the second falling rate period which begins from a moisture content (Mc_2) of 502.15 (%db) and ends at a moisture content (Mc_3) of 273.49 (%db) is characterised by the exponential function

$$M = 592.16\exp(-0.15t)$$

Between the first and second falling rate periods, the drying rate which spans a 1 hour period is characterised by the linear function

$$M = 496.15t - 490.15$$

After the second falling rate period, another drying period spanning 1 hour indicates inactivity, hence,

$$M = 273.49$$

This result is in close conformity with findings of Lewis (1921). Since the linear part of the drying rate is insignificant, it can be concluded that the entire drying rate falls within the falling rate period.

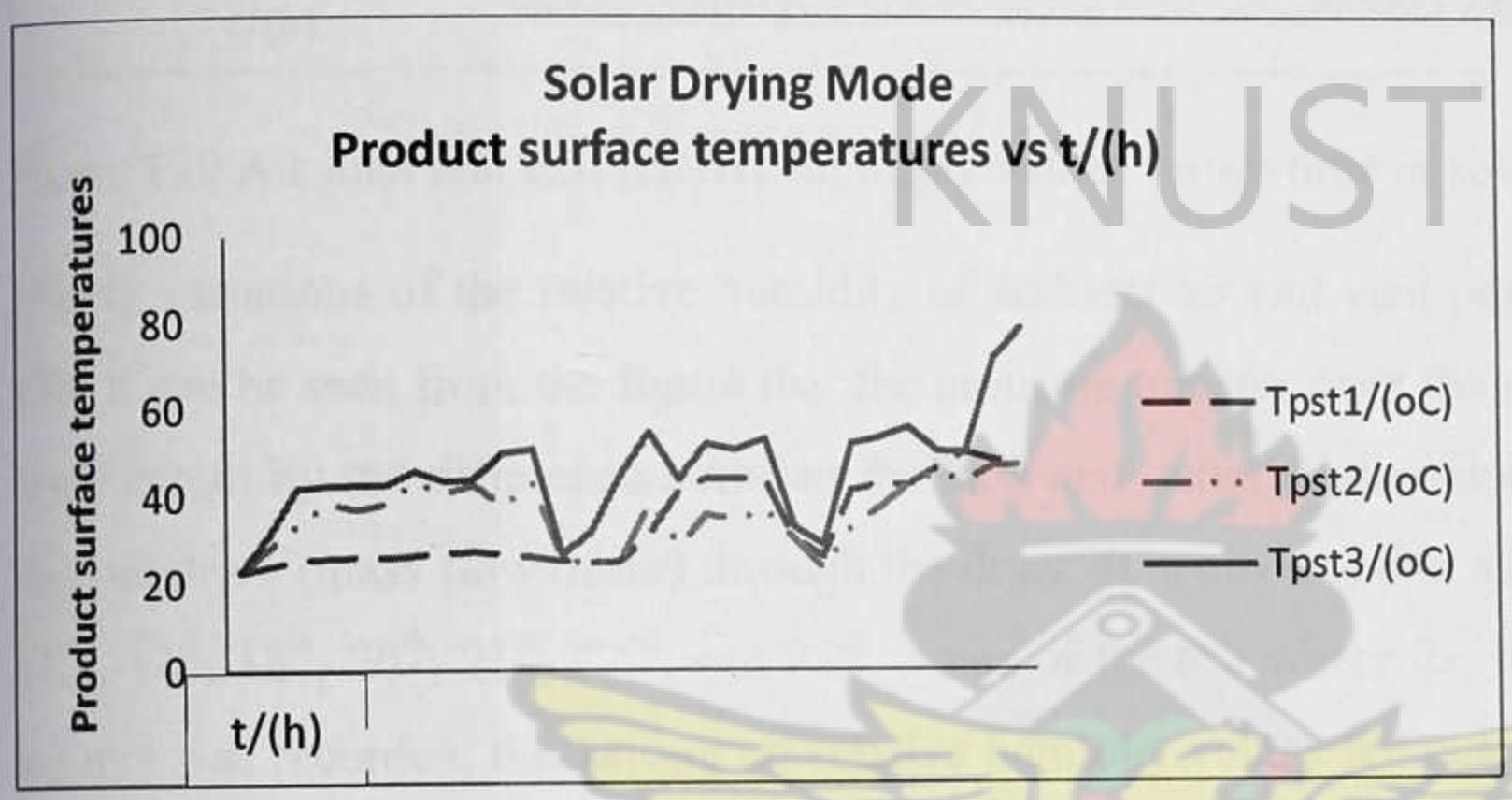

Figure 119 Product surface temperatures in trays 1, 2, and 3 versus time in solar drying mode

Hourly product surface temperature variations are shown in figure 119 with all product surface temperatures starting from an initial value of 22.7 °C at all tray levels. It is obvious the top tray (tray3) experienced the highest product surface temperature throughout the entire duration of the test with the minimum and maximum values being 22.7 and 72 °C respectively.

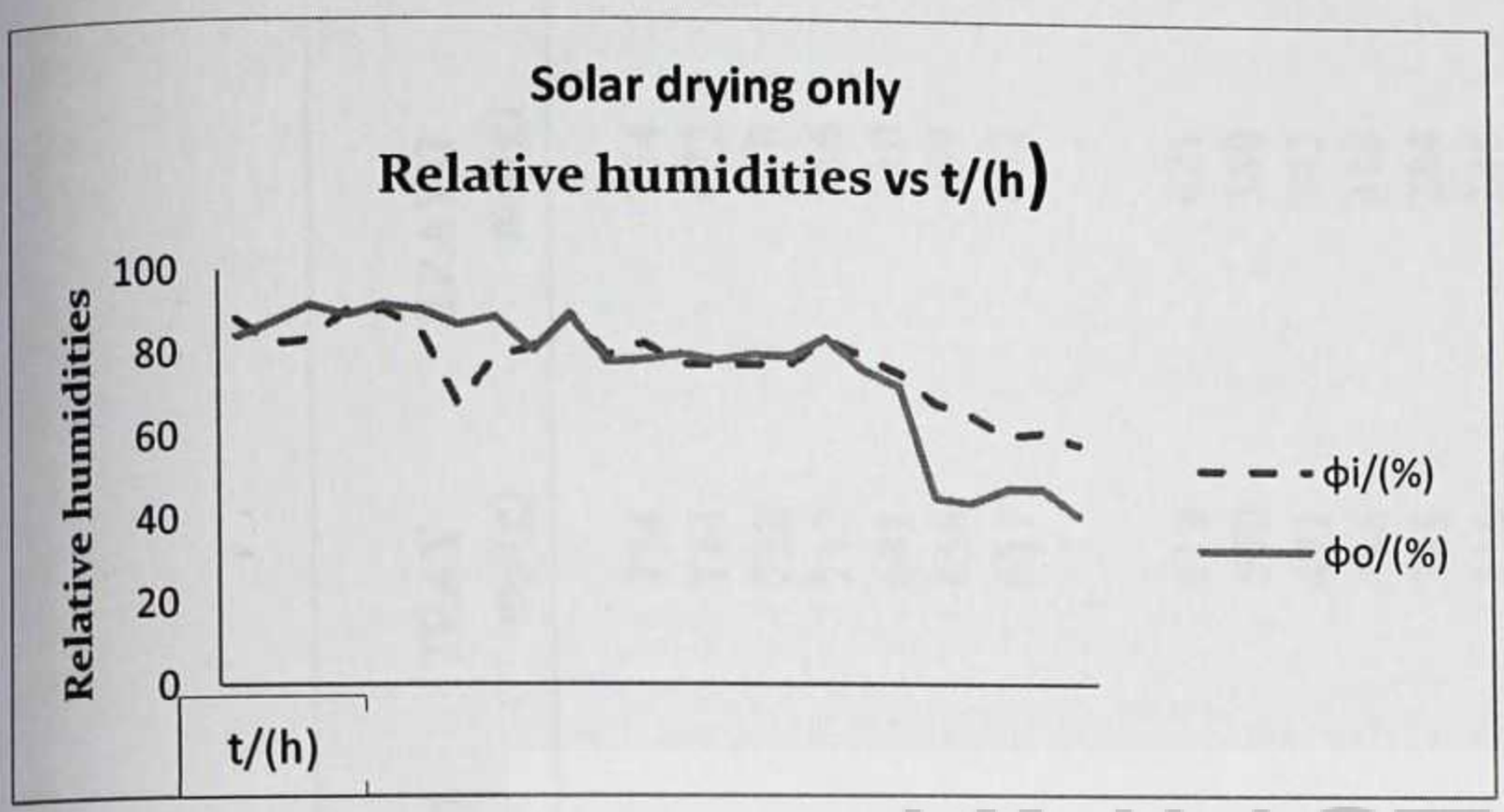

Figure 120 Air inlet and exit relative humidity values versus time in solar drying mode

Hourly variations of the relative humidity of ambient air and vent outlet air is shown in figure 120. It can be seen from the figure that the moisture transfer from the products as represented to some extent by the difference between the inlet and outlet relative humidity values responds to thermal drive (mass flow of air) through the dryer. It is obvious that at the 0^{th}, 1st, 4th, 9th, 10^{th}, 11^{th} , 12^{th}, 18^{th}, 20^{th}, 21^{st}, 22^{nd}, and 23^{rd} hours of the test where the lowest air inlet velocity of 0.3 m/s was recorded, the exiting air relative humidity values fell below the corresponding inlet values.

SOLAR DRYING AT DAY TIME WITH BACK-UP HEATING AT NIGHT (SCENARIO 2)

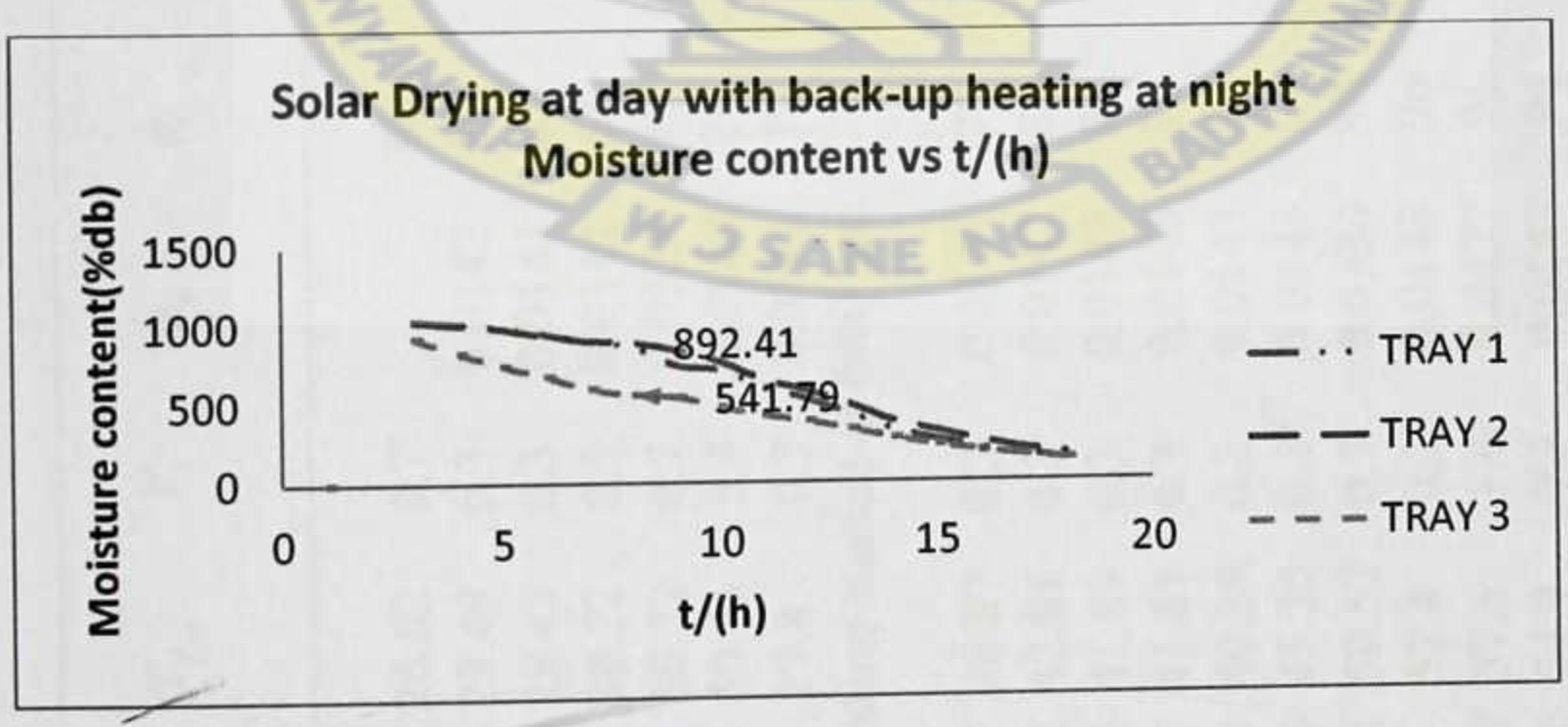

Figure 121 Percentage moisture content on dry basis versus time in back-up heating mode

Table 7 Solar drying with back up heating; loading density = 14.54 kg/m2; radiation intensity used: 350 W/m^2 for the first 1 hour and 450 W/m^2 between 12:00 GMT and 17:00 GMT; Average Volume flow rate = 73.63 m^3/h

Test date: July 21, 2012; Time started: 11:40 am

$T/(h)$	$T_{f,i}$ ±0.1 °C	$T_{f,o}$	V_i	$\dot{m}_o$	ϕ_i	ϕ_o	P_{atm}	ηp	ηd	TRAY 1 m_1/(g)	TRAY m_2/(g)	TRAY 3 m_3/(g)
										754	754	754
0	26.02	26.02	0.7		66	58.1	983.4			741	744	672
1	27.49	27.49	0.3	0.0142	59	62.1	980.1	0.9988	1.818	728	732	610
2	29.43	29.43	0.3	0.0141	65	69.1	980.0	0.2870	0.7465	715	712	556
3	30.22	30.22	0.3	0.0141	61	80.0	982.0	0.4371	0.4954	688	681	510
4	30.72	30.72	0.7	0.0328	63	74.5	981.3	0.2565	0.4448	657	658	459
5	30.91	30.91	0.3	0.0140	74	78.1	981.2	0.1025	0.3590	631	651	432
6	29.8	27.8	0.3	0.0141	79	77.9	981.2	0.1124	0.1712			
Backed up heating started at 6:00 pm												
7	28.87	28.87	0.3	0.0141	79	91.8	981.9	0.2096	0.2963	599	618	621
8	27.62	42.81	0.3	0.0142	84	92.5	982.5	0.0158	-3.9133	533	570	380
9	26.55	41.89	0.3	0.0143	92	91.8	982.9	0.3452	4.1261	459	491	343
10	25.87	41.61	0.3	0.0143	92	93.5	983.8	0.0046	1.1245	410	446	318
11	25.64	40.39	0.3	0.0143	92	93.0	984.1	0.1276	1.2848	347	385	284
12	25.59	45.25	0.3	0.0143	94	83.0	983.8	0.0052	1.2893	279	318	246
13	25.61	50.57	0.7	0.0334	94	92.9	983.1	0.0006	0.8999	240	274	216
14	25.6	52.4	0.3	0.0143	96	86.7	982.2	0.0024	0.7650	201	232	190
15	25.39	57.5	1.0	0.0477	96	73.4	982.3	0.0002	0.6745	176	201	171
16	25.06	54.9	0.3	0.0143	96	72.4	982.2	0.0006	0.6764	155	175	153
17	24.71	62.2	0.3	0.0143	97	70.4	982.1	0.0002	0.4427	145	158	141
18	24.48	65.1	0.7	0.0335	97	87.0	982.5	6.8×10^{-5}	0.2245	140	144	143

LIBRARY
KWAME NKRUMAH
UNIVERSITY OF SCIENCE & TECHNOLOGY
KUMASI

Table 8 Solar drying with back up heating -system component temperatures

Test date: July 21, 2012; Time started: 11:40 am; plenum inlet gap = 6cm, vent outlet gap = 4 cm

Day	Hour	T_{fi}	T_{bg}	T_{lw}	T_{rp}	T_{ab-rp}	T_{ab}	T_{uw}	T_f	T_{pst1}	T_{pst2}	T_{pst3}	T_{fo}
203	1100	26.02	26.02	26.02	26.02	26.02	26.02	26.02	26.02	26.02	26.02	26.02	26.02
203	1200	27.49	27.49	27.49	27.49	27.49	27.49	27.49	27.49	27.49	28.87	27.49	27.49
203	1300	29.43	29.43	29.43	29.43	29.43	29.43	29.43	29.43	29.43	45.93	32.18	29.43
203	1400	30.22	30.22	30.22	30.22	30.22	30.22	45.33	30.22	30.22	46.7	42.58	30.22
203	1500	30.72	30.72	30.72	30.72	30.72	30.72	47.18	30.72	30.72	47.18	37.58	30.72
203	1600	30.91	30.91	30.91	30.91	30.91	30.91	47.37	32.91	30.91	47.37	39.14	30.91
203	1700	29.8	29.8	29.8	29.8	29.8	29.8	46.29	31.88	29.8	46.29	36.68	27.8
203	1800	28.87	28.87	28.87	28.87	28.87	28.87	45.4	28.87	28.87	57.39	45.4	28.87
203	1900	27.62	27.62	42.81	71.8	50.88	41.35	63.83	37.29	38.68	35.91	34.53	42.81
203	2000	26.55	26.55	44.5	92.5	57.89	73.5	119.2	43.16	47.18	43.16	43.16	41.89
203	2100	25.87	25.87	47.88	104.2	58.61	94.4	141.1	53.24	54.59	42.51	42.51	41.61
203	2200	25.64	25.64	49	111.3	62.29	104	99.6	42.29	47.65	42.29	42.29	40.39
203	2300	25.59	25.59	58.34	119.7	70.1	114.9	74	52.98	58.3	55.66	58.34	45.25
204	0	25.61	25.61	57.02	128	77.8	119.7	86.6	63.57	57.02	58.36	58.36	50.57
204	100	25.6	25.6	58.35	132.7	76.5	123.2	89.2	59.66	54.33	60.96	57.01	52.4
204	200	25.39	25.39	58.16	132.5	81.4	118.3	89	69.89	60.77	68.58	58.16	57.5
204	300	25.06	25.06	57.86	132.3	86.2	118.1	88.7	68.28	68.28	60.46	57.86	54.9
204	400	24.71	24.71	57.53	132	88.4	117.7	88.4	71.9	57.53	66.66	57.53	62.2
204	500	24.48	24.48	57.32	131.8	86.9	123.5	88.2	73	73	73	65.15	65.1
204	600	24.19	24.19	57.04	131.6	87.9	125.6	87.9	72.7	72.7	70.1	66.18	56.04
204	700	24.59	24.59	42.63	100.6	60.03	110.4	89.5	66.56	66.56	75.5	61.3	56.04

Figure 121 shows the dehydration curves for the bottom, top and middle trays in solar drying mode with back up heating at night. In this drying mode, effective drying time was reduced from 23 hours in solar drying mode to 19 hours. The dryer was operated in this mode at full capacity with an average volumetric air flow rate of 73.63 m^3/h being recorded. The moisture pick up efficiency ranged between 0.0068% and 99.88% giving an average value of 15.30%. At the initial stage of drying (solar mode of operation) drying rate was highest in the top tray (tray 3) followed by the middle tray with the bottom tray recording the lowest initial drying rate. This is due to the exposure of the top tray products to direct infra red radiation. However, with the operation of the backup heater the gap between the drying rates narrowed because of increased heating effect in the plenum. The pick- up efficiency across the three trays ranged between 0.0055% and 99.88%. It can be observed that the moisture pick- up efficiency generally decreases as drying proceeds because of the high water molecule binding energies that prevail at low moisture contents. It becomes increasingly difficult to cause moisture to move to the surface of the product. For the drying rate in the top tray, the entire drying period falls within the falling rate period with two different falling rate regimes manifesting. The point of transition between the two falling rate regimes occurs at a critical moisture content of 541.79 at the 8th hour from the start of drying as shown on figure 121. The critical moisture content for the middle and bottom trays both occurred at the 7th hour with a value of 892.41.

The two falling rate regimes are characterised by the following equations:

$M_1 = 994.77\exp(-0.093t)$ and $M_2 = 677.7\exp(-0.158t)$

The graphs showing these deductions are shown in figures 122 and 123.

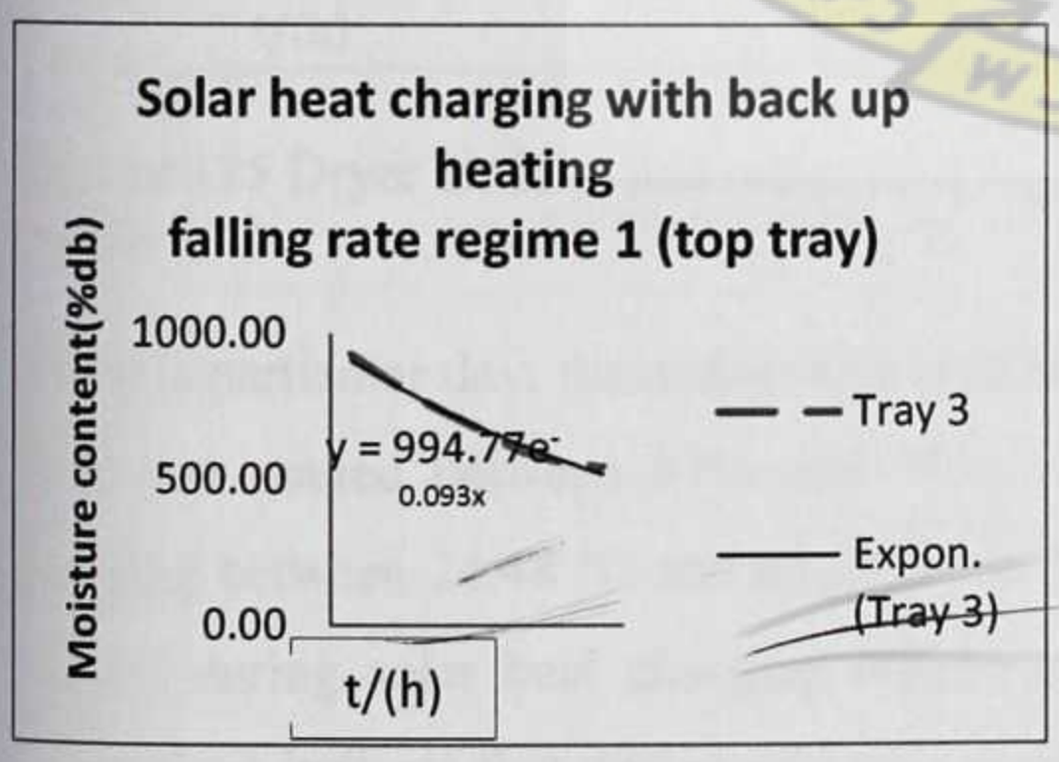

Figure 122 falling rate regime 1(top tray)

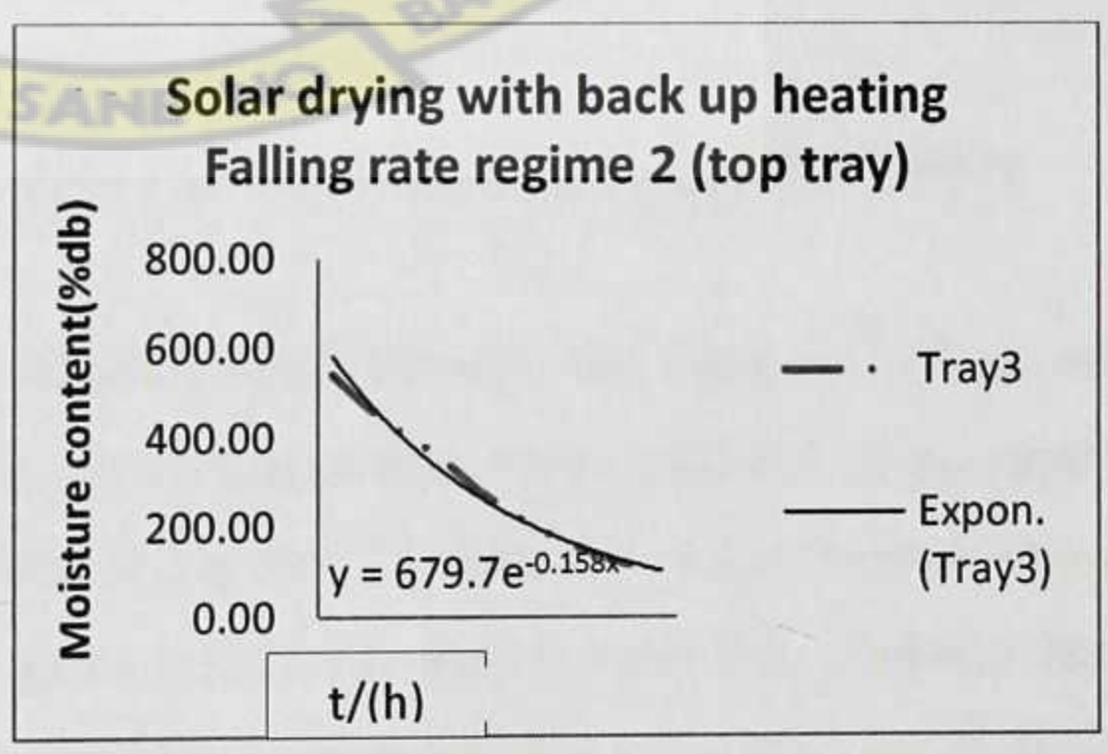

Figure 123 Falling rate regime 2(top tray)

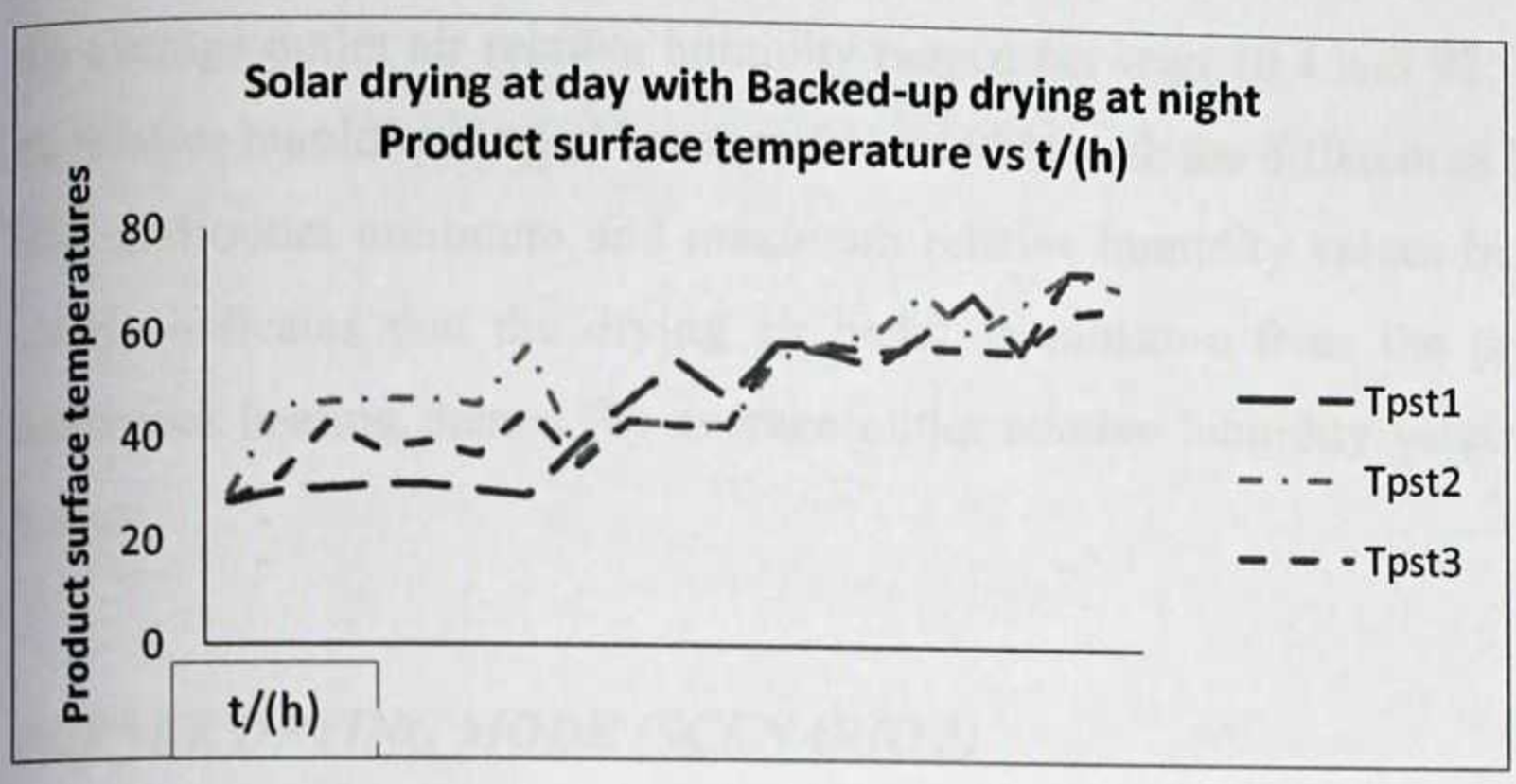

Figure 124 Product surface temperatures at trays 1, 2, and 3 versus time in back-up heating mode

The hourly variation of product surface temperatures at the three tray levels are shown on figure 124. After the 7th hour of drying, the middle tray product surface temperature falls whereas the top tray product surface temperature leads the values for the bottom and middle trays for a significant period of the second half of drying.

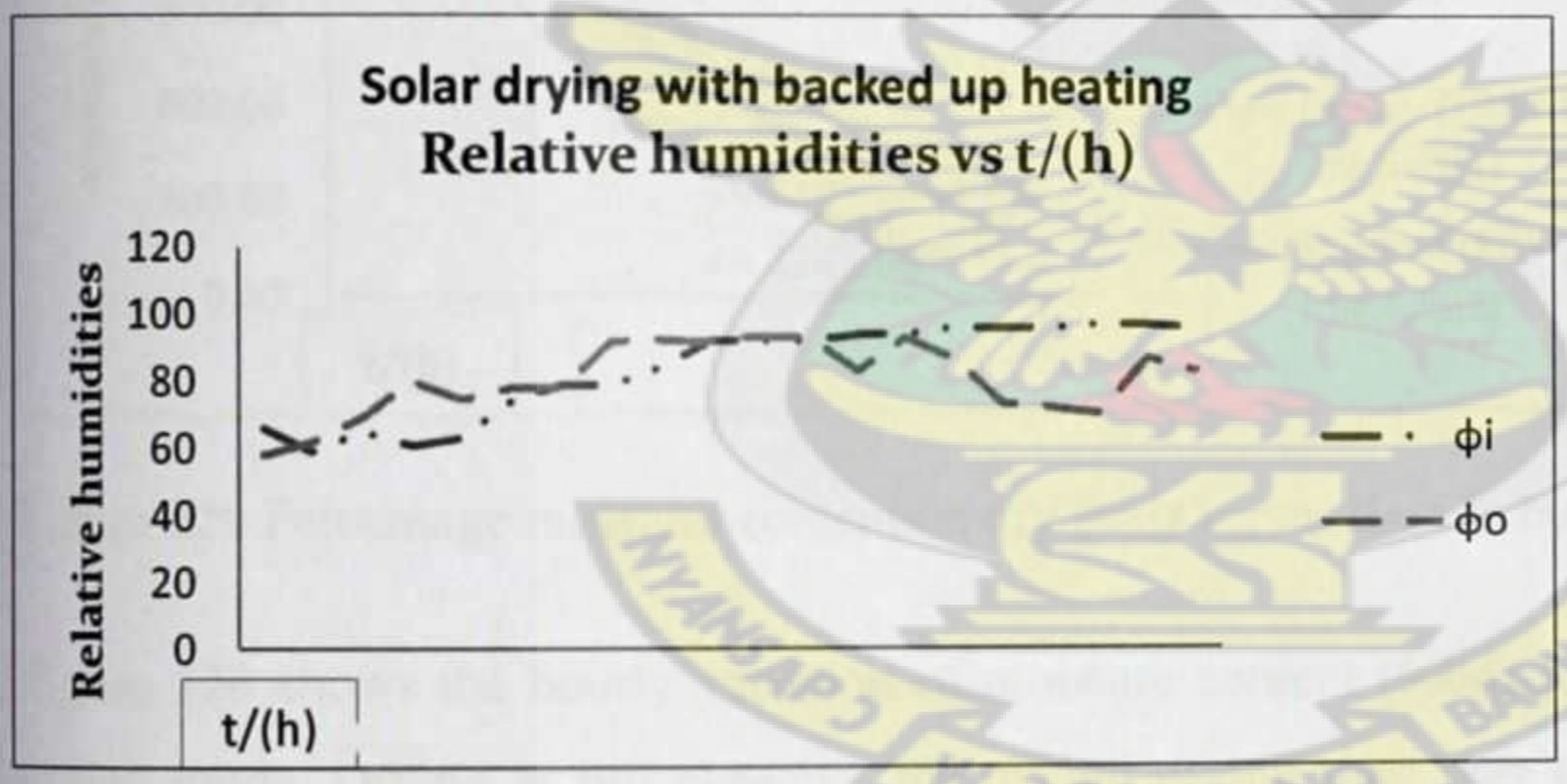

Figure 125 Dryer air inlet and outlet relative humidity values versus time in back-up heating mode

On this particular day, the ambient air relative humidity range between the hours of 7:00 pm and 5:00 am ranged between 84% and 97% with the corresponding mean ambient temperatures ranging between 24.48 °C and 27.62 °C as shown in figure 125. The calculated thermal energy stored during solar heat charging ranged between 0.1242 MJ and 0.2044 MJ. Clearly, these conditions indicate that drying will not be effective if back up heating is not employed. Between 11:00 pm (July 21, 2012) and 5:00 am (July 22, 2012) (during the peak back up heating period)

the average outlet air relative humidity ranged between 70.4 and 92.9% while the average inlet air relative humidity ranged between 94 and 97% with the differences between the corresponding inlet and outlet minimum and maximum relative humidity values being 23.6% and 41%. This clearly indicates that the drying air picks up moisture from the product and simultaneously undergoes heating, hence the average outlet relative humidity values being less than the inlet values.

BURNER DRYING MODE (SCENARIO 3)

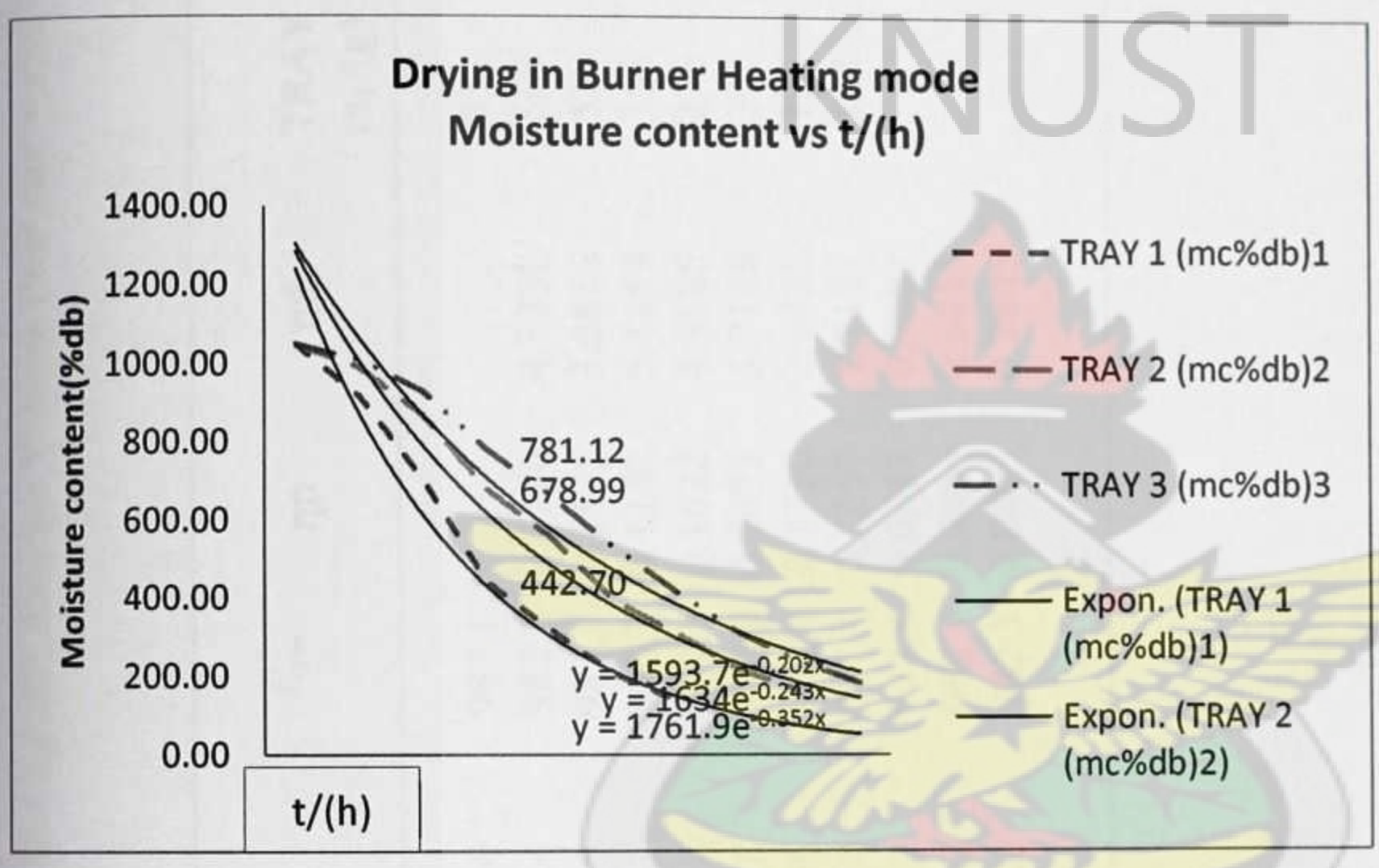

Figure 126 Percentage moisture content on dry basis versus time in burner drying mode

Figure 126 shows the hourly variation of moisture content (%bd) for the three trays in burner drying mode. Drying at full capacity, the overall drying time was 10 hours which is less than twice the total drying time recorded in solar drying mode of operation. Moisture pick up efficiency over the drying period ranged between 0.053 and 63% with an average value of 17.22% and an average volumetric air flow rate of 156.78 m^3/h. Obviously, drying rate was highest in the bottom tray (tray 1) due to the relatively high heating effect and, hence, improved thermal buoyancy in the plenum. The products in the middle tray (tray 2) recorded the second highest drying rate followed by the last tray. The critical moistures contents for the trays 1, 2, and 3 are 781.12, 678.99, and 442.70, respectively. The dehydration curves for the bottom, middle, and top trays are

Table 9 Drying in burner mode; loading density = 14.54 kg/m2; Average Volume flow rate = 156.78 m^3/h; Burner rating: 1800 W

Test date: July 22, 2012; Time started: 12:12 pm

$T/(h)$	$T_{f,i}$	$T_{f,o}$	V_i	$\dot{m}_o$	ϕ_i	ϕ_o	P_{atm}	ηp	ηd	TRAY 1 m_1/(g)	TRAY 2 m_2/(g)	TRAY 3 m_3/(g)
0	28.35	28.35	0.3		65	75.4	982.1			754	754	754
1	29.39	44.42	1.4	0.0142	63	89.4	982.2	0.6266	4.3332	668	716	728
2	30.2	66.5	1.4	0.0659	68	87.5	981.1	0.1135	3.0816	528	636	676
3	30.4	77	2.0	0.0657	70	86.2	980.3	0.1102	5.4159	356	511	578
4	30.28	78.2	0.7	0.0936	70	91.4	979.7	0.1622	4.9585	276	432	502
5	29.83	77.8	0.3	0.0327	71	92.8	980.0	0.2691	5.7148	201	324	415
6	29.27	77.3	0.3	0.0141	77	79.6	980.6	0.1730	2.8425	156	269	340
7	28.57	76.6	1.0	0.0141	79	79.0	981.4	0.2567	1.7121	134	210	271
8	27.93	76.1	0.3	0.0473	82	80.2	981.8	0.0017	0.9882		173	221
9	27.51	73.1	0.7	0.0143	85	71.2	982.4	0.0086	0.6413		151	186
10	26.91	73.9	0.3	0.0334	92	74.0	982.3	0.0005	0.2805			163

KNUST

Table 10 Drying in burner mode – system component temperatures

Test date: July 22, 2012; Time started: 12:12 pm; plenum inlet gap = 6cm, vent outlet gap = 4 cm

Day	Hour	T_{fi}	T_{bg}	T_{lw}	T_{rp}	T_{ab-rp}	T_{ab}	T_{uw}	T_f	T_{pst1}	T_{pst2}	T_{pst3}	T_{fo}
204	1200	28.35	28.35	28.35	44.89	28.35	44.89	39.38	29.73	28.35	28.35	28.35	28.35
204	1300	29.39	30.76	52.46	72	55.08	43.14	48.46	32.14	29.39	29.39	29.39	44.42
204	1400	30.2	31.58	62.63	115.1	76.8	75.5	84.4	46.68	35.7	31.58	32.95	66.5
204	1500	30.4	31.78	64.1	133.1	90.9	100.7	98.2	57.46	46.83	37.27	41.38	77
204	1600	30.28	34.4	74.3	142.3	92	108	104.3	67.82	53.4	46.75	44.01	78.2
204	1700	29.83	40.82	77.8	148.8	92.9	108.8	105.1	59.62	58.29	46.32	47.61	77.8
204	1800	29.27	33.4	77.3	149.5	92.4	113.1	102.2	72.1	60.43	45.78	48.4	77.3
204	1900	28.57	28.57	68.87	146.7	91.8	121	105.3	86.7	61.11	55.78	59.78	76.6
204	2000	27.93	27.93	63.11	135.7	89.9	119.2	94.9	78.6	60.51	59.18	60.51	76.1
204	2100	27.51	27.51	60.12	134.2	87	116.5	90.8	75.7	66.61	60.13	60.13	73.1
204	2200	26.91	28.3	59.57	133.8	85.3	112.3	90.3	75.2	73.9	71.3	60.87	73.

Tpst: Product surface temperature; all temperatures are in degrees Celsius; numbers 204 represent day of the year (i.e. 203+1 for a Leap year)

$$M = 1761.9\exp(-0.352t),$$

$$M = 1634\exp(-0.243t), \text{ and}$$

$$M = 1761.9\exp(-0.352t) \text{ respectively}$$

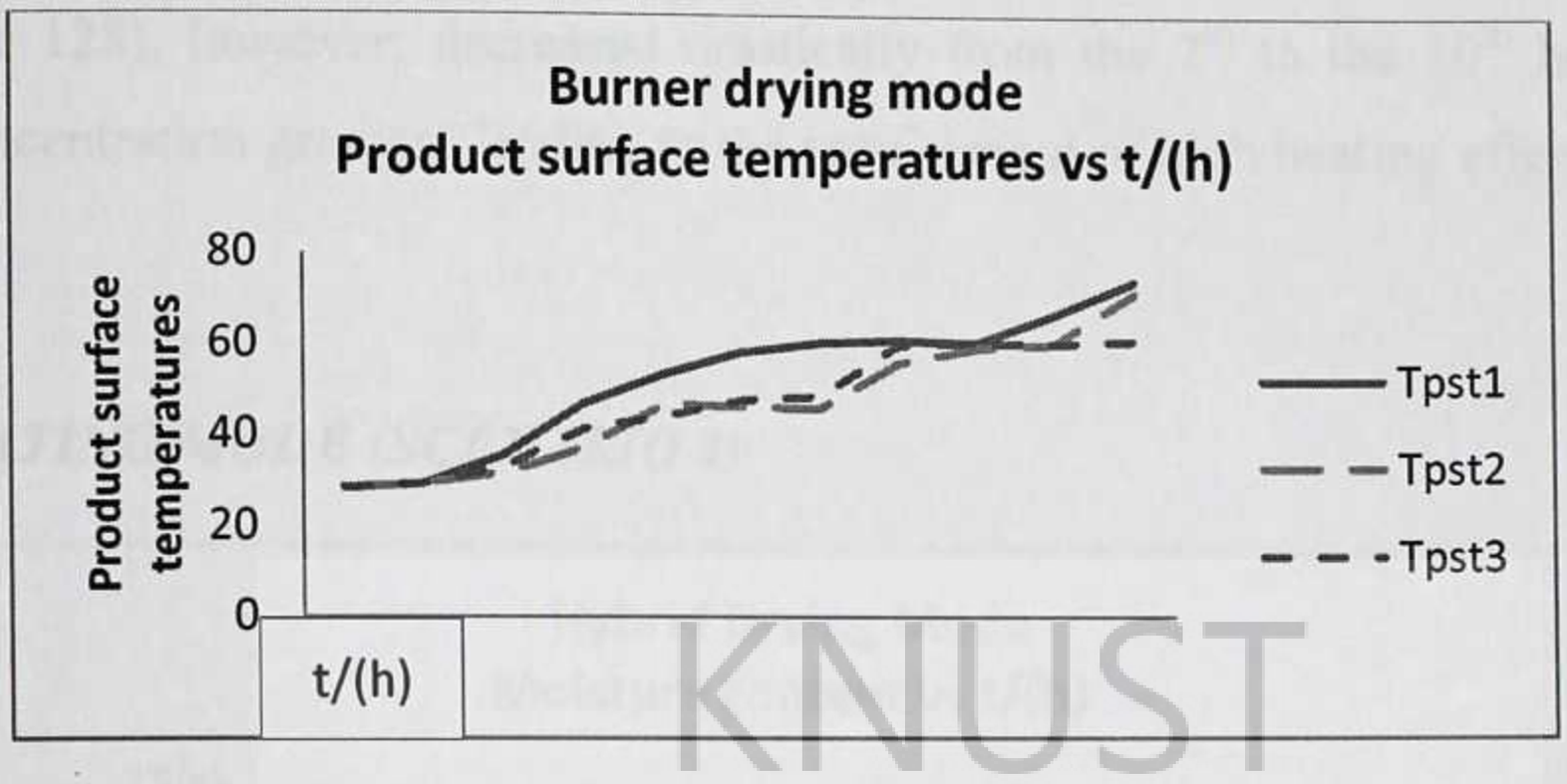

Figure 127 Product surface temperatures versus time in burner drying mode

Figure 127 shows the hourly variation of the product surface temperatures at the various tray levels. Obviously, the product surface temperatures at tray 1 (the bottom tray) are comparatively higher than at tray 2 (the middle tray). The top tray recorded the lowest product surface temperatures. This observation can be attributed to the fact that the bottom tray products are closer to the thermal mass so that the bottom tray products experience more heating than at subsequent tray levels.

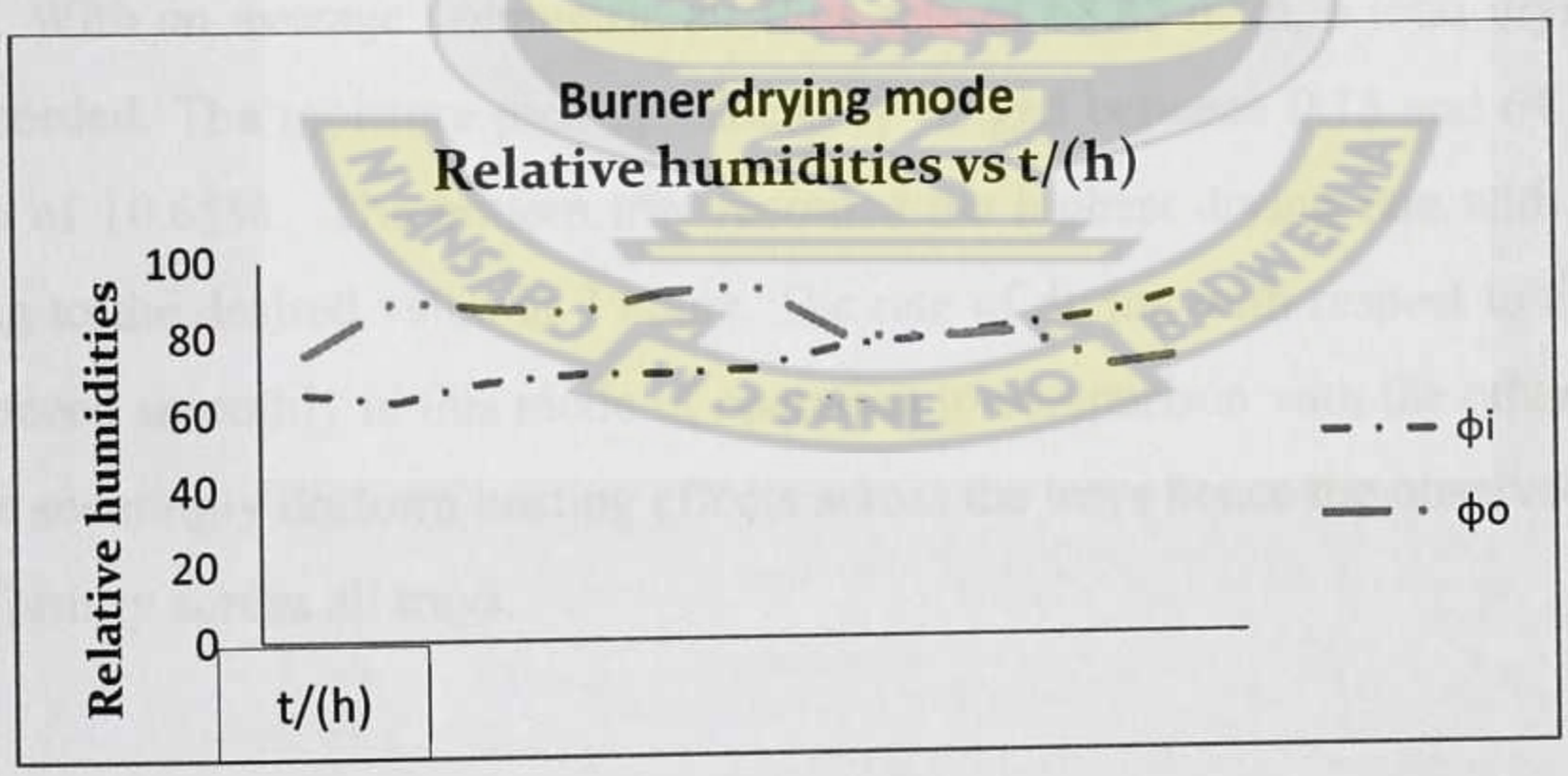

Figure 128 Dryer inlet and outlet relative humidity values versus time in burner drying mode

Figure 128 represents the hourly variation in average fluid inlet and vent outlet relative humidity values over the period of drying. Up to the 6th hour of drying the rate of dehydration was significantly high with the outlet air relative humidity reaching 92.8% from a corresponding average inlet relative humidity value of 71% at the 5th hour of drying. The rate of dehydration (refer to figure 128), however, decreased drastically from the 7th to the 10th hour due to the decrease in concentration gradient leading to the requirement of high heating effects for moisture migration.

HYBRID HEATING MODE (SCENARIO 4)

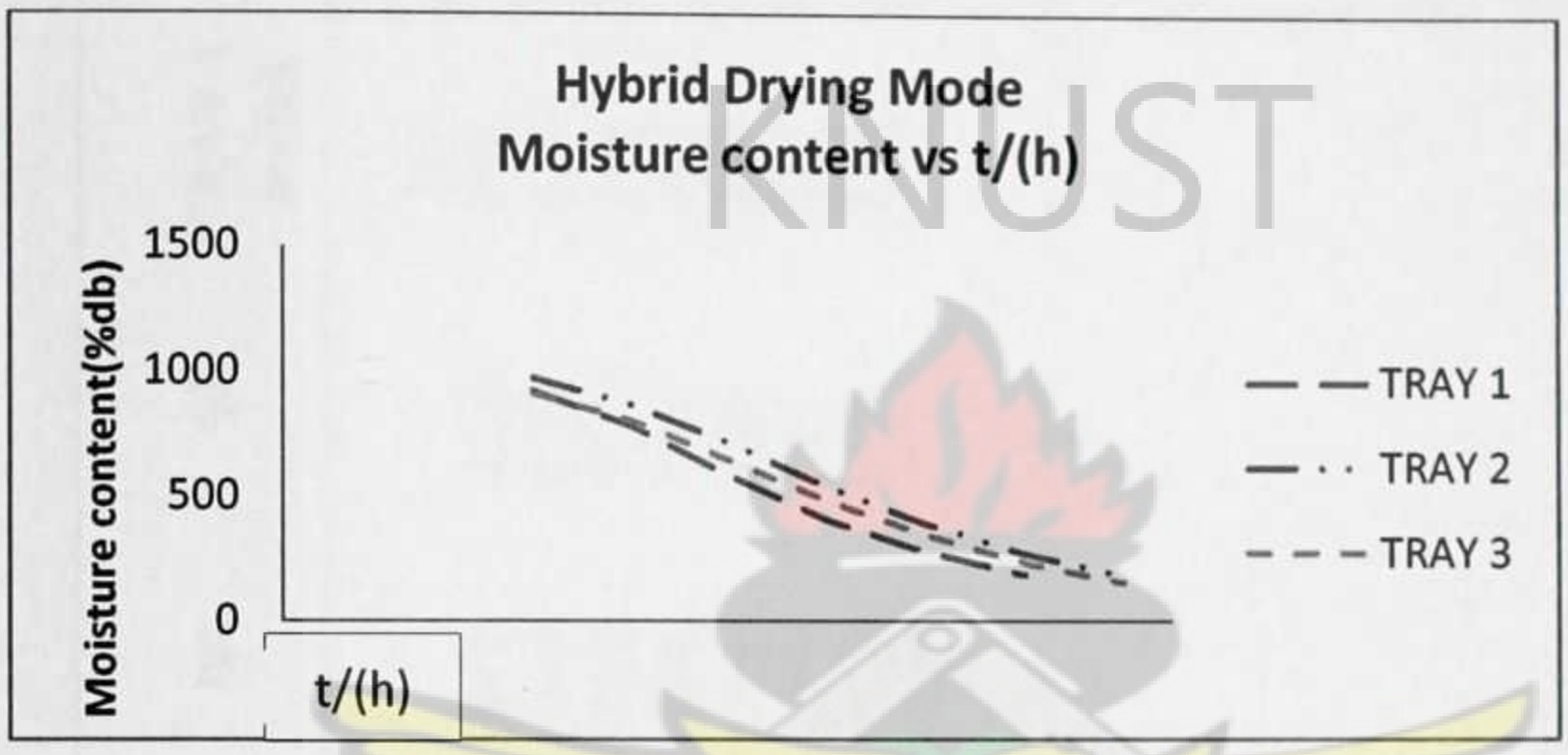

Figure 129 Percentage moisture content on dry basis versus time in hybrid drying mode

The dehydration curves for the three trays at full capacity in hybrid mode of operation are shown in figure 129. With an average volumetric air flow rate of 68.85 m^3/h, a total drying time of 8 hours was recorded. The moisture pick up efficiency ranged between 0.15 and 64.75% with an average value of 10.65%. The bottom tray recorded the highest drying rate with the moisture content getting to the desired value in 7 hours. The rate of drying with respect to the three trays appears to proceed smoothly in this mode of operation in comparison with the other three modes because of the seemingly uniform heating effects across the trays hence the observed consistency in drying uniformity across all trays.

Table 11 Hybrid drying; loading density = 14.54 kg/m^2; radiation intensity used: 350 W/m^2 for the first 2 hours and 450 W/m^2 between 12:00 GMT and 17:00 GMT; Average Volume flow rate = 68.85 m^3/h; Burner rating: 1800 W

Test date: July 23, 2012; Time started: 10:40 am

$T/(h)$	$T_{f,i}$	$T_{f,o}$	V_i	$\dot{m}_o$	ϕ_i	ϕ_o	P_{atm}	ηp	ηd	TRAY 1 m_1/(g)	TRAY 2 m_2/(g)	TRAY 3 m_3/(g)
0	24.57	24.57	1.0		73	78.4	982.7			754	754	754
1	27.55	31.69	0.3	0.0142	70	89.7	982.0	0.6474	-13.81	669	704	664
2	28.74	50.6	0.3	0.0141	70	85.4	981.2	0.0608	-6.53	577	632	591
3	29.74	64.78	0.3	0.0141	67	88.8	980.6	0.0185	91.39	446	533	488
4	30.45	77.1	1.0	0.0468	63	81.6	979.7	0.0082	4.83	331	419	382
5	32.08	79.8	0.3	0.0140	69	82.9	979.7	0.0052	5.02	248	321	293
6	31.72	79.5	0.3	0.0140	70	79.8	979.3	0.0040	2.63	187	244	220
7	31.23	79	0.3	0.014	76	72.0	979.5	0.0015	1.81	147	184	167
8	30.52	78.4	0.3	0.0140	86	78.4	980.3	0.0000			84	125

KNUST

Table 12 Drying in hybrid mode-system component temperatures

Test date: July 23, 2012; Time started: 10:40 am; plenum inlet gap = 6cm, vent outlet gap = 4 cm

Day	Hour	T_{fi}	T_{bg}	T_{lw}	T_{rp}	T_{ab-rp}	T_{ab}	T_{uw}	T_f	T_{pst1}	T_{pst2}	T_{pst3}	T_{fo}
204	2300	25.49	25.49	47.51	111	68.6	105.1	81.5	66.06	66.06	52.8	55.53	60.82
205	0	25.03	25.03	41.7	76	48.41	89.9	61.73	56.48	53.79	41.7	41.7	41.7
205	100	24.64	24.64	37.15	57.46	41.32	67.86	52.08	41.32	41.32	35.76	37.15	41.32
205	200	23.99	23.99	25.38	50.12	40.7	51.47	40.7	40.7	40.7	23.99	29.55	33.73
205	300	23.65	23.65	23.65	40.37	36.19	40.37	40.37	33.4	29.22	23.65	23.65	23.65
205	400	23.5	23.5	23.5	40.23	23.5	40.23	34.65	23.5	23.5	23.5	23.5	23.5
205	500	23.34	23.34	23.34	37.29	23.34	30.31	23.34	23.34	23.34	23.34	23.34	23.34
205	600	23.19	23.19	23.19	23.19	23.19	23.19	23.19	23.19	23.19	23.19	23.19	23.19

KNUST

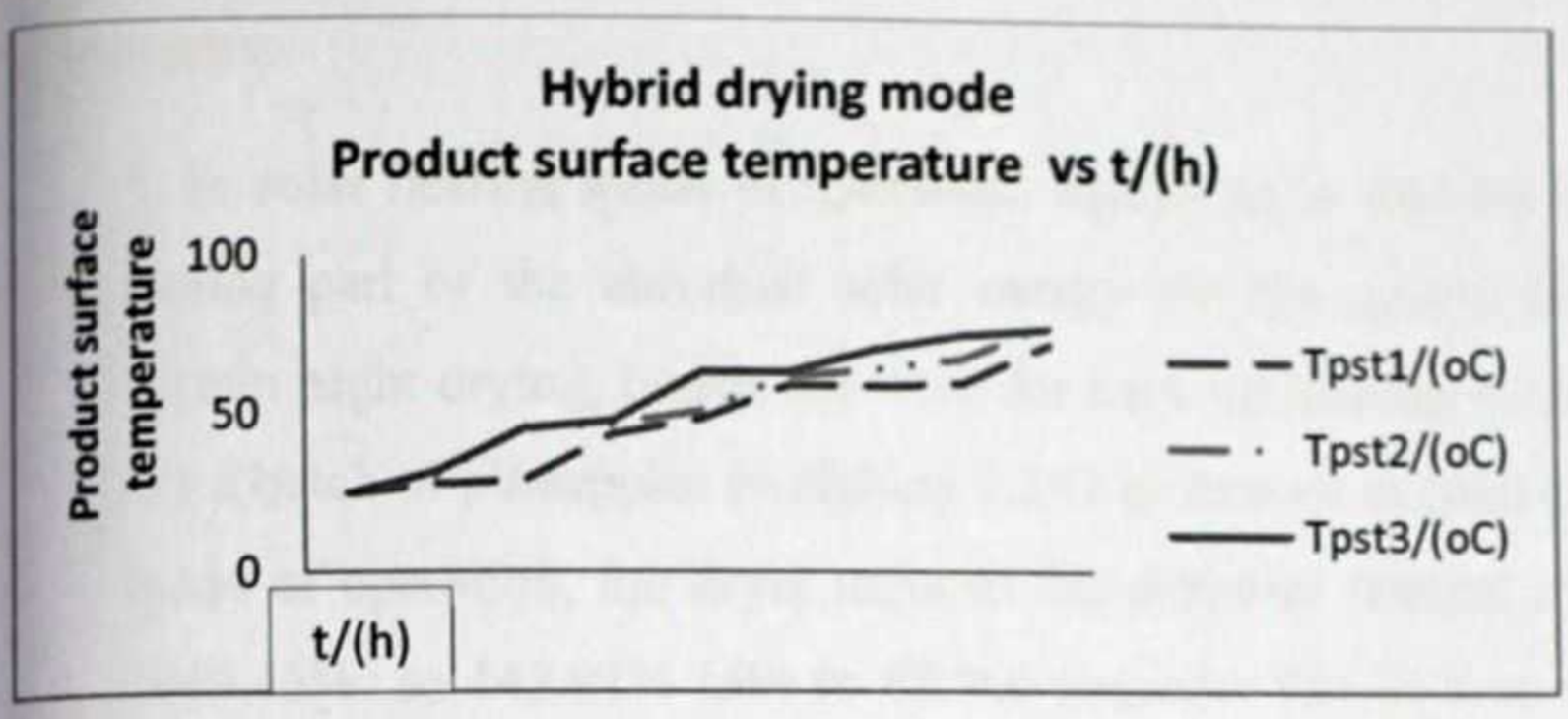

Figure 130 Product surface temperatures versus time in hybrid drying mode

Figure 130 shows the hourly variations in product surface temperature with respect to the three trays. It can be seen from figure 130 that the product surface temperature in the bottom tray leads the middle and bottom trays. This can be attributed to the comparatively high heating effect of the thermal mass on plenum fluid as opposed to the heating effect on the top tray due to direct heating from the infra red lamps.

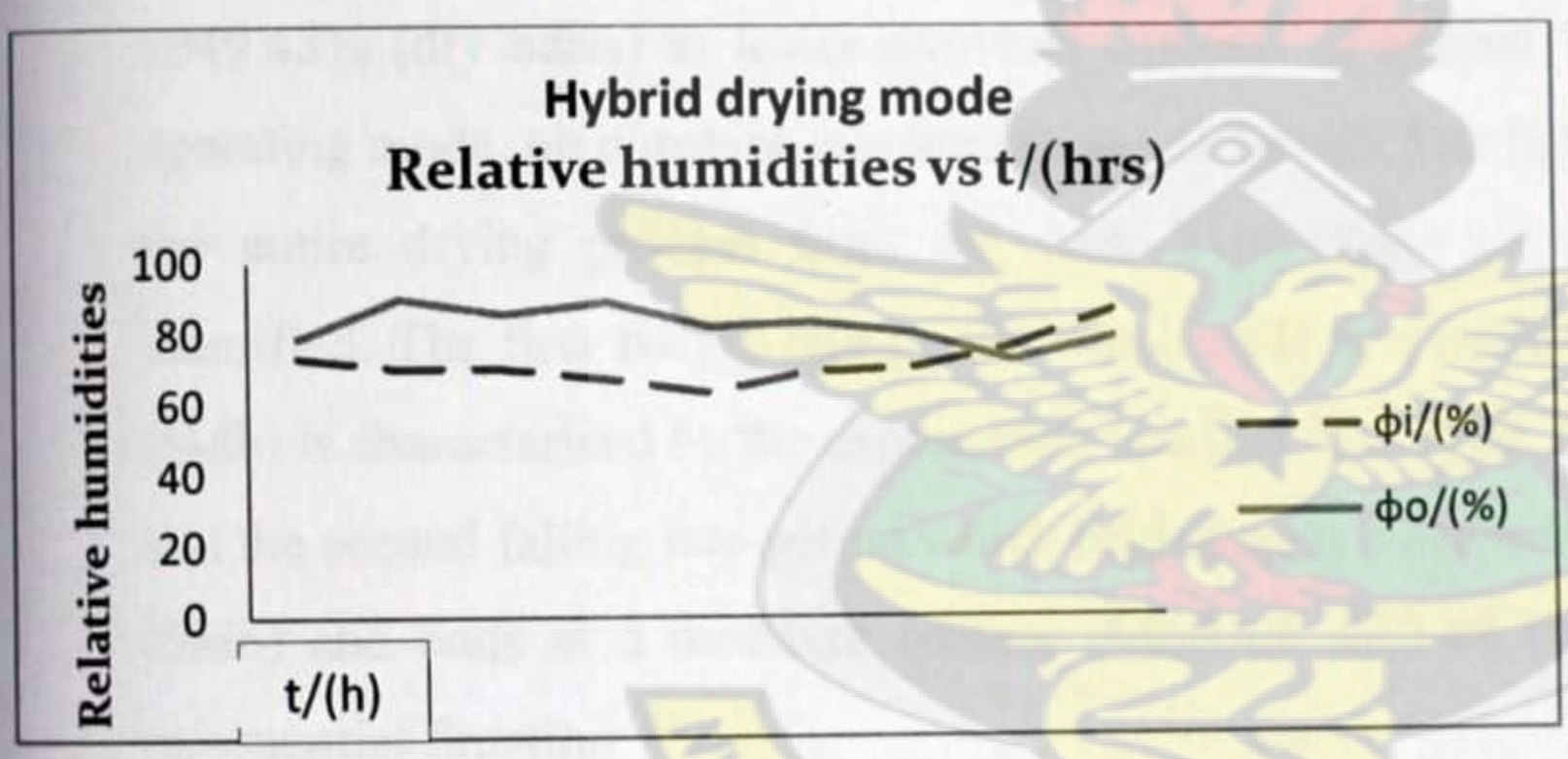

Figure 131 Dryer inlet and outlet relative humidity values versus time in hybrid drying mode

Figure 131 shows the hourly variations in the dryer inlet air and vent outlet air relative humidity values. The dehydration rate from the start of the drying to the 6th hour was very high as indicated by the difference in relative humidity values shown in figure 131. However, the dehydration rate decreased significantly between the 7th and the 8th hour because of the drastic decrease in concentration gradient

Comments:

1. In solar heating mode of operation, results show that the thermal mass was capable of storing part of the absorbed solar energy but the quantities involved are insufficient to sustain night drying, hence, the need for back up heating in solar drying. It was possible to dry a batch of pineapples (weighing 2,262 grammes) in each mode of operation. In the solar mode of operation, the dryer reduced the moisture content of pineapple slices from about 1049.43% to 143.91% (db) in 82,800 seconds; 924.42% to 105.80% in solar drying with back up heating mode in 68,400 seconds; 1049.43% to 183.55% in burner drying mode in 36,000 seconds; and 912.23% to 154.58% in hybrid drying mode in 25,200 seconds. The average values of the moisture pickup efficiency were 15.24%, 15.30%, 17.22%, and 13% in the solar, solar with back up heating, biomass, and hybrid modes of operation respectively.

KNUST

2. During the natural convection solar drying of pineapple from a moisture content of 1049.43% (dry basis) to lower moisture contents of around 143.91% (dry basis) in solar operating mode, no constant-rate period was observed. The falling-rate period characterised the entire drying process from the start. Two stages of the falling-rate period were identified. The first falling rate period which ends at a moisture content (Mc_1) of 624.11 (%db) is characterised by the exponential function M = 1205.7exp (-0.131t)
and the second falling rate period which begins from a moisture content (Mc_2) of 502.15 (%db) and ends at a moisture content (Mc_3) of 273.49 (%db) is characterised by the exponential function

$$M = 592.16\exp(-0.15t)$$

In solar dryer mode with back up heating, the entire dehydration curve falls within the falling rate period with two distinct falling rate regimes manifesting. These falling rate regimes are characterised by the falling equations: The two falling rate regimes are characterised by the underlisted two rate equations:

$$M_1 = 994.77\exp(-0.093t) \text{ and}$$

$$M_2 = 677.7\exp(-0.158t)$$

The point of transition between the two falling rate regimes occurs at a critical moisture content of 541.79 at the 8th hour from the start of drying.

3. In burner drying mode, the rate of dehydration was highest in the bottom tray (tray 1) due to the relatively high heating effect and, hence, improved thermal buoyancy in the plenum. Again dehydration at the bottom, middle, and top trays were all within the falling rate period with the following characteristic functions:

$$M = 1761.9\exp(-0.352t), M = 1634\exp(-0.243t), \text{ and}$$

$$M = 1761.9\exp(-0.352t) \text{ respectively}$$

Hence, it can be concluded that the dehydration of pineapple occurs entirely in the falling rate period.

KNUST

CHAPTER SIX

COMPUTER SIMULATION: PROGRAMS, RESULTS AND DISCUSSION

6.0 Computer simulation code

A complete testing of the air-heating mathematical models developed in chapter 3 to predict the expected performance of the system was carried out by means of three computer simulation codes integrated on one platform - SHM, BHM, and HHM- written using MATLAB. The simulations begin with the selection of a particular programme (SHM, BHM or HHM). The program SHM is for studying the performance of the air-heater in solar heating mode; BHM for investigating the performance of the air heater in burner heating mode; and HHM for predicting the performance of the air heater in hybrid heating mode. Each of the air heater models consists of three elements– AIRFM (the air flow model), DCHM (the drying chamber heating model), and the air heater model (i.e. SHM, BHM or HHM). The air heater model, serves to determine the average temperatures of the air heater and burner components right from inlet to the plenum. The component DCHM takes care of the pertinent drying chamber performance parameters under no load conditions.The data required as user-supplied or internally-generated input in the execution of each of the air heater models are as follows:

a) the temperature of heated air entering the drying chamber which is equal to the mean temperature of plenum air, T_f
b) guess values for the average operating temperatures of the air heater components,
c) the velocity of heated air entering the drying chamber,
d) the intensity of radiation reaching the dryer from the solar simulator,
e) the ambient conditions (temperature of ambient air and the wind speed)
f) the physical and thermal properties of the materials used for constructing the dryer, and
g) the dimensions of the system (plenum inlet gap, vent outlet gap, concrete absorber surface area, plenum glass cover surface area(solar aperture), and upper and lower wall surface areas).

LIBRARY
KWAME NKRUMAH
UNIVERSITY OF SCIENCE & TECHNOLOGY
KUMASI

The general flow chart of the MATLAB programme designed for the air heater model in each heating mode is shown in figure 132. The flow chart shows the simulation procedure

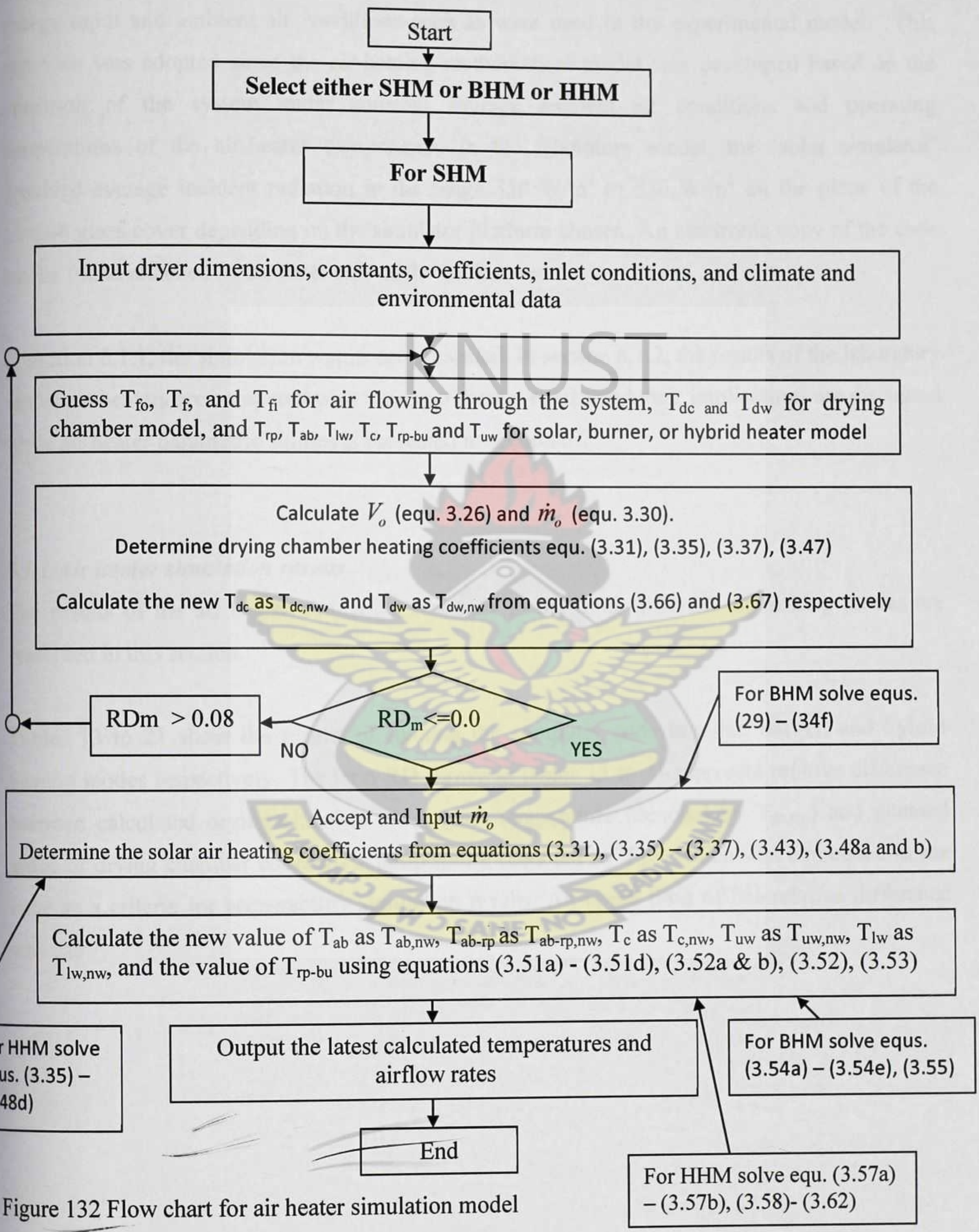

Figure 132 Flow chart for air heater simulation model

6.1 Air-heater performance simulations

The performance of the air-heater was simulated using constant operating values of the incident energy input and ambient air conditions such as were used in the experimental model. This approach was adopted since the air-heating mathematical model was developed based on the operation of the system under constant average ambient air conditions and operating temperatures of the air-heater components. In the laboratory model, the 'solar simulator' provided average incident radiation in the range 350 W/m^2 to 550 W/m^2 on the plane of the plenum glass cover depending on the simulator platform chosen. An electronic copy of the code can be found attached to the inner side of the back cover.

In section 6.1.1, the simulation results are presented. In section 6.1.2, the results of the laboratory model air-heaters are compared with the experimental results and their implications are discussed while air heater parametric studies is presented in section 6.2

6.1.1 Air heater simulation results

The results of the air heater simulation test runs in the three different air heating modes are presented in this section.

Tables 13 to 21 show the results of running the computer code in solar, burner, and hybrid heating modes respectively. The term RD shown in tables 13 to 21 represent relative difference between calculated drying chamber cover glass temperature (denoted by $T_{dc,nw}$) and guessed value of drying chamber cover glass temperature (denoted by T_{dc}) which was embedded in the code as a criteria for acceptability simulation results. An upper limit of 8% relative difference was use

Table 13: SIMULATION RESULTS: ***Solar heating mode 1***

	Plenum inlet gap 0.02 m and vent outlet gap of 0.02 m				
	T_{fi} = 299.5 K, V_i = 0.3 m/s	T_{fi} = 301, V_i = 0.3 m/s	T_{fi} = 303K, V_i = 0.7 m/s	T_{fi} = 302, V_i = 0.7 m/s	T*fi*=302, V*i*= 1m/s
T_{ab} /(K)	296.07	297.26	297.44	298.39	301.47
T_{ab-rp} /(K)	298.21	299.63	300.91	300.6	303.67
T_{rp-bu} /(K)	299.5	301	303	302	305
T_{lw} /(K)	341.34	345.4	370.83	346.04	346.4
T_{dc} /(K)	286.52	288.66	291.54	334.56	335
T_{dw} /(K)	302.56	304.77	307.7	304.4	302
v_o/(m/s)	0.056	0.07	0.09	0.0635	0.068
$\dot{m}_o$ /(kg/s)	0.0065	0.008	0.01	0.072	0.0076
$\dot{Q}_{tm}$ /(W)	300	240.7	138.44	188.42	242.3
$\Delta\dot{\psi}$ /(kW)	2569.7	2128.6	1532	2460	1560
η_c/(%)	0.14	0.15	0.14	0.15	0.1
$(\Delta S)_T$/(kJ/K)	-334.44	-251.76	-177.67	-246.13	-246.13
RD	0.073	0.07	0.06	0.066	0.006

Table 14 SIMULATION RESULTS: ***Solar heating mode 2***

	Plenum inlet gap 0.04 m and vent outlet gap of 0.03 m				
	T_{fi} = 297.9 K, V_i = 1.4 m/s	T_{fi} = 298.9, V_i = 1.7 m/s	T_{fi} = 298.6K, V_i = 2.0 m/s	T_{fi} = 299.9, V_i = 1 m/s	T_{fi}=299.3, V_i= 1m/s
T_{ab} /(K)	294.89	295.08	294.46	296.3	395.23
T_{ab-rp} /(K)	296.77	297.5	297.05	298.53	297.8
T_{rp-bu} /(K)	297.9	298.1	298.6	299.4	299.3
T_{lw} /(K)	333.54	346.1	351.3	345.1	350.02
T_{dc} /(K)	325.4	324.96	323.03	330.07	329.42
T_{dw} /(K)	302.3	292.1	292.69	299.9	291.8
v_o/(m/s)	0.184	0.339	0.475	0.39	0.45
$\dot{m}_o$ /(kg/s)	0.0026	0.0047	0.0065	0.0054	0.006
$\dot{Q}_{tm}$ /(W)	456.64	541.5	363.24	475.90	731.86
$\Delta\dot{\psi}$ /(kW)	2415	3755	2460	3080	3420
η_c/(%)	0.056	0.15	0.14	0.14	0.18
$(\Delta S)_T$ /(kJ/K)	-589.57	-378	-125.7	-201.1	-302.96
RD	0.074	0.027	0.033	0.066	0.01

Table 15 SIMULATION RESULTS: ***Solar heating mode 3***

	Plenum inlet gap 0.06 m and vent outlet gap of 0.04 m		
	$T_{fi} = 303$ K, $V_i = 2.4$ m/s	$T_{fi} = 295.7$, $V_i = 2.7$ m/s	$T_{fi} = 302$K, $V_i = 0.7$ m/s
T_{ab} /(K)	299.6	291.97	298.25
T_{ab-rp} /(K)	301.72	294.3	300.59
T_{rp-bu} /(K)	303	295.7	302
T_{lw} /(K)	343.72	343.1	347.72
T_{dc} /(K)	325.71	517.25	332.57
T_{dw} /(K)	300.4	290	295.71
v_o/(m/s)	0.311	0.449	0.315
$\dot{m}_o$ /(kg/s)	0.057	0.0083	0.0058
$\dot{Q}_{tm}$ /(W)	453.2	348.35	358.52
$\Delta\dot{\psi}$ /(kW)	3120	2280	3420
η_c/(%)	0.15	0.17	0.166
$(\Delta S)_T$ /(kJ/K)	-188	-391.76	-196.3
RD	0.007	0.045	0.01

Table 16 SIMULATION RESULTS: ***Burner heating mode 1***

	Plenum inlet gap 0.02 m and vent outlet gap of 0.02 m		
	T_{fi} = 297.3 K, V_i = 0.7 m/s	T_{fi} = 297.4, V_i = 1 m/s	T_{fi} = 297.2K, V_i = 1.0 m/s
T_{ab} /(K)	387	391.45	391.8
T_{ab-rp} /(K)	357.66	356.42	356.2
T_{rp-bu} /(K)	339.99	335.33	334.7
T_{lw} /(K)	337	337	391.8
T_{dc} /(K)	329.96	327.78	327
T_{dw} /(K)	299.6	299.49	296.1
v_o/(m/s)	0.351	0.41	0.476
$\dot{m}_o$ /(kg/s)	0.0033	0.00375	0.0043
Q_{tm} /(W)	407413.9	458813.6	517155.62
$\Delta\dot{\psi}$ /(kW)	4470	3490	4820
η_c/(%)	0.0000012	0.000000.96	0.0000013
$(\Delta S)_T$ /(kJ/K)	881.54	1061.18	1080.73
RD	0.082	0.064	0.038

Table 17 SIMULATION RESULTS: ***Burner heating mode 2***

	Plenum inlet gap 0.04 m and vent outlet gap of 0.04 m		
	T_{fi} = 297.5 K, V_i = 0.7 m/s	T_{fi} = 298.3, V_i = 1 m/s	T_{fi} = 298 K, V_i = 0.3 m/s
T_{ab} /(K)	393.2	395.45	413.42
T_{ab-rp} /(K)	356.4	357.58	360.59
T_{rp-bu} /(K)	334.33	334.78	328.77
T_{lw} /(K)	337.2	338	337.7
T_{dc} /(K)	329.64	327.98	333.16
T_{dw} /(K)	296.53	291.48	296.61
v_o/(m/s)	0.496	0.52	0.51
$\dot{m}_o$ /(kg/s)	0.0068	0.007	0.0069
Q_{tm} /(W)	531939.97	553299.86	767825.2
$\Delta\dot{\psi}$ /(kW)	4700	61500	3000
η_c/(%)	0.00000198	0.00000.25	0.0000009
$(\Delta S)_T$ /(kJ/K)	1114.18	1146.2	1606.60
RD	0.047	0.003	0.042

Table 18 SIMULATION RESULTS: ***Burner heating mode***

	Plenum inlet gap 0.06 m and vent outlet gap of 0.04 m		
	T_{fi} = 298.2 K, V_i = 0.7 m/s	T_{fi} = 298.5, V_i = 1.4 m/s	T_{fi} = 298.9 K, V_i = 0.7 m/s
T_{ab} /(K)	396.08	417.15	421.41
T_{ab-rp} /(K)	358.23	362.24	363.6
T_{rp-bu} /(K)	335.44	329.17	328.81
T_{lw} /(K)	337.9	338.2	338.6
T_{dc} /(K)	329.8	325.3	328.55
T_{dw} /(K)	289.9	286.91	286.1
v_o/(m/s)	0.63	0.63	0.54
$\dot{m}_o$ /(kg/s)	0.01	0.011	0.0096
Q_{tm} /(W)	571209.31	793246.34	350155.77
$\Delta\dot{\psi}$ /(kW)	7530	7790	15890
η_c/(%)	0.00000462	0.00000.345	0.00000529
$(\Delta S)_T$ /(kJ/K)	1143.57	1665.13	1749.92
RD	0.0057	0.032	0.014

Table 19 SIMULATION RESULTS: ***Hybrid heating mode 1***

	Plenum inlet gap 0.02 m and vent outlet gap of 0.02 m		
	T_{fi} = 298.2 K, V_i = 0.3 m/s	T_{fi} = 298.5, V_i = 0.7 m/s	T_{fi} = 299.4 K, V_i = 0.3 m/s
T_{rp-bu} /(K)	386.9	387.6	396.8
T_{dc} /(K)	334	330.62	332.8
T_{dw} /(K)	295	292.53	277.78
v_o/(m/s)	0.215	0.357	0.41
$\dot{m}_o$ /(kg/s)	0.002	0.0033	0.0037
$\dot{Q}_{tm}$ /(W)	183727	244354.8	368490.7
$\Delta\dot{\psi}$ /(kW)	201860	214700	232700
η_c/(%)	0.00000412	0.0000053	0.0000042
$(\Delta S)_T$/(kJ/K)	55763.7	244354.8	368490.7
RD	0.028	0.01	0.05

Table 20 SIMULATION RESULTS: ***Hybrid heating mode 2***

	Plenum inlet gap 0.04 m and vent outlet gap of 0.04 m		
	T_{fi} = 299.8 K, V_i = 0.3 m/s	T_{fi} = 299.3, V_i = 0.3 m/s	T_{fi} = 298.9 K, V_i = 1.4 m/s
T_{rp-bu} /(K)	404.81	396.34	390.4
T_{dc} /(K)	334.49	333.6	325.4
T_{dw} /(K)	295.4	292.24	284.43
v_0/(m/s)	0.28	0.22	0.62
$\dot{m}_o$ /(kg/s)	0.0039	0.003	0.008
$\dot{Q}_{tm}$ /(W)	358138.65	478632	512876
$\Delta\dot{\psi}$ /(kW)	156890	192280	150200
η_c/(%)	0.0000034	0.0000022	0.0000047
$(\Delta S)_T$ /(kJ/K)	85913.27	78205	104655
RD	0.001	0.01	0.04

Table 21 SIMULATION RESULTS: ***Hybrid heating mode 3***

	Plenum inlet gap 0.06 m and vent outlet gap of 0.04 m		
	T_{fi} = 299.4 K, V_i = 0.3 m/s	T_{fi} = 301.2, V_i = 0.3 m/s	T_{fi} = 300.1 K, V_i = 0.3 m/s
T_{rp-bu} /(K)	401.1	419.1	403.9
T_{dc} /(K)	333.7	335.34	333.8
T_{dw} /(K)	288.4	291.6	293.6
v_0/(m/s)	0.58	0.55	0.42
$\dot{m}_o$ /(kg/s)	0.01	0.0098	0.0076
$\dot{Q}_{tm}$ /(W)	570158.8	615591.96	655142.8
$\Delta\dot{\psi}$ /(kW)	130530	134020	146800
η_c/(%)	0.0000048	0.0000093	0.0000034
$(\Delta S)_T$/(kJ/K)	110683.6	997.02	88499.5
RD	0.018	0.017	0.0036

UST

6.1.2 Comparison of simulation and experimental results on air heater

In order to gain confidence in the simulation code as a tool for predicting the ventilation performance of the dryer, a validation process is performed to ascertain the accuracy of the code within acceptable limits. Results of the solar, burner, and hybrid air heating simulations are compared with experimental results and presented in tables 22 to 25. Causes of any wide deviation between the recorded and simulated values are examined for adjustments to be made where necessary. For the experimental results, the lower wall, drying chamber cover glass, drying chamber wall, absorber top surface, rock pile – absorber interface and rock pile –burner interface temperatures are determined form average values recorded. These average values are confirmed with those obtained using the model equations for each heating mode. The same dimensions and the prevailing environmental conditions in the trial of the physical MNCSCDBBH model have been used to run the simulation code. The general input simulation parameters are listed in table 5.1. Tables 22 and 23 compare the simulation results (headed Sim) with those recorded from experiment (headed expt) of the model in solar heating mode whereas tables 24 and 25 compare results for burner and hybrid heating modes respectively. The solar heater simulation code (SHM) predicts the temperatures to within 0.03% and 18.2% relative difference (RD). The deviation of the predicted lower temperature in solar heating mode at a plenum inlet gap of 0.02, fluid inlet velocity of 0.7 m/s, and a fluid inlet temperature of 303 K resulted in the extreme relative difference of 18.2%. In burner heating mode, the simulation code (BHM) predicts the temperatures to within 1.1% and 29.5%. The extreme case of 29.5% relative difference occurred at a plenum inlet gap of 0.02 m for the rock bed –burner interface temperature at a fluid inlet temperature of 297.2 K. and a velocity of 1 m/s

The relative difference range was 2.5% to 20% for hybrid heating mode with the extreme relative difference value of 20% occurring at a plenum inlet opening of 0.04 m and inlet temperature of 298.9 K.

Results Comparison of simulation results (headed Sim) and experimental results (headed expt) each with the relative difference D below it. $D = \left|\{(\text{Sim} - \text{expt})/\text{exptR}\}\right| \times 100\%$

Table 22 Comparison of simulation results (headed Sim) and experimental results (headed expt)-Solar heating mode 1

	Plenum inlet gap 0.02 m		and vent outlet gap 0.02 m							
$T_{f,i}$/(K)	299.5		301		303		302		302	
V_i/(m/s)	0.3		0.3		0.7		0.7		1	
	EXPT	SIM	EXPT	SIM	EXPT	SIM	EXPT	SIM	EXPT	SIM
T_{ab}	299.4	296.04	316.8	297.3	325	297.4	324	298.4	325	301.5
D/%	1.12		6.2		8.5		7.9		7.2	
T_{ab-rp}	300.6	298.2	308.3	299.6	305.7	300.9	301.6	300.6	307.9	303.7
D/%	0.798		2.8		1.6		1.0		1.4	
T_{rp-bu}	298.7	299.5	308.1	301	305	303	305	302	308	305
D/%	0.27		2.3		0.66		0.98		0.97	
T_{lw}	298.6	341.3	305.2	345.4	303.3	370.8	302.8	346	304	346.4
D/%	12.5		11.6		18.2		12.5		12.2	
T_{dc}	302.1	286.5	337.8	288.7	328	291.5	335.3	334.6	332	335
D/%	5.2		14.5		11.1		0.21		0.896	
T_{dw}	298.9	302.6	306.3	304.8	315	307.7	316.5	304.4	315	302
D/%	1.2		0.49		2.3		3.8		3.8	

Table 23 Comparison of simulation results (headed Sim) and experimental results (headed expt) - solar heating mode 2

Plenum inlet gap 0.04 m and vent outlet gap 0.03 m

T_{fi}/(K)	297.9		298.9		298.6		299.9		299.3	
V_i/(m/s)	1.4		1.7		2.0		1.0		1.0	
	EXPT	SIM	EXPT	SIM	EXPT	SIM	EXPT	SIM	EXPT	SIM
T_{ab}	309.8	294.9	319	295.1	317	294.5	321	296.3	318	395.2
D/%	4.8		7.5		7.1		7.7		19.5	
T_{ab-rp}	298.8	296.8	301.3	297.5	300.5	297.1	303.3	298.5	301.2	297.8
D/%	0.67		1.3		1.1		1.06		1.1	
T_{rp-bu}	298	297.9	301	298.9	299.2	298.6	302.8	299.4	300	299.3
D/%	0.03		0.37		0.2		1.13		0.23	
T_{lw}	298.3	333.5	300.7	346.1	299.2	351.3	300.8	345.1	299.5	350.0
D/%	10.6		13.1		14.8		12.8		14.4	
T_{dc}	328	325.4	336	325.0	334.6	323.0	334.5	330.1	335	329.4
D/%	0.79		3.3		3.5		1.3		1.7	
T_{dw}	303	302.3	313.1	292.1	311.2	292.7	314	299.9	311.4	291.8
D/%	0.23		6.7		5.9		4.5		6.3	

Table 24: Comparison of simulation results (headed Sim) and experimental results (headed expt) ***-Burner heating mode 1***

	Plenum inlet gap 0.02 m and vent outlet gap of 0.02 m					
	T_{fi} = 297.3 K, V_i = 0.7 m/s		T_{fi} = 297.4, V_i = 1 m/s		T_{fi} = 297.2K, V_i = 1.0 m/s	
	EXPT	SIM	EXPT	SIM	EXPT	SIM
T_{ab} /(K)	387	314	391.45	338	391.8	341
D/(%)	18.9		13.7		12.97	
T_{ab-rp} /(K)	357.66	314.3	356.42	337.9	356.2	345.8
D/(%)	2.1		5.2		2.9	
T_{rp-bu} /(K)	339.99	356	335.33	452	334.7	475
D/(%)	4.5		25.8		29.5	
T_{lw} /(K)	337	326.7	337	328.4	391.8	321.2
D/(%)	3.1		2.6		18.0	
T_{dc} /(K)	329.96	309.5	327.78	314	327	341
D/(%)	6.2		4.2		4.1	
T_{dw} /(K)	299.6	303	299.49	308	296.1	309
D/(%)	1.1		2.8		4.2	

Table 25 Comparison of simulation results (headed Sim) and experimental results (headed expt) -***Hybrid heating mode 2***

	Plenum inlet gap 0.04 m and vent outlet gap of 0.04 m					
	T_{fi} = 299.8 K, V_i = 0.3 m/s		***T_{fi} = 299.3, V_i = 0.3 m/s***		***T_{fi} = 298.9 K, V_i = 1.4 m/s***	
	SIM	EXPT	SIM	EXPT	SIM	EXPT
T_{rp-bu} /(K)	404.81	464	396.34	476	390.4	488
D/(%)	12.8		16.7		20	
T_{dc} /(K)	334.5	343	333.6	347	325.4	349
D/(%)	2.5		3.9		6.7	
T_{dw} /(K)	295.4	315	292.24	318	284.43	321
D/(%)	6.2		8.1		11.4	

KNUST

6.2 Parametric studies and optimization of air ventilation process

In order to determine the optimum plenum inlet area to vent outlet area ratio of the dryer for effective ventilation, the air flow through the dryer is examined in relation to various design parameters of the dryer, under a given irradiation condition in solar heating mode. Figures 133, 134, and 135 show the graphs of air mass flow rate, air outlet velocity and collector efficiency versus inlet fluid temperature for the plenum inlet to vent outlet area ratios (A_p/A_o) of 1, 1.33, and 1.5 respectively. In each parametric study, and for each area ratio the simulation code was run a number of times with different values of fluid inlet temperature at a constant insolation of 350 W/m^2 on the middle plane of the plenum cover glass while observing changes in the air mass flow rate (mo), air outlet velocity (vo), and collector efficiency.

KNUST

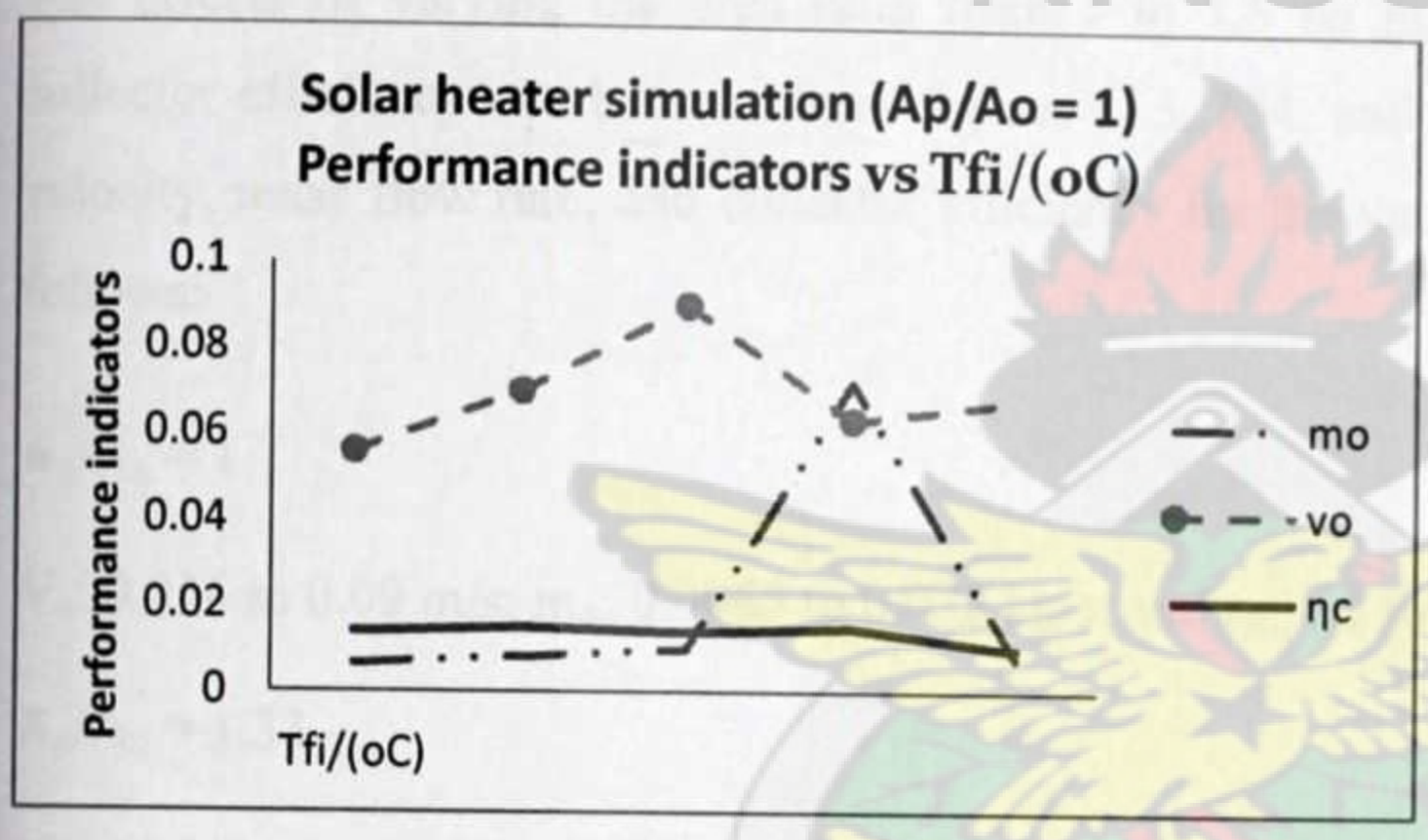

Figure 133 Parametric studies-solar heating mode 1

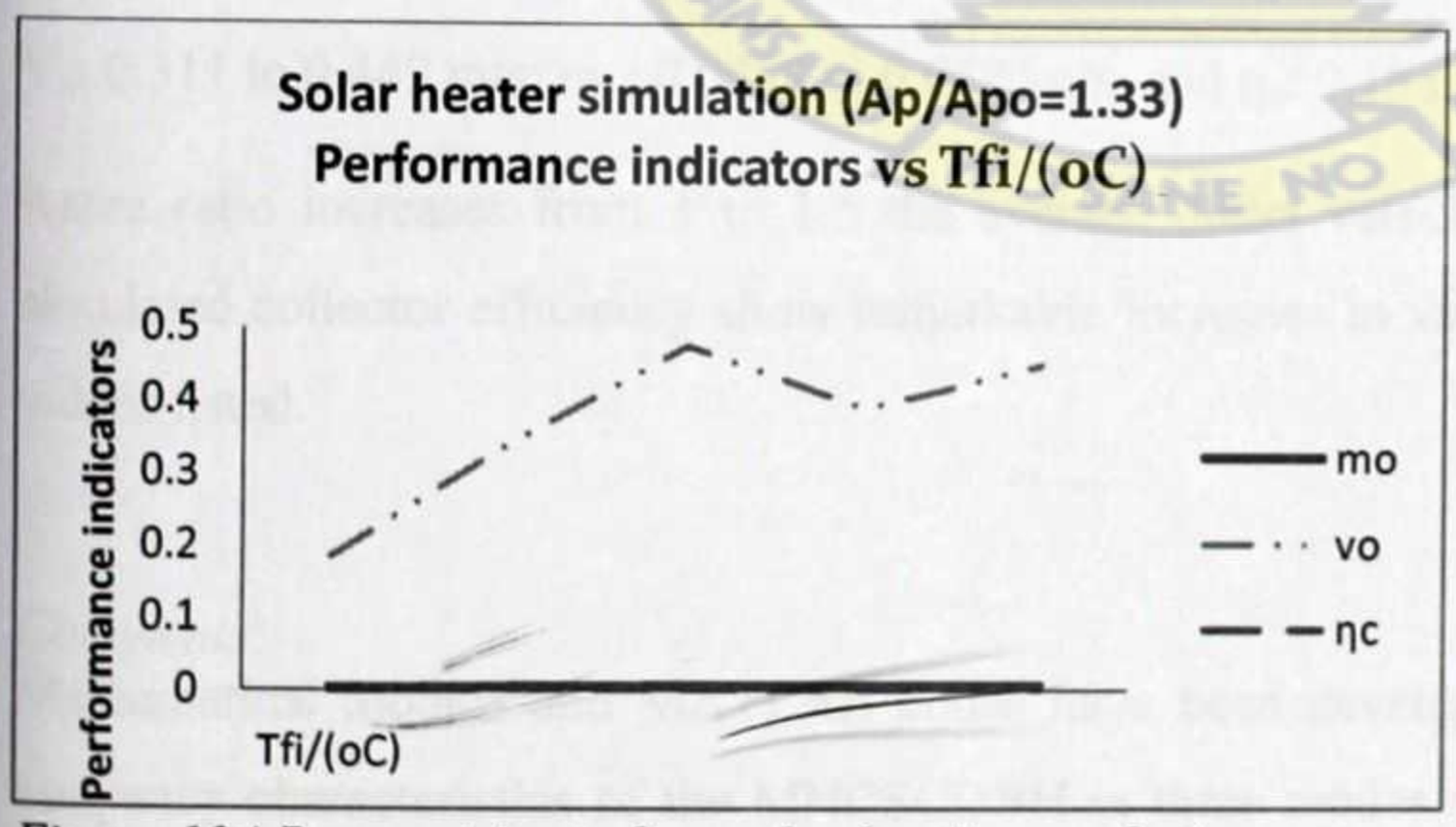

Figure 134 Parametric studies-solar heating mode 2

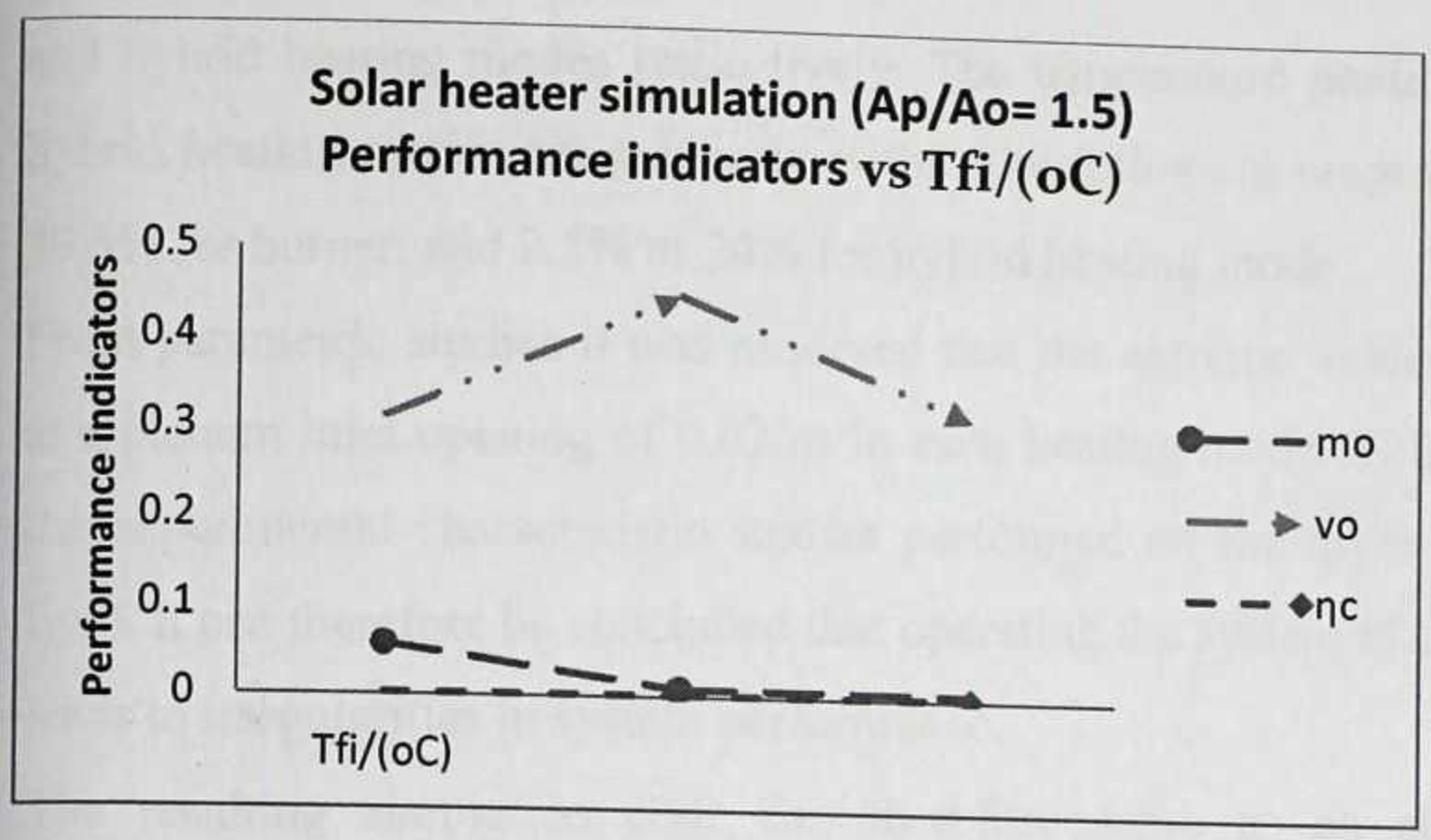

Figure 135 Parametric studies-solar heating mode 3

KNUST

The effects of varying the area ratio from 1 to 1.5 on mass flow rate, outlet velocity, and collector efficiency can be seen from figures 133, 134, and 135. The range of values of outlet velocity, mass flow rate, and collector efficiency for the various area ratios are summarized as follows:

$A_p/A_o = 1$

V_o: 0.056 to 0.09 m/s; m_o: 0.0065 to 0.072 kg/s; and η_c: 0.1 to 0.15

$A_p/A_o = 1.33$

V_o: 0.184 to 0.475 m/s; m_o: 0.0026 to 0.0065 kg/s; and η_c: 0.056 to 0.15

$A_p/A_o = 1.5$

V_o: 0.311 to 0.449 m/s; m_o: 0.0058 to 0.057 kg/s; and η_c: 0.15 to 0.17

Aarea ratio increases from 1 to 1.5 the average outlet velocity, average mass flow rate, and simulated collector efficiency show remarkable increases in value as indicated by the ranges of values listed.

Comments:

Mathematical models and MATLAB codes have been developed to simulate the thermal and buoyancy characteristics of the MNCSCDBH in three modes of heating namely, solar, burner,

and hybrid heating modes respectively. The temperature predictions for the solar, burner, and hybrid heating modes are generally within the following ranges 0.03 to 18.2 for solar; 1.1% to 29.5% for burner; and 2.5% to 20% for hybrid heating mode.

From parametric studies it was observed that the extreme values of relative difference occurred at a plenum inlet opening of 0.02 m in each heating mode. This result confirms the findings of the experimental characteristic studies performed on the dryer (refer to section 5.1 of chapter five). It can therefore be concluded that operating the system at a plenum inlet opening of 0.02 m leads to irregularities in system performance.

The resulting simulation code can therefore serve as an effective tool for designing the MNCSCDBH for optimum performance.

KNUST

CHAPTER SEVEN

CONCLUSIONS AND SUGGESTIONS FOR FURTHER WORK

7.0 Conclusions

The main objective of the research was to study the thermal buoyancy characteristics and possible drying conditions of a mixed-mode natural convection solar crop dryer with integrated collector-storage and back-backup heater through modeling and experimental studies.

. A typical small-scale mixed-mode natural convection solar crop dryer (MNCSCDBH) was designed and constructed. Two categories of experimental investigations were carried out on the laboratory model of the MNCSCDBH with six (6) infra- red lamps and a 1800 Watts electric heater as heat sources. The first category of experiments was conducted under no load conditions as part of a general thermal characteristics study of the experimental dryer under varied plenum inlet and vent outlet gap conditions. The second category of tests which was conducted at maximum loading capacity of 2,262 grammes using fresh pineapples in four heating modes namely, solar drying mode, solar drying with back up heating, drying in backup heating mode only, and hybrid drying mode, to determine the effect of the heating modes on drying time and drying effectiveness. The control drying test for the second category of test is the solar drying mode since results obtained in solar drying mode were used as baseline values for comparative analysis. An integrated mathematical model was developed and used for simulating the performance of the air-heating system in the three heating modes employed. The validity of the predicted results was checked by comparing some pertinent simulation results of the air-heating processes with experimental data. The models were fine tuned and used for some parametric studies the results of which were presented in chapter six. Considering the results of the present study, the following conclusions can be drawn:

1. The dryer characteristic study has shown for plenum inlet gap to vent outlet gap ratios of 1:1 and 1.33 in each of the three heating modes that the air flow through the dryer is inadequate and that temperatures in the system components become high giving rise to relatively high plenum inlet temperatures and low air heater

efficiency. It was also noticed under these conditions that the relative humidity of the air exiting the vent did not follow any particular pattern.

2. In solar heating mode the ambient air relative humidity values covering the 9 experiments conducted ranged between 51% and 95% whereas the mean ambient temperature values ranged between 22.7 °C and 32.2 °C. The calculated thermal energy stored during solar heat charging ranged between 0.029 MJ and 0.251 MJ. Clearly, these conditions indicate that drying will not be effective on some days if back up heating is not employed since the quantities of energy absorbed are too small to sustain night drying.
3. At a plenum inlet gap to vent outlet gap ratio of 1.5:1 comparatively high mass flow rates of between 0.0141 and 0.0798 kg/s were recorded with comparatively high air heater efficiency values of between 0.093% and 1.89%. Against this background it is concluded that a plenum inlet gap of 6 cm and a vent outlet gap of 4 cm optimises the thermal performance of the dryer. For design purposes a plenum inlet gap to vent outlet gap ratio of 1.5:1 optimises air flow through the dryer.
4. It was possible to dry a batch of pineapples (weighing 2,262 grammes) in each mode of operation. In the solar mode of operation, the dryer reduced the moisture content of pineapple slices from about 1049.43% to 143.91% (db) in 23 hours; 924.42% to 105.80% in solar drying with back up heating mode in 19 hours; 1049.43% to 183.55% in burner drying mode in 10 hours; and 912.23% to 154.58% in hybrid drying mode in 7 hours. These results are in close conformity with the observations of Madhlopa et al (2006). The average values of the moisture pickup efficiency were 15.24%, 15.30%, 17.22%, and 13% in the solar, solar with back up heating, biomass, and hybrid modes of operation, respectively. These results are in conformity with the observations of Madhlopa et al. (2006) and Elepano and Satairapan (2001). In solar- biomass mode of drying, Elepano and Satairapan 2001) noted that the dryer dried 50 kilograms of sliced pineapple fruit from a moisture content of 85% w.b. down to 20% w.b. in 18 hours.
5. The falling-rate period characterised the entire drying process in solar drying mode. Two stages of the falling-rate period were identified. The first falling rate period which ended at a moisture content (Mc_1) of 624.11 (%db) was characterised by the exponential function $M = 1205.7\exp(-0.131t)$, whereas the second falling rate period which started from a moisture content (Mc_2) of 502.15 (%db) and ended at a

moisture content (Mc_3) of 273.49 (%db) was characterised by the exponential function $M = 592.16 \exp(-0.15t)$

6. In solar dryer mode with back up heating, the entire dehydration curve fell within the falling rate period with two distinct falling rate regimes manifesting. These falling rate regimes were characterised by the following equations:

$$M_1 = 994.77 \exp(-0.093t) \text{ and}$$

$$M_2 = 677.7\exp(-0.158t)$$

7. In burner drying mode, the rate of dehydration was highest in the bottom tray (tray 1) due to the relatively high heating effect and, hence, improved thermal buoyancy in the plenum. Again dehydration at the bottom, middle, and top trays were all within the falling rate period with the following characteristic functions:

$$M = 1761.9\exp(-0.352t),$$

$$M = 1634\exp(-0.243t), \text{ and}$$

$$M = 1761.9\exp(-0.352t), \text{ respectively.}$$

Hence, it can be concluded that the dehydration of pineapple occurs entirely in the falling rate period. These conclusions are in conformity with the observations of Ayensu (1997) and Aggary *et al* (2013) that no constant rate period occurs in the drying curves for unblanched and blanched pineapple samples.

8. Mathematical models and MATLAB codes have been developed to predict the thermal and buoyancy characteristics of the MNCSCDBH. The temperature predictions for the solar, burner, and hybrid heating modes are generally accurate within the following ranges 0.03 to 18.2% for solar; 1.1% to 29.5% for burner; and 2.5% to 20% for hybrid heating mode
9. Even though some discrepancies were found between the experimental performance indicators and their corresponding values predicted by the model as presented in this study, the code can be considered to be quite satisfactory in predicting the thermal and buoyancy performance of the dryer under no load conditions
10. From the parametric studies it was observed that the extremely large values of relative difference occurred at a plenum inlet opening of 0.02 m in each heating mode. This result confirms the findings of the experimental characteristic studies performed on the dryer. It can further be concluded that a plenum inlet area gap to vent outlet gap ratio of 1.5 optimises the performance of the dryer.

7.1 Suggestions for further studies

A prototype of the dryer could not be built as a result of time and financial constraints. It is apparent from the findings of this study that some further work is necessary in refining and verifying some of the deductions made. The following areas require further work in order to consolidate the observations made.

1. A horizontal arrangement was adopted for building the thermal mass. It is recommended that further model studies be conducted to investigate the effects of varying the orientation of the thermal mass on system availability (exergy), collector efficiency, and the overall performance of the dryer.

2. It is recommended that a commercial scale type of the dryer be built to investigate the effect of loading density on the dryer. Adequate experimental data on the full capacity of the dryer must be established and used to validate the performance of the system in order to establish conclusively the findings of this study.

3. The model developed only investigates the performance of the dryer under no load conditions because of time constraints. However, a comprehensive algorithm has been developed to that effect in section 2.9 of chapter two. Secondly, sufficient experimental data has been collected from the load tests on the laboratory model. It is therefore recommended that a model capable of predicting the performance of the dryer under load conditions be built and validated against the data collected on the small scale model for each operating mode.

KNUST

LIST OF REFERENCES

ABOUL-ENEIN, S., EL-SEBAII, RAMADAN, M.R.I., EL-GOHARY, H.G., 2000. Parametric study of a solar air heater with and without thermal storage for solar drying. Renewable Energy 21, 505–522.

Akyurt, M., Selc¸uk, M.K., 1973. A solar drier supplemented with auxiliary heating systems for continuous operation. Solar Energy 14, 313–320.

AKYURT, M., SELC¸UK, M.K., 1973. A solar drier supplemented with auxiliary heating systems for continuous operation. Solar Energy 14, 313–320.

ALAM, A. and SHOVE, G.C. 1973. Simulation of soybean drying. *Trans. am. Soc. agric. Engrs*., vol. 16, no. 1, p.134-136.

ANON. 1962. *Wealth of India, Raw Materials*. vol. 6 (L-M), p.293-297. Coun. Sci. ind. Res., New Delhi. Quoted by Ingram and Humphries, 1972.

ASHRAE 1977. *Handbook and Product directory*:. *Fundamentals*: ASHRAE, Inc., Atlanta, USA.

ASHRAE. 1989. *Fundamentals handbook* (SI edition). ASHRAE Inc., Atlanta, USA.

ASHRAE 1993. *Fundamentals handbook*, ASHRAE Inc., Atlanta, USA

ASHRAE. 2009. *Fundamentals handbook* (SI edition). ASHRAE Inc., Atlanta, USA.

AYENSU, A., 1997. Dehydration of food crops using a solar dryer with convective heat flow. Solar Energy 59, 121–126

AYENSU, A., ASIEDU-BONDZIE, V., 1986. Solar drying with convective self flow and energy storage. Solar & Wind Technology 3, 273–279.

BALA, B.K. and WOODS, J.L. 1984. Simulation of Deep Bed Malt Drying. *J. agric. Engng. Res*., vol. 30, p. 235-244.

BANSAL, N.K. and GEORGE, O.P. (1993) Solar drying in India and other Asian countries, in Drying '80 (ed. A.S. Mujumdar), Hemisphere, New York, p. 117

BAKER, C.G.J. (1997) Industrial drying of foods. Blackie academy and professional, an imprint of Chapman and Hall, London, p.16 – 21.

BAKKER-ARKEMA, BROOK, R.C, and LEREW, L.E. 1978. Cereal grain drying. In *Advances in Science and Technology*, (Y. Pomeranz ed.), vol. 2. American Association of Cereal Chemists Incorporated, St. Paul, Minnesota, p. 1-90.

BARNELL, H.B. (1974). *Biology and the food industry in the institute of Biology studies in Biology No 45*. Edward Arnold Publishers, London.

BARRE, H.J., BAUGHMAN, G.R. and HAMDY, M.Y. 1971. Application of the logarithmic model to cross-flow bed grain drying. *ASAE*, vol. 14, p.1061-1064.

BARRE, H.J. and HAMDY, M.Y. 1974. Optimal filling rates for in-storage drying. *Trans. ASAE*, vol. 17, no. 4, p.705-710.

BASSEY, M.W., WHITFIELD, M.J., KORAMA, E.Y., 1987. Problems and solutions for natural convection solar crop drying. In: Bassey, M.W., Schmidt, O.G. (Eds.), Solar Crop Drying in Africa – Proceedings of Food Drying Workshop, Dakar, IDRC, Ottawa, Canada.

BABBITT, J.D. 1949. Observations on the adsorption of water vapour by wheat. *Can. J. Res. Sec.* F. 27: 55-72.

BECKER, H.A. and SALLANS, H. R. 1956. A study of desorption isotherms of wheat at 25°C and 50°C. *Cereal Chem*., vol. 33, no. 2, p. 79-91.

BENA, B., FULLER, R.J., 2002. Natural convection solar dryer with biomass backup heater. Solar Energy 72, 75–83.

BLOOME, P. D. and SHOVE, G. C. 1971. Near Equilibrium Simulation of Shelled Corn Drying. *Transactions of the ASAE*, Vol. 14, No. 4,pp. 709-712.

BOYCE, D.S. 1965. Grain moisture and temperature changes with position and time during through drying. *J. agric. Engng. Res*., 10(4): 333-341.

BRAMHALL, G. 1979. Sorption diffusion in wood. *Wood Sci*. 12(1): 3-13

BRENNDORFER, B., KENNEDY, L., OSWIN BATEMAN, C.O., TRIM, D.S., MREMA, G.C. and WEREKO-BROBBY, C. 1987. *SOLAR DRYERS- their role in post-harvest processing*. London: Commonwealth Science Secretariat.

BROOKER, D.B., BAKKER-ARKEMA, F.W. and HALL, C.W. 1974. *Drying Cereal Grains*. Westport, Connecticut: AVI Publishing Co., Inc.

BRUIN, S. and LUYBEN, K.Ch.A.M. (1980). Drying of food materials: a review of recent developments, in Advances in Drying, Vol. 1 (ed. A.S. Mujumdar), Hemisphere, NY, pp. 115-216.

BUNN, J.M., HENSON Jr., W.H. and WALTON, L.R. 1972. Drying equation for high moisture materials. *J. agric. Engng. Res*., 17, 343-347.

ÇENGEL, Y. A. and BOLES, M. A. *Thermodynamics: An Engineering Approach, 2nd* ed, McGraw-Hill, 2006, pp. 606 - 631

KNUST

CENKOWSKI, S., JAYAS, D.S. and PABIS, S. 1993 Deep-bed grain drying:- a review of particular theories. *Drying Technology*, 11(7), 1553-1581.

CHIANG, WIN-CHIN and PETERSEN, J.N. 1985. Thin-layer air drying of French fried potatoes. *Journal of Food Technology,* vol. 20, p.67-78.

CHINNAN, M.S. and YOUNG, J.H. 1977. A Study of diffusion equations describing moisture movement in peanut pods- I: comparison of vapour and liquid diffusion equations. *Trans. of ASAE* 20, 3, 539-546.

CHHINNAN, M.S. 1984. Evaluation of selected mathematical models for describing thin-layer drying of in-shell pecans. *Trans. ASAE* 27, 610-619.

CHIRIFE, J. and CACHERO, R.A. 1970. Through-circulation drying of tapioca root. *Journal of Food Science* 35, 364-368.

CHIRIFE, J. 1971. Diffusional process in the drying of tapioca root. *Journal of Food Science* 36, 327-330.

CHUNG, D.S. and PFOST, H.B. 1967. Adsorption and desorption of water vapour by cereal grains and their products. Part I: Heat and free energy change of adsorption and desorption. *Trans. am. Soc. agric. Engrs.*, 10 (4), 549-551 and 555.

CHUNG, D.S. and PFOST, H.B. 1967. Adsorption and desorption of water vapour by cereal grains and their products. Part II: Development of the general isotherm equation. *Trans. am. Soc. agric. Engrs.*, 10 (4), 552-555.

CLARK, R.G. and LAMOND, W.J. 1968. Drying of wheat in 2ft beds. I. *J. agric. Engng. Res.*, vol. 13, no. 2, p. 141.

CRANK, J. 1975. *The mathematics of diffusion*, 2nd Ed., Oxford University Press, Oxford.

DAPAAH, S.K. 1991. *Evaluation of Post-production Systems for Cereals in Ghana.* Phase One Report Prepared for National Energy Board (now Ministry of Mines and Energy), Ghana, October, 1991.

DAY, D.L, and NELSON, G.L. 1965. Desorption isotherms for wheat. *Trans. am. Soc. agric. Engrs.*, vol. 8, no. (2), p.293-297.

DALY, B.B. 1992. *Woods Practical Guide to Fan Engineering.* 3rd edn. Ipswich, Suffolk: Woods of Colchester Limited, UK.

DICKERSON, R.W. 1972. Computing heating and cooling rates of food: Symposium on Prediction of Cooling/Freezing Times for Food ducts. ASHRAE Bulletin No-72-3, p. 5.

KNUST

DIAMANTE, L.M. and MUNRO, P.A. 1991a. Mathematical modelling of the thin layer solar drying of sweet potato slices. *Solar Energy,* 2, 4, 271-276.

DIAMANTE, L.M. and MUNRO, P.A. 1991b. Mathematical modelling of hot Air drying of sweet potato slices. *Int. J. Food Science & Technology* 26, 99-109.

DUFFIE, J.A. and BECKMAN, W.A. (1993). Solar Engineering of Thermal Processes, Wiley, New York.

EKECHUKWU, O.V. and NORTON, B. (1993). Design and Measured Performance of a Solar Chimney for Natural-circulation Solar Dryers, in Proceedings of ISES Solar World Congress, Budapest, Hungary, Vol. 8, p. 78.

EL-SEBAII, A.A., ABOUL-ENEIN, S., RAMADAN, M.R.I., EL-GOHARY, H.G., 2002. Experimental investigation of an indirect type natural convection solar dryer. Energy Conversion and Management 43, 2251–2266.

ELSAYED, M.M. 1990. Mathematical modelling of a thin layer solar kiln. *TRANS. ASME, J. Solar Energy Engng*. 12, 196-203.

ENIBE, O.S., 2002. Performance of a natural circulation solar air heating system with phase change material energy storage. Renewable Energy 27, 69–86.

ESPER, A. and M*ü* hlbauer, W. (1993). Development and dissemination of Solar tunnel dryers, Proceedings of the Expert Workshop on Drying and Conservation with Solar Energy, Budapest, Hungary, ISES, Budapest, p. 63.

FAO. Food and Agriculture Organisation of the United Nations, Assessment collection of data on post-harvest food-grain losses. Econ. Social Development Paper 13, 1980. 1–70.

FLOOD, C.A., SABBAH, M.A., MECKER, D. and PEART, R.M. 1972. Simulation of natural air corn-drying system. *Trans. ASAE*, vol. 15, p. 156-159, & 162.
FORSON, F.K., NAZHA, M.A.A. and AKUFFO, F.O. 1996. Natural convection solar crop dryers of commercial scale in Ghana: design, construction and performance. *Ambient Energy*, vol. 17, no. 3, p. 123-130.

FORTES, M. and OKOS, M.R. (1980). Drying theories: their bases and limitations as applied to foods and grains, in Advances in Drying, vol. 3 (ed. A.S. Mujumdar), Hemisphere, NY, pp. 119-154

GANE, R. 1936. The thermal conductivity of the tissue of fruits. Ann Report, Food Investigation Board, Great Britain, p. 211.

ALL, C.W. and RODGRIGUEZ-ARIAS 1958. Application of Newton's equation to moisture removal from shelled corn at 40- 140° F. *J. agric. Engng. Res*., 3, 275-280.

KNUST

HALL, D.W. 1975. *Manual handling and storage of food grains in tropical and sub- tropical areas*., F.A.O. Development Paper No. 90.

HALL, C.W. 1980. *Drying and storage of agricultural crops*. Connecticut, Westport: AVI Publishing Company, Inc.

HEISLER, M.P. 1947. Temperature charts for induction and constant temperature heating. ASME Transactions, Vol. 69, p. 227.

HENDERSON, S.M. 1952. A basic concept of equilibrium moisture. *Agric. Engng*., 29-32.

HUSTRULID, A. and FLIKKE, A.M. 1959. Theoretical drying curve for shelled corn. *Trans. ASAE* 3, 112-114.

HENDERSON, S. M. and PABIS, S. 1961. Grain drying theory I: -temperature effect on drying coefficient. *J. agric. Engng. Res*., 6, 169-174.

HENDERSON, S.M. and PABIS, S. 1962. Grain drying theory IV: the effect of airflow rate on the drying index. *J. agric. Engng. Res*., 7, 85-89.

HOUGEN, O.A., McCAULEY, H.J., and MARSHALL, W.R. 1940. Limitations of diffusion equation in drying. *AIChE Transactions* 36(2):183-209.

HUKILL, W.V. 1954. Grain drying. AACC Monograph II. Storage of Cereal Grains. Am. Assoc. Cereal Chemists, St. Paul, Minn. (Cited by Bakker-Arkema *et. al*. 1974.)

HUKILL, W.V. and SCHMIDT, J.L. 1960. Drying rate of fully exposed grain kernels. *Transactions of ASAE* 3(2): 71-77 & 80.

HUSAIN, ASHFAQ, CHEN, C.S., CLAYTON, J.T. and WHITNEY, L.F. 1972. Mathematical simulation of mass and heat transfer in high moisture foods. *Trans. of the ASAE*, 15, pp.732-736.

IGLESIAS, H.A. and CHIRIFE, J. 1982. *Hanbook of food isotherms*. Academic Press, New York.

IGBEKA, J.C. 1982. Simulation of moisture movement during drying a starchy food product-cassava *J. Fd Technol*. 17, 27-36.

IHEKORONYE, A.I. and NGODDY, P.O. (1985). *Integrated Food Science and Technology for the Tropics*. Macmillan Publishers, London. Pp. 245

ILO. Solar drying: practical methods of food preservation, International Labour Office-Geneva, 1986.

ILOEJE, O.C., EKECHUKWU, O.V. and EZEIKE, G.O.I. 1993. Design, construction and test run of a two-tonne capacity soler rice dryer with rice-husk-fired auxialliary heater. Paper

submitted at the Second training workshop on solar drying technologies for agriculture and industry, 24-27 November 1993, Nsukka-Nigeria

IMRE, L. (1981). Heat transfer simulation of composite devices, in Numerical Methods in Heat Transfer, Vol. I (ed. R.W> Lewis, K. Morgan and O. Zienkiewicz), Wiley, Chichester, Chap. 3.

IMRE, L. (1988a) Interpretation of the Economy Evaluation of Solar Dryers, in Proceedings of the Tenth Congress on Energy, Opatija, pp. 23-28

IMRE, L. (1989). Solar Drying in Hungary, in Proceedings of ASRE '89 Symposium, Cairo, Egypt, Vol. 2, p. 1029.

IMRE, L. (1993). General Aspects for Designing Solar Dryers, in Proceedings of an Expert Workshop on Drying and Conservation with Solar Energy, Budapest, Hungary, p. 7.

ISLAM, M.N. and FLINK, J.M. 1982. Dehydration of Potato. *J. Fd Technol*. 17, 373-385.

JINDAL, V.K. and GUNASEKARAN, S. 1982. Estimating Air Flow and Drying Rate due to Natural Convection in Solar Rice Dryers. *Renewable Energy Review Journal* 4, 2, 1-9.

KAREL, M., FENNEMA, O.R. and LUND, D.B. 1975. *Physical principles of food preservation*. vol. 4 part 2, Marcel Dekker, New York

KHANNA, M.L., 1967. Design data for solar heating of air using a heat exchange and storage system. Solar Energy 11, 142–144.

KING, C.J. 1971. Freeze Drying of Foods, CRC Press, Cleveland.

KIRANOUDIS, C.T., MAROULIS, Z.B. and MARINOS-KOURIS, D. 1993. Mass transfer model building in drying, 11(6): 1251-1270.

KLEIN, S.A. 1979. Calculation of the Monthly-Average Transmittance-Absorptance Product. *Solar Energy* 23, 6, 547-551.

KRISTOFERSON, L.A., BOKALDERS, V., 1991. Renewable Energy Technologies: Their Applications in Developing Countries. Intermediate Technology Publications, Southmpton, pp. 3–19.

KUMAR, A. and SODHA, M.S. 1986. Computer siumulation models for solar drying processes. In: Reviews of renewable energy resources (M.S. Sodha, Mathur, S.S. and M.A. Malik, eds.), vol. 3, p.269-344: New Delhi, Wiley Eastern Ltd.

LAWS, N. and PARRY, J.L. 1983. Mathematical modelling of heat and mass transfer in agricultural grain drying. *Proc. R. Soc. Lon.*, A385, 169-187.

LEON, M.A., KUMAR, S. and BHATTACHARYA, S.C. 2002. A comprehensive procedure for performance evaluation of solar food dryers. I.: Renewable and sustainable energy reviews, 6 (2002) 367 – 393.

LEWIS, W.K., 1921. The Rate of Drying of Solid Materials. *Industrial and Engineering Chemistry* 13, 5, 427-432.

LILEY, P.E. and GAMBILL, W.R. 1973. Physical and chemical data. In *Chemical Engineers' Handbook*, 5th edition (Perry, R.H and Chilton, C.H. eds.) McGraw-Hill Book Company, Section 3.

LI, H and MOREY, R.V. 1984. Thin-layer drying of yellow dent corn. *Trans. ASAE,* 27:581-585.

LIU, B.Y.H. and JORDAN, R.C. 1977. Availability of solar energy for flat-plate solar heat collector. In *Application of Solar Energy for Heating and Cooling of Buildings*,

LOF, G.O.G., 1962. Recent Investigations in the Use of Solar Energy for the Drying of Solids. *Solar Energy*, 6, 4, 122-128.

LUNDE, P.J. (1980). Solar Thermal Engineering, Wiley, New York.

MADHLOPA, A., NGWALO, G., 2006. Solar dryer with thermal storage and biomass-backup heater. Solar Energy 81(2007), 449 – 462.

MARINOS-KOURIS, D and MAROULIS, Z.B. 1995. Transport properties in the drying of solids. In: *Handbook of Industrial Drying* Volume1 (Arun S. Mujumdar ed.), 2nd edition, Marcel Dekker, Inc. New York, pp 113-160.

McLEAN, K.A. 1980. *Drying and storage of combinable crops*, Farm Press Ltd., Ipswich, Suffolk, UK.

M'EWEN, EWEN and O'CALLAGHAN, J.R. 1954. Through Drying of Deep Beds of Wheat Grain. *The Engineer* 198, 817-819.

MISRA, M.K. and BROOKER, D.B. 1980. Thin-Layer Drying and Rewetting Equations for Shelled Yellow Corn. *Trans ASAE* 23, 1254-1260.

MUJUMDAR, A.S. 1995. *Hanbook of Industrial Drying*, Volume 1, 2nd edn., Marcel Dekker, Inc., New York, 1995.

O'CALLAGHAN, J.R. 1954. Drying of wheat grain: Effects of air condition on through drying. M.Sc. Thesis, university of Durham.

O'CALLAGHAN, J.R., MENZIES, D.J. and BAILEY, P.H. 1971. Digital Simulation of Agricultural Drier Performance. *J. agric. Engng. Res*. 16, 3, 223-244.

KNUST

OTHMER, D.F. 1940. Correlating Vapour Pressure and Latent Heat Data. *Industrial and Chemical Engineering* 32, 16, 841-856

OVERHULTS, D.G., WHITE, H.E., HAMILTON, H.E., and ROSS, I.J. 1973. Drying soybeans with heated air. Trans. ASAE, Vol. 16, p.112-113.

PABIS, S., and HENDERSON, S.M. 1961. Grain drying theory II: A critical analysis of the drying curve for shelled maize. *J. agric. Engng. Res.*, vol. 6, no. 4, p. 272-277.

PAGE, G.E. 1949. *Factors influencing the maximum rate of air drying shelled corn in thin layers*. M.S. Thesis. Mechanical Engineering Department, Purdue University, Lafayette, IN.

PARRY, J.L. 1985. Mathematical modelling and computer simulation of heat and mass transfer in agricultural grain drying: A Review. *J. agric. Engng.Res.* Vol. 32, pp. 1-29.

PIXTON, S.W. and HOWE, R.W. 1983. The Suitability of Various Linear Transformations to Represent the Sigmoid Relationship of Humidity and Moisture Content. *J. Stored Prod. Res*. 19, 1, 1-18.

PRASAD, J., VIJAY, V.K., 2005. Experimental studies on drying of Zingiber officinale, Curcuma l. and Tinosopora cordifolia in solar–biomass hybrid drier. Renewable Energy 30, 2097–2109

PORTER, H.F, McCORMICK, P.Y., LUCAS, R.L and WELLS, D.F. 1973. Gas-Solid Systems In *Chemical Engineers' Handbook*, 5th edition (Perry, R.H and Chilton, C.H. eds.) McGraw-Hill Book Company, Section 20.

PUIGGALI, J.R. and LARA, M.A. (1982). Some Experiments about Small Country Solar Dryers, in 7th International Congress on Chemical Engineering, Prague, Czech Republic, p. 390.

RAMALLO, L. A., and MASCHERONI, R.H. (2012). Quality evaluation of pineapple fruit during drying process. *Food and Bioproducts Processing,* **90:** 275-283.

RATTI, C. and MUJUMDAR, A.S. 1995. Simulation of Packed Bed Drying of Foodstuffs with Airflow Reversal. *Journal of Food Engineering*, 26, 3, 259-271.

REID, R.C., PRAUNSNITZ, J.M. and POLING, B.E. 1987. *The Properties of Gases and Liquids*, 4th Ed., McGraw-Hill Book Company, New York, chapter 11 pp577-631(diffusion), Chapter 7pp205-240(latent heat of vaporisation)

REUSS, M. (1993). Solar Drying in Europe, in Proceedings of an Expert Workshop on Drying and Conservation with Solar Energy, Budapest, Hungary, p. 89.

ROA, G. (1974). Natural drying of cassava. PhD thesis, Michigan State University, USA.

KNUST

RODRIGUEZ-ARIAS, J.H. 1956. Moisture equilibria of shelled corn. Unpubl. Ph.D. Thesis, Michigan State University. Cited by Bakker-Arkema et. al., 1974.

ROMAN, G.N., ROTSTEIN, E., and URBICAIN, M.J. 1979. Kinetics of water desorption from apples J. Food Sci. 44:193-197.

ROSS, I.J. and WHITE, G.M. 1972. Thin layer drying characteristics of white corn. *Trans ASAE* 15, 175-176 & 179.

SABBAH, M.A., MEYER, G.E., KEENER, H.M., and ROLLER, W.L. 1976. Reversed-air drying for fixed bed of soybean seed. Am. Soc. Agr. Emg. Paper 76-3023.

SABBAH, M.A., KEENER, H.M. and MEYER, G.E. 1979. Simulation of solar drying of shelled corn using the logarithmic model. *Trans. ASAE*, vol. 22, no. 3, 637-643.

SCHNEIDER, P.J. 1955. Conduction Heat Transfer. Addison-Wesley Publishing Co., Reading, MA, p. 15.

SCHNEIDER, P.J. 1963. Temperature Response Charts. John Wiley and Sons, New York.

SHARP, J.R. (1982) A Review of Low Temperature Drying Simulation Models. J. agric. Engng. Res. 27, 169-190.

SHARAF-ELDEEN, Y.I., BLAISDELL, J.L. and HAMDY, M.Y. 1980. A modeo for ear corn drying. *TRANSACTIONS of the ASAE*, Vol. 23, No. 5, p. 1261-1265, 1271.

SHERWOOD, T.K., (1936). Air Drying of Solids. *Trans. Amer. Inst. Chem. Engrs*. 12, 150-168

SIEBEL, J.E. (1892). Specific heat of various products. *Ice and Refrigeration*, vol. 2, p. 256-257.

SIMMONDS, W.H.C., WARD, G.T. and McEWEN, EWEN (1953a). The drying of wheat grain Part I: Through-drying of deep beds. *Trans. Instn. Chem. Engrs*. 31, 3, 265-279.

SLAVICEK, E., K. HANDA and M. KMINEK. 1962. Measurements of the thermal diffusivity of sugar beets. Cukrovarnicke Listy, Vol. 78, Czechoslovakia, p. 116.

SMITH, S.E. 1947. The sorption of water vapour by high polymers. *J. am. chem. Soc*., 69, 646-651.

SMITH, R.E., G.L. NELSON and R.L. HENRICKSON. 1967. Analysis on transient heat transfer from anomalous shapes. ASAE Transactions, Vol. 10, No. 2, p. 236

SMITH, R.E., G.L. NELSON and R.L. HENRICKSON. 1968. Applications of geometry analysis of anomalous shapes to problems in transient heat transfer from anomalous shapes. . ASAE Transactions, Vol. 10, No. 2, p. 296.

KNUST

SOPONRONNARIT, S., 1995. Solar drying in Thailand. Energy for Sustainable Development 2, 19–25.

TANG, J. and SOKHANSANJ, S. (1993). Drying parameter effect on lentil seed viability. Trans. ASAE, **36**(3), 855-61. . *J. agric. Engng. Res.* 17, 189-194.

STATEMENT (1992). Environmental Policy Statement, '92 Global Forum, Rio de Janeiro, Brazil.

STEFFE, J.F. and SINGH, R.P. 1982. Diffusion Coefficients for Predicting Rice Drying Behaviour. *J. agric. Engng. Res.* 27, 489-493.

STROHMAN, R.D. and YOERGER, R.R. 1967. A new equilibrium moisture content equation. *Trans. am. Soc. agric. Engrs.*, 10(5), 675-677.

SUAREZ, C., VIOLLAZ, P. and CHIRIFE, J. 1980. Diffusional Analysis of air Drying of Grain Sorghum. *Journal of . Food Technology* 15, 523-531.

SYARIEF, A.M., GUSTAFSON, R.J., and MOREY, R.V. 1987. Moisture diffusion coeficient s for yellow-dent corn components. *Trans. ASAE*, Vol., 30, p. 522-528.

SYARIEF, A.M., MOREY, R.V. and GUSTASON, R.J. (1984). Thin-Layer Drying of Sunflower Seed. *Trans ASAE* 27, 195-200.

TETER, C.N. and CITELLY, F. 1970. Biongenieria. Mimeo. Instituto Colombiano Agropecuario, Universidad Nacional, Tibaitata, Colombia. Cited by Roa, 1974.

TROEGER, J.M., and HUKILL, W.V. 1971. Mathematical description of the drying rate of fully exposed corn. Trans. ASAE, vol. 11, p.582-586.

THOMPSON, T.L. 1967. *Predicted Performances and Optimal Designs of Convection Grain Dryers*, PhD Thesis, Purdue University, Lafayette Ind., USA

THOMPSON, T.L. and PEART, R.M. 1968. Useful search techniques to save research time. *Trans. of ASAE* 2, 4, 461-467.

VACCAREZZA, L.M., LOMBARDI, J.L. and CHIRIFE, J. 1974. Kinetics of moisture movement during air drying of sugar beet root. *Journal of Food Science* 9, 317-327.

VAN ARSDEL, W.B. 1947. Approximate diffusion calculation for the falling-rate phase of drying. *Chem. Eng. Progr.*, vol. 43, 13-24.

VAN REST, D.J. and ISACCS, G.W. 1968. Exposed layer drying rates of grain. *Trans. am. Soc. Engrs.*, 11 (2) 236-239.

KNUST

VAN BRAKEL, J. 1980. Mass transfer in convective drying. In: Mujumdar, A.S. (ed.). Advances in drying, Vol. 1, Hemisphere Publishing Corp., New York.

VERMA, L.R., BUCKLIN, R.A., ENDAN, J.B. and WRATTEN, F.T. 1985. Effects of Drying Air Parameters on Rice Drying Models. *Trans. of the ASAE* 28, 296-301.

WAANANEN, K.M., LITCHFIELD, J.B. and OKOS, M.R. 1993. Classification of Drying Models for Porous Solids. *Drying Technology*, 11(1), 1-40.

WALKER, L.P. 1977. *Optimization of rice dryers*. Ph.D. Thesis, Mich. State Uni. Uni. Mocrifilms, Ann Arbor, Mich.

WALLAPAPAN, K. 1986. Thermal properties of porous foods. In: *Physical and chemical properties of food* (Edited by M.R. Okos), St. Joseph Michigan, ASAE, pp. 78-119.

WANG, J.K. and HALL, C.W. 1961. Moisture movement in microscopic materials and mathematical analysis. *Trans. of the ASAE*, 42, pp. 33-36.

WATSON, E.L. and BHARGAVA, V.K. 1974. Thin layer drying studies on wheat. *Can. Agric. Eng.,* Vol. 16, no. 1, p. 18-22.

WESTERMAN, P.W., WHITE, G.M. and ROSS, I.J. 1973. Relative humidity effect on high temperature drying of shelled corn. *Trans. am. Soc. agric. Engrs.*, 1136 1139 of ASAE

WHITE, G.M., ROSS, I.J. and WESTERMAN, P.W. 1973. Drying Rate and Quality of White Shelled Corn as influenced by Dew Point Temperature. *Trans. ASAE* 16, 118-120.

WHITE, G.M., BRIDGES, T.C., LOEWER, O.J., and ROSS, I.J., 1981. Thin layer drying model for soybeans. Trans. am. Soc. agric. Engrs., 1643-1646.

WHITE, G.M., BRIDGES, T.C., LOEWER, O.J., and ROSS, I.J., 1981. Thin layer drying model for soybeans. Trans. am. Soc. agric. Engrs., 1643-1646.

WIBULSWAS, P. and Niyomkarn, C. (1980) Development of Solar Air-heaters for a Cabinet-type Solar Dryer, in Regional Workshop on Solar Drying, CNED-UNESCO, Manilla, Phillipines, p.1.

WIJEYSUNDERA, N.E., Ah, L.L. and TIJOE, L.E. (1982). Thermal performance study of two-pass solar air heaters. Solar Energy, 28, 363.

WISNIEWSKI, G.D. (1993) Methods of Rational Solar Collectors Selection for Crop Drying, in Proceedings of ISES Solar World Congress, Budapest, Hungary, Vol. 8, p. 97.

XIONG, X., NARSIMHAN, G. and OKOS, M.R. 1992. Effect of Composition and Pore Structure on Binding Energy and Effective Diffusity of Moisture in Porous Food., *Journal of Food Engineering*, vol. 15, no. 3, p.187-208.

YOUNG, J.H. and WHITAKER, T.B. 1971a. Evaluation of the diffusion equation for describing thin-layer drying of peanuts in the hull. *Trans. of the ASAE*, vol. 14, no. 2,

ZAHED, A.H. and ELSAYED, M.M. 1994. Transient Performance of a Natural Ventilation Solar Kiln. *Renewable Energy,* vol. 4, no. 2, p.189-198.

ZAMAN, M.A. and BALA, B.K. 1989. Thin Layer Solar Drying of Rough Rice. *Solar Energy,* vol. 42, no. 2, p.167-171.

KNUST

APPENDICES

Appendix A

Table A1: Head loss coefficients for a range of pipe fittings

Fitting	Loss coefficient, K
Gate valve (open to 75 per cent shut)	0.25 →25
Globe valve	10
Spherical plug valve (fully open)	0.1
Pump foot valve	1.5
Return bend	2.2
90° elbow	0.9
45° elbow	0.4
Large-radius 90° bend	0.6
Tee junction	1.8
Sharp pipe entry	0.5
Radiused pipe entry	→0.0
Sharp pipe exit	0.5

KNUST

Table A2 Monthly Solar Irradiance (W/m^2) Data for Kumasi

Month	Monthly Irradiance (W/m^2)
January	266.7
February	333.33
March	380.25
April	405.08
May	413.75
June	341.33
July	300.42
August	236.75
September	292.00
October	374.67
November	351.50
December	303.30
Average	333.30

Source: F.K. Forson *et al* (2004), "*Solar Resource Assessment for Ghana*", *Journal of the Ghana Institution of Engineers.*

APPENDIX B

SAMPLE DESIGN CALCULATION

The size of the collector was based on meteorological and crop parameters.

Some of the following characteristics were established experimentally while others were adopted from literature:

Initial mass of fresh pineapples, $m_1 = 30\ kg$

Drying air inlet temperature, $T_{f,i} = 30\,^{o}C$

Drying air inlet relative humidity, $\phi_i = 75\%$

Initial moisture content of pineapple, $M_i = 85\%$

Desired final moisture content of dried pineapple, $M_f = 20\%$

To dehydrate a fresh food with an initial mass (m_1), the required mass of dry air (m_a) to vaporise water of mass (mw) from the fresh food can be calculated by (Ayensu, 1997)

$$m_w = (M_1 - M_2)/(100 - M_2) \quad (1)$$

$$m_a = m_w (W_2 - W_1) \quad (2)$$

Under the stated design conditions, $m_w = 24.375\ kg$

Using pyschrometric principles, ambient air is heated from point A (temperature $T_{f,i} = 303$ K, relative humidity $\phi_i = 80\%$, specific volume $v_a = 0.888\ m^3/kg$, $h_i = 86\ ^{kJ}/_{kg}$, $W_i = 0.0215\ ^{kg\,H_2O}/_{kg\,dry\,air}$) to point B ($T_{f,p} = 315$ K, $\phi_{db,i} = 42\%$) at constant humidity ratio ($W_i = W_{db,i}$) as shown in Fig. 1. The heated air (in the plenum) passes through the drying bed and picks up moisture from the fresh food at constant enthalpy, increasing humidity ratio (W_o) to

KNUST

A climate of innovation.
NAUTICA DEHUMIDIFIERS
NAUTICA DEHUMIDIFIERS, INC.
www.NauticaDehumid.com
1.866.628.8424

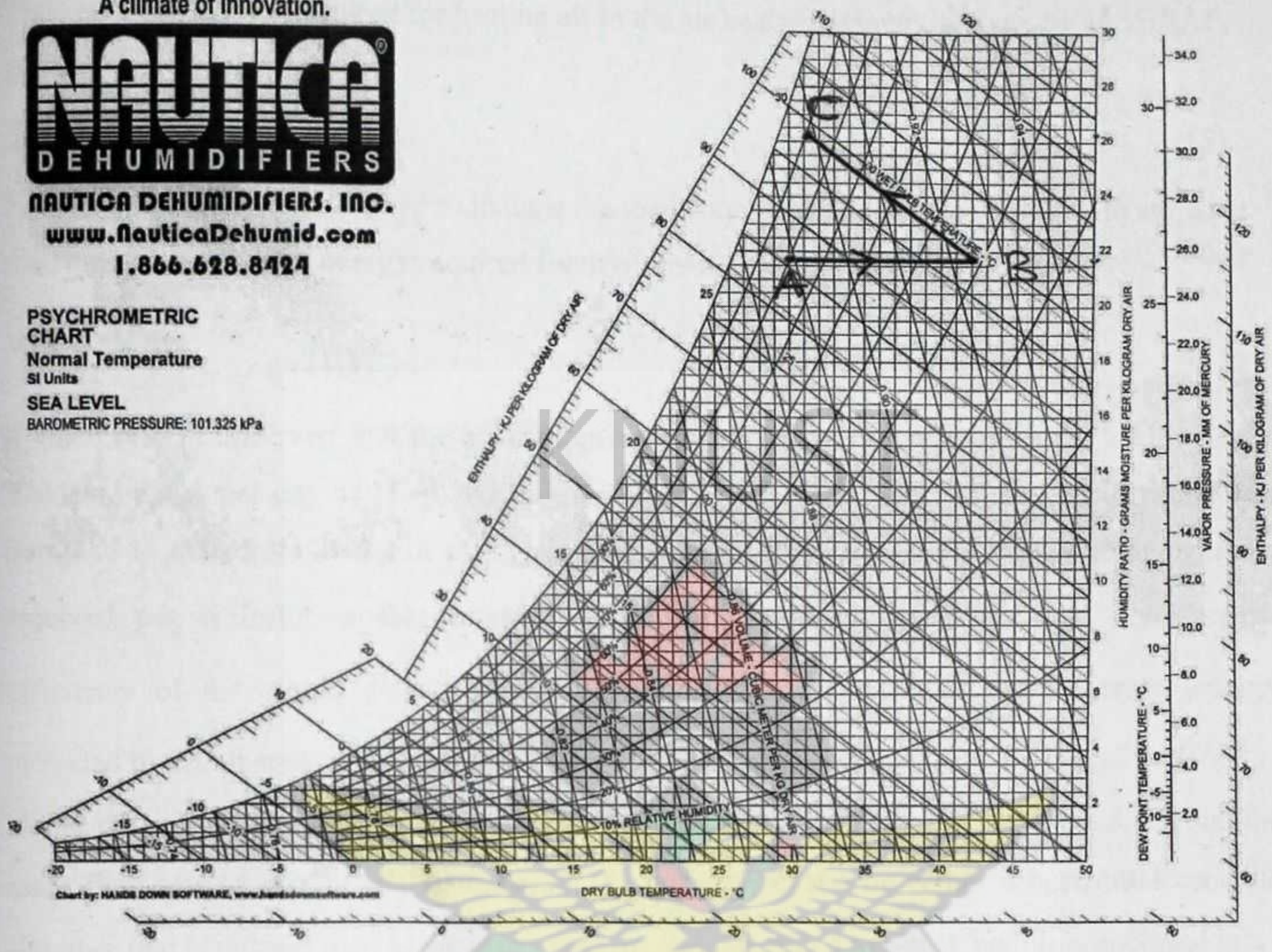

Fig. 1 Illustration of psychrometric drying

$0.0264\,^{kg\,H_2O}/_{kg\,dry\,air}$ at point C where it is assumed to exit the drying chamber at $\phi_o = 90\%$ and $T_{f,o} = 304.2$ K ($h_{f,o} = 98.8\,^{kJ}/_{kg}$) above the drying bed.

Therefore, to dehydrate 30 kg of pineapple at $M_i = 85\%$ to $M_f = 20\%$, means removing $m_w =$ 24.38 kg of moisture requiring $m_a = 4{,}974.49\ kg$ of dry air. The corresponding volume of drying air required for dehydration,

$$V_a = {m_a R T_{f,o}}/{P} = {(4974.49\,kg)\times(0.2871\,^{kJ}/_{kg.K})\times(304.2\,K)}/{(101.3\,kPa)} = 4{,}288.76\,m^3.$$

The heat transfer rate required for heating air in the air heater passages is given by (ASHRAE, 2001)

$$\dot{Q} = \dot{m}_a \left(h_{db,i} - h_{f,i} \right) \qquad (3)$$

Equation (3) can be transformed to include the total concrete absorber area required to store the total amount of thermal energy required for drying within a period of time *t*, as

$$A = {m_a \left(h_{db,i} - h_{f,i} \right)} \Big/ {\left(\eta_t H_d \right)} \qquad (4)$$

Ayensu (1997) observed that the solar intensity ranges from 550 to 1075 W m $^{-2}$ with a total incident energy per day of 15-30 MJ m -2 in Ghana. The solar system under consideration was designed to dehydrate 30 kg of pineapple in 259,200 s (3 days). Using a daily solar radiation received per collector surface area of $25 \mathrm{MJ}/\left(\mathrm{m}^2\right)$ and assuming the total opto-thermal efficiency of the single glazing-collector system, $\eta_t \cong 25\%$ then the total thermal energy provided by a unit area of the collector during the drying period (3 days) is 3 x 0.3 x 28 MJ/m^2 . Under the stated meteorological conditions, the total collector area required, A = 2.5 m^2, and the mass flow rate of dry air is $0.0192\, kg/s$. The collector of the dryer has a horizontal concrete absorber that is painted matt black on its top part and integrated to a rock bed. It is enclosed in a wooden frame (constructed from block board) mounted on the top part of the brick wall that houses the burner using metal straps mortared into the top part of the brick wall. The exterior part of the woodwork was covered with a painted galvanized iron sheet (6×10^{-4} m thick) to protect the wood from weathering.

The standard storage capacity of a solar air heater is 0.25 m^3 of pebbles (including void space) per unit area of the collector (Duffie and Beckman, 1991). For A = 2.5 m^2 in the present study, the required pebble volume and depth would be about 0.63 m^3 and 0.25 m respectively.

According to Forson et al (2007), the effective drying bed area A_{db} is obtained from first principles by relating the solid density of the wet material to its mass and the corresponding volume as

$$A_{db} = \frac{m_p}{\rho_{gr} h_L \xi \left(1 - \varepsilon_v\right)} \qquad (5)$$

where m_p is the mass of the crop to be dried, ρ_{gr} the bulk density of the crop on wet basis, h_L depth of drying bed, ε_v the loading bed void fraction, and ξ the crop porosity. Putting $m_p = 30\ kg$, $\rho_{gr} = 964\ \text{kg/m}^3$, $h_L = 0.15m$, $\varepsilon_v = 0.267$, and $\xi = 0.11$ @85% *moisture content* (Dull, 1971), the drying bed (A_{db}) area is given as 11m^2. The corresponding loading density ($L_D = m_p / A_{db}$) is 11.66 kg/m^2, the value of which falls within the acceptable range of 5–18 kg/m^2. Hence, each of the three trays to be used in the drying chamber will have a total surface area of 0.86 m^2 (i.e. 0.86 m × 1 m) and a depth of 0.05 m. The width has been adjusted to 0.90 m whereas the length has been adjusted to 1.64 m given a new drying tray surface area of 1.476 m^2 per tray.

The free flow of air through the drying bed is caused by a pressure drop across it resulting from the difference between the densities of relatively cool ambient air and the warm air inside the dryer. As shown in figure 2A, P_1, P_2, P_3, and P_4 represent the pressure levels and while ρ_i and ρ_h are the respective densities of ambient and heated air. The density difference equation is given as

$$\Delta\rho = \rho_i - \rho_h = P\left(T_A^{-1} - T_B\right)/R$$

Where $T_B = 315\ \text{K}$, $T_A = 303\text{K}$, $P = 101.3\,Pa$, $R = 0.287\,\text{kJ}/(\text{kg K})$ and, therefore $\Delta\rho = 4.4\times10^{-2}\ kg/m^3$. If the total height, h= 2.4 m, the corresponding pressure difference because of convection is $\Delta p = h(\Delta\rho)g = 0.693\ \text{Nm}^{-2}$, where g is the acceleration due to gravity.

CALCULATION OF RELEVANT GEOMETRIC PARAMETERS OF THE PROTOTYPE USED IN THE SIMULATON

$$\text{Characteristic length, } L_{rp\text{-}f} = \frac{A_{rp}}{P_{rp}} = \frac{1.4\times1.8}{6.4} = 0.394\,\text{m}$$

$$\text{Characteristic length, } L_{c\text{-}f} = A_s/P = \frac{1.7486}{5.298} = 0.33\ \text{m}$$

$$l_{hw} = \frac{(1.54\times0.62)\times2 + (2.03\times0.62)\times2}{(1.54\times4) + (0.62\times4) + (2.03\times4)} = 0.264\ m$$

Lower wall total surface area, $A_{lw} = (1.54\times0.62\times2) + (2.03\times0.62\times2) = 4.427\ m^2$

$A_{ab} = 1.4\times1.8 = 2.52 m^2$, $A_c = 1.64\times1.249 = 2.048 m^2$

$$A_{uw} = 2\times\left\{(0.1\times2.13) + \frac{(2.13 + 0.94)\times0.217}{2}\right\} + (0.1\times1.64) + (1.64\times0.317)$$

$= 1.776\ m^2$

KNUST

Dryer air inlet area, $A_i = 1.54\times0.1 = 0.154\ m^2$

Dryer cross-sectional area, $A_{cdd} = 1.64\times0.9 = 1.476\ m^2$

Calculation of Various plenum inlet and vent outlet openings used in the simulation:

Plenum inlet openings

$A_{pi_1} = 1.54\times0.09 = 0.139\ m^2$ $A_{pi_2} = 1.54\times0.07 = 0.108\ m^2$ $A_{pi_3} = 1.54\times0.05 = 0.077\ m^2$

Vent outlet openings

$A_{o_1} = 1.6\times0.1 = 0.16\ m^2$ $A_{o_2} = 1.6\times0.08 = 0.128\ m^2$ $A_{o_3} = 1.6\times0.06 = 0.096\ m^2$

$A_p = 0.423\ m^2$

Drying chamber wall inner surface area:

$A_{dw} = 2(1.64\times0.41) + 2(0.9\times0.41) = 2.08\ m^2$

Total height of dryer excluding the flue gas chimney,

Total height of dryer (excluding flue gas chimney pipe), $H = 1.605$ m

$H_{bu} = 620$ mm, $H_{cu} = 317$ mm, $H_{dd} = 410$ mm, $H_{vu} = 158$ mm

Hydraulic Radius for drying chamber, $R_{dd} = \frac{A}{P} = \frac{0.9\times1.64}{(0.9\times2) + (1.64\times2)} = 0.291$ m

Characteristic length for drying chamber cover glass,

$$L_{dc} = \frac{A_{c,dc}}{P_{dc}} = \frac{0.9 \times 1.64}{(0.9 \times 2) + (1.64 \times 2)} = 0.95 \text{ m}$$

Estimation of Loss Coefficients

1. *Burner unit loss coefficient* (K_{bu})

$$K_{bu} = K_{entry} + K_{bending} + K_{exp}$$

For sharp rectangular entry, $K_{entry} = 0.50$

For 90^{o} bend, $K_{bending} = 0.9$

For sudden expansion losses, $K_{exp} = \left(1 - \frac{A_1}{A_2}\right)^2 = \left(1 - \frac{0.154}{0.9548}\right)^2 = 0.7034$

Therefore, $K_{bu} = 0.9 + 0.7 + 0.5 = 2.1$

2. Collector unit loss coefficient (K_{cu})

$$K_{cu} = K_{exp} + K_{contr}$$

For sudden enlargement losses at plenum entrance,

$$K_{exp} = \left(1 - \frac{A_1}{A_2}\right)^2 = \left(1 - \frac{0.126}{2.52}\right)^2 = 0.9025$$

For contraction losses along plenum glass cover roof, $K_{cont} = 0.17$

$$K_{cu} = K_{exp} + K_{contr} = 0.9025 + 0.17 = 1.07$$

3. Drying chamber loss coefficient (K_{dd})

Under no load conditions, $K_{dd} = \frac{H_{dd} f}{R_{dd}}$

Under load conditions

Pressure drop due to resistance offered by crop bed,

$$\Delta P_{cb} = R_{air}(\rho_2 T_2 - \rho_1 T_1) = 0.2871 \times ((1/0.889) \times 304.2 - (1/0.924) \times 315) = 0.366 \text{ kPa}$$

KNUST

Specific volumes at outlet and inlet to drying bed corresponding to the psychometric diagram shown in Fig. 1 of appendix B are $v_2 = 0.924\ m^3/kg$ and $v_1 = 0.889\ m^3/kg$ respectively

4. Bending and contraction losses at dryer exit (K_{vu})

$$K_{vu} = K_{bending} + K_{cont}$$

Bending losses, $K_{bending} = 0.9$

Contraction losses at air vent outlet, $K_{cont} = 0.795$

$$K_{vu} = K_{bending} + K_{cont} = 0.9 + 0.795 = 1.695$$

KNUST

Table B 1: Design parameters for a designed Prototype solar crop dryer with biomass back-up heater

Design parameter	Dimension
Absorber surface area, $A_{ab} = 2.5\ m^2$ (dimensions: 1.8 m × 1.4 m) Absorber: concrete slab (0.03 m thick)	
Thermal mass: granite pebble bed (360 kg, 0.09 m thick)	
Drying chamber External dimensions of a drying tray: 1.64 m × 0.90 m × 0.05 m Dryer external dimensions: 0.94 m long × 1.64 m wide × 0.410 m high on the front side : 0.94 m long × 1.64 m wide × 0.568 m high on the back side Effective tray area: 4.428 m^2 (for three trays) Loading density: 11.66 kg/m^2	
Air outlet vent dimensions: 1.64 m × 0.1 m	
Glass cover for drying chamber: Thickness = 0.003 m Tilt angle = 10° Absorber glass cover dimensions: 1.249 m × 1.640 m	
Biomass burner Burner housing external dimensions: 2.17 m long × 1.68 m wide × 0.62 m high	
Drum Diameter = 0.60 m Length = 1.4 m Burner door = 0.55 m × 0.54 m	
Air inlet vent dimensions = 1.4 m × 0.09 m	
Flue gas chimney	
Total height = 2.005 m Diameter = 0.12 m	

KNUST

Date: June 30, 2012; Time started: 9:00 am. ***Results cover solar heating mode under no load conditions***

Table C1 SOLAR HEATING MODE 1

Vent outlet gap: 0.02 m; plenum entry gap: 0.02 m
An insolation of 350W/m^2 was maintained on the inclined plane of the plenum glass cover for this experiment

$T_{f,i}$	26.5	24.9	25.8	27.5	27.4	27.2	27.6	28.3	28.0	27.6	27.9	28.4	27.6	27.8	27.4	27.2
T_{ab-rp}	27.6	27.2	27.3	31.2	30.3	31.8	33.8	37	35.3	34	37.9	37	33.6	33.5	33.8	35.5
T_{uw}	25.8	27.3	27.3	28.9	29.2	29.5	33	45	45	45.4	45	45	45	45	43	44.5
T_{lw}	25.6	26	26.9	28.5	29.6	29.3	29.2	30.4	32.2	30.3	30.2	32	30.6	30	30.6	31.1
T_{bg}	24	24	24	24.6	24.6	25	25	25	25.5	26.9	26.8	26.8	28.9	27	29.1	29
T_f	26.8	26.8	27	28.4	30.2	30.5	31.9	33.6	36.2	40.6	41.6	35.9	37.1	43	43	43
T_{rp-f}	25.7	26.3	27.3	28.6	30.6	32.3	34.9	33.8	35.1	35.5	36.6	38.6	35.7	33.9	33.5	34.5
$T_{p,c}$	35	39	39.8	40.1	42	41.1	44	46	45.4	46.5	47	47	48	48	45	46.5
$T_{d,w}$	25.9	27	28.5	28.7	28.9	30.2	31.8	35.4	33.3	33.2	34.4	39	37.1	35.3	36.6	38.6
$T_{f,o}$	27	28.5	28.9	29.4	29.9	30.7	30.7	35.2	30.5	31.3	36.5	40.8	43.7	43.5	44.6	45.7
T_{ab-f}	26.4	27.5	28.7	30.3	32.6	32.4	41.5	44.6	43.8	34.9	44.9	46	56	56	54	55
$T_{c,d}$	29.1	26.8	28.5	30.6	30.8	53	57.8	69	64.8	67	70	72	73.4	72.5	71.8	77.5
V_i	0.3	0.7	0.7	0.7	1.4	0.7	0.3	0	0.28	1.0	0.0	0.0	0.3	0.3	0.0	0.0
V_o	1.56	3.68	3.68	3.66	7.34	3.68	1.58	1.60	1.47	5.26	1.60	1.62	1.64	1.65	1.66	
$\dot{m}_o$ x 10^{-2}	1.42	3.34	3.33	3.31	6.63	3.32	1.42	1.41	1.32	4.74	1.42	1.42	1.42	1.42	1.42	
η_{c} x 10^{-3}	0.1	1.7	1.0	0.8	4.9	2.9	1.6	2.0	2.8	6.1	5.1	2.8	5.6	5.8	5.9	
ϕ_i	70	69	61	59	57	60	60	56	59	61	62	62	62	63	65	66
ϕ_o	67.8	71.3	73	66	62	65	67	63	67	69	70	70	70	73	75	76
P_{atm}	981.1	981.4	980.9	980.6	980.8	979.8	980.8	980.9	979.8	979.8	979.5	982	982	982	981.5	980.3	979.1
Q_T/(W)	7.20	22.13	12.82	14.57	14.62	16.30	24.97	25.87	21.82	13.97	21.55	19.39	19.28	17.72	18.61	
$\Delta\psi$	93.09	578.12	367.69	276.52	859.05	987.83	1275.40	1565.08	2410.35	3807.24	3990.95	2204.72	4418.46	4537.64	4597.29	

Table 2C ***SOLAR HEATING MODE 2*** (Date: July 01, 2012, Time started: 9:20 am; Gi = 350 W/m^2)

Vent outlet gap: 0.03 m; plenum entry gap: 0.02 m

$T_{f,i}$	24.9	25.3	25.6	25.9	26.4	27.7	27.7	26.5	27.0	29	28.6	28.2	28.5	28.6	28.4	28.1	
T_{ab-rp}	25.8	26.6	27.5	28.3	29.4	29.8	30.4	28.6	28.6	28.6	32.8	33.3	33.9	34.4	34.1	34.3	
T_{uw}	35.5	39	38	40	40	43	42	42.2	43	43.2	44	45	45.1	44.8	44.8	44	
T_{lw}	25.3	25.9	26.6	27.7	28.2	28	28.8	28.6	28.6	29.8	30.5	30.5	30.8	31.1	31.4	30.8	
T_{bg}	24	24	29	25	25	25	25	25	25	26	26	26	27	26.5	26.8	26	
T_f	36	36.2	38	38	39.5	41	41	41	41	41.2	42	42	43	42	43	42	
T_{rp-f}	25	26	26	28	28.5	30	30	30	32	32	33	32	35	34	35	36	
$T_{p,c}$	39	40.2	39	42	42	44	44.1	44.5	43	44.5	45	44.5	45	45	44.3	44.5	
$T_{d,w}$	30	38	39	40.1	41.1	42.5	43	43.2	41.1	43.5	44	45	44.8	45	44.3	38.6	
$T_{f,o}$	32.2	37.4	31.6	36.4	36.8	35.9	46.9	44.5	45.6	45.3	41.2	41.9	38.8	42.4	35.7	36	
T_{ab-f}	36.8	43	44	46	48	50	50	50	50	51	53	53	54	54	54	55	
$T_{c,d}$	55	55.4	55	63	60	64	66	66	62	62.3	58.5	61	62.3	60	61	57	
V_i	0.3	0.7	0.7	0.3	1.7	0.7	0.7	0.3	0.7	2.4	1.7	0.7	0.7	1.0	1.7	1.0	
V_o	1.07	2.53	2.48	1.08	6.10	2.49	2.58	1.10	2.58	8.77	6.14	2.54	2.50	3.63	6.04	3.56	
$\dot{m}_o$ x10^{-2}	1.43	3.34	3.33	1.43	8.07	3.31	3.31	1.42	3.31	11.27	7.99	3.29	3.29	4.70	7.99	4.71	
η_c x10^{-3}	4.16	9.51	10.81	4.52	27.64	11.51	11.50	5.39	12.12	35.96	28.01	11.89	12.48	16.47	30.53	17.12	
ϕ_i	74	73	72	69	65	64	65	67	67	62	60	60	60	61	61	64	
ϕ_o	67.9	62.1	70.5	30	43.5	43.6	43.6	32.9	34.3	40.5	44.5	35	28.7	42.1	40.5	35.8	
Patm	981.2	981.2	980.9	980.8	980.2	980.9	979.7	979.5	979.1	978.5	978.4	978.1	978.2	978	977.9	978.1	
Q_T/(W)	80.74	60.96	43.64	38.24	33.59	27.32	24.28	22.00	19.33	13.99	18.73	17.92	17.93	16.58	15.81	15.95	
$\Delta\dot{\psi}$	3278.9	3219.1	3648.9	3556.7	3854.53	3881.1	3881.4	4236.9	4090.1	3584.6	3912.8	4017.2	4211.9	3901 5	4255.5	4049.8	

LIBRARY

Table 3C SOLAR HEATING MODE 3, Date: July 02, 2012; Time started: 10:00 am

Vent outlet gap: 0.04 m; plenum entry gap: 0.02 m

An insolation of 350W/m^2 was maintained on the inclined plane of the plenum glass cover for this experiment

$T_{f,i}$	26.1	26.5	27.3	27	27.5	27.7	28.9	28.9	29.1	30	29.1	30	29.3	29.6	29.1	29.1
T_{ab-rp}	26.6	27.1	28.1	29.1	29.8	30.3	31.2	31.8	32.6	32.5	33.8	32.7	33.9	34.4	34.9	34.1
T_{uw}	35	35.2	38.9	40	40	40	43	42	44	44.8	44.2	44.2	44	43	43	44
T_{lw}	25.9	26.4	26.9	27.3	27.7	28	28.8	29.6	29.4	29.5	29.8	30.3	30.7	31.1	31	31
T_{bg}	24.8	25	25	25	25	25.2	25.2	26	26.8		26	26	27	26.8	27	27
T_f	35	35	36	37.5	37	38	40	39.9	40	40	41	41	40.1	40.2	41	40.7
T_{rp-f}	26	26.5	27	28	29	30	31	30.7	31.5	32	33	32	33	34	35	35
$T_{p,c}$	37.1	38	40.2	41	41.6	41	44	43	43.2	44.2	42	44	44.4	43.5	42.5	43.8
$T_{d,w}$	34.5	36.2	36	38	38	39	40.2	41	41.2	41.5	41.8	42	41.5	42	42	42
$T_{f,o}$	28.6	31.6	37.4	34.8	35.4	36.8	38.2	42.3	35.6	35.7	37.8	35.4	38.8	33.5	34.8	40.4
T_{ab-f}	37	40	43	45	46	47	49	50	50	51	52	52	52	52	52	53
$T_{c,d}$	44.7	50	61	61	60.4	58	58.4	60	56	55.4	56	55	60.5	52	59	57.2
V_i	0.7	1.0	0.7	0.7	0.3	1.4	0.3	1.4	1.7	1.0	0.7	1.0	1.4	1.4	1.4	1.0
V_o	1.84	2.64	1.88	1.87	0.80	3.75	0.80	3.80	4.52	2.65	1.87	2.65	3.75	3.69	3.71	2.70
$\dot{m}_o$ x10^{-2}	3.32	4.74	3.31	3.31	1.42	6.61	1.41	6.58	7.98	4.68	3.29	4.68	6.56	6.55	6.57	4.69
η_c x10^{-2}	0.77	1.05	0.75	0.91	0.35	1.78	0.41	1.89	2.28	1.22	1.02	1.35	1.85	1.82	2.04	1.42
ϕ_i	75	72	66	66	65	63	61	61	60	62	59	61	60	60	61	63
ϕ_o	70.1	60.9	60.3	70.2	60	59.7	54.2	54.5	60.1	58.6	60.2	61	52.2	54.5	57.6	59.1
P_{atm}	980	979.9	979.8	980	979.9	979.5	979.1	978.9	978.7	978.6	978.5	978	977.7	977.3	977.4	977.0
Q_T/(W)	69.39	43.46	33.63	33.23	27.99	25.16	21.71	20.34	22.23	15.90	18.18	13.91	15.16	14.29	15.61	13.57
$\Delta\dot{\psi}$	2629.6	2511.4	2561.4	3084.6	2789.9	3024.5	3236.2	3213.6	3185.4	2913.2	3463.8	3198.9	3152.0	3091.6	3468.2	3379.8

Date: July 04, 2012; Time started: 01:50 pm

Table 4C SOLAR HEATING MODE 4

Vent outlet gap: 0.02 m; plenum entry gap: 0.04 m
An insolation of 350W/m^2 was maintained on the inclined plane of the plenum glass cover for this experiment

$T_{f,i}$	28	28.7	28.6	29.3	26.0	24.3	23.4	24.1	24.1	24.1	24.1	24.1
T_{ab-rp}	28.6	29.1	29.5	29.7	29.7	29.8	29.8	29.6	29.6	30.0	30.5	30.1
T_{uw}	37	39	45.0	39	36.2	36	37	36	36	37	37	37
T_{lw}	28.4	28.2	28.4	29.2	29.9	27.1	27.2	26.4	27.9	27.0	26.7	27.3
T_{bg}	25	25	25.1	26	25	24	24	25.4	25.1	25.7	25.6	25.7
T_f	37	38	39	38	36	34	35	35	35.2	36	36	36
T_{rp-f}	27	28	29	29	28.5	28	28	28	30	30	30	30
$T_{p,c}$	42	42.5	43	42	47.5	47	40	40	40.1	41	41	42
$T_{d,w}$	38.1	39.9	40	40.2	39.8	38	37.5	38	38.9	39	39	39
$T_{f,o}$	26.3	26.3	26.3	33.5	27	26.2	26.2	26.2	26.2	26.2	26.2	26.9
T_{ab-f}	39	40	42	42	41	42	43	42	43	44	45	45
$T_{c,d}$	65.5	66	65	57	42	56.2	60	62	63.2	64	62.2	65.2
V_i	0.7	0.3	1.4	2.7	0.9	0.7	0.7	0.3	0.3	0.0	0.7	0.3
V_o	1.87	0.80	3.73	7.12	2.35	1.83	1.84	0.79	0.79	0.00	1.83	0.79
$\dot{m}_o$ x10^{-2}	1.65	0.70	3.28	6.32	2.13	1.67	1.67	0.71	0.71	0.00	1.67	0.71
η_c x10^{-4}	38.74	17.11	8.91	143.69	55.73	42.27	50.69	20.38	20.74	0	5.19	22.25
ϕ_i	62	65	64	63	65	77	64	60	58	55	54	57
ϕ_o	63.2	63.8	56.6	54.4	82.3	82.2	86	83.4	84.1	84.1	82.5	82.8
P_{atm}	976.5	976.3	976	975.7	977	976.7	976.4	976.9	976.6	978.6	976.8	977
Q_T/(W)	67.91	34.46	30.31	19.73	27.41	29.35	28.59	22.26	21.35	20.21	19.37	17.43
$\Delta\dot{\psi}$	2642.2	2721.4	3044.3	2564.9	2950.7	2878.8	3441.6	3229.2	3287.3	3519.2	3520.6	3519.5

Table 5C SOLAR HEATING MODE 5, Date: July 05, 2012; Time started: 02:20 pm

Vent outlet gap: 0.03 m; plenum entry gap: 0.04 m
An insolation of 350W/m^2 was maintained on the inclined plane of the plenum glass cover for this experiment

$T_{f,i}$	28.7	28.5	28.4	28.7	28.4	28.1	28.2	27.0	26.6	27.0	27.0	26.3	25.9
T_{ab-rp}	28.1	28.6	29.4	29.5	30.4	30.6	31.3	31.1	30.8	31.0	31.0	30.8	31.8
T_{uw}	37	37.5	39.8	41	41	42	41	40	40.7	40	40	40	40.8
T_{lw}	27.7	28.1	28.5	28.3	28.6	28.9	28.9	27.7	27.6	27.3	27.4	27.9	27.4
T_{bg}	25	25	25	25	25	26	26	25.5	26	26	26	26	25.5
T_f	36	36.5	37	39	38	40	37	36.5	38	37	37	38	38.2
T_{rp-f}	26	27	27	28	29	29	29	28.8	29	30	30	31	31
$T_{p,c}$	41	42	44	44.6	46	46	46.1	43	43.1	42.5	42.7	44	44
$T_{d,w}$	37	39	40.5	41.8	42	42.4	42.3	41.1	41.1	40.9	41	41.2	41.1
$T_{f,o}$	32.9	34.9	39.3	34	39.8	35.2	39.9	35.9.	36.9	36.5	33.7	34.9	32.2
T_{ab-f}	37	40	41	43	45	45	45.5	46	46	47	48	48.8	49
$T_{c,d}$	56.5	62	64	59	64	60.2	59	56	55	57	55	54.1	57
V_i	0.7	0.3	0.7	1.0	0.3	0.3	2	1.4	1.7	1.0	1.7	2.0	0.3
V_o	2.46	1.06	2.51	3.53	1.08	1.06	7.20	5.00	6.10	3.58	6.01	7.13	1.06
$\dot{m}_o$ x10^{-2}	0.94	0.40	0.92	1.33	0.39	0.40	2.61	1.85	2.24	1.32	2.27	2.65	0.40
η_c x10^{-4}	17.87	8.33	20.6	35.86	9.84	12.38	60.12	46.03	66.78	34.53	59.24	81.23	12.93
ϕ_i	60	61	61	60.4	61	57	62	64	67	70	70	74	75
ϕ_o	60.1	60.1	63.9	58.0	52.7	55.7	58.6	62.9	70.9	67.3	72	67.3	69.9
P_{atm}	978.1	977.8	977.6	977.4	977.4	977.3	977.5	977.4	976.6	977.4	977.5	977.5	977.8
Q_T/(W)	32.86	31.94	26.63	22.72	24.39	21.66	19.71	20.27	18.67	17.20	16.18	16.57	16.78
$\Delta\psi$	2146.1	2348.1	2524.7	3014.4	2810.8	3474.1	2605.2	2805.7	3363.8	2944.63	2955.4	3459.8	3614.2

Date: July 06, 2012; Time started: 06:50 am

Table 6C ***SOLAR HEATING MODE 6***

Vent outlet gap: 0.04 m; plenum entry gap: 0.04 m

An insolation of 350W/m^2 was maintained on the inclined plane of the plenum glass cover for this experiment

$T_{f,i}$	22.7	22.9	23.3	23.9	24.3	24.6	25.3	26.7	26.1	26.9	26.3	26.7	26.8	27.1
T_{ab-rp}	24.7	25.1	25.5	26.3	27.1	27.2	27.8	28.3	29.3	30.4	30.5	30.4	30.9	31.2
T_{uw}	34	34.8	36	37	38.7	38	39	41.5	41	41	41	41	41.8	43
T_{lw}	23.5	23.7	24.1	24.3	24.8	24.9	25.5	26	26.5	26.7	27	26.6	27.3	27.7
T_{bg}	23	23.4	23.8	24	24	24	24	25	25	25	25	25	25	25
T_f	30.5	31.7	32	33	34.2	34	34.8	36.5	36	37	37.5	39	38	38
T_{rp-f}	23	23.8	24.8	25	26	27	27	28	28.8	29	30	31	31.1	31
$T_{p,c}$	39	40.3	42	42.5	43	42	43.2	44	44.5	45	45.5	46.5	46.5	45.2
$T_{d,w}$	33	34.4	36	36.5	37.5	37	38.2	39.4	39.9	39.2	40.8	41	40.8	41.2
$T_{f,o}$	34.1	35	33.1	37	36.7	32	37.6	35.8	34.1	34.2	36.7	35.5	33.5	36.9
T_{ab-f}	37	39	40.3	43	43	43.5	45	47	48	49	49	49	48.1	50.1
$T_{c,d}$	59.1	57.2	61.5	60.5	57	48	60	56	57	58	60.2	63	59	59
V_i	0.2	0.3	0.3	0.3	0.3	0.7	0.7	1.0	1.0	1.0	1.0	0.3	0.3	0.7
V_o	0.54	0.81	0.81	0.81	0.81	1.87	1.90	2.68	2.67	2.66	2.69	0.80	0.80	1.88
$\dot{m}_o$ x10^{-2}	0.96	1.44	1.44	1.44	1.44	3.35	3.34	4.75	4.76	4.75	4.76	1.43	1.42	3.32
η_c x10^{-4}	19.62	33.19	32.78	34.22	37.18	82.33	82.99	121.73	123.25	125.43	139.36	45.85	41.73	94.67
ϕ_i	95	93	91	87	82	83	79	75	66	71	68	69	65	65
ϕ_o	82.5	81.9	76.5	77.7	74.5	73.2	57.9	56.8	61	68.9	63	58.2	56.6	63.4
P_{atm}	981.1	981.6	981.8	981.8	982.0	982.4	982.1	982.1	982.4	982.6	982.5	982.4	982.3	982.3
Q_T/(W)	106.94	61.08	43.32	35.73	29.39	24.83	21.42	17.87	19.35	7.58	8.44	7.32	14.31	13.90
$\Delta\dot{\psi}$	2333.9	2626.9	2594.1	2706.1	2936.0	2788.6	2811.3	2886.9	2921.5	2971.6	3295.4	3604.6	3287.2	3198.9

Date: July 06, 2012; Time started: 02:10 pm

Table 7C SOLAR HEATING MODE 7

Vent outlet gap: 0.02 m; plenum entry gap: 0.06 m

$T_{f,i}$	32.0	31.0	29.6	30.1	29.4	30.1	32.2	32	27.9	27.5	27.3	26.9
T_{ab-rp}	31.5	31.4	31.6	31.8	32.3	29.5	32.4	32.9	33.2	33.2	33.4	32.8
T_{uw}	40.1	41.6	42.1	42.5	48	43	43	43	43	44.5	44	44.2
T_{lw}	29.3	29	29.6	29.3	29.5	31	30.5	30.1	29.5	28.9	30.3	29.8
T_{bg}	25.7	26	26	26	26	26	28	27	26	28	26.9	26
T_f	37	38.7	39.6	40.1	40	39	40	40	40	41	40.1	40.2
T_{rp-f}	30	30	31	31.5	32	31	31.8	32.5	33	33	33	32
$T_{p,c}$	45.5	46.5	46.2	45	46.7	47	47.8	48	48	48.5	49	49
$T_{d,w}$	39	40.5	40.1	41	41	42	42	42.3	42.1	41.8	42.5	42.6
$T_{f,o}$	40.6	40.6	42.1	39.6	44.6	44.2	43.8	44.1	40.5	44.3	43.6	45.6
T_{ab-f}	43	45	46	47	48	49	49	50	49	51	52	43
$T_{c,d}$	60	61.2	60.1	57.2	63	63	62.5	65.2	64.2	65.5	68	68.5
V_i	0.7	0.3	1.0	1.4	0.28	0.3	0.7	0.28	0.0	0.0	0.3	0.3
V_o	3.74	1.61	5.41	7.51	1.53	1.63	3.78	1.51	0.00	0.00	1.64	1.66
$\dot{m}_o \times 10^{-2}$	3.26	1.42	4.69	6.56	1.31	1.40	3.25	1.30	0.00	0.00	1.42	1.42
$\eta_c \times 10^{-2}$	0.43	0.32	1.23	1.71	0.36	0.33	0.66	0.27	0.00	0.00	0.47	0.49
ϕ_i	54	54	56	59	61	59	52	51	53	55	57	61
ϕ_o	57	46.4	48.1	56	58.8	58.3	60.6	51.4	56	55	59	60.2
P_{atm}	979.9	979.9	979.7	979.	979.1	978.9	978.9	978.7	978.9	979.0	978.9	979.2
Q_T/(W)	52.86	51.96	41.32	30.99	30.20	18.48	14.44	14.86	22.23	22.01	21.10	14.68
$\Delta\dot{\psi}$	1465.3	2538.7	2928.2	2936.5	3088.86	2595.36	2269.2	2322.2	3533.0	3937.9	3741.7	3889.7

Date: July 07, 2012; Time started: 08:20 am

Table 8C SOLAR HEATING MODE 8

Vent outlet gap: 0.03 m; plenum entry gap: 0.06 m
An insolation of 350W/m^2 was maintained on the inclined plane of the plenum glass cover for this experiment

$T_{f,i}$	24.4	24.6	25.2	25.9	25.6	26.3	26.6	26.6	26.9	27.4	27.3	27.4
T_{ab-rp}	24.9	25.6	2.6	26.9	27.5	28.2	28.9	30.2	30.3	30.4	31.4	31.5
T_{uw}	34	35.4	36	37.7	38	39	41	39	41	41	41.3	41
T_{lw}	24.4	25.1	25.2	25.6	26.2	26.5	27.8	27.7	27.8	28.8	28.4	28.4
T_{bg}	24	24	24.1	24.8	25	25	25	25	25	25	25	25
T_f	32	34	33.8	33.8	35.1	35	37	36.5	38.2	38	38.6	38
T_{rp-f}	23.5	24	25	25.5	26.2	27	28	29	29.8	30	30	29.7
$T_{p,c}$	40.1	40.2	42.4	44	43	43.8	44.8	45	45.2	46.6	47	47.7
$T_{d,w}$	32	35	36	37.2	38.2	38.4	39.8	39.8	41	41.1	41.6	42
$T_{f,o}$	33.2	30.1	37.6	36.4	37.7	37.8	39	39.6	33.3	40.5	40.7	41.5
T_{ab-f}	36	39	41	42	44	45	46	46.2	48	49	49	50
$T_{c,d}$	58.5	57.1	61.7	61	61.6	62	56.4	60.8	61.5	65.2	66	65.2
V_i	0.3	0.3	0.7	0.3	0.3	1.0	0.7	0.3	1.4	0.3	0.3	0.3
V_o	1.07	1.06	2.53	1.08	1.08	3.60	2.53	1.09	4.96	1.09	1.09	1.09
$\dot{m}_o$ x10^{-2}	1.44	1.44	3.34	1.43	1.43	4.76	3.33	1.43	6.65	1.42	1.42	1.42
η_c x10^{-2}	0.29	0.35	0.75	0.30	0.36	1.08	0.90	0.37	1.96	0.39	0.42	0.39
ϕ_i	83	79	80	74	73	71	71	69	67	67	67	65
ϕ_o	77.3	76.3	57.9	63	64.5	54.6	64.6	60.2	60.1	56.4	57.7	51.4
P_{atm}	982.1	982.3	982.4	982.5	982.5	982.1	982.3	978.7	982.3	982.2	982.2	981.8
Q_T/(W)	70.91	46.95	-44.18	26.22	26.34	22.32	20.71	20.40	19.13	17.00	16.54	15.48
$\Delta\dot{\psi}$	2262.3	2787.6	2551.3	2338.9	2807.6	2574.2	3061.2	2914.2	3325.9	3108.4	3310.8	3108.4

Date: July 07, 2012; Time started: 02:35 pm

Table 9C SOLAR HEATING MODE 9

Vent outlet gap: 0.04 m; plenum entry gap: 0.06 m
An insolation of 350W/m^2 was maintained on the inclined plane of the plenum glass cover for this experiment

$T_{f,i}$	28.9	29.0	28.9	28.6	28.7	28.3	28.1	27.7	27.7	27.5	27.7	27.5
T_{ab-rp}	32.1	31.8	32.6	32.6	33	33.6	34	33.5	34.0	33.3	34.3	34.3
T_{uw}	40.1	43	41.2	42	41.8	41	43	41	40.2	41	41	41
T_{lw}	30.3	30.4	30.5	30.1	31.4	31.3	30.5	30.2	30.8	29.6	31.2	30.8
T_{bg}	25.5	26	26	26	26	26	26	26	26	26	27	27
T_f	37.5	40	38.2	39	39.8	39	40	39	39	38.2	39	40
T_{rp-f}	30.1	31	30.1	31	31	32.6	32.5	33	32	32	32	32
$T_{p,c}$	46	47	47	46.5	48	46.5	47.8	47	46.7	47	47	47
$T_{d,w}$	39	40.8	41	42	42.8	42.1	42.2	41.1	42	42.2	42	42
$T_{f,o}$	38.3	34.8	41.3	41.1	42.3	39.2	38.9	40.1	39.1	38.7	43.3	40.8
T_{ab-f}	43	46	47	48.5	49	49	50	50	50	50	51	51
$T_{c,d}$	61.2	63	65.1	63	69	66.5	70	69.4	64	65	70	70.2
V_i	0.3	1.4	0.3	0.3	0.0	0.0	0.0	0.0	0.0	0.0	0.0	0.0
V_o	0.80	3.71	0.81	0.81	0.00	0.00	0.00	0.00	0.00	0.00	0.00	0.00
$\dot{m}_o$ x10^{-2}	1.41	6.58	1.41	1.41	0.00	0.00	0.00	0.00	0.00	0.00	0.00	0.00
η_c x10^{-4}	31.75	189.35	34.3	38.4	0.00	0.00	0.00	0.00	0.00	0.00	0.00	0.00
ϕ_i	58	57	56	56	54	55	58	62	63	63	61	64
ϕ_o	52.8	50.4	50.2	55.2	55.9	57.9	58.8	57.2	59.8	59.9	58	60.2
P_{atm}	980	979.6	979.3	979.3	978.9	979	978.9	978.8	978.8	978.7	978.8	978.7
Q_T/(W)	121.39	68.99	50.12	42.25	34.80	32.41	29.72	26.64	23.79	21.11	20.28	18.92
$\Delta\dot{\psi}$	2518.0	3212.2	2719.7	3038.6	3238.0	3127.5	3473.5	3306.0	3306.0	3135.6	3306.0	3652.2

Date: July 08, 2012; Time started: 09:00 am

Table 10C BURNER HEATING MODE 1

Vent outlet gap: 0.02 m; plenum entry gap: 0.02 m. An 1800 Watts electrical resistance heater, attached to the base of the thermal m

$T_{f,i}$	25.7	27.4	27.5	26.8	28.0	28.4	26.6	26.3	28.1	28.1	28.4	28.7
T_{ab-rp}	24.9	36.1	38.4	47.5	54.7	59.8	60.6	60.2	72.6	68.8	70.5	76.2
T_{uw}	31.7	36	40.5	44	52	52.2	56	56	55	59	60.2	59.8
T_{lw}	34.1	51.6	41.5	44.7	50.7	51.2	51.1	48.2	66.5	73.3	66.1	59.8
T_{bg}	44	51	48	57	60.1	60.1	66	64	56	68.4	75	64
T_f	34.5	41.1	43.8	51.5	57.1	58	61	61.8	60.2	67	67	67.2
T_{rp-f}	89	115	127	162	178	174	187	180	160	201	199	185
$T_{p,c}$	30	34	48	41.2	48.5	51	52	52	51.8	54.6	54	55
$T_{d,w}$	26	28	30.1	34	36	38	40	40	41	42	43	45
$T_{f,o}$	27	30.8	35.2	38.3	41.8	46.0	46.7	48.8	49.3	52.3	52	52.2
T_{ab-f}	25	30.1	37	45	57	60	65	66	66	69	71	70.2
$T_{c,d}$	27	29.8	33	36.2	40.8	43	41.8	46	46	48.7	48.8	48.8
V_i	0.7	0.3	0.7	0.7	0.7	0.3	2.4	0.7	1.4	1.7	0.7	0.3
V_o	13.26	5.88	13.56	13.75	14.04	6.17	49.11	14.29	28.32	34.98	14.37	6.31
$\dot{m}_o$ x10^{-2}	11.91	5.21	11.84	11.86	11.81	5.19	40.79	11.87	23.55	28.76	11.78	5.71
η_c x10^{-4}	23.3	22.76	84.87	121.32	159.04	86.49	806.4	282.78	671.83	848.84	372.2	196.28
ϕ_i	83	76	75	77	70	70	75	79	71	72	69	69
ϕ_o	78.3	77.8	88.4	86.9	90.5	84.8	87.3	93.4	87.7	93.7	83.7	86.8
P_{atm}	981.5	981.5	981.7	981.5	980.9	980.7	980.4	980.4	979.5	979.5	979.5	979.2
Q_T/(W)	423	316	229	243	218	179	175	150	113	133	123	102
$\Delta\dot{\psi}$	2687.3	4012.9	4821.8	7184.2	8363.2	8411.2	10906.3	10140.5	9464	11478.3	10896.2	10779

Date: July 08, 2012; Time started: 02:10 am

Table 11C ***BURNER HEATING MODE 2***

Vent outlet gap: 0.03 m; plenum entry gap: 0.02 m. A 1800 Watts electrical resistance heater, attached to the base of the thermal mass was used to generate heat for this experiment.

$T_{f,i}$	28.4	28.6	29.1	29.1	30.1	30.3	30.4	29.3	29.5	29.2	30.0	28.4	
T_{ab-rp}	76.8	75.5	81.7	78.9	80.7	87.8	88.2	92.6	93.8	89.8	90.4	90.8	
T_{uw}	56	59	62	64	66	69	6 6	65	66	67	70	68	
T_{lw}	66.5	66.1	68.2	62.9	57.2	73.3	74.3	81.5	73.3	63.9	71.2	67.3	
T_{bg}	64	69	64	69	69	76	82	76	78	81	80	76	
T_f	64.8	66	67.8	69	71	72	73	73	74.2	73.8	74.2	75.1	
T_{rp-f}	178	198	207	198	205	215	220	200	224	222	222	223	
$T_{p,c}$	52	53	56	68	59	62	60.6	59.9	62	61	63	61	
$T_{d,w}$	43	46	42	42	43	44	44	45	45	45	45	45	
$T_{f,o}$	51.8	50.4	49.9	44.3	48.7	46.2	49.7	53.8	54.1	49.3	47.7	53	
T_{ab-f}	67	69	71	74	77	80	79	78	80	81	85	84	
$T_{c,d}$	46	49	51	52	51.8	51	53.2	55	55	54	55	54	
V_i	0.7	1.4	0.7	1.7	1.0	1.4	0.7	0.28	0.7	0.7	1.0	0.3	
V_o	9.34	18.59	9.26	22.21	13.25	18.24	9.22	3.75	9.37	9.24	13.21	4.12	
$\dot{m}_o$ x10^{-2}	11.76	23.51	11.73	28.62	16.83	23.36	11.68	4.69	11.71	11.72	16.83	5.71	
η_c x10^{-3}	3.27	12.7	9.33	31.77	23.23	36.39	21.46	10.23	27.42	31.08	48.25	16.75	
ϕ_i	69	68	67	66	64	62	60	65	66	64	62	69	
ϕ_o	76.1	82.4	86.4	81.8	87.3	53.8	66.4	84.3	57.1	85.5	70.1	82.3	
P_{atm}	978.5	978.3	978	977.9	977.8	977.7	977.7	977.7	977.5	977.5	977.2	977.3	
Q_T/(W)	1318	697	490	362	298	270	233	202	192	169	155	145	
$\Delta\dot{\psi}$	10255	10633.0	10838.7	11341.9	11421.5	11695.2	11810.4	12102.9	12388.1	12372.5	12280.2	12913.4	

Date: July 09, 2012; Time started: 08:10 am

Table 12C ***BURNER HEATING MODE 3***

Vent outlet gap: 0.04 m; plenum entry gap: 0.02 m. A 1800 Watts electrical resistance heater, attached to the base of the thermal mass was used to generate heat for this experiment.

$T_{f,i}$	23.9	24.2	24.2	24.5	25.1	24.5	24.3	24.4	25.3	25.2	24.8	25.5	
T_{ab-rp}	26.1	23.8	41.3	47.8	53.0	63.5	64.9	72.8	79.9	74.1	82.9	77.8	
T_{uw}	40	42	47	47	49	53	54	57	57	61	63	63	
T_{lw}	46.6	41.8	53.7	54.4	63.8	59.7	55.4	48.2	49.2	46.7	63.7	52.1	
T_{bg}	53	38	58	51	61	64	63	65	60	65	68	72	
T_f	40.8	42	49.2	53	57.2	58	58.2	62	62	65.2	67	68	
T_{rp-f}	42	49	83	188	198	194	179	202	183	215	228	214	
$T_{p,c}$	35	38	42.4	43	44	48	58	50	50	53.5	56	56.7	
$T_{d,w}$	28	28	30	31.8	33	34	35	36	36	39	40	40	
$T_{f,o}$	24.7	30.2	29.8	35.4	37.1	39.8	37.1	41.1	39.9	40.7	43.6	42.1	
T_{ab-f}	28	34	41	48	55	60.1	65	68	72	75	80	81	
$T_{c,d}$	29	30.8	36.5	36.2	37.2	37	41	43	43	49	51	48	
V_i	0.3	1.0	1.0	0.7	0.7	0.7	0.7	0.7	0.7	0.3	1.4	1.0	
V_o	9.34	18.59	9.26	22.21	13.25	18.24	9.22	3.75	9.37	9.24	13.21	4.12	
$\dot{m}_o$ x10^{-2}	11.76	23.51	11.73	28.62	16.83	23.36	11.68	4.69	11.71	11.72	16.83	5.17	
η_c x10^{-3}	3.27	12.7	9.33	31.77	23.23	36.39	21.46	10.23	27.42	31.08	48.25	16.75	
ϕ_i	91	89	88	89	85	86	87	89	86	86	89	87	
ϕ_o	79.4	87.3	85.1	80.5	84.7	86.7	84.8	84.5	81.7	85.3	80.8	83.4	
P_{atm}	980.5	980.8	981	981.0	980.7	980.8	981.0	981.1	980.8	980.9	980.7	980.7	
QT/(W)	435	166	191	141	139	119	99.54	89.48	74.65	72.58	76.21	67.63	
$\Delta\dot{\psi}$	4964	5254.2	7280	8216.9	9183.4	9581.3	9695.8	10688.1	10417.4	11280.9	11967.2	11974.0	

Date: July 09, 2012; Time started: 02:30 pm

Table 13C BURNER HEATING MODE 4

Vent outlet gap: 0.02 m; plenum entry gap: 0.04 m. A 1800 Watts electrical resistance heater, attached to the base of the thermal mass was used to generate heat for this experiment.

$T_{f,i}$	30.3	30.2	29.0	27.5	28.7	28.7	30.2	28.5	27.4	26.9	27.6	26.5
T_{ab-rp}	50.7	52.4	57.7	66.7	76.1	79.9	86.8	77.2	92.0	95.3	93.3	96.8
T_{uw}	40	45	48	50.8	49	52	51	52	53	50	53	53
T_{lw}	50.6	44.6	45.5	47.5	60.7	58.7	46.9	41.3	47.9	52.8	69.7	50.9
T_{bg}	56	72	72	79	74	75	59	41.3	66	53	82	66
T_f	52	57.5	63	67	65	70	66	68	70	62	73.2	69.8
T_{rp-f}	131	169	192	210	185	211	181	187	200	145	215	191
$T_{p,c}$	43	48	51	53	51	54	51.4	54	54	52	57	56
$T_{d,w}$	35	37	39	41	41	43	43	44	45	43	45	45
$T_{f,o}$	38.5	46.2	45.6	52.6	41.2	57.9	57.2	58.9	59.1	55.8	54.3	43
T_{ab-f}	51	41	64	51	41	51	51.6	51.5	51.6	51	52	51.6
$T_{c,d}$	39	43	46	47	47	48	47	50	51	48	50.1	53
V_i	1.0	1.0	1.0	1.4	0.3	0.3	0.7	0.3	1.0	0.7	0.3	1.0
V_o	19.32	19.63	19.90	28.02	1.66	6.16	13.89	6.17	20.32	14.00	6.20	20.38
$\dot{m}_o$ x10^{-2}	16.83	16.84	16.91	23.59	1.41	5.17	11.69	5.17	16.99	11.81	5.19	17.04
η_c x10^{-4}	76.31	129.36	220.47	474.62	44.04	196.92	779.15	387.21	1342.84	1328.94	396.35	1882.62
ϕ_i	64	64	67	73	73	72	67	71	76	78	78	79
ϕ_o	41.1	67.0	67.6	74.1	74.6	69.9	73.8	75.3	78.3	76.4	77.3	78.9
P_{atm}	978.5	978.5	978.4	978.3	978.2	978.1	977.9	977.9	977.9	977.7	977.8	977.8
QT/(W)	435.2	291	221.6	196.2	152.8	135.3	85.50	65.50	82.29	61.23	86.58	64.06
$\Delta\dot{\psi}$	6371.5	7910.4	9749.3	11443.8	10179.8	11512.4	10092.4	11047.9	12080.6	10010.5	12671.8	12298.3

LIBRARY
KWAME NKRUMAH
UNIVERSITY OF SCIENCE & TECHNOLOGY
KUMASI

Date: July 10, 2012; Time started: 08:10 am

Table 14 C ***BURNER HEATING MODE 5***

Vent outlet gap: 0.03 m; plenum entry gap: 0.04 m. A 1800 Watts electrical resistance heater, attached to the base of the thermal mass was used to generate heat for this experiment.

$T_{f,i}$	24.6	24.8	25.2	25.3	26.0	26.7	27.1	28.0	28.4	28.2	28.6	28.4	
T_{ab-rp}	27.9	34.9	46.5	57.9	67.3	68.8	82.7	88.4	90.9	100.2	97.6	100.2	
T_{uw}	33	37	40	44	47	50	51	54	55	51	55	58	
T_{lw}	37.8	32.9	36	38.6	38.9	35.4	37.7	42.7	57	42.3	49.2	55.4	
T_{bg}	66	63	52	56	70	74	76		82	80	62	86	86
T_f	44	48	55	60	63	67	70	72	75	64	74	78	
T_{rp-f}	138	173	192	210	220	228	235	240	243	165	229	239	
$T_{p,c}$	37	39	44.8	46.5	51	53	56	58	60	53	59	62	
$T_{d,w}$	28	30	32	35	37	39	40	42	44	45	45	48	
$T_{f,o}$	31.0	37.8	46.0	46.6	54.5	57.1	55.9	58.6	60.1	51.2	66.2	65.6	
T_{ab-f}	30	38	49.8	51	51	51	51	51	51	51	51	51	
$T_{c,d}$	31	34	38.8	42	47	47	50	50	52	49	53	55	
V_i	1.4	0.7	0.7	1.0	0.7	0.3	1.0	0.7	0.7	0.3	0.3	1.4	
V_o	3.72	1.90	1.95	2.79	1.99	0.86	2.85	2.01	2.01	0.84	0.88	4.09	
$\dot{m}_o$ x10^{-2}	6.69	3.34	3.34	4.77	3.33	1.42	4.74	3.31	3.30	1.42	1.41	6.61	
η_c x10^{-2}	0.25	0.20	0.29	0.54	0.46	0.25	0.93	0.73	0.86	0.36	0.44	2.33	
ϕ_i	87	85	84	83	80	78	76	72	69	67	67	68	
ϕ_o	81.7	80.7	82.7	81.7	77.7	76.7	72.7	69.6	68.8	68	67.9	66.6	
P_{atm}	981.3	981.4	981.5	981.6	981.5	981.4	981.4	981.3	981.3	981.3	981.3	981.3	
QT/(W)	521.9	388.5	344.1	306.0	268.9	229.6	219.6	199.6	180.6	140.9	148.4	141.9	
$\Delta\dot{\psi}$	5663.8	6722.4	8534.7	9861.6	10453.5	11302.9	11973.8	12224.7	12881.5	10061.9	12562.9	13656.2	

Date: July 10, 2012; Time started: 03:20 pm

Table 15C BURNER HEATING MODE6

Vent outlet gap: 0.04 m; plenum entry gap: 0.04 m. A 1800 Watts electrical resistance heater, attached to the base of the thermal mass was used to generate heat for this experiment.

$T_{f,i}$	31.6	32.8	31.7	31.6	32.4	32.6	31.7	30.3	29.6	29.4	28.1	27.2	
T_{ab-rp}	46.9	40.6	50.6	64.5	69.6	72.8	81.7	80.1	91.9	88.8	82.8	87.5	
T_{uw}	40	44	47	50.1	52	55	57	52	51	48	50	53	
T_{lw}	40.2	38.8	39.7	40.1	39.2	43.2	43.9	36.9	58.8	50	39.6	46.5	
T_{bg}	48	61	74	74	81	65	86	66	56	50	53	73	
T_f	46	53	59	65	67	70	74	64.5	62	58	69	72	
T_{rp-f}	110	152	172	198	209	221	232	238	170	139	211	243	
$T_{p,c}$	41	47	49	52	54	58	59	55	52	50	55	57	
$T_{d,w}$	35	38	40	41	45	46	45	45	43	42	48	45	
$T_{f,o}$	35.8	37.5	38.6	58.6	53.7	61.3	60.2	46.9	48	46.7	55.0	57.9	
T_{ab-f}	52	54	59	69	72	79	85	86	81	80	75	85	
$T_{c,d}$	36	41	41	46	48	49	51	49	67	45.5	48	49	
V_i	0.7	0.7	2.0	1.0	1.0	0.3	1.0	0.7	0.3	0.7	1.0	0.7	
V_o	3.69	3.70	10.64	5.66	5.56	1.71	5.69	3.84	1.65	3.85	5.66	4.01	
$\dot{m}_o$ x10^{-2}	3.27	3.26	9.33	4.67	4.66	1.40	4.66	3.28	1.41	3.29	4.73	3.32	
η_c x10^{-2}	0.08	0.19	0.84	0.51	0.61	0.22	0.85	0.54	0.28	0.71	1.37	0.99	
ϕ_i	52	49	51	56	49	53	54	56	60	61	64	70	
ϕ_o	53	55.3	56.4	56.8	56.1	58.7	55.7	52.9	59.4	58.8	55.6	69.2	
P_{atm}	978.4	978.4	978.4	978.4	978.4	978.3	978.3	978.3	978.4	978.6	978.6	978.4	
Q_T/(W)	591.2	342.5	305.9	305.9	264.2	239.9	232.4	208.6	166.4	134.0	142.3	151.6	
$\Delta\dot{\psi}$	4145.8	5738	7742.4	9337.3	9630.4	10345.2	11662.4	9579.3	9114.3	8103.3	11426.3	12469.1	

Date: July 11, 2012; Time started: 08:25 pm

Table 16C ***BURNER HEATING MODE 7***

Vent outlet gap: 0.02 m; plenum entry gap: 0.06 m. A 1800 Watts electrical resistance heater, attached to the base of the thermal mass was used to generate heat for this experiment.

T_{fi}	24.8	25.2	25.4	26	29.6	25.6	25.3	26.5	25.8	26.8	28.1	29.3
T_{ab-rp}	26.4	34.2	47.4	60.7	63.9	69.1	80.6	84.8	91.6	89.4	91.1	98
T_{uw}	33	38	41	45	49	50	53	56	51	56	59	53
T_{lw}	27.9	29.7	33.1	39.5	44.1	52.3	58.3	52.4	52.4	65.2	58.3	53.6
T_{bg}	57	62	69	75	66	62	80	86	47	71	77	55
T_f	43	50.6	56	61	66	68	72	74	62	73.6	76	64
T_{rp-f}	110	153	179	196	208	217	226	237	175	215	233	168
$T_{p,c}$	38	43	46	51	53	55	58	60.5	54	63	65	55
$T_{d,w}$	28	30	32	35	38	40	41	43	43	44	46	45
$T_{f,o}$	33	41.2	43	46.6	52.1	51.5	55.3	59	54.4	57.4	57.3	57.1
T_{ab-f}	32	39.6	48	58	64	69	76	80.2	81	85.5	88	84.8
$T_{c,d}$	35	38	41	46	48	49	52.7	57	48	55	56.6	50
V_i	0.3	0.3	0.3	0.3	0.3	1.4	0.3	1.4	0.7	1.0	1.7	1.4
V_o	1.60	1.64	1.65	1.67	1.68	7.91	1.72	8.07	3.99	5.73	9.70	7.95
$\dot{m}_o$ x10^{-2}	1.43	1.43	1.43	1.43	1.41	6.67	1.43	6.65	3.33	4.47	8.02	6.58
η_c x10^{-2}	0.07	0.11	0.14	0.16	0.20	1.17	0.28	1.45	0.69	1.29	2.35	1.75
ϕ_i	84	81	79	76	73	75	80	72	76	72	67	61
ϕ_o	74.3	70.1	76.6	71.4	69.3	64	65.6	68.5	68.8	68.9	65.4	59.9
P_{atm}	981.9	981.9	981.7	981.3	981.5	981.7	981.3	981.2	981.1	981.1	980.5	980.5
Q_T/(W)	402.2	345.5	324.7	306.0	253.6	244.4	238.0	219.2	176.7	173.7	165	131.6
$\Delta\dot{\psi}$	5316	7324.6	8747	9918.3	10177.7	11925.3	13031.3	13219.8	10252.4	13011.2	13271.6	9765.7

Date: July 11, 2012; Time started: 01:50 pm

BURNER HEATING MODE 8

Vent outlet gap: 0.03 m; plenum entry gap: 0.06 m. A 1800 Watts electrical resistance heater, attached to the base of the thermal mass was used to generate heat for this experiment.

$T_{f,i}$	30.4	31.3	30.8	30.7	30.3	30.4	30.2	32.4	32.4	31.7	32.4	32.5
T_{ab-rp}	53.5	55.9	62.4	66.6	71.9	77.0	81.6	85.2	81.4	79.9	79.7	78.3
T_{uw}	45	49	53	55	57	58	60	61	58	53	50	49
T_{lw}	41.8	43.7	43.8	40.8	45.4	48.4	55.5	42.4	49.4	44.8	40.6	40.3
T_{bg}	57	72	84	73	86	89	88	90	63	54	52	59
T_f	36.7	62.5	67	70	72	73	77.6	79	67	65	58.5	58
T_{rp-f}	149	180	204	213	222	228	234	240	184	152	132	118
$T_{p,c}$	50	54	57	60	62	62	66	66	59	54	53	51
$T_{d,w}$	39	40	44	45	47	49	50	51	51	4 9	47	40
$T_{f,o}$	46.5	47	58.5	63.5	66.8	68.1	68.5	59.1	42.8	53.1	53.2	52.9
T_{ab-f}	59	62	69	73	78	80.2	85	88	87	86	82	79
$T_{c,d}$	45	48	51	52	52	53	55.5	57	52.2	50.2	49	47
V_i	1.0	0.3	0.3	0.3	0.7	0.0	0.0	0.0	0.3	0.0	0.0	0.0
V_o	3.65	1.09	1.13	1.15	2.72	0.00	0.00	0.00	1.08	0.00	0.00	0.00
$\dot{m}_o$ x10^{-2}	4.68	1.40	1.40	1.40	3.27	0.00	0.00	0.00	1.39	0.00	0.00	0.00
η_c x10^{-3}	0.34	0.85	1.23	1.65	4.66	0.00	0.00	0.00	3.06	0.00	0.00	0.00
ϕ_i	58	55	55	57	58	58	58	52	52	51	53	52
ϕ_o	55.5	51.9	55.6	52.6	53.2	54.3	55.6	49.5	53	49.9	51.8	45.2
P_{atm}	979.1	978.6	978.8	979	978.8	978.6	978.6	978.6	978.5	978.5	978.4	978.2
Q_T/(W)	880.3	514.5	414.3	336.8	294.9	260.1	237.7	212.2	158.7	129.3	106.6	90.1
$\Delta\dot{\psi}$	1849	8745.5	10086.4	10903	11544.7	11771.1	13013.5	12723.1	9615.9	9292.4	7347.3	7182.8

Date: July 12, 2012; Time started: 08:35 pm

Table 18C BURNER HEATING MODE 9

Vent outlet gap: 0.04 m; plenum entry gap: 0.06 m. A 1800 Watts electrical resistance heater, attached to the base of the thermal mass was used to generate heat for this experiment.

$T_{f,i}$	24.3	24.4	24.2	24.5	25.3	25	25.2	25.5	25.9	26.4	26.8	26.6
T_{ab-rp}	25.8	33.3	48.5	58.4	60.5	72.7	78.2	85.7	93.3	98.4	105.5	107.2
T_{uw}	32	37	40.2	44	47	50	53	56	51	56	59	53
T_{lw}	39.3	40.6	40.7	40.9	46.4	49	57.3	61.3	58.3	57.7	57.4	55.7
T_{bg}	54	54	60	58	63	66	62	70	74	68	78	78
T_f	44	49.8	54.5	58.7	62	64	69	69	72.4	75	70.2	75.6
T_{rp-f}	114	154	181	196	209	215	224	231	237	242	212	240
$T_{p,c}$	39	43	47	50	52	56	57.8	60	62	65	61	62
$T_{d,w}$	27	30	32	34	36	38	40	41	43	45	45	46
$T_{f,o}$	31.8	34.4	35.5	37.9	40.3	45.8	48.1	48.9	48.7	53	51.9	53.9
T_{ab-f}	31	38	48	56	62	68	74	75	83	85.2	85	88
$T_{c,d}$	32	35.1	39.8	42	43	46.8	50	50	51	55	50.2	55
V_i	0.7	1.0	1.0	0.7	1.0	0.3	0.7	1.4	0.7	0.7	0.3	1.0
V_o	1.87	2.69	2.70	1.90	2.73	0.83	1.96	3.93	1.96	1.98	0.85	2.84
$\dot{m}_o$ x10^{-2}	3.35	4.79	4.79	3.35	4.77	1.43	3.34	6.67	3.33	3.33	1.42	4.75
η_c x10^{-4}	15.96	35.35	43.07	37.62	67.16	22.49	63.52	135.4	75.19	83.82	36.33	138.14
ϕ_i	86	85	85	84	81	82	75	79	77	75	74	73
ϕ_o	81.6	81.1	65.7	64.4	65.8	70.2	56.3	74.7	70.8	70.8	71	70.2
P_{atm}	981.5	981.9	981.6	981.8	981.6	981.7	981.8	981.6	981.5	981.3	981.1	981.1
Q_T/(W)	416.3	346.2	339.1	304.7	262.4	250.1	232	215.9	207.5	194.2	171.2	169.6
$\Delta\dot{\psi}$	5749.7	7345.2	8700.3	9695.8	10397.9	11018.3	12279.1	12194.1	12955.4	13477.7	12112.3	13574.0

Date: July 14, 2012; Time started: 12:30 pm

Table 19C ***HYBRID HEATING MODE 1***

Vent outlet gap: 0.02 m; plenum entry gap: 0.02 m. A 1800 Watts electrical resistance heater, attached to the base of the thermal mass was used to generate heat for this experiment.

$T_{f,i}$	29.8	28.8	30.4	30.8	30.4	29.8	29.1	28.7	28.5	28.2	28.3	28.2
T_{ab-rp}	35.1	42.2	53.7	66.4	77.6	88.7	99.4	107.1	113	112.4	107.4	103.3
T_{uw}	40	44	49	52	56	59	60	58	55	54	58	60
T_{lw}	43.6	56	52.7	62.9	58.9	62.3	63.5	64.8	61.5	52.7	72.6	62.8
T_{bg}	55	82	78	76	78	82	83	62	51	45	65	84
T_f	49	53	59	67	73	75	79	70	66	64	75	77.8
T_{rp-f}	114	154	181	196	209	215	224	231	237	242	212	240
$T_{p,c}$	49	53	56	41	65	68	70	66	65	63	67	69
$T_{d,w}$	39	41	45	48	51	53	55	57	56	55	56	56
$T_{f,o}$	44.2	49.8	51.6	52.6	66.2	67.5	69.2	48.9	47	47.5	61.8	61.1
T_{ab-f}	43	50	59	69	79.8	87	92.6	95	96	96	98	98.8
$T_{c,d}$	52	57	59	62.5	69	70	72	69.5	69	66	71	73
V_i	1.7	0.7	1.0	2.0	0.3	1.4	0.3	1.4	2.0	2.4	0.3	0.3
V_o	9.26	3.89	5.56	11.15	1.74	8.19	1.77	7.77	11.04	13.27	1.73	1.73
$\dot{m}_o$ x10^{-2}	7.98	3.30	4.68	9.35	1.40	6.56	1.41	6.59	9.41	11.29	1.41	1.41
η_c x10^{-4}	30.26	19.06	35.9	97.03	17.91	93.83	23.15	95.11	131.23	162.07	30.77	33.98
ϕ_i	59	65	58	57	59	59	61	62	64	63	65	67
ϕ_o	48.1	63.8	60	62.9	57.2	61.1	53.4	56.8	57.6	54.1	43	51.3
P_{atm}	980.3	980.1	980.0	979.6	979.1	978.9	979	978.8	978.7	978.3	978	978
QT/(W)	471.2	382.7	337.0	312.7	297.6	279.7	267.1	249.7	232.3	210.5	177.3	169
$\Delta\dot{\psi}$	5549.9	6917.9	8085.7	10145.9	11772.6	12497.3	13697.5	11523.23	10523.2	10057.5	12910.9	13658.7

Date: July 15, 2012; Time started: 09:10 am

Table 20C ***HYBRID HEATING MODE 2***

Vent outlet gap: 0.03 m; plenum entry gap: 0.02 m. A 1800 Watts electrical resistance heater, attached to the base of the thermal mass was used to generate heat for this experiment.

$T_{f,i}$	24.7	24.7	24.8	25.2	25.6	25.7	25.8	25.1	25.5	25.4	26.6	26.9
T_{ab-rp}	29.2	35.2	42.4	56.4	62.1	67.5	75.1	82.7	84.2	91.4	87.6	89.5
T_{uw}	36	41	45	47	51	55	59	61	59	59	60	63
T_{lw}	34.9	42	43.1	46.9	57.3	46.4	55.5	55.5	45.8	51	52.8	53.6
T_{bg}	50	56	57	72	61	72	86	80	68	77	82	78
T_f	44	54	58	61	66.8	72	75	78.8	70.8	73	78	72
T_{rp-f}	121	163	190	200	202	221	235	242	205	195	233	204
$T_{p,c}$	45	51	53	54.5	60	66	67.3	69.8	66	69.6	71	70
$T_{d,w}$	32	37	40	42	43	47	49	51	51	52	53	53
$T_{f,o}$	37.1	44.5	41.3	45.4	54.5	60.8	46.1	56.3	40.7	61.6	51.8	68
T_{ab-f}	41.5	50	60	65.2	78	86	93	99	101.8	109	113	111
$T_{c,d}$	48	54	54	53	58	62.5	62	65	63	65	66	65
V_i	1.4	0.7	1.4	1.0	1.7	1.4	2.4	2.0	2.4	1.7	2.4	2.7
V_o	5.06	2.59	5.12	3.70	6.46	5.42	8.89	7.66	8.74	6.61	9.02	10.64
$\dot{m}_o$ x10^{-2}	6.68	3.34	6.68	4.77	8.09	6.66	11.41	9.53	11.42	8.09	11.38	12.78
η_c x10^{-4}	22.71	22.14	57.38	48.74	106.07	103.66	197.06	187.38	221.77	173.98	271.38	302.12
ϕ_i	86	88	86	84	82	81	80	83	83	83	79	76
ϕ_o	74.3	75.8	72.3	77.2	74	70	67	72.5	69.1	70.1	62	57
P_{atm}	980.5	980.6	980.6	980.6	980.5	980.4	980.2	980.4	980.1	980.2	979.8	979.7
QT/(W)	533.4	406.8	350.8	314	278.0	261.1	248.4	236.6	196.4	184.5	178.2	153.7
$\Delta\dot{\psi}$	5639.6	8412.9	9480.9	10163.2	11598.6	12923.6	13692	14866	12693	13279.5	14223.1	12603.8

Date: July 15, 2012; Time started: 01:05 pm

Table 21C HYBRID HEATING MODE 3

Vent outlet gap: 0.04 m; plenum entry gap: 0.02 m. A 1800 Watts electrical resistance heater, attached to the base of the thermal mass was used to generate heat for this experiment.

$T_{f,i}$	26.7	27.1	28.3	29	28.4	27.1	26.4	25.4	25.4	25.3	25	24.6
T_{ab-rp}	71.2	79.8	84	81.1	93.1	89.5	92.8	85.7	85.5	87.4	92.5	92.5
T_{uw}	60	65	70	73.4	64	59	56	64	68	67	68	73
T_{lw}	61.0	52.7	58.3	61.1	49.6	49	46.7	54.7	55.2	48.6	59.1	52.1
T_{bg}	72	70	80	79	56	50	48	80	68	77	82	78
T_f	68.8	74	79.8	81	68	65	62	68	82	82	80	88
T_{rp-f}	184	214	231	241	178	144	128	187	214	230	239	246
$T_{p,c}$	61.8	68	69	73	68	66	64	67	68	70	72	73
$T_{d,w}$	43	48	40	42	43	47	49	51	51	52	53	53
$T_{f,o}$	38.7	45.7	52	54	54	53	52	52	53	54	55	57
T_{ab-f}	95	101	104	109	111	108	106	107	106	109	111	117
$T_{c,d}$	56	62	61	66	63	62	61	62	63	66	68	68
V_i	3.1	2.7	3.4	1.4	0.7	3.1	0.3	0.7	0.3	2.4	0.3	1.7
V_o	10.40	9.25	11.83	4.89	2.45	10.86	1.05	2.46	1.06	8.48	1.06	6.08
$\dot{m}_o$ x10^{-2}	18.21	15.83	20.05	8.15	4.08	18.17	1.76	4.13	1.77	14.15	1.77	10.05
η_c x10^{-4}	50.55	83.06	160.5	84.98	42.01	229.6	24.28	69.08	41.4	346.25	43.55	297.55
ϕ_i	76	75	71	67	71	74	78	80	80	81	82	83
ϕ_o	63.4	56	55.1	60	62.4	60.5	53	70	64.3	72.7	69.9	74.6
P_{atm}	979	978.7	978.1	977.9	978	978.1	978.1	978.3	978.2	978	978.2	978.4
Q_T/(W)	1488.4	861.6	609.2	463.7	349.1	263.4	221.6	217.7	204.9	194.8	186.7	177.1
$\Delta\dot{\psi}$	11824.9	13048.1	1 4201.1	14244.3	11062	10708.8	10065.6	11957.8	15560.5	15623.1	15174.4	17319.3

Date: July 16, 2012; Time started: 09:15 am

Table 22C ***HYBRID HEATING MODE 4***

Vent outlet gap: 0.02 m; plenum entry gap: 0.04 m. A 1800 Watts electrical resistance heater, attached to the base of the thermal mass was used to generate heat for this experiment.

T_{fi}	24.3	24.6	24.6	24.9	25.4	25.4	24.8	25.6	27.1	27.7	27.6	28.3
T_{ab-rp}	26.2	30.8	41.2	48.8	58.3	69.1	80.4	84.4	86.4	97.8	97.8	90.9
T_{uw}	36	41	46	49	53	56	58	61	62.5	65	59	57
T_{lw}	36.4	38.4	48.8	47.4	51.8	48.7	56.7	58.6	58.8	59.9	50.0	50.1
T_{bg}	52	65	63	66	72	70	77	85	79	76	57	48
T_f	45	51.6	57	63	67	72	74	77.5	80.2	82	69.5	65
T_{rp-f}	108	149	176	193	206	216	224	231	238	240	173	145
$T_{p,c}$	45	49	53	58	63	65	67	71	72.5	75	68.5	68
$T_{d,w}$	39	34	38	41	43	46	49	51	52	54	54	53
$T_{f,o}$	41.4	42.7	46.8	56.4	60.9	62.8	59.6	54.2	65.5	67.8	49.4	49.6
T_{ab-f}	39	46	60	71	81	89	95	102	107	110	109	109
$T_{c,d}$	55	55	57	60	66.2	67.5	69.8	70.8	73	75	68	67.2
V_i	0.7	0.3	1.0	1.4	1.0	0.7	0.7	0.3	0.3	0.3	0.3	1.4
V_o	3.85	1.65	5.59	8.05	5.82	4.10	4.07	1.71	1.76	1.77	1.67	7.79
$\dot{m}_o$ x10^{-2}	3.35	1.44	4.79	6.69	4.77	3.34	3.35	1.43	1.42	1.42	1.42	6.61
η_c x10^{-4}	14.49	10.16	42.45	76.29	63.17	51.75	56.65	27.42	30.2	31.89	29.97	143.57
ϕ_i	88	85	85	83	81	81	83	82	76	71	72	68
ϕ_o	74.5	78	68.2	70.9	66.6	65.9	58.4	59.8	59.6	55.4	55.6	58.7
P_{atm}	982.8	982.6	982.7	982.7	982.5	982.4	982.5	982.5	982.3	982.2	982.2	981.9
Q_T/(W)	444.1	345.6	329.3	298.1	278.0	264.4	254.2	234.2	213.6	205.0	161.5	131.7
$\Delta\dot{\psi}$	6037.5	7781.3	9273.0	10813.3	11708.3	13008	13706	14358.4	14597.3	14873.9	11691.8	10326.7

Date: July 16, 2012; Time started: 01:05 pm

Table 23C ***HYBRID HEATING MODE 5***

Vent outlet gap: 0.03 m; plenum entry gap: 0.04 m. A 1800 Watts electrical resistance heater, attached to the base of the thermal mass was used to generate heat for this experiment.

T_{fi}	30	30.5	30.1	30.6	30.1	31.9	31.4	31.4	30.9	30.1	31.2	30.8
T_{ab-rp}	65.3	69.6	74.6	75.5	88.4	92.8	94.4	92.8	98.4	94.9	93.1	88.1
T_{uw}	53	58	60	63	63	65	67	63	61	59	55	60
T_{lw}	45.8	51.5	55.5	53	56.4	55.8	59.2	56.6	53.9	49.4	44.3	51.8
T_{bg}	67	59	72	79	80	87	75	60	56	50	46	70
T_f	66	71	75	77	79	81.5	82	72.8	67	65	62	74
T_{rp-f}	161	190	207	219	225	235	240	179	149	141	116	178
$T_{p,c}$	61	65	68.5	70	73	75	77	71	68	67	65	70
$T_{d,w}$	45	50	51	54	56	58	60	59	57	56	53	54
$T_{f,o}$	57.4	49.6	57	48.6	48.1	47.2	53.8	51.3	43.7	45.4	47.5	61.3
T_{ab-f}	84	90	96	101	104	108	111	113	111	111	106	108
$T_{c,d}$	64	62	69	70	74	76	76	72	65	66	64	70
V_i	0.0	2.7	0.7	1.0	0.3	0.3	0.3	0.3	0.3	1.0	1.0	0.3
V_o	0.00	9.949	2.642	3.672	1.102	1.092	1.117	1.108	1.084	3.642	3.652	1.14
$\dot{m}_o$ x10^{-2}	0.00	12.64	3.28	4.68	1.41	1.40	1.40	1.40	1.40	4.69	4.67	1.40
η_c x10^{-4}	0.00	70.27	26.68	49.01	17.27	19.8	22.51	23.26	23.18	83.78	86.88	35.01
ϕ_i	59	57	58	56	60	59	56	54	55	54	52	51
ϕ_o	45	46.1	44.9	38	49.3	51.3	33	39.1	45.5	31.2	31.5	35.6
P_{atm}	980.5	980.4	980.3	980	980	979.9	979.7	979.7	979.7	979.8	979.9	980
Q_T/(W)	1204.6	695.2	517.6	407.6	362.3	314.0	278.3	212.3	181.30	158.1	128.2	135.8
$\Delta\dot{\psi}$	10058.1	11268.0	12379.3	12748.2	13400.7	13504.5	13777.8	11425.2	10056.9	9770	8647	11912.3

Date: July 17, 2012; Time started: 07:55 am

Table 24C ***HYBRID HEATING MODE 6***

Vent outlet gap: 0.04 m; plenum entry gap: 0.04 m. A 1800 Watts electrical resistance heater, attached to the base of the thermal mass was used to generate heat for this experiment.

T_{fi}	25.2	25.5	26.4	26.8	26.3	25.9	26.4	28.2	27.1	29.2	29.3	29.5
T_{ab-rp}	26.9	34.7	43	53.1	57.3	62.8	78.7	79.2	86	90.7	98.9	102.1
T_{uw}	37.2	43	48	50	53	55	58	60	61	63	65	65.5
T_{lw}	31.7	37.5	41.7	42.5	49.1	50.9	46.1	56	56.4	59.6	52.5	48.6
T_{bg}	51	58	63	63	73	71	75	75	74	84	72	78
T_f	46	53	57.8	62	70	73	75	75	78	81	82	86
T_{rp-f}	116	154	177	191	203	215	220	226	231	237	239	243
$T_{p,c}$	45	48	53	57	60	63	65	67	69	70	72	73
$T_{d,w}$	32	37	40	42	45	48	49	52	53	55	56	48
$T_{f,o}$	39.1	33.4	37	53.2	50.6	47.3	55.1	45.6	66.1	55.2	65	75
T_{ab-f}	40	50	57	61	64	66	67	68	69	73	73	74
$T_{c,d}$	52	54	69	70	74	76	76	72	65	66	64	70
V_i	0.0	0.7	0.3	0.3	0.3	1.4	0.0	0.0	0.0	0.0	0.7	0.0
V_o	0.00	1.87	0.81	0.85	0.84	3.90	0.00	0.00	0.00	0.00	2.03	0.00
$\dot{m}_o$ x10^{-2}	0.00	3.35	1.43	1.43	1.43	6.69	0.00	0.00	0.00	0.00	3.30	0.00
η_c x10^{-4}	0.00	18.33	12.67	15.78	21.86	118.8	0.00	0.00	0.00	0.00	70.19	0.00
ϕ_i	82	77	73	74	72	72	71	64	66	61	60	59
ϕ_o	63	62.1	67.5	57.9	62.1	60	51.7	42	46.1	48.2	36.2	40.5
P_{atm}	985.1	985.1	985.1	985	985.2	985.3	985.4	985.0	985	984.8	984.6	984.8
Q_T/(W)	471.3	381.2	318.7	282.4	249.6	228.5	221.0	193.2	184.7	171.6	164.0	154.5
$\Delta\dot{\psi}$	6040.9	6602.2	8935.1	9945.8	12209.6	13115.9	13476	12939.2	13009	14930.2	11838.9	13322.6

Date: July 17, 2012; Time started: 02:50 pm

Table 25C ***HYBRID HEATING MODE 7***

Vent outlet gap: 0.02 m; plenum entry gap: 0.06 m. A 1800 Watts electrical resistance heater, attached to the base of the thermal mass was used to generate heat for this experiment.

$T_{f,i}$	30.6	32.9	32.7	32.3	30.4	30.2	30.9	32.2	32.3	31.8	31.1	30.0
T_{ab-rp}	49.7	56.3	64.9	71.8	76.8	86.3	90.6	101.3	108.5	111.3	111.6	108.4
T_{uw}	48	54	61	62	64	66	67	70	71	65	68	70
T_{lw}	51.1	50.6	47.7	48.1	55.5	45.6	54.8	63.2	59.0	55.4	59.6	59.3
T_{bg}	56	60	76	80	84	90	95	92	90	67	86	88
T_f	56.6	64	70	73	76	78	79	82	83	73	80	83
T_{rp-f}	136	172	191	206	218	225	230	236	243	187	221	241
$T_{p,c}$	50	57	61	64	65	67	70	71	73	67	70	72
$T_{d,w}$	42	46	51	54	56	58	60	62	63	63	63	65
$T_{f,o}$	51.5	56.1	62.9	60	68	70	72	73	75	68	73	75
T_{ab-f}	62	72	82	89	96	112	110	109	112	109	111	113
$T_{c,d}$	66	72	72	76	78	80	82	83	85	80	82	86
V_i	0.0	0.0	1.0	0.7	0.7	0.0	0.0	0.0	0.0	0.0	0.0	0.0
V_o	0.00	0.00	5.71	3.97	4.09	0.00	0.00	0.00	0.00	0.00	0.00	0.00
$\dot{m}_o$ x10^{-2}	0.00	0.00	4.65	3.26	3.28	0.00	0.00	0.00	0.00	0.00	0.00	0.00
η_c x10^{-4}	0.00	0.00	38.21	33.62	41.7	0.00	0.00	0.00	0.00	0.00	0.00	0.00
ϕ_i	50	44	45	45	52	53	51	48	48	48	51	55
ϕ_o	42.8	39.1	42.4	33.8	32.6	48.2	44.4	43.9	46.2	41.5	46.2	50.4
P_{atm}	981.0	980.6	980.5	980.5	980.7	981.0	980.8	980.7	980.7	980.8	980.9	981.3
Q_T/(W)	803.9	514.4	418.4	358.7	322.7	306.1	267.7	246.6	232.1	188.4	186.4	177.7
$\Delta\psi$	7361.8	8674.9	10330.4	11219.6	12552.7	13115.6	13164.0	13542.2	13764.9	11358.8	13359.3	14442.1

Date: July 18, 2012; Time started: 07:55 am

Table 26C HYBRID HEATING MODE 8

Vent outlet gap: 0.03 m; plenum entry gap: 0.06 m. A 1800 Watts electrical resistance heater, attached to the base of the thermal mass was used to generate heat for this experiment.

T_{fi}	23.4	23.8	24.1	24.6	25	25.6	25.9	25.9	26.2	26.6	26.9	27.2
T_{ab-rp}	27.8	34.2	41.8	58.3	67.3	68.7	76.0	89.1	86.1	90.5	91.7	98.8
T_{uw}	37	42	48	50	53	58	60	62	63	65	66	67
T_{lw}	33.1	37.8	44.5	48.6	40.7	48.7	57.8	50.2	56	52.4	51.3	43.2
T_{bg}	55	60	67	69	74	76	81	80	82	83	75	88
T_f	44	51	55	61	63	68	71	73	76	75	79	79
T_{rp-f}	113	150	174	189	200	208	215	220	226	232	232	236
$T_{p,c}$	39	45	49	52	54	58	61	62	63	65	67	68
$T_{d,w}$	30	35	38	43	44	46	53	50	52	55	55	57
$T_{f,o}$	47	53	51	58	61	64	62	69	70	66	71	73
T_{ab-f}	42	52	65	75	83	91	97	102	105	108	111	111
$T_{c,d}$	46	53	53	56	59	62	64	66	68	68	70	70
V_i	0.0	0.3	0.7	0.3	0.7	1.7	0.7	0.0	1.0	1.0	0.7	0.3
V_o	0.00	1.42	2.65	1.16	2.72	6.65	2.72	0.00	3.97	3.92	2.78	
$\dot{m}_o$ x10^{-2}	0.00	1.44	3.36	1.44	3.35	8.12	3.34	0.00	4.77	4.76	3.33	1.42
η_c x10^{-4}	0.00	9.20	22.47	14.48	38.4	200.79	54.2	0.00	96.74	99.12	79.94	35.36
ϕ_i	88	87	85	83	81	79	78	76	73	71	67	66
ϕ_o	77.7	78.1	72.8	74.5	71	67.7	66	47.9	56	61.7	54	53.1
P_{atm}	983.8	983.8	983.8	983.9	983.6	983.5	983.9	983.8	983.7	983.6	983.6	983.5
Q_T/(W)	516.3	390.6	342.0	325.4	295.2	134	241.3	233.8	208.5	195.5	179.9	171.7
$\Delta\dot{\psi}$	6019.7	7855.9	8867.2	10337.9	10755.2	11915.7	12593.3	13109.2	13800.3	13423.4	14354.2	14261.7

Date: July 18, 2012; Time started: 12:55 pm

Table 27C HYBRID HEATING MODE 9

Vent outlet gap: 0.04 m; plenum entry gap: 0.06 m. A 1800 Watts electrical resistance heater, attached to the base of the thermal mass was used to generate heat for this experiment.

$T_{f,i}$	31.4	30.7	30.1	30.1	29.9	30.1	30.2	30	30	30.5	30.3	29.9
T_{ab-rp}	64.9	64.2	73.2	80	83.4	91.3	89.4	98.8	103.7	107.8	105.2	104.7
T_{uw}	52	60	60	62	63	63	66	68	70	70	70	70
T_{lw}	48.0	53.9	48.7	60	64.7	53.2	66.1	63.4	68.4	61	72.1	58.2
T_{bg}	70	85	75	85	80	86	91	97	91	77	86	86
T_f	62	68	68	72	75	75	76.5	79	84	80.2	80	78
T_{rp-f}	150	189	191	208	215	220	227	231	233	235	238	241
$T_{p,c}$	54	60	60	63	65	65	67	68	70	69	70	70
$T_{d,w}$	42	49	50	52	54	56	58	59	60	61.8	62	62
$T_{f,o}$	53	59	64	69	70	72	70	74	70	75	74	72
T_{ab-f}	71	85	88	94	101	105	107	110	117	113	116	116
$T_{c,d}$	59	65	66	69	71	72	72	73	75	75	74	73
V_i	0.7	1.0	0.0	0.7	0.7	0.7	0.0	0.0	1.7	1.7	0.3	0.3
V_o	1.95	2.84	0.00	2.05	2.06	2.07	0.00	0.00	5.00	5.07	0.89	0.89
ϕ_i	53	54	56	56	56	56	55	56	55	52	54	57
ϕ_o	45.9	47.6	47.4	51.7	46.9	52.5	47.6	46.8	46.8	47.4	47.4	45
P_{atm}	982.0	981.5	981.3	981.1	981.0	980.7	980.8	980.7	980.7	980.4	980.2	979.7
Q_T/(W)	1050.4	649.2	475.5	399.8	341.5	304.4	276.5	247.2	230.8	209.2	190.9	176.3
$\Delta\dot{\psi}$	8583.5	10382	10555.5	11602.2	12437.1	12378	12732	13429.6	14704.5	13598.3	13595.6	13204.6

APPENDIX D

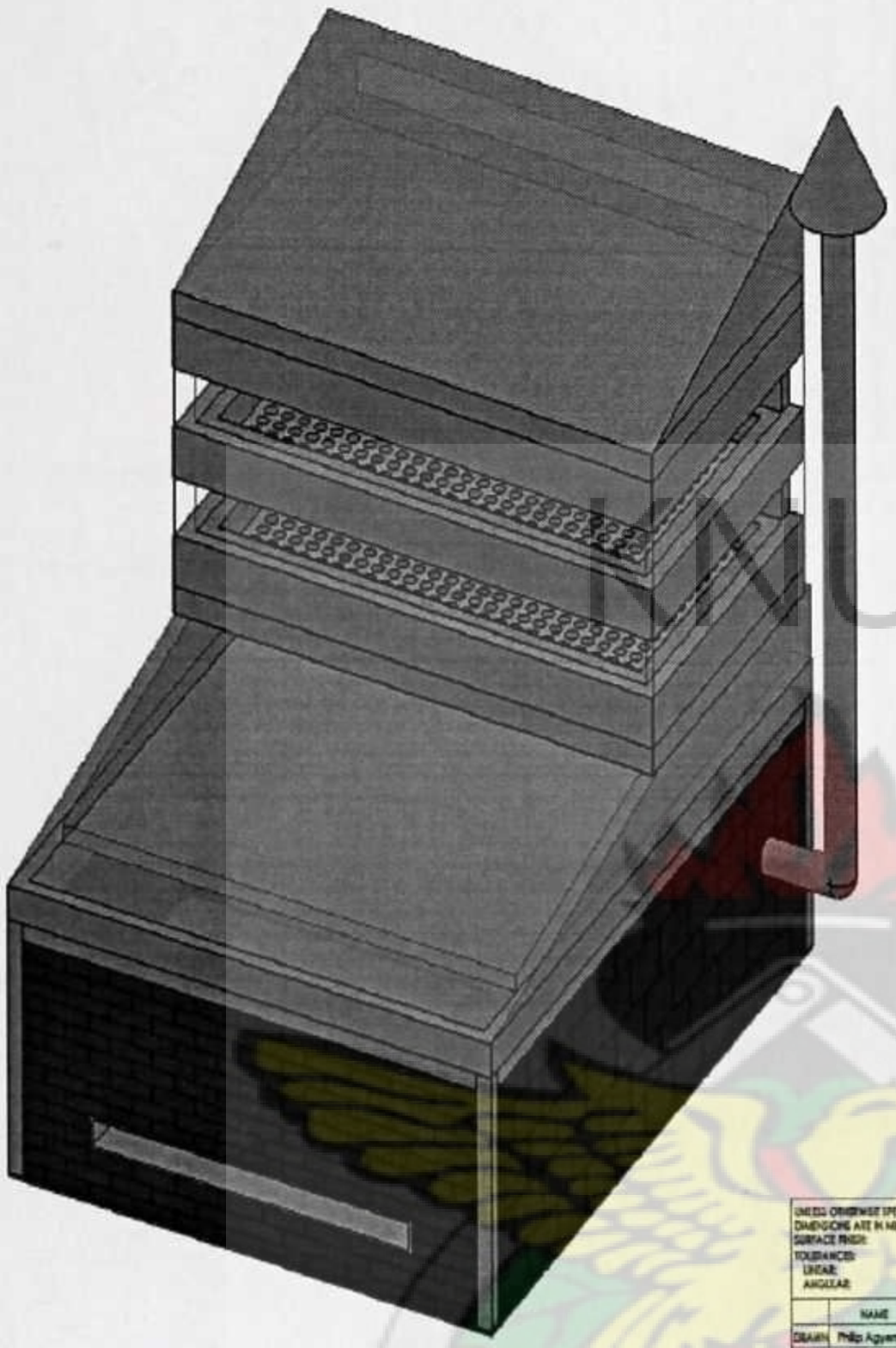

UNLESS OTHERWISE SPECIFIED: DIMENSIONS ARE IN MILLIMETERS SURFACE FINISH: TOLERANCES: LINEAR: ANGULAR:	FINISH:	DEBUR AND BREAK SHARP EDGES	DO NOT SCALE DRAWING	REVISION	
	NAME	SIGNATURE	DATE	TITLE: Mixed mode Solar crop dryer with Biomass backup heater	
DRAWN	Philip Agyeman		13/06/2012		
CHKD					
APPVD	C.E.K. Sekyere				
MFG					
QA					
				MATERIAL: Wood and Glass	DWG NO. 20 of 20
				WEIGHT:	SCALE:1:50 SHEET 20 OF 20

KNUST

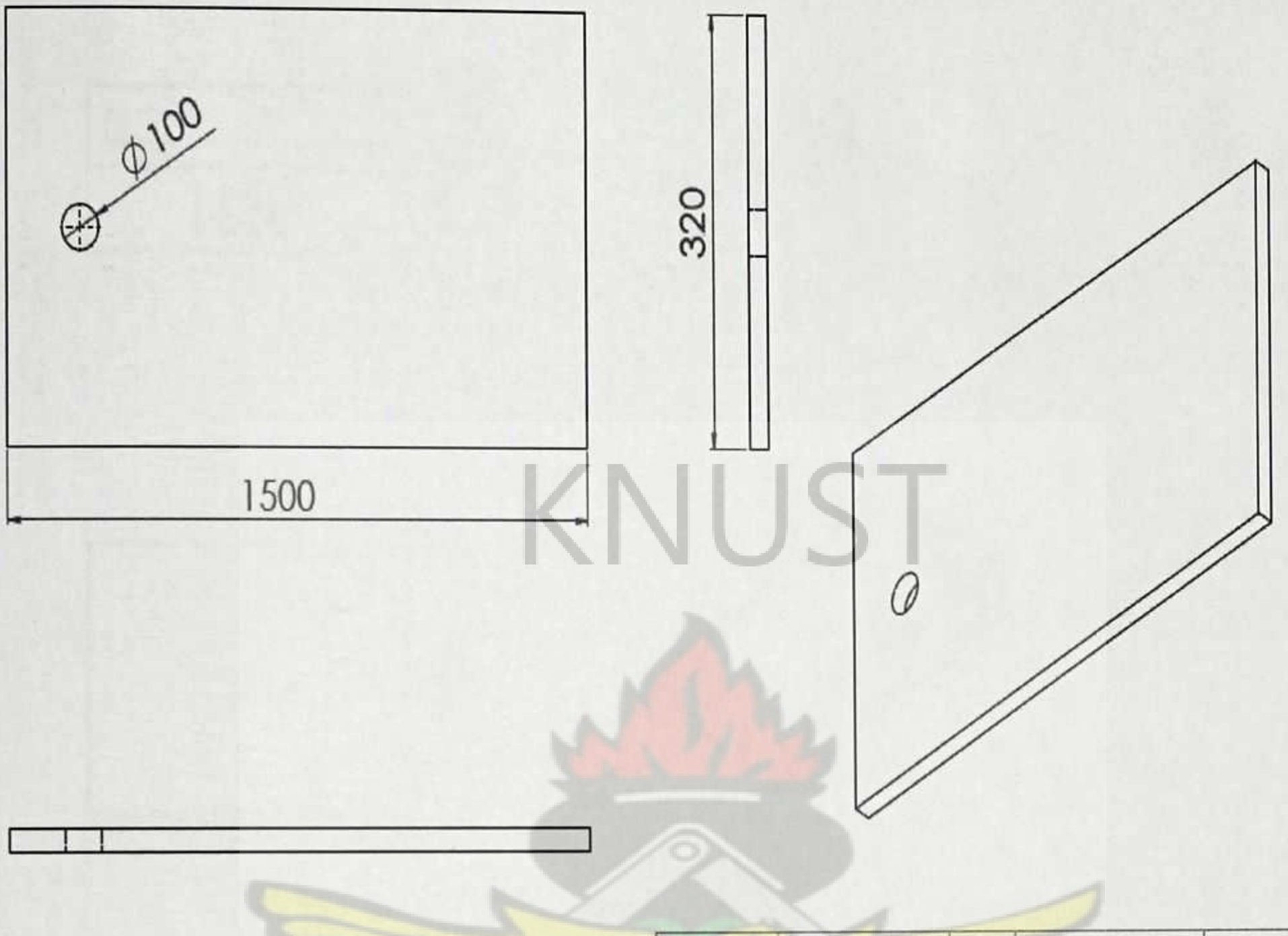

KNUST
NYANSAPO WOSANE NO BADWENMA

LIBRARY
KWAME NKRUMAH
UNIVERSITY OF SCIENCE & TECHNOLOGY
KUMASI

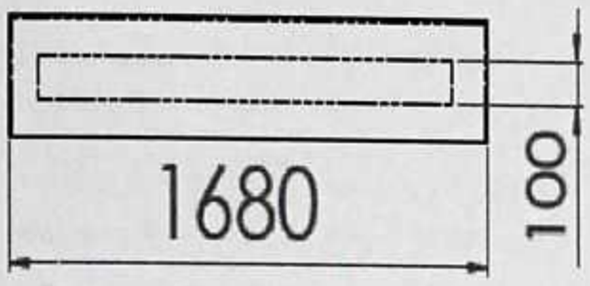

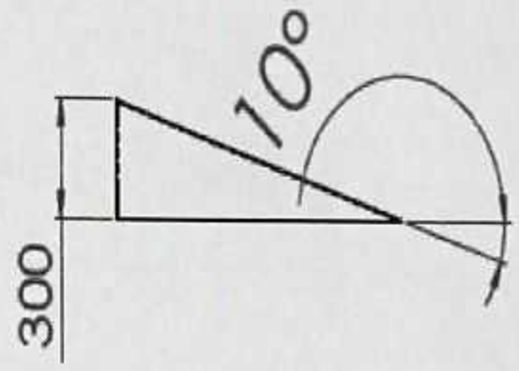

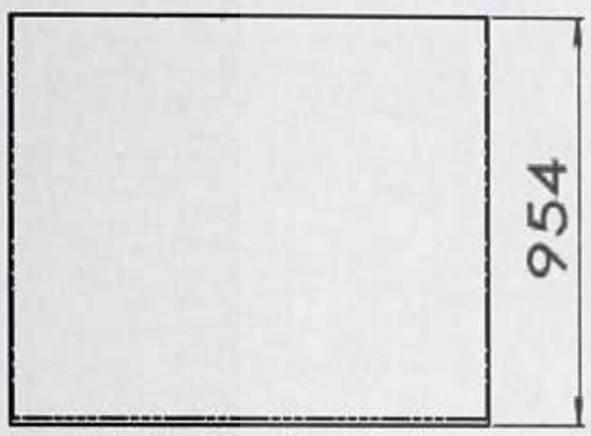

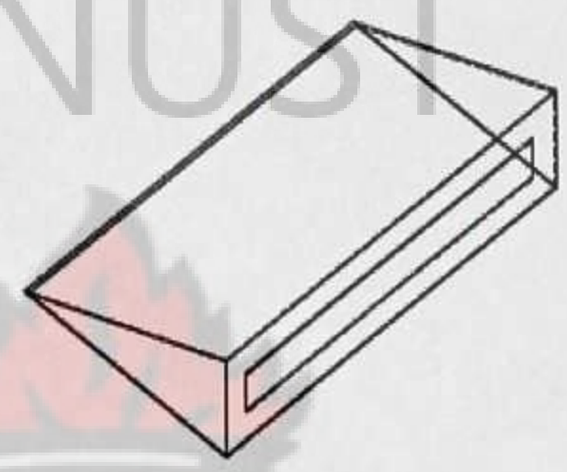

KNUST

UNLESS OTHERWISE SPECIFIED: DIMENSIONS ARE IN MILLIMETERS SURFACE FINISH: TOLERANCES: LINEAR: ANGULAR:			FINISH:				DO NOT SCALE DRAWING
							PART NAME: Air outlet vent
	NAME	SIGNATURE	DATE				TITLE: Mixed mode solar crop dryer with biomass backup heater
DRAWN	Philip Agyeman		12/04/2012				
CHKD							
APPVD	C.K.K. Seltzerer						
MFG							
QA				MATERIAL: WOOD AND GLASS			DWG NO. 6 of 20
				WEIGHT:			SCALE:1:20 SHEET 6 OF 20

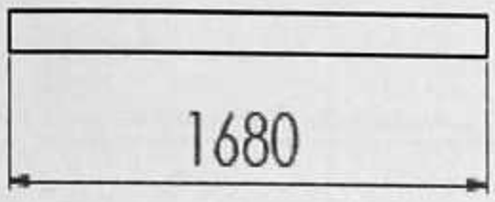

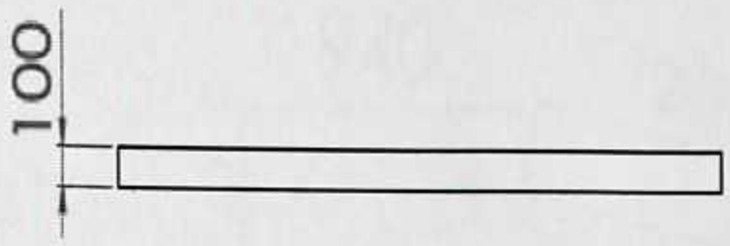

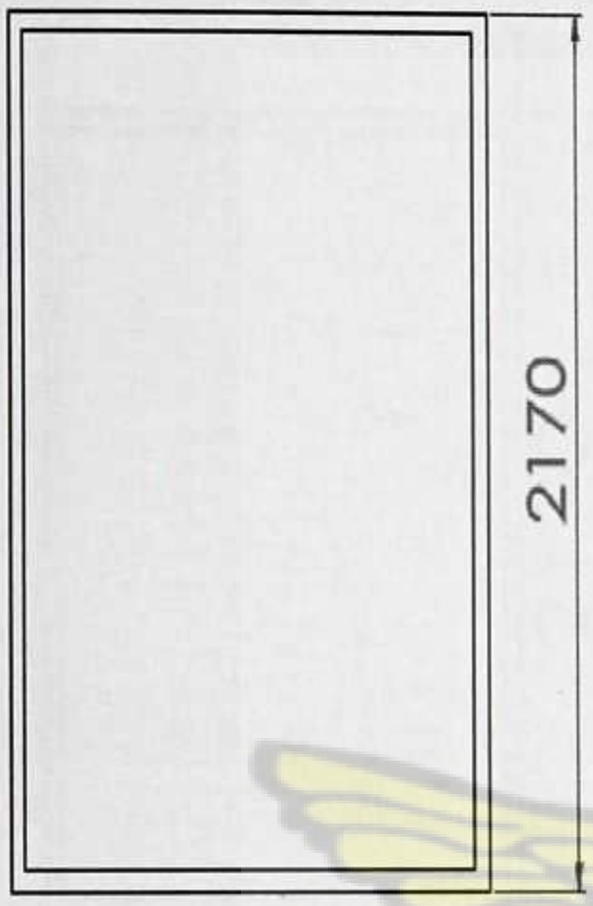

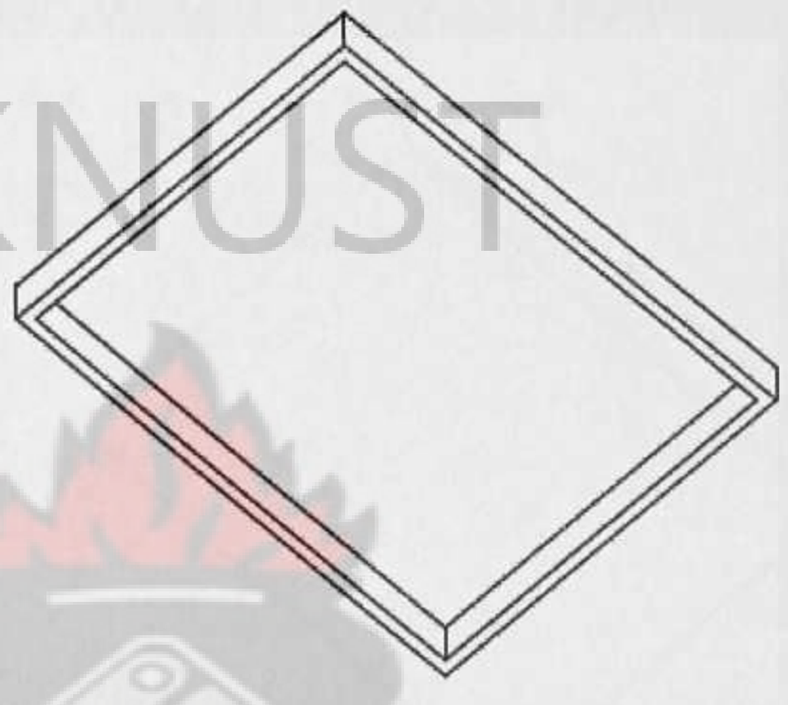

KNUST

UNLESS OTHERWISE SPECIFIED: DIMENSIONS ARE IN MILLIMETERS SURFACE FINISH: TOLERANCES: LINEAR: ANGULAR:	FINISH				DO NOT SCALE DRAWING	REVISION
					PART NAME: Plenum glass cover support	
	NAME	SIGNATURE	DATE		TITLE: Mixed mode solar crop dryer with biomass backup heater	
DRAWN	Philip Agyeman		12/04/2018			
CHKD						
APPVD	C.K.K. Sekyere					
MFG						
Q.A				MATERIAL: WOOD	DWG NO. 11 of 20	
				WEIGHT:	SCALE:1:20	SHEET 11 OF 20

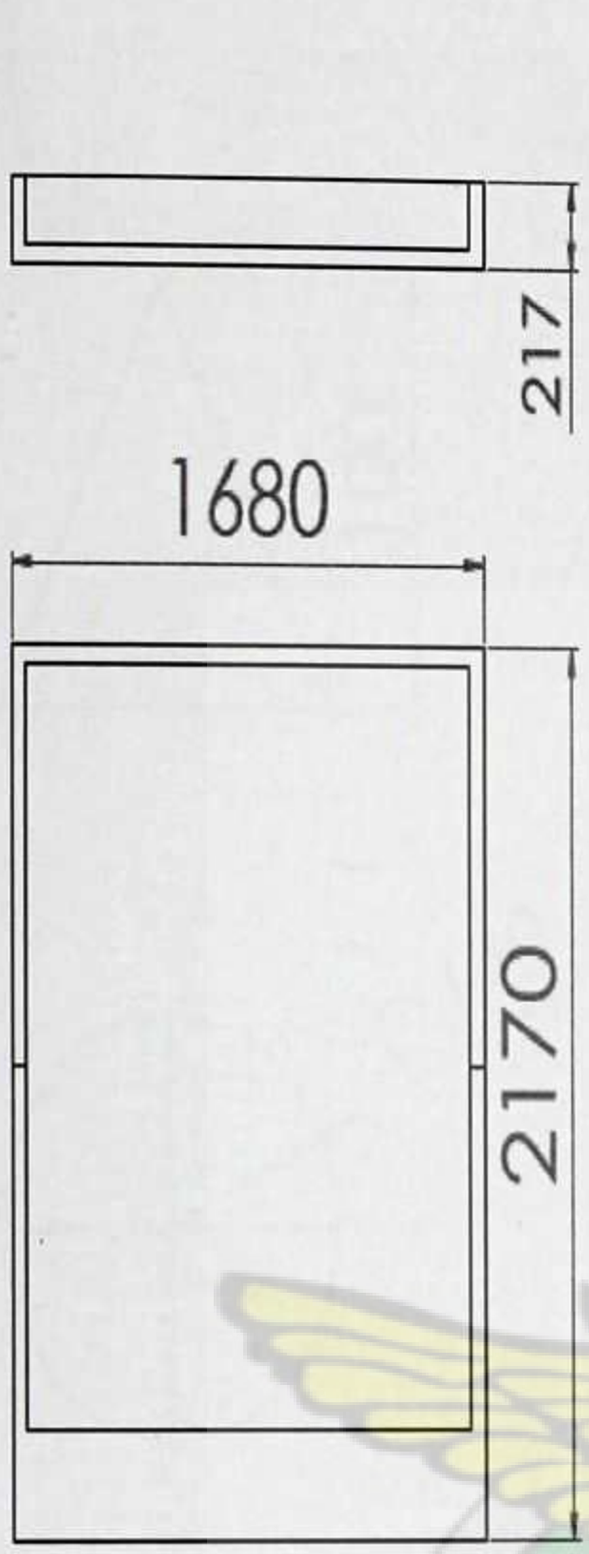

KNUST

UNLESS OTHERWISE SPECIFIED: DIMENSIONS ARE IN MILLIMETERS SURFACE FINISH: TOLERANCES: LINEAR: ANGULAR:	FINISH:					DO NOT SCALE DRAWING	REVISION
						PART NAME: Plenum cover glass assembly	
	NAME	SIGNATURE	DATE			TITLE: Mixed mode solar crop dryer with biomass backup heater	
DRAWN	Philip Aguerron		13/dec/2012				
CHKD							
APPVD	C.K.K. Sekyere						
MFG							
Q.A							
				MATERIAL: WOOD AND GLASS		DWG NO. 10 of 20	
				WEIGHT:		SCALE:1:20	SHEET 10 OF 20

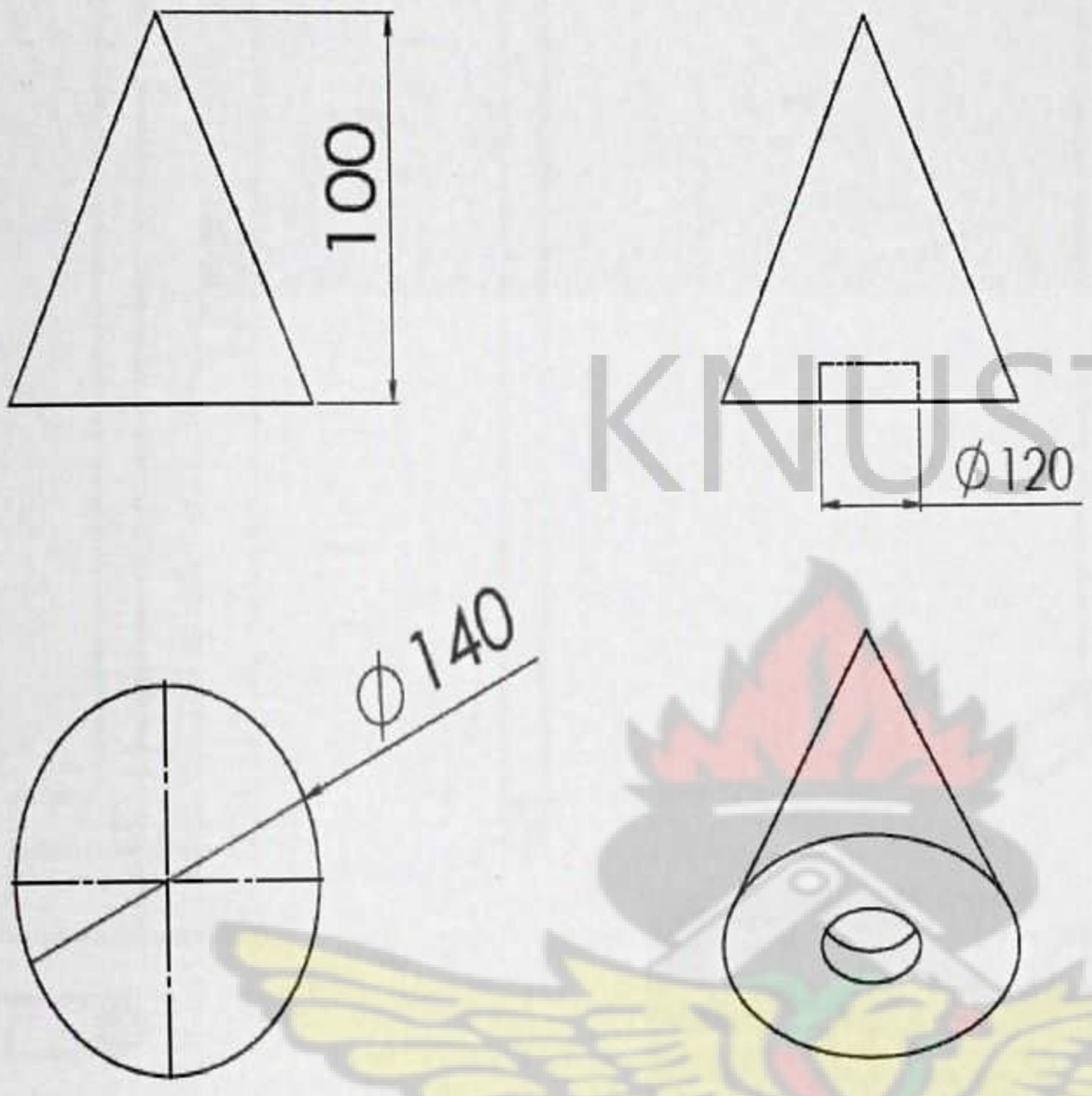

KNUST

UNLESS OTHERWISE SPECIFIED: DIMENSIONS ARE IN MILLIMETERS SURFACE FINISH: TOLERANCES: LINEAR: ANGULAR:	FINISH				DO NOT SCALE DRAWING	REVISION
					PART NAME: Flue gas chimney cover	
	NAME	SIGNATURE	DATE		TITLE: Mixed mode solar crop dryer with biomass backup heater	
DRAWN	Philip Agyeman		12/MAR/13			
CHKD						
APPVD	C.K.K. Sekyere					
MFG						
Q.A						
				MATERIAL: Galvanised Steel	DWG NO. 9 of 20	
				WEIGHT:	SCALE:1:5	SHEET 9 OF 20

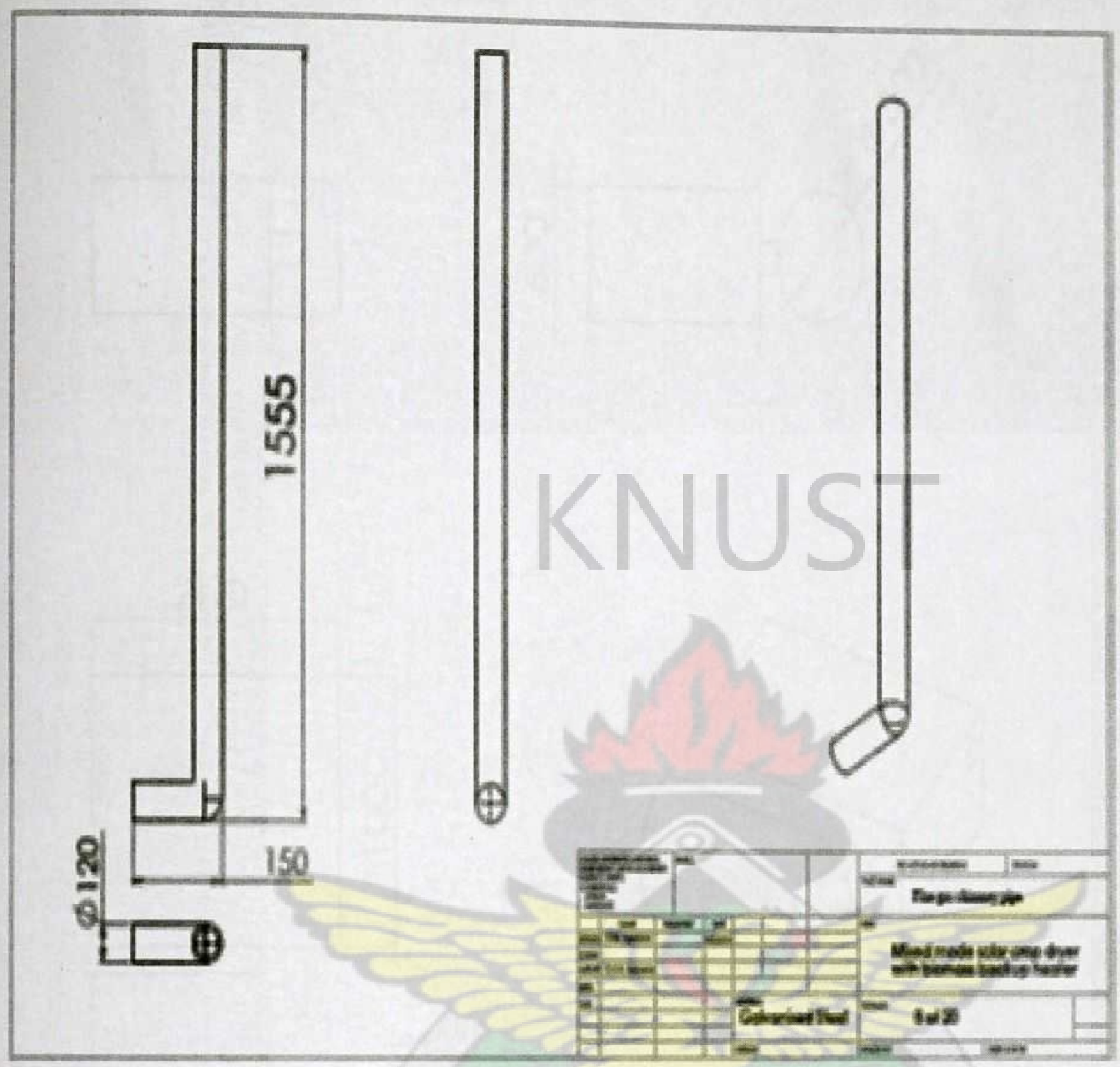

KNUST

11

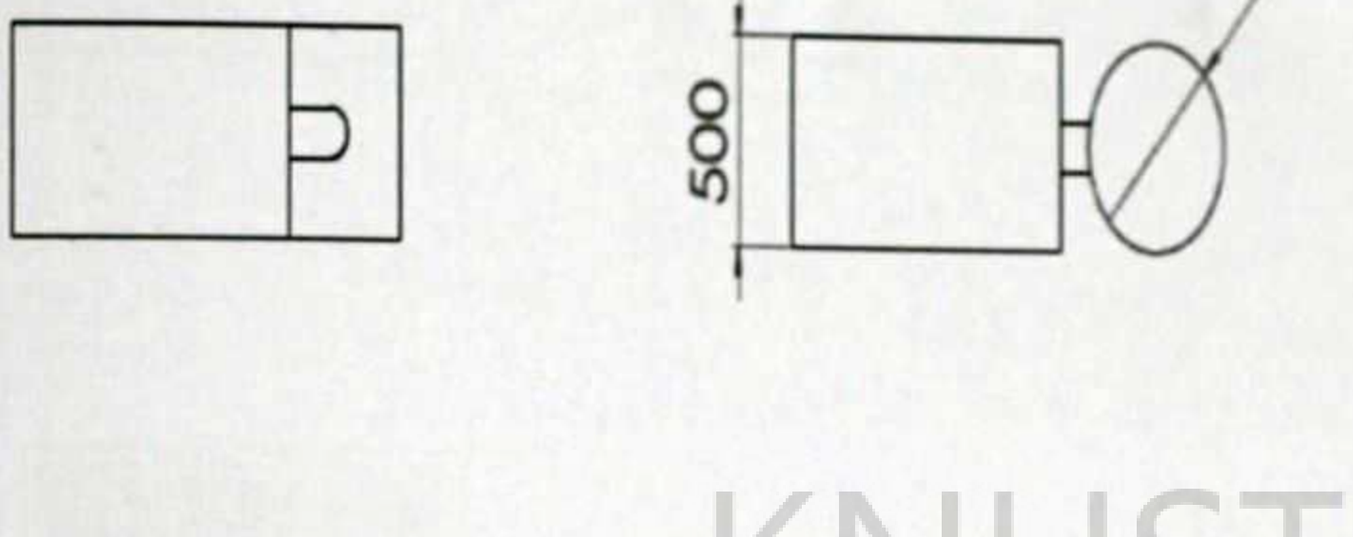

KNUST

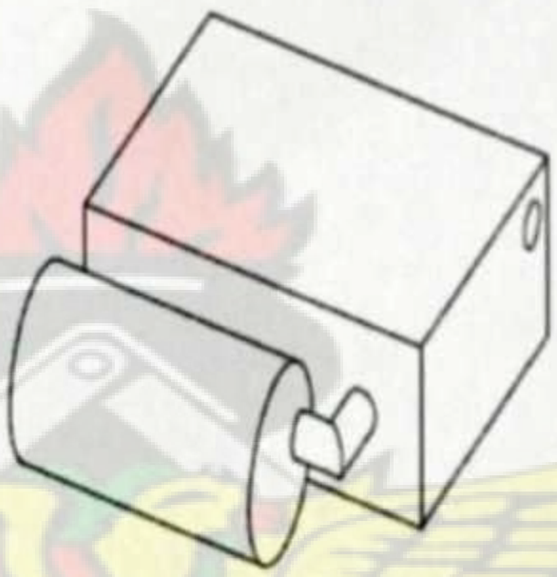

UNLESS OTHERWISE STATED DIMENSIONS ARE IN MILLIMETRES SURFACE FINISH TOLERANCES LINEAR ANGULAR	FINISH				DO NOT SCALE DRAWING	REVISION
					PART NAME: Burner with rectangular duct	
	NAME	SIGNATURE	DATE		TITLE: Mixed mode solar crop dryer with biomass backup heater	
DRAWN	Philip Agyeman					
CHKD						
APPVD	C.K.K. Saleyere					
MFG						
QA						
				MATERIAL: Stainless steel	DWG NO. 19 of 20	
				WEIGHT	SCALE:1:20	SHEET 19 OF 20

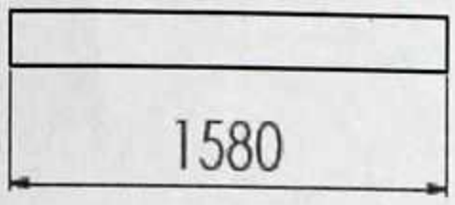

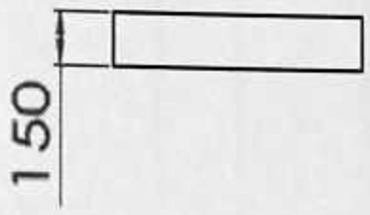

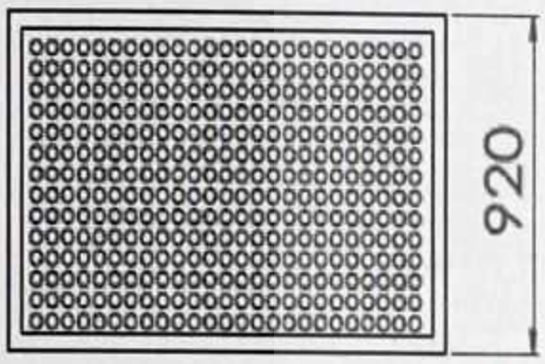

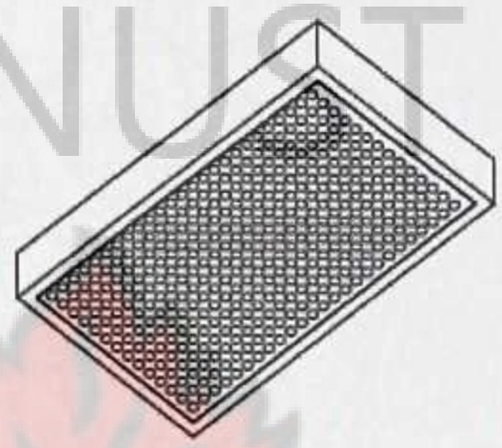

KNUST

UNLESS OTHERWISE SPECIFIED: DIMENSIONS ARE IN MILLIMETERS SURFACE FINISH: TOLERANCES: LINEAR: ANGULAR:	FINISH:				DO NOT SCALE DRAWING	REVISION
					PART NAME: Drying tray	
	NAME	SIGNATURE	DATE		TITLE: Mixed mode solar crop dryer with biomass backup heater	
DRAWN	Philo Agyeman		13/06/2013			
CHK'D						
APP'D	C.K.K. Sekyere					
MFG						
Q.A						
				MATERIAL: Wire mesh and wood	DWG NO. 5 of 20	
				WEIGHT:	SCALE:1:20	SHEET 5 OF 20

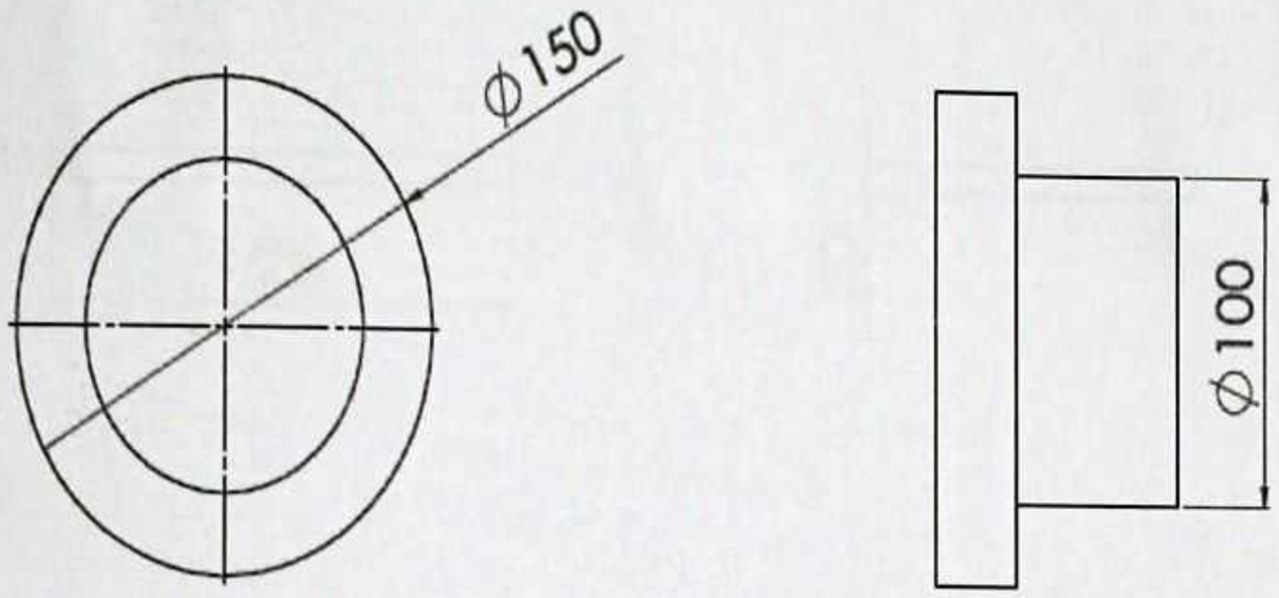

KNUST

UNLESS OTHERWISE SPECIFIED: DIMENSIONS ARE IN MILLIMETRES SURFACE FINISH: TOLERANCES: LINEAR: ANGULAR:				DO NOT SCALE DRAWING	REVISION
				PART NAME: Drying chamber door knop	
	NAME	SIGNATURE	DATE	TITLE: Mixed mode solar crop dryer with biomass backup heater	
DRAWN	Philo Agyeman				
CHKD					
APPVD	C.K.K. Sekyere				
MFG					
Q.A				MATERIAL: WOOD	DWG NO. 2 of 20
				WEIGHT:	SCALE:1:2 SHEET 2 OF 20

NYANSAPO WJSANE NO BADWENMA

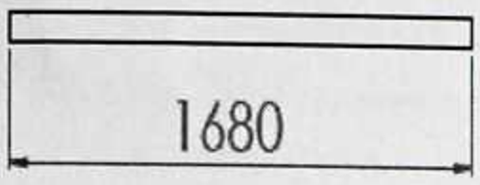

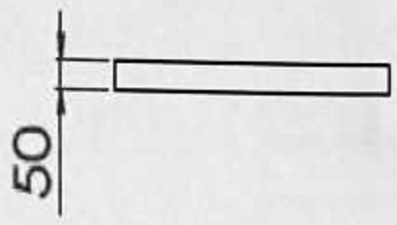

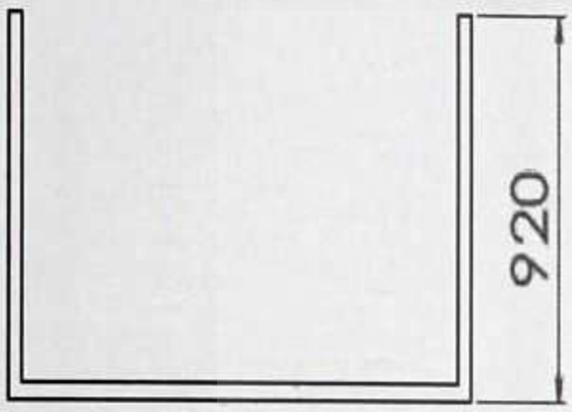

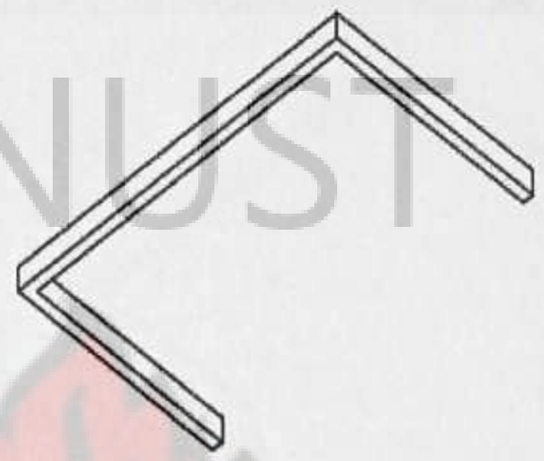

KNUST

UNLESS OTHERWISE SPECIFIED: DIMENSIONS ARE IN MILLIMETERS SURFACE FINISH: TOLERANCES: LINEAR: ANGULAR:				FINISH:			DO NOT SCALE DRAWING
							REVISION
							PART NAME: Spacing before first tray and after last tray
	NAME	SIGNATURE	DATE				TITLE: Mixed mode solar crop dryer biomass backup heater
DRAWN	Philip Agyeman						
CHK'D							
APPV'D	C.K.K. Sekyere						
MFG							
Q.A				MATERIAL: WOOD			DWG NO. 7 of 20
				WEIGHT:			SCALE:1:20 SHEET 7 OF 20

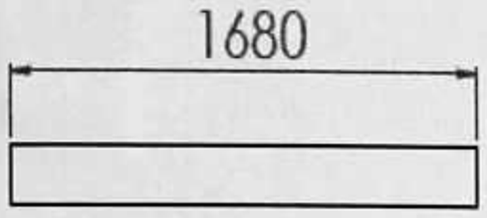

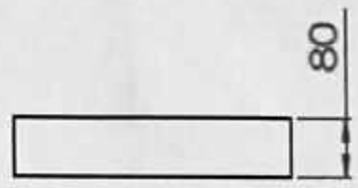

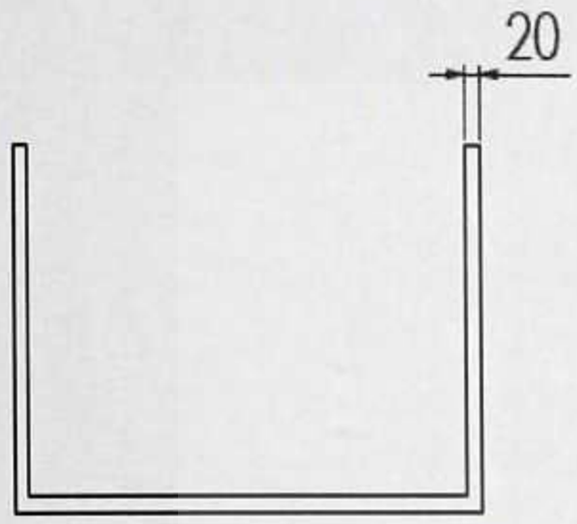

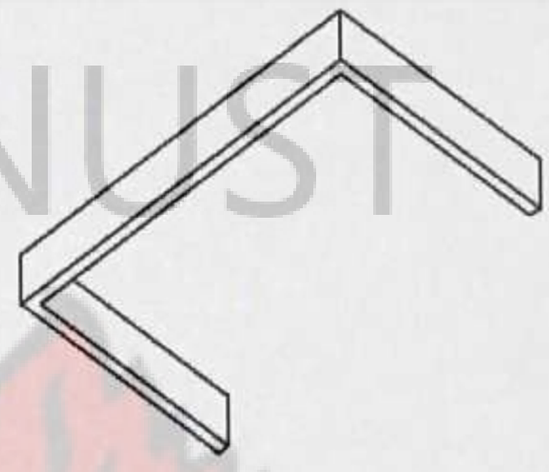

KNUST

UNLESS OTHERWISE SPECIFIED: DIMENSIONS ARE IN MILLIMETERS SURFACE FINISH: TOLERANCES: LINEAR: ANGULAR:				FINISH:			DO NOT SCALE DRAWING / REVISION
	NAME	SIGNATURE	DATE				PART NAME: Tray interspacing
DRAWN	Philip Agyeman		[illegible]				TITLE: Mixed mode solar crop dryer with biomass backup heater
CHKD							
APPVD	C.K.K. Sekyere						
MFG							
Q.A				MATERIAL: Space			DWG NO. 3 of 20
				WEIGHT:			SCALE:1:20 / SHEET 3 OF 20